


Spring 1996

A One-Dimensional Model for Storm Breaching of Barrier Islands

Cheol Shik Shin
Old Dominion University

Follow this and additional works at: https://digitalcommons.odu.edu/cee_etds

 Part of the [Civil Engineering Commons](#), [Geology Commons](#), [Mechanical Engineering Commons](#), and the [Oceanography Commons](#)

Recommended Citation

Shin, Cheol S.. "A One-Dimensional Model for Storm Breaching of Barrier Islands" (1996). Doctor of Philosophy (PhD), dissertation, Civil/Environmental Engineering, Old Dominion University, DOI: 10.25777/3cyj-xw31
https://digitalcommons.odu.edu/cee_etds/44

This Dissertation is brought to you for free and open access by the Civil & Environmental Engineering at ODU Digital Commons. It has been accepted for inclusion in Civil & Environmental Engineering Theses & Dissertations by an authorized administrator of ODU Digital Commons. For more information, please contact digitalcommons@odu.edu.

**A ONE - DIMENSIONAL MODEL FOR STORM BREACHING
OF BARRIER ISLANDS**

by

Cheol Shik Shin

B.C.E. February 1986, Seoul City University, Seoul, Korea
M.S. February 1988, Seoul City University, Seoul, Korea
M.S. December 1991, University of Delaware, Newark, USA

A Dissertation Submitted to the Faculty of
Old Dominion University in Partial Fulfillment of the
Requirement for the Degree of

DOCTOR OF PHILOSOPHY

CIVIL ENGINEERING

OLD DOMINION UNIVERSITY

May 1996

Approved by :

David R. Basco, Ph.D.
Chair of Committee

A. Osman Akan, Ph.D.

Ronald E. Johnson, Ph.D.

George F. Oertel, Ph.D.

ABSTRACT

A ONE - DIMENSIONAL MODEL FOR STORM BREACHING OF BARRIER ISLANDS

Cheol Shik Shin
Old Dominion University, 1996
Advisor : Dr. David R. Basco

A set of numerical models is developed for simulating the four stages of barrier breaching characterized by one horizontal spatial dimension.

The SBEACH model is employed for the first stage of dune/beach erosion. The Lax-Wendroff two-step explicit scheme for Stage II is developed to simulate initiation of ocean flood propagation on initially dry barrier islands and the method of characteristics (MOC) is employed to compute additional boundary data. The development of the Preissmann implicit scheme for water motion and a forward time centered space explicit scheme for sediment motion in Stages III and IV provide a tool to study the volume change and centroid movements of barrier dune during various levels of storm activity.

The accuracy and correctness of numerical codes have been verified by conducting a series of standard tests and numerous volume conservation tests.

The sensitivity studies show that the most sediments are transported landward by larger peak storm surge difference between ocean and bay with shorter time lag and longer duration, and seaward by smaller peak storm surge difference with longer time lag and shorter storm duration

Finally, the integrated numerical model is found to produce reasonable results from the various sensitivity tests which reveal that the numerical model has properly responded to the changes of each model parameter.

ACKNOWLEDGMENTS

The author wishes to express sincere appreciation to his advisor, Professor David R. Basco, for his constant guidance and thoughtfulness. The topic and content of this material originated from his idea. Without his invaluable advice and assistance, this dissertation could not have been possible.

Also, the author would like to acknowledge Dr. George Oertel, Dr. Osman Akan and Dr. Ronald Johnson for their generous advice and assistance.

Special thanks go to all my friends in the Coastal Engineering Group.

The author would like to express his gratitude to his parents, uncle and aunt for their love, encouragement and financial support throughout this research.

Finally, the author is eternally grateful to his wife, Mee Sung and son, Jang Ho for their understanding, patience and love.

TABLE OF CONTENTS

	Page
ABSTRACT	
ACKNOWLEDGMENTS	ii
TABLE OF CONTENTS	iii
LIST OF TABLES	vii
LIST OF FIGURES	x
NOMENCLATURE	xxi
Chapter	
1.0 INTRODUCTION	1
1.1 Background	1
1.2 Objectives	2
1.3 Scope	3
1.4 Limitations	4
2.0 LITERATURE REVIEW	7
2.1 Inlet / Barrier Islands Process	7
2.2 Dune / Beach Erosion	9
2.3 Overwash / Overland Flow	13
2.4 Non-cohesive Sediment Transport	15

3.0	ONE-DIMENSIONAL MODEL DEVELOPMENT (THEORY)	20
3.1	Stage I - Dune/Beach Erosion	24
3.1.1	Water Wave Model	24
3.1.2	Transport Rate Model	29
3.1.3	Profile Change Model	33
3.2	Stage II - Overwash / Overland Flow	34
3.2.1	Water Motion in Overland Flow	34
3.2.2	Sediment Movement and Profile Change	38
3.3	Stage III and IV - Storm Tides	39
3.3.1	Water Motion	40
3.3.2	Sediment Motion	43
3.3.3	Sediment Transport Formula	44
	3.3.3.1 Bed Load Transport	46
	3.3.3.2 Suspended Load Transport	49
4.0	NUMERICAL INTEGRATION PROCEDURES	55
4.1	Stage I - Dune / Beach Erosion	55
4.1.1	Water Wave Model	55
4.1.2	Profile Change Model	57
4.2	Stage II - Overwash / Overland Flow	59
4.2.1	The Lax-Wendroff Two-Step Scheme	59

4.2.2	Method of Characteristics (MOC)	65
4.2.3	Stability	74
4.3	Stage III and IV - Storm Tides	77
4.3.1	Water Motion - The Preissmann Scheme	77
4.3.2	Sediment Motion - FTCS Explicit Scheme	85
4.3.3	Stability	87
4.4	Standard Tests for Computer Codes	89
4.4.1	Static Test	89
4.4.2	Cosine Swing Test	91
4.4.3	Shock Test	92
4.5	Dissipative Interface	96
5.0	INITIAL AND BOUNDARY CONDITIONS	105
5.1	Stage I - SBEACH Model	105
5.2	Stage II - Lax-Wendroff Scheme	108
5.3	Stage III and IV - Preissmann / FTCS Schemes	111
6.0	MODEL TESTS AND RESULTS	114
6.1	Volume Conservation Tests	114
6.2	Model Results	138
6.2.1	Stage I - Dune / Beach Erosion	138
6.2.2	Stage II - Overwash / Overland Flow	139

6.2.3	Stage III and IV - Storm Tides	151
7.0	DISCUSSIONS AND ANALYSES OF RESULTS	275
7.1	Stage I - Dune / Beach Erosion	275
7.2	Stage II - Overwash / Overland Flow	275
7.3	Stage III and IV - Storm Tides	276
7.3.1	Storm Surge Level	277
7.3.2	Time Lag	282
7.3.3	Sediment Grain Size	286
7.3.4	Storm Duration	290
7.4	General Discussion	290
8.0	CONCLUSIONS AND RECOMMENDATIONS	295
8.1	Conclusions	295
8.2	Recommendations	298
	REFERENCES	300
	APPENDIX A	309
	APPENDIX B	314
	BIOGRAPHY	

LIST OF TABLES

TABLE	PAGE
6.1 Volume Losses at Intermediate Time Steps Using Dirichlet Type Boundary Conditions. ($\Delta x=20\text{m}$, $\Delta t=8\text{sec}$, $\gamma=1/200$ and $mmm=20$)	117
6.2 Volume Losses at Intermediate Time Steps Using Dirichlet Type Boundary Conditions. ($\Delta x=20\text{m}$, $\Delta t=8\text{sec}$, $\gamma=1/100$ and $mmm=20$)	117
6.3 Volume Losses at Intermediate Time Steps Using Dirichlet Type Boundary Conditions. ($\Delta x=20\text{m}$, $\Delta t=8\text{sec}$, $\gamma=1/50$ and $mmm=20$)	118
6.4 Volume Losses at Intermediate Time Steps Using Dirichlet Type Boundary Conditions. ($\Delta x=20\text{m}$, $\Delta t=8\text{sec}$, $\gamma=1/40$ and $mmm=20$)	118
6.5 Volume Losses at Intermediate Time Steps Using Dirichlet Type Boundary Conditions. ($\Delta x=20\text{m}$, $\Delta t=8\text{sec}$, $\gamma=1/30$ and $mmm=20$)	119
6.6 Volume Losses at Intermediate Time Steps Using Dirichlet Type Boundary Conditions. ($\Delta x=20\text{m}$, $\Delta t=8\text{sec}$, $\gamma=1/20$ and $mmm=20$)	119
6.7 Volume Losses at Intermediate Time Steps Using Dirichlet Type Boundary Conditions. ($\Delta x=20\text{m}$, $\Delta t=8\text{sec}$, $\gamma=1/10$ and $mmm=20$)	120
6.8 Volume Losses at Intermediate Time Steps Using Dirichlet Type Boundary Conditions. ($\Delta x=10\text{m}$, $\Delta t=4\text{sec}$, $\gamma=1/200$ and $mmm=20$)	121
6.9 Volume Losses at Intermediate Time Steps Using Dirichlet Type Boundary Conditions. ($\Delta x=10\text{m}$, $\Delta t=4\text{sec}$, $\gamma=1/100$ and $mmm=20$)	121
6.10 Volume Losses at Intermediate Time Steps Using Dirichlet Type Boundary Conditions. ($\Delta x=10\text{m}$, $\Delta t=4\text{sec}$, $\gamma=1/50$ and $mmm=20$)	122
6.11 Volume Losses at Intermediate Time Steps Using Dirichlet Type Boundary Conditions. ($\Delta x=10\text{m}$, $\Delta t=4\text{sec}$, $\gamma=1/40$ and $mmm=20$)	122
6.12 Volume Losses at Intermediate Time Steps Using Dirichlet Type Boundary Conditions. ($\Delta x=10\text{m}$, $\Delta t=4\text{sec}$, $\gamma=1/30$ and $mmm=20$)	123
6.13 Volume Losses at Intermediate Time Steps Using Dirichlet Type Boundary Conditions. ($\Delta x=10\text{m}$, $\Delta t=4\text{sec}$, $\gamma=1/20$ and $mmm=20$)	123

6.14	Volume Losses at Intermediate Time Steps Using Dirichlet Type Boundary Conditions. ($\Delta x=10\text{m}$, $\Delta t=4\text{sec}$, $\gamma=1/10$ and $mmm=20$)	124
6.15	Volume Losses at Intermediate Time Steps Using Dirichlet Type Boundary Conditions. ($\Delta x=5\text{m}$, $\Delta t=2\text{sec}$, $\gamma=1/4$ and $mmm=2$)	125
6.16	Volume Losses at End of Simulation Using Various γ , mmm and Grid Sizes Using Dirichlet Type Boundary Conditions.	126
6.17	Volume Losses at Intermediate Time Steps Using Neumann Type Boundary Conditions. ($\Delta x=20\text{m}$, $\Delta t=8\text{sec}$, $\gamma=1/200$ and $mmm=20$)	128
6.18	Volume Losses at Intermediate Time Steps Using Neumann Type Boundary Conditions. ($\Delta x=20\text{m}$, $\Delta t=8\text{sec}$, $\gamma=1/100$ and $mmm=20$)	128
6.19	Volume Losses at Intermediate Time Steps Using Neumann Type Boundary Conditions. ($\Delta x=20\text{m}$, $\Delta t=8\text{sec}$, $\gamma=1/50$ and $mmm=20$)	129
6.20	Volume Losses at Intermediate Time Steps Using Neumann Type Boundary Conditions. ($\Delta x=20\text{m}$, $\Delta t=8\text{sec}$, $\gamma=1/40$ and $mmm=20$)	129
6.21	Volume Losses at Intermediate Time Steps Using Neumann Type Boundary Conditions. ($\Delta x=20\text{m}$, $\Delta t=8\text{sec}$, $\gamma=1/30$ and $mmm=20$)	130
6.22	Volume Losses at Intermediate Time Steps Using Neumann Type Boundary Conditions. ($\Delta x=20\text{m}$, $\Delta t=8\text{sec}$, $\gamma=1/20$ and $mmm=20$)	130
6.23	Volume Losses at Intermediate Time Steps Using Neumann Type Boundary Conditions. ($\Delta x=20\text{m}$, $\Delta t=8\text{sec}$, $\gamma=1/10$ and $mmm=20$)	131
6.24	Volume Losses at Intermediate Time Steps Using Neumann Type Boundary Conditions. ($\Delta x=10\text{m}$, $\Delta t=4\text{sec}$, $\gamma=1/200$ and $mmm=20$)	132
6.25	Volume Losses at Intermediate Time Steps Using Neumann Type Boundary Conditions. ($\Delta x=10\text{m}$, $\Delta t=4\text{sec}$, $\gamma=1/100$ and $mmm=20$)	132
6.26	Volume Losses at Intermediate Time Steps Using Neumann Type Boundary Conditions. ($\Delta x=10\text{m}$, $\Delta t=4\text{sec}$, $\gamma=1/50$ and $mmm=20$)	133
6.27	Volume Losses at Intermediate Time Steps Using Neumann Type Boundary Conditions. ($\Delta x=10\text{m}$, $\Delta t=4\text{sec}$, $\gamma=1/40$ and $mmm=20$)	133
6.28	Volume Losses at Intermediate Time Steps Using Neumann Type	

	Boundary Conditions. ($\Delta x=10\text{m}$, $\Delta t=4\text{sec}$, $\gamma=1/30$ and $mmm=20$)	134
6.29	Volume Losses at Intermediate Time Steps Using Neumann Type Boundary Conditions. ($\Delta x=10\text{m}$, $\Delta t=4\text{sec}$, $\gamma=1/20$ and $mmm=20$)	134
6.30	Volume Losses at Intermediate Time Steps Using Neumann Type Boundary Conditions. ($\Delta x=10\text{m}$, $\Delta t=4\text{sec}$, $\gamma=1/10$ and $mmm=20$)	135
6.31	Volume Losses at Intermediate Time Steps Using Neumann Type Boundary Conditions. ($\Delta x=5\text{m}$, $\Delta t=2\text{sec}$, $\gamma=1/16$ and $mmm=5$)	136
6.32	Volume Losses at Intermediate Time Steps Using Neumann Type Boundary Conditions. ($\Delta x=5\text{m}$, $\Delta t=2\text{sec}$, $\gamma=1/8$ and $mmm=5$)	136
6.33	Volume Losses at End of Simulation Using Various γ , mmm and Grid Sizes Using Neumann Type Boundary Conditions.	137
6.34	Summary of Employed Storm Surge Levels, Wave Heights and Periods.	138
6.35	SBEACH Simulation Results for Various Storm Surge Levels and Wave Conditions.	140
6.36	Running Table for Various Combinations of Important Parameters	156
6.37	Volume Changes, Retreat Speeds and Centroid Positions of Barrier Islands above MLLW in Stages III and IV with Various Storm Surge Elevations. ($t_{lag}=3\text{hr}$, $D_{50}=0.3\text{mm}$ and $T=24\text{hr}$)	160
6.38	Volume Changes, Retreat Speeds and Centroid Positions of Barrier Islands above MLLW in Stages III and IV with Various Time Lags. ($h_{om}=4.0\text{m}$, $h_{bm}=3.0\text{m}$, $D_{50}=0.3\text{mm}$ and $T=24\text{hr}$)	162
6.39	Volume Changes, Retreat Speeds and Centroid Positions of Barrier Islands above MLLW in Stages III and IV with Various Sand Daimaters. ($h_{om}=4.0\text{m}$, $h_{bm}=3.0\text{m}$, $t_{lag}=3\text{hr}$ and $T=24\text{hr}$)	164
6.40	Volume Changes, Retreat Speeds and Centroid Positions of Barrier Islands above MLLW in Stages III and IV with Various Storm Durations. ($h_{om}=4.0\text{m}$, $h_{bm}=3.0\text{m}$, $t_{lag}=3\text{hr}$ and $D_{50}=0.3\text{mm}$)	165

LIST OF FIGURES

FIGURE	PAGE
3.1 Schematic of Barrier Bay System, (a); Localized Breach - Barrier remains above storm surge flood elevation, (b); Inundated Barrier - Barrier submerged below storm surge flood elevation, (c).	21
3.2 Schematic Representation of Key Independent Variables for a Typical Sandbridge, Virginia Cross-section : (a) distorted scale and (b) undistorted scale	23
3.3 Principal Zones of Cross-shore Transport	29
3.4 Definition Sketch of Flow in Alluvial Channel	42
4.1 Schematic Operator of Lax-Wendroff, Two-step Scheme	60
4.2 Left Hand Boundary Data Obtained by Method of Characteristics	66
4.3 Right Hand Boundary Data Obtained by Method of Characteristics	71
4.4 The Box or Preissmann Scheme Drawn for $\theta=\psi=1/2$	79
4.5 Static Test Results for the Lax-Wendroff and Preissmann Scheme at Six Different Time Steps. ($t=1, 200, 400, 600, 800$ and $1,000$)	90
4.6 Cosine Swing Test Results for the Lax-Wendroff and Preissmann Scheme at Five Different Time Steps. ($T=0, T/4, T/2, 3T/4$ and T)	93
4.7 Shock Test Results for the Preissmann Scheme at Six Different Time Steps	95
4.8 Amplitude Portrait for Dissipative Interface	99
4.9 Instability from Dirichlet Type B.C. without Dissipative Interface	100
4.10 Instability from Neumann Type B.C. without Dissipative Interface	101
4.11 Results Using Dirichlet Type B.C. with Dissipative Interface ($\gamma=1/20$) . . .	102
4.12 Results Using Neumann Type B.C. with Dissipative Interface ($\gamma=1/20$) . .	103

5.1	Storm Surge Hydrographs for the Three Synthetic Storms	107
5.2	Storm Surge Hydrographs between Ocean and Bay with $t_{lag}=3hr$, $h_{om}=5m$ and $h_{bm}=5m$	109
5.3	Storm Surge Hydrographs between Ocean and Bay with $t_{lag}=3hr$, $h_{om}=5m$ and $h_{bm}=3m$	110
6.1	SBEACH Results for $h_{om}=5m$, $H_{mo}=5.54m$, $T_p=15.25s$ and $t_1=28,800s$. . .	141
6.2	SBEACH Results for $h_{om}=4.5m$, $H_{mo}=5.45m$, $T_p=15.01s$ and $t_1=29,700s$. .	142
6.3	SBEACH Results for $h_{om}=4m$, $H_{mo}=5.32m$, $T_p=14.78s$ and $t_1=30,720s$. . .	143
6.4	SBEACH Results for $h_{om}=3.5m$, $H_{mo}=5.20m$, $T_p=14.54s$ and $t_1=31,950s$. .	144
6.5	SBEACH Results for $h_{om}=3m$, $H_{mo}=5.08m$, $T_p=14.31s$ and $t_1=33,480s$. . .	145
6.6	Zoomed Profiles for $h_{om}=5m$, $H_{mo}=5.54m$, $T_p=15.25s$ and $t_1=28,800s$	146
6.7	Zoomed Profiles for $h_{om}=4.5m$, $H_{mo}=5.45m$, $T_p=15.01s$ and $t_1=29,700s$	147
6.8	Zoomed Profiles for $h_{om}=4m$, $H_{mo}=5.32m$, $T_p=14.78s$ and $t_1=30,720s$	148
6.9	Zoomed Profiles for $h_{om}=3.5m$, $H_{mo}=5.20m$, $T_p=14.54s$ and $t_1=31,950s$	149
6.10	Zoomed Profiles for $h_{om}=3m$, $H_{mo}=5.08m$, $T_p=14.31s$ and $t_1=33,480s$	150
6.11	Water Surface Profile Changes on Initially Dry Bed during Stage II. ($h_{om}=5m$, $h_{bm}=4m$, $t_{lag}=3hr$ and $D_{50}=0.3mm$ with $h_{ini}=0.05m$)	152
6.12	Water Velocity Changes on Initially Dry Bed during Stage II. ($h_{om}=5m$, $h_{bm}=4m$, $t_{lag}=3hr$ and $D_{50}=0.3mm$ with $h_{ini}=0.05m$)	153
6.13	Bed Elevation Changes in Stages III and IV at $t=0, 1000, 3000, 6000,$ 9000 and 11563 . ($h_{om}=5m$, $h_{bm}=5m$, $t_{lag}=0hr$ and $D_{50}=0.3mm$)	166
6.14	Bed Elevation Changes in Stages III and IV at $t=0, 1000, 3000, 6000,$	

	9000 and 14125. ($h_{om}=5m, h_{bm}=5m, t_{lag}=1hr$ and $D_{50}=0.3mm$)	167
6.15	Bed Elevation Changes in Stages III and IV at $t=0, 1000, 3000, 6000,$ 9000 and 14125. ($h_{om}=5m, h_{bm}=5m, t_{lag}=2hr$ and $D_{50}=0.3mm$)	168
6.16	Bed Elevation Changes in Stages III and IV at $t=0, 1000, 3000, 6000,$ 9000 and 14125. ($h_{om}=5m, h_{bm}=5m, t_{lag}=3hr$ and $D_{50}=0.3mm$)	169
6.17	Bed Elevation Changes in Stages III and IV at $t=0, 1000, 3000, 6000,$ 9000 and 14125. ($h_{om}=5m, h_{bm}=5m, t_{lag}=4hr$ and $D_{50}=0.3mm$)	170
6.18	Bed Elevation Changes in Stages III and IV at $t=0, 1000, 3000, 6000,$ 9000 and 14125. ($h_{om}=5m, h_{bm}=5m, t_{lag}=5hr$ and $D_{50}=0.3mm$)	171
6.19	Bed Elevation Changes in Stages III and IV at $t=0, 1000, 3000, 6000,$ 9000 and 14125. ($h_{om}=5m, h_{bm}=5m, t_{lag}=6hr$ and $D_{50}=0.3mm$)	172
6.20	Bed Elevation Changes in Stages III and IV at $t=0, 1000, 3000, 6000,$ 9000 and 11111. ($h_{om}=4.5m, h_{bm}=4.5m, t_{lag}=0hr$ and $D_{50}=0.3mm$)	173
6.21	Bed Elevation Changes in Stages III and IV at $t=0, 1000, 3000, 6000,$ 9000 and 13890. ($h_{om}=4.5m, h_{bm}=4.5m, t_{lag}=1hr$ and $D_{50}=0.3mm$)	174
6.22	Bed Elevation Changes in Stages III and IV at $t=0, 1000, 3000, 6000,$ 9000 and 13890. ($h_{om}=4.5m, h_{bm}=4.5m, t_{lag}=2hr$ and $D_{50}=0.3mm$)	175
6.23	Bed Elevation Changes in Stages III and IV at $t=0, 1000, 3000, 6000,$ 9000 and 13890. ($h_{om}=4.5m, h_{bm}=4.5m, t_{lag}=3hr$ and $D_{50}=0.3mm$)	176
6.24	Bed Elevation Changes in Stages III and IV at $t=0, 1000, 3000, 6000,$ 9000 and 13890. ($h_{om}=4.5m, h_{bm}=4.5m, t_{lag}=4hr$ and $D_{50}=0.3mm$)	177
6.25	Bed Elevation Changes in Stages III and IV at $t=0, 1000, 3000, 6000,$ 9000 and 13890. ($h_{om}=4.5m, h_{bm}=4.5m, t_{lag}=5hr$ and $D_{50}=0.3mm$)	178
6.26	Bed Elevation Changes in Stages III and IV at $t=0, 1000, 3000, 6000,$ 9000 and 13890. ($h_{om}=4.5m, h_{bm}=4.5m, t_{lag}=6hr$ and $D_{50}=0.3mm$)	179
6.27	Bed Elevation Changes in Stages III and IV at $t=0, 1000, 3000, 6000,$ and 7131. ($h_{om}=4.0m, h_{bm}=4.0m, t_{lag}=0hr$ and $D_{50}=0.3mm$)	180
6.28	Bed Elevation Changes in Stages III and IV at $t=0, 1000, 3000, 6000,$ 9000 and 13628. ($h_{om}=4.0m, h_{bm}=4.0m, t_{lag}=1hr$ and $D_{50}=0.3mm$)	181

6.29	Bed Elevation Changes in Stages III and IV at $t=0$, 1000, 3000, 6000, 9000 and 13628. ($h_{om}=4.0m$, $h_{bm}=4.0m$, $t_{lag}=2hr$ and $D_{50}=0.3mm$)	182
6.30	Bed Elevation Changes in Stages III and IV at $t=0$, 1000, 3000, 6000, 9000 and 13628. ($h_{om}=4.0m$, $h_{bm}=4.0m$, $t_{lag}=3hr$ and $D_{50}=0.3mm$)	183
6.31	Bed Elevation Changes in Stages III and IV at $t=0$, 1000, 3000, 6000, 9000 and 13628. ($h_{om}=4.0m$, $h_{bm}=4.0m$, $t_{lag}=4hr$ and $D_{50}=0.3mm$)	184
6.32	Bed Elevation Changes in Stages III and IV at $t=0$, 1000, 3000, 6000, 9000 and 13628. ($h_{om}=4.0m$, $h_{bm}=4.0m$, $t_{lag}=5hr$ and $D_{50}=0.3mm$)	185
6.33	Bed Elevation Changes in Stages III and IV at $t=0$, 1000, 3000, 6000, 9000 and 13628. ($h_{om}=4.0m$, $h_{bm}=4.0m$, $t_{lag}=6hr$ and $D_{50}=0.3mm$)	186
6.34	Bed Elevation Changes in Stages III and IV at $t=0$, 1000, 3000, 6000, and 7167. ($h_{om}=3.5m$, $h_{bm}=3.5m$, $t_{lag}=0hr$ and $D_{50}=0.3mm$)	187
6.35	Bed Elevation Changes in Stages III and IV at $t=0$, 1000, 3000, 6000, 9000 and 13312. ($h_{om}=3.5m$, $h_{bm}=3.5m$, $t_{lag}=1hr$ and $D_{50}=0.3mm$)	188
6.36	Bed Elevation Changes in Stages III and IV at $t=0$, 1000, 3000, 6000, 9000 and 13312. ($h_{om}=3.5m$, $h_{bm}=3.5m$, $t_{lag}=2hr$ and $D_{50}=0.3mm$)	189
6.37	Bed Elevation Changes in Stages III and IV at $t=0$, 1000, 3000, 6000, 9000 and 13312. ($h_{om}=3.5m$, $h_{bm}=3.5m$, $t_{lag}=3hr$ and $D_{50}=0.3mm$)	190
6.38	Bed Elevation Changes in Stages III and IV at $t=0$, 1000, 3000, 6000, 9000 and 13312. ($h_{om}=3.5m$, $h_{bm}=3.5m$, $t_{lag}=4hr$ and $D_{50}=0.3mm$)	191
6.39	Bed Elevation Changes in Stages III and IV at $t=0$, 1000, 3000, 6000, 9000 and 13312. ($h_{om}=3.5m$, $h_{bm}=3.5m$, $t_{lag}=5hr$ and $D_{50}=0.3mm$)	192
6.40	Bed Elevation Changes in Stages III and IV at $t=0$, 1000, 3000, 6000, 9000 and 13312. ($h_{om}=3.5m$, $h_{bm}=3.5m$, $t_{lag}=6hr$ and $D_{50}=0.3mm$)	193
6.41	Bed Elevation Changes in Stages III and IV at $t=0$, 1000, 3000, 6000, and 6348. ($h_{om}=3.0m$, $h_{bm}=3.0m$, $t_{lag}=0hr$ and $D_{50}=0.3mm$)	194
6.42	Bed Elevation Changes in Stages III and IV at $t=0$, 1000, 3000, 6000, 9000 and 11286. ($h_{om}=3.0m$, $h_{bm}=3.0m$, $t_{lag}=1hr$ and $D_{50}=0.3mm$)	195
6.43	Bed Elevation Changes in Stages III and IV at $t=0$, 1000, 3000, 6000,	

	9000 and 12897. ($h_{om}=3.0m$, $h_{bm}=3.0m$, $t_{lag}=2hr$ and $D_{50}=0.3mm$)	196
6.44	Bed Elevation Changes in Stages III and IV at $t=0$, 1000, 3000, 6000, 9000 and 12897. ($h_{om}=3.0m$, $h_{bm}=3.0m$, $t_{lag}=3hr$ and $D_{50}=0.3mm$)	197
6.45	Bed Elevation Changes in Stages III and IV at $t=0$, 1000, 3000, 6000, 9000 and 12897. ($h_{om}=3.0m$, $h_{bm}=3.0m$, $t_{lag}=4hr$ and $D_{50}=0.3mm$)	198
6.46	Bed Elevation Changes in Stages III and IV at $t=0$, 1000, 3000, 6000, 9000 and 12897. ($h_{om}=3.0m$, $h_{bm}=3.0m$, $t_{lag}=5hr$ and $D_{50}=0.3mm$)	199
6.47	Bed Elevation Changes in Stages III and IV at $t=0$, 1000, 3000, 6000, 9000 and 12897. ($h_{om}=3.0m$, $h_{bm}=3.0m$, $t_{lag}=6hr$ and $D_{50}=0.3mm$)	200
6.48	Bed Elevation Changes in Stages III and IV at $t=0$, 1000, 3000, 6000, 9000 and 14125. ($h_{om}=5.0m$, $h_{bm}=4.0m$, $t_{lag}=0hr$ and $D_{50}=0.3mm$)	201
6.49	Bed Elevation Changes in Stages III and IV at $t=0$, 1000, 3000, 6000, 9000 and 14125. ($h_{om}=5.0m$, $h_{bm}=4.0m$, $t_{lag}=1hr$ and $D_{50}=0.3mm$)	202
6.50	Bed Elevation Changes in Stages III and IV at $t=0$, 1000, 3000, 6000, 9000 and 14125. ($h_{om}=5.0m$, $h_{bm}=4.0m$, $t_{lag}=2hr$ and $D_{50}=0.3mm$)	203
6.51	Bed Elevation Changes in Stages III and IV at $t=0$, 1000, 3000, 6000, 9000 and 14125. ($h_{om}=5.0m$, $h_{bm}=4.0m$, $t_{lag}=3hr$ and $D_{50}=0.3mm$)	204
6.52	Bed Elevation Changes in Stages III and IV at $t=0$, 1000, 3000, 6000, 9000 and 14125. ($h_{om}=5.0m$, $h_{bm}=4.0m$, $t_{lag}=4hr$ and $D_{50}=0.3mm$)	205
6.53	Bed Elevation Changes in Stages III and IV at $t=0$, 1000, 3000, 6000, 9000 and 14125. ($h_{om}=5.0m$, $h_{bm}=4.0m$, $t_{lag}=5hr$ and $D_{50}=0.3mm$)	206
6.54	Bed Elevation Changes in Stages III and IV at $t=0$, 1000, 3000, 6000, 9000 and 14125. ($h_{om}=5.0m$, $h_{bm}=4.0m$, $t_{lag}=6hr$ and $D_{50}=0.3mm$)	207
6.55	Bed Elevation Changes in Stages III and IV at $t=0$, 1000, 3000, 6000, 9000 and 14125. ($h_{om}=5.0m$, $h_{bm}=3.0m$, $t_{lag}=0hr$ and $D_{50}=0.3mm$)	208
6.56	Bed Elevation Changes in Stages III and IV at $t=0$, 1000, 3000, 6000, 9000 and 14125. ($h_{om}=5.0m$, $h_{bm}=3.0m$, $t_{lag}=1hr$ and $D_{50}=0.3mm$)	209
6.57	Bed Elevation Changes in Stages III and IV at $t=0$, 1000, 3000, 6000, 9000 and 14125. ($h_{om}=5.0m$, $h_{bm}=3.0m$, $t_{lag}=2hr$ and $D_{50}=0.3mm$)	210

6.58	Bed Elevation Changes in Stages III and IV at $t=0$, 1000, 3000, 6000, 9000 and 14125. ($h_{om}=5.0m$, $h_{bm}=3.0m$, $t_{lag}=3hr$ and $D_{50}=0.3mm$)	211
6.59	Bed Elevation Changes in Stages III and IV at $t=0$, 1000, 3000, 6000, 9000 and 14125. ($h_{om}=5.0m$, $h_{bm}=3.0m$, $t_{lag}=4hr$ and $D_{50}=0.3mm$)	212
6.60	Bed Elevation Changes in Stages III and IV at $t=0$, 1000, 3000, 6000, 9000 and 14125. ($h_{om}=5.0m$, $h_{bm}=3.0m$, $t_{lag}=5hr$ and $D_{50}=0.3mm$)	213
6.61	Bed Elevation Changes in Stages III and IV at $t=0$, 1000, 3000, 6000, 9000 and 14125. ($h_{om}=5.0m$, $h_{bm}=3.0m$, $t_{lag}=6hr$ and $D_{50}=0.3mm$)	214
6.62	Bed Elevation Changes in Stages III and IV at $t=0$, 1000, 3000, 6000, 9000 and 13628. ($h_{om}=4.0m$, $h_{bm}=3.0m$, $t_{lag}=0hr$ and $D_{50}=0.3mm$)	215
6.63	Bed Elevation Changes in Stages III and IV at $t=0$, 1000, 3000, 6000, 9000 and 13628. ($h_{om}=4.0m$, $h_{bm}=3.0m$, $t_{lag}=1hr$ and $D_{50}=0.3mm$)	216
6.64	Bed Elevation Changes in Stages III and IV at $t=0$, 1000, 3000, 6000, 9000 and 13628. ($h_{om}=4.0m$, $h_{bm}=3.0m$, $t_{lag}=2hr$ and $D_{50}=0.3mm$)	217
6.65	Bed Elevation Changes in Stages III and IV at $t=0$, 1000, 3000, 6000, 9000 and 13628. ($h_{om}=4.0m$, $h_{bm}=3.0m$, $t_{lag}=3hr$ and $D_{50}=0.3mm$)	218
6.66	Bed Elevation Changes in Stages III and IV at $t=0$, 1000, 3000, 6000, 9000 and 13628. ($h_{om}=4.0m$, $h_{bm}=3.0m$, $t_{lag}=4hr$ and $D_{50}=0.3mm$)	219
6.67	Bed Elevation Changes in Stages III and IV at $t=0$, 1000, 3000, 6000, 9000 and 13628. ($h_{om}=4.0m$, $h_{bm}=3.0m$, $t_{lag}=5hr$ and $D_{50}=0.3mm$)	220
6.68	Bed Elevation Changes in Stages III and IV at $t=0$, 1000, 3000, 6000, 9000 and 13628. ($h_{om}=4.0m$, $h_{bm}=3.0m$, $t_{lag}=6hr$ and $D_{50}=0.3mm$)	221
6.69	Bed Elevation Changes in Stages III and IV at $t=0$, 1000, 3000, 6000, 9000 and 11635. ($h_{om}=4.5m$, $h_{bm}=4.0m$, $t_{lag}=0hr$ and $D_{50}=0.3mm$)	222
6.70	Bed Elevation Changes in Stages III and IV at $t=0$, 1000, 3000, 6000, 9000 and 13890. ($h_{om}=4.5m$, $h_{bm}=4.0m$, $t_{lag}=1hr$ and $D_{50}=0.3mm$)	223
6.71	Bed Elevation Changes in Stages III and IV at $t=0$, 1000, 3000, 6000, 9000 and 13890. ($h_{om}=4.5m$, $h_{bm}=4.0m$, $t_{lag}=2hr$ and $D_{50}=0.3mm$)	224
6.72	Bed Elevation Changes in Stages III and IV at $t=0$, 1000, 3000, 6000,	

	9000 and 13890. ($h_{om}=4.5m$, $h_{bm}=4.0m$, $t_{lag}=3hr$ and $D_{50}=0.3mm$)	225
6.73	Bed Elevation Changes in Stages III and IV at $t=0$, 1000, 3000, 6000, 9000 and 13890. ($h_{om}=4.5m$, $h_{bm}=4.0m$, $t_{lag}=4hr$ and $D_{50}=0.3mm$)	226
6.74	Bed Elevation Changes in Stages III and IV at $t=0$, 1000, 3000, 6000, 9000 and 13890. ($h_{om}=4.5m$, $h_{bm}=4.0m$, $t_{lag}=5hr$ and $D_{50}=0.3mm$)	227
6.75	Bed Elevation Changes in Stages III and IV at $t=0$, 1000, 3000, 6000, 9000 and 13890. ($h_{om}=4.5m$, $h_{bm}=4.0m$, $t_{lag}=6hr$ and $D_{50}=0.3mm$)	228
6.76	Bed Elevation Changes in Stages III and IV at $t=0$, 1000, 3000, 6000, 9000 and 13890. ($h_{om}=4.5m$, $h_{bm}=3.0m$, $t_{lag}=0hr$ and $D_{50}=0.3mm$)	229
6.77	Bed Elevation Changes in Stages III and IV at $t=0$, 1000, 3000, 6000, 9000 and 13890. ($h_{om}=4.5m$, $h_{bm}=3.0m$, $t_{lag}=1hr$ and $D_{50}=0.3mm$)	230
6.78	Bed Elevation Changes in Stages III and IV at $t=0$, 1000, 3000, 6000, 9000 and 13890. ($h_{om}=4.5m$, $h_{bm}=3.0m$, $t_{lag}=2hr$ and $D_{50}=0.3mm$)	231
6.79	Bed Elevation Changes in Stages III and IV at $t=0$, 1000, 3000, 6000, 9000 and 13890. ($h_{om}=4.5m$, $h_{bm}=3.0m$, $t_{lag}=3hr$ and $D_{50}=0.3mm$)	232
6.80	Bed Elevation Changes in Stages III and IV at $t=0$, 1000, 3000, 6000, 9000 and 13890. ($h_{om}=4.5m$, $h_{bm}=3.0m$, $t_{lag}=4hr$ and $D_{50}=0.3mm$)	233
6.81	Bed Elevation Changes in Stages III and IV at $t=0$, 1000, 3000, 6000, 9000 and 13890. ($h_{om}=4.5m$, $h_{bm}=3.0m$, $t_{lag}=5hr$ and $D_{50}=0.3mm$)	234
6.82	Bed Elevation Changes in Stages III and IV at $t=0$, 1000, 3000, 6000, 9000 and 13890. ($h_{om}=4.5m$, $h_{bm}=3.0m$, $t_{lag}=6hr$ and $D_{50}=0.3mm$)	235
6.83	Bed Elevation Changes in Stages III and IV at $t=0$, 1000, 3000, 6000, 9000 and 13628. ($h_{om}=4.0m$, $h_{bm}=3.0m$, $t_{lag}=3hr$ and $D_{50}=0.1mm$)	236
6.84	Bed Elevation Changes in Stages III and IV at $t=0$, 1000, 3000, 6000, 9000 and 13628. ($h_{om}=4.0m$, $h_{bm}=3.0m$, $t_{lag}=3hr$ and $D_{50}=0.2mm$)	237
6.85	Bed Elevation Changes in Stages III and IV at $t=0$, 1000, 3000, 6000, 9000 and 13628. ($h_{om}=4.0m$, $h_{bm}=3.0m$, $t_{lag}=3hr$ and $D_{50}=0.3mm$)	238
6.86	Bed Elevation Changes in Stages III and IV at $t=0$, 1000, 3000, 6000, 9000 and 13628. ($h_{om}=4.0m$, $h_{bm}=3.0m$, $t_{lag}=3hr$ and $D_{50}=0.4mm$)	239

6.87	Bed Elevation Changes in Stages III and IV at $t=0$, 1000, 3000, 6000, 9000 and 13628. ($h_{om}=4.0m$, $h_{bm}=3.0m$, $t_{lag}=3hr$ and $D_{50}=0.6mm$)	240
6.88	Bed Elevation Changes in Stages III and IV at $t=0$, 1000, 3000, 6000, 9000 and 13628. ($h_{om}=4.0m$, $h_{bm}=3.0m$, $t_{lag}=3hr$ and $D_{50}=1.0mm$)	241
6.89	Bed Elevation Changes in Stages III and IV at $t=0$, 500, 1500, 3000, 4500 and 6633. ($h_{om}=4.0m$, $h_{bm}=3.0m$, $t_{lag}=3hr$, $D_{50}=0.3mm$ and $T=12hr$)	242
6.90	Bed Elevation Changes in Stages III and IV at $t=0$, 1000, 3000, 6000, 9000 and 13628. ($h_{om}=4.0m$, $h_{bm}=3.0m$, $t_{lag}=3hr$, $D_{50}=0.3mm$ and $T=24hr$)	243
6.91	Bed Elevation Changes in Stages III and IV at $t=0$, 2000, 6000, 12000, 18000 and 27681. ($h_{om}=4.0m$, $h_{bm}=3.0m$, $t_{lag}=3hr$, $D_{50}=0.3mm$ and $T=48hr$)	244
6.92	Bed Elevation Changes with Centroid of the Dune above MLLW in Stages III and IV at $t=0$, 1000, 3000, 6000, 9000 and 14125. ($h_{om}=5.0m$, $h_{bm}=5.0m$, $t_{lag}=3hr$ and $D_{50}=0.3mm$)	245
6.93	Bed Elevation Changes with Centroid of the Dune above MLLW in Stages III and IV at $t=0$, 1000, 3000, 6000, 9000 and 13890. ($h_{om}=4.5m$, $h_{bm}=4.5m$, $t_{lag}=3hr$ and $D_{50}=0.3mm$)	246
6.94	Bed Elevation Changes with Centroid of the Dune above MLLW in Stages III and IV at $t=0$, 1000, 3000, 6000, 9000 and 13628. ($h_{om}=4.0m$, $h_{bm}=4.0m$, $t_{lag}=3hr$ and $D_{50}=0.3mm$)	247
6.95	Bed Elevation Changes with Centroid of the Dune above MLLW in Stages III and IV at $t=0$, 1000, 3000, 6000, 9000 and 13312. ($h_{om}=3.5m$, $h_{bm}=3.5m$, $t_{lag}=3hr$ and $D_{50}=0.3mm$)	248
6.96	Bed Elevation Changes with Centroid of the Dune above MLLW in Stages III and IV at $t=0$, 1000, 3000, 6000, 9000 and 12897. ($h_{om}=3.0m$, $h_{bm}=3.0m$, $t_{lag}=3hr$ and $D_{50}=0.3mm$)	249
6.97	Bed Elevation Changes with Centroid of the Dune above MLLW in Stages III and IV at $t=0$, 1000, 3000, 6000, 9000 and 13890. ($h_{om}=4.5m$, $h_{bm}=4.0m$, $t_{lag}=3hr$ and $D_{50}=0.3mm$)	250
6.98	Bed Elevation Changes with Centroid of the Dune above MLLW in Stages III and IV at $t=0$, 1000, 3000, 6000, 9000 and 14125. ($h_{om}=5.0m$, $h_{bm}=4.0m$, $t_{lag}=3hr$ and $D_{50}=0.3mm$)	251

6.99	Bed Elevation Changes with Centroid of the Dune above MLLW in Stages III and IV at $t=0, 1000, 3000, 6000, 9000$ and 13628. ($h_{om}=4.0m, h_{bm}=3.0m, t_{lag}=3hr$ and $D_{50}=0.3mm$)	252
6.100	Bed Elevation Changes with Centroid of the Dune above MLLW in Stages III and IV at $t=0, 1000, 3000, 6000, 9000$ and 13890. ($h_{om}=4.5m, h_{bm}=3.0m, t_{lag}=3hr$ and $D_{50}=0.3mm$)	253
6.101	Bed Elevation Changes with Centroid of the Dune above MLLW in Stages III and IV at $t=0, 1000, 3000, 6000, 9000$ and 14125. ($h_{om}=5.0m, h_{bm}=3.0m, t_{lag}=3hr$ and $D_{50}=0.3mm$)	254
6.102	Bed Elevation Changes with Centroid of the Dune above MLLW in Stages III and IV at $t=0, 1000, 3000, 6000, 9000$ and 13628. ($h_{om}=4.0m, h_{bm}=3.0m, t_{lag}=0hr$ and $D_{50}=0.3mm$)	255
6.103	Bed Elevation Changes with Centroid of the Dune above MLLW in Stages III and IV at $t=0, 1000, 3000, 6000, 9000$ and 13628. ($h_{om}=4.0m, h_{bm}=3.0m, t_{lag}=1hr$ and $D_{50}=0.3mm$)	256
6.104	Bed Elevation Changes with Centroid of the Dune above MLLW in Stages III and IV at $t=0, 1000, 3000, 6000, 9000$ and 13628. ($h_{om}=4.0m, h_{bm}=3.0m, t_{lag}=2hr$ and $D_{50}=0.3mm$)	257
6.105	Bed Elevation Changes with Centroid of the Dune above MLLW in Stages III and IV at $t=0, 1000, 3000, 6000, 9000$ and 13628. ($h_{om}=4.0m, h_{bm}=3.0m, t_{lag}=3hr$ and $D_{50}=0.3mm$)	258
6.106	Bed Elevation Changes with Centroid of the Dune above MLLW in Stages III and IV at $t=0, 1000, 3000, 6000, 9000$ and 13628. ($h_{om}=4.0m, h_{bm}=3.0m, t_{lag}=4hr$ and $D_{50}=0.3mm$)	259
6.107	Bed Elevation Changes with Centroid of the Dune above MLLW in Stages III and IV at $t=0, 1000, 3000, 6000, 9000$ and 13628. ($h_{om}=4.0m, h_{bm}=3.0m, t_{lag}=5hr$ and $D_{50}=0.3mm$)	260
6.108	Bed Elevation Changes with Centroid of the Dune above MLLW in Stages III and IV at $t=0, 1000, 3000, 6000, 9000$ and 13628. ($h_{om}=4.0m, h_{bm}=3.0m, t_{lag}=6hr$ and $D_{50}=0.3mm$)	261
6.109	Bed Elevation Changes with Centroid of the Dune above MLLW in Stages III and IV at $t=0, 1000, 3000, 6000, 9000$ and 13628. ($h_{om}=4.0m, h_{bm}=3.0m, t_{lag}=3hr$ and $D_{50}=0.1mm$)	262

6.110	Bed Elevation Changes with Centroid of the Dune above MLLW in Stages III and IV at $t=0$, 1000, 3000, 6000, 9000 and 13628. ($h_{om}=4.0m$, $h_{bm}=3.0m$, $t_{lag}=3hr$ and $D_{50}=0.2mm$)	263
6.111	Bed Elevation Changes with Centroid of the Dune above MLLW in Stages III and IV at $t=0$, 1000, 3000, 6000, 9000 and 13628. ($h_{om}=4.0m$, $h_{bm}=3.0m$, $t_{lag}=3hr$ and $D_{50}=0.3mm$)	264
6.112	Bed Elevation Changes with Centroid of the Dune above MLLW in Stages III and IV at $t=0$, 1000, 3000, 6000, 9000 and 13628. ($h_{om}=4.0m$, $h_{bm}=3.0m$, $t_{lag}=3hr$ and $D_{50}=0.4mm$)	265
6.113	Bed Elevation Changes with Centroid of the Dune above MLLW in Stages III and IV at $t=0$, 1000, 3000, 6000, 9000 and 13628. ($h_{om}=4.0m$, $h_{bm}=3.0m$, $t_{lag}=3hr$ and $D_{50}=0.6mm$)	266
6.114	Bed Elevation Changes with Centroid of the Dune above MLLW in Stages III and IV at $t=0$, 1000, 3000, 6000, 9000 and 13628. ($h_{om}=4.0m$, $h_{bm}=3.0m$, $t_{lag}=3hr$ and $D_{50}=1.0mm$)	267
6.115	Bed Elevation Changes with Centroid of the Dune above MLLW in Stages III and IV at $t=0$, 500, 1500, 3000, 4500 and 6633. ($h_{om}=4.0m$, $h_{bm}=3.0m$, $t_{lag}=3hr$, $D_{50}=0.3mm$, $T=12hr$)	268
6.116	Bed Elevation Changes with Centroid of the Dune above MLLW in Stages III and IV at $t=0$, 1000, 3000, 6000, 9000 and 13628. ($h_{om}=4.0m$, $h_{bm}=3.0m$, $t_{lag}=3hr$, $D_{50}=0.3mm$, $T=24hr$)	269
6.117	Bed Elevation Changes with Centroid of the Dune above MLLW in Stages III and IV at $t=0$, 2000, 6000, 12000, 18000 and 27681. ($h_{om}=4.0m$, $h_{bm}=3.0m$, $t_{lag}=3hr$, $D_{50}=0.3mm$, $T=48hr$)	270
6.118	Bed Elevations Changes in Stages III and IV at $t=0$ and 14125. ($h_{om}=4.5m$, $h_{bm}=4.0m$, $t_{lag}=1hr$ and $D_{50}=0.3mm$)	271
6.119	Bed Elevations Changes in Stages III and IV at $t=0$ and 14125. ($h_{om}=4.5m$, $h_{bm}=4.0m$, $t_{lag}=2hr$ and $D_{50}=0.3mm$)	271
6.120	Water Depth and Velocity Variation at the Initial Top of Dune. ($h_{om}=4.0m$, $h_{bm}=3.0m$, $t_{lag}=3hr$, $D_{50}=0.3mm$ and $\Delta t=4sec$)	272
6.121	Suspended Sediment Transport Ratio at the Initial Top of Dune. ($h_{om}=4.0m$, $h_{bm}=3.0m$, $t_{lag}=3hr$, $D_{50}=0.3mm$ and $\Delta t=4sec$)	273

6.122	Total Sediment Transport Rates for Various Time Lags at the Initial Top of Dune. ($h_{om}=4.0m$, $h_{bm}=3.0m$, $D_{50}=0.3mm$ and $\Delta t=4sec$)	274
7.1	Volume Changes above MLLW for Five Different Storm Surge Levels. ($t_{lag}=3hr$, $D_{50}=0.3mm$ and $T=24hr$)	278
7.2	Dune Retreat Speeds above MLLW for Five Different Storm Surge Levels. ($t_{lag}=3hr$, $D_{50}=0.3mm$ and $T=24hr$)	279
7.3	Volume Changes above MLLW for Five Different Storm Surge Levels. ($t_{lag}=3hr$, $D_{50}=0.3mm$ and $T=24hr$)	280
7.4	Dune Retreat Speeds above MLLW for Five Different Storm Surge Levels. ($t_{lag}=3hr$, $D_{50}=0.3mm$ and $T=24hr$)	281
7.5	Volume Changes above MLLW for Various Time Lags. ($h_{om}=4.0m$, $h_{bm}=3.0m$, $D_{50}=0.3mm$ and $T=24hr$)	283
7.6	Dune Retreat Speeds above MLLW for Various Time Lags. ($h_{om}=4.0m$, $h_{bm}=3.0m$, $D_{50}=0.3mm$ and $T=24hr$)	284
7.7	Volume Changes and Dune Retreat Speeds above MLLW for Various Time Lags at $t=3000$. ($h_{om}=4.0m$, $h_{bm}=3.0m$, $D_{50}=0.3mm$ and $T=24hr$)	285
7.8	Volume Changes above MLLW for Various Sand Diameters. ($h_{om}=4.0m$, $h_{bm}=3.0m$, $t_{lag}=3.0hr$ and $T=24hr$)	287
7.9	Dune Retreat Speeds above MLLW for Various Sand Diameters. ($h_{om}=4.0m$, $h_{bm}=3.0m$, $t_{lag}=3.0hr$ and $T=24hr$)	288
7.10	Volume Changes and Dune Retreat Speeds above MLLW for Various Sand Diameters at $t=3000$. ($h_{om}=4.0m$, $h_{bm}=3.0m$, $t_{lag}=3.0hr$ and $T=24hr$)	289
7.11	Volume Changes above MLLW for Various Storm Durations. ($h_{om}=4.0m$, $h_{bm}=3.0m$, $t_{lag}=3.0hr$ and $D_{50}=0.3mm$)	291
7.12	Dune Retreat Speeds above MLLW for Various Storm Durations. ($h_{om}=4.0m$, $h_{bm}=3.0m$, $t_{lag}=3.0hr$ and $D_{50}=0.3mm$)	292
7.13	Volume Changes above MLLW in Each Stage for 24 Hours Storm Duration. ($h_{om}=4.0m$, $h_{bm}=3.0m$, $t_{lag}=3.0hr$ and $D_{50}=0.3mm$)	294

NOMENCLATURE

- a** Reference level, L.
Wave amplitude, L.
- A** Amplification factor.
Empirical coefficient found from large scale laboratory tests (Kajima et al., 1983), (=1.14).
Grain size (or fall velocity) parameter.
- B** Empirical coefficient found from large scale laboratory tests (Kajima et al, 1983), (=0.21).
- $\bar{\mathbf{B}}$ Coefficient matrix.
- C** Wave celerity, L/T.
Empirical constant.
- C_a Reference concentration, M/L^3 .
- C_b Bed-load concentration, M/L^3 .
- C_c Chezy coefficient.
- C_g Wave group celerity, L/T.
- C_0 Maximum bed concentration, M/L^3 .
- C_r Courant number.
- C_s Sediment concentration, M/L^3 .
- C_{\pm} Characteristic speeds, L/T.
- C' Overall Chezy coefficient.
- CF** Control function.
- d** Local water depth to SWL, L.
- d_b Initial bay boundary water depth, L.
- d_o Initial ocean boundary water depth, L.
- D** Wave energy dissipation per unit volume, $F/L^2 \cdot T$.
Empirical coefficient.

D_{50}	Mean particles diameter, L.
D_{90}	Diameter of bed material with 90 percent finer, L.
D_c	Dune crest elevation above MLLW, L.
D_{eq}	Equilibrium wave energy dissipation per unit water volume, F-L/L ³ -T.
D_s	Representative particle diameter of suspended sediment, L.
D^*	Wave energy dissipation, F/L-T.
D_*	Particle parameter.
E	Total wave energy per wave, F-L/L.
\bar{E}	Wave energy density, F-L/L ² .
\bar{E}_s	Stable wave energy density, F-L/L ² .
f	General function.
\bar{f}	Vector of flow variables.
f_j^n	Arbitrary function at grid point j and time level n .
F	Wave energy flux, L-F/L-T.
	Correction factor for suspended load.
	Auxiliary variable.
$\bar{F}(\bar{V})$	Vector of flow variables.
F_r	Froude number.
F_s	Stable wave energy flux, L-F/L-T.
g	Gravity constant, L/T ² .
$g_{1,2}$	Eigenvalues of matrix \bar{G} .
G	Auxiliary variable.
\bar{G}	Amplification matrix.
$\bar{G}(\bar{V})$	Vector of flow variables.
h	Total water depth (= $d+\bar{\eta}$), L.
h^*	Local quasi-constant flow depth in stage III and IV, L.
	Average flow depth from nearest four corners, L.
h_b	Bay boundary water depth, L.
	Breaking water depth, L.

h'_b	Water level rise at bay boundary, L.
h_{bm}	Peak storm surge height in the bay, L.
h_o	Ocean boundary water depth, L. Total storm surge plus tidal elevation above datum, L. Still water depth, L.
h'_o	Water surface elevation above MSL at ocean boundary, L.
h_{om}	Peak (maximum) storm surge height in the ocean, L.
H	Wave height, L.
H_b	Wave height at the breaker point, L.
H_{mo}	Significant wave height, L.
H_o	Deep water wave height, L.
H_p	Wave height at the plunge point, L.
H_s	Stable wave height, L.
H_z	Wave height at the end of the surf zone, L.
J_{\pm}	Riemann invariant, L/T.
k_s	Effective bed roughness ($=3D_{90}$), L.
K	Empirical transport rate coefficient, L^4/F . Profile diffusion coefficient for stage II.
L	Wave length, L. Length of the channel, L.
L_o	Deep water wave length, L.
Δt	Alternate time step.
M	Empirically determined coefficient.
n	Coefficient. $=1/2\{1+(2\pi d/L)/(\sinh 2\pi d/L)\}$.
p	Porosity of the bed.
P	Auxiliary variable.
\bar{P}	Coefficient matrix.
q	Cross-shore sand transport rate, $L^3/L-T$.

	Volumetric flowrate per unit width, $L^3/L-T$.
q^*	Average flow rate from the nearest four corners, $L^3/L-T$.
q_b	Bed-load transport per unit width, L^2/T .
	Transport rate at the breaker point, $L^3/L-T$.
q_L	Lateral sediment inflow, $L^3/L-T$.
q_p	Transport rate at the plunge point, $L^3/L-T$.
q_s	Suspended load transport per unit width, L^2/T .
q_t	Total sediment transport rate, L^2/T .
q_z	Transport rate at the end of the broken wave region, $L^3/L-T$.
Q	Auxiliary variable.
R	Reynolds' number.
	Auxiliary variable.
R_b	Hydraulic radius of the bed, L .
S	Total volume of bottom profile, L^3/L .
S_f	Friction slope.
S_o	Representative, averaged, bottom slope across the barrier.
S_s	Specific gravity of the sediment.
S_{xx}	Radiation stress component directed onshore, F/L .
t_1	SBEACH simulation time, T .
t_2	Simulation time in Stage I and II, T .
T	Storm duration, T .
	Transport stage parameter.
	Wave period, T .
T_p	Spectral peak period, T .
$\tan\beta$	Beach slope seaward of break point.
u	Water velocity, L/T .
u^*	Local quasi-constant flow velocity, L/T .
u_*	Overall bed-shear velocity, L/T .
$u_{*,cr}$	Critical bed-shear velocity, L/T .

u'	Effective bed-shear velocity, L/T.
u_b	Particle velocity, L/T.
V	Cross-section volume, L ³ .
\bar{V}	Vector of flow variables.
V_{ini}	Total cross-section volume of initial profile, L ³ /L.
V_{fin}	Total cross-section volume of final profile, L ³ /L.
w	Dune base width, L. The representative fall velocity for the characteristic grain size in the profile, L/T.
w_s	Fall velocity of suspended sediment in Stage III and IV, L/T.
W	Barrier width, L.
x	Cross-shore coordinate, L.
x_b	Location of wave breaker point, L.
x_p	Location of plunge point, L.
x_r	Runup distance, L.
x_z	Location of the end of the broken wave region, L ³ /L-T.
y	Water surface elevation above a datum, L.
z	Bed elevation above an arbitrary datum, L.
z_j^*	Smoothed or filtered bed elevation at a time level, L.
Z	Suspension parameter.
Z'	Adjusted suspension parameter.
α	Dimensionless wave number.
β	A factor.
γ	Dissipative interface weighting factor ($K\Delta t/\Delta x^2$), L. Ratio between wave height and water depth at the breaker point.
Γ	Stable wave height coefficient.
δ_b	Thickness of bed-load layer, L.
Δ	Bed-form height, L.
Δh	Stage difference between ocean and bay, L.
Δt	Time step, T.

ΔV	Total cumulative volume change, L^3/L .
ΔV_1	Total cumulative volume change, %.
ΔV_2	Cumulative volume outgoing through both boundaries, %.
ΔV_3	Cumulative volume loss due to numerical error, %.
Δx	Space step, L.
Δz	$= z^{n+1} - z^n$, L.
ϵ	Empirical transport rate coefficient for the slope-dependent term, L^2/T .
$\bar{\eta}$	Time -averaged, mean water level change (set up or set down), L.
θ	Characteristic distance, L. Particle mobility parameter. Wave angle (crest) relative to bottom contour. Weighting coefficient.
θ_{cr}	Critical mobility parameter.
κ	Breaker, decay model coefficient. Von Karman constant (=0.40).
λ_1	Empirical spatial decay coefficient, L^{-1} .
λ_2	Empirical spatial decay coefficient, L^{-1} .
ν	Kinematic viscosity coefficient, L^2/T .
$\bar{\xi}$	Fourier coefficient.
ξ_0	Deep water surf-similarity parameter, $\tan\beta/(H_0/L_0)^{1/2}$.
ρ	Water density, M/L^3 .
σ_s	Geometric standard deviation of bed material.
τ	Time lag, T.
φ	Overall correction factor.
Ψ	Bed-form steepness. Weighting coefficient.

1.0 INTRODUCTION

1.1 Background

Barrier islands protect the bays, lagoons and estuaries that lie behind them. The reduced wave energy environment permits the retention of cohesive sediments and grasses to survive in the tidal marsh areas. About 35 percent of the U.S. coastline is composed of barrier island - bay systems. At many locations, landward migration (transgression) of barrier islands toward the mainland is occurring and is attributed to sea level rise.

Two mechanisms for landward migration have been put forward: namely (1) rollover due to washover events during storms; and (2) the creation of *new tidal inlets* and sand trapping in the tidal deltas (Leatherman, 1988). Thus new tidal inlets interrupt the longshore sediment transport processes and play a major role in sediment budgets and shoreline erosion.

Dune/beach erosion, wave overwash and hydraulic (flood/ebb) flows that create a *low* profile section across a barrier island but *not* necessarily a new tidal inlet are herein defined as a "breach" event. New tidal inlet formation is therefore defined as a breach event such that the *entire* low profile section lies *below* the mean lower low water (MLLW) elevation at the conclusion of the storm event. Each successive, normal, flood-ebb tidal cycle will cause water to flow through the new inlet.

In general, four modeling stages are involved, namely: (1) storm surge, wave attack and the dune/beach physics; (2) overwash and overland island flow; (3) storm tidal flooding

from ocean to bay; and (4) storm tidal ebbing from bay to ocean.

This study emphasizes the development of a set of numerical models to simulate the four stages of barrier breaching for the *unit width of inundated breaching* mode characterized by one horizontal spatial dimension. The sensitivity tests will be carried out to understand which conditions or parameters are critical for the breaching of barrier islands. The problem is fully nonlinear, unsteady in time and involves both short wave and long wave motions over a variable-positioned bottom boundary.

1.2 Objectives

The focal point of this study is the development of integrated numerical models of the conservation equations for wave motions, water flows and sediment transports that take place during four process stages of dune/beach erosion, dune breach and the cutting of a new tidal inlet through a barrier island. Recent successes in the development, calibration and verification of dune/beach erosion models give confidence that computer simulations of the remaining stages in the process can be achieved. These computer models will provide insight regarding the storm energy levels, barrier and back bay geometry and sediment dynamics necessary to produce a break-through event. Knowledge will be gained to understand why new inlets are created at certain locations along barrier-bay systems during major storms.

The ultimate goal is to provide a simulation and prediction tool to study how global climate change will alter the number and frequency of barrier island breaches on littoral drift coasts. Mitigation and modification techniques such as dune strengthening, beach nourishment and underwater, shore-parallel sand berm construction may then be

economically focused at vulnerable locations to minimize impacts on the coastal zone.

1.3 Scope

The following work tasks are carried out in this study.

Task No.1 - Develop, Link and Test Codes. The dune/beach erosion model, SBEACH, for Stage I is run on the PC workstation. After each time step, a check is made to determine if the water levels exceed the eroded dune crest elevation. If true, the output of Stage I is linked to Stage II developed for overland flow computation. The Lax-Wendroff two-step explicit scheme has been considered as an approximation to the differential equations and the method of characteristics is elaborated to compute additional boundary data.

The major task is to develop the Preissmann implicit codes for water motion and a forward time centered space (FTCS) explicit scheme for sediment motion (Stage III and IV). Standard tests for a fixed boundary aid in the calibration and verification of the numerical models.

All the stages are then linked and run together as one model to study the sensitivity of the important variables on the breaching of barrier islands.

Task No.2 - Develop Sensitivity Tests. The barrier island cross-section volume above the Mean Lower Low Water (MLLW) level can be considered as the fundamental indicator of the state of the barrier to withstand attack by various storm intensities. A typical geometric section at Sandbridge, Virginia is employed to study the influence of key variables. The most important variables are the maximum elevation of the storm surge height, phase lag between

ocean and bay, duration of coastal storm, and sediment diameter. A volume conservation check will be made for the whole spatial computational domain from ocean boundary to bay to verify existing numerical errors. Various synthetic storms will be devised to test the sensitivity of the model. In Task No.2, the volume losses, barrier islands retreat speeds and the locations of centroid of dune above MLLW will be produced for each test.

Task No.3 - Analyze and Critique Results. The results from Tasks No.1 and 2 will be analyzed and critiqued to learn if the model can produce reasonable results. The sensitivity tests will help to reveal which boundary conditions or variables are critical in the transport of the most sediment landward (Stage III) and seaward (Stage I and IV) in the model.

1.4 Limitations

The fundamental limitation of overall studies comes from the one-dimensional formulation representing only longitudinal bed profiles (across barrier islands), free surface profiles and sediment transports as a function of time and hydraulic flow conditions. Major limitations and assumptions for each stage have been verified as:

Stage I - Dune / Beach Erosion Model.

- Sediment transport is not affected by the fluid velocity (*i.e.*, storm induced cross-shore current) because the breaking of short period waves is assumed to be the major cause of profile change, and thus the major part of cross-shore sand transport takes place only in the surf zone.
- Constant wave height and period are assumed for this study in terms of input conditions at the ocean boundary.

- The gradient of the longshore sediment transport is assumed to be negligibly small at the site so that profile change is solely affected by cross-shore sediment transport.
- Waves on the bay are assumed negligible.

Stage II - Overland Flow Model.

- Zero flow depth is not allowed by introducing small base flows on the initial flood plains.
- Water wave motion is considered secondary in importance to translation processes advecting both water and sediment in the overland direction.
- Breach width is constant (*i.e.*, unit) in time and space.
- No sediment transport is assumed in either direction during the extremely short time period for Stage II.

Stage III and IV - Storm Tide Model.

- Water wave motion is considered secondary.
- A lateral distribution of deposits or erosions related to the tractive force is not introduced.
- It is assumed for the water motion calculation that the bottom elevations do not change during a time step (*i.e.*, uncoupled model).
- Within a short period of time, the change in bed slope is assumed very small.
- Suppression of the convective acceleration term in equation of motion is assumed to give little effect on the results.
- Dissipative interface is introduced for all stages to stabilize the originally

unstable numerical scheme when and where flows change rapidly.

- Proposed sediment transport formulas are assumed to give a reliable estimate of the whole computational and physical ranges in this study.

2.0 LITERATURE REVIEW

2.1 Inlet / Barrier Islands Process

Early studies of tidal inlets focused on their hydraulics and sedimentation characteristics regarding ship pathways to protected harbors within the estuary (O'Brien, 1931; Escoffier, 1940 and 1972; Keulegan, 1967). Pierce (1970) discussed the conditions under which washover fans or tidal inlets form and which conditions permit inlet formation from the seaward side or from the lagoon side. Bruun (1978) has written an entire book devoted to their stability. Oertel (1988) presented qualitative analyses and reviews for the processes of sediment exchange between tidal inlets, ebb deltas and barrier islands.

The barrier island spit called Nauset Beach separating Pleasant Bay from the Atlantic Ocean at the town of Chatham, Maryland was breached during a severe northeaster on 2 January 1987. A new inlet formed just south of the location predicted by Giese (1978). Analysis of historical map data for the spit shows a cyclic phenomenon on the order of 140 - 150 years for (1) tidal inlet formation (2) southerly drift of the inlet (3) eventual disintegration of the southern segment, (4) continued longshore drift and spit growth, and (5) eventual re-establishment of a continuous Nauset Beach Spit as existed prior to the new breach in 1987 (Goldsmith, 1972; McClennen, 1979). This cyclic pattern was used by Giese (1978) for his *new inlet* location prediction. However, there is no way to generalize these results for application at other locations. In addition, accelerated sea level rise could considerably alter the period of the cycle even at this location.

Stauble *et al.* (1990) described some of the morphological changes that occurred

along the South Carolina coast to the beaches, dunes, inlets and barrier island areas during Hurricane Hugo, 22 September 1989. Several beaches were breached across narrow sections of barrier islands. Overwash processes in many locations transported sand into the back beach areas and in some instances completely across narrow barrier islands. A chronological overview of aspects of the meteorology, climatology, sea-state, storm-surge and coastal morphologic impact associated with Hurricane Andrew, 26 August 1992 was provided (Stone *et al.*, 1993). Storm surge inundation, breaching and overwash were most notable along the barrier island arc.

When a new inlet forms, significant environmental hazards may be created. Increased currents, wave energy, salinity levels, etc., transform the protected embayment ecology into an open coast, ocean ecology. Pros and cons exist regarding the environmental impact and ecological value or destruction caused by a new tidal inlet through a barrier-bay system (Stauble, 1989; Giese, Liu and Aubrey, 1989; Fessenden and Scott, 1989; Basco, 1990).

The temporal and spatial distribution of over three hundred historic and active tidal inlets along the entire North Atlantic seaboard (Long Island to Florida) were analyzed from published information in McBride (1986). This reference source will be extremely valuable for field verification of the developed models.

The most recent international symposium on tidal inlets was held at the Woods Hole Oceanographical Institute (1986) with a compendium of the scientific papers edited by Aubrey and Weishar (1988). The editors state in their Preface that this volume provides a broad overview of present day tidal inlet research but it *fails* to answer some major questions such as : “ Why are new inlets formed....?” and “ How is climate change going to alter the

hydrodynamic balances within tidal inlets and their distribution?” To these questions a third may be added, namely, “ Will global climate and sea level change increase the number and frequency of barrier islands breaches and the cutting of new tidal inlets during major storm events ? ”

The initial step toward attempting to answer these questions is the main focus of the research herein. Presently, no generally applicable, empirical and/or semi-theoretical models exist for the prediction of a new tidal inlet along a barrier island coast. Site specific predictions of a new tidal inlet have been made upon *historical records* (Giese, 1978) or using a crude, *width-of-island* approach (Dolan, 1985). However, none incorporated the physics of coastal storm energy, barrier island geometry, and sediment transport physics within the general conservation laws of mass, momentum and energy to study the *potential* for island breaching and/or new inlet formation as a *break-through* event.

Recent major advances in the physical problem formulation and numerical modeling of (1) dune/beach response to coastal storm events and (2) riverine, mobile-bed and sediment dynamics have made it now possible to solve the barrier island, break-through problem.

2.2 Dune / Beach Erosion

The theory of erosion by rise of sea level was first advanced in 1962 (Bruun, 1962) and briefly concerns a long-term budget of onshore/offshore movement of material. The rule is based on the assumption of a closed material balance system between the (1) beach and nearshore, and (2) the offshore bottom profile. Bruun (1983) discussed boundary conditions and made adjustments which make the rule more *practical* or *realistic*.

Edelmann (1968, 1972) observed that during severe storms: (1) beach change is mainly the result of sand transport perpendicular to the shoreline; and (2) transfer of sand occurs from the berm and dune to the seaward edge of the surf zone where it is limited by incoming breaking waves. Swart (1976) developed predictive equations for both longshore and onshore-offshore sediment transport, which are being used in practical applications.

Dean (1976, 1977) proposed that short-term, storm-induced erosion may also be determined graphically from a knowledge of pre- and post-storm equilibrium beach profiles, the maximum storm surge level, and breaking wave height.

Vellinga (1982, 1983) has proposed a procedure that has been shown to agree reasonably well with measured post-storm profiles associated with the 1953 storm event in the Netherlands.

Moore (1982) developed a numerical model to predict beach profile change produced by breaking waves. He assumed the transport rate to be proportional to the energy dissipation from breaking waves per unit water volume above an equilibrium value of Dean (1977).

Kriebel (1982, 1986) and Kriebel and Dean (1984, 1985) developed a numerical model to predict beach and dune erosion using the same transport relationship as Moore (1982). The amount of erosion was primarily determined by water-level variation and breaking wave height. They also applied their model to estimate the probability distribution of dune recession due to hurricanes using a Monte Carlo simulation method. Kobayashi (1987) supplemented their work and showed that the problem of beach and dune erosion by a storm could be formulated as a one-dimensional diffusion problem with moving boundaries at the breaker line and shoreline.

Kriebel, Dally and Dean (1986a and b) studied beach recovery after storm events both during laboratory and field conditions, noting the rapid process of berm formation. They found marked differences in profile response depending on the initial shape's being planar or equilibrium profile type. An initially plane beach produced a more pronounced bar and steeper offshore slopes. The fall speed parameter and the deepwater wave steepness were used to distinguish erosional and accretionary profiles using large wave tank data.

The numerical model originally developed by Kriebel (1982,1986), and Kriebel and Dean (1985) has been revised by Kriebel and named EDUNE. The model predicts the time-dependent evolution of existing or design beach and dune profiles for specified storm surges and storm wave conditions. The sediment transport rate is based on the equilibrium beach profile theory of Dean (1977, 1984) and the surf zone energy dissipation mechanism. The wave height is assumed to be related to water depth in a fixed ratio, and the wave period does not directly enter in the model. The time dependent profile response is obtained by solving the equation for conservation of sediment in finite-difference form, along with a simplified expression for cross shore sediment transport rates. The model also allows a wide range of pre-storm profiles to be simulated , including (1) input of either schematic pre-storm profiles or arbitrary survey profiles, (2) simulation of design beach fill cross-sections, (3) simulation of low dunes that may be overtopped, (4) simulation of narrow dunes that may erode completely, and (5) simulation of dunes backed by vertical or sloping seawalls. The model has been widely accepted in the United States for predicting the erosion impact of severe storms on the open-coast.

Larson (1988), and Larson and Kraus (1989) developed and revised (1994, **SBEACH**

3.0) the model that simulates the macro-scale profile change, such as growth and movement of bars and berms by storm waves and water levels. The model is empirically based and was first developed from a large data set of net cross-shore sand transport rates and geomorphic change observed in large wave tanks, then verified using high quality field data. A new criterion was developed for predicting erosion and accretion, and the model uses this criterion to calculate net sand transport rates in four regions of the nearshore extending from deep water to the limit of wave runup. The wave height distribution is calculated across the shore by applying small-amplitude wave theory up to the point of breaking, and then the breaker decay model of Dally, Dean, and Dalrymple (1985a, 1985b) is used to provide the wave height in regions of breaking waves. Also, SBEACH 3.0 contains an upgraded wave model for more realistic simulation of beach change under random waves. Changes in beach profile are calculated from the distribution of the cross shore sand transport rate and the equation of mass conservation of sand.

Recent research in the Netherlands has developed a new time dependent computation model, DUROSTA (Steezel, 1993), for dune and beach erosion during severe storm surges. The basic equation for the net local sediment transport is a depth-integrated, time-averaged suspended sediment transport equation with time-averaged flow profiles. Starting with the conditions at the seaward boundary, the momentary wave height decay is computed using the procedure as described in Battjes and Janssen (1978). The basic equations describing this wave height decay while taking account of the wave induced cross-shore water level set-up are the wave action equation and the cross-shore momentum equation. The model is able to simulate a bar formation, but the swash-induced onshore direction sand transport mechanism

is not working well. Bottom changes are computed using the conservation equation of sediment mass incorporated with the porosity of the settled bed material. Both the effect of structures and longshore transports on the cross-shore profile development are incorporated in the model.

A study was undertaken to evaluate ten of the most well-known mathematical cross-shore transport models with regard to different model requirements (Schoonees *et al.*, 1995). They evaluated each model with regard to their theoretical basis (mainly sediment transport) and the associated verification data (mainly morphodynamics). In their evaluation the SBEACH (Larson *et al.*, 1989) model was classified into *best group* with respect to the reproduction of the observed profile behavior.

In the present work, an empirically-based model of beach profile change, SBEACH (Storm Induced BEAch Change) developed by Larson and Kraus (1989) is employed for the first stage of dune/beach erosion.

2.3 Overwash / Overland Flow

The simulation of flood wave propagation on a dry bed has many engineering applications, including the investigation of overland flow, irrigation and initiation of coastal flooding on barrier islands.

A two-dimensional model based on the method of characteristics was constructed and tested for its capability for simulating dambreak flood waves on a dry channel (Katopodes *et al.*, 1978).

Cunge, Holly and Verwey (1980) presented the numerical treatment of particular

situations related to the fact that one tries to simulate continuous nature with a discontinuous, or discrete model. They discussed some aspects of computational problems (*i.e.* small depth, weir oscillation) in river modeling.

Akan and Yen (1981) developed a physically based mathematical model to simulate a conjunctive surface - subsurface flow system. In the model a four-point implicit finite difference scheme was employed for the solution of surface runoff equations, and an implicit finite difference scheme based on the successive line over-relaxation method (SLOR) was employed to solve the subsurface flow equation. In the case of overland flow developing on an initially dry surface, a very thin water film was assumed to be ponded before the flow is initiated. The results are not affected by the assumed thickness of this very thin film (Akan, 1976).

A model was presented for the simulation of shallow water flow and, specifically, flood waves propagating on a dry bed (Akanbi and Katopodes, 1988). The governing equations are transformed to an equivalent system valid on a deforming coordinate system and are solved by dissipative finite element techniques. A difficult problem encountered in the simulation of flood waves on a dry bed pertains to the expanding flow domain. It is difficult to properly account for an expanding domain in some of the available numerical schemes, so a very small depth of water everywhere was assumed as the initial condition. However, overland flow occurs in only a portion of the plain until the flow reaches the downstream end of the maximum possible extent of the flood.

The conditions of observability and field-parameter identifiability for surface irrigation advance are examined by analytical techniques and the linearized zero-inertia

model (Katopodes, 1990). Also, the controllability of surface irrigation advance is examined by analytical means and numerical tests based on the linearized zero-inertia model (Katopodes *et al.*, 1990).

The physics-based modeling of overland flow was accomplished through the numerical solution of the St. Venant equations (Tayfur *et al.*, 1993). In their study, the full St. Venant equations, the kinematic wave and diffusion wave approximations were used to route flow over experimental plots, and numerical results were compared with the observed hydrographs. This study brought out the limitations of the surface flow equations when applied to irregular topography. The implicit centered finite difference scheme for the full St. Venant equations also broke down when the flow surface changed rapidly. To avoid singularity problems when flow started with an initially dry bed, an artificial small uniform flow depth was imposed.

In this study, the conservation form of St. Venant equations using the Lax-Wendroff, two-step scheme is employed to simulate initiation of ocean flooding propagation on initially dry barrier islands starting with an initial uniform base flow as justified above.

2.4 Non-cohesive Sediment Transport

Presented in this section is a summarized literature review of the water, sediment transport model and sediment transport formulas under nonsteady conditions.

The numerical solution of *water motion* can proceed in the following two directions. Either an attempt can be made to convert the original system of partial differential equations into an equivalent system of ordinary differential equations by using the method of

characteristics (Chang *et al.*, 1971), or one can replace the partial derivatives in the original system with quotients of finite-differences by using the explicit or implicit scheme (Mahmood *et al.*, 1975). Many computational river models are based upon the Preissmann (1961) scheme which is a four-point implicit finite difference method.

A generalization of the implicit method which is identical with Preissmann (1961) was presented for application to irregular channels in which the cross-sectional geometry and bottom elevation can vary from section to section (Amein, 1968; Amein *et al.*, 1970). Further efforts to summarize implicit methods were made by Basco (1977). The reference books (Mahmood *et al.*, 1975; Abbott, 1979; Cunge *et al.*, 1980; Abbott *et al.*, 1989) give extensive coverage to the implicit method.

Aggradation in a stream due to increase in sediment load was studied *analytically* using a simplified diffusion equation under the assumption of quasi-steady water motion and uniform flow (de Vries, 1973; Soni *et al.*, 1980). A nonlinear parabolic model for nonequilibrium processes in alluvial rivers was presented for more appropriate boundary conditions (Jain, 1981), and analytical expressions for the characteristic parameters of relevant aggradation and degradation processes were derived (Jaramillo *et al.*, 1984). However, simplified analytical models are seldom used in practical applications for complex geometry of the channel.

Most of the existing practical applications of mobile bed modeling are based on the finite difference approach. In practice, this may be done in two different ways : either by solving for the water surface profile and then adjusting the bed elevation using the sediment continuity equation (uncoupled mode), or by simultaneously solving the sediment continuity

equation and water motion equations (coupled mode).

Chen (1973) modified the method of Amein and Fang (1970) and derived linear implicit equations which give a stable scheme for large time increments. In his model, changes in bed elevation are assumed to be negligible within each iteration of each time step so that hydraulic equations are solved first and then the sediment continuity equation is applied to produce a new bed elevation for use as the fixed boundary in the next time step in computation of the hydraulics. Simplified uncoupled modeling technique was developed using the implicit scheme to solve the ordinary differential equation of water momentum and the forward time centered space explicit scheme to solve the unsteady sediment continuity equation (de Vries, 1973). He introduced a dissipative interface in the sediment continuity equation, stabilizing an otherwise numerically unstable scheme.

The rate and extent of bed aggradation resulting from sediment overloading were determined using the uncoupled Preissmann implicit scheme for water motion and an explicit scheme for bed elevation (Park *et al.*, 1986 and 1987).

It has long been recognized that the water motion celerities are much larger in absolute magnitude and of more disproportionate scales than the celerity for a disturbance at the bed (de Vries, 1965). This has led to decoupling of the hydraulic and sediment equations.

However, within a time step, when changes in bed elevations are important, the water-surface transients disappear and a quasi-steady flow was assumed and solved simultaneously (de Vries, 1975; Mahmood *et al.*, 1976; Ponce *et al.*, 1979).

Lyn (1987) has formally shown that above approaches are not capable of satisfying

either a general boundary condition or an arbitrary initial condition. He investigated more closely this coupling, where relatively rapid changes in both fluid and sediment discharge are imposed at the upstream boundary. The stability and convergence characteristics of Preissmann scheme were examined and the analysis was made for a general linear hyperbolic system, but it was restricted to the homogeneous or frictionless case (Lyn *et al.*, 1987).

Holly and Rahuel (1990) were among the first to lay out a new physical frame-work that distinctly separated the bed-load transport at a relatively slow propagation speed from the suspended-load sediment transport at essentially the orders-of-magnitude-larger water velocities. Sediment sorting and armoring can then be accommodated along with the simulation of important interactions among suspended-loads, bed-loads and the bed material making up the bed elevation variation in space and time. The modeling approach is also discussed in Rahuel *et al.* (1989) and its verification for sediment mixtures by flume experiments is reviewed in Hsu and Holly (1992). These researchers also recognized the need to incorporate higher order accuracy numerical methods for advection of suspended-loads with steep gradients as found in flushing operations for reservoirs. Another recent approach for a fully coupled model by Correia *et al.* (1992) incorporated a term for the rate of change of bed level in the water flow continuity equation along with inclusion of the alluvial roughness effects on the friction slope. However, total sediment load was used for ease in model development.

The above coupling models use the implicit Preissmann scheme for numerical integration of the equations. Lai (1989, 1991) suggested that the method of characteristics approach, labeled the multimode characteristics method, is more appropriate because of its

inherent ability to automatically apply the most appropriate computational mode to the disparate celerities involved.

All of the above mentioned researchers have employed classical, empirically based formulations for the sediment transport rates, which in turn control the accuracy and reliability of the model. Several studies have shown (White *et al.*, 1973; Bathurst *et al.*, 1987; Voogt *et al.*, 1991) that there is no one transport formula valid for all ranges of natural conditions. Correia *et al.* (1992) provided seven options in their model which can be selected by the user for a particular set of conditions. For high shear stresses (*i.e.* high velocities) Wilson (1987) and Wilson *et al.* (1990) have proposed modifications of the classical coefficients for transport rate and friction slope. Similar investigations in the Netherlands for velocities up to 2.7 m/s and fine sand (0.1 - 0.4 mm) found that the formulas of Engelund and Hansen (1967) and Ackers and White (1973) overpredicted the sediment transport rates by a considerable amount (Voogt, van Rijn and van den Berg, 1991). Application of the formulas by van Rijn (1984a, b and c) gave the best agreement and have been employed in models for hyper concentrated sand-water mixtures (10 - 50% sand concentration by volume) to simulate mixed subcritical and supercritical flows over on erodible bed during the closure of the Eastern Scheldt (Philipsdam) in the Netherlands.

In this study, the implicit four-point Preissmann scheme will be employed for Stages III and IV to solve the continuity and momentum equations. The water depths and velocities found from the first step are then used to solve the first order partial differential equation describing propagation of the bottom sand wave being approximated with the forward time centered space explicit finite difference scheme.

3.0 ONE-DIMENSIONAL MODEL DEVELOPMENT (THEORY)

Dune/beach erosion, wave overwash and hydraulic (flood/ebb) flows create a *low* profile section across a barrier island. Figure 3.1(a) schematically depicts a barrier-bay system with one existing tidal inlet. A potential new inlet location is also indicated. Many factors determine its location. The coastal orientation, offshore bathymetry and exposure to storm energy are factors; mainland topography, the planform geometry of the bay and barrier width and elevation are factors and; the location of the existing inlet is a factor in that the distance will cause lags in storm tide amplitude and phase between the ocean and the bay. For example, the narrow restriction in the bay will create phase lags in the ocean and bay storm tides for both storm flooding and storm ebbing cycles. Storm ebb flows in the northern bay may take a path of least resistance to turn a breach into a new inlet at the *potential* location shown.

Two simplified modes for break-through events are considered.

Localized Breach. The barrier generally remains above the maximum storm surge flood elevation except at *localized* spots where breaching occurs. The situation is depicted in Figure 3.1(b) for the same barrier-beach schema. Storm flood flows create a mainland flooded region and storm ebb flows return only through the existing inlet and the breaching location(s). One (or more) new inlets may form at the end of a storm event. Clearly, flow is concentrated through the localized breach for the entire storm event.

Inundated barrier. A second possibility exists if the barrier becomes generally submerged below the maximum storm surge flood elevation as depicted in Figure 3.1(c).

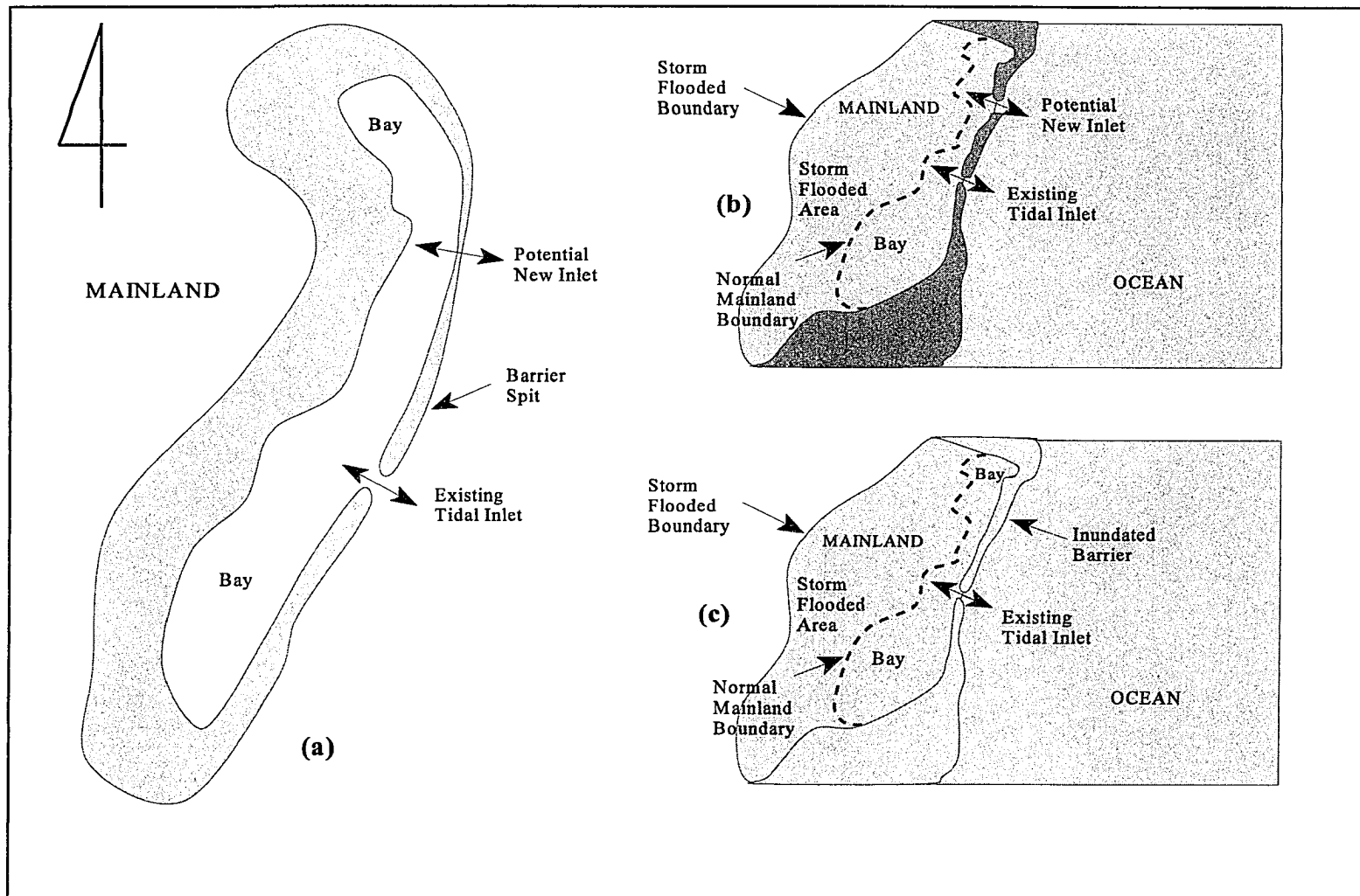


Figure 3.1 Schematic of Barrier Bay System, (a); Localized Breach - Barrier remains above storm surge flood elevation, (b); Inundated Barrier - Barrier submerged below storm surge flood elevation, (c).

The storm flooded area may be similar but now the early storm ebb flows return across the entire barrier. Eventually, the storm ebbs only through the existing inlet and the lowest breaching locations. The return ebb flow also covers the barrier until the topography constricts it to the breach location(s). Again one (or more) new inlets may form.

These two modes for potential, new inlet formation are helpful in formulating a general plan for the overall, *long range* investigation of the breaching and new inlet formation problem.

In this study, the development of an integrated set of numerical models to simulate the four stages of barrier breaching for the *unit width of inundated breaching* mode characterized by one horizontal spatial dimension is emphasized.

The integrated set of numerical models will permit the study of transport mechanics, coefficients, time scales, and the key *independent* variables responsible for dune breaching and new inlet formation. These key variables are basically: (1) barrier volume above MLLW (island width, dune crest elevation, barrier profile); (2) ocean storm level (storm surge hydrograph, storm duration, storm wave characteristics); (3) bay storm surge head and phase differential relative to ocean conditions; and (4) sediment grain size as schematically represented in Figure 3.2. At distorted scales, Figure 3.2(a) taken from actual field measurements at Sandbridge, Virginia depicts the barrier section volume above MLLW that must be spread laterally in both directions for a breaching event. At undistorted scales, Figure 3.2(b) presents a true perspective of the relatively thin barrier volume involved.

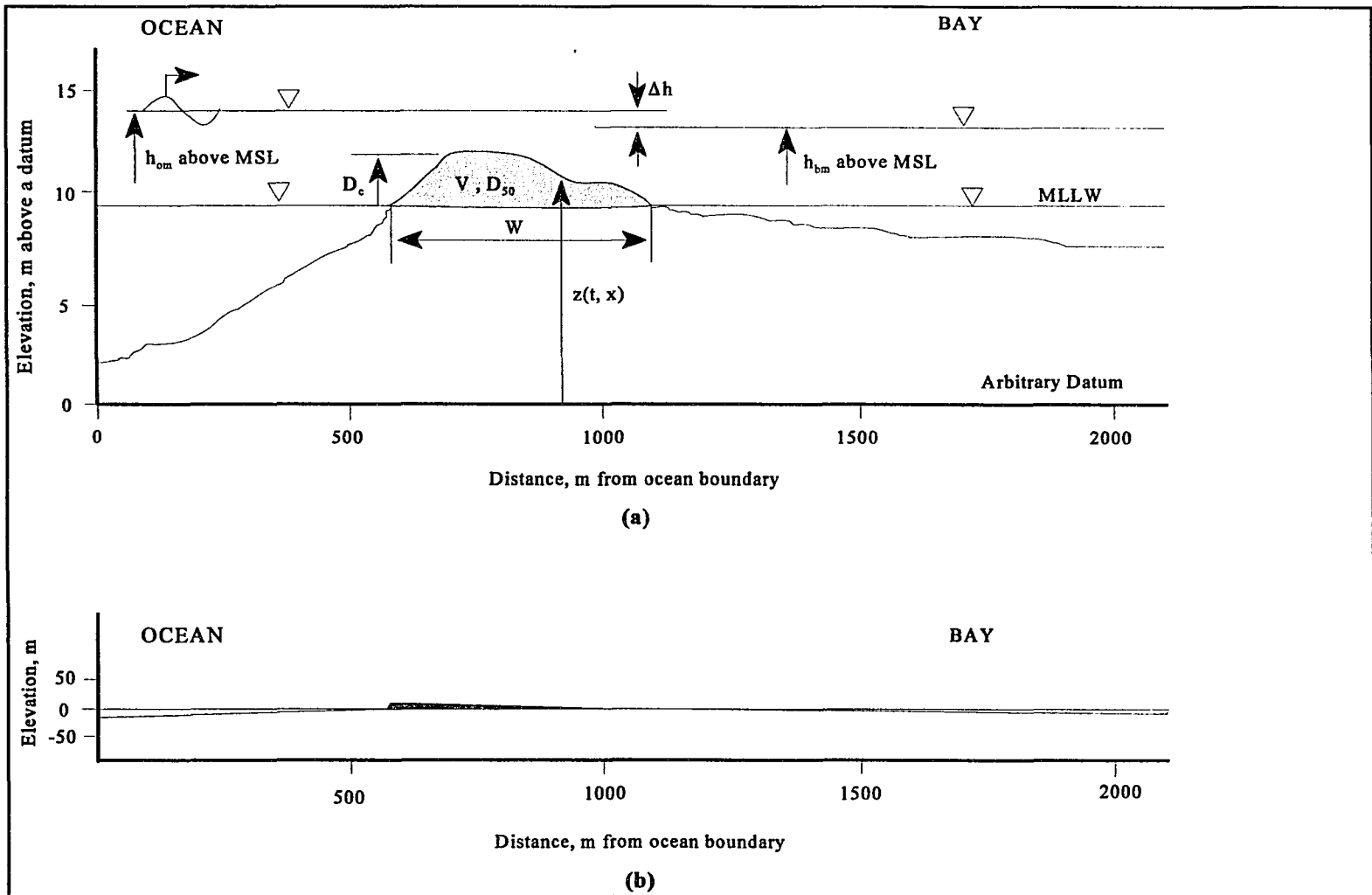


Figure 3.2 Schematic Representation of Key Independent Variables for a Typical Sandbridge, Virginia
 Cross-section : (a) distorted scale and (b) undistorted scale.

3.1 Stage I - Dune/Beach Erosion

Morphologic changes exhibited by beaches are on a spatial scale of meters and on a time scale of hours for storm events. Therefore, a macro scale approach based upon a sound, *empirical* foundation was followed to develop the beach profile change, numerical simulation model **SBEACH** (Larson and Kraus, 1989). In this study, the SBEACH model is employed to simulate dune/beach erosion processes. However, water wave motion is based upon classical wave theory.

3.1.1 Water Wave Model

The wave model provides input to calculate cross-shore sediment transport rates from which profile change is obtained. To begin, for steady state single frequency, wave conditions (H , T , θ) along straight and parallel bottom contours, the conservation laws of time-averaged, depth-integrated wave motion can be written as follows.

Wave Action (Number) Equation

$$\frac{d}{dx} \left(\frac{\sin \theta}{L} \right) = 0 \quad (3.1)$$

Linear Momentum Equation

$$\frac{d}{dx} (S_{xx}) = -\rho g d \frac{d\bar{\eta}}{dx} \quad (3.2)$$

Energy Equation

$$\frac{d}{dx} (F \cos\theta) = \begin{cases} 0 & , \text{ outside surf zone} \\ D^* & , \text{ inside surf zone} \end{cases} \quad (3.3)$$

where:

H = wave height, L

T = wave period, T

θ = wave angle (crest) relative to bottom contour

L = wave length, L

d = total water depth = $h + \bar{\eta}$, L

h = local water depth to SWL, L

$\bar{\eta}$ = time-averaged, mean water level change (set up or set down), L

ρ = water density, M / L^3

g = gravity constant, L / T^2

and with

S_{xx} = radiation stress component directed onshore, F / L

F = wave energy flux, $L \cdot F / L \cdot T$

D^* = wave energy dissipation, $F / L \cdot T$.

At this level of approximation and boundary conditions, waves can shoal, refract (bend) and lose energy (breaking and bottom friction) over variable mean-water depths but cannot either laterally spread energy (diffract) or interact with currents. To proceed further

requires specification of the wave "theory" that relates L , F and S_{xx} to the wave characteristics (H , T).

Classical, small-amplitude, linear wave theory (Airy, 1845) provides the simplest, yet physically correct description of water motion beneath waves. The dispersion relation defines the wave length, L as

$$L \equiv \frac{g T^2}{2 \pi} \tanh \left(\frac{2 \pi d}{L} \right) \quad (3.4)$$

and all the remaining relationships (see, e.g. Wiegel, 1964) such as

$$\begin{aligned} F &\equiv \bar{E} \cdot C_g \\ \bar{E} &= \text{wave energy density, } \frac{F \cdot L}{L^2} \\ &= \frac{E}{L} = \frac{1}{8} \rho g H^2 \\ C_g &= \text{wave group celerity, } \frac{L}{T} \\ &= n \cdot C \\ n &= \frac{1}{2} \left(1 + \frac{2 \pi d / L}{\sinh 2 \pi d / L} \right) \\ C &\equiv \frac{L}{T}, \text{ the wave celerity} \end{aligned} \quad (3.5)$$

with E the wave energy over one wave length, L and depth integrated. And finally, the radiation stress is obtained as

$$S_{xx} = \bar{E} \left[n (\cos^2 \theta + 1) - \frac{1}{2} \right] \quad (3.6)$$

All the above equations hold *outside* the surf zone where bottom friction is very small and neglect giving zero energy dissipation. An extensive literature exists to describe and develop empirical models of incipient wave breaking and breaker height decay for realistic, bar/trough beach profiles *inside* the surf zone (see, e.g. Dally, 1990). For incipient breaking, Larson and Kraus (1989) for SBEACH use the relationship:

$$\frac{H_b}{h_b} = A \xi_0^B \quad , \quad (A, B) = (1.14, 0.21) \quad (3.7)$$

where H_b and h_b are the breaking wave height and water depth, respectively, and A and B are empirical coefficients found from large scale laboratory tests (Kajima *et al.*, 1983). The ξ_0 is the deep water surf-similarity parameter which is defined as

$$\xi_0 = \frac{\tan \beta}{\sqrt{H_0 L_0}} \quad (3.8)$$

where H_0 and L_0 are the deep water wave height and wave length, respectively, and $\tan\beta$ is the beach slope seaward of break point.

After the waves break, the model of Dally, Dean and Dalrymple (1985a and b) is employed to estimate the wave energy dissipation *per unit volume*, D where:

$$D \equiv \frac{D^*}{d} = \frac{\kappa}{d^2} (F - F_s) \quad (3.9)$$

with κ = the breaker, decay model coefficient, and

F_s = the "stable" wave energy flux,

$$= \bar{E}_s \cdot C_g$$

and $\bar{E}_s =$ the "stable" wave energy density,

$$= 1/8 \rho g H_s^2$$

such that

$$H_s \equiv \Gamma d, \text{ the "stable" wave height,}$$

$$\Gamma \equiv \text{the "stable" wave height coefficient.}$$

Stable means a *state* in which energy dissipation during breaking *stops* allowing waves to reform, i.e., when $F = F_s$, $D = 0$. Thus this model permits waves to break over bars with energy dissipation and then the energy dissipation to cease as the wave reforms in the trough. The two empirical coefficients (κ , Γ) have been field verified (Ebersole, 1987) and typically taken as (0.15, 0.40) respectively.

Equations (3.1) through (3.9) above describe a model which gives the wave height distribution $H(x)$ inside and outside the surf zone as depicted in Figure 3.3, which in turn is used to calculate the spatial variation in wave energy dissipation per unit volume, $D(x)$. The $D(x)$ is needed to predict the cross-shore sand transport rate as described below. This macro scale approach recognizes that turbulence is introduced in the surf zone after breaking and stirs up the sand bottom but does not resolve the internal structure of the water motion. Turbulence is thus assumed to be in local equilibrium (production balances dissipation) which is a first-order approximation for the breaker transition zone.

In summary, the water wave model requires four empirical coefficients (A , B for incipient breaking and κ , Γ for wave height decay) to describe $D(x)$ for a specified wave (H ,

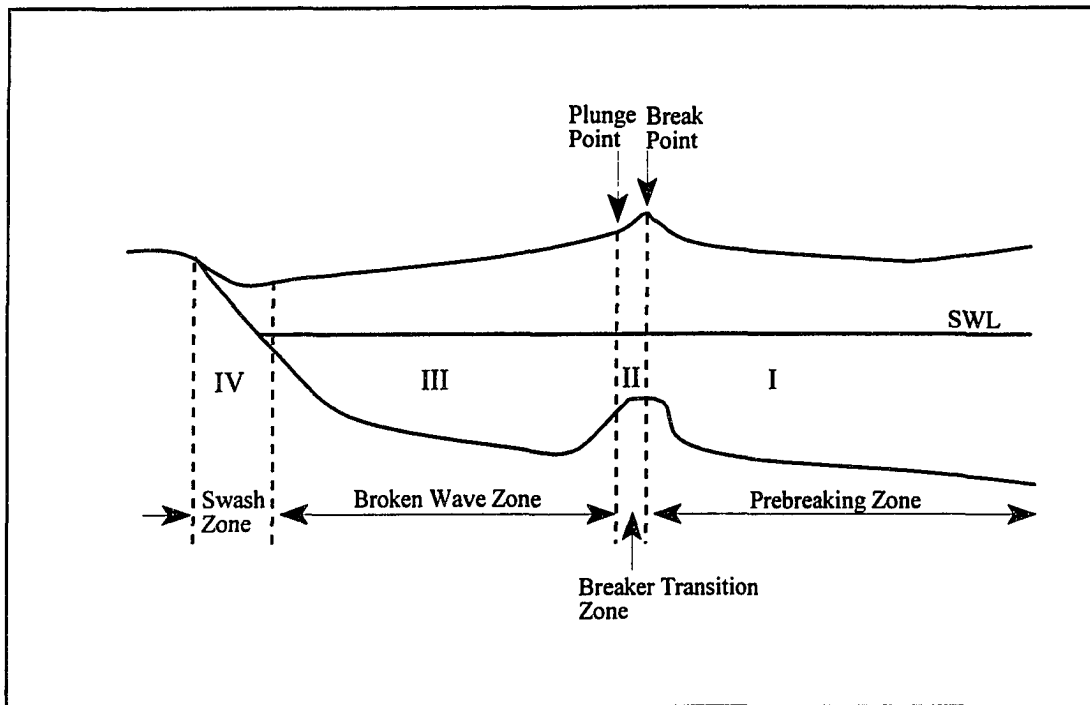


Figure 3.3 Principal Zones of Cross-shore Transport.

T, θ) entering the nearshore zone.

3.1.2 Transport Rate Model

The fundamental assumption is that inside the surf zone (Figure 3.3, Zone III, Broken Waves) the rate of cross-shore sediment transport is proportional to the *excess* energy dissipation per unit volume, D relative to an equilibrium energy dissipation, D_{eq} associated with an equilibrium profile shape undergoing little or no cross-shore adjustment. This formulation follows the pioneering efforts of Moore (1982) and Kriebel (1982). It is built upon the *equilibrium beach profile* concept of Dean (1977) expressed as

$$h = A x^{2/3} , L \quad (3.10)$$

and its related *equilibrium* wave energy dissipation per unit volume formulation of Dean (1977),

$$D_{eq} = \frac{5}{24} \rho g^{3/2} \gamma^2 A^{3/2} , \frac{F \cdot L}{L^3 \cdot T} \quad (3.11)$$

where: A = *grain size (or fall velocity) parameter*

$$= 0.067 w^{0.44}$$

γ = *(H/h)_b, at the breaker point*

as further evaluated from hundreds of fields measurements of beach profiles (Dean, 1977, 1987) with

w = *the representative fall velocity for the characteristic grain size in the profile, L / T.*

For the region of fully broken waves (Figure 3.3, Zone III), the transport rate model of Moore (1982) and Kriebel (1982) was slightly modified to include (add) an extra term to account for the effect of local slope. The modified relationship for the transport rate, q (Larson and Kraus, 1989) is

$$q = \left\{ \begin{array}{ll} K(D - D_{eq}) + \epsilon \frac{dh}{dx} & , D > \left(D_{eq} - \frac{\epsilon}{K} \frac{dh}{dx} \right) \\ 0 & , D \leq \left(D_{eq} - \frac{\epsilon}{K} \frac{dh}{dx} \right) \end{array} \right\} \quad (3.12)$$

where K is an empirical transport rate coefficient, and ϵ is an empirical transport rate

coefficient for the slope-dependent term.

A steeper slope was expected to increase the transport rate down the slope as justification for the $\epsilon dh/dx$ term (Larson and Kraus, 1989). No transport occurs when D becomes less than D_{eq} , corrected for the slope term.

The transport *direction* is also determined by an empirical criterion that relates the offshore wave steepness (H_0/L_0) with the dimensionless, Dean number (H_0/wT) such that

$$\frac{H_0}{L_0} = M \left[\frac{H_0}{wT} \right]^3 \quad (3.13)$$

with $M = 0.00070$ as the empirically determined coefficient. From studies of laboratory and field data it was found (Larson, 1988, Larson and Kraus, 1989) that for erosion (bar building)

$$\frac{H_0}{L_0} > 0.00070 \left[\frac{H_0}{wT} \right]^3 \quad \text{for erosion} \quad (3.14a)$$

and for accretion (berm building)

$$\frac{H_0}{L_0} < 0.00070 \left[\frac{H_0}{wT} \right]^3 \quad \text{for accretion} \quad (3.14b)$$

Further details for setting $q = 0$ when $D < D_{eq}$ and cases for mixed transport directions along the same profile can be found in Larson and Kraus (1989).

For the prebreaking transport region (Figure 3.3, ZONE I), a simple exponential rate decay was found to adequately model the measured results from the full scale experiments.

Hence in

$$q = q_b e^{-\lambda_1 (x - x_b)} \quad , \quad x_b < x$$

$$\lambda_1 = C \left(\frac{d_{50}}{H_b} \right)^D \quad (3.15)$$

where q_b is the transport rate at the breaker point, and λ_1 is an empirical spatial decay coefficient such that from the prototype-scale tests (C, D) equals $(0.4, 0.47)$, respectively. Because so little information was available about transport beneath breaking waves in the transition region (Figure 3.3, ZONE II), the data suggested using for

$$q = q_p e^{-\lambda_2 (x - x_p)} \quad , \quad x_p < x \leq x_b \quad (3.16)$$

where: $\lambda_2 = 0.2 \lambda_1$

$q_p =$ the transport rate at the plunge point,

taken such that the plunge distance, $x_b - x_p$ was about $3H_b$.

Finally, transport in the swash region on the beach face (Figure 3.3, ZONE IV) was simply taken as a linear decay from that found at the end of the broken wave region (x_z) or surf zone (ZONE III) such that

$$q = q_z \left[\frac{x - x_r}{x_z - x_r} \right] \quad (3.17)$$

where x_r is the runup distance.

In summary, the transport rate models for the four zones are spatially related to the location of the wave heights at the break point, H_b , plunge point, H_p , end of the surf zone, H_z and run up limit $H_r = 0$, respectively. Four empirical coefficients are needed (K, ϵ for

Zones III and IV and C, D or (λ_1, λ_2) for Zones I and II to describe the $q(x)$ distribution for a given $D(x)$ and specified wave (H, T, θ) entering the nearshore zone. It should also be noted that a fifth empirical parameter to limit the maximum dune slope during *avalanching* is also required in the model.

3.1.3 Profile Change Model

Changes in the beach profile are determined from the equation of mass conservation for the bottom (sand) material written simply for one-dimensional motion as

$$\frac{\partial z}{\partial t} + \frac{\partial q}{\partial x} = 0 \quad (3.18)$$

where $z(x, t)$ is the bed elevation above an arbitrary datum. Here, the porosity is included in the transport rate, q .

The standard boundary conditions are *no* sand transport shoreward of the runup limit and seaward of the depth where significant sand movement occurs. An implicit, finite-difference algorithm with simple, first-order time marching is employed to numerically integrate Equation (3.18). Complete details can be found in Larson *et al.* (1990).

The model has performed exceedingly well during the erosional stages of storm events (Larson, Kraus and Byrnes, 1990, p.104) which is of utmost concern for this study. Onshore transport during slower beach recovery stages following storm events is less accurately predicted by the present formulation of the SBEACH model.

Development of the SBEACH model has taken many man-years of effort and although still under development, its availability and quantitative success in modeling dune

and beach profile change during storm events will give added confidence to the overall chances of success for this effort to model barrier islands breaching.

3.2 Stage II - Overwash / Overland Flow

Continued rising water level accompanied by irregular wave runup will eventually create landward directed flows and sediment movements across the barrier when the water levels exceed the eroded dune crest elevation.

A simple model without sediment transport will be followed for Stage II to basically develop the *initial conditions* (water motions and topographic profile) for the subsequent stages (III and IV) of the flow and sediment simulation model.

3.2.1 Water Motion in Overland Flow

The fundamental notions and hypotheses used in the mathematical modeling of rivers are formalized in the equations of unsteady open channel flow. These equations are simple models of extremely complex phenomena: they incorporate only the most important real-life flow influences, discarding those which are thought to be of secondary importance in view of the purpose of modeling.

The fundamental equations for spatially-varied, unsteady flow over a plane bed are derived from the de St Venant (1871) hypotheses which we consider to be valid throughout this study except when some corrective factors which depart from the hypotheses are introduced. The differential equations of gradually varied unsteady flow can be obtained from integral equations if one assumes that the dependent variables are continuous,

differentiable functions. The de St Venant equations for unsteady flow in non-conservation form are as follows:

Water Continuity Equation

$$\frac{\partial h}{\partial t} + u \frac{\partial h}{\partial x} + h \frac{\partial u}{\partial x} = 0 \quad (3.19)$$

Equation of Motion

$$\frac{\partial u}{\partial t} + u \frac{\partial u}{\partial x} + g \frac{\partial h}{\partial x} = g \frac{\partial z}{\partial x} - g S_f \quad (3.20)$$

Friction Slope

$$S_f = \frac{u |u|}{C_c^2 h} \quad (3.21)$$

Chezy-coefficient

$$C_c = 18 \log \left(\frac{12 R_b}{k_s} \right) \quad (3.22)$$

where: $u(t, x)$ = local water velocity, L/T

$h(t, x)$ = local water depth, L

R_b = hydraulic radius of the bed, L

k_s = hydraulic roughness of a movable bed surface, L

$\equiv 3D_{90}$

D_{90} = diameter of bed material with 90 percent finer, L

$$g = \text{acceleration of gravity, } L/T^2$$

$$z(x, t) = \text{local elevation of the bed from the arbitrary datum, } L$$

The above equations are based upon the following series of assumptions (Cunge *et al.*, 1980):

1. The flow is one-dimensional *i.e.* the velocity is uniform over the cross-section and the water level across the section is horizontal.
2. The streamline curvature is small and vertical accelerations are negligible, hence the pressure is hydrostatic.
3. The effects of boundary friction and turbulence can be accounted for through resistance laws analogous to those used for steady state flow.
4. The average channel bed slope is small so that the cosine of the angle it makes with the horizontal may be replaced by unity.

In Stage II, the flow variables, $u(t, x)$ and $h(t, x)$, are not continuous (*i.e.*, hydraulic jump, bore) at certain locations due to shallow water depth and steep bottom slope. It is possible to obtain valid discontinuous (weak) solutions of the differential equations only if the differential flow equations are written under the divergent momentum conservation forms and conserved relevant physical quantities (*i.e.*, momentum). Then the primitive forms (Eulerian forms) of Equations (3.19) and (3.20) can also be derived in conservation forms (divergent forms) as follows:

Water Continuity Equation

$$\frac{\partial h}{\partial t} + \frac{\partial q}{\partial x} = 0 \quad , \quad q = u h \quad (3.23)$$

Equation of Motion

$$\frac{\partial q}{\partial t} + \frac{\partial}{\partial x} \left(\frac{q^2}{h} + \frac{1}{2} g h^2 \right) = g h \frac{\partial z}{\partial x} - g h S_f \quad (3.24)$$

Friction Slope

$$S_f = \frac{q |q|}{C_c^2 h^3} \quad (3.25)$$

The dependent variables are now water depth, $h(t, x)$ and volumetric flowrate per unit width, $q(t, x)$. Consequently, Equations (3.23) and (3.24) may be rewritten in vector notation.

$$\frac{\partial \bar{V}}{\partial t} + \frac{\partial \bar{F}(\bar{V})}{\partial x} = \bar{G}(\bar{V}) \quad (3.26)$$

$$\bar{V} = \begin{bmatrix} h \\ q \end{bmatrix} \quad (3.27)$$

$$\bar{F}(\bar{V}) = \begin{bmatrix} q \\ \frac{q^2}{h} + \frac{1}{2} g h^2 \end{bmatrix} \quad (3.28)$$

$$\bar{G}(\bar{V}) = \begin{bmatrix} 0 \\ g h \frac{\partial z}{\partial x} - g h S_f \end{bmatrix} \quad (3.29)$$

Equation (3.26) is employed for the discretization of an explicit finite difference scheme, namely the *Lax-Wendroff two-step scheme*.

In the beginning of Stage II, computational difficulties may develop when physical flow depths are zero across the barrier islands (*i.e.*, dry bed condition). At the early stage of study, this was a prime concern which should be handled by the program to as great an extent as possible. Never allowing zero flow situations to occur can be accomplished by introducing small base flows on the flood plain.

Oscillatory water wave motion, while still present to produce irregular overwash events, is assumed secondary in importance to translation processes advecting both water and sediment in the overland direction.

Equations (3.26) through (3.29) will provide a rough estimate for both the short, initial time required for flow to advect across the barrier width and the initial conditions ; $u(x)$, $h(x)$ for use in the Stage III and IV model.

3.2.2 Sediment Movement and Profile Change

During the extremely short time period for Stage II (generally less than 10 minutes), wave overtopping, overwash and overland flows will generally *smooth* out the pre-breach

profile landward of the dune crest. Consequently, profile change will be modeled as a *diffusion* process with no advection or transport in either direction.

For the profile elevation, z which is relative to the datum, a diffusion equation is employed as

$$\frac{\partial z}{\partial t} = K \frac{\partial^2 z}{\partial x^2} \quad (3.30)$$

where K is a profile *diffusion* coefficient for Stage II. For the numerical methods, use of Equation (3.30) is equivalent to using a numerical *filter* to smooth the bottom profile and *simulate* the movement of sediment from peaks to adjacent low regions. Mass over the computational domain is conserved by artificial means during this process.

At the end of Stage II, the initial conditions, $u(x)$, $h(x)$ and $z(x)$ will be known across the entire length of the simulation from the ocean to the bay for use in the final stages of the model.

The coefficients required are a uniform flow, open channel friction coefficient, C_c and a profile diffusion coefficient, K to smooth the bottom contours during the first few minutes of overland flow.

3.3 Stage III and IV - Storm Tides

The long wave, shallow-water equations of free-surface, open channel flow (de St Venant, 1871) are employed to simulate time varying water motions from the ocean to the bay (flooding, Stage III). The water elevation (head) difference between the bay and the

ocean reverses so that the velocity and the resulting sediment movement also reverse direction to become *ebbing* flows and transports (Stage IV). At these stages, it is initially assumed that waves are of only minor influence for the sediment transport process.

3.3.1 Water Motion

The one-dimensional non-conservation forms of differential equations of gradually varied unsteady flow in unit width rectangular channel are governed for Stage III and IV. Introducing a *control function* and a *linearization* of local variables in Equations (3.19) and (3.20) then provides

Water Continuity Equation

$$\frac{\partial h}{\partial t} + u^* \frac{\partial h}{\partial x} + h^* \frac{\partial u}{\partial x} = 0 \quad (3.31)$$

Equation of Motion

$$\frac{\partial u}{\partial t} + CF \cdot u^* \frac{\partial u}{\partial x} + g \frac{\partial h}{\partial x} = g \frac{\partial z}{\partial x} + g S_f \quad (3.32)$$

Control Function

$$CF = \begin{cases} 1 - Fr^2 & , & Fr < 1 \\ 0 & , & Fr \geq 1 \end{cases} \quad (3.33)$$

Froude Number

$$Fr = \frac{u^*}{\sqrt{g h^*}} \quad (3.34)$$

Friction Slope

$$S_f = g \frac{u |u|}{C_c^2 h^*} \quad (3.35)$$

where: u^* = local quasi-constant flow velocity, L/T

h^* = local quasi-constant flow depth, L

Fr = local Froude Number.

Figure 3.4 shows a definition sketch for one-dimensional flow in the alluvial channel. The set of differential equations (3.31 and 3.32) links the three unknown functions $h(t, x)$, $u(t, x)$ and $z(t, x)$ with the independent variables t and x . They incorporate a series of hypotheses concerning both water flow and solid transport. The de St Venant hypotheses, *i.e.*, the hydrostatic distribution of pressure and the uniformity of velocity within a section, are accepted for the liquid phase.

There is normally no risk of the flow becoming super-critical, unless the natural slope of the channel is greater than the critical slope. The super-critical flow condition is exceedingly rare in river modeling and requires a special algorithm. However, in this study, bed slopes at certain locations in ocean-side and the barrier islands are generally steeper than the critical slope, and bay-side slopes are normally sub-critical ranges so that mixed-type flows, sub-critical (ocean), super-critical (barrier islands) and sub-critical (bay) again, occur. It is not easy to solve the partial differential equations system ((3.31) and (3.32)) in this situation due to insufficient boundary data at the control sections (*i.e.*, the locations of critical

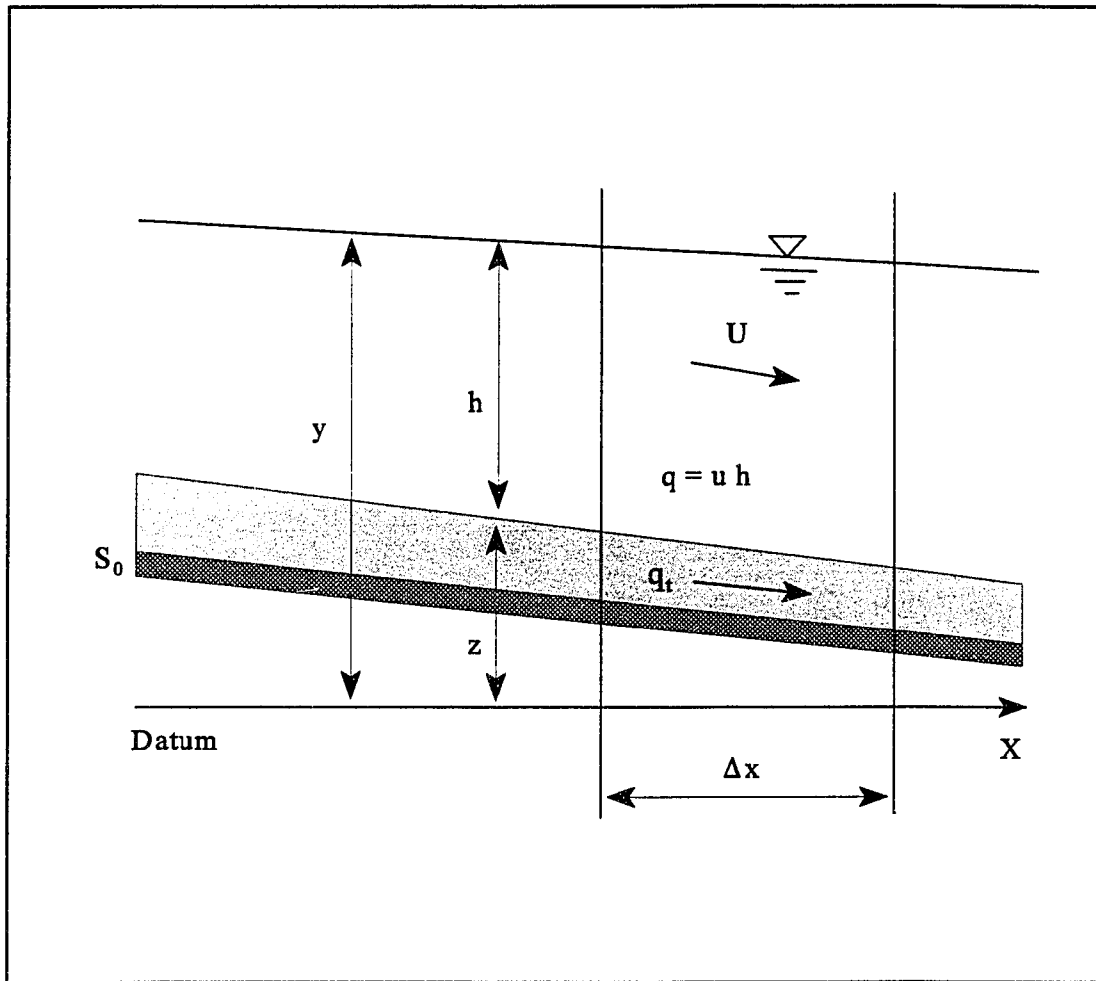


Figure 3.4 Definition Sketch of Flow in Alluvial Channel.

depth).

The problem of combining different algorithmic structures can be avoided altogether through a technique described by Havnø and Brorsen (1986), whereby the influence of a convective acceleration term in the water momentum equation is reduced (or suppressed) by a *Control Function*. By this means it is certainly possible to maintain a sub-critical flow characteristic structure and data structure over the whole domain of the solution, including

subdomains of super-critical flow. The dominance of the resistance term for small depths means that the suppression of the convective acceleration term will have little effect on the results. The quasi-constant values, u^* and h^* are obtained from the averaging at the nearest four grid points and will be further discussed in Chapter 4.3.1.

The water depth and velocity found from the water motion equations are first used in the sediment transport formula, and then the first-order sediment continuity equation describing propagation of the bottom sand wave is numerically solved.

3.3.2 Sediment Motion

In natural channels, the phenomena of sediment motion are of a three-dimensional nature. If it is assumed that the net deposition or erosion of sediment between two neighboring sections is uniformly distributed over the channel bed in both the longitudinal (*i.e.*, across the barrier islands) and the transverse (*i.e.*, along the barrier islands) directions, the three-dimensional nature could be simulated by a one-dimensional approach (Mahmood, *et al.*, 1975). The one-dimensional sediment continuity equation, expressed *per unit of width*, is

$$(1 - p) \frac{\partial z}{\partial t} + \frac{\partial}{\partial t} (C_s h) + \frac{\partial q_t}{\partial x} = q_L \quad (3.36)$$

where: C_s = sediment concentration, M/L^3

q_t = total sediment transport rate for both bed- and suspended-load transport, $L^3/L \cdot T$

$$\begin{aligned}
 &= q_t(u, h) \\
 q_L &= \text{lateral sediment inflow, } L^3/T \cdot L \\
 p &= \text{porosity of bed materials.}
 \end{aligned}$$

According to Mahmood and Ponce (1976), Ponce *et al.* (1979) and Lyn (1987), in river flow the temporal concentration variation term, the second term in Equation (3.36) is very small when compared with the remaining terms; therefore, it is neglected. Also, q_L can be neglected due to the one-dimensional assumption. Equation (3.36) is reduced to

$$(1 - p) \frac{\partial z}{\partial t} + \frac{\partial q_t}{\partial x} = 0 \quad (3.37)$$

which is subjected to discretization.

The sediment transport rate, q_t can be estimated from the field surveys or from the available theories. In this study, an available empirical theory (van Rijn, 1984a and b) based on field measurements is used to compute the sediment transport rate for both bed- and suspended-load transport.

3.3.3 Sediment Transport Formula

The transport of sediment particles by a flow of water can be in the form of bed- and suspended-load, depending on the size of the bed material particles and the flow conditions. Although in natural conditions there will be no sharp division between the bed-load transport and suspended-load transport, it is necessary to define a layer with bed-load transport for

mathematical representation. Usually, three modes of particle motion are distinguished: (1) rolling and sliding motion, or both ; (2) saltation motion ; and (3) suspended particle motion, in continuous contact with the bed. For increasing values of the bed-shear velocity, the particles will be moving along the bed by more or less regular jumps, which are called saltations. When the value of the bed-shear velocity exceeds the fall velocity of the particles, the sediment particles can be lifted to a level at which the upward turbulent forces will be comparable with or of higher order than the submerged weight of the particles, and as a result the particles may go in suspension (van Rijn, 1984a).

A method was developed which enables the computation of the bed-load transport as the product of the saltation height, the particle velocity and the bed-load concentration (van Rijn, 1984a) and which enables the computation of the suspended-load as the depth-integration of the product of the local concentration and flow velocity (van Rijn, 1984b).

The predictive capability of the sediment transport formulas of Engelund and Hansen (1967), Ackers and White (1973) ,and van Rijn (1984b) at high velocities was investigated (Voogt *et. al.*, 1991). The method of van Rijn yields the best results from comparisons with the field measurements within the high velocity range of 1 - 3 m/sec and bed material in the range of 0.1 - 0.4 mm. In addition, predicted transport rates according to his formulas are less sensitive to the Nikuradse bed roughness, which is difficult to estimate under tidal flows. The van Rijn formulas are employed for the computation of the sediment transport rate.

3.3.3.1 Bed Load Transport

The steady uniform flow of water and sediment particles is defined by the following input parameters: mean flow velocity, mean flow depth, particle diameters, density of water and sediment, viscosity coefficient, etc...

In this analysis, it is assumed that the bed-load transport rate can be described sufficiently accurately by two dimensionless parameters only, a dimensionless particle parameter, D_* and a transport stage parameter, T . The computation procedure of the bed-load transport is as follows (van Rijn, 1984a).

1. Particle Parameter, D_*

The D_* -parameter can be derived by eliminating the shear velocity from the particle mobility parameter, $\theta = u_*^2 / (S_s - 1)gD_{50}$ and the particle Reynolds' number, $R = u_*D_{50} / \nu$.

$$D_* = D_{50} \left[\frac{(S_s - 1)g}{\nu^2} \right]^{1/3} \quad (3.38)$$

where: S_s = *specific density of sediment*
= 2.58
 ν = *kinematic viscosity*
= $1.0 \times 10^{-6} \text{ m}^2/\text{sec}$
 u_* = *bed shear velocity, L/T*

2. Critical Bed-Shear Velocity, $u_{*,cr}$ according to Shields (1936)

$$\begin{aligned}
D_* \leq 4 & , \quad \theta_{cr} = 0.24 (D_*)^{-1} \\
4 < D_* \leq 10 & , \quad \theta_{cr} = 0.14 (D_*)^{-0.64} \\
10 < D_* \leq 20 & , \quad \theta_{cr} = 0.04 (D_*)^{-0.10} \\
20 < D_* \leq 150 & , \quad \theta_{cr} = 0.013 (D_*)^{0.29} \\
D_* > 150 & , \quad \theta_{cr} = 0.055
\end{aligned} \tag{3.39}$$

$$u_{*,cr} = \sqrt{\theta_{cr} (S_s - 1) g D_{50}}$$

3. Chezy-coefficient Related to Grains, C_c

$$C_c = 18 \log \left(\frac{12 R_b}{3 D_{90}} \right) \tag{3.40}$$

where: R_b = hydraulic radius of channel bed (\equiv water depth, h), L

4. Effective Bed-Shear Velocity, u_*'

The u_*' -parameter is described in terms of the mean flow velocity and a Chézy-coefficient related to the grains of the bed.

$$u_*' = \frac{(g^{0.5} u)}{C_c} \tag{3.41}$$

5. Transport Stage Parameter, T

The T -parameter expresses the mobility of the particles in terms of the stage of

movement relative to the critical stage for initiation of motion.

$$T = \frac{(u_*')^2 - (u_{*,cr})^2}{(u_{*,cr})^2} \quad (3.42)$$

6. Bed-Load Concentration, C_b

Extensive analysis of the data showed that the bed-load concentration can be represented by:

$$C_b = 0.18 \frac{T}{D_*} C_0 \quad (3.43)$$

where: C_0 = maximum bed concentration
= 0.65

7. Particle Velocity, u_b

The particle velocity is defined as a function of the flow conditions and sediment size from the experiments.

$$u_b = 1.5 T^{0.6} [(S_s - 1) g D_{50}]^{0.5} \quad (3.44)$$

8. Thickness of Bed-Load Layer, δ_b

For each set of hydraulic conditions, the T - and D_* -parameters are computed and related to the computed saltation height resulting thickness of the bed-load layer with an inaccuracy of about 10% by the following simple expression.

$$\delta_b = 0.3 D_*^{0.7} T^{0.5} D_{50} \quad (3.45)$$

9. Finally, *Bed-Load Transport*, q_b

The bed-load transport for particles in the range 200 - 2,000 μm can be computed as:

$$\begin{aligned} q_b &= C_b u_b \delta_b \\ &= 0.053 \frac{T^{2.1}}{D_*^{0.3}} [(S_s - 1) g]^{0.5} D_{50}^{1.5} \end{aligned} \quad (3.46)$$

van Rijn (1984a) reported that the proposed equations predict a reliable estimate of the bed-load transport in the particle range 200 - 2,000 μm , which is based on a verification study using 580 flume and field data.

3.3.3.2 Suspended Load Transport

The method is based on the computation of the reference concentration from the bed-load transport. The procedures in bed-load transport computation, No.1 through No.5 are employed to compute particle parameter, D_* and transport stage parameter, T . The computation procedure of the suspended-sediment transport is as follows (van Rijn, 1984b).

1. *Reference Level, a*

The concentration profile is relatively sensitive to small variations (about 20%) in the suspension parameter, particularly for a reference level, a which is very close to the bed, $a=0.001h$ where h is water depth. It is evident that a reference level smaller than $0.01h$ leads

to large errors in the concentration profile. The reference level is assumed to be equal to half the bed-form height, Δ or the equivalent roughness height, k_s , if the bed-form dimensions are not known, while a minimum value $a=0.01h$ is used for reasons of accuracy.

$$a = 0.5 \Delta \quad \text{or} \quad a = k_s, \quad (\text{with } a_{\min} = 0.01 h) \quad (3.47)$$

2. Reference Concentration, C_a

$$C_a = 0.015 \frac{D_{50}}{a} \frac{T^{1.5}}{D_*^{0.3}} \quad (3.48)$$

which is obtained from the field and experiment data.

3. Representative Particle Diameter of Suspended Sediment, D_s

Observations in flume and field conditions have shown that the sediments transported as bed load and as suspended load have different particle size distributions. Usually, the suspended sediment particles are considerably smaller than the bed-load particles. The parameter is related to the D_{50} of the bed material and the geometric standard deviation of bed material, σ_s ,

$$\frac{D_s}{D_{50}} = 1 + 0.011 (\sigma_s - 1) (T - 25) \quad (3.49)$$

where: σ_s = *geometric standard deviation of bed material*
 \cong 1.5 ~ 2.5

= 2.5 for best result.

4. Fall Velocity of Suspended Sediment, w_s

The main controlling hydraulic parameters for the suspended-load are the particle fall velocity and the sediment diffusion coefficient.

In a clear, still fluid the particle fall velocity, w_s , of a solitary sand particle smaller than about $100\mu\text{m}$ can be described by:

$$w_s = \frac{1}{18} \frac{(S_s - 1) g D_s^2}{\nu} \quad (3.50)$$

For suspended sand particles in the range of $100 - 1,000\mu\text{m}$, the following type of equation, as proposed by Zanke (1977) is used:

$$w_s = 10 \frac{\nu}{D_s} \left\{ \left[1 + \frac{0.01 (S_s - 1) g D_s^3}{\nu^2} \right]^{0.5} - 1 \right\} \quad (3.51)$$

For particles larger than about $1,000\mu\text{m}$ the following simple equation is used:

$$w_s = 1.1 [(S_s - 1) g D_s]^{0.5} \quad (3.52)$$

5. Overall Bed-Shear Velocity, u .

If bed-form steepness, Ψ is negligible (≈ 0), then overall Chezy coefficient, C' can be replaced to Chezy coefficient related to grains, C_c

$$C' = C_c = 18 \log \left(\frac{12 R_b}{k_s} \right) \quad (3.53)$$

where: k_s = *effective roughness height*

$$= 3D_{90} + 1.1\Delta (1 - e^{-25\psi})$$

$$\equiv 3D_{90}$$

and

$$u_* = (g h S_f)^{0.5} = \sqrt{g} \frac{u}{C_c} \quad , \quad S_f = \frac{u^2}{C_c^2 h} \quad (3.54)$$

6. β -Factor

β -factor describes the difference in the diffusion of a discrete sediment particle and the diffusion of a fluid particle (or small coherent fluid structure) and is assumed to be constant over the flow depth. This factor is obtained from the results of Coleman (1970).

$$\beta = 1 + 2 \left[\frac{w_s}{u_*} \right]^2 \quad \text{for} \quad \frac{u_*}{w_s} > 2$$

$$= 1 \quad \text{for} \quad \frac{u_*}{w_s} \leq 2 \quad (3.55)$$

7. φ -Factor

φ -Factor is an overall correction factor representing all additional effects (volume occupied by particles, reduction of particle fall velocity and damping of turbulence). The φ value has been determined by means of a trial and error method which implies the numerical

computation of concentration profiles for various sets of hydraulic conditions and the determination of the φ -value that yields a concentration profile similar to the concentration profile based on the numerical method. Therefore, for each set of hydraulic conditions (w_s , u_* , c_a) a φ -value is obtained. Analysis of the φ -values showed a simple relationship with the main hydraulic parameter, as follows (inaccuracy of about 25%):

$$\varphi = 2.5 \left[\frac{w_s}{u_*} \right]^{0.8} \left[\frac{C_a}{C_0} \right]^{0.4} \quad \text{for} \quad 0.01 \leq \frac{w_s}{u_*} \leq 1 \quad (3.56)$$

where C_0 is the maximum bed sediment concentration (≈ 0.65).

8. Suspension Parameters, Z and Z'

To describe the suspended-load transport, a suspension parameter which expresses the influence of the upward turbulent fluid forces and the downward gravitational forces, is defined as:

$$Z = \frac{w_s}{\beta \kappa u_*} \quad , \quad Z' = Z + \varphi \quad (3.57)$$

where κ is the constant of Von Karman (≈ 0.40) and Z' is an adjusted suspension parameter.

9. F - Factor

This is a correction factor for suspended-load and is defined as:

$$F = \frac{\left[\frac{a}{h}\right]^{Z'} - \left[\frac{a}{h}\right]^{1.2}}{\left[1 - \frac{a}{h}\right]^{Z'} (1.2 - Z')} \quad (3.58)$$

10. Suspended-Load Transport, q_s

Full integration of suspended transport equation can be represented with an inaccuracy of about 25% by:

$$q_s = F u h C_a \quad (3.59)$$

($0.3 \leq Z' \leq 3$ and $0.01 \leq a/h \leq 0.1$)

Finally, *the total sediment transport rate, q_t* is obtained from:

$$q_t = q_s + q_b \quad (3.60)$$

From the results of the verification analysis it was concluded that the proposed formulas for both bed- and suspended-load transport have a good predictive ability for a range of flow conditions ($u=0.5-2.5m/s$, $h=0.1-3.5m$, $D_{50}=100-500\mu m$) using 783 flume and field data.

4.0 NUMERICAL INTEGRATION PROCEDURES

4.1 Stage I - Dune / Beach Erosion

The model SBEACH consists of three calculation modules that are executed consecutively at each time step in a simulation. The modules calculate wave height across-shore, net cross-shore sand transport rate and profile change, respectively.

4.1.1 Water Wave Model

An explicit finite-difference scheme is used to solve the equations for determining cross-shore wave height. In the model, a quasi-stationary approach is applied, implying that a steady-state solution of the wave height distribution is determined at every time step.

Numerical calculations start at the seaward end of the grid and proceed onshore through an explicit solution scheme in which quantities known at a specific grid point are used to determine corresponding quantities at the next grid point. The wave height, period, and incident angle must be known at the most seaward grid point prior to starting the calculation.

Wave refraction is first determined if the incident wave approaches with an angle to the bottom contours. From the wave action Equation (3.1), the angle, θ , between the wave crests and the bottom contours is given by

$$\theta_i = \arcsin \left(\frac{L_i}{L_{i+1}} \sin \theta_{i+1} \right) \quad (4.1)$$

where L_i and L_{i+1} are the wavelengths at grid point i and $i+1$, respectively. Note that grid point numbering increases in the seaward direction since the x-axis points offshore, but the calculation proceeds from offshore in the shore-ward direction. Wave lengths are computed using Equation (3.4).

The next step in the calculation is to determine the energy flux and thus the wave height. Equation (3.3) with Equation (3.9) is written in difference form as:

$$\frac{F_{i+1} \cos\theta_{i+1} - F_i \cos\theta_i}{\Delta x} = \frac{\kappa}{h_i + \bar{\eta}_{i+1}} \left(\frac{F_{i+1} + F_i}{2} - F_{s,i} \right) \quad (4.2)$$

$$F_i = \frac{1}{\cos\theta_i + 0.5 A_{c,i}} [F_{i+1} (\cos\theta_{i+1} - 0.5 A_{c,i}) + A_{c,i} F_{s,i}] \quad (4.3)$$

where Δx is length step and

$$A_{c,i} = \frac{\kappa \Delta x}{h_i + \bar{\eta}_{i+1}} \quad (4.4)$$

The stable energy flux at grid point I , is determined from

$$F_{s,i} = \frac{1}{8} \rho g [\Gamma(h_i + \bar{\eta}_{i+1})]^2 \frac{C_{g,i} + C_{g,i+1}}{2} \quad (4.5)$$

After the energy flux has been calculated at a specific point, the corresponding wave height is determined from Equation (3.5) as

$$H_i = \left(\frac{8 F_i}{\rho g C_{g,i}} \right)^{1/2} \quad (4.6)$$

Using the wave height, radiation stress is calculated from Equation (3.6) and setdown (or setup) given from Equation (3.2) expressed in difference form as

$$\bar{\eta}_i = \bar{\eta}_{i+1} + \frac{(S_{xx})_{i+1} - (S_{xx})_i}{\rho g (h_i + \bar{\eta}_{i+1})} \quad (4.7)$$

At every calculation step, a check is made to determine if wave breaking has occurred according to Equations (3.7) and (3.8). Once breaking is initiated, the wave decay coefficient is set for $\kappa=0.15$, and energy dissipation takes place.

Wave height is used to calculate the transport rate from which profile change is calculated.

4.1.2 Profile Change Model

Profile change is calculated from the mass conservation equation using the net transport rate distribution determined from Equation (3.12) through (3.17).

The location of the break point is given directly from the wave height calculations, and the plunge point is computed as $3H_b$ based on findings by Galvin (1969) and Svendsen (1987).

To determine the transport rate distribution, sand transport is first calculated in zones of fully broken waves (Figure 3.3, Zone III) according to Equation (3.12) , written in

difference form,

$$q_i = K \left[\frac{(D_i + D_{i-1})}{2} - D_{eq} + \frac{\epsilon}{K \Delta x} (h_i - h_{i-1}) \right] \quad (4.8)$$

Calculation of the transport rate in zones of fully broken waves defines the boundaries of Zone III, from which the transport rate may be calculated in the other zones. After these values are determined at the plunge point and at the end of the surf zone, Equations (3.15), (3.16) and (3.17) are applied to completely define the transport rate distribution. In discretizing the mass conservation equation, transport rate distributions from two time levels are used and the difference equation is expressed as

$$\frac{h_i^{k+1} - h_i^k}{\Delta t} = \frac{1}{2} \left[\frac{q_{i+1}^{k+1} - q_i^{k+1}}{\Delta x} + \frac{q_{i+1}^k - q_i^k}{\Delta x} \right] \quad (4.9)$$

Since the transport rate distribution is determined from different relationships depending on the zone of transport, its spatial derivative will generally be discontinuous at the boundaries between the zones. To obtain a smoother, more realistic transport distribution, a three-point filter is applied to the calculated transport rates on grid cells away from boundaries by

$$q_i^* = 0.25 q_{i-1} + 0.5 q_i + 0.25 q_{i+1} \quad (4.10)$$

where star denotes the smoothed transport rate.

The concept of avalanching, as discussed by Allen (1970), is incorporated in the

numerical model, and a routine was included to account for transport induced by slope failure.

The time interval and length step are not independent because they both govern the stability of the numerical solution scheme. Generally, a shorter length step requires a smaller time interval. An explicit criterion for the relation between time and length step for numerical stability could not be determined due to the non-linearity of the equations and the smoothing of the transport rate.

4.2 Stage II - Overwash / Overland Flow

Conservation form of water continuity and momentum equations are numerically solved using the Lax-Wendroff two-step method in this stage. Also, the Method of Characteristics is employed to compute additional boundary data at both boundaries.

4.2.1 The Lax-Wendroff Two-Step Scheme

Lax and Wendroff (1960) introduced a second-order scheme, $O(\Delta t^2, \Delta x^2)$, with two time levels, n to $n+1/2$ and $n+1/2$ to $n+1$. The original derivation of Lax and Wendroff was based on a Taylor series expansion in time up to the third order to achieve second-order accuracy. This is called a *leapfrog* operator because some intermediate grid values are not employed in the computation. (Figure 4.1)

Governing equations in conservation form are rewritten in vector notation.

$$\frac{\partial \bar{V}}{\partial t} + \frac{\partial \bar{F}(\bar{V})}{\partial x} = \bar{G}(\bar{V}) \quad (4.11)$$

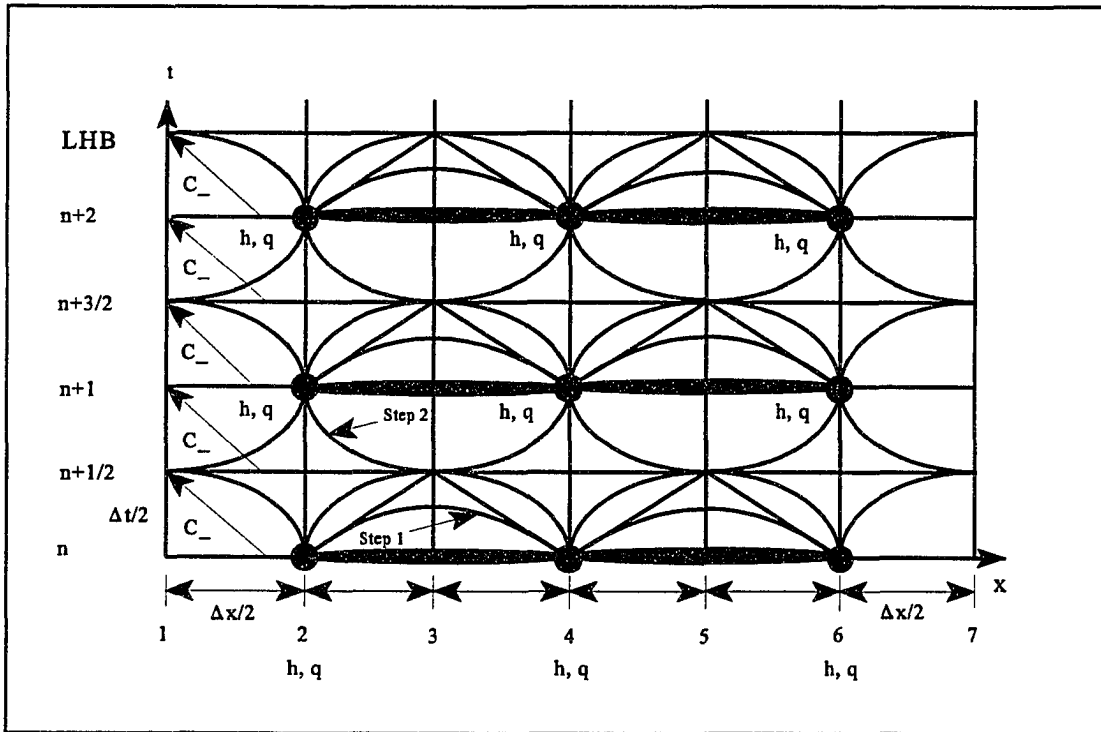


Figure 4.1 Schematic Operator of Lax-Wendroff, Two-step Scheme.

$$\bar{V} = \begin{bmatrix} h \\ q \end{bmatrix}$$

$$\bar{F}(\bar{V}) = \begin{bmatrix} q \\ \frac{q^2}{h} + \frac{1}{2} g h^2 \end{bmatrix} \quad (4.12)$$

$$\bar{G}(\bar{V}) = \begin{bmatrix} 0 \\ g h \frac{\partial z}{\partial x} - g h S_f \end{bmatrix}$$

We shall now use the scalar notation.

$$F = \frac{q^2}{h} + \frac{1}{2} g h^2 \quad (4.13)$$

$$G = g h \frac{\partial z}{\partial x} - g h S_f$$

Step 1, n to $n+1/2$

The Lax operator is used for the first stage

$$\frac{\bar{V}_{j+1/2}^{n+1/2} - \left(\frac{\bar{V}_{j+1}^n + \bar{V}_j^n}{2} \right)}{\Delta t/2} + \frac{\bar{F}_{j+1}^n - \bar{F}_j^n}{\Delta x} = \frac{\bar{G}_{j+1}^n + \bar{G}_j^n}{2} \quad (4.14)$$

which translates to the following equation pair for computational purposes:

$$\frac{h_{j+1/2}^{n+1/2} - \left(\frac{h_{j+1}^n + h_j^n}{2} \right)}{\Delta t/2} + \frac{q_{j+1}^n - q_j^n}{\Delta x} = 0 \quad (4.15)$$

and

$$\frac{q_{j+1/2}^{n+1/2} - \left(\frac{q_{j+1}^n + q_j^n}{2} \right)}{\Delta t/2} + \frac{F_{j+1}^n - F_j^n}{\Delta x} = \frac{G_{j+1}^n + G_j^n}{2} \quad (4.16)$$

Rearranging Equations (4.15) and (4.16) here as

$$h_{j+1/2}^{n+1/2} = \left(\frac{h_{j+1}^n + h_j^n}{2} \right) - \frac{\Delta t}{2 \Delta x} (q_{j+1}^n - q_j^n) \quad (4.17)$$

$$q_{j+1/2}^{n+1/2} = \left(\frac{q_{j+1}^n + q_j^n}{2} \right) - \frac{\Delta t}{2 \Delta x} (F_{j+1}^n - F_j^n) + \frac{\Delta t}{4} (G_{j+1}^n + G_j^n) \quad (4.18)$$

where:

$$F_j^n = \frac{(q_j^n)^2}{h_j^n} + \frac{1}{2} g (h_j^n)^2 \quad (4.19)$$

$$F_{j+1}^n = \frac{(q_{j+1}^n)^2}{h_{j+1}^n} + \frac{1}{2} g (h_{j+1}^n)^2 \quad (4.20)$$

and

$$G_j^n = g h_j^n \frac{z_j - z_{j+1/2}}{\Delta x/2} - g \frac{q_j^n |q_j^n|}{(C_c h_j^n)^2}, \quad C_c = 18 \log \left(\frac{12 h_j^n}{3 D_{90}} \right) \quad (4.21)$$

$$G_{j+1}^n = g h_{j+1}^n \frac{z_{j+1} - z_{j+3/2}}{\Delta x/2} - g \frac{q_{j+1}^n |q_{j+1}^n|}{(C_c h_{j+1}^n)^2}, \quad C_c = 18 \log \left(\frac{12 h_{j+1}^n}{3 D_{90}} \right) \quad (4.22)$$

The values of $h_{j+1/2}^{n+1/2}$ and $q_{j+1}^{n+1/2}$ calculated from Step 1 used as input in Step 2.

Step 2, $n+1/2$ to $n+1$

The leapfrog operator is employed for the second stage.

$$\frac{\bar{V}_j^{n+1} - \bar{V}_j^n}{\Delta t} + \frac{\bar{F}_{j+1/2}^{n+1/2} - \bar{F}_{j-1/2}^{n+1/2}}{\Delta x} = \frac{\bar{G}_{j+1/2}^{n+1/2} + \bar{G}_{j-1/2}^{n+1/2}}{2} \quad (4.23)$$

Then Equation (4.23) becomes

$$\frac{h_j^{n+1} - h_j^n}{\Delta t} + \frac{q_{j+1/2}^{n+1/2} - q_{j-1/2}^{n+1/2}}{\Delta x} = 0 \quad (4.24)$$

$$\frac{q_j^{n+1} - q_j^n}{\Delta t} + \frac{F_{j+1/2}^{n+1/2} - F_{j-1/2}^{n+1/2}}{\Delta x} = \frac{G_{j+1/2}^{n+1/2} + G_{j-1/2}^{n+1/2}}{2} \quad (4.25)$$

Rearranging Equations (4.24) and (4.25) here as

$$h_j^{n+1} = h_j^n - \frac{\Delta t}{\Delta x} (q_{j+1/2}^{n+1/2} - q_{j-1/2}^{n+1/2}) \quad (4.26)$$

$$q_j^{n+1} = q_j^n - \frac{\Delta t}{\Delta x} (F_{j+1/2}^{n+1/2} - F_{j-1/2}^{n+1/2}) + \frac{\Delta t}{2} (G_{j+1/2}^{n+1/2} + G_{j-1/2}^{n+1/2}) \quad (4.27)$$

where:

$$F_{j-1/2}^{n+1/2} = \frac{(q_{j-1/2}^{n+1/2})^2}{h_{j-1/2}^{n+1/2}} + \frac{1}{2} g (h_{j-1/2}^{n+1/2})^2 \quad (4.28)$$

$$F_{j+1/2}^{n+1/2} = \frac{(q_{j+1/2}^{n+1/2})^2}{h_{j+1/2}^{n+1/2}} + \frac{1}{2} g (h_{j+1/2}^{n+1/2})^2 \quad (4.29)$$

and

$$G_{j-1/2}^{n+1/2} = g h_{j-1/2}^{n+1/2} \frac{z_{j-1/2} - z_j}{\Delta x/2} - g \frac{q_{j-1/2}^{n+1/2} |q_{j-1/2}^{n+1/2}|}{(C_c h_{j-1/2}^{n+1/2})^2}, \quad C_c = 18 \log \left(\frac{12 h_{j-1/2}^{n+1/2}}{3 D_{90}} \right) \quad (4.30)$$

$$G_{j+1/2}^{n+1/2} = g h_{j+1/2}^{n+1/2} \frac{z_{j+1/2} - z_{j+1}}{\Delta x/2} - g \frac{q_{j+1/2}^{n+1/2} |q_{j+1/2}^{n+1/2}|}{(C_c h_{j+1/2}^{n+1/2})^2}, \quad C_c = 18 \log \left(\frac{12 h_{j+1/2}^{n+1/2}}{3 D_{90}} \right) \quad (4.31)$$

Note that both the volume and momentum equations are used in each step but the steps are alternating in space so that, in effect, one of them *leaps over* one time level of intermediate grid points, in the manner of the children's game that is commonly called *leapfrog* (Abbott and Basco, 1989).

The Lax-Wendroff, two-step scheme is also amplitude dissipative despite being of second order, and it is often used to model flows with moving shocks and discontinuities. In this study, the Lax-Wendroff scheme employs a numerical filtering device that has been called a *dissipative interface* so as to add a small amount of additional dissipation for each dependent variable. By this means, the scheme which initially has small base flow ($h \approx 0.03m$) can certainly control nonlinear instabilities mainly coming from extremely small local water depth and complex flow situations (*i.e.*, stationary jump at certain location) over the computational domain. The stability and dissipative interface will be further discussed in Ch.

4.2.3 and 4.5, respectively.

4.2.2 Method of Characteristics (MOC)

The Lax-Wendroff, two-step scheme presents problems at both boundaries for a solution.

The characteristic directions together with the Riemann relations, J_{\pm} along these characteristics provide the solution technique. There is a physical significance of the process in which we trace the propagation of flow information in the $x-t$ plane. The Riemann invariants are constant along each characteristic trace in the frictionless, horizontal channels. However, when boundary slope and shear are taken into account then, the Riemann invariant will no longer be constant along characteristics, C_{\pm} . In such a case the bottom slope is acting as a momentum source while the boundary shear is behaving as a momentum drain or sink.

Subcritical flows require the specification of one-point boundary data (q or h) at each boundary if a unique solution is to be obtained. In this study, water depths, h are specified at both boundaries, but both q and h are required to find F and G at these points. A special boundary method is then needed to provide flow rates, q at the boundary points so that the solution procedure can continue. The method of characteristics (MOC) provides a particularly transparent procedure for this purpose, and it is commonly used within the Lax-Wendroff, two step scheme as follows (Abbott and Basco, 1989).

LHB, at $n+1/2$ The $h_1^{n+1/2}$ is specified as the left-hand boundary data as indicated in Figure 4.2. The starting location, θ on the C_- characteristic striking the boundary exactly

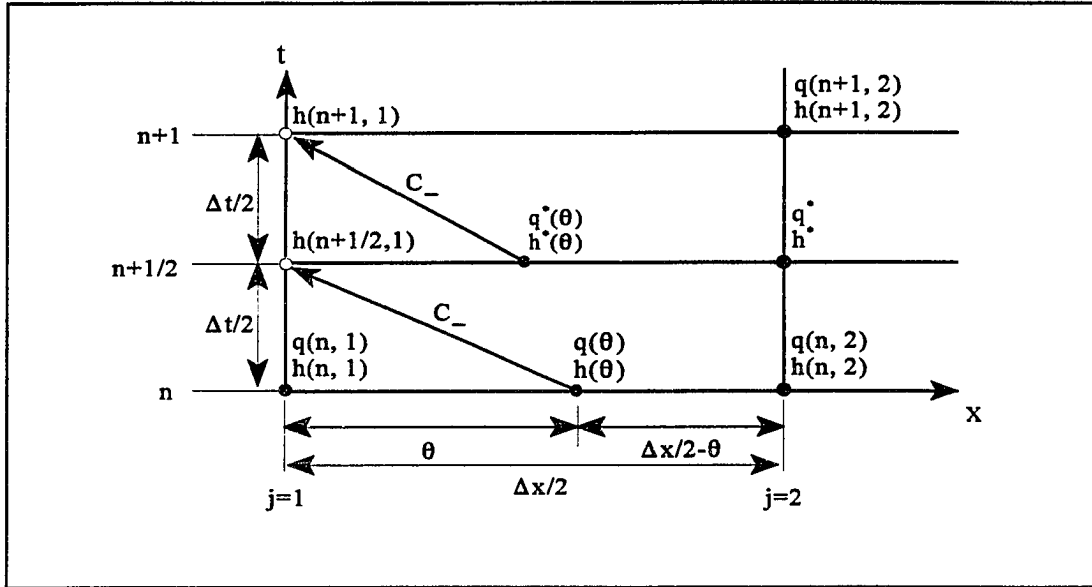


Figure 4.2 Left Hand Boundary Data Obtained by Method of Characteristics.

at $(n+1/2, 1)$ is unknown; therefore, the Newton-Raphson iteration method is employed to find $q(\theta)$ and $h(\theta)$ at the location, θ .

The characteristic speed, C_- is given as

$$C_- = - \frac{dx}{dt} = \frac{-\theta}{\Delta t/2} \quad (4.32)$$

and consequently, along C_- characteristic, celerity (value) of the C_- is unchanged as

$$C_- = u - \sqrt{gh} = \frac{q}{h} - \sqrt{gh} \quad (4.33)$$

Water depth and flow rate at point θ are computed from

$$\begin{aligned}
q(\theta) &= \frac{[\theta q_2^n + (\Delta x/2 - \theta) q_1^n]}{\Delta x/2} \\
h(\theta) &= \frac{[\theta h_2^n + (\Delta x/2 - \theta) h_1^n]}{\Delta x/2}
\end{aligned}
\tag{4.34}$$

Equations (4.32), (4.33) and (4.34) are then used to compute the characteristic distance, θ ,

$$\theta = -\frac{\Delta t}{2} \left\{ \frac{\theta q_2^n + \left(\frac{\Delta x}{2} - \theta\right) q_1^n}{\theta h_2^n + \left(\frac{\Delta x}{2} - \theta\right) h_1^n} - \left[g \frac{\theta h_2^n + \left(\frac{\Delta x}{2} - \theta\right) h_1^n}{\frac{\Delta x}{2}} \right]^{1/2} \right\}
\tag{4.35}$$

Newton-Raphson iteration continues according to some convergence criterion. A subroutine makes this relatively straightforward on the computer. Finally, the value of the Riemann Invariant, $J_-(\theta)$ can be found and, together with, $h_1^{n+1/2}$ the other boundary value $q_1^{n+1/2}$ can be determined as follows:

Riemann Invariant at θ

$$J_-(\theta) = \frac{q(\theta)}{h(\theta)} - 2\sqrt{gh(\theta)}
\tag{4.36}$$

Riemann Invariant at $(n+1/2, 1)$

$$J_-(n+1/2, 1) = \frac{q_1^{n+1/2}}{h_1^{n+1/2}} - 2\sqrt{gh_1^{n+1/2}}
\tag{4.37}$$

When boundary slope and boundary shear are taken into account , the *quasi-invariant* along

the C_c characteristic is derived as

$$\left(\frac{q_1^{n+1/2}}{h_1^{n+1/2}} - 2\sqrt{g h_1^{n+1/2}} \right) - \left(\frac{q(\theta)}{h(\theta)} - 2\sqrt{g h(\theta)} \right) = \int_{t_1}^{t_2} g(S_0 - S_f) dt \quad (4.38)$$

Rearranging and taking small enough time steps, $t_2 - t_1 = \Delta t/2$, Equation (4.38) gives additional boundary data as

$$\begin{aligned} q_1^{n+1/2} = h_1^{n+1/2} & \left[2\sqrt{g h_1^{n+1/2}} + \left(\frac{q(\theta)}{h(\theta)} - 2\sqrt{g h(\theta)} \right) \right] \\ & + g h_1^{n+1/2} \left(\frac{z_1^n - z_2^n}{\Delta x/2} - \frac{q(\theta) |q(\theta)|}{C_c^2 h^3(\theta)} \right) \frac{\Delta t}{2} \end{aligned} \quad (4.39)$$

where C_c is the Chezy coefficient at point θ defined as

$$C_c = 18 \log \left(\frac{12 h(\theta)}{3 D_{90}} \right) \quad (4.40)$$

LHB, at $n+1$ The step is the identical one as in the above procedures and is indicated in Figure 4.2. The h_1^{n+1} is specified as the left-hand boundary data at $n+1$ time level. After the second step, water depths and flow rates at $n+1$ time level are obtained over the computational domain except at the both boundaries. The starred values q^* and h^* are evaluated from the latest information available at the four corners as

$$q^* = \frac{q_1^{n+1/2} + q_2^n + q_2^{n+1} + q_3^{n+1/2}}{4} \quad (4.41)$$

$$h^* = \frac{h_1^{n+1/2} + h_2^n + h_2^{n+1} + h_3^{n+1/2}}{4}$$

Water depth and flow rate at point θ are computed from

$$q^*(\theta) = \frac{[\theta q^* + (\Delta x/2 - \theta) q_1^{n+1/2}]}{\Delta x/2} \quad (4.42)$$

$$h^*(\theta) = \frac{[\theta h^* + (\Delta x/2 - \theta) h_1^{n+1/2}]}{\Delta x/2}$$

The characteristic distance, θ is then derived from the Equations (4.32), (4.33) and (4.42) as

$$\theta = -\frac{\Delta t}{2} \left\{ \frac{\theta q^* + \left(\frac{\Delta x}{2} - \theta\right) q_1^{n+1/2}}{\theta h^* + \left(\frac{\Delta x}{2} - \theta\right) h_1^{n+1/2}} - \left[g \frac{\theta h^* + \left(\frac{\Delta x}{2} - \theta\right) h_1^{n+1/2}}{\frac{\Delta x}{2}} \right]^{1/2} \right\} \quad (4.43)$$

Riemann Invariant at θ

$$J_-(\theta) = \frac{q^*(\theta)}{h^*(\theta)} - 2\sqrt{g h^*(\theta)} \quad (4.44)$$

Riemann Invariant at $(n+1, 1)$

$$J_-(n+1, 1) = \frac{q_1^{n+1}}{h_1^{n+1}} - 2\sqrt{g h_1^{n+1}} \quad (4.45)$$

The *quasi-invariant* along the C_- characteristic is derived as

$$\left(\frac{q_1^{n+1}}{h_1^{n+1}} - 2\sqrt{g h_1^{n+1}} \right) - \left(\frac{q^*(\theta)}{h^*(\theta)} - 2\sqrt{g h^*(\theta)} \right) = \int_{t_2}^{t_3} g(S_0 - S_f) dt \quad (4.46)$$

Rearranging Equation (4.46) gives additional boundary data as

$$\begin{aligned} q_1^{n+1} = h_1^{n+1} & \left[2\sqrt{g h_1^{n+1}} + \left(\frac{q^*(\theta)}{h^*(\theta)} - 2\sqrt{g h^*(\theta)} \right) \right] \\ & + g h_1^{n+1} \left(\frac{z_1^n - z_2^n}{\Delta x/2} - \frac{q^*(\theta) |q^*(\theta)|}{C_c^2 h^{*3}(\theta)} \right) \frac{\Delta t}{2} \end{aligned} \quad (4.47)$$

where:

$$C_c = 18 \log \left(\frac{12 h^*(\theta)}{3 D_{90}} \right) \quad (4.48)$$

RHB, at $n+1/2$ The $h_{ij}^{n+1/2}$ is specified as the right-hand boundary data as indicated in Figure 4.3.

The characteristic speed, C_+ is given as

$$C_+ = \frac{dx}{dt} = \frac{\theta}{\Delta t/2} \quad (4.49)$$

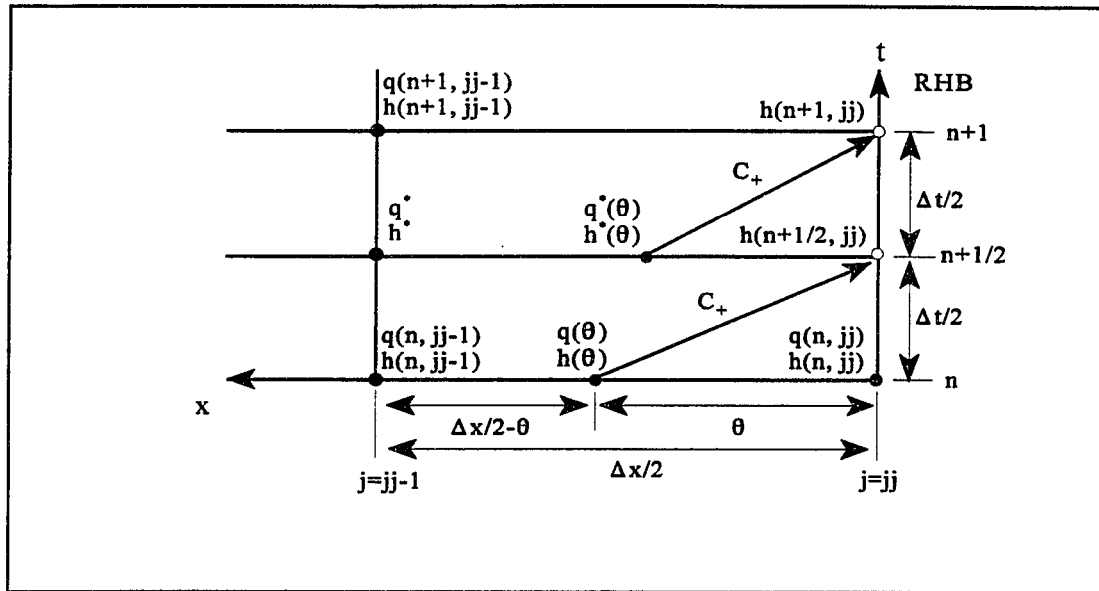


Figure 4.3 Right Hand Boundary Data Obtained by Method of Characteristics.

and

$$C_+ = u + \sqrt{gh} = \frac{q}{h} + \sqrt{gh} \quad (4.50)$$

Water depth and flow rate at point θ are computed from

$$q(\theta) = \frac{[\theta q_{jj-1}^n + (\Delta x/2 - \theta) q_{jj}^n]}{\Delta x/2} \quad (4.51)$$

$$h(\theta) = \frac{[\theta h_{jj-1}^n + (\Delta x/2 - \theta) h_{jj}^n]}{\Delta x/2}$$

The characteristic distance, θ is derived as

$$\theta = -\frac{\Delta t}{2} \left\{ \frac{\theta q_{jj-1}^n + \left(\frac{\Delta x}{2} - \theta\right) q_{jj}^n}{\theta h_{jj-1}^n + \left(\frac{\Delta x}{2} - \theta\right) h_{jj}^n} + \left[g \frac{\theta h_{jj-1}^n + \left(\frac{\Delta x}{2} - \theta\right) h_{jj}^n}{\frac{\Delta x}{2}} \right]^{1/2} \right\} \quad (4.52)$$

Riemann Invariant at θ

$$J_+(\theta) = \frac{q(\theta)}{h(\theta)} + 2\sqrt{gh(\theta)} \quad (4.53)$$

Riemann Invariant at $(n+1/2, jj)$

$$J_+(n+1/2, jj) = \frac{q_{jj}^{n+1/2}}{h_{jj}^{n+1/2}} + 2\sqrt{gh_{jj}^{n+1/2}} \quad (4.54)$$

Finally, additional right-hand boundary value, $q_{jj}^{n+1/2}$ at $n+1/2$ time level is computed from

$$\begin{aligned} q_{jj}^{n+1/2} = h_{jj}^{n+1/2} & \left[\left(\frac{q(\theta)}{h(\theta)} + 2\sqrt{gh(\theta)} \right) - 2\sqrt{gh_{jj}^{n+1/2}} \right] \\ & + g h_{jj}^{n+1/2} \left(\frac{z_{jj-1}^n - z_{jj}^n}{\Delta x/2} - \frac{q(\theta) |q(\theta)|}{C_c^2 h^3(\theta)} \right) \frac{\Delta t}{2} \end{aligned} \quad (4.55)$$

RHB, at $n+1$ The h_{jj}^{n+1} is specified as the right-hand boundary data at $n+1$ time level.

The starred values q^* and h^* are evaluated from the latest information available at the four corners as

$$\begin{aligned}
q^* &= \frac{q_{jj}^{n+1/2} + q_{jj-1}^n + q_{jj-1}^{n+1} + q_{jj-2}^{n+1/2}}{4} \\
h^* &= \frac{h_{jj}^{n+1/2} + h_{jj-1}^n + h_{jj-1}^{n+1} + h_{jj-2}^{n+1/2}}{4}
\end{aligned}
\tag{4.56}$$

Water depth and flow rate at point θ are computed from

$$\begin{aligned}
q^*(\theta) &= \frac{[\theta q^* + (\Delta x/2 - \theta) q_{jj}^{n+1/2}]}{\Delta x/2} \\
h^*(\theta) &= \frac{[\theta h^* + (\Delta x/2 - \theta) h_{jj}^{n+1/2}]}{\Delta x/2}
\end{aligned}
\tag{4.57}$$

The characteristic distance, θ is then derived from the Equations (4.49), (4.50) and (4.57) as

$$\theta = -\frac{\Delta t}{2} \left\{ \frac{\theta q^* + \left(\frac{\Delta x}{2} - \theta\right) q_{jj}^{n+1/2}}{\theta h^* + \left(\frac{\Delta x}{2} - \theta\right) h_{jj}^{n+1/2}} + \left[g \frac{\theta h^* + \left(\frac{\Delta x}{2} - \theta\right) h_{jj}^{n+1/2}}{\frac{\Delta x}{2}} \right]^{1/2} \right\} \tag{4.58}$$

Riemann Invariant at θ

$$J_+(\theta) = \frac{q^*(\theta)}{h^*(\theta)} + 2\sqrt{g h^*(\theta)} \tag{4.59}$$

Riemann Invariant at $(n+1, jj)$

$$J_+(n+1, jj) = \frac{q_{jj}^{n+1}}{h_{jj}^{n+1}} + 2\sqrt{g h_{jj}^{n+1}} \quad (4.60)$$

From the Equations (4.59) and (4.60), additional boundary data, q_{jj}^{n+1} is obtained as

$$\begin{aligned} q_{jj}^{n+1} = h_{jj}^{n+1} & \left[\left(\frac{q^*(\theta)}{h^*(\theta)} + 2\sqrt{g h^*(\theta)} \right) - 2\sqrt{g h_{jj}^{n+1}} \right] \\ & + g h_{jj}^{n+1} \left(\frac{z_{jj-1}^n - z_{jj}^n}{\Delta x/2} - \frac{q^*(\theta) |q^*(\theta)|}{C_c^2 h^{*3}(\theta)} \right) \frac{\Delta t}{2} \end{aligned} \quad (4.61)$$

Therefore, four boundary modules are employed to compute all required boundary data within each time level (*i.e.* n to $n+1$) and then, the numerical computation moves to the next time level.

4.2.3 Stability

For the homogeneous linearized vector equations for the Lax-Wendroff scheme,

$$\frac{\bar{f}_{j+1/2}^{n+1/2} - \left(\frac{\bar{f}_{j+1}^n + \bar{f}_j^n}{2} \right)}{\Delta t/2} + \bar{\bar{B}} \frac{\bar{f}_{j+1}^n - \bar{f}_j^n}{\Delta x} = 0 \quad (4.62a)$$

$$\frac{\bar{f}_j^{n+1} - \bar{f}_j^n}{\Delta t} + \bar{\bar{B}} \frac{\bar{f}_{j+1/2}^{n+1/2} - \bar{f}_{j-1/2}^{n+1/2}}{\Delta x} = 0 \quad (4.62b)$$

with

$$\bar{f} = \begin{bmatrix} h \\ u h \end{bmatrix}, \quad \bar{\bar{B}} = \begin{bmatrix} 0 & 1 \\ (gh - u^2) & 2u \end{bmatrix} \quad (4.63)$$

From Equation (4.62a),

$$\begin{aligned} \bar{f}_{j+1/2}^{n+1/2} &= -\frac{\Delta t \bar{\bar{B}}}{2 \Delta x} (\bar{f}_{j+1}^n - \bar{f}_j^n) + \frac{1}{2} (\bar{f}_{j+1}^n + \bar{f}_j^n) \\ \bar{f}_{j-1/2}^{n+1/2} &= -\frac{\Delta t \bar{\bar{B}}}{2 \Delta x} (\bar{f}_j^n - \bar{f}_{j-1}^n) + \frac{1}{2} (\bar{f}_j^n + \bar{f}_{j-1}^n) \end{aligned} \quad (4.64)$$

Putting Equation (4.64) into (4.62b) gives

$$\bar{f}_j^{n+1} = \frac{1}{2} \left(\frac{\Delta t \bar{\bar{B}}}{\Delta x} \right)^2 (\bar{f}_{j+1}^n - 2\bar{f}_j^n + \bar{f}_{j-1}^n) - \frac{\Delta t \bar{\bar{B}}}{2 \Delta x} (\bar{f}_{j+1}^n - \bar{f}_{j-1}^n) + \bar{f}_j^n \quad (4.65)$$

The amplification matrix of Equation (4.65) is determined by the linear stability analysis method which determines how each Fourier coefficient, $\bar{\xi}$, behaves (grows, decays, or stays constant) in time for any wave number, k .

Let,

$$\bar{f}_j^n = \sum_{k=1}^{kk} \bar{\xi}_k^n \exp(i\alpha_j) \quad (4.66)$$

be a finite, Fourier series representation of $\bar{f}(j, n)$ for all dimensionless wave numbers, $\alpha(k)$, $k=1, 2, \dots, kk$, at time level, n . It is simply shown at any wave number (say $k=1$) giving

$$\bar{f}_j^n = \bar{\xi}^n e^{i\alpha j} \quad (4.67)$$

where $\bar{\xi}^n$ is the Fourier coefficient for wave number l at time-level n , and substitute into Equation (4.65) then, amplification matrix is obtained as,

$$\bar{G} = \frac{\bar{\xi}^{n+1}}{\bar{\xi}^n} = \bar{I} - (1 - \cos\alpha) \left(\frac{\Delta t \bar{B}}{\Delta x} \right)^2 - i \left(\frac{\Delta t \bar{B}}{\Delta x} \right) \sin\alpha \quad (4.68)$$

and eigenvalues of matrix \bar{G} , $g_{1,2}$ now become

$$g_{1,2} = 1 - (1 - \cos\alpha) C_r^2 - i C_r \sin\alpha \quad (4.69)$$

with Courant number,

$$C_r = (u \pm \sqrt{gh}) \frac{\Delta t}{\Delta x} \quad (4.70)$$

The von Neumann and Courant-Friedrichs-Lewy (CFL) conditions for stability of equation systems give

$$|g_{1,2}| \leq 1 \quad \text{and} \quad C_r \leq 1 \quad (4.71)$$

, respectively.

Further details of the amplitude and phase portraits for the finite difference scheme are found in Richtmyer and Morton (1967), and Abbott and Basco (1989).

The main restriction on the use of explicit schemes for the solution of unsteady, one-dimensional, real fluid flows is a time step limitation. In this study, time step, Δt is defined

from Equation (4.71) as,

$$\Delta t \leq \frac{\Delta x}{|u_{\max}| + \sqrt{g h_{\max}}} \quad (4.72)$$

Maximum values of u and h are unknown before a solution is obtained so that some safety margin is needed to prevent the computation from going unstable.

4.3 Stage III and IV - Storm Tides

In the first step (*i.e.* water motion calculation), bottom elevation is considered to be constant during the time interval Δt , and $u(t+\Delta t, x)$ and $h(t+\Delta t, x)$ are computed using the Preissmann scheme (1961). In the second step, a forward time and centered space explicit scheme is employed for the sediment continuity equation using known water depths and velocities.

4.3.1 Water Motion - The Preissmann Scheme

Non-conservation (Eulerian) form of governing equations are rewritten here.

Water Continuity Equation

$$\frac{\partial h}{\partial t} + h \cdot \frac{\partial u}{\partial x} + u \cdot \frac{\partial h}{\partial x} = 0 \quad (4.73)$$

Equation of Motion

$$\frac{\partial u}{\partial t} + (1 - Fr^2) u^* \frac{\partial u}{\partial x} + g \frac{\partial h}{\partial x} = g \frac{\partial z}{\partial x} - g S_f \quad (4.74)$$

Friction Slope and Chezy-coefficient

$$S_f = \frac{u |u|}{C_c^2 h} \quad , \quad C_c = 18 \log \left(\frac{12 R_b}{k_s} \right) \quad (4.75)$$

A schematic representation of the Preissmann operator is shown in Figure 4.4. Let $f(t, x)$ be any one fluid-flow dependent variable, its time derivative and space derivative by the difference formulas represented by

$$\begin{aligned} \frac{\partial f}{\partial t} &\approx (1 - \psi) \frac{f_j^{n+1} - f_j^n}{\Delta t} + \psi \frac{f_j^{n+1} - f_{j+1}^n}{\Delta t} \\ \frac{\partial f}{\partial x} &\approx (1 - \theta) \frac{f_{j+1}^n - f_j^n}{\Delta x} + \theta \frac{f_{j+1}^{n+1} - f_j^{n+1}}{\Delta x} \end{aligned} \quad (4.76)$$

with

$$\begin{aligned} u^* &\approx \frac{(u_j^{n+1} + u_j^n + u_{j+1}^{n+1} + u_{j+1}^n)}{4} \\ h^* &\approx \frac{(h_j^{n+1} + h_j^n + h_{j+1}^{n+1} + h_{j+1}^n)}{4} \end{aligned} \quad (4.77)$$

where ψ and θ are the weighting factors for space and time, respectively. The starred values u^* and h^* are local, *quasi-constants*, evaluated from the latest information available at the four corners of the scheme in an iterative process. Using Equation (4.76) as general operation, the following two finite difference equations are obtained.

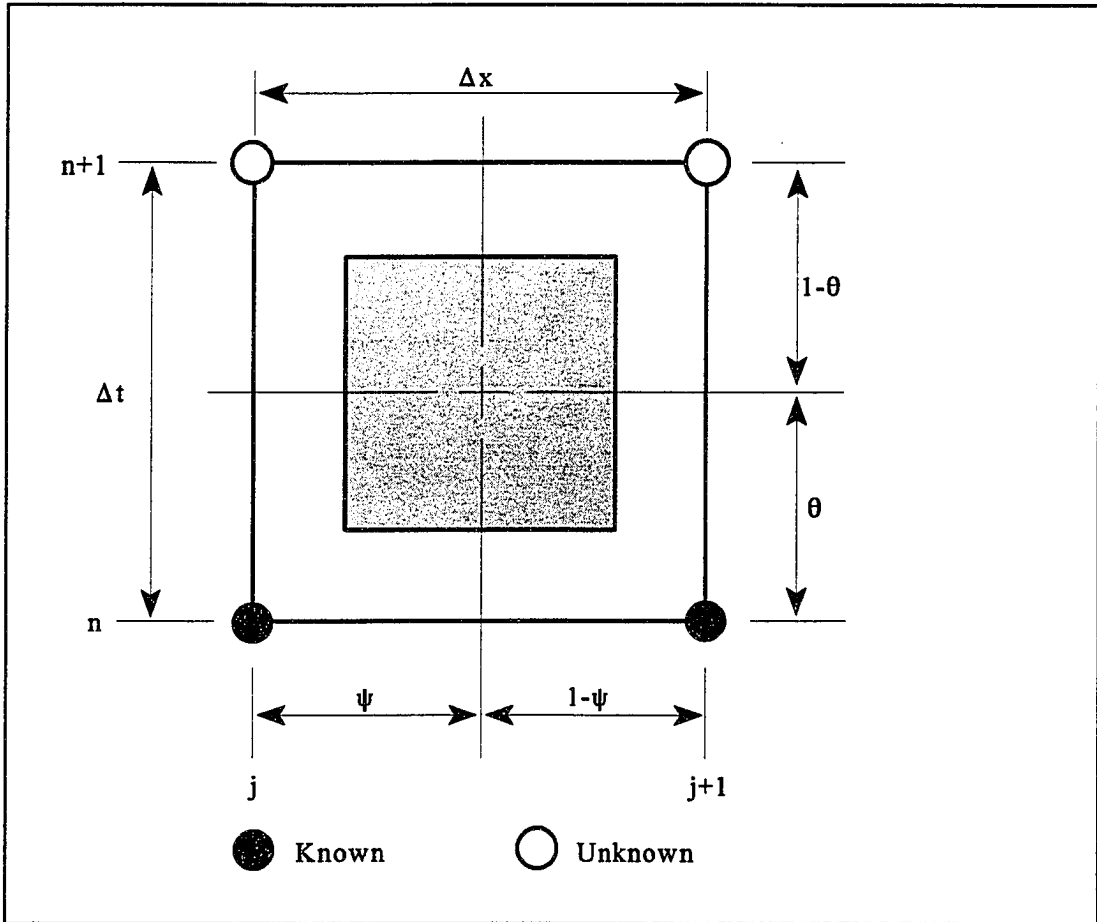


Figure 4.4 The Box or Preissmann Scheme Drawn for $\theta = \psi = 1/2$.

Motion

$$\begin{aligned}
 & (1 - \psi) \frac{u_j^{n+1} - u_j^n}{\Delta t} + \psi \frac{u_{j+1}^{n+1} - u_{j+1}^n}{\Delta t} \\
 & + (1 - Fr^2) u^* \left[(1 - \theta) \frac{u_{j+1}^n - u_j^n}{\Delta x} + \theta \frac{u_{j+1}^{n+1} - u_j^{n+1}}{\Delta x} \right] \\
 & + g \left[(1 - \theta) \frac{h_{j+1}^n - h_j^n}{\Delta x} + \theta \frac{h_{j+1}^{n+1} - h_j^{n+1}}{\Delta x} \right] \\
 & = g \frac{z_j^n - z_{j+1}^n}{\Delta x} - B_s (u_j^{n+1} + u_{j+1}^{n+1})
 \end{aligned} \tag{4.78}$$

Volume

$$\begin{aligned}
& (1 - \psi) \frac{h_j^{n+1} - h_j^n}{\Delta t} + \psi \frac{h_{j+1}^{n+1} - h_{j+1}^n}{\Delta t} \\
& + u^* \left[(1 - \theta) \frac{h_{j+1}^n - h_j^n}{\Delta x} + \theta \frac{h_{j+1}^{n+1} - h_j^{n+1}}{\Delta x} \right] \\
& + h^* \left[(1 - \theta) \frac{u_{j+1}^n - u_j^n}{\Delta x} + \theta \frac{u_{j+1}^{n+1} - u_j^{n+1}}{\Delta x} \right] = 0
\end{aligned} \tag{4.79}$$

where:

$$B_s = \frac{g}{4 C_c^2 h^*} |u_j^n + u_{j+1}^n| \tag{4.80}$$

Rearranging and collecting all higher time level terms on the left side of the equations give

$$\text{Motion} : A1 u_j^{n+1} + B1 h_j^{n+1} + C1 u_{j+1}^{n+1} + D1 h_{j+1}^{n+1} = E1 \tag{4.81}$$

$$\text{Mass} : A2 u_j^{n+1} + B2 h_j^{n+1} + C2 u_{j+1}^{n+1} + D2 h_{j+1}^{n+1} = E2 \tag{4.82}$$

where:

$$\begin{aligned}
A1 &= \frac{1 - \psi}{\Delta t} - (1 - Fr^2) \frac{u^* \theta}{\Delta x} + B_s \\
B1 &= -D1 = -\frac{g \theta}{\Delta x} \\
C1 &= \frac{\psi}{\Delta t} + (1 - Fr^2) \frac{u^* \theta}{\Delta x} + B_s \\
A2 &= -C2 = -\frac{h^* \theta}{\Delta x} \\
B2 &= \frac{1 - \psi}{\Delta t} - \frac{u^* \theta}{\Delta x} , \quad D2 = \frac{\psi}{\Delta t} - \frac{u^* \theta}{\Delta x}
\end{aligned} \tag{4.83}$$

and on the right side, at the lower (known) time level,

$$\begin{aligned}
 E1 = & u_j^n \left[\frac{1-\Psi}{\Delta t} + (1-Fr^2) \frac{u^*(1-\theta)}{\Delta x} \right] + u_{j+1}^n \left[\frac{\Psi}{\Delta t} - (1-Fr^2) \frac{u^*(1-\theta)}{\Delta x} \right] \\
 & + h_j^n \left[\frac{g(1-\theta)}{\Delta x} \right] - h_{j+1}^n \left[\frac{g(1-\theta)}{\Delta x} \right] + g \frac{z_j^n - z_{j+1}^n}{\Delta x}
 \end{aligned} \tag{4.84}$$

and

$$\begin{aligned}
 E2 = & u_j^n \left[\frac{h^*(1-\theta)}{\Delta x} \right] - u_{j+1}^n \left[\frac{h^*(1-\theta)}{\Delta x} \right] \\
 & + h_j^n \left[\frac{1-\Psi}{\Delta t} + \frac{u^*(1-\theta)}{\Delta x} \right] + h_{j+1}^n \left[\frac{\Psi}{\Delta t} - \frac{u^*(1-\theta)}{\Delta x} \right]
 \end{aligned} \tag{4.85}$$

Equations (4.81) and (4.82) constitute a system of two nonlinear algebraic equations which provide a pentadiagonal matrix structure. Formally

$$\bar{P} \cdot \bar{f}_j^{n+1} = \bar{E}_j^n \tag{4.86}$$

where:

$$\bar{f}_j^{n+1} = \begin{bmatrix} u_j \\ h_j \end{bmatrix}^{n+1}, \quad \bar{E}_j^n = \begin{bmatrix} E1_j \\ E2_j \end{bmatrix}^n \tag{4.87}$$

and \bar{P} is the coefficient matrix. Equations (4.81) and (4.82) represent a system of $2(N-1)$ nonlinear equations involving $2N$ unknowns, where N is the number of grid points along the x-axis. Two additional equations for determining all the unknowns are supplied by the boundary conditions.

To solve a nonlinear equation system by iterations, the system is usually first linearized. The linearized system is then solved, giving initial estimates of the new flow variables at time level $(n+1)\Delta t$. The new linear system can then be solved using the same piece of code, so as to obtain improved estimates of all coefficients, and indeed this iteration process can be continued until some established criterion is satisfied, such as one corresponding to the accuracy that is desired.

The *double sweep solution method* is proposed herein for the solution of this system. This is now widely accepted as the most efficient way to solve systems of nonlinear as well as linear equations.

Water depths are specified at both ocean and bay boundaries in this study.

The First Sweep (j = jj to 1)

First, introduce auxiliary variables F_j and G_j so as to linearly relate h_j^{n+1} and u_j^{n+1} at right hand boundary:

$$h_{j+1}^{n+1} = F_{j+1} u_{j+1}^{n+1} + G_{j+1} \quad (4.88a)$$

$$h_{jj}^{n+1} = F_{jj} u_{jj}^{n+1} + G_{jj} \quad , \quad \text{at RHB} \quad (4.88b)$$

To ensure the independence of the necessary coefficients, we can take $F_{jj}=0$ giving

$$G_{jj} = h_{jj}^{n+1} \quad (4.89)$$

Substituting Equation (4.88a) into Equations (4.81) and (4.82) gives

$$\begin{aligned}
A1 u_j^{n+1} + B1 h_j^{n+1} + (C1 + D1 F_{j+1}) u_{j+1}^{n+1} &= E1 - D1 G_{j+1} \\
A2 u_j^{n+1} + B2 h_j^{n+1} + (C2 + D2 F_{j+1}) u_{j+1}^{n+1} &= E2 - D2 G_{j+1}
\end{aligned} \tag{4.90}$$

Now eliminate u_{j+1}^{n+1} in equation (4.90), then

$$h_j^{n+1} = F_j u_j^{n+1} + G_j \tag{4.91}$$

where:

$$F_j = \frac{-[A1(C2 + D2 F_{j+1}) - A2(C1 + D1 F_{j+1})]}{[B1(C2 + D2 F_{j+1}) - B2(C1 + D1 F_{j+1})]} \tag{4.92}$$

and

$$G_j = \frac{[(C2 + D2 F_{j+1})(E1 - D1 G_{j+1}) - (C1 + D1 F_{j+1})(E2 - D2 G_{j+1})]}{[B1(C2 + D2 F_{j+1}) - B2(C1 + D1 F_{j+1})]} \tag{4.93}$$

Equations (4.92) and (4.93) define a set of recurrence relations to calculate the initial sweep coefficients, $(F_{jj-1}, G_{jj-1}), (F_{jj-2}, G_{jj-2}), \dots, (F_2, G_2), (F_1, G_1)$, since each successive pair, (F_j, G_j) , only depends upon the previous pair, (F_{j+1}, G_{j+1}) and other known information.

The Second Sweep (j = 1 to jj)

To begin the second, reverse, return sweep in the double sweep procedure, we pick up the boundary data, h_1^{n+1} from the other end (*i.e.* ocean boundary) and Equation (4.91) is used to solve directly for the missing values as,

$$u_1^{n+1} = \frac{(h_1^{n+1} - G_1)}{F_1} \quad (4.94)$$

To find the remaining values, Equation (4.90) is utilized to establish an auxiliary relation, and we introduce three additional non-recursive relations that must also be calculated during the initial sweep. Rearranging the first equation in (4.90) gives

$$u_{j+1}^{n+1} = P_{j+1} u_j^{n+1} + Q_{j+1} h_j^{n+1} + R_{j+1} \quad (4.95)$$

where:

$$\begin{aligned} P_{j+1} &= \frac{-A1}{C1 + D1 F_{j+1}} \\ Q_{j+1} &= \frac{-B1}{C1 + D1 F_{j+1}} \\ R_{j+1} &= \frac{E1 - D1 G_{j+1}}{C1 + D1 F_{j+1}} \end{aligned} \quad (4.96)$$

The three new auxiliary coefficients are computed initially for all j , from $j=jj-1$ to $j=1$, since they depend only on the known coefficients. Equation (4.95) is then used, starting at $j=1$ (which in this example is the left-hand ocean boundary) to calculate water velocities, and Equation (4.88a) is used to calculate water depths.

This completes the second sweep of the double sweep procedure. Velocities and water depths are now known at time level $n+1$ for all grid points including both boundaries. Since these new values update the u^* and h^* values used in the coefficients, a first and

possibly a second iteration may then be required to satisfy the accuracy that is desired.

4.3.2 Sediment Motion - FTCS Explicit Scheme

Once the water depths and velocities at the new time level are known, the sediment transport rates for bed- and suspended-loads are computed based on the available theory (van Rijn, 1984a and b). These computed loads are then used to compute channel bed elevation by solving sediment continuity equation.

The Sediment Continuity Equation

$$(1 - p) \frac{\partial z}{\partial t} + \frac{\partial q_t}{\partial x} = 0 \quad (4.97)$$

is solved using a forward time and centered space (FTCS) explicit scheme usually on the same computational grid as the water motion calculation.

The above partial differential equation is approximated as

$$(1 - p) \frac{z_j^{n+1} - z_j^n}{\Delta t} + \frac{q_{t,j+1}^{n+1} - q_{t,j-1}^{n+1}}{2 \Delta x} = 0 \quad (4.98)$$

which can be expanded to yield

$$z_j^{n+1} = z_j^n - \frac{1}{1 - p} \frac{\Delta t}{2 \Delta x} (q_{t,j+1}^{n+1} - q_{t,j-1}^{n+1}) \quad (4.99)$$

where:

$$\begin{aligned}
z_j^n &= \text{bottom elevation above a datum at time level } n, L \\
z_j^{n+1} &= \text{bottom elevation above a datum at time level } n+1, L \\
p &= \text{porosity of bed materials} \\
q_{t,j+1}^{n+1} &= \text{total sediment transport rate at } (t, x) = (n+1, j+1), L^3/L \cdot T \\
q_{t,j-1}^{n+1} &= \text{total sediment transport rate at } (t, x) = (n+1, j-1), L^3/L \cdot T
\end{aligned}$$

Equation (4.99) generally produces unstable results (*i.e.* wiggles) when and where water flow is rapidly changed. The wiggles are growing with time marching and eventually give an uncontrollable situation. To avoid this situation a dissipative interface is introduced at alternate time steps so as to add a small amount of local dissipation such as:

$$z_j^{n*} = \gamma z_{j-1}^n + (1 - 2\gamma) z_j^n + \gamma z_{j+1}^n, \quad 0 \leq \gamma \leq 1/2 \quad (4.100)$$

where z_j^{n*} is updated value and γ is a weighting factor. The dissipative interface will be further discussed in Ch.4.5.

Equation (4.99) requires both upstream (ocean) and downstream (bay) boundary conditions and the boundary conditions are treated in Ch.5.3 in detail.

After bed level computations are finished at the time level $n+1$, the following adjustments of the flow characteristics in the reach are performed as,

$$\begin{aligned}
q^{n+1} &= u^{n+1} \cdot h^{n+1} \\
\Delta z &= z^{n+1} - z^n \\
h^{n+1} &= h^n - \Delta z \\
u^{n+1} &= q^{n+1} / h^{n+1}
\end{aligned}
\tag{4.101}$$

The above adjusted variables give the final values of u and h at the $n+1$ time level and are used for the next time step water flow computations.

4.3.3 Stability

The standard technique for the analysis of the stability and convergence of a difference scheme is the Fourier series method attributed to von Neumann.

Fread (1974) conducted an early von Neumann analysis of the linearized mass equation and the momentum equation including a linearized boundary shear stress term. As expected, the friction produces more damping, some of it physically justified, some of it arising numerically from the form of the resistance term.

Evans (1977) considered the full nonlinear equations of de St. Venant with bed slope and boundary shear.

Ponce and Simons (1977) also included bed slope and boundary shear in the full equations and made extensive comparisons between the amplification factor and the continuum response function in the dissipative range, $0.5 \leq \theta \leq 1.0$. They concluded that numerical amplification or attenuation can occur depending upon the Froud number, Courant number, and the wave number in a very complicated way.

Lyn and Goodwin (1987) examined the stability and convergence characteristics of the Preissmann's four-point implicit finite difference scheme. The analysis was made for a general linear hyperbolic system of n first-order equations, but is restricted to the homogeneous or frictionless case. In particular, the effect of a weighting factor in space, as well as in time, is considered.

A linear stability analysis for the homogeneous de St. Venant equations is fully discussed in Abbott and Basco (1989).

The detailed stability analysis for the *non-homogeneous* equations are beyond the intended scope of this investigation. However, from the various numerical experiments, actual computations in water motion have shown that the theoretically better value of the time weighting factor, $\theta=0.5$ is impractical from the stability viewpoint, and that in practice following criteria are recommended.

$$\psi = 0.5 \quad \text{and} \quad \theta \geq 0.65 \quad (4.102)$$

The weighting factors of $\psi=0.5$ and $\theta=0.75$ are used in this study.

An explicit criterion for the relation between time and length step for numerical stability could not be determined due to the nonlinearity of the sediment transport continuity equation and the smoothing of the bed elevations. However, it was empirically found that the use of the dissipative interface greatly improves stability of the solution; otherwise, numerical oscillations may originate from the top of the barrier dune where flows change rapidly.

4.4 Standard Tests for Computer Codes

The numerical tests provide a tool to check program correctness. Very many different testing tools can be employed and each of these is run over a wide range of flow conditions and discretization conditions during the development process.

The *static* and *cosine swing tests* for the Lax-Wendroff and Preissmann schemes, and a *shock test* for the Preissmann scheme are employed to check the conservation law and the growth of round off errors for each numerical code.

4.4.1 Static Test

It is the simplest tool to confirm the accuracy of the scheme and the computer code using the concept of conservation of mass. For ease of use the frictionless horizontal bed is considered and test conditions are as follows.

Initial Conditions

$$u(1, x) = 0 \quad , \quad h(1, x) = 10m \quad (4.103)$$

Boundary Conditions

$$u(t, 1) = 0 \quad , \quad u(t, jj) = 0 \quad (4.104)$$

with $\Delta x=100m$, $\Delta t=10sec$ and channel length, $L=2,000m$, and $\psi=0.5$ and $\theta=0.5$ for the Preissmann scheme.

Figure 4.5 shows test results for the Lax-Wendroff and Preissmann schemes at

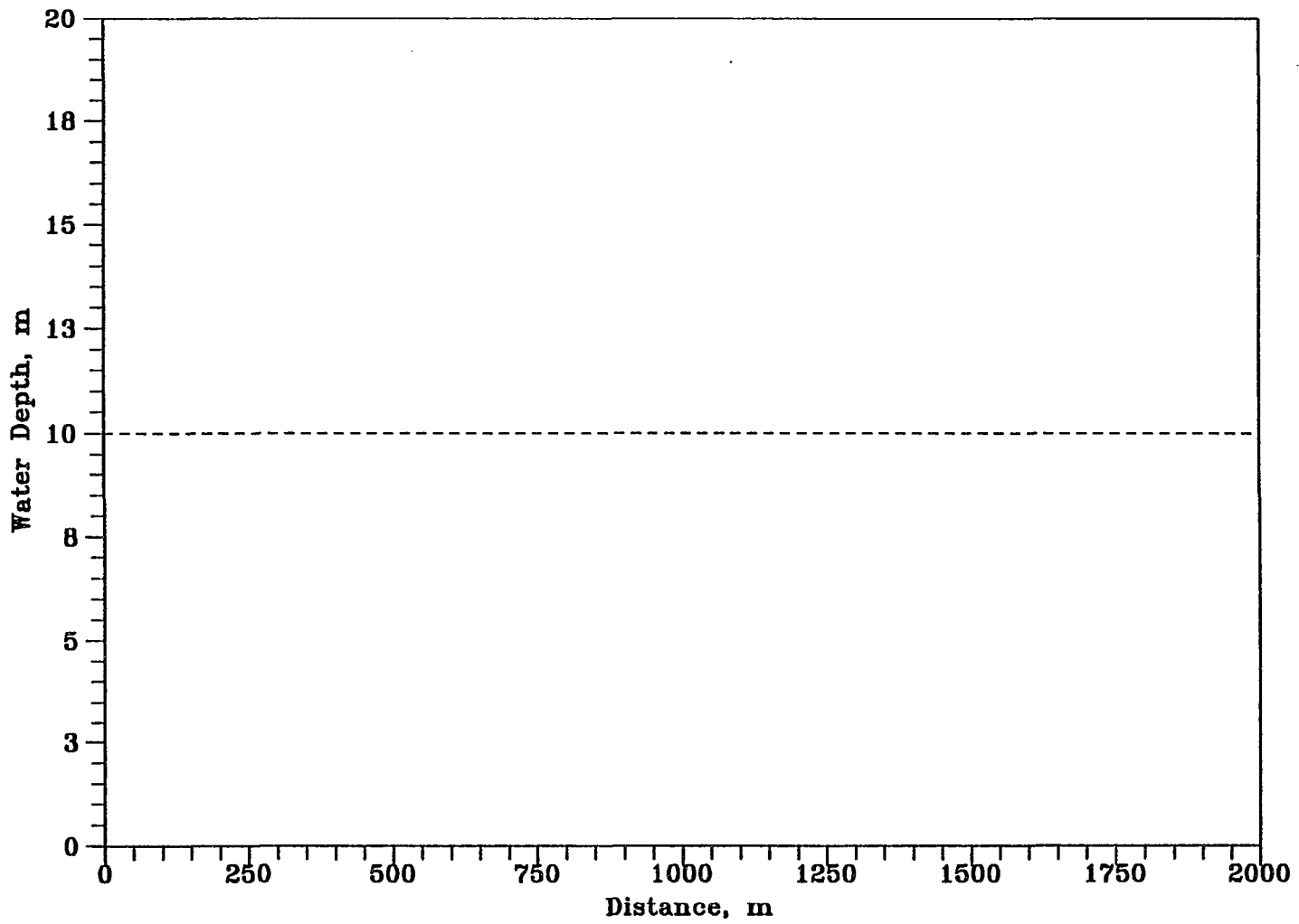


Figure 4.5 Static Test Results for Lax-Wendroff and Preissmann Scheme at Six Different Time Steps. ($t=1, 200, 400, 600, 800$ and 1000)

various time levels. No depth change is shown at all time levels and the mass (*i.e.* volume of water) is well conserved over the computational domain. From these tests, both numerical codes should be regarded as correct and applicable for further numerical integration.

4.4.2 Cosine Swing Test

An example of one-dimensional testing for amplitude and phase error is a cosine swing test using the concept of periodic standing wave phenomenon.

Water Profile Equation and Wave Period

$$\eta(x) = a \cos\left(\frac{\pi x}{L}\right) \quad , \quad T = \frac{2L}{\sqrt{g h_0}} \quad (4.105)$$

Initial Conditions

$$h(1, x) = a \cos\left(\frac{\pi x}{L}\right) + h_0 \quad , \quad q(1, x) = 0 \quad (4.106)$$

Boundary Conditions

$$q(t, 1) = 0 \quad , \quad q(t, jj) = 0 \quad (4.107)$$

where: a = amplitude of standing wave (= 0.1m)

L = length of the channel (=2,000m)

h_0 = still water depth (=10m)

$$\begin{aligned}
S_0 &= \text{bottom slope (=0)} \\
S_f &= \text{energy slope (=0)} \\
T &= \text{wave period (=404sec)} \\
(\Delta x, \Delta t) &= (100m, 10.1sec) \\
(\theta, \psi) &= (0.5, 0.5)
\end{aligned}$$

For the Lax-Wendroff scheme, the method of characteristics that is discussed in Ch.4.2.2 is employed to compute additional boundary data at each boundary.

No amplitude and phase errors in both schemes are shown in Figure 4.6.

4.4.3 Shock Test

The shock test is more realistic than those previously employed because a bed slope and boundary shear are embodied. Introducing a sudden shock at downstream boundary may give an unstable situation at the early stage; however, after a certain time level a *new steady state* will be obtained over the whole computational domain.

Test conditions are as follows.

Chezy Coefficient and Steady Uniform Velocity

$$C_c = 18 \log \left(\frac{12 h}{3 D_{90}} \right) \quad , \quad V = C_c \sqrt{h S_0} \quad (4.108)$$

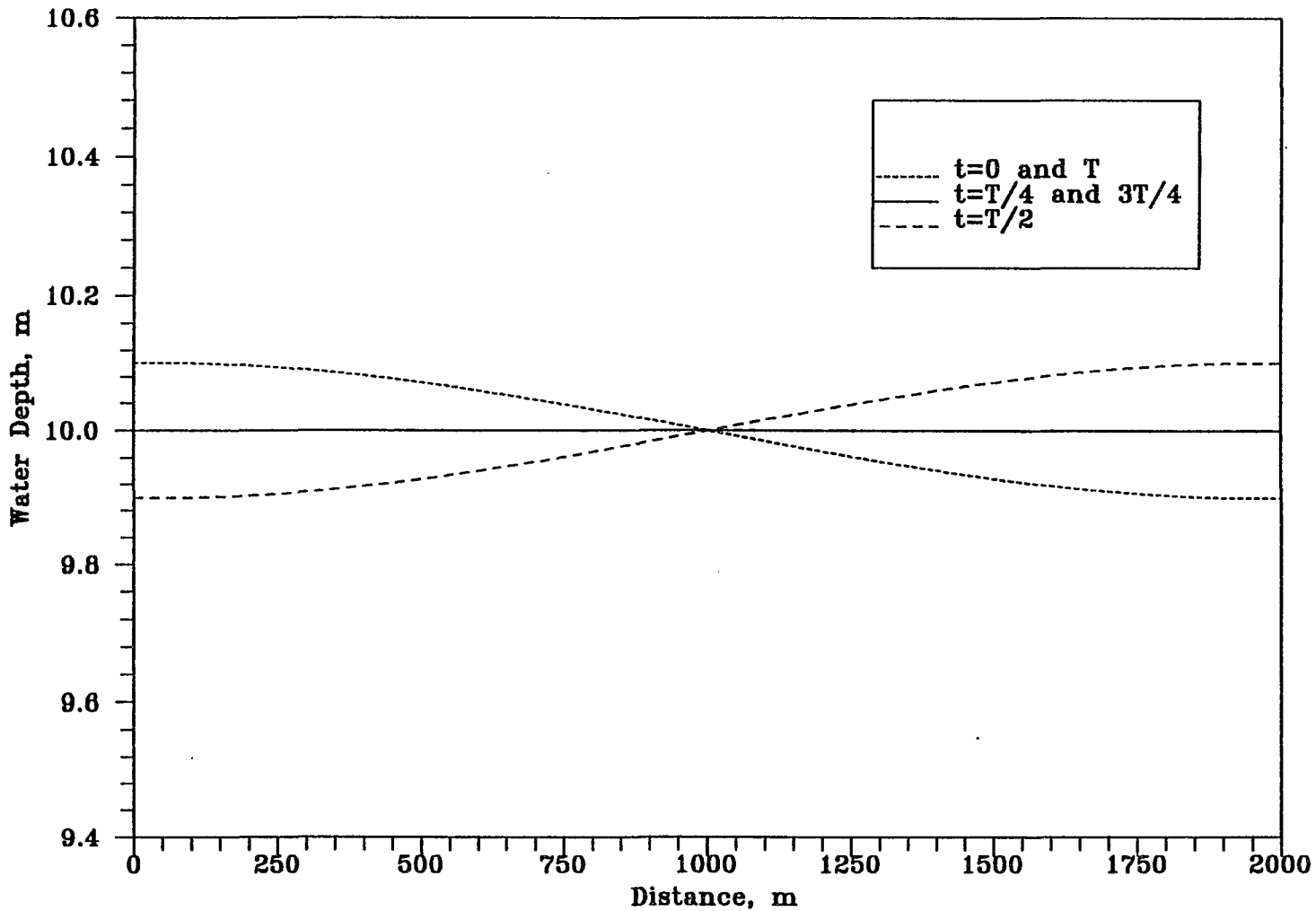


Figure 4.6 Cosine Swing Test Results for Lax-Wendroff and Preissmann Scheme at Five Different Time Steps. ($t=0$, $T/4$, $T/2$, $3T/4$ and T)

Initial Conditions

$$u(1, x) = V = 6.72\text{m/sec} \quad , \quad h(1, x) = 10\text{m} \quad (4.109)$$

Boundary Conditions

$$u(t, 1) = V = 6.72\text{m/sec} \quad , \quad h(t, jj) = h(1, x) + \Delta h = 11.0\text{m} \quad (4.110)$$

$$\begin{aligned} \text{where: } S_0 &= 5 \times 10^{-4} \\ D_{90} &= 4 \times 10^{-4}\text{m} \\ (\Delta t, \Delta x) &= (50\text{sec}, 100\text{m}) \\ (\theta, \psi) &= (1.0, 0.5) \end{aligned}$$

Shock test results are graphically presented in Figure 4.7 for the Preissmann scheme at various time steps. Initially unstable water depths in the domain go to a new steady state as we expected.

The above three tests are instrumental in determining the usefulness of the given finite difference scheme and computer codes. The utilities of the θ parameter in the Preissmann scheme and the method of characteristics in the Lax-Wendroff scheme became apparent. In the cases of static and swing tests for the Preissmann scheme, the most accurate solution in both amplitude and phase was produced with $\theta=0.5$. However, after adding boundary shear and bed slope in shock test $\theta=1.0$ increased the convergence rate for the final steady state without affecting the accuracy but using $\theta=1.0$ gives the largest numerical dampening for unsteady flow problems.

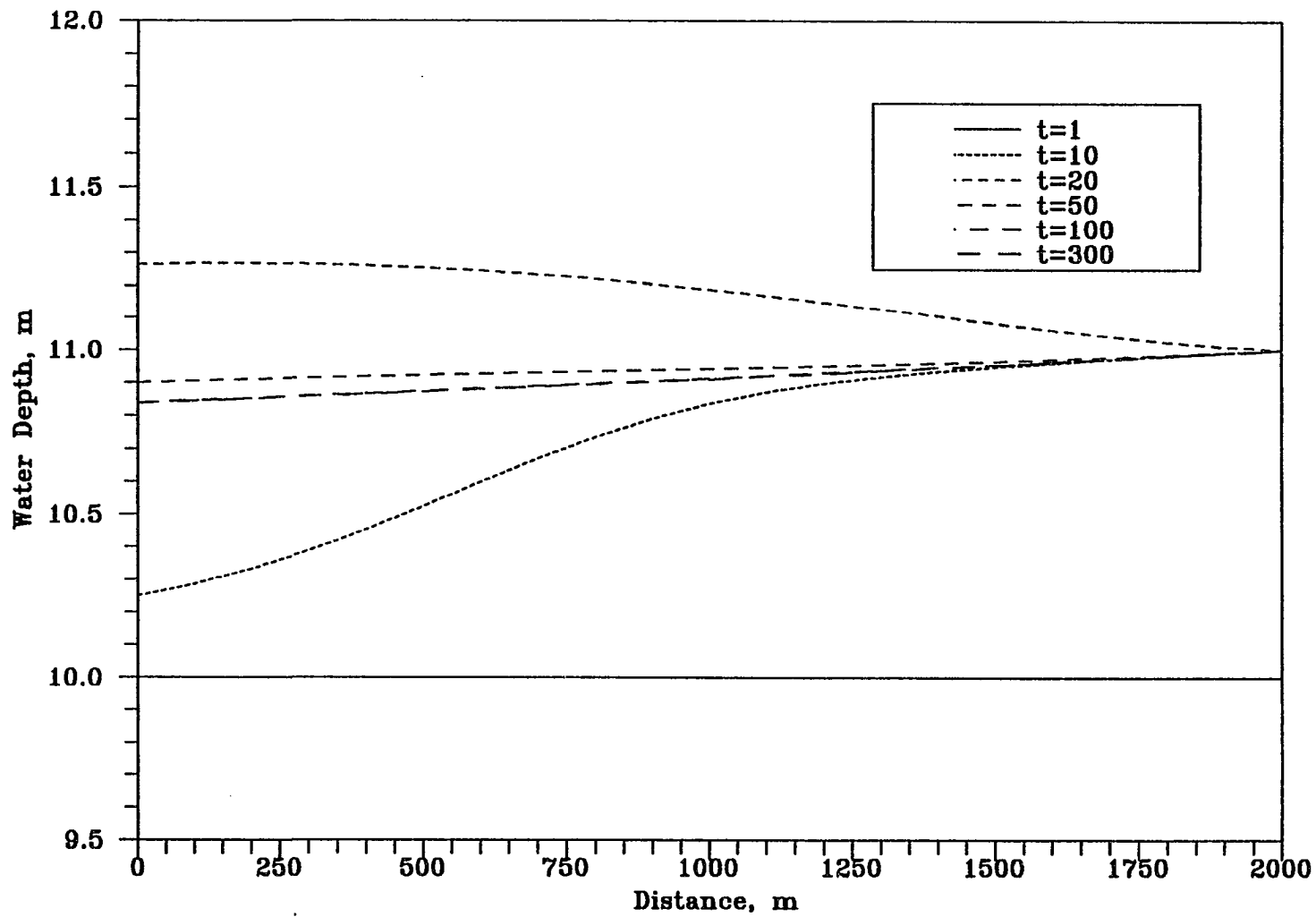


Figure 4.7 Shock Test Results for Preissmann Scheme at Six Different Time Steps.

4.5 Dissipative Interface

The non-dissipative scheme accounts for the saw-tooth solutions obtained with this method when the shock waves are computed. In this study, large velocity, shallow water depth, and bottom elevation gradient when the flow approaches the top of dune result in growing oscillations (*i.e.*, *wiggles*). The oscillations are steadily growing with time increment. In order to avoid these oscillations, supplementary dissipative terms should be added to the finite difference equations.

As shown by Abbott (1979, p.155), the Richtmyer (1963) version of the Lax-Wendroff, two-step scheme employs a numerical filtering device that has been called a *dissipative interface*, applied at alternate time steps so as to add a small amount of additional dissipation. What is done, in effect, is to average out the values of each dependent variable obtained after alternate time steps. For each dependent variable, $f(t, x)$, separately, this simplest of such filters is given by

$$f_j^{n*} = \gamma f_{j+1}^n + (1 - 2\gamma) f_j^n + \gamma f_{j-1}^n \quad , \quad 0 \leq \gamma \leq 1 \quad (4.111)$$

where γ is a weighting factor. The dissipative interface can be useful to provide some dissipation to the non-dissipative scheme and to suppress nonlinear instabilities (Abbott and Basco, 1989).

The amplification factor of Equation (4.111) is determined by the linear stability analysis method which determines how each Fourier coefficient, ξ , behaves (grows, decays, or stays constant) in time for any wave number, k .

Let,

$$f_j^n = \sum_{k=1}^{kk} \xi_k^n \exp(i\alpha_j) \quad (4.112)$$

be a finite, Fourier series representation of $f(j, n)$ for all dimensionless wave numbers, $\alpha(k)$, $k=1, 2, \dots, kk$, at time level, n . It is simply shown at any wave number (say $k=1$) giving

$$f_j^n = \xi^n e^{i\alpha_j} \quad (4.113)$$

where ξ^n is the Fourier coefficient for wave number 1 at time-level n , and substitute into the *dissipative interface* discretized equation then,

$$\xi_*^n e^{i\alpha_j} = \gamma \xi^n e^{i\alpha(j-1)} + (1 - 2\gamma) \xi^n e^{i\alpha_j} + \gamma \xi^n e^{i\alpha(j+1)} \quad (4.114)$$

and introducing also Euler's equation, $e^{i\theta} = \cos\theta + i \sin\theta$, we obtain

$$\begin{aligned} \frac{\xi_*^n}{\xi^n} &= A = 1 - 2\gamma(1 - \cos\alpha) \\ &= 1 - 2\gamma\left(1 - \cos\frac{2\pi}{N}\right) \end{aligned} \quad (4.115)$$

where A is *amplification factor*, $\alpha=2\pi/N$ and N is the number of grid points.

For stable finite-difference schemes, the Fourier coefficients, ξ , cannot grow without bound, so that

$$|A| \leq 1 \quad \text{for stability.} \quad (4.116)$$

Figure (4.8) shows amplitude portrait for dissipative interface for five values of γ . Taking $\gamma=1/4$ and $\gamma=0$ gives a fully centered and an exact solution, respectively. Since amplitude portrait has no imaginary part, it cannot give any phase distortion. Also, from the discretized equation the following sum may then be constructed.

$$\begin{aligned}
 f_0^* &= (1 - \gamma) f_0 + \gamma f_1 \\
 f_1^* &= \gamma f_0 + (1 - 2\gamma) f_1 + \gamma f_2 \\
 f_2^* &= \gamma f_1 + (1 - 2\gamma) f_2 + \gamma f_3 \\
 &\quad \vdots \\
 &\quad \vdots \\
 f_{jj-1}^* &= \gamma f_{jj-2} + (1 - 2\gamma) f_{jj-1} + \gamma f_{jj} \\
 f_{jj}^* &= \gamma f_{jj-1} + (1 - \gamma) f_{jj}
 \end{aligned}
 \tag{4.117}$$

$$\sum_{j=0}^{jj} f_j^* = f_0 + f_1 + f_2 + \dots + f_{jj-1} + f_{jj}$$

Thus, at least for a uniform grid spacing Δx , the total quantity of f over the computational domain is not changed by the dissipative interface but only its distribution is altered.

Figures (4.9) and (4.10) show instabilities of a scheme which is forward time and centered space without a dissipative interface using Dirichlet type and Neumann type boundary conditions, respectively. All data points beyond grid boundaries were excluded on the figures. Clearly, the numerical solution needs some mechanism to dissipate the short wave energy produced that is comparable to a natural, internal turbulence dissipator. After a dissipative interface ($\gamma=1/20$) is added in unstable scheme, the instabilities are apparently suppressed in a controlled manner. This is shown in Figures (4.11) and (4.12) using Dirichlet type and Neumann type boundary conditions, respectively. In Figure (4.11), some unstable

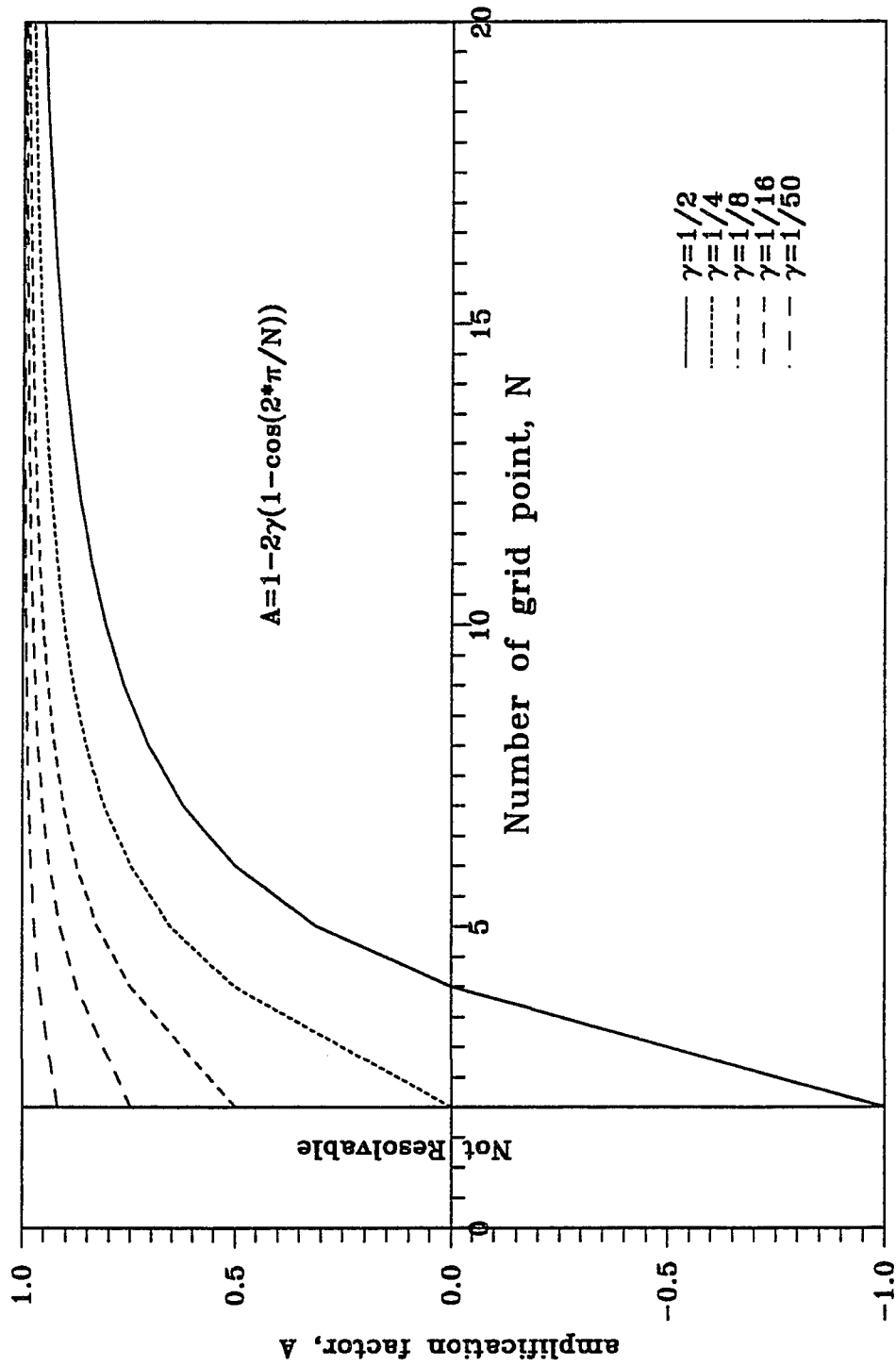


Figure 4.8 Amplitude Portrait for Dissipative Interface.

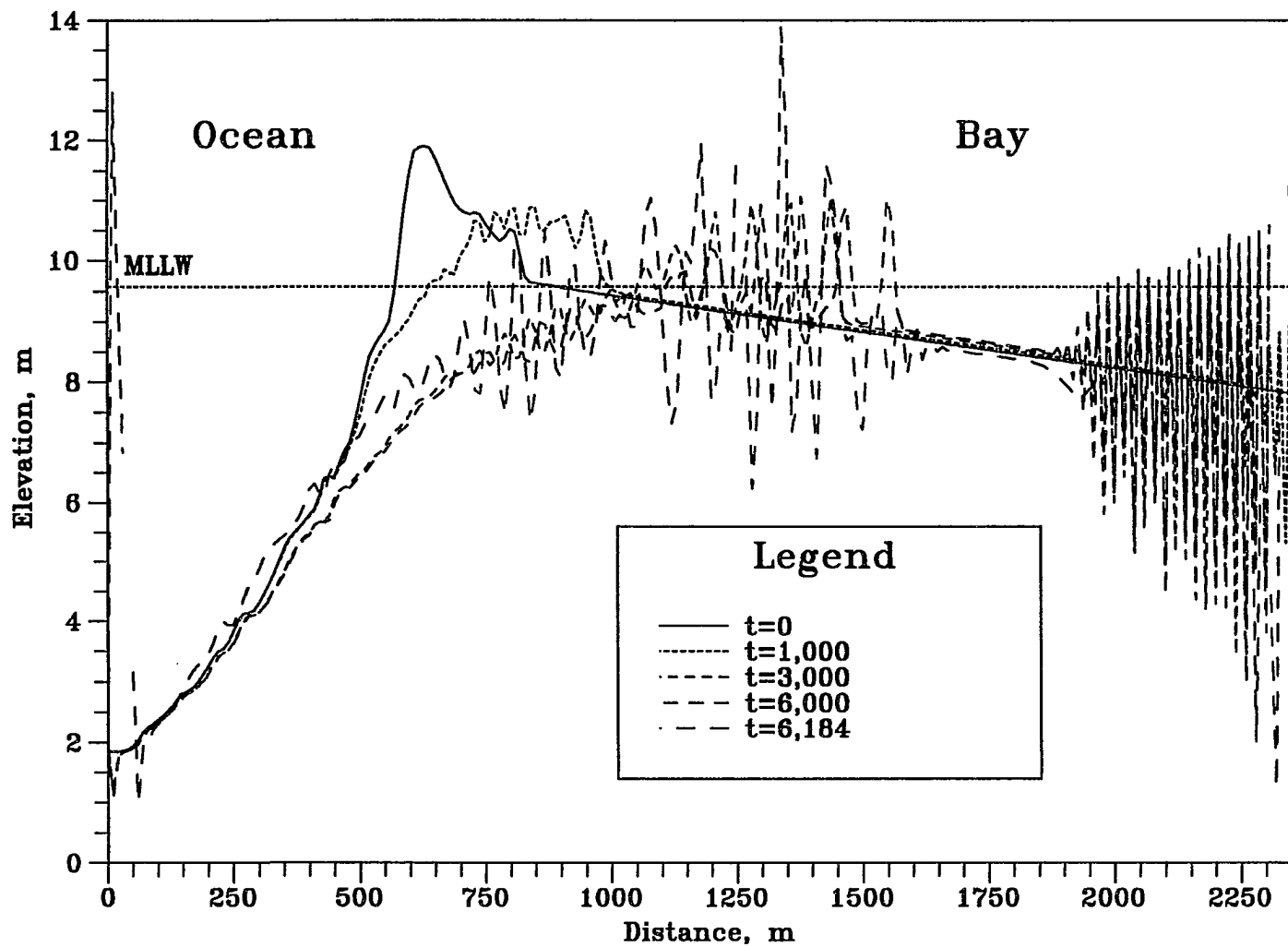


Figure 4.9 Instability from Dirichlet Type B.C. without Dissipative Interface.

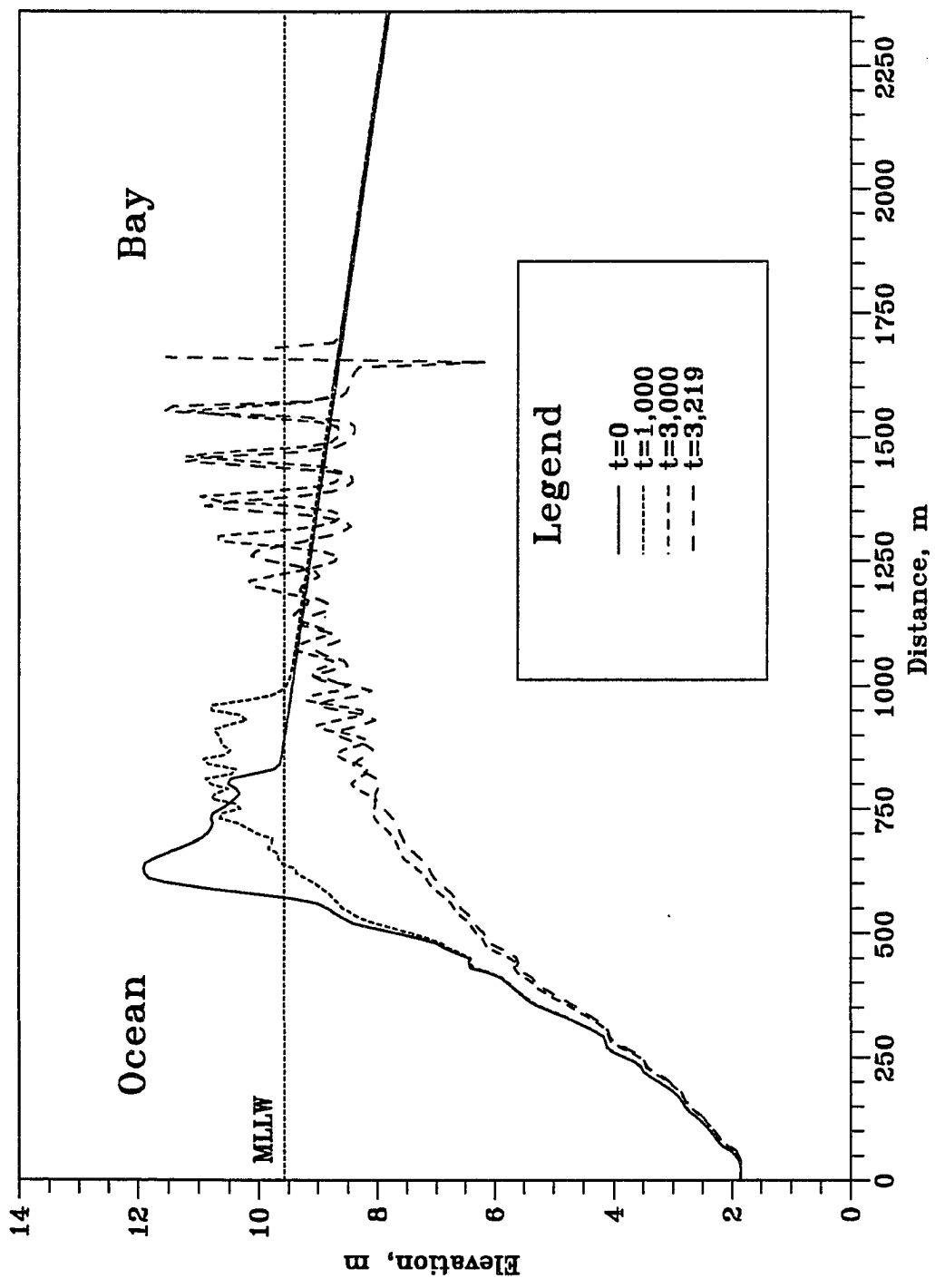


Figure 4.10 Instability from Newmann Type B.C. without Dissipative Interface.

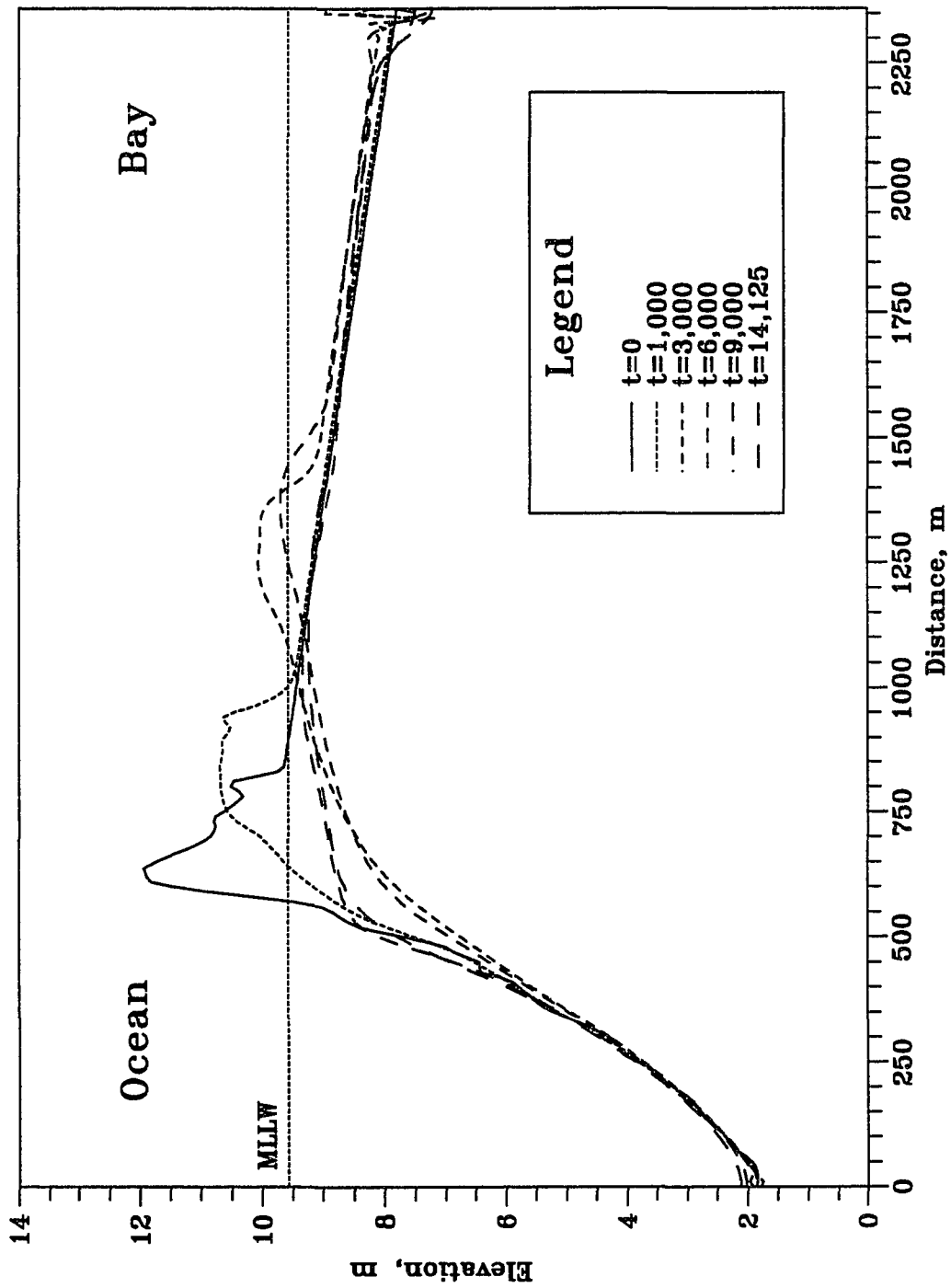


Figure 4.11 Results Using Dirichlet Type B.C. with Dissipative Interface. ($\gamma=1/20$)

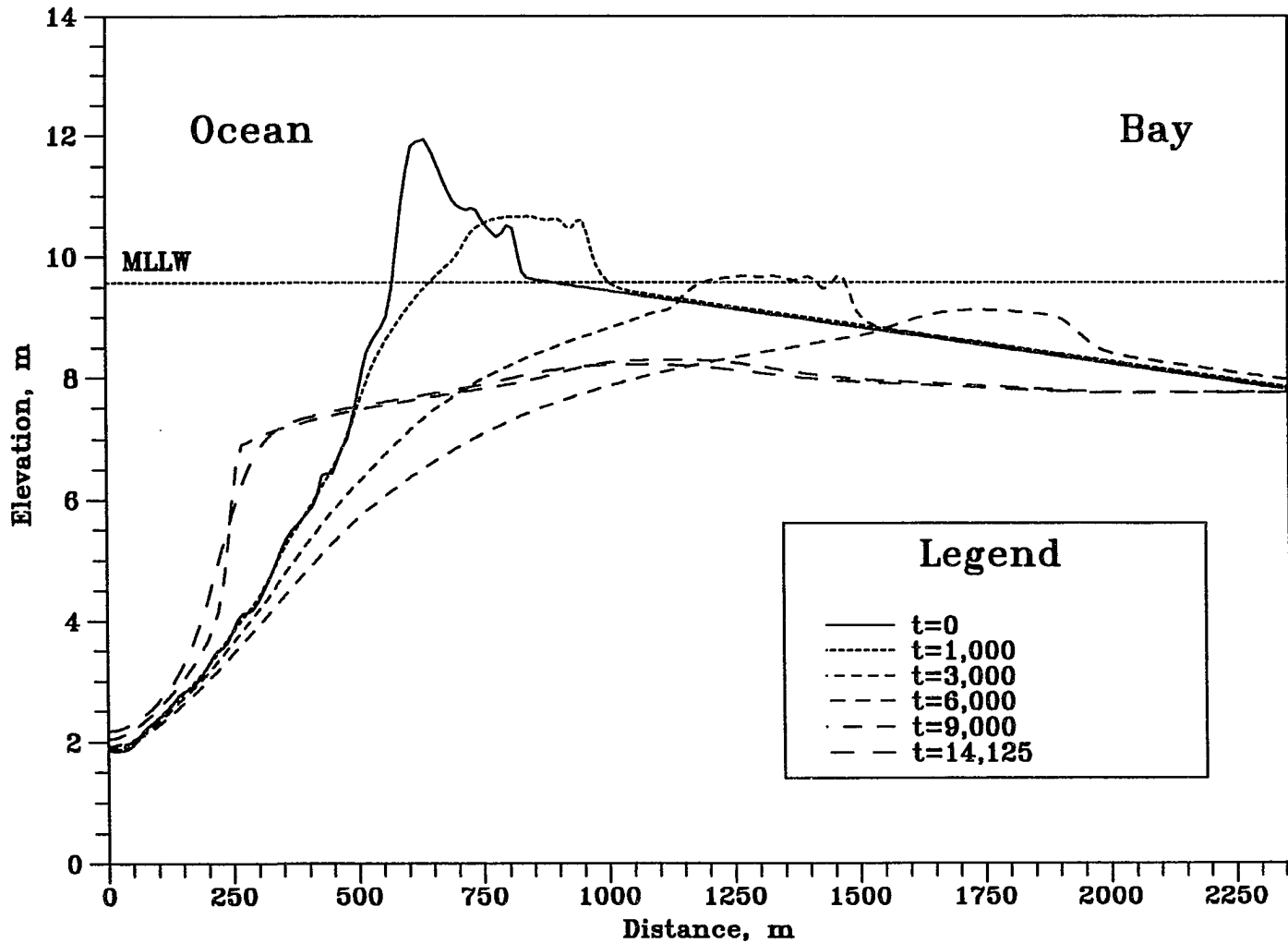


Figure 4.12 Results Using Neumann Type B.C. with Dissipative Interface. ($\gamma=1/20$)

results are still shown at both boundaries due to ill posed boundary conditions (*i.e.*, Dirichlet type boundary conditions).

The selection of γ is the negotiation between an accuracy (*i.e.*, dissipation) and a stability limit. The minimum γ which makes the scheme stable is the most generous stability condition of the sediment continuity finite difference equation. It will be further discussed in Ch.6.1.

5.0 INITIAL AND BOUNDARY CONDITIONS

5.1 Stage I - SBEACH Model

Numerical calculations start at the seaward end of the grid and proceed onshore through an explicit solution scheme for determining cross-shore wave height and a two time level explicit scheme for the sediment continuity equation.

Initial water depths over the computational domain are determined within the routine from the initial beach profile data which is surveyed above an arbitrary datum (MSL, NGVD, MLW, etc...).

The wave height, H_{mo} period, T_p and incident angle must be known at the most seaward grid point (given or calculated from some reference depth offshore) prior to starting the calculation. In this study, constant wave heights and periods with incident angles normal to the shoreline are used for wave boundary conditions.

The key ocean boundary condition is the storm surge hydrograph which for synthetic hurricane storms can be analytically described as an inverse hyperbolic squared,

$$h_o'(t) = h_{om} \frac{1}{\cosh^2 \left[\frac{2\pi(t - T/2)}{T} \right]} \quad (5.1)$$

where: $h_o'(t)$ = *water surface elevation above MSL at ocean boundary, L*

h_{om} = *peak ocean storm surge height, L*

T = *storm duration, T*

Figure 5.1 shows an example of surge hydrographs for the synthetic hurricanes for 24 hours duration with three different peak ocean storm surge levels.

The total simulation time for SBEACH and storm surge elevation at the end of simulation are obtained from the many runs by trial and error until the water level at the ocean boundary exceeds the eroded dune crest elevation.

The astronomical tidal variation is not considered in this study because surge hydrograph itself includes the effects of mean tidal variation.

The ocean boundary water depth, $h_o(t_1)$ at the end of Stage I is defined as,

$$h_o(t_1) = d_o + h_o'(t_1) \quad (5.2)$$

where: t_1 = *SBEACH simulation time for Stage I, T*

d_o = *initial ocean boundary water depth defined below MSL, L*

$h_o'(t_1)$ = *water level rise at ocean boundary at the end of Stage I, L*

Standard boundary conditions in the profile change model are no sand transport shoreward of the runup limit and seaward of the depth where significant sand movement occurs. The runup height is determined from an empirical expression derived from the large wave tank experiment data relating the height of the active profile to the surf similarity parameter and the deep water wave height. The depth of significant sand movement is determined through the exponential decay of the transport rate with distance seaward from the break point. If the transport rate decreases to a small predetermined value, the calculation stops, and the transport rate is set to zero at the next cell, making that cell the seaward

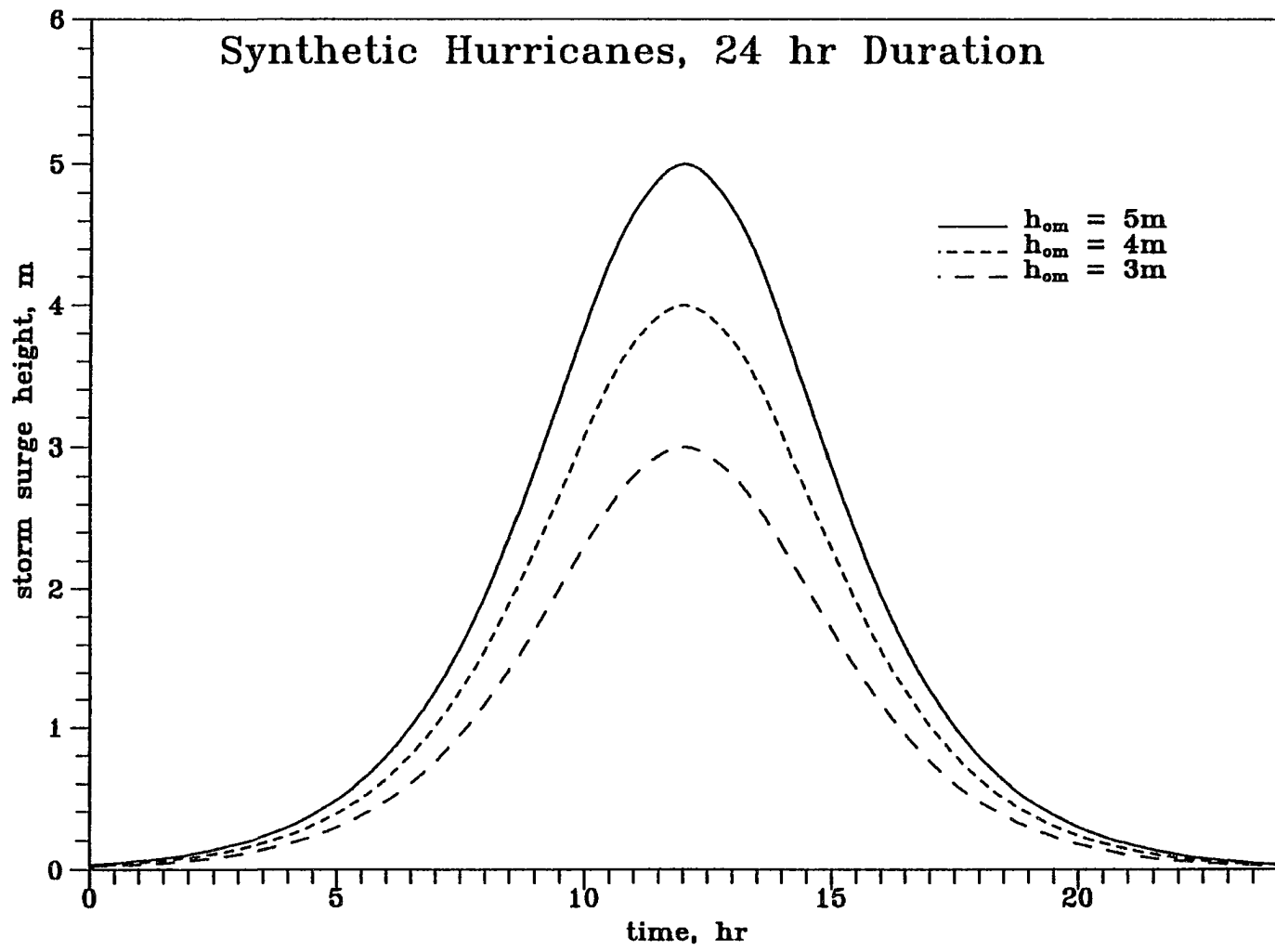


Figure 5.1 Storm Surge Hydrographs for the Three Synthetic Storms.

boundary.

5.2 Stage II - Lax-Wendroff Scheme

At the end of Stage I, ocean boundary water depth from Equation (5.2) and eroded dune/beach profile data are obtained. Boundary water depth in the bay is also determined from the bay storm surge hydrographs during SBEACH simulation period as,

$$h'_b(t_1) = h_{bm} \frac{1}{\cosh^2 \left[\frac{2\pi(t_1 - \tau - T/2)}{T} \right]} \quad (5.3)$$

$$h_b(t_1) = d_b + h'_b(t_1) \quad (5.4)$$

where: $h'_b(t_1)$ = *water level rise at bay boundary at the end of Stage I, L*

$h_b(t_1)$ = *bay boundary water depth at time t_1 , L*

h_{bm} = *peak bay storm surge height, L*

τ = *time lag between ocean and bay, T*

d_b = *initial bay boundary water depth, L*

with an assumption of no wave actions in the bay.

Figures 5.2 and 5.3 show storm surge hydrographs for both ocean and bay for a three-hour time lag with same and different energy levels, respectively.

Water level rises at the end of Stage I in ocean side are assumed to be constant for the initial water depth calculations in Stage II so that the water depth at the eroded dune crest becomes zero. Water level rises in bay side also assumed to be constant.

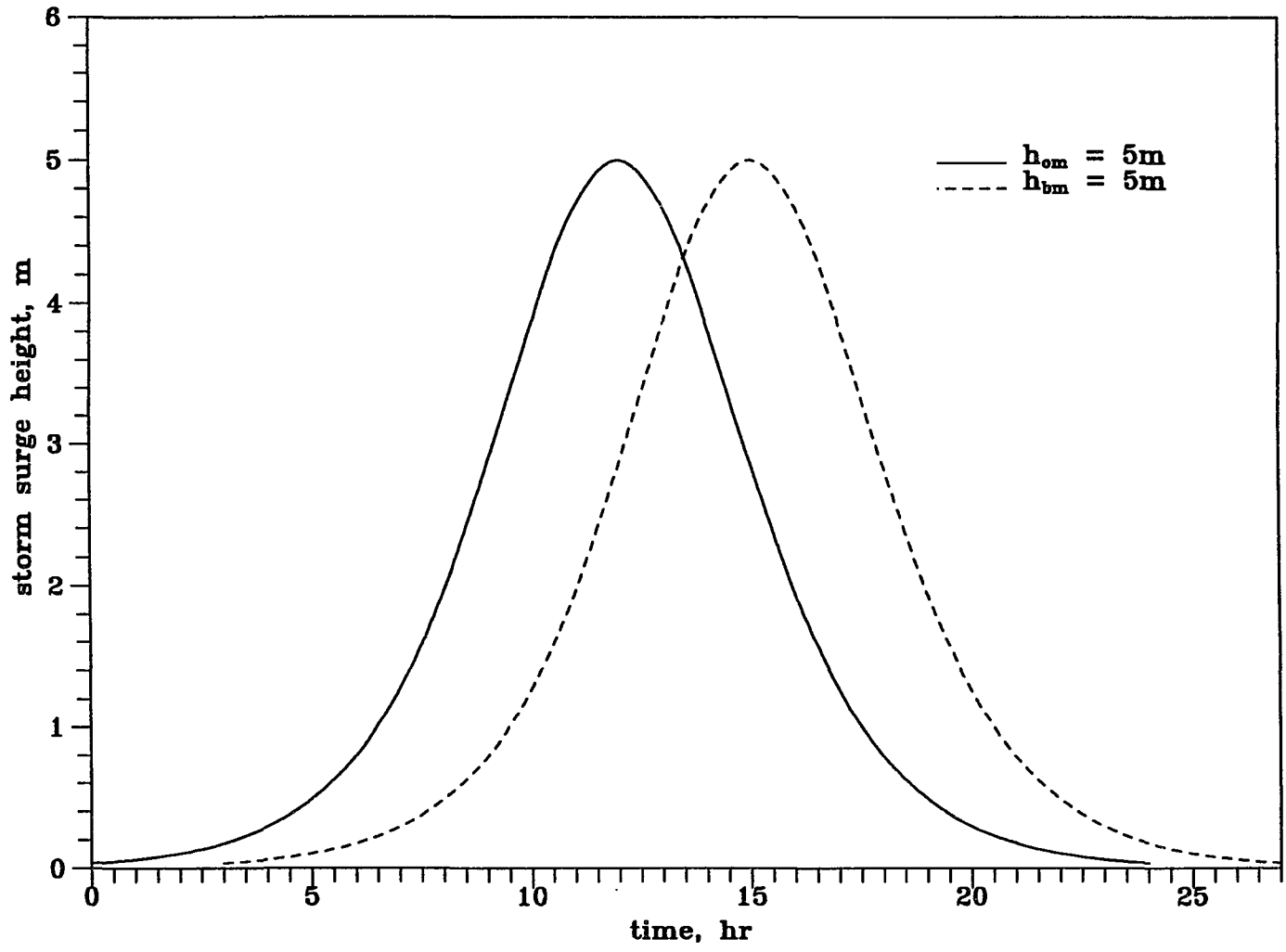


Figure 5.2 Storm Surge Hydrographs between Ocean and Bay with $T_{lag}=3$ hr.

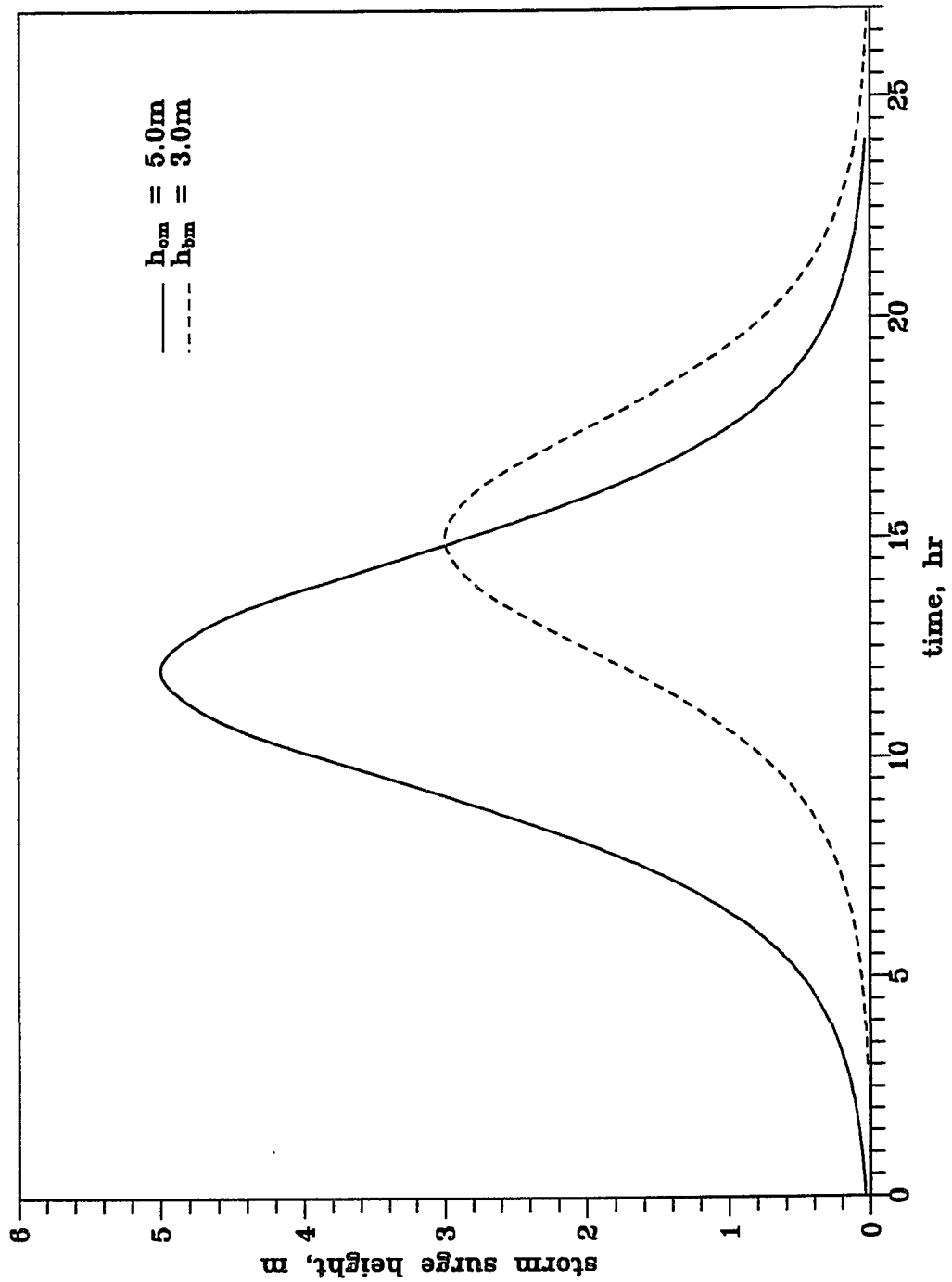


Figure 5.3 Storm Surge Hydrographs between Ocean and Bay with $T_{lag}=3$ hr.

A small uniform water depth (0.03 - 0.05m) is imposed on the dry bed between eroded dune crest and end of barrier islands. Water velocity over computational domain is initially set to zero.

For the water motion calculations, the ocean boundary condition is computed as,

$$h_o(t) = h_o(t_1) + h_{om} \left\{ \frac{1}{\cosh^2 \left\{ \frac{2\pi[(t_1+t)-T/2]}{T} \right\}} - \frac{1}{\cosh^2 \left\{ \frac{2\pi(t_1-T/2)}{T} \right\}} \right\} \quad (5.5)$$

A similar formulation can be developed for the bay side of the barrier with now time, $t = t - \tau$ for the boundary condition as,

$$h_b(t) = h_b(t_1) + h_{bm} \left\{ \frac{1}{\cosh^2 \left\{ \frac{2\pi[(t_1+t)-(\tau+T/2)]}{T} \right\}} - \frac{1}{\cosh^2 \left\{ \frac{2\pi[t_1-(\tau+T/2)]}{T} \right\}} \right\} \quad (5.6)$$

where $t = t_1 + 1, \dots, t_2$ and t_2 is total simulation time in Stage I and II.

Additional boundary value, q (flow rate) at both boundaries can be computed using the method of characteristics in Ch.4.2.2.

There is no sediment transport in either direction in this extremely short time period for Stage II (generally less than 10 minutes) so that bottom boundary conditions are not necessary herein.

5.3 Stage III and IV - Preissmann / FTCS Schemes

At the end of Stage II, the initial conditions, $u(x)$, $h(x)$ and $z(x)$ will be known across

the entire length of the simulation from the ocean to the bay for use in Stages III and IV of the model. Note that in Lax-Wendroff scheme grid points which contain water flow information are not evenly spaced at both boundaries. Linear interpolation is employed to generate alternate grid points for Stages III and IV.

For the water motion, water depths from the storm surge hydrograph are provided for the boundary conditions at ocean, $h_o(t)$ and bay, $h_b(t)$ as,

$$h_o(t) = h_o(t_2) + h_{om} \left\{ \frac{1}{\cosh^2 \left\{ \frac{2\pi[(t_2+t)-T/2]}{T} \right\}} - \frac{1}{\cosh^2 \left\{ \frac{2\pi(t_2-T/2)}{T} \right\}} \right\} + \sum_{t=t_2}^T \Delta z_1 \quad (5.7)$$

and

$$h_b(t) = h_b(t_2) + h_{bm} \left\{ \frac{1}{\cosh^2 \left\{ \frac{2\pi[(t_2+t)-(\tau+T/2)]}{T} \right\}} - \frac{1}{\cosh^2 \left\{ \frac{2\pi[t_2-(\tau+T/2)]}{T} \right\}} \right\} + \sum_{t=t_2}^T \Delta z_{jj} \quad (5.8)$$

where: t_2 = total simulation time for Stages I and II, T

Δz_1 = bed elevation difference between n and $n+1$ time level at ocean boundary, L

$$= z_1^n - z_1^{n+1}$$

Δz_{jj} = bed elevation difference between n and $n+1$ time level at bay

$$\begin{aligned} & \text{boundary, } L \\ = & z_{jj}^n - z_{jj}^{n+1} \end{aligned}$$

Water depths are adjusted from the cumulative bed level differences for both boundaries.

There are no specific boundary conditions required for the sediment transport formulas because sediment transport rates for both bed- and suspended-load can be computed from the known two variables (water depth and velocity). However, for the sediment continuity equation which is discretized in forward time and centered space (FTCS) explicit scheme, Neumann type boundary conditions are introduced at both boundaries as,

$$\frac{\partial z}{\partial t} \Big|_{j=1} - \frac{\partial z}{\partial t} \Big|_{j=2} = \frac{\partial z}{\partial t} \Big|_{j=2} - \frac{\partial z}{\partial t} \Big|_{j=3} \quad (5.9)$$

$$\frac{\partial z}{\partial t} \Big|_{j=jj} - \frac{\partial z}{\partial t} \Big|_{j=jj-1} = \frac{\partial z}{\partial t} \Big|_{j=jj-1} - \frac{\partial z}{\partial t} \Big|_{j=jj-2}$$

In difference form, Equation (5.9) can be written as,

$$z_1^{n+1} = z_1^n + 2(z_2^{n+1} - z_2^n) - (z_3^{n+1} - z_3^n) \quad (5.10)$$

$$z_{jj}^{n+1} = z_{jj}^n + 2(z_{jj-1}^{n+1} - z_{jj-1}^n) - (z_{jj-2}^{n+1} - z_{jj-2}^n)$$

From the numerous experiments, Equation (5.10) is found to give excellent boundary data without any disturbances which can appear from ill-posed boundary conditions.

6.0 MODEL TESTS AND RESULTS

6.1 Volume Conservation Tests

In this section, particular attention is paid to the considerations of numerical accuracy. Although numerical errors are only partially responsible for model uncertainty, it is considered important to prevent them from becoming dominant. As a general rule, it can be required that numerical errors be an order of magnitude smaller than errors from physical sources, so that the model performances can be entirely attributed to the latter (Abbott and Cunge, 1982).

It is a desirable property that the solution of the finite difference equations satisfies the (discrete form of) overall mass-balance equation. This can be used as a check on program correctness.

The accumulation of volume of the element is computed from the difference between the leaving and entering amounts of sediment volume through both boundaries. If the change of the total volume during one time step is considered, the following equation may then be established.

$$\frac{dS(t)}{dt} = \frac{1}{(1 - p)} [q_r(t, jj) - q_l(t, 1)] \quad (6.1)$$

where $S(t)$ is the total volume of bottom profile above a datum over the computational domain at time level t , p is a porosity, and $q_l(t, 1)$ and $q_r(t, jj)$ are the sediment transport rates at the left hand and right hand boundaries, respectively. Equation (6.1) can be written in the form of discretization as follows.

$$\frac{S(t+\Delta t)-S(t)}{\Delta t} = \frac{1}{(1-p)} \left[\frac{q_i(t, jj)+q_i(t+\Delta t, jj)}{2} - \frac{q_i(t, 1)+q_i(t+\Delta t, 1)}{2} \right] \quad (6.2)$$

$$\Delta S=S(t+\Delta t)-S(t) = \frac{\Delta t}{(1-p)} \left[\frac{q_i(t, jj)+q_i(t+\Delta t, jj)}{2} - \frac{q_i(t, 1)+q_i(t+\Delta t, 1)}{2} \right]$$

The total volume change, ΔS in Equation (6.2) gives an exact result over the entire computational domain at time level $t+\Delta t$ without any numerical error. This is an excellent tool to check the volume conservation of a numerical scheme.

In this study, a trapezoidal rule is used for volume calculation of bottom profiles produced in discrete form of the sediment continuity equation. The volume change from the numerical computation should contain a numerical inaccuracy due to numerical dissipations and instabilities, mainly coming from the truncation errors and ill-posed boundary conditions or the physics of the problem itself (*i.e.*, hydraulic bores, breaking waves and flow separation, etc.).

Let $V(t)$ be the total volume of a bottom profile calculated from the numerical integration at time level t , then the volume change, $\Delta V(t)$ between an initial profile (*i.e.*, $t=0$), V_{ini} and an intermediate profile, $\Delta V(t)$ is computed as

$$\Delta V(t) = V_{ini} - V(t) \quad (6.3)$$

The total cumulative volume change over the computational domain, ΔV_1 , the cumulative volume outgoing through both boundaries, ΔV_2 , and the cumulative volume change from the *numerical errors*, ΔV_3 in percent are defined as follows.

$$\begin{aligned}
\Delta V_1 &= \frac{\Delta V(t)}{V_{ini}} \times 100, & \% \\
\Delta V_2 &= \frac{V_{ini} - S(t)}{V_{ini}} \times 100, & \% \\
\Delta V_3 &= \frac{S(t) - V(t)}{V_{ini}} \times 100, & \% \\
\Delta V_1 &= \Delta V_2 + \Delta V_3
\end{aligned} \tag{6.4}$$

For all simulations in volume conservation tests, an ocean side maximum storm surge level ($=h_{om}$) of 5 m and a bay side maximum storm surge level ($=h_{bm}$) of 4 m with 3 hours time lag are used for Stage III and IV periods ($t=15.7$ hrs).

Tables 6.1 through 6.15 show the results of volume losses at intermediate time steps using Dirichlet type boundary conditions (*i.e.*, $z(t)=\text{constant}$ at both boundaries). Grid sizes of $\Delta x=20$ m, $\Delta t=8$ sec (Tables 6.1 - 6.7), $\Delta x=10$ m, $\Delta t=4$ sec (Tables 6.8 - 6.14), and $\Delta x=5$ m, $\Delta t=2$ sec (Table 6.15) are employed. A dissipative interface has been applied with seven different weighting factors, γ at every 20 time steps ($mmm=20$) except Table 6.15 that has $\gamma=1/4$ and $mmm=2$. In these tables, ΔV_1 is total volume losses in percent. Since there are no incoming and outgoing sediment transports, total volume losses come entirely from numerical errors due to the instabilities by an ill-posed boundary condition. Table 6.16 shows volume losses at the end of simulation with various γ , mmm and grid sizes. The weighting factor of $\gamma=1/20$ gives minimum volume losses except the case of Table 6.15 which is only stable at $\gamma=1/4$, $mmm=2$. Figure 4.11 (p.102) shows bottom profile changes at six different time levels with $\Delta x=10$ m, $\Delta t=4$ sec, and $\gamma=1/20$ but some instabilities are shown at both

Table 6.1 Volume Losses at Intermediate Time Steps Using Dirichlet Type Boundary Conditions. ($\Delta x=20$ m, $\Delta t=8$ sec, $\gamma=1/200$, and $mmm= 20$)

Time Step	V_{ini} , m^3/m	$V(t)$, m^3/m	ΔV , m^3/m	ΔV_1 , %
500	18,819	18,756	63	0.33
1,500		17,819	999	5.31
3,000		17,311	1,507	8.01
4,500		16,755	2,064	10.97
6,893*		14,915	3,903	20.74

* Scheme is unstable after 6,894 time step.

Table 6.2 Volume Losses at Intermediate Time Steps Using Dirichlet Type Boundary Conditions. ($\Delta x=20$ m, $\Delta t=8$ sec, $\gamma=1/100$, and $mmm= 20$)

Time Step	V_{ini} , m^3/m	$V(t)$, m^3/m	ΔV , m^3/m	ΔV_1 , %
500	18,819	18,759	60	0.32
1,500		17,979	840	4.46
3,000		17,719	1,100	5.85
4,500		17,736	1,083	5.75
7,062		17,590	1,229	6.53

Table 6.3 Volume Losses at Intermediate Time Steps Using Dirichlet Type Boundary Conditions. ($\Delta x=20$ m, $\Delta t=8$ sec, $\gamma=1/50$, and $mmm=20$)

Time Step	V_{ini} , m^3/m	$V(t)$, m^3/m	ΔV , m^3/m	ΔV_1 , %
500	18,819	18,763	56	0.30
1,500		18,159	660	3.51
3,000		17,999	820	4.36
4,500		18,029	790	4.20
7,062		18,015	804	4.27

Table 6.4 Volume Losses at Intermediate Time Steps Using Dirichlet Type Boundary Conditions. ($\Delta x=20$ m, $\Delta t=8$ sec, $\gamma=1/40$, and $mmm=20$)

Time Step	V_{ini} , m^3/m	$V(t)$, m^3/m	ΔV , m^3/m	ΔV_1 , %
500	18,819	18,765	54	0.29
1,500		18,203	616	3.27
3,000		18,060	759	4.04
4,500		18,090	729	3.87
7,062		18,080	739	3.93

Table 6.5 Volume Losses at Intermediate Time Steps Using Dirichlet Type Boundary Conditions. ($\Delta x=20$ m, $\Delta t=8$ sec, $\gamma=1/30$, and $mmm=20$)

Time Step	V_{ini} , m^3/m	$V(t)$, m^3/m	ΔV , m^3/m	ΔV_1 , %
500	18,819	18,767	52	0.28
1,500		18,249	570	3.03
3,000		18,118	701	3.73
4,500		18,149	670	3.56
7,062		18,140	679	3.61

Table 6.6 Volume Losses at Intermediate Time Steps Using Dirichlet Type Boundary Conditions. ($\Delta x=20$ m, $\Delta t=8$ sec, $\gamma=1/20$, and $mmm=20$)

Time Step	V_{ini} , m^3/m	$V(t)$, m^3/m	ΔV , m^3/m	ΔV_1 , %
500	18,819	18,769	50	0.27
1,500		18,292	527	2.80
3,000		18,166	653	3.47
4,500		18,198	621	3.30
7,062		18,188	631	3.35

Table 6.7 Volume Losses at Intermediate Time Steps Using Dirichlet Type Boundary Conditions. ($\Delta x=20$ m, $\Delta t=8$ sec, $\gamma=1/10$, and $mmm=20$)

Time Step	V_{ini} , m^3/m	$V(t)$, m^3/m	ΔV , m^3/m	ΔV_1 , %
500	18,819	18,770	49	0.26
1,500		18,304	515	2.74
3,000		18,151	668	3.55
4,500		18,193	626	3.33
7,062		18,173	646	3.43

Table 6.8 Volume Losses at Intermediate Time Steps Using Dirichlet Type Boundary Conditions. ($\Delta x=10$ m, $\Delta t=4$ sec, $\gamma=1/200$, and $mmm=20$)

Time Step	V_{ini} , m^3/m	$V(t)$, m^3/m	ΔV , m^3/m	ΔV_1 , %
1,000	18,819	18,751	68	0.36
3,000		18,002	817	4.34
6,000		17,774	1,045	5.55
9,000		17,774	1,045	5.55
14,125		17,572	1,247	6.63

Table 6.9 Volume Losses at Intermediate Time Steps Using Dirichlet Type Boundary Conditions. ($\Delta x=10$ m, $\Delta t=4$ sec, $\gamma=1/100$, and $mmm=20$)

Time Step	V_{ini} , m^3/m	$V(t)$, m^3/m	ΔV , m^3/m	ΔV_1 , %
1,000	18,819	18,759	61	0.32
3,000		18,197	623	3.31
6,000		18,058	762	4.05
9,000		18,070	749	3.98
14,125		18,051	768	4.08

Table 6.10 Volume Losses at Intermediate Time Steps Using Dirichlet Type Boundary Conditions. ($\Delta x=10$ m, $\Delta t=4$ sec, $\gamma=1/50$, and $mmm=20$)

Time Step	V_{ini} , m^3/m	$V(t)$, m^3/m	ΔV , m^3/m	ΔV_1 , %
1,000	18,819	18,767	52	0.28
3,000		18,327	492	2.62
6,000		18,223	596	3.17
9,000		18,235	584	3.11
14,125		18,233	586	3.12

Table 6.11 Volume Losses at Intermediate Time Steps Using Dirichlet Type Boundary Conditions. ($\Delta x=10$ m, $\Delta t=4$ sec, $\gamma=1/40$, and $mmm=20$)

Time Step	V_{ini} , m^3/m	$V(t)$, m^3/m	ΔV , m^3/m	ΔV_1 , %
1,000	18,819	18,770	49	0.26
3,000		18,356	463	2.46
6,000		18,256	563	3.00
9,000		18,268	551	2.93
14,125		18,266	553	2.94

Table 6.12 Volume Losses at Intermediate Time Steps Using Dirichlet Type Boundary Conditions. ($\Delta x=10$ m, $\Delta t=4$ sec, $\gamma=1/30$, and $mmm=20$)

Time Step	V_{ini} , m^3/m	$V(t)$, m^3/m	ΔV , m^3/m	ΔV_1 , %
1,000	18,819	18,773	46	0.25
3,000		18,384	435	2.31
6,000		18,286	533	2.84
9,000		18,299	520	2.76
14,125		18,297	522	2.77

Table 6.13 Volume Losses at Intermediate Time Steps Using Dirichlet Type Boundary Conditions. ($\Delta x=10$ m, $\Delta t=4$ sec, $\gamma=1/20$, and $mmm=20$)

Time Step	V_{ini} , m^3/m	$V(t)$, m^3/m	ΔV , m^3/m	ΔV_1 , %
1,000	18,819	18,777	42	0.23
3,000		18,407	412	2.19
6,000		18,305	514	2.73
9,000		18,321	498	2.65
14,125		18,318	501	2.66

Table 6.14 Volume Losses at Intermediate Time Steps Using Dirichlet Type Boundary Conditions. ($\Delta x=10$ m, $\Delta t=4$ sec, $\gamma=1/10$, and $mmm=20$)

Time Step	V_{ini} , m^3/m	$V(t)$, m^3/m	ΔV , m^3/m	ΔV_1 , %
1,000	18,819	18,779	40	0.21
3,000		18,407	412	2.19
6,000		18,283	536	2.85
9,000		18,306	513	2.73
14,125		18,302	517	2.75

Table 6.15 Volume Losses at Intermediate Time Steps Using Dirichlet Type Boundary Conditions. ($\Delta x=5$ m, $\Delta t=2$ sec, $\gamma=1/4$, and $mmm=2$)

Time Step	V_{ini} , m^3/m	$V(t)$, m^3/m	ΔV , m^3/m	ΔV_1 , %
2,000	18,819	18,743	76	0.41
6,000		17,979	840	4.47
12,000		17,405	1,414	7.51
18,000		17,431	1,388	7.38
28,250		17,039	1,780	9.46

Table 6.16 Volume Losses at End of Simulation Using Various γ , mmm and Grid Sizes Using Dirichlet Type Boundary Conditions.

α , mmm	Δx , m	Δt , sec	V_{ini} , m^3/m	V_{end} , m^3/m	ΔV , m^3/m	ΔV_1 , %
1/200, 20	20	8	18,819	14,916	3,903	20.74
	10	4	18,819	17,572	1,247	6.63
	5	2	Unstable			
1/100, 20	20	8	18,819	17,590	1,229	6.53
	10	4	18,819	18,051	768	4.08
	5	2	Unstable			
1/50, 20	20	8	18,819	18,015	804	4.27
	10	4	18,819	18,233	586	3.11
	5	2	Unstable			
1/40, 20	20	8	18,819	18,080	739	3.93
	10	4	18,819	18,266	553	2.94
	5	2	Unstable			
1/30, 20	20	8	18,819	18,140	679	3.61
	10	4	18,819	18,297	522	2.77
	5	2	Unstable			
1/20, 20	20	8	18,819	18,188	631	3.35
	10	4	18,819	18,319	500	2.66
	5	2	Unstable			
1/10, 20	20	8	18,819	18,173	646	3.43
	10	4	18,819	18,302	517	2.75
	5	2	Unstable			
1/4, 2	5	2	18,819	17,039	1,780	9.46

boundaries due to an ill-posed boundary condition. From the above results the Dirichlet type boundary condition for volume conservation checks is not suitable in this physical system.

Tables 6.17 through 6.32 show the results of volume losses at intermediate time steps using *Neumann type* boundary conditions. The results for ΔV , ΔV_1 , ΔV_2 , and ΔV_3 are obtained from the Equations (6.3) and (6.4). In this case, a volume loss from the numerical error, ΔV_3 is greatly reduced to the order of 10^{-3} in percent. The negative and positive number in ΔV_3 mean a volume increase and loss due to numerical dissipation, respectively. Therefore, total volume losses over the computational domain are mainly based on the losses through both boundaries. Table 6.33 shows volume losses at the end of simulation with various γ , mmm and grid sizes using *Neumann type* boundary conditions. A grid size of $\Delta x=10$ m, $\Delta t=4$ sec and a weighting factor of $\gamma=1/50$ give most satisfactory results among overall simulations. Figure 4.12 (p.103) shows bottom profile changes at six different time levels with $\Delta x=10$ m, $\Delta t=4$ sec and $\gamma=1/20$.

From the above volume conservation checks using both Dirichlet and Neumann type boundary conditions with different grid sizes and weighting factors, it can be concluded that the Dirichlet type boundary condition is not suitable for this study. Larger grid sizes in time and space give greater volume changes and numerical dissipation. A fine grid size of $\Delta x=5$ m, $\Delta t=2$ sec gives unsatisfactory results because this results in severe instabilities and requires more artificial dissipation for stability.

For the model tests, a grid size of $\Delta x=10$ m, $\Delta t=4$ sec and $\gamma=1/50-1/20$ with $mmm=20$ are employed with various combinations of model parameters.

Table 6.17 Volume Losses at Intermediate Time Steps Using Neumann Type Boundary Conditions. ($\Delta x=20$ m, $\Delta t=8$ sec, $\gamma=1/200$, and $mmm=20$)

Time Step	V_{ini} , m^3/m	$V(t)$, m^3/m	ΔV , m^3/m	ΔV_1 , %	ΔV_2 , %	ΔV_3 , %
500	18,819	18,752	67	0.36	0.36	0.00
1,500		17,728	1,091	5.80	5.80	0.00
3,000		16,944	1,875	9.96	9.97	-0.01
4,500		17,314	1,505	7.80	8.01	-0.01
7,062		17,324	1,495	7.94	7.95	-0.01

Table 6.18 Volume Losses at Intermediate Time Steps Using Neumann Type Boundary Conditions. ($\Delta x=20$ m, $\Delta t=8$ sec, $\gamma=1/100$, and $mmm=20$)

Time Step	V_{ini} , m^3/m	$V(t)$, m^3/m	ΔV , m^3/m	ΔV_1 , %	ΔV_2 , %	ΔV_3 , %
500	18,819	18,752	67	0.36	0.36	0.00
1,500		17,724	1,095	5.82	5.82	0.00
3,000		16,938	1,881	10.00	10.01	-0.01
4,500		17,327	1,492	7.93	7.94	-0.01
7,062		17,339	1,480	7.87	7.88	-0.01

Table 6.19 Volume Losses at Intermediate Time Steps Using Neumann Type Boundary Conditions. ($\Delta x=20$ m, $\Delta t=8$ sec, $\gamma=1/50$, and $mmm=20$)

Time Step	V_{ini} , m^3/m	$V(t)$, m^3/m	ΔV , m^3/m	ΔV_1 , %	ΔV_2 , %	ΔV_3 , %
500	18,819	18,751	68	0.36	0.36	0.00
1,500		17,708	1,111	5.90	5.90	0.00
3,000		16,893	1,926	10.23	10.24	-0.01
4,500		17,300	1,519	8.07	8.08	-0.01
7,062		17,324	1,495	8.02	8.02	0.00

Table 6.20 Volume Losses at Intermediate Time Steps Using Neumann Type Boundary Conditions. ($\Delta x=20$ m, $\Delta t=8$ sec, $\gamma=1/40$, and $mmm=20$)

Time Step	V_{ini} , m^3/m	$V(t)$, m^3/m	ΔV , m^3/m	ΔV_1 , %	ΔV_2 , %	ΔV_3 , %
500	18,819	18,751	68	0.36	0.36	0.00
1,500		17,697	1,121	5.96	5.96	0.00
3,000		16,862	1,957	10.40	10.41	-0.01
4,500		17,273	1,546	8.21	8.22	-0.01
7,062		17,282	1,537	8.17	8.17	0.00

Table 6.21 Volume Losses at Intermediate Time Steps Using Neumann Type Boundary Conditions. ($\Delta x=20$ m, $\Delta t=8$ sec, $\gamma=1/30$, and $mmm=20$)

Time Step	V_{ini} , m^3/m	$V(t)$, m^3/m	ΔV , m^3/m	ΔV_1 , %	ΔV_2 , %	ΔV_3 , %
500	18,819	18,750	69	0.36	0.36	0.00
1,500		17,676	1,143	6.07	6.07	0.00
3,000		16,803	2,016	10.71	10.72	-0.01
4,500		17,219	1,600	8.50	8.50	0.00
7,062		17,224	1,595	8.48	8.48	0.00

Table 6.22 Volume Losses at Intermediate Time Steps Using Neumann Type Boundary Conditions. ($\Delta x=20$ m, $\Delta t=8$ sec, $\gamma=1/20$, and $mmm=20$)

Time Step	V_{ini} , m^3/m	$V(t)$, m^3/m	ΔV , m^3/m	ΔV_1 , %	ΔV_2 , %	ΔV_3 , %
500	18,819	18,749	70	0.37	0.37	0.00
1,500		17,627	1,192	6.33	6.33	0.00
3,000		16,667	2,152	11.44	11.44	0.00
4,500		17,086	1,733	9.21	9.21	0.00
7,062		17,079	1,740	9.25	9.23	0.02

Table 6.23 Volume Losses at Intermediate Time Steps Using Neumann Type Boundary Conditions. ($\Delta x=20$ m, $\Delta t=8$ sec, $\gamma=1/10$, and $mmm=20$)

Time Step	V_{ini} , m^3/m	$V(t)$, m^3/m	ΔV , m^3/m	ΔV_1 , %	ΔV_2 , %	ΔV_3 , %
500	18,819	18,742	77	0.41	0.40	0.01
1,500		17,455	1,364	7.25	7.24	0.01
3,000		16,184	2,635	14.00	13.99	0.01
4,500		16,587	2,232	11.86	11.84	0.02
7,062		16,517	2,302	12.23	12.20	0.03

Table 6.24 Volume Losses at Intermediate Time Steps Using Neumann Type Boundary Conditions. ($\Delta x=10$ m, $\Delta t=4$ sec, $\gamma=1/200$, and $mmm=20$)

Time Step	V_{ini} , m^3/m	$V(t)$, m^3/m	ΔV , m^3/m	ΔV_1 , %	ΔV_2 , %	ΔV_3 , %
1,000	18,819	18,753	66	0.36	0.36	0.00
3,000		17,732	1,087	5.78	5.78	0.00
6,000		16,945	1,874	9.96	9.97	-0.01
9,000		17,333	1,486	7.90	7.91	-0.01
14,125		17,350	1,469	7.81	7.82	-0.01

Table 6.25 Volume Losses at Intermediate Time Steps Using Neumann Type Boundary Conditions. ($\Delta x=10$ m, $\Delta t=4$ sec, $\gamma=1/100$, and $mmm=20$)

Time Step	V_{ini} , m^3/m	$V(t)$, m^3/m	ΔV , m^3/m	ΔV_1 , %	ΔV_2 , %	ΔV_3 , %
1,000	18,819	18,752	67	0.36	0.36	0.00
3,000		17,730	1,089	5.79	5.79	0.00
6,000		16,942	1,877	9.98	9.99	-0.01
9,000		17,358	1,461	7.76	7.77	-0.01
14,125		17,379	1,440	7.65	7.66	-0.01

Table 6.26 Volume Losses at Intermediate Time Steps Using Neumann Type Boundary Conditions. ($\Delta x=10$ m, $\Delta t=4$ sec, $\gamma=1/50$, and $mmm=20$)

Time Step	V_{ini} , m^3/m	$V(t)$, m^3/m	ΔV , m^3/m	ΔV_1 , %	ΔV_2 , %	ΔV_3 , %
1,000	18,819	18,753	66	0.36	0.36	0.00
3,000		17,726	1,093	5.81	5.81	0.00
6,000		16,930	1,889	10.04	10.05	-0.01
9,000		17,371	1,448	7.69	7.70	-0.01
14,125		17,394	1,425	7.57	7.58	-0.01

Table 6.27 Volume Losses at Intermediate Time Steps Using Neumann Type Boundary Conditions. ($\Delta x=10$ m, $\Delta t=4$ sec, $\gamma=1/40$, and $mmm=20$)

Time Step	V_{ini} , m^3/m	$V(t)$, m^3/m	ΔV , m^3/m	ΔV_1 , %	ΔV_2 , %	ΔV_3 , %
1,000	18,819	18,752	67	0.36	0.36	0.00
3,000		17,722	1,097	5.83	5.83	0.00
6,000		16,919	1,900	10.10	10.11	-0.01
9,000		17,366	1,453	7.72	7.73	-0.01
14,125		17,389	1,430	7.60	7.60	0.00

Table 6.28 Volume Losses at Intermediate Time Steps Using Neumann Type Boundary Conditions. ($\Delta x=10$ m, $\Delta t=4$ sec, $\gamma=1/30$, and $mmm=20$)

Time Step	V_{ini} , m^3/m	$V(t)$, m^3/m	ΔV , m^3/m	ΔV_1 , %	ΔV_2 , %	ΔV_3 , %
1,000	18,819	18,752	67	0.36	0.36	0.00
3,000		17,714	1,105	5.87	5.87	0.00
6,000		16,895	1,924	10.22	10.23	-0.01
9,000		17,347	1,472	7.82	7.82	0.00
14,125		17,368	1,451	7.71	7.71	0.00

Table 6.29 Volume Losses at Intermediate Time Steps Using Neumann Type Boundary Conditions. ($\Delta x=10$ m, $\Delta t=4$ sec, $\gamma=1/20$, and $mmm=20$)

Time Step	V_{ini} , m^3/m	$V(t)$, m^3/m	ΔV , m^3/m	ΔV_1 , %	ΔV_2 , %	ΔV_3 , %
1,000	18,819	18,752	67	0.36	0.36	0.00
3,000		17,692	1,127	5.99	5.99	0.00
6,000		16,831	1,988	10.57	10.57	0.00
9,000		17,286	1,533	8.15	8.15	0.00
14,125		17,302	1,518	8.06	8.06	0.00

Table 6.30 Volume Losses at Intermediate Time Steps Using Neumann Type Boundary Conditions. ($\Delta x=10$ m, $\Delta t=4$ sec, $\gamma=1/10$, and $mmm=20$)

Time Step	V_{ini} , m^3/m	$V(t)$, m^3/m	ΔV , m^3/m	ΔV_1 , %	ΔV_2 , %	ΔV_3 , %
1,000	18,819	18,749	70	0.37	0.37	0.00
3,000		17,602	1,217	6.47	6.46	0.01
6,000		16,586	2,233	11.87	11.87	0.00
9,000		17,030	1,789	9.51	9.50	0.01
14,125		17,021	1,798	9.55	9.54	0.01

Table 6.31 Volume Losses at Intermediate Time Steps Using Neumann Type Boundary Conditions. ($\Delta x=5$ m, $\Delta t=2$ sec, $\gamma=1/16$, and $mmm=5$)

Time Step	V_{ini} , m^3/m	$V(t)$, m^3/m	ΔV , m^3/m	ΔV_1 , %	ΔV_2 , %	ΔV_3 , %
2,000	18,819	18,747	72	0.38	0.38	0.00
6,000		17,548	1,271	6.76	6.75	0.01
12,000		16,434	2,385	12.68	12.67	0.01
18,000		16,878	1,941	10.32	10.31	0.01
28,250		16,855	1,964	10.44	10.43	0.01

Table 6.32 Volume Losses at Intermediate Time Steps Using Neumann Type Boundary Conditions. ($\Delta x=5$ m, $\Delta t=2$ sec, $\gamma=1/8$, and $mmm=5$)

Time Step	V_{ini} , m^3/m	$V(t)$, m^3/m	ΔV , m^3/m	ΔV_1 , %	ΔV_2 , %	ΔV_3 , %
2,000	18,819	18,737	82	0.44	0.44	0.00
6,000		17,280	1,539	8.18	8.17	0.01
12,000		15,629	3,190	16.95	16.94	0.01
18,000		16,080	2,739	14.55	14.53	0.02
28,250		15,936	2,883	15.32	15.30	0.02

Table 6.33 Volume Losses at End of Simulation Using Various γ , mmm and Grid Sizes Using Neumann Type Boundary Conditions.

α , mmm	Δx , m	Δt , sec	V_{ini} , m^3/m	V_{end} , m^3/m	ΔV , m^3/m	ΔV_1 , %	ΔV_2 , %	ΔV_3 , %
1/200, 20	20	8	18,819	17,324	1,495	7.94	7.95	-0.01
	10	4	18,819	17,350	1,469	7.81	7.82	-0.01
	5	2	Unstable					
1/100, 20	20	8	18,819	17,339	1,480	7.87	7.88	-0.01
	10	4	18,819	17,379	1,440	7.65	7.66	-0.01
	5	2	Unstable					
1/50, 20	20	8	18,819	17,310	1,509	8.02	8.02	0.00
	10	4	18,819	17,394	1,425	7.57	7.57	0.00
	5	2	Unstable					
1/40, 20	20	8	18,819	17,282	1,537	8.17	8.17	0.00
	10	4	18,819	17,389	1,430	7.60	7.60	0.00
	5	2	Unstable					
1/30, 20	20	8	18,819	17,224	1,595	8.48	8.48	0.00
	10	4	18,819	17,368	1,451	7.71	7.71	0.00
	5	2	Unstable					
1/20, 20	20	8	18,819	17,079	1,740	9.24	9.23	0.01
	10	4	18,819	17,301	1,518	8.06	8.06	0.00
	5	2	Unstable					
1/10, 20	20	8	18,819	16,517	2,302	12.24	12.20	0.04
	10	4	18,819	17,021	1,798	9.55	9.54	0.01
	5	2	Unstable					
1/16, 5	5	2	18,819	16,855	1,964	10.44	10.43	0.01
1/8, 5	5	2	18,819	15,936	2,883	15.32	15.30	0.02

6.2 Model Results

A typical barrier island's profile at Sandbridge, Virginia which is about 300m wide is used for the bathymetry input. The elevation of the top of the dune is 2.07m above mean sea level (MSL).

Five different storm surge levels are selected from the probabilities of exceedance curves (U.S. Army, 1989), and equivalent wave heights are taken from the annual cumulative wave height distributions curve (Leffler *et al.*, 1993). Wave periods can be computed using the assumption that the local wave steepness, H_{mo}/L where L is the local wave period, is constant for all waves. The number of values derived for each energy level is shown in Table 6.34.

Table 6.34 Summary of Employed Storm Surge Levels, Wave Heights and Periods.

Return period in year	100	350	500	800	1,000
h_{om} , m	3.0	3.5	4.0	4.5	5.0
H_{mo} , m	5.08	5.20	5.32	5.45	5.54
T_p , sec	14.31	14.54	14.78	15.01	15.25

6.2.1 Stage I - Dune / Beach Erosion

In Stage I, the following parametric coefficients (from Basco and Shin, 1992 and 1993) are used for SBEACH simulation with $\Delta x=5.0m$ and $\Delta t=5.0min$.

- *Transport rate coefficient, $K=1.5 \times 10^{-6} m^4/N$.*

- *Coefficient for slope-dependent term, $\epsilon=0.002 \text{ m}^2/\text{sec}$.*
- *Transport rate decay coefficient multiplier, $\lambda=0.40$.*
- *Maximum profile slope prior to avalanching in degrees, $B_{max}=15^\circ$.*
- *Effective grain size diameter, $D_{50}=0.3\text{mm}$.*
- *Constant wave heights and periods.*
- *Variable water levels.*

SBEACH simulation results are summarized in Table 6.35 for various storm surge levels and wave conditions. The volume changes between initial profile, V_{ini} and final profile, V_{fin} are investigated in volume, ΔV and percent volume, $\Delta V\%$ losses with the changes of dune crest elevations, Δz . In Stage I, it is assumed that wave actions in the bay are negligible so that no sediment transport takes place. Simulation results are shown in Figures 6.1 through 6.5 for the initial and final profiles with five different storm surge and wave energy levels. Also, Figures 6.6 through 6.10 show zoomed barrier island cross-sectional profiles.

6.2.2 Stage II - Overwash / Overland Flow

In this stage, the Lax-Wendroff two-step explicit scheme is used for the water motion calculation and the profile change is modeled as a diffusion process (diffusion coefficient, $K=1/16$) with no sediment transport in either direction. From the stability analyses, the space step, $\Delta x=10\text{m}$ and time step, $\Delta t=0.5\text{sec}$ are used for all simulations.

The simulation time is about ten minutes; however, it can be extended, depending on the stability condition of the numerical scheme under given storm surge levels. Required

Table 6.35 SBEACH Simulation Results for Various Storm Surge Levels and Wave Conditions.

Storm No.	V_{ini} , m^3/m	V_{fin} , m^3/m	ΔV , m^3/m	ΔV_1 , %	Δz , m
1 $h_{om} = 5.0$ m $H_{mo} = 5.54$ m $T_p = 15.25$ sec $t = 8$ hr	349	347.8	1.20	0.34	0.14
2 $h_{om} = 4.5$ m $H_{mo} = 5.45$ m $T_p = 15.01$ sec $t = 8.25$ hr	349	347.6	1.40	0.40	0.14
3 $h_{om} = 4.0$ m $H_{mo} = 5.32$ m $T_p = 14.78$ sec $t = 8.53$ hr	349	347.3	1.70	0.49	0.15
4 $h_{om} = 3.5$ m $H_{mo} = 5.20$ m $T_p = 14.54$ sec $t = 8.87$ hr	349	347.5	1.50	0.43	0.16
5 $h_{om} = 3.0$ m $H_{mo} = 5.08$ m $T_p = 14.31$ sec $t = 9.3$ hr	349	346.6	2.40	0.69	0.16

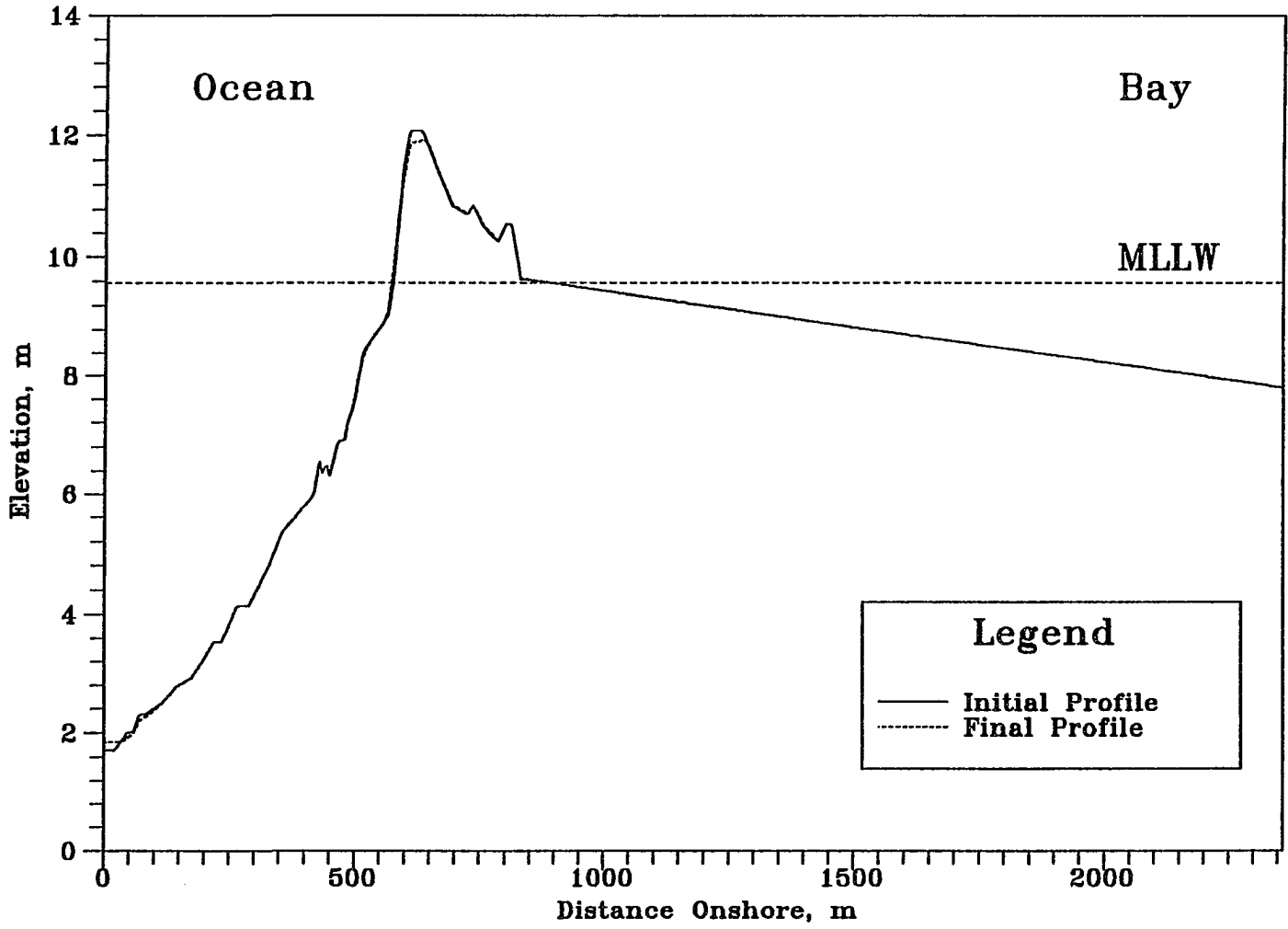


Figure 6.1 SBEACH Results for $h_{om}=5m, H_{mo}=5.54m, T_p=15.25s$ and $t_1=28,800s$.

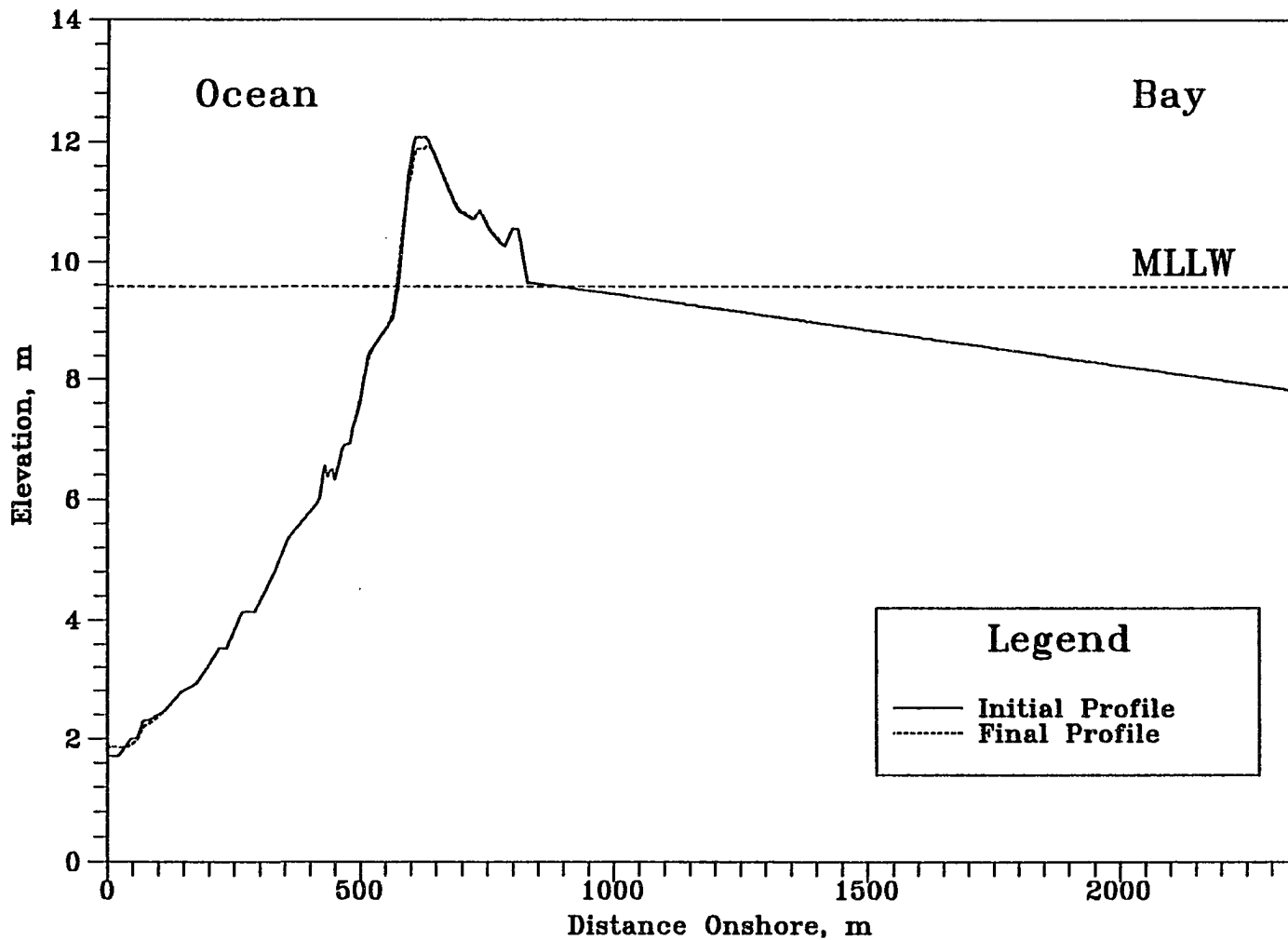


Figure 6.2 SBEACH Results for $h_{om}=4.5m, H_{mo}=5.45m, T_p=15.01s$ and $t_1=29,700s$.

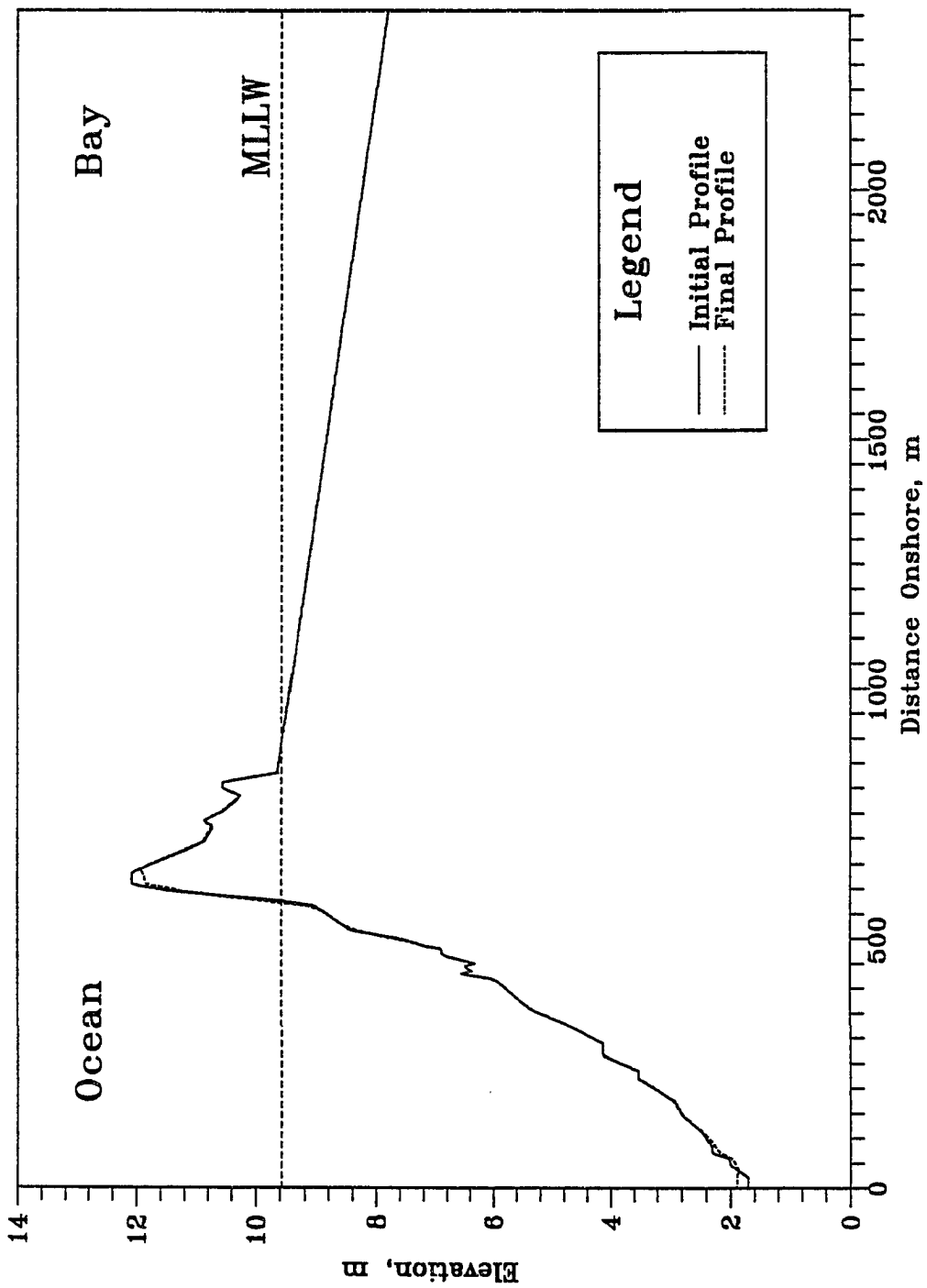


Figure 6.3 SBEACH Results for $h_{mo}=4m, H_{mo}=5.32m, T_p=14.78s$ and $t_1=30,720s$.

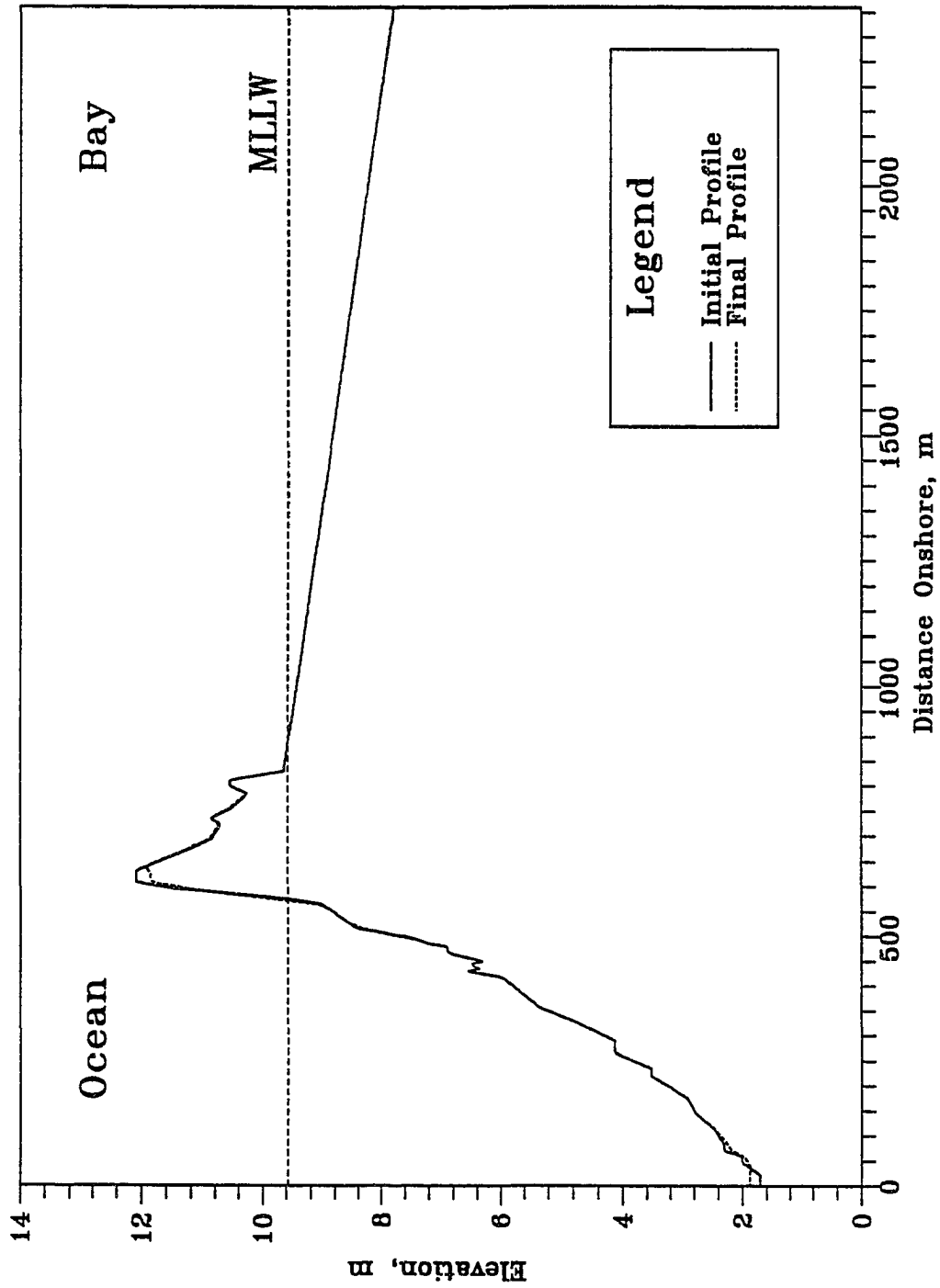


Figure 6.4 SBEACH Results for $h_{om}=3.5m, H_{mo}=5.20m, T_p=14.54s$ and $t_1=31,950s$.

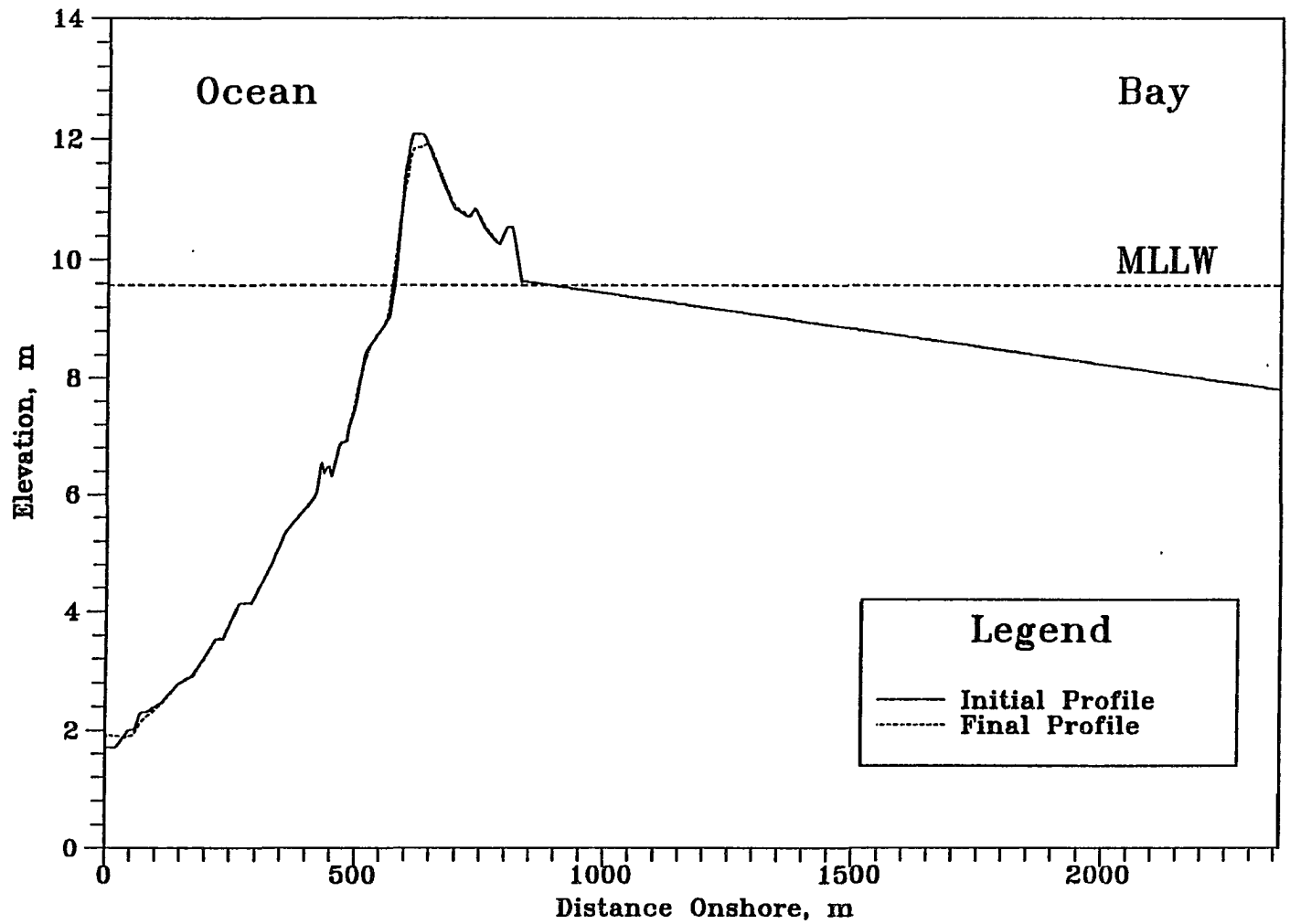


Figure 6.5 SBEACH Results for $h_{om}=3m, H_{mo}=5.08m, T_p=14.31s$ and $t_1=33,480s$.

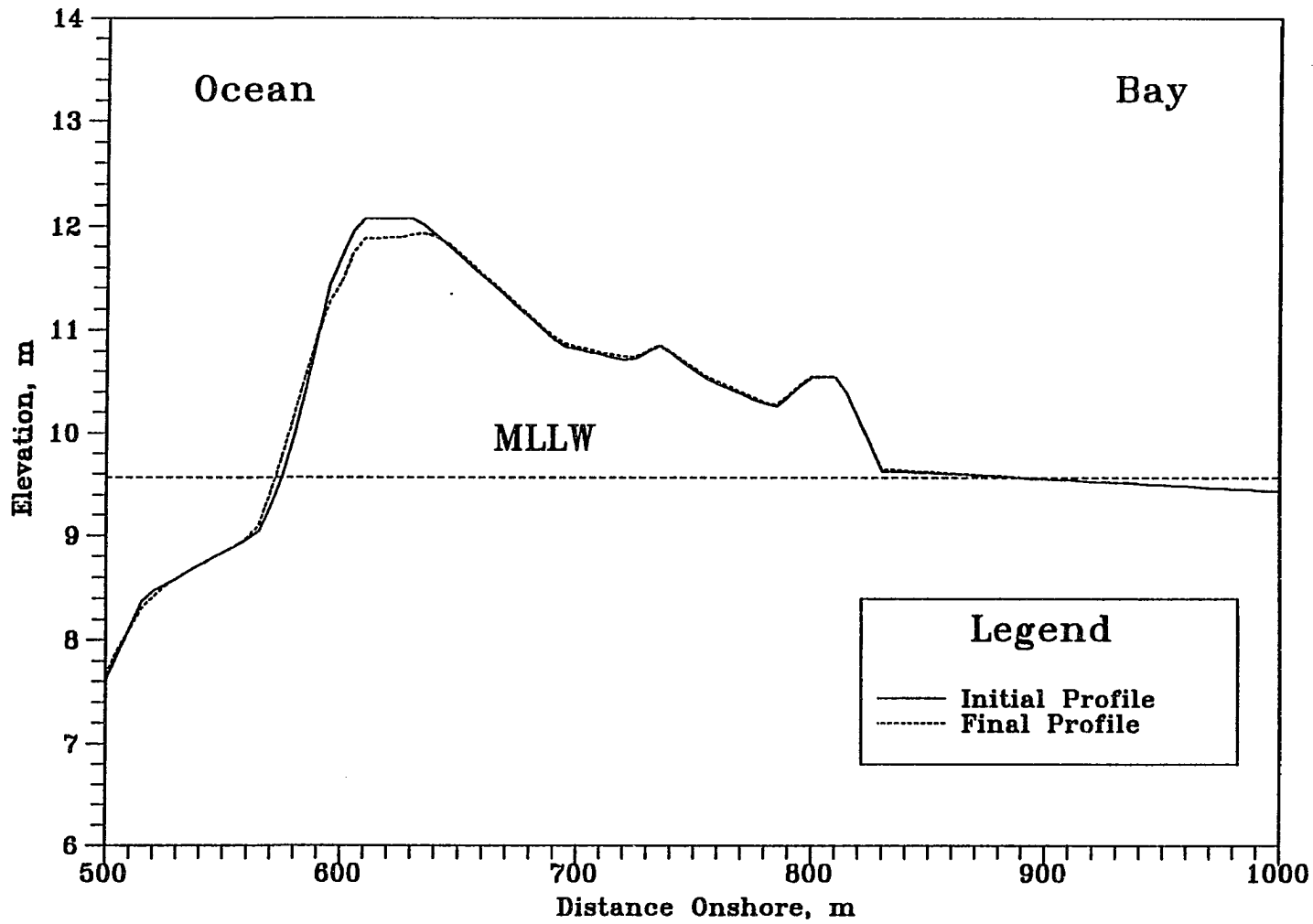


Figure 6.6 Zoomed Profiles for $h_{om}=5m, H_{mo}=5.54m, T_p=15.25s$ and $t_1=28,800s$.

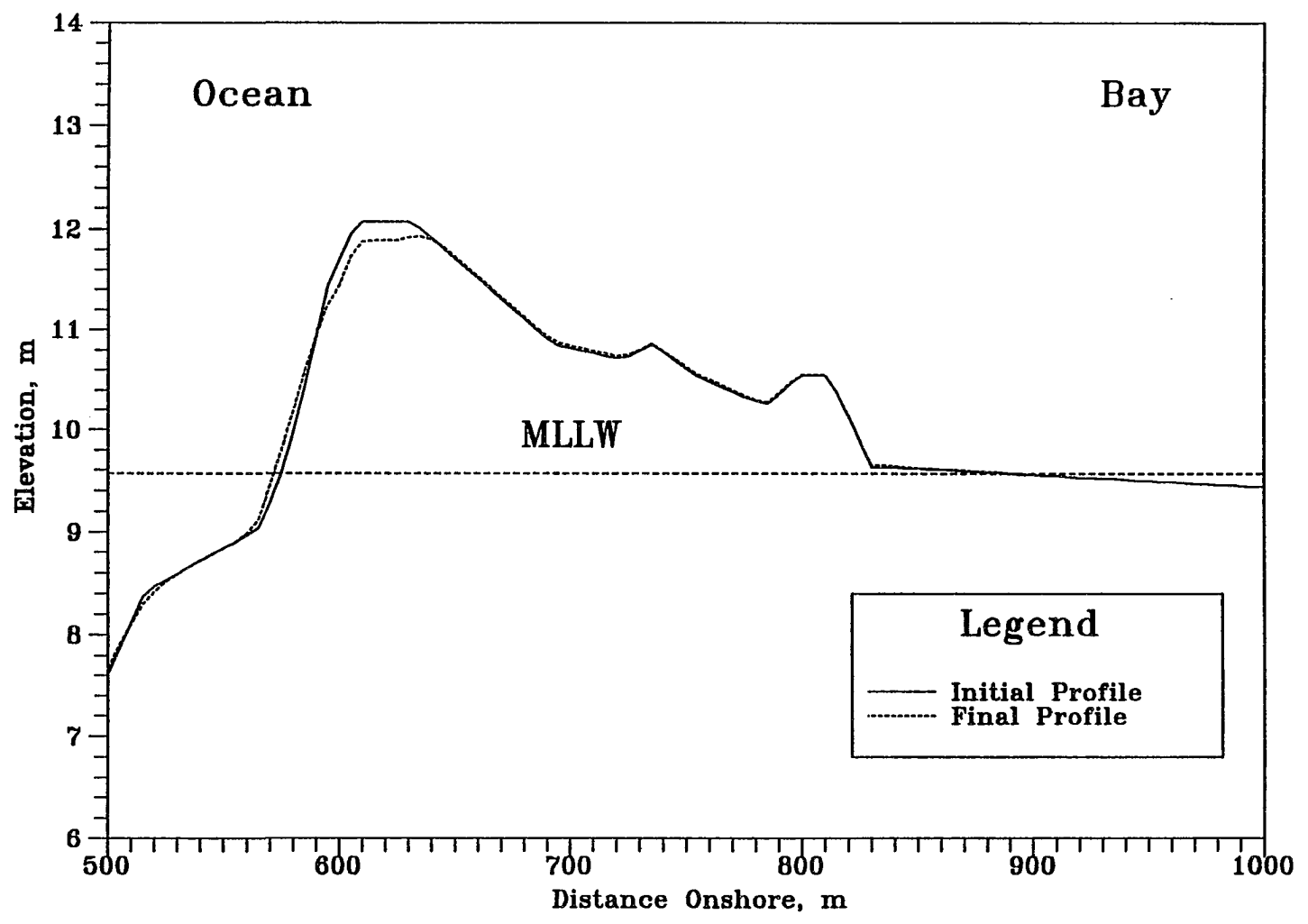


Figure 6.7 Zoomed Profiles for $h_{om}=4.5m, H_{mo}=5.45m, T_p=15.01s, t_1=29,700s$.

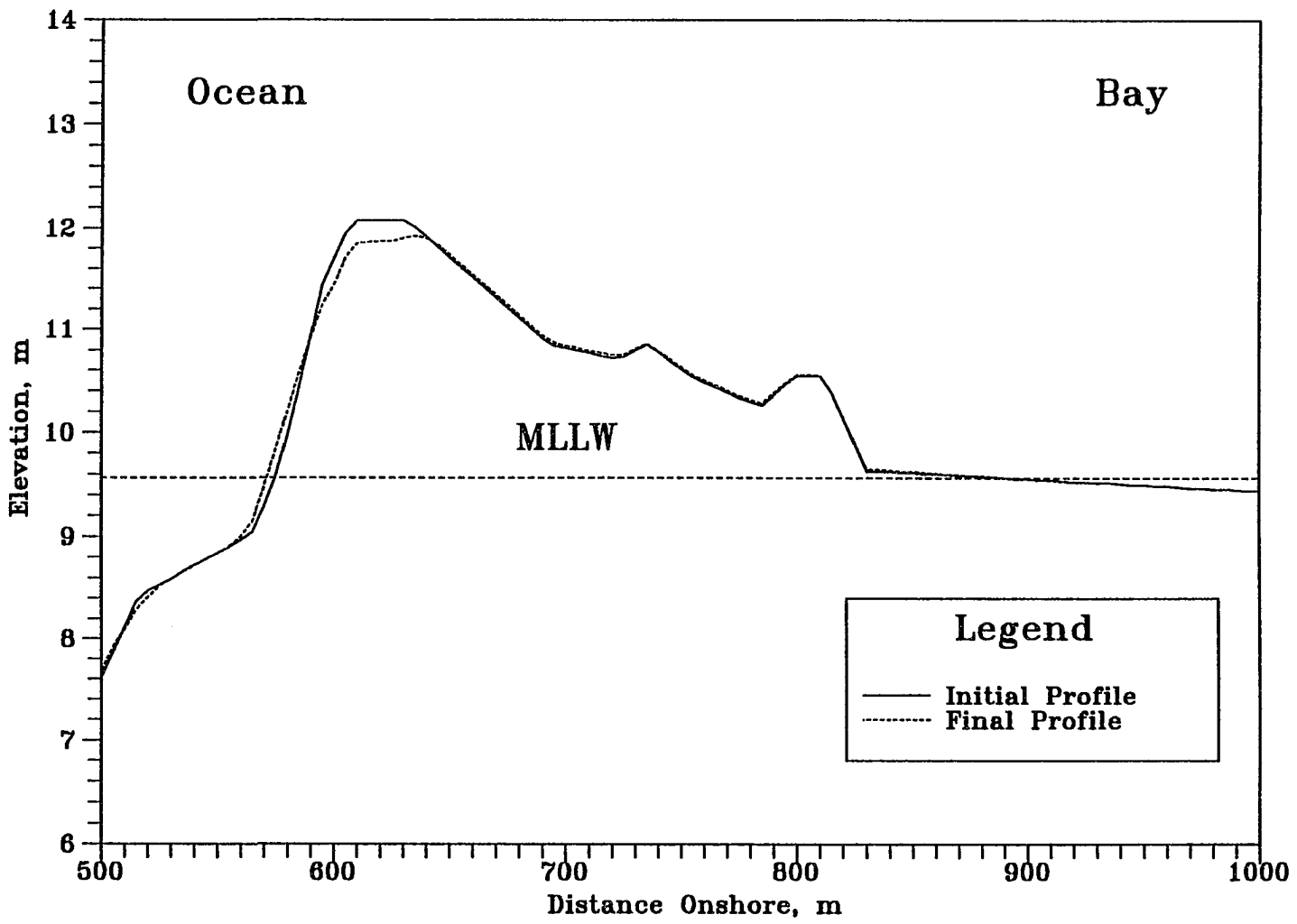


Figure 6.8 Zoomed Profiles for $h_{om}=4m, H_{mo}=5.32m, T_p=14.78s$ and $t_1=30,720s$

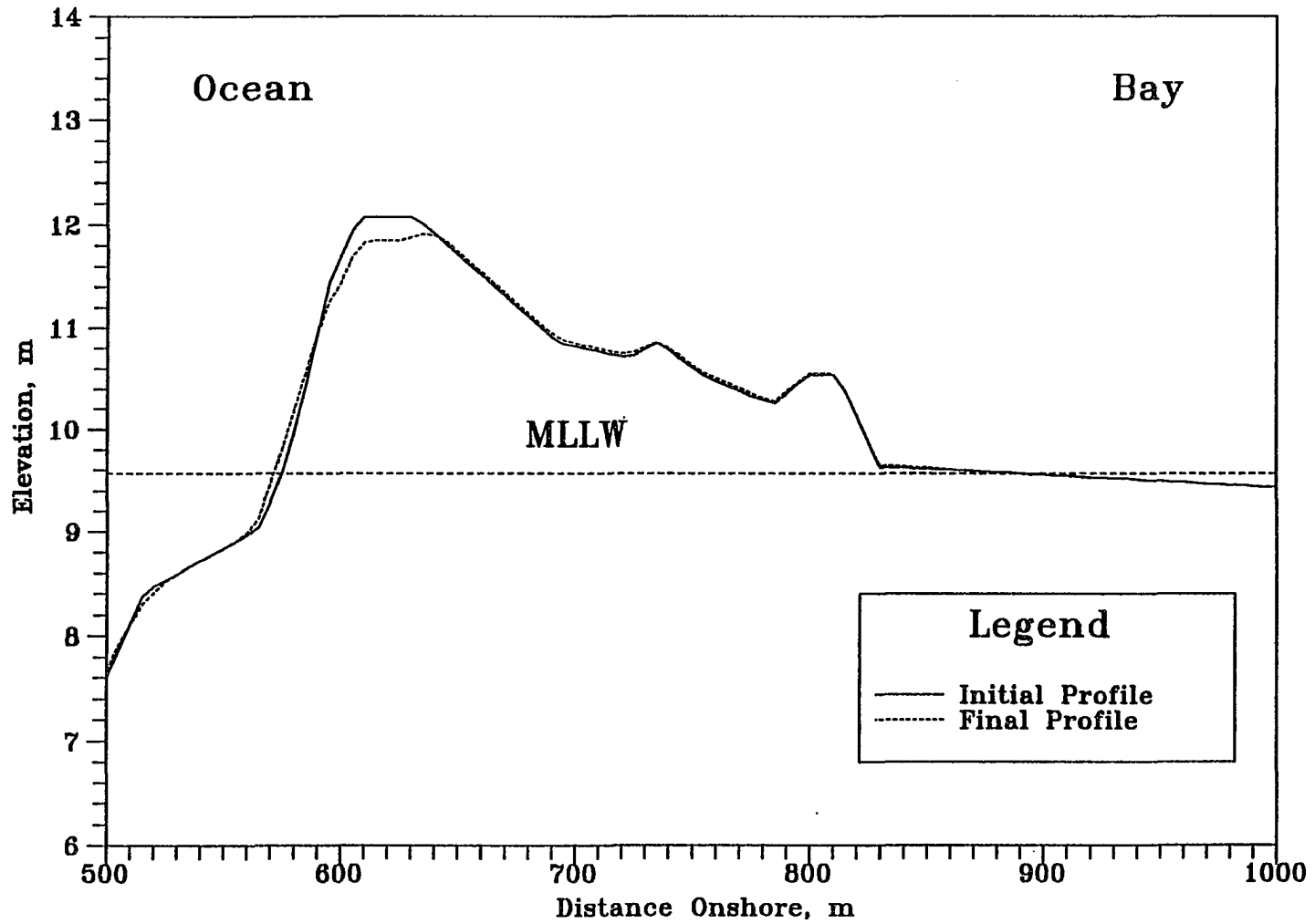


Figure 6.9 Zoomed Profiles for $h_{om}=3.5m, H_{mo}=5.20m, T_p=14.54s, t_1=31,950s$

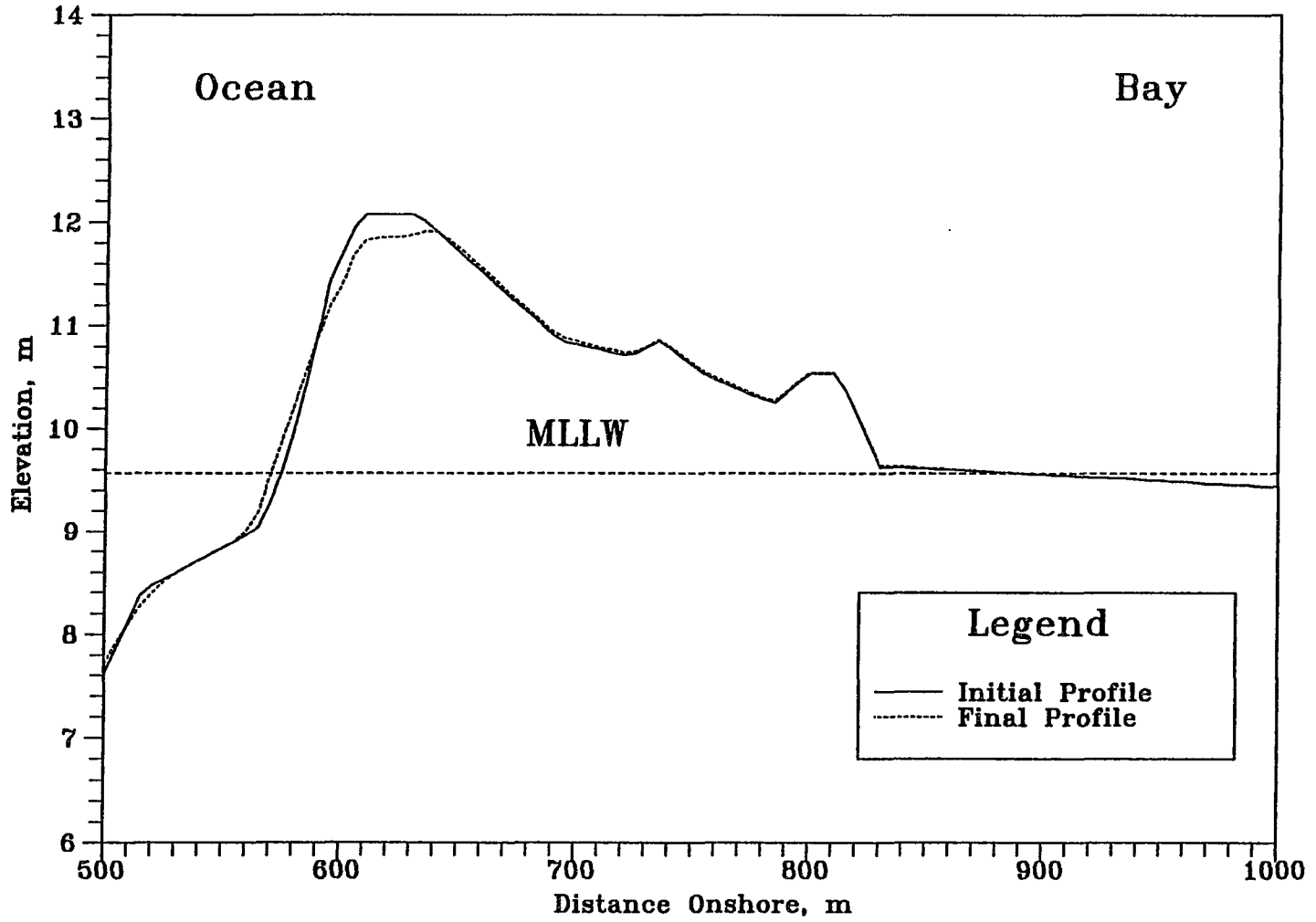


Figure 6.10 Zoomed Profiles for $h_{om}=3m, H_{mo}=5.08m, T_p=14.31s, t_1=33,480s$.

input data for the simulations are as follows.

- *Dune crest elevation above MSL to compute water depth at both ocean and bay sides.*
- *Elevation of MSL above an arbitrary datum.*
- *Distance between ocean boundary and eroded dune crest.*
- *Distance between ocean boundary and the most landward point of barrier island after SBEACH simulation to define dry bed distances from eroded dune crest.*
- *Initial water depth on dry bed is about 0.03-0.05m which is changed depending on the stability in each simulation.*
- *Weighting factor in dissipative interface, $\gamma=0.25$.*

Figure 6.11 illustrates an example of the water surface profile changes between eroded (*i.e.* by the SBEACH simulations) dune crest and end of barrier islands cross-section for ten minutes duration. Water velocity changes are also shown in Figure 6.12.

6.2.3 Stage III and IV - Storm Tides

The Preissmann scheme for the water motion, and the forward time and centered space explicit scheme for the sediment transport are used to compute profile changes. The space step of ten meters and time step of four seconds are chosen for the entire simulations.

Required input data in these stages are as follows.

- *Weighting factor for space in Preissmann scheme, $\psi=0.5$.*
- *Weighting factor for time in Preissmann scheme, $\theta=0.75$.*

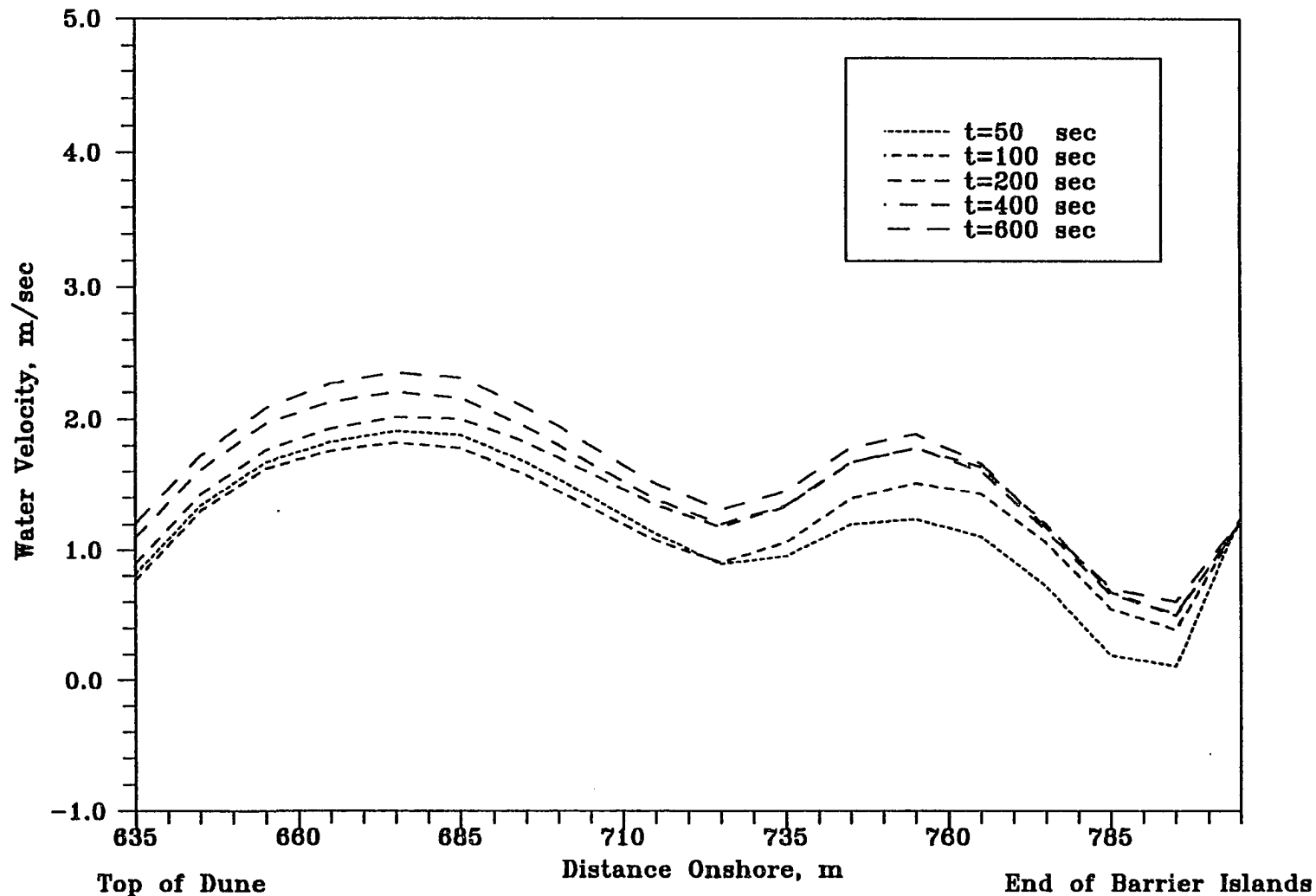


Figure 6.12 Water Velocity Changes on Initially Dry Bed During Stage II.
 ($h_{om}=5m$, $h_{bm}=4m$, $Timelag=3hr$, $D_{60}=0.3mm$ and $h_{lm}=0.05m$)

- *Porosity of bed materials, $p=0.35$.*
- *Maximum volumetric bed concentration, $C_0=0.65$.*
- *Weighting factor in dissipative interface, $\gamma=1/50 - 1/20$.*

The simulation stops when the flow depth is smaller than initial base flow depth ($\approx 0.03m$) at the eroded dune crest in order to overcome numerical instability which comes from zero depth situation.

Table 6.36 shows various simulation cases depending on the ocean and bay peak storm surge levels, time lags between ocean and bay storm surge rising, sediment diameters, and storm durations. The relationship between D_{50} and D_{90} ($D_{90} \approx 1.3D_{50}$) was obtained from the grain size analysis at Dam Neck Naval Facility, Virginia (Basco, 1996).

Figures 6.13 through 6.91 show bed profile changes in Stages III and IV for the various combinations of parameters which are indicated in Table 6.36.

The volume changes, retreat speeds and centroid positions of barrier islands above MLLW with various storm surge elevations are summarized in Table 6.37 and graphically presented in Figures 6.92 through 6.101. The large black dots indicate the centroid positions. The results of model sensitivity tests for the various time lags are shown in Table 6.38 and Figures 6.102 through 6.108. The results of model tests for the various sand diameters and storm durations are summarized in Tables 6.39 and 6.40, and graphically presented in Figures 6.109 through 6.114 and 6.115 through 6.117, respectively.

All the above graphical results are plotted at a large distorted scale (elevation to distance) about 1:125, so some confusion may arise when the profile changes are read. Therefore, less

distorted scaled (1:25) plots are provided in Figures 6.118 and 6.119.

Water depth and velocity variations at the initial top of dune in Figure 6.120 (p.272) show directional changes of water flows from ocean to bay (positive velocity) and bay to ocean (negative velocity).

The suspended sediment transport ratio, q_s/q_t , is shown in Figure 6.121 (p.273) and total sediment transport rates, q_t , at the initial top of dune are presented in Figure 6.122 (p.274) for various time lags.

Table 6.36 Running Table for Various Combinations of Important Parameters.

Fig. No.	h_{om} , m	h_{bm} , m	t_{lag} , hr	D_{50} , mm	D_{90} , mm	Duration, hr
6.1	5	5	0	0.3	0.4	24
6.2	5	5	1	0.3	0.4	24
6.3	5	5	2	0.3	0.4	24
6.4	5	5	3	0.3	0.4	24
6.5	5	5	4	0.3	0.4	24
6.6	5	5	5	0.3	0.4	24
6.7	5	5	6	0.3	0.4	24
6.8	4.5	4.5	0	0.3	0.4	24
6.9	4.5	4.5	1	0.3	0.4	24
6.10	4.5	4.5	2	0.3	0.4	24
6.11	4.5	4.5	3	0.3	0.4	24
6.12	4.5	4.5	4	0.3	0.4	24
6.13	4.5	4.5	5	0.3	0.4	24
6.14	4.5	4.5	6	0.3	0.4	24
6.15	4	4	0	0.3	0.4	24
6.16	4	4	1	0.3	0.4	24
6.17	4	4	2	0.3	0.4	24
6.18	4	4	3	0.3	0.4	24
6.19	4	4	4	0.3	0.4	24
6.20	4	4	5	0.3	0.4	24
6.21	4	4	6	0.3	0.4	24
6.22	3.5	3.5	0	0.3	0.4	24
6.23	3.5	3.5	1	0.3	0.4	24
6.24	3.5	3.5	2	0.3	0.4	24

6.25	3.5	3.5	3	0.3	0.4	24
6.26	3.5	3.5	4	0.3	0.4	24
6.27	3.5	3.5	5	0.3	0.4	24
6.28	3.5	3.5	6	0.3	0.4	24
6.29	3	3	0	0.3	0.4	24
6.30	3	3	1	0.3	0.4	24
6.31	3	3	2	0.3	0.4	24
6.32	3	3	3	0.3	0.4	24
6.33	3	3	4	0.3	0.4	24
6.34	3	3	5	0.3	0.4	24
6.35	3	3	6	0.3	0.4	24
6.36	5	4	0	0.3	0.4	24
6.37	5	4	1	0.3	0.4	24
6.38	5	4	2	0.3	0.4	24
6.39	5	4	3	0.3	0.4	24
6.40	5	4	4	0.3	0.4	24
6.41	5	4	5	0.3	0.4	24
6.42	5	4	6	0.3	0.4	24
6.43	5	3	0	0.3	0.4	24
6.44	5	3	1	0.3	0.4	24
6.45	5	3	2	0.3	0.4	24
6.46	5	3	3	0.3	0.4	24
6.47	5	3	4	0.3	0.4	24
6.48	5	3	5	0.3	0.4	24
6.49	5	3	6	0.3	0.4	24
6.50	4	3	0	0.3	0.4	24

6.51	4	3	1	0.3	0.4	24
6.52	4	3	2	0.3	0.4	24
6.53	4	3	3	0.3	0.4	24
6.54	4	3	4	0.3	0.4	24
6.55	4	3	5	0.3	0.4	24
6.56	4	3	6	0.3	0.4	24
6.57	4.5	4	0	0.3	0.4	24
6.58	4.5	4	1	0.3	0.4	24
6.59	4.5	4	2	0.3	0.4	24
6.60	4.5	4	3	0.3	0.4	24
6.61	4.5	4	4	0.3	0.4	24
6.62	4.5	4	5	0.3	0.4	24
6.63	4.5	4	6	0.3	0.4	24
6.64	4.5	3	0	0.3	0.4	24
6.65	4.5	3	1	0.3	0.4	24
6.66	4.5	3	2	0.3	0.4	24
6.67	4.5	3	3	0.3	0.4	24
6.68	4.5	3	4	0.3	0.4	24
6.69	4.5	3	5	0.3	0.4	24
6.70	4.5	3	6	0.3	0.4	24
6.71	4	3	3	0.1	0.13	24
6.72	4	3	3	0.2	0.26	24
6.73	4	3	3	0.3	0.4	24
6.74	4	3	3	0.4	0.52	24
6.75	4	3	3	0.6	0.78	24
6.76	4	3	3	1.0	1.3	24

Table 6.36 : continued

6.77	4	3	3	0.3	0.4	12
6.78	4	3	3	0.3	0.4	24
6.79	4	3	3	0.3	0.4	48

Table 6.37 Volume Changes, Retreat Speeds and Centroid Positions of Barrier Islands above MLLW in Stages III and IV with Various Storm Surge Elevations. ($t_{lag}=3$ hr, $D_{50}=0.3$ mm and $T=24$ hr)

h_{om} , m	h_{bm} , m	Time level ($\Delta t=4$ sec)	Volume, m^3/m	x_c , m	z_c , m	Speed, m/sec
5.0	5.0	0	348.88	682.64	10.37	0
		1,000	296.24	805.06	10.07	0.031
		3,000	84.75	1,234.03	9.74	0.054
4.5	4.5	0	348.58	682.66	10.37	0
		1,000	298.36	801.21	10.07	0.030
		3,000	103.12	1,200.65	9.77	0.050
4.0	4.0	0	348.33	682.86	10.37	0
		1,000	301.94	794.71	10.07	0.028
		3,000	129.94	1,152.86	9.79	0.045
3.5	3.5	0	348.68	683.03	10.37	0
		1,000	306.87	787.79	10.07	0.026
		3,000	165.83	1,089.43	9.81	0.038
		6,000	6.45	949.75	9.59	-0.012
3.0	3.0	0	347.43	682.85	10.37	0
		1,000	311.87	777.58	10.08	0.024
		3,000	216.24	1,002.64	9.85	0.028
		6,000	19.23	813.75	9.62	-0.016
5.0	4.0	0	348.88	682.64	10.37	0
		1,000	292.07	808.91	10.06	0.032
		3,000	55.54	1,251.88	9.68	0.055
5.0	3.0	0	348.88	682.64	10.37	0
		1,000	287.42	812.31	10.05	0.032

Table 6.37 : continued

5.0	3.0	3,000	8.28	1,531.94	9.60	0.090
4.0	3.0	0	348.33	682.86	10.37	0
		1,000	296.49	799.75	10.06	0.029
		3,000	93.79	1,180.12	9.75	0.048
		6,000	10.18	1,377.62	9.60	0.016
4.5	4.0	0	348.58	682.66	10.37	0
		1,000	295.81	803.39	10.06	0.030
		3,000	88.82	1,210.32	9.75	0.051
4.5	3.0	0	348.58	682.66	10.37	0
		1,000	291.26	807.23	10.05	0.031
		3,000	58.93	1,227.16	9.68	0.052

Table 6.38 Volume Changes, Retreat Speeds and Centroid Positions of Barrier Islands above MLLW in Stages III and IV with Various Time Lags. ($h_{om}=4.0$ m, $h_{bm}=3.0$ m, $D_{50}=0.3$ mm and $T=24$ hr)

Time lag, hr	Time level ($\Delta t=4$ sec)	Volume, m^3/m	x_c , m	z_c , m	Speed, m/sec
	0	348.33	682.86	10.37	0
0.0	1,000	336.66	733.51	10.22	0.013
	3,000	285.16	941.37	9.97	0.026
	6,000	183.29	1,159.06	9.75	0.018
	9,000	155.39	1,178.55	9.72	0.002
	13,628	142.60	1,169.88	9.71	0.000
1.0	1,000	322.27	772.31	10.13	0.022
	3,000	217.95	1,055.60	9.88	0.035
	6,000	166.07	1,184.63	9.78	0.011
	9,000	156.29	1,177.50	9.76	-0.001
	13,628	145.33	1,171.49	9.75	0.000
2.0	1,000	306.47	790.82	10.08	0.027
	3,000	144.38	1,139.09	9.80	0.044
	6,000	80.59	1,281.66	9.71	0.012
	9,000	32.75	1,140.41	9.63	-0.012
	13,628	27.74	1,130.44	9.62	-0.001
3.0	1,000	296.49	799.75	10.06	0.029
	3,000	93.79	1,180.12	9.75	0.048
	6,000	10.18	1,377.62	9.60	0.016
4.0	1,000	290.18	804.61	10.04	0.030
	3,000	60.77	1,197.76	9.69	0.049

Table 6.38 : continued

5.0	1,000	286.62	807.05	10.03	0.031
	3,000	27.14	1,180.00	9.63	0.047
6.0	1,000	284.44	808.41	10.03	0.031
	3,000	6.52	1,183.44	9.59	0.047

Table 6.39 Volume Changes, Retreat Speeds and Centroid Positions of Barrier Islands above MLLW in Stages III and IV with Various Sand Diameters. ($h_{om}=4.0$ m, $h_{bm}=3.0$ m, $t_{lag}=3.0$ hr and $T=24$ hr)

D_{50} , mm	Time level ($\Delta t=4$ sec)	Volume, m^3/m	x_c , m	z_c , m	Speed, m/sec
	0	348.33	682.86	10.37	0
0.1	1,000	305.06	719.97	10.23	0.009
	3,000	229.92	823.50	10.09	0.013
	6,000	167.90	903.16	9.96	0.007
	9,000	86.36	837.19	9.76	-0.005
	13,628	25.79	695.73	9.65	-0.008
0.2	1,000	309.15	772.43	10.10	0.022
	3,000	155.71	1,057.14	9.84	0.036
	6,000	73.79	1,202.18	9.71	0.012
0.3	1,000	296.49	799.75	10.06	0.029
	3,000	93.79	1,180.12	9.75	0.048
	6,000	10.18	1,377.62	9.60	0.016
0.4	1,000	288.26	819.69	10.02	0.034
	3,000	43.70	1,288.13	9.67	0.059
0.6	1,000	298.41	798.98	10.04	0.029
	3,000	73.37	1,207.84	9.70	0.051
1.0	1,000	317.69	754.47	10.11	0.018
	3,000	180.36	996.42	9.83	0.030
	6,000	101.74	1,114.09	9.72	0.010
	9,000	2.35	987.74	9.58	-0.011

Table 6.40 Volume Changes, Retreat Speeds and Centroid Positions of Barrier Islands above MLLW in Stages III and IV with Various Storm Durations. ($h_{om}=4.0$ m, $h_{bm}=3.0$ m, $t_{lag}=3.0$ hr and $D_{50}=0.3$ mm)

Duration, hr	Time level ($\Delta t=4$ sec)	Volume, m^3/m	x_c , m	z_c , m	Speed, m/sec
12	0	349.83	682.04	10.38	0
	500	315.25	760.54	10.15	0.039
	1,500	175.71	988.00	9.85	0.057
	3,000	59.79	1,185.68	9.68	0.033
24	0	348.33	682.86	10.37	0
	1,000	296.49	799.75	10.06	0.029
	3,000	93.79	1,180.12	9.75	0.048
	6,000	10.18	1,377.62	9.60	0.016
48	0	349.92	682.53	10.35	0
	1,000	324.91	752.63	10.11	0.018
	2,000	274.28	863.38	9.95	0.028
	3,000	204.55	998.70	9.83	0.034
	6,000	0.511	1,556.93	9.57	0.043

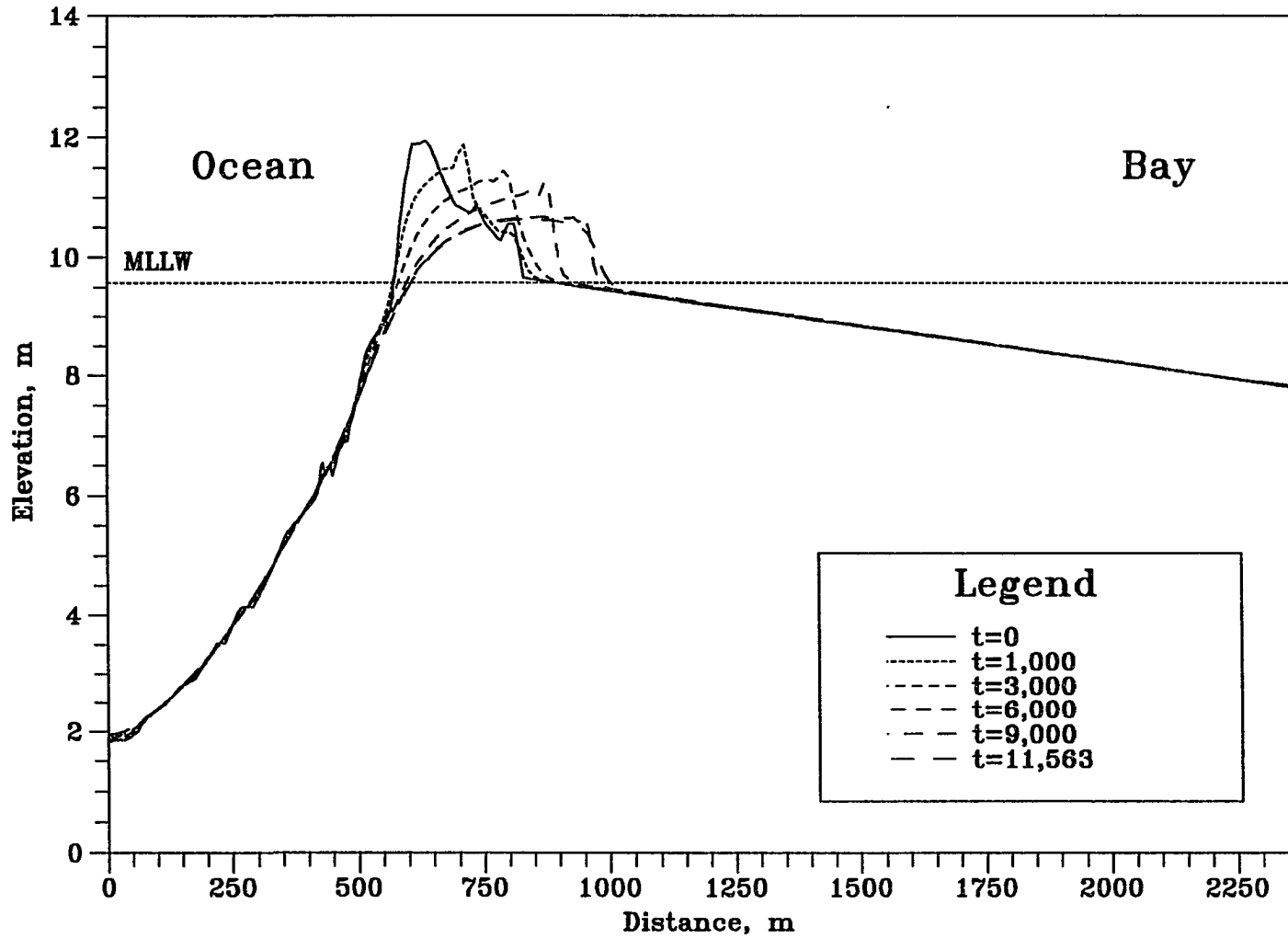


Figure 6.13 Bed Elevation Changes in Stage III/IV at t=0, 1000, 3000, 6000, 9000 and 11563. ($h_{om}=5m$, $h_{bm}=5m$, $t_{lag}=0hr$, $D_{50}=0.3mm$)

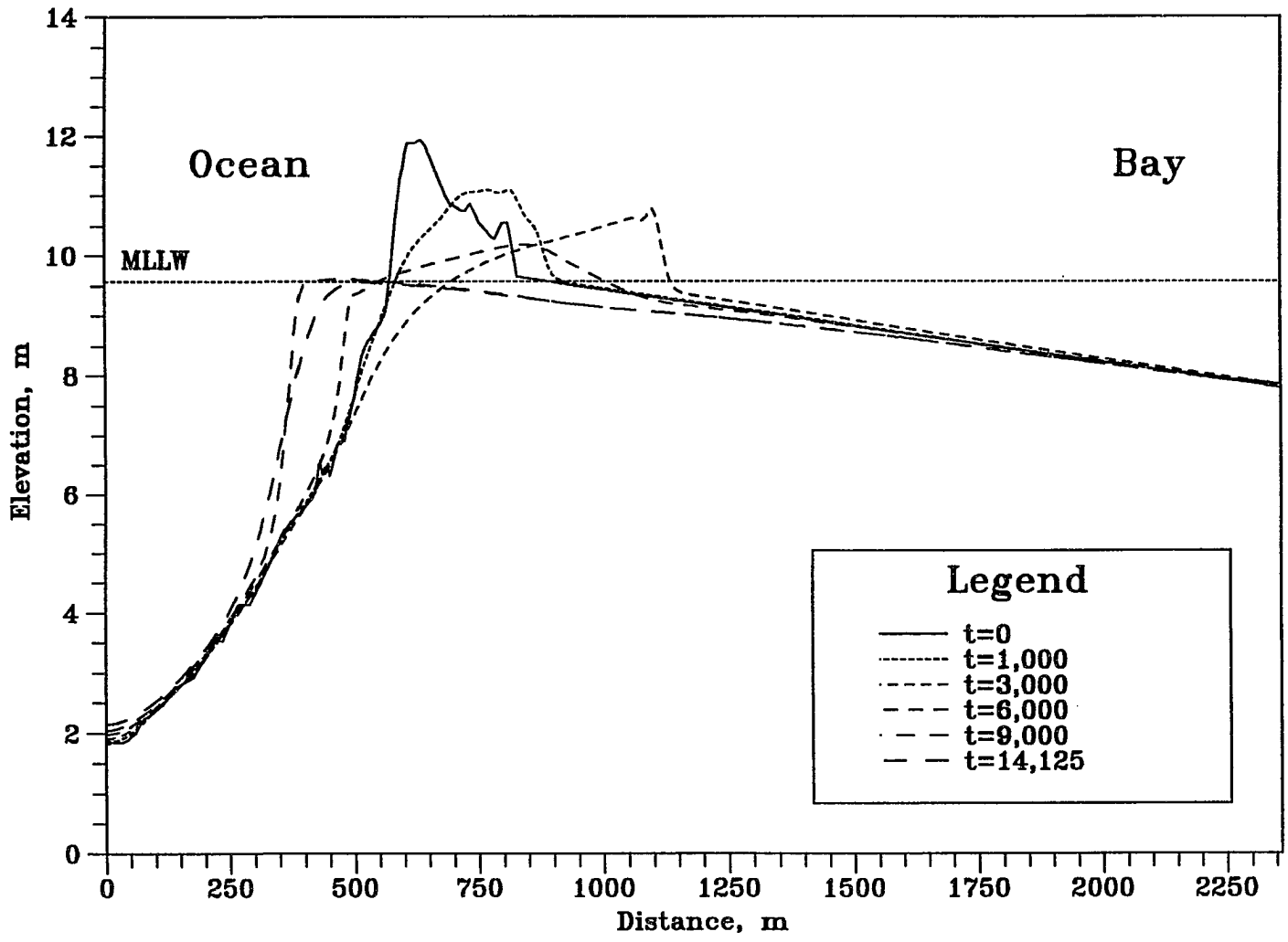


Figure 6.14 Bed Elevation Changes in Stage III/IV at t=0, 1000, 3000, 6000, 9000 and 14125. ($h_{om}=5m$, $h_{bm}=5m$, $t_{lag}=1hr$, $D_{50}=0.3mm$)

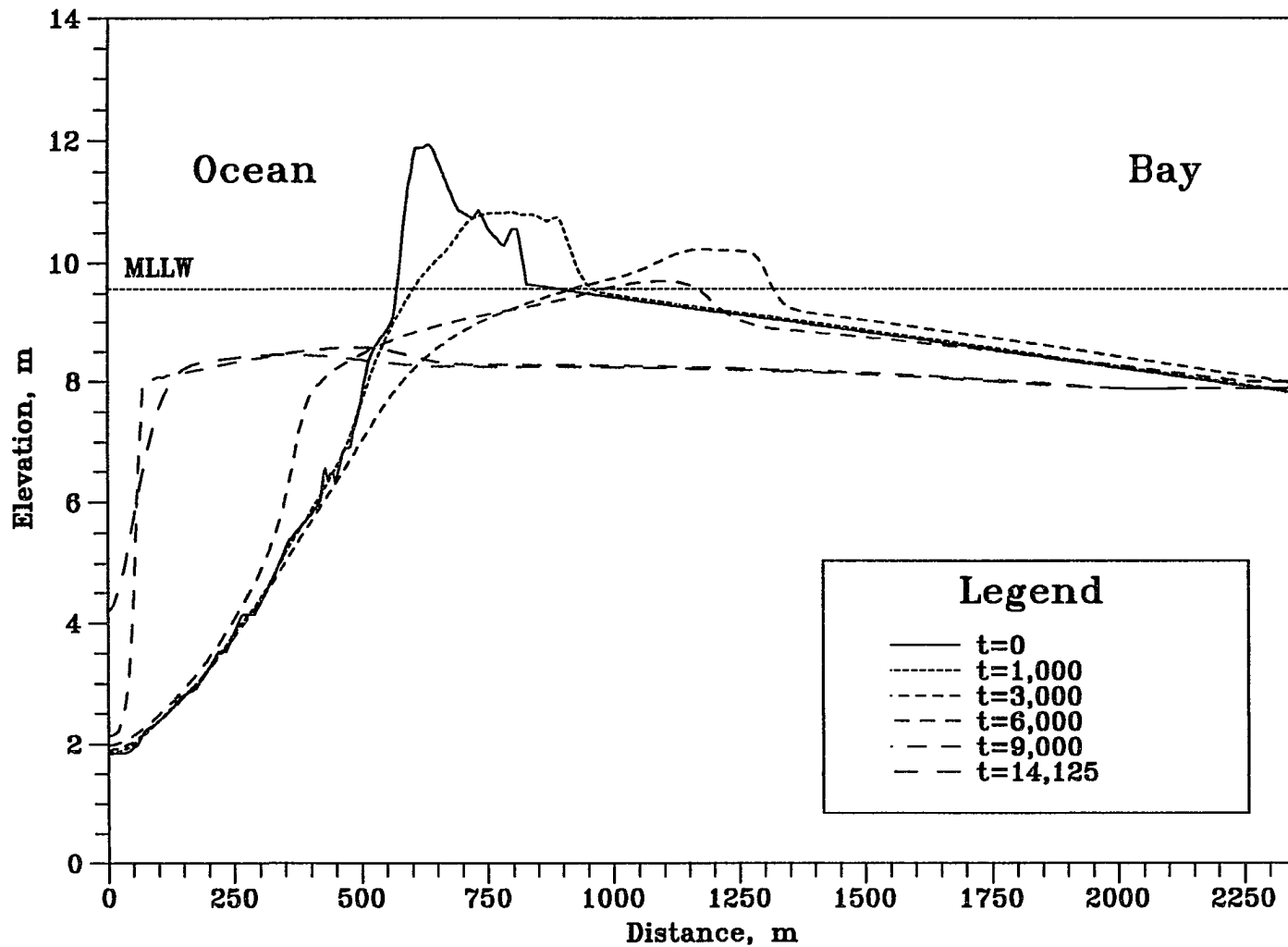


Figure 6.15 Bed Elevation Changes in Stage III/IV at $t=0$, 1000, 3000, 6000, 9000 and 14125. ($h_{om}=5m$, $h_{bm}=5m$, $t_{lag}=2hr$, $D_{50}=0.3mm$)

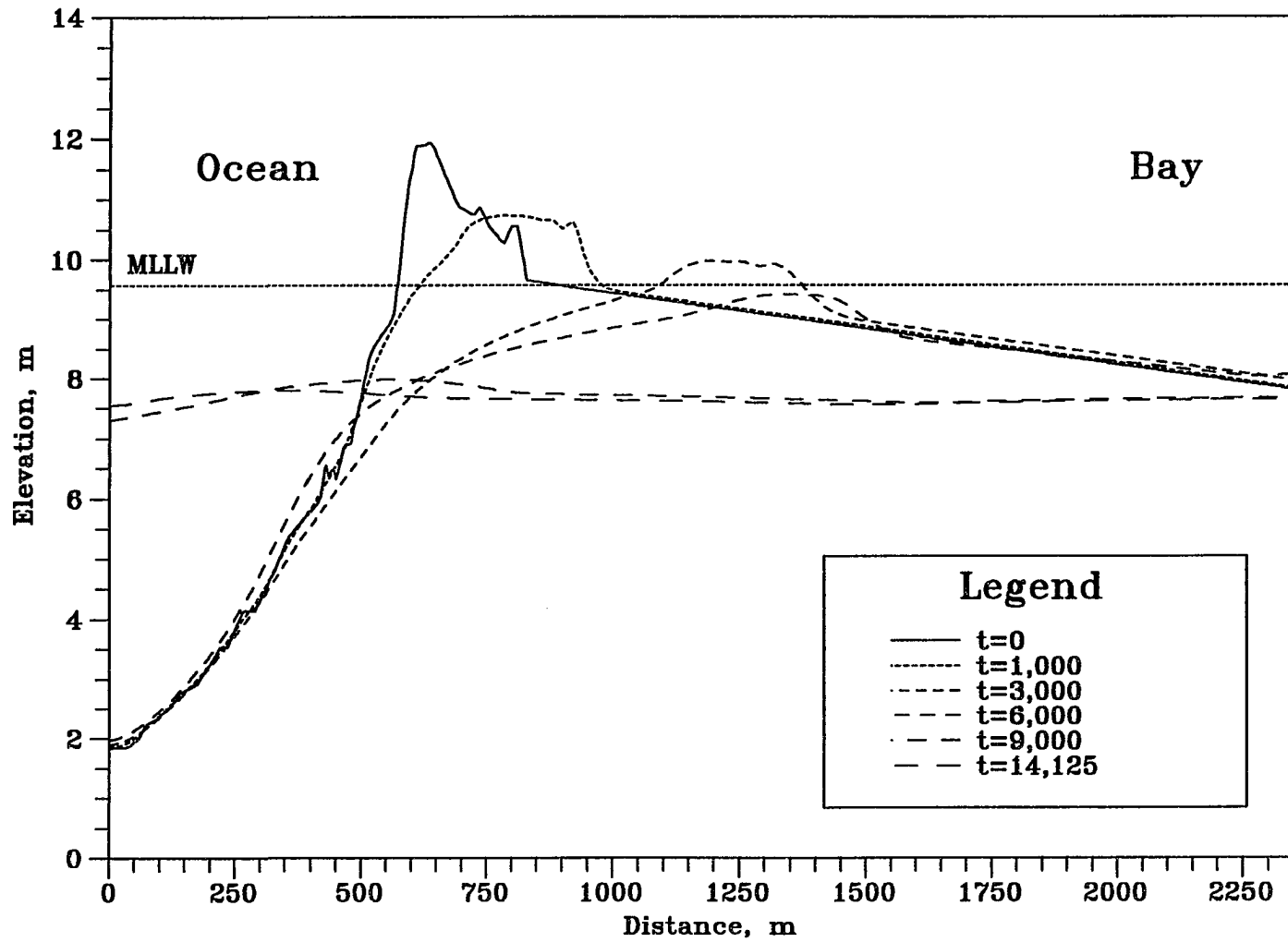


Figure 6.16 Bed Elevation Changes in Stage III/IV at t=0, 1000, 3000, 6000, 9000 and 14125. ($h_{om}=5m$, $h_{bm}=5m$, $t_{lag}=3hr$, $D_{50}=0.3mm$)

170

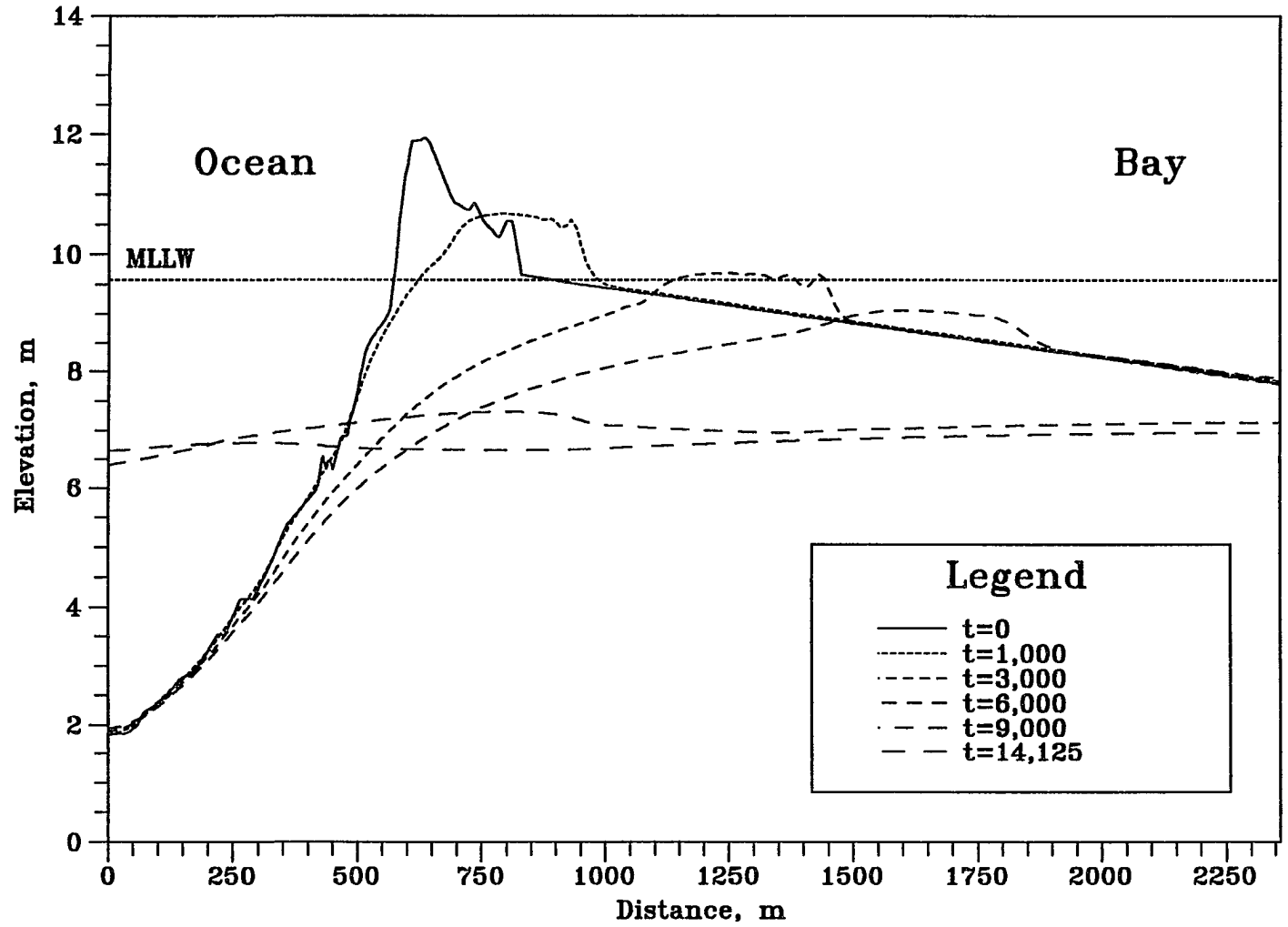


Figure 6.17 Bed Elevation Changes in Stage III/IV at t=0, 1000, 3000, 6000, 9000 and 14125. ($h_{om}=5m$, $h_{bm}=5m$, $t_{lag}=4hr$, $D_{50}=0.3mm$)

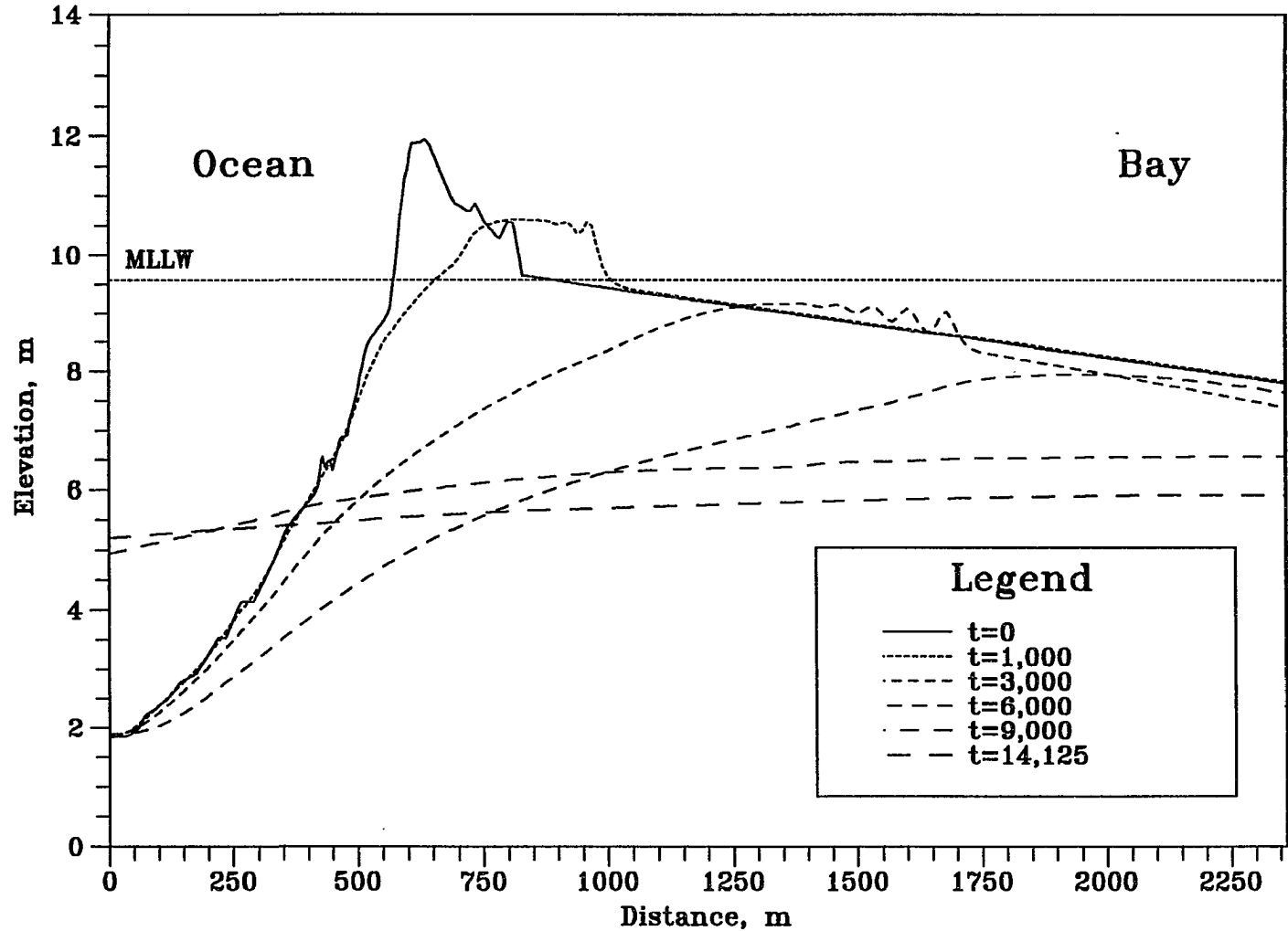


Figure 6.18 Bed Elevation Changes in Stage III/IV at t=0, 1000, 3000, 6000, 9000 and 14125. ($h_{om}=5m$, $h_{bm}=5m$, $t_{lag}=5hr$, $D_{50}=0.3mm$)

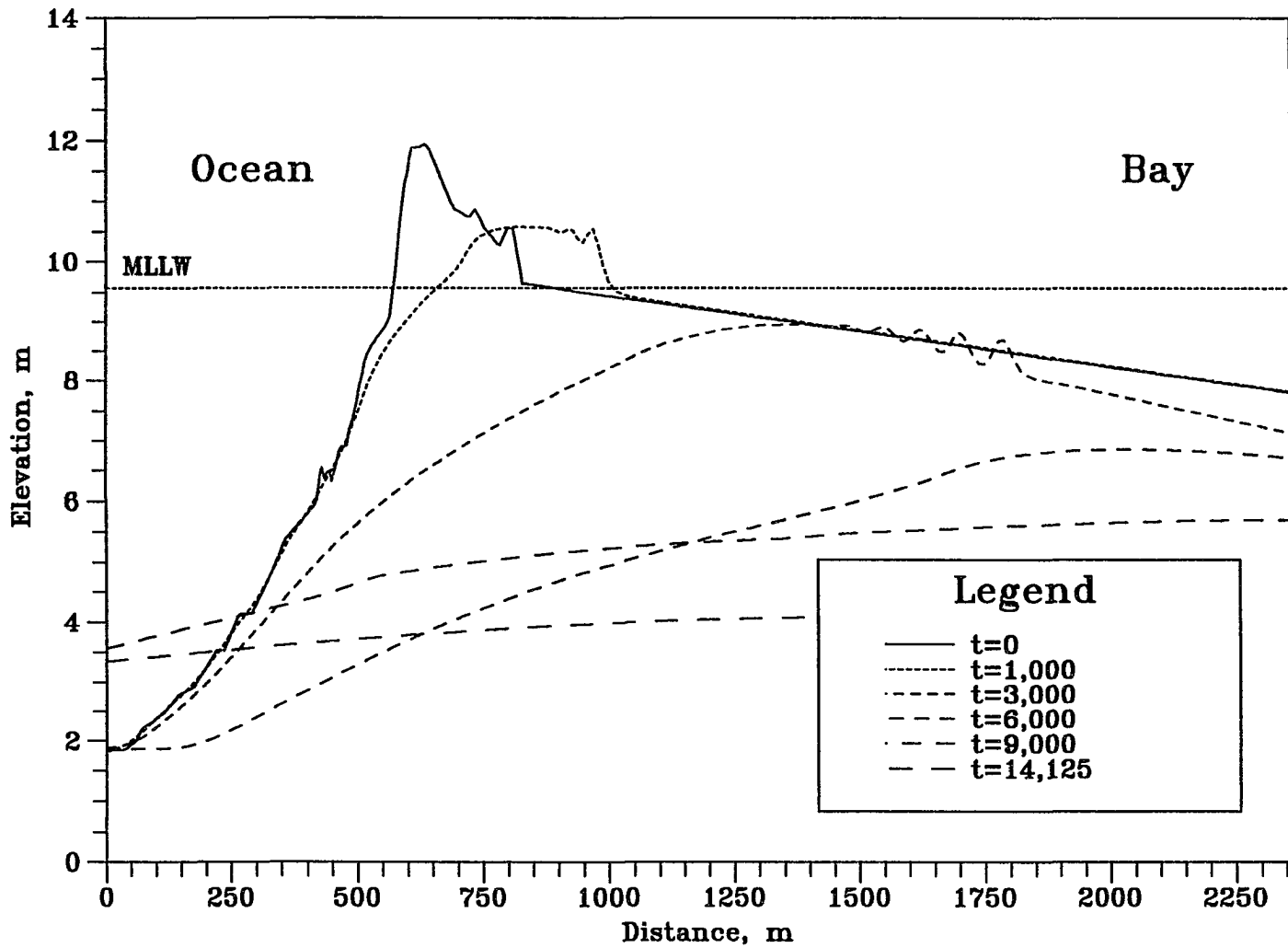


Figure 6.19 Bed Elevation Changes in Stage III/IV at t=0, 1000, 3000, 6000, 9000 and 14125. ($h_{om}=5m$, $h_{bm}=5m$, $t_{lag}=6hr$, $D_{50}=0.3mm$)

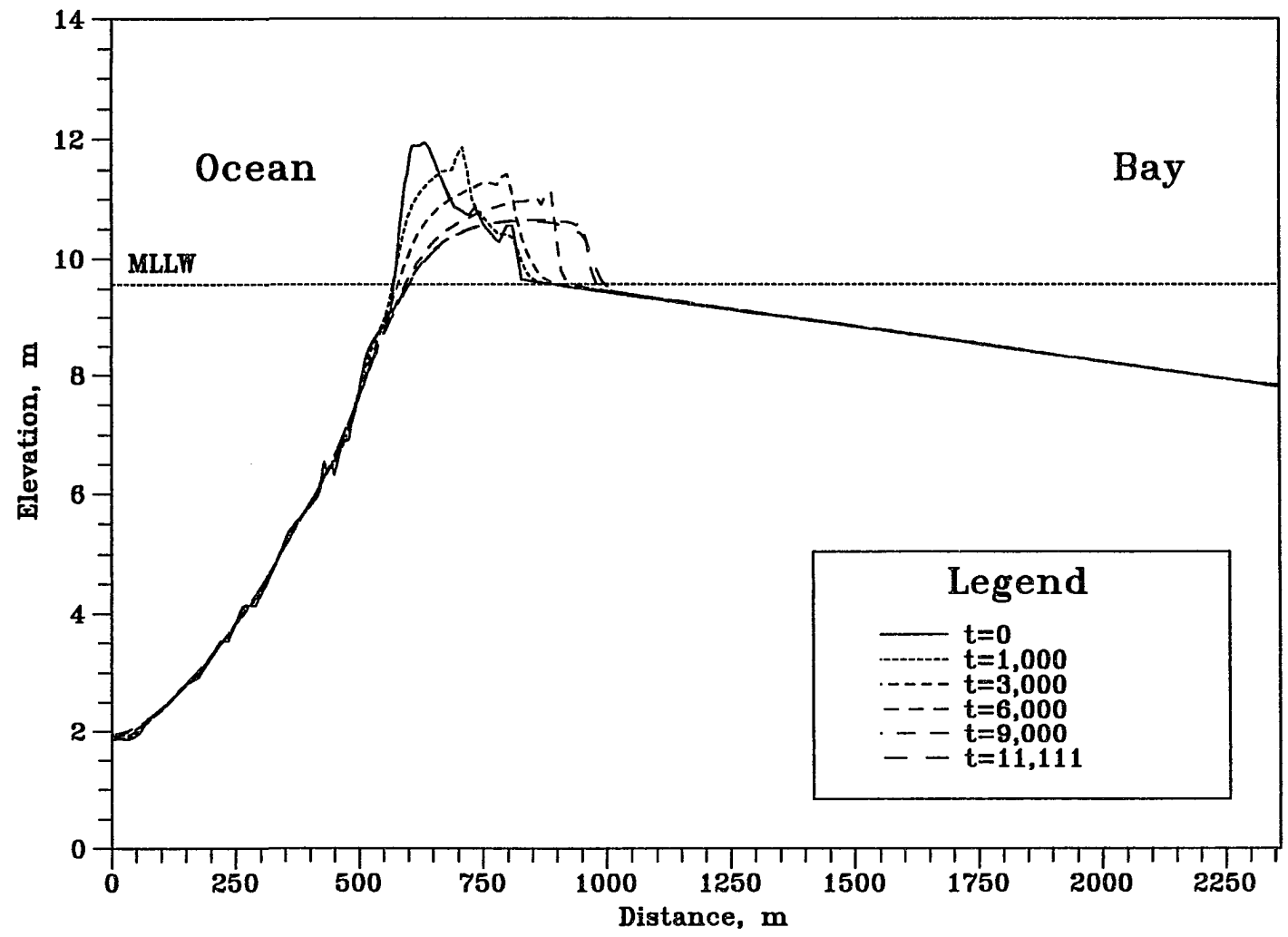


Figure 6.20 Bed Elevation Changes in Stage III/IV at t=0, 1000, 3000, 6000, 9000 and 11111. ($h_{om}=4.5m$, $h_{bm}=4.5m$, $t_{lag}=0hr$, $D_{50}=0.3mm$)

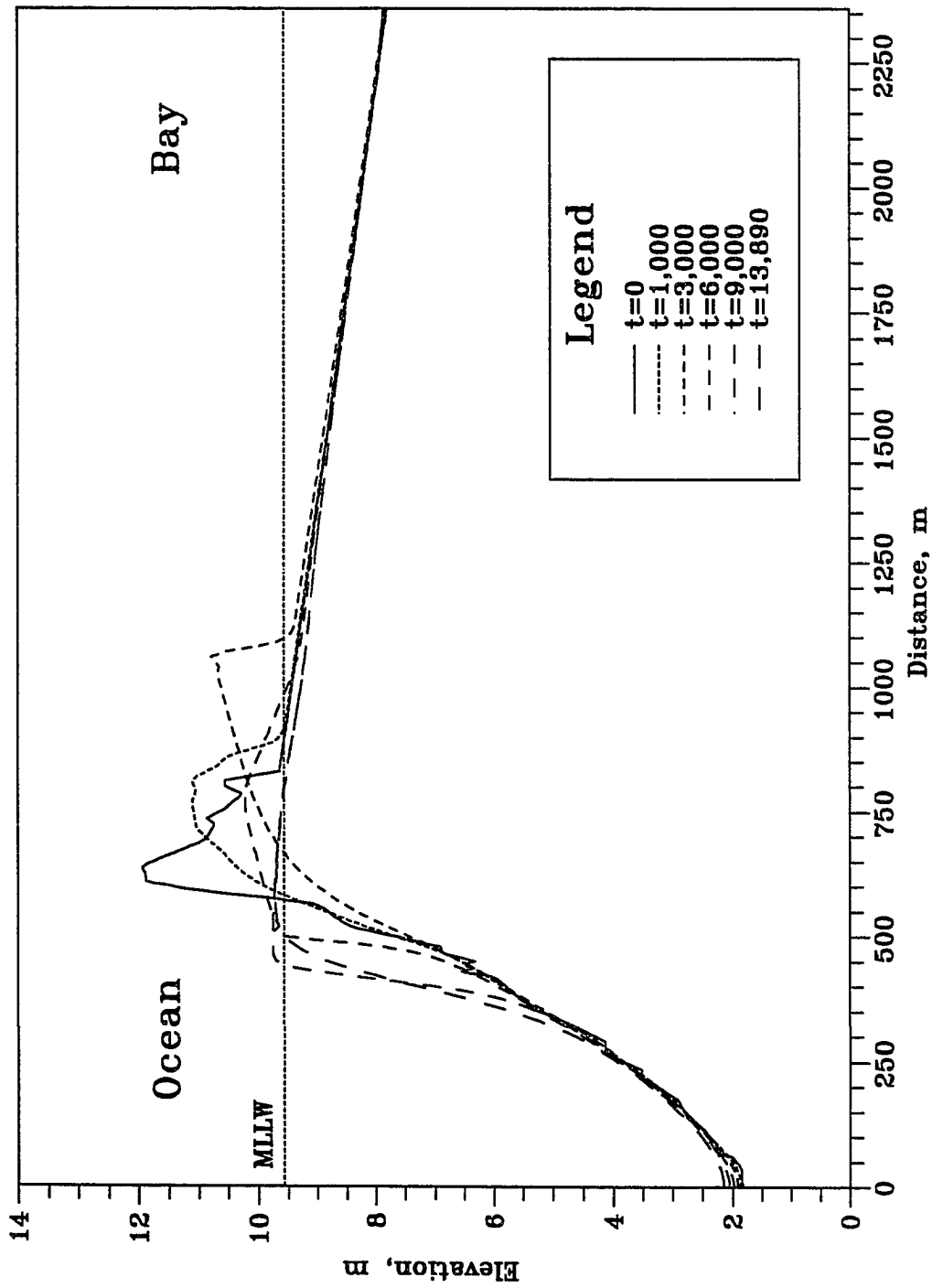


Figure 6.21 Bed Elevation Changes in Stage III/IV at t=0, 1000, 3000, 6000, 9000 and 13890. ($h_{om}=4.5m$, $h_{bm}=4.5m$, $t_{lag}=1hr$, $D_{50}=0.3mm$)

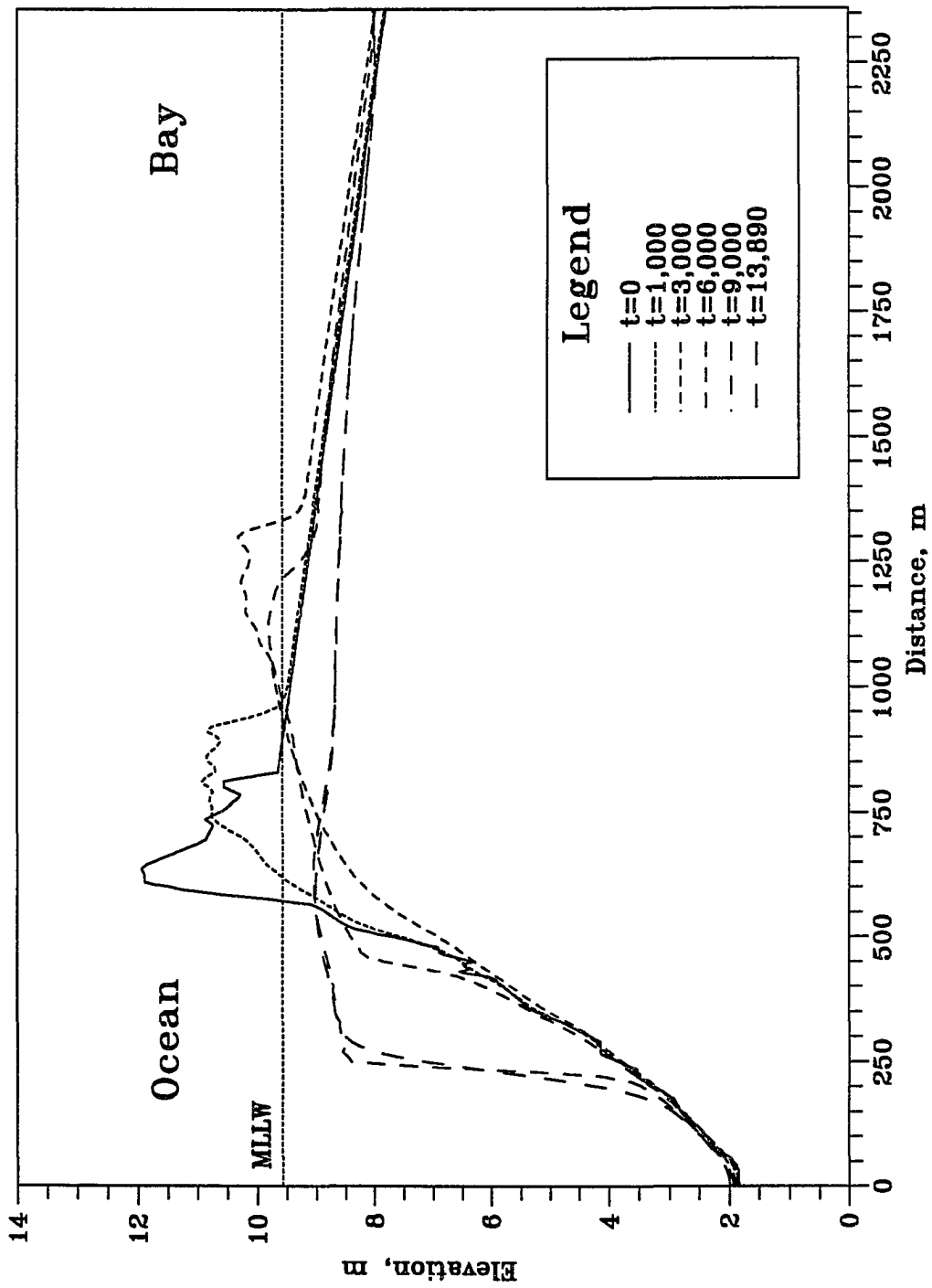


Figure 6.22 Bed Elevation Changes in Stage III/IV at t=0, 1000, 3000, 6000, 9000 and 13890. ($h_{om}=4.5m$, $h_{bm}=4.5m$, $t_{lag}=2hr$, $D_{50}=0.3mm$)

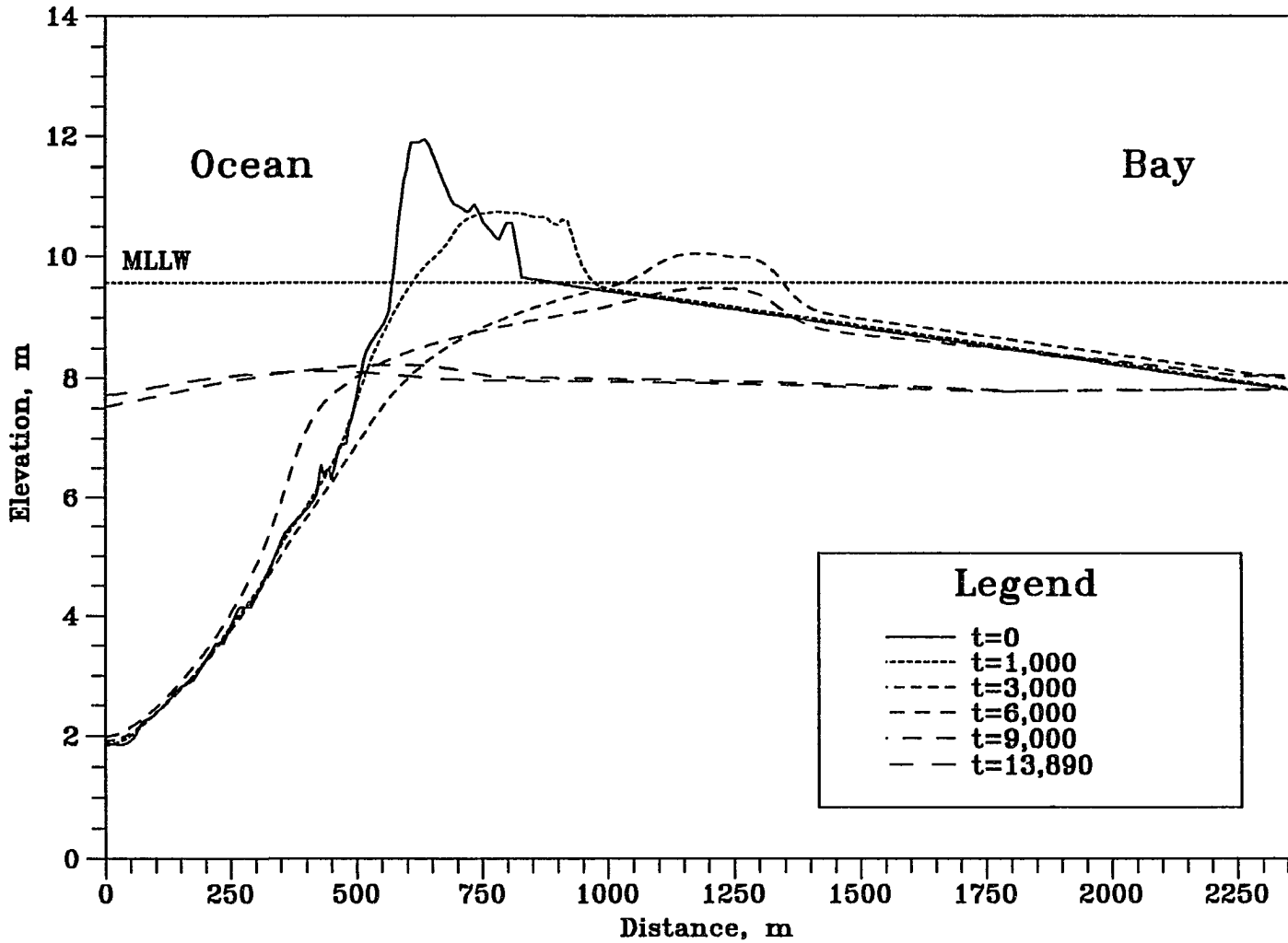


Figure 6.23 Bed Elevation Changes in Stage III/IV at t=0, 1000, 3000, 6000, 9000 and 13890. ($h_{om}=4.5m$, $h_{bm}=4.5m$, $t_{lag}=3hr$, $D_{50}=0.3mm$)

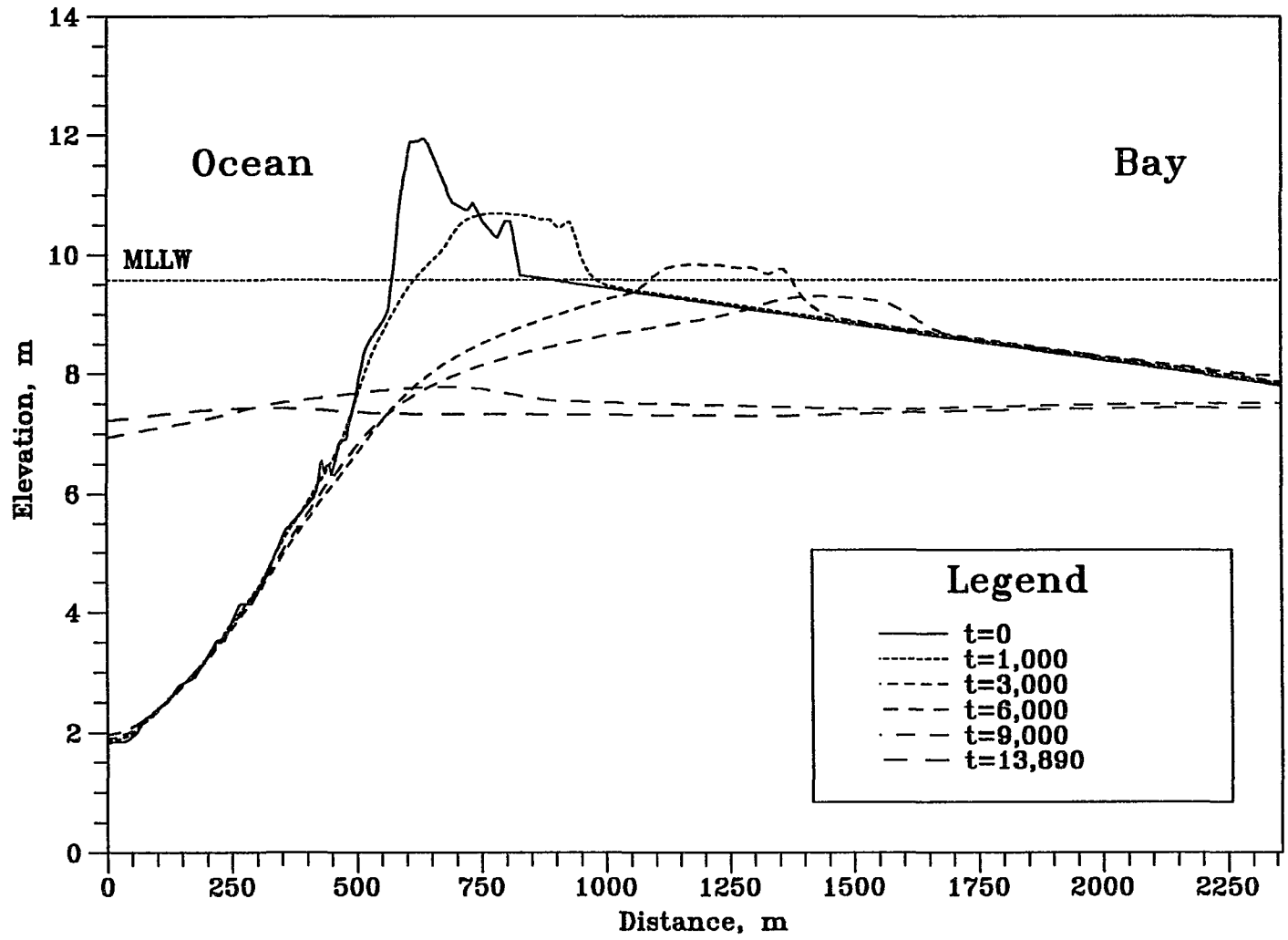


Figure 6.24 Bed Elevation Changes in Stage III/IV at t=0, 1000, 3000, 6000, 9000 and 13890. ($h_{om}=4.5m$, $h_{bm}=4.5m$, $t_{lag}=4hr$, $D_{50}=0.3mm$)

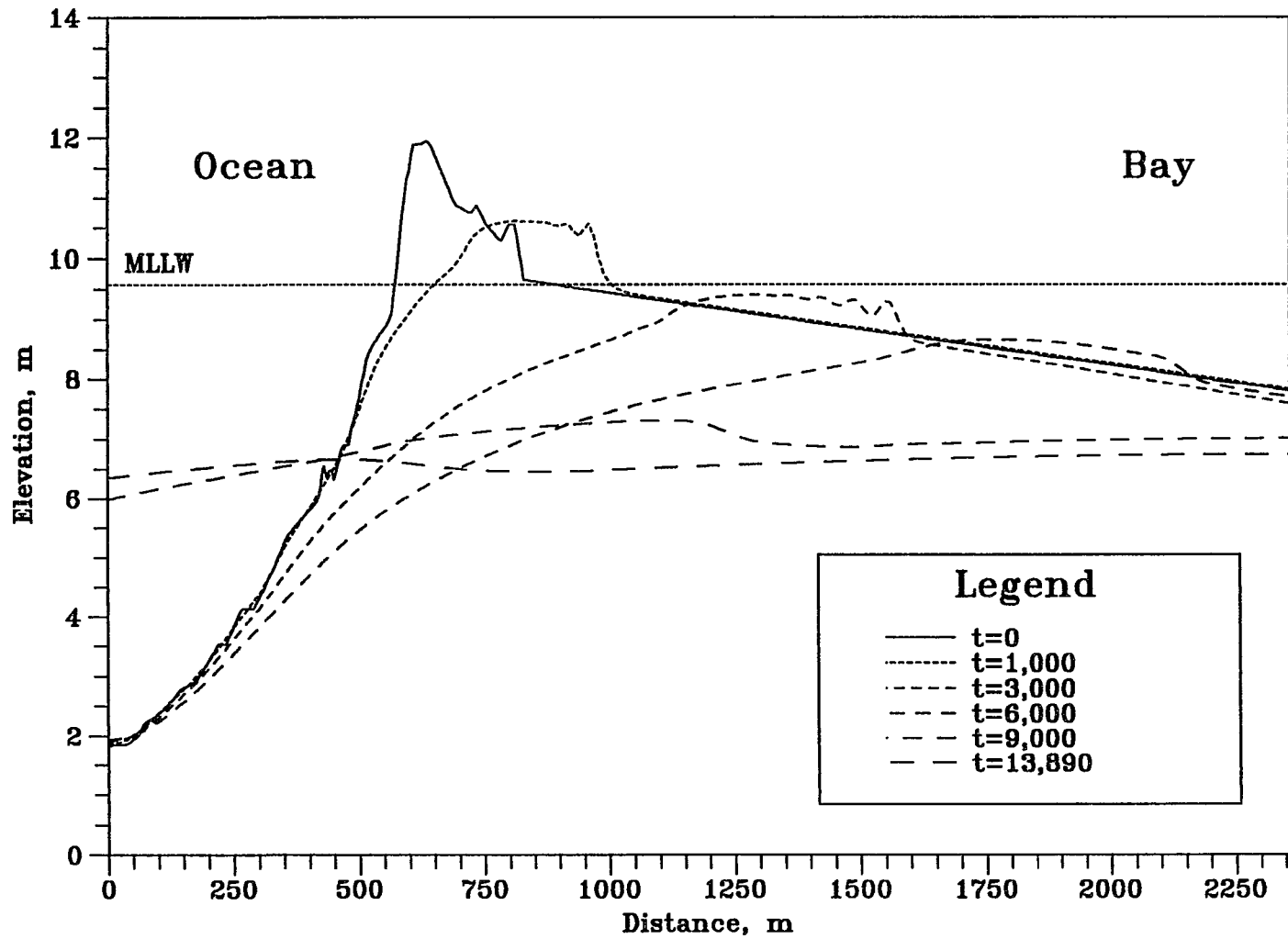


Figure 6.25 Bed Elevation Changes in Stage III/IV at t=0, 1000, 3000, 6000, 9000 and 13890. ($h_{om}=4.5m$, $h_{bm}=4.5m$, $t_{lag}=5hr$, $D_{50}=0.3mm$)

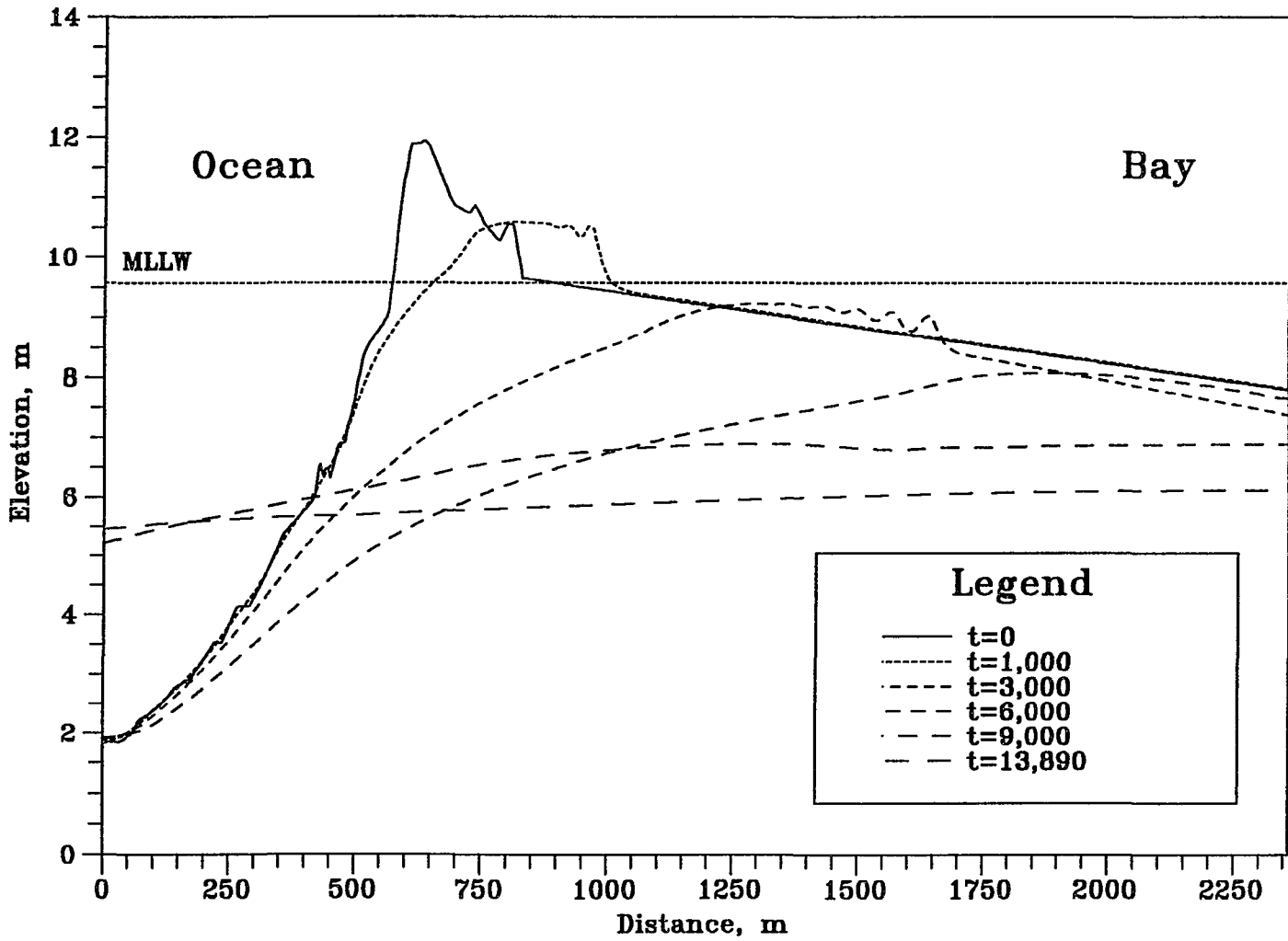


Figure 6.26 Bed Elevation Changes in Stage III/IV at $t=0, 1000, 3000, 6000, 9000$ and 13890 . ($h_{om}=4.5\text{m}$, $h_{bm}=4.5\text{m}$, $t_{lag}=6\text{hr}$, $D_{50}=0.3\text{mm}$)

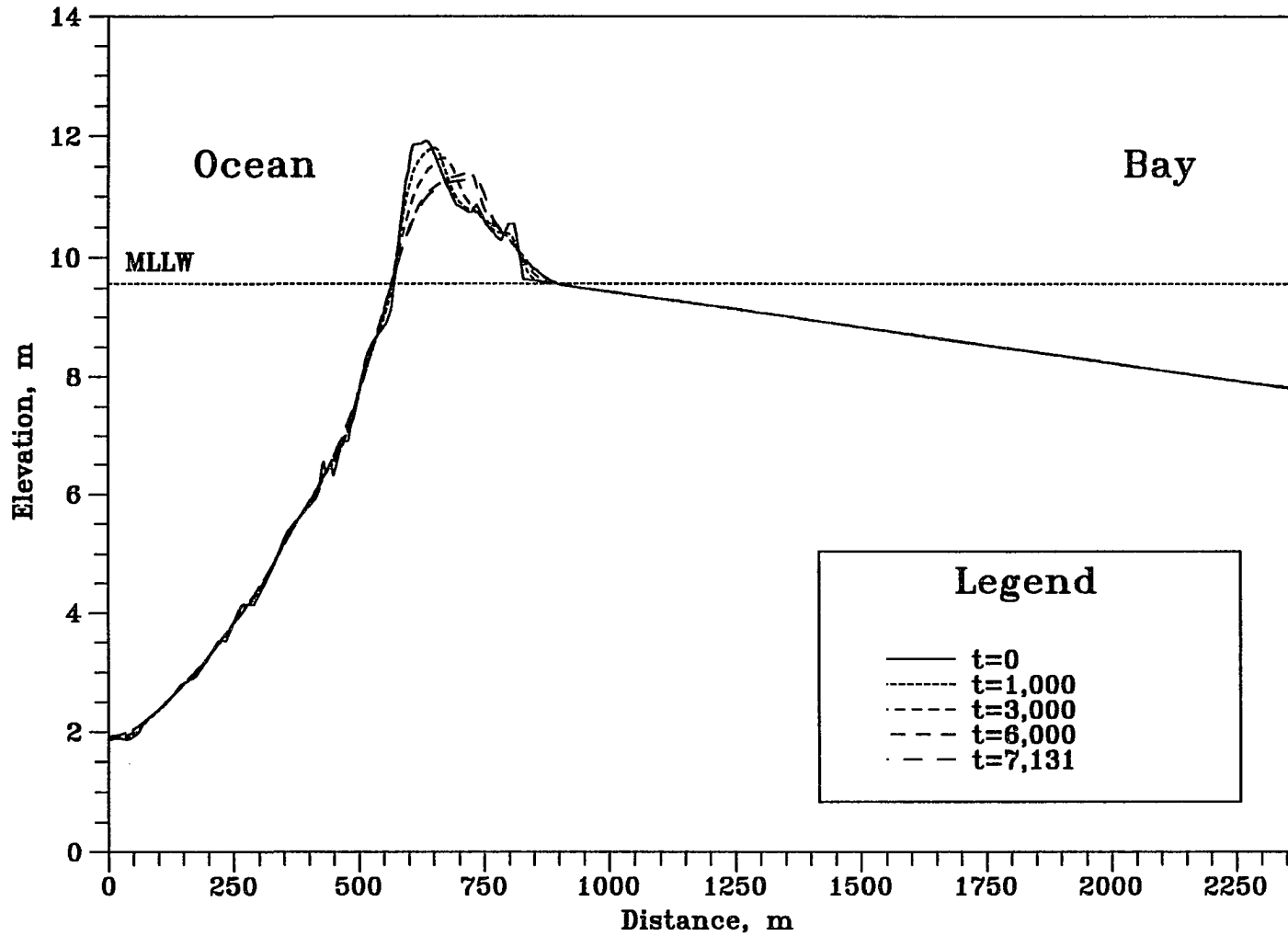


Figure 6.27 Bed Elevation Changes in Stage III/IV at t=0, 1000, 3000, 6000, and 7131. ($h_{om}=4.0m$, $h_{bm}=4.0m$, $t_{lag}=0hr$, $D_{50}=0.3mm$)

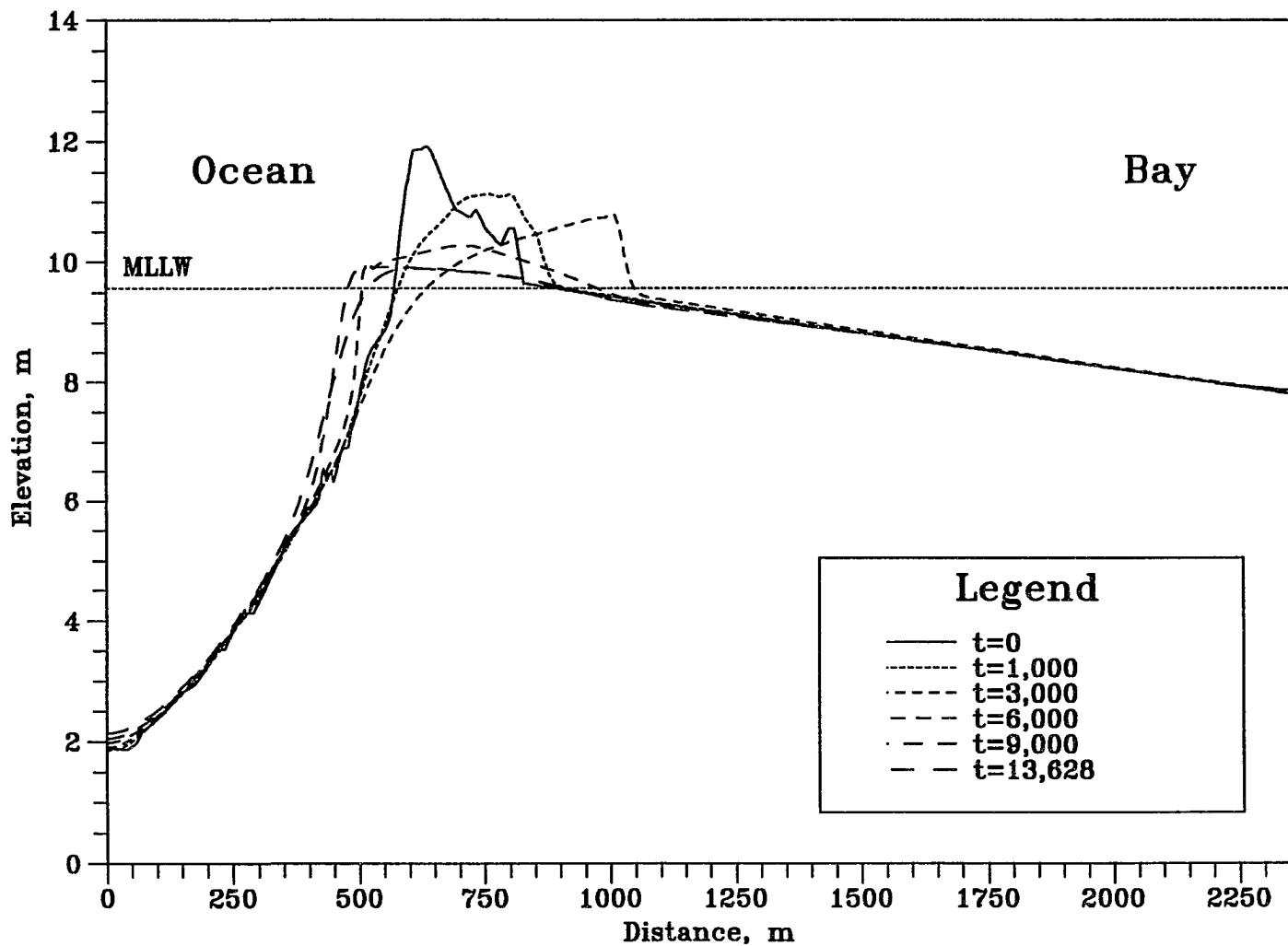


Figure 6.28 Bed Elevation Changes in Stage III/IV at t=0, 1000, 3000, 6000, 9000 and 13628. ($h_{om}=4.0m$, $h_{bm}=4.0m$, $t_{lag}=1hr$, $D_{50}=0.3mm$)

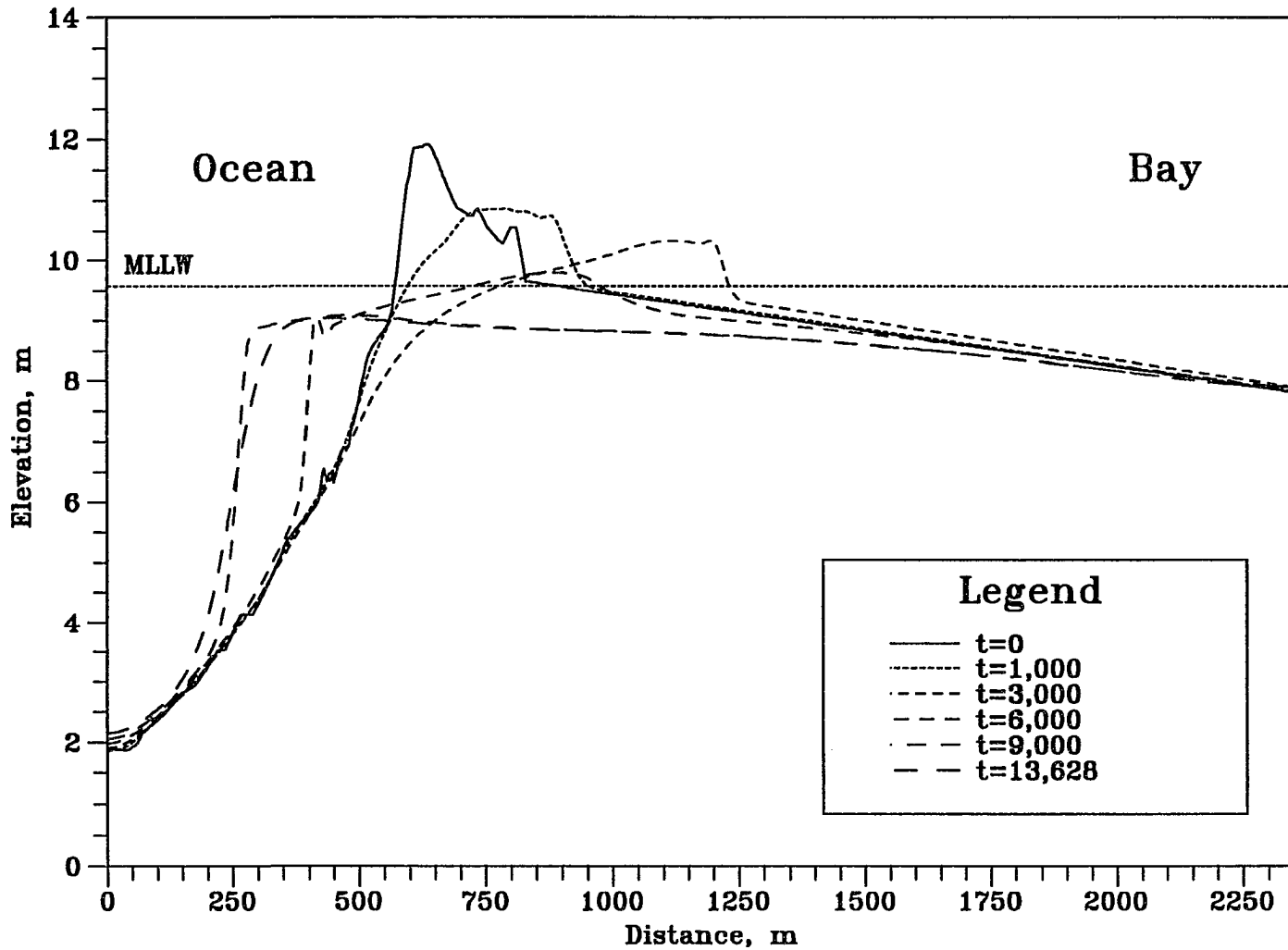


Figure 6.29 Bed Elevation Changes in Stage III/IV at t=0, 1000, 3000, 6000, 9000 and 13628. ($h_{om}=4.0m$, $h_{bm}=4.0m$, $t_{lag}=2hr$, $D_{50}=0.3mm$)

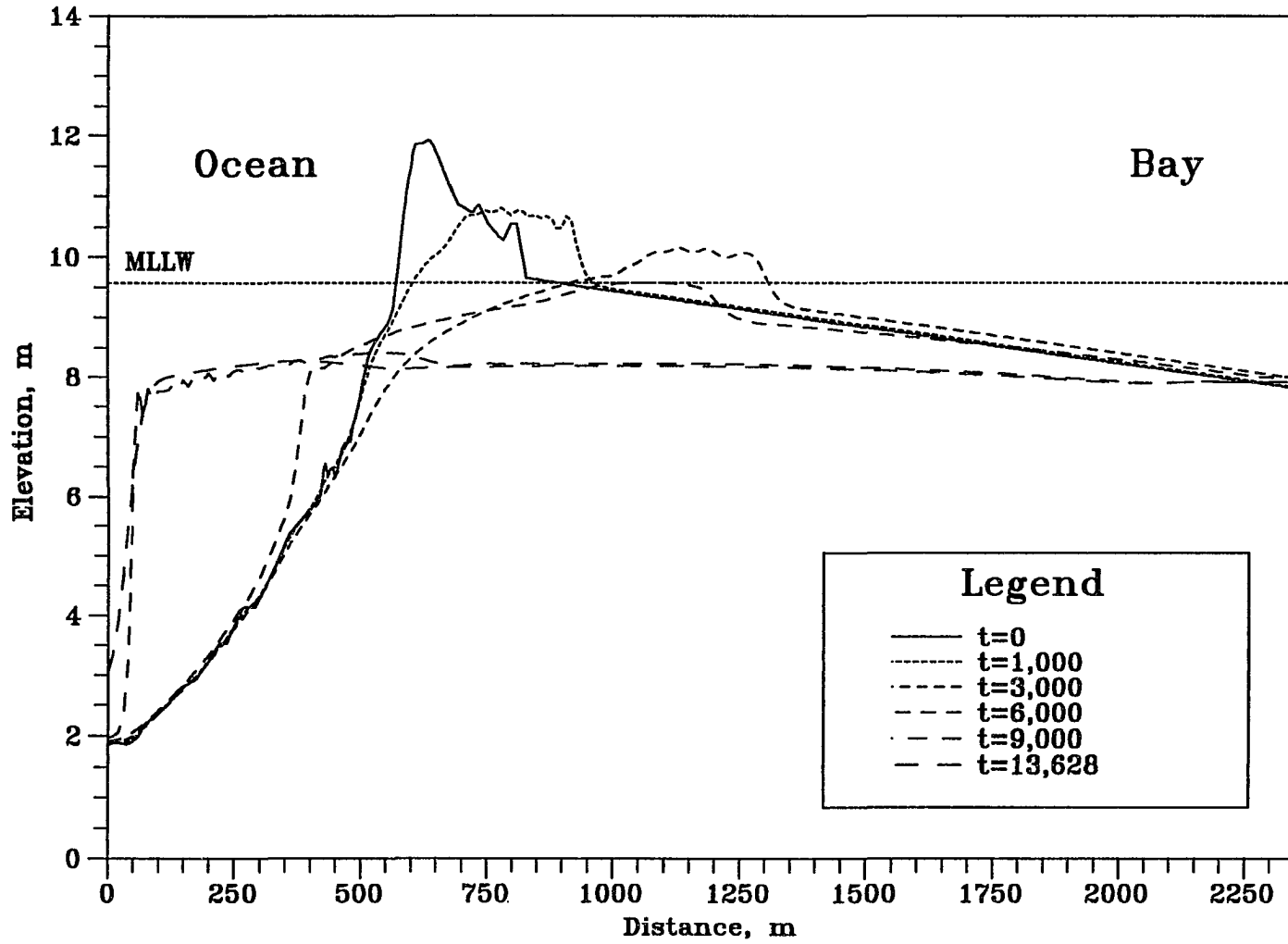


Figure 6.30 Bed Elevation Changes in Stage III/IV at t=0, 1000, 3000, 6000, 9000 and 13628. ($h_{om}=4.0m$, $h_{bm}=4.0m$, $t_{lag}=3hr$, $D_{50}=0.3mm$)

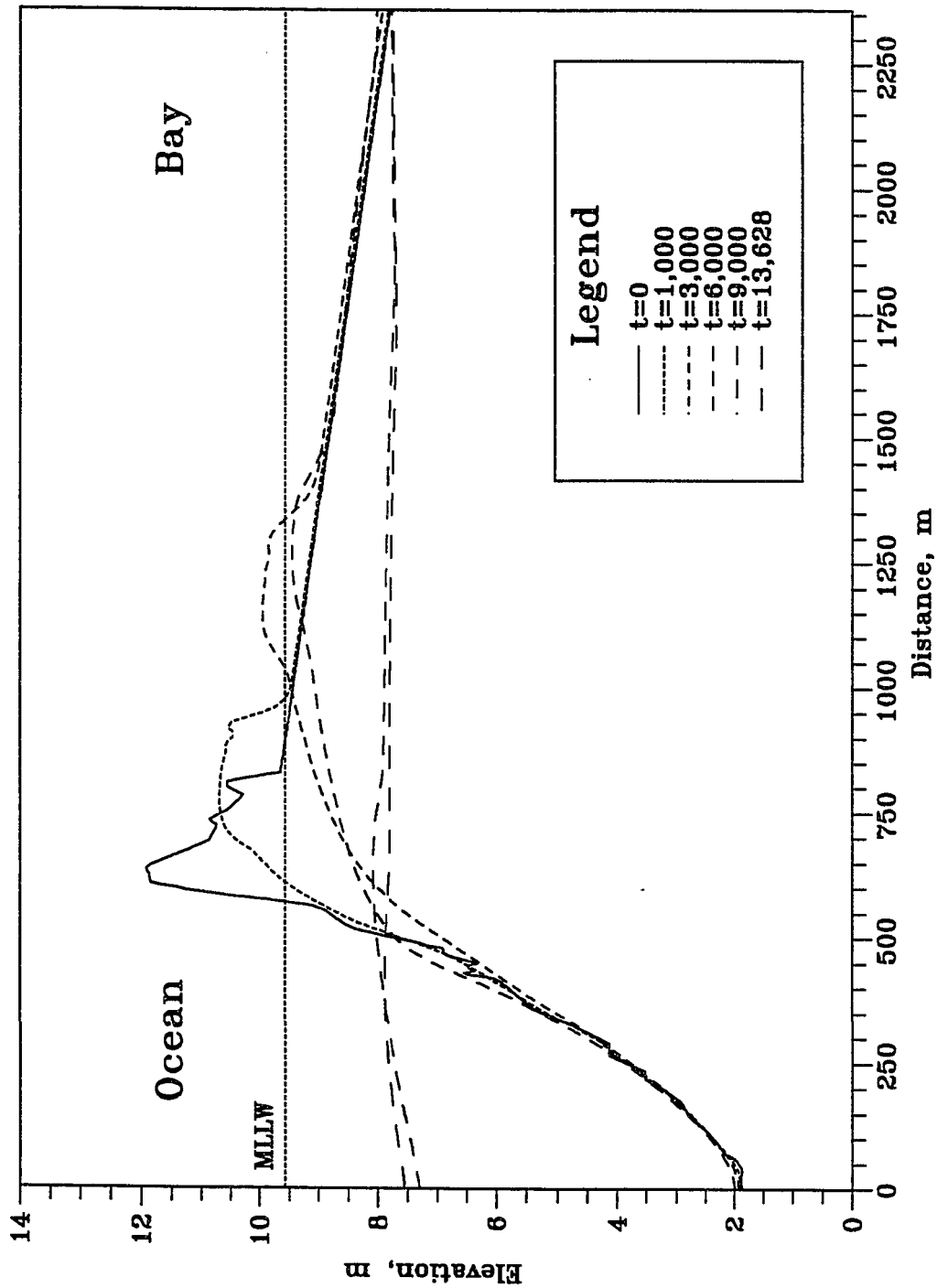


Figure 6.31 Bed Elevation Changes in Stage III/IV at t=0, 1000, 3000, 6000, 9000 and 13628. ($h_{om}=4.0\text{m}$, $h_{bm}=4.0\text{m}$, $t_{ag}=4\text{hr}$, $D_{50}=0.3\text{mm}$)

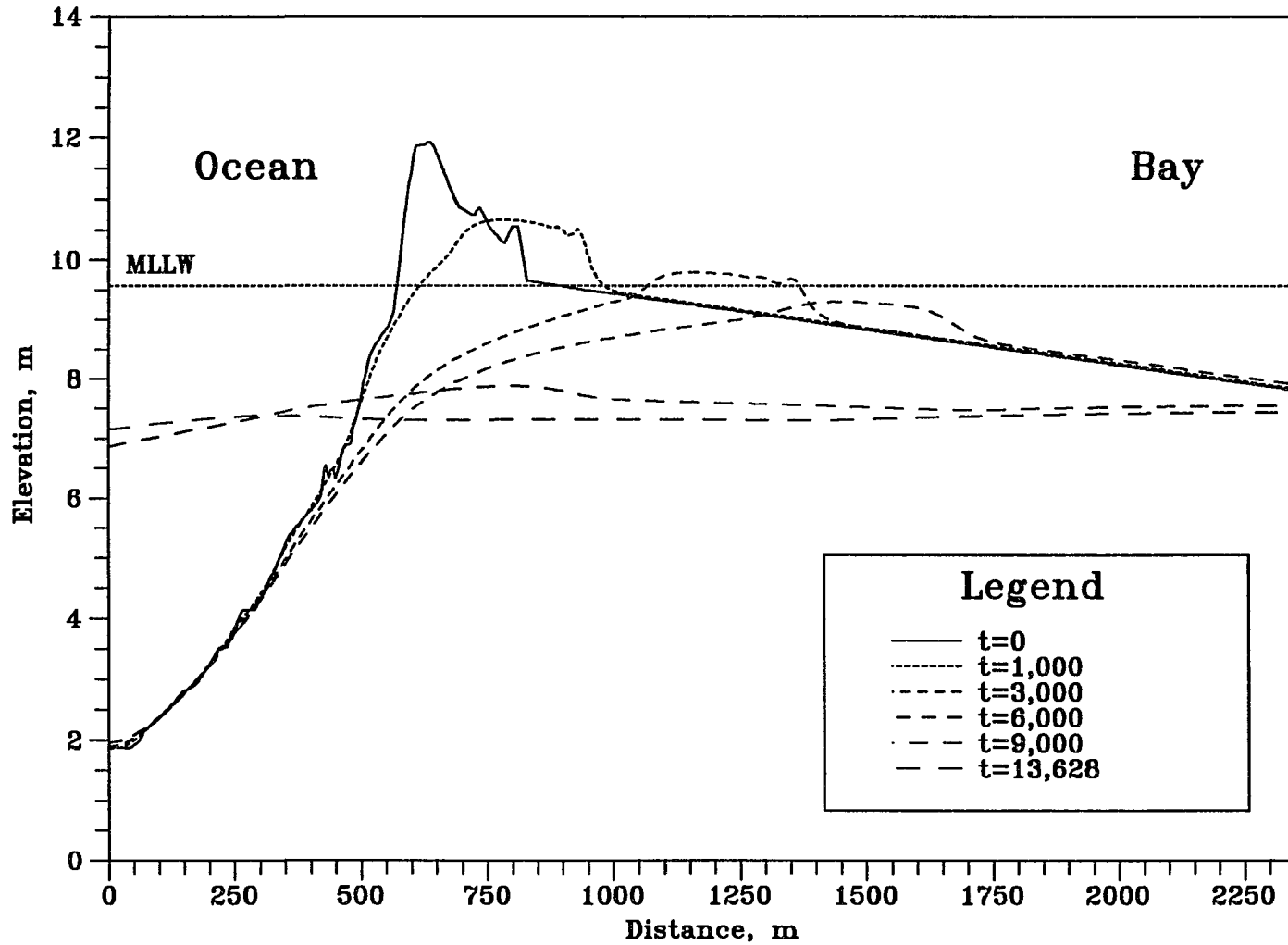


Figure 6.32 Bed Elevation Changes in Stage III/IV at t=0, 1000, 3000, 6000, 9000 and 13628. ($h_{om}=4.0\text{m}$, $h_{bm}=4.0\text{m}$, $t_{lag}=5\text{hr}$, $D_{50}=0.3\text{mm}$)

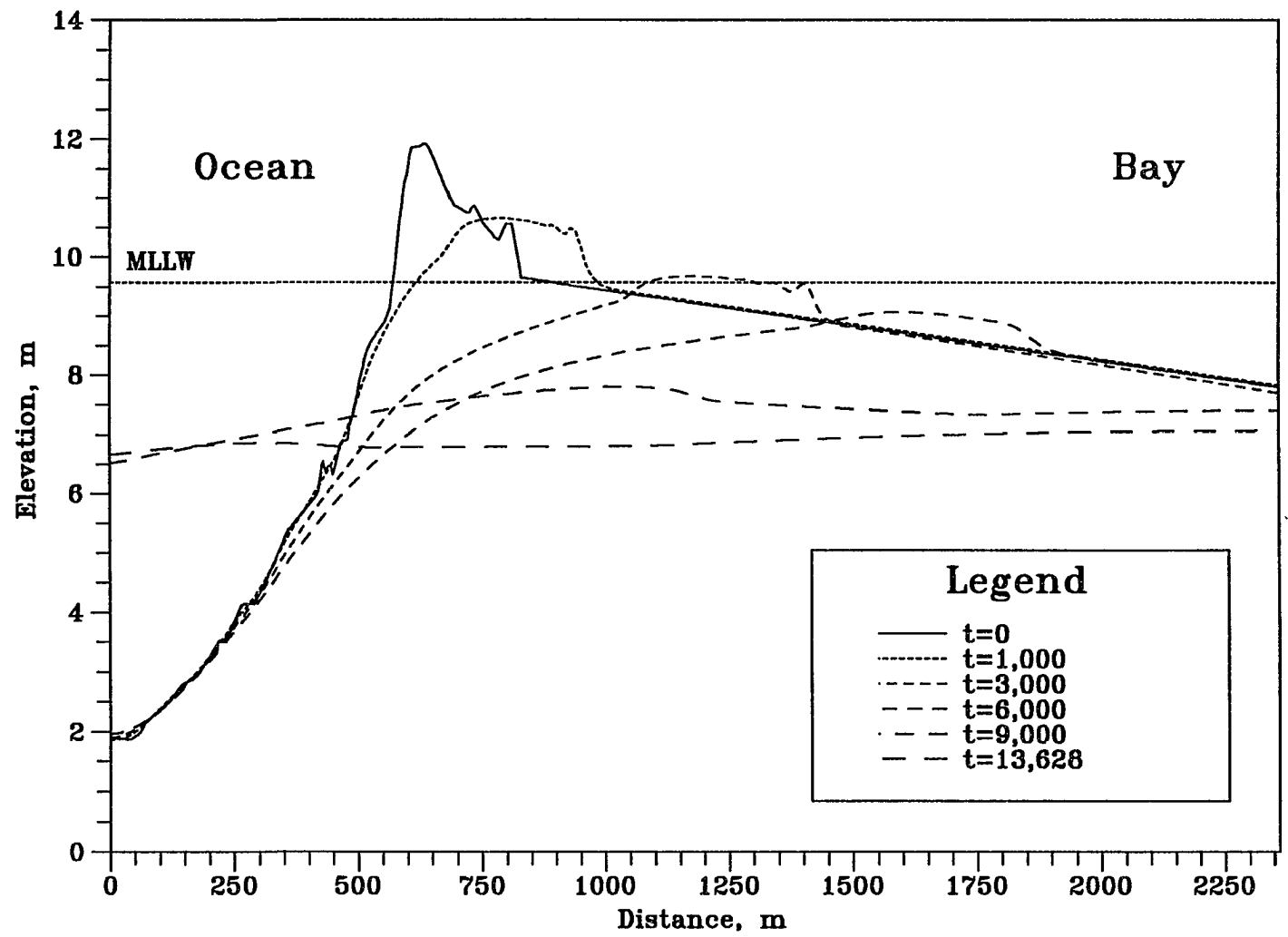


Figure 6.33 Bed Elevation Changes in Stage III/IV at t=0, 1000, 3000, 6000, 9000 and 13628. ($h_{om}=4.0m$, $h_{bm}=4.0m$, $t_{lag}=6hr$, $D_{50}=0.3mm$)

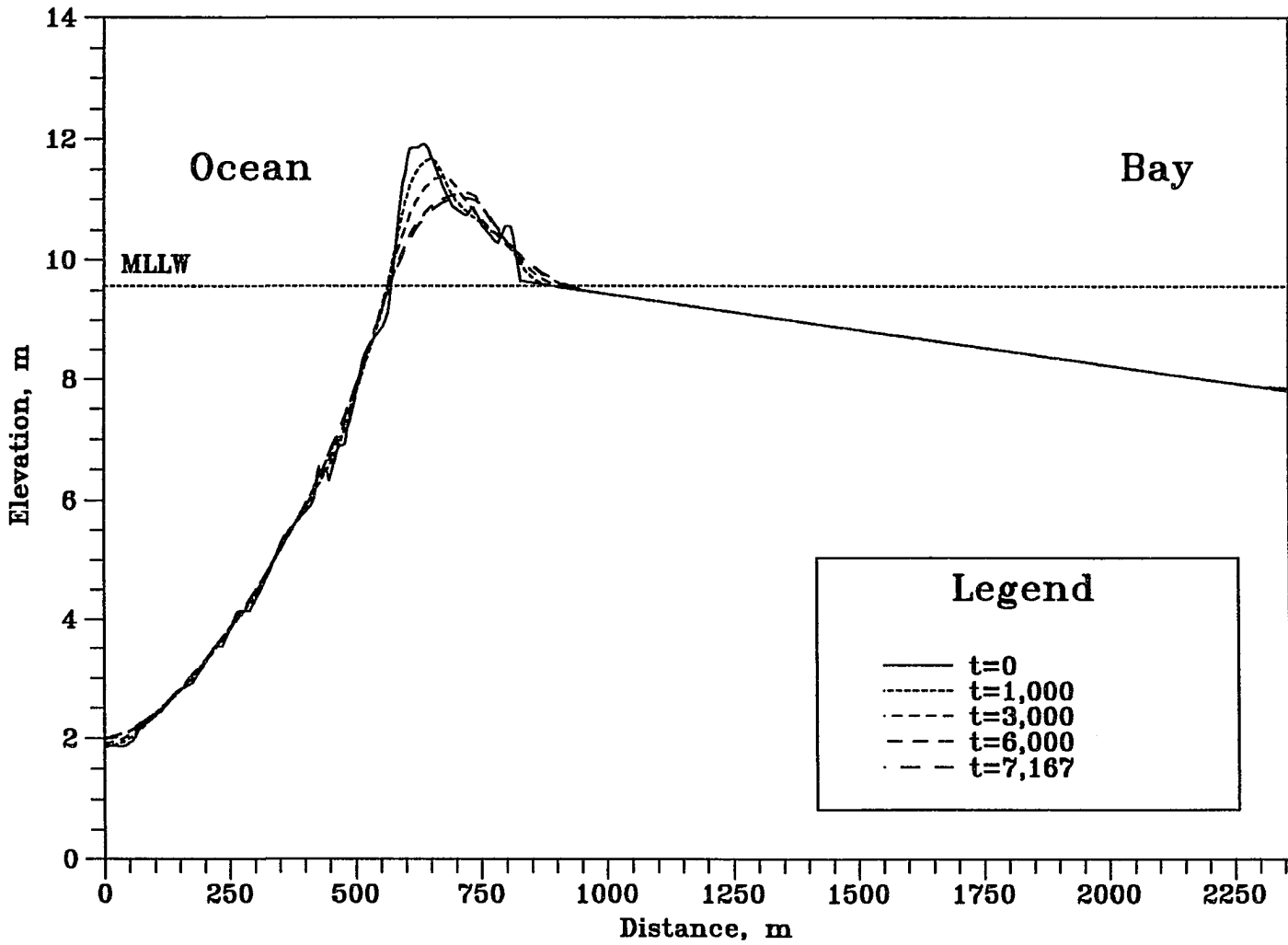


Figure 6.34 Bed Elevation Changes in Stage III/IV at t=0, 1000, 3000, 6000, and 7167. ($h_{om}=3.5m$, $h_{bm}=3.5m$, $t_{lag}=0hr$, $D_{50}=0.3mm$)

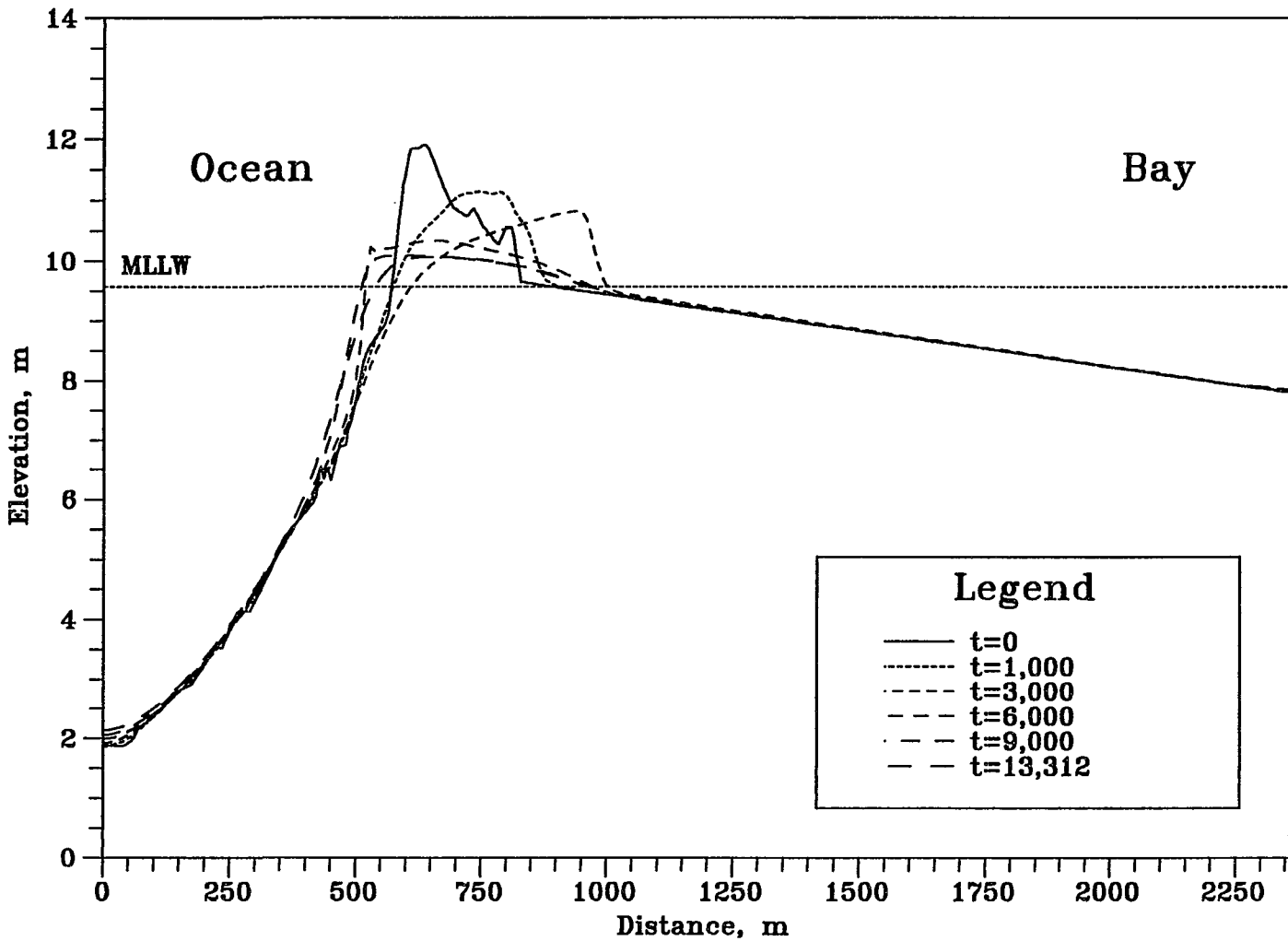


Figure 6.35 Bed Elevation Changes in Stage III/IV at $t=0, 1000, 3000, 6000, 9000$ and 13312 . ($h_{om}=3.5m, h_{bm}=3.5m, t_{lag}=1hr, D_{50}=0.3mm$)

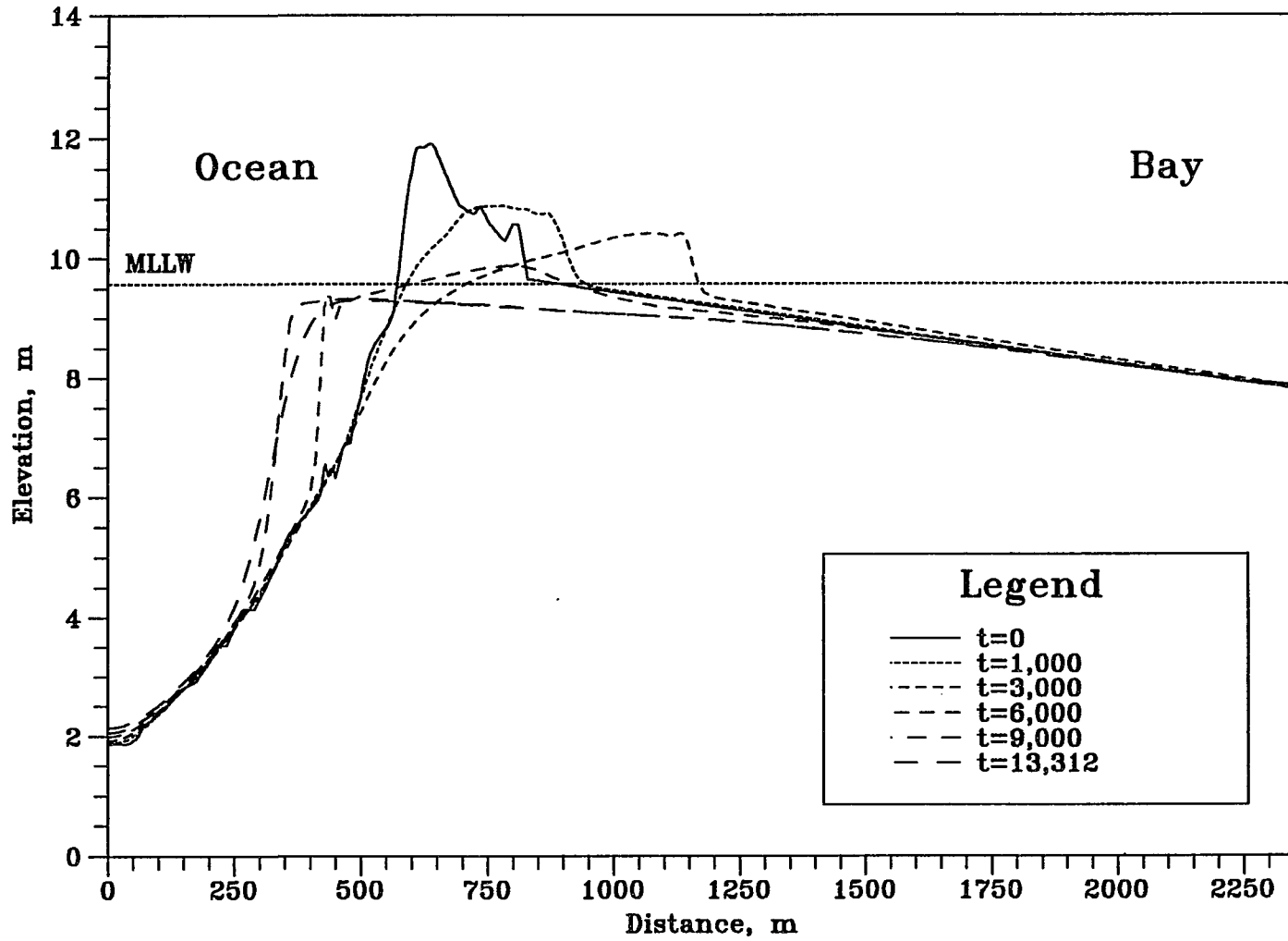


Figure 6.36 Bed Elevation Changes in Stage III/IV at t=0, 1000, 3000, 6000, 9000 and 13312. ($h_{om}=3.5m$, $h_{bm}=3.5m$, $t_{lag}=2hr$, $D_{50}=0.3mm$)

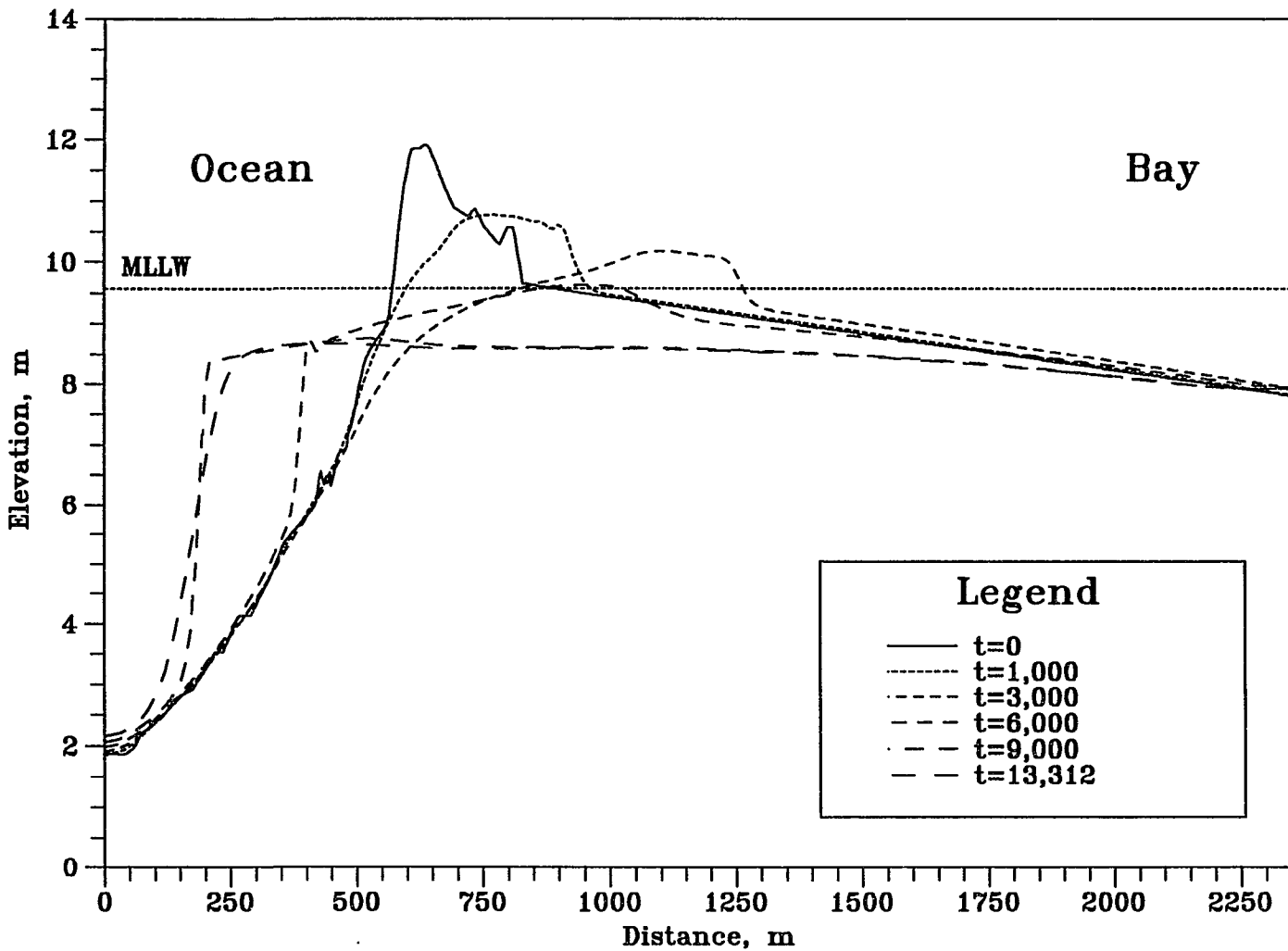


Figure 6.37 Bed Elevation Changes in Stage III/IV at t=0, 1000, 3000, 6000, 9000 and 13312. ($h_{om}=3.5m$, $h_{bm}=3.5m$, $t_{lag}=3hr$, $D_{50}=0.3mm$)

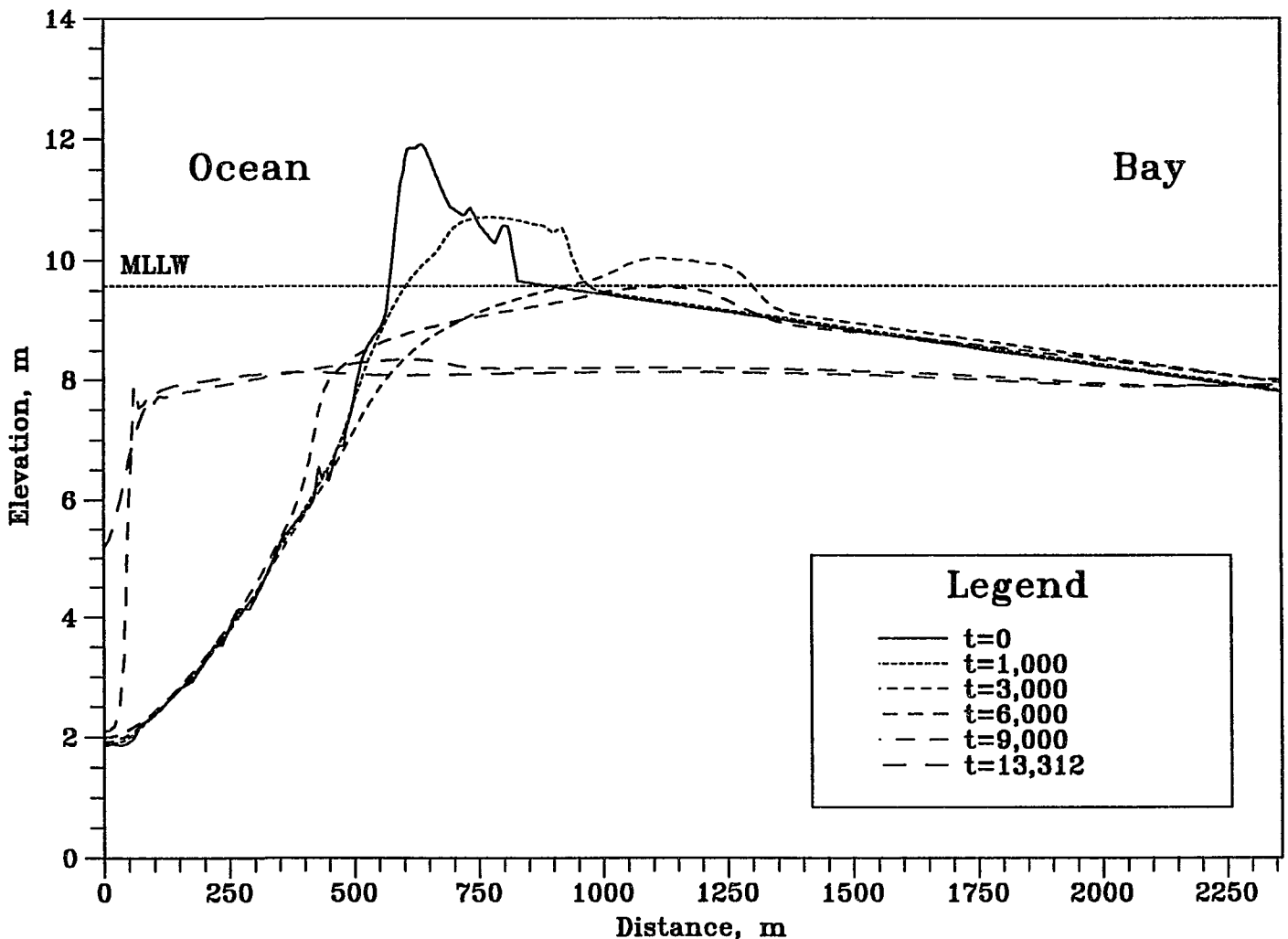


Figure 6.38 Bed Elevation Changes in Stage III/IV at t=0, 1000, 3000, 6000, 9000 and 13312. ($h_{om}=3.5m$, $h_{bm}=3.5m$, $t_{lag}=4hr$, $D_{50}=0.3mm$)

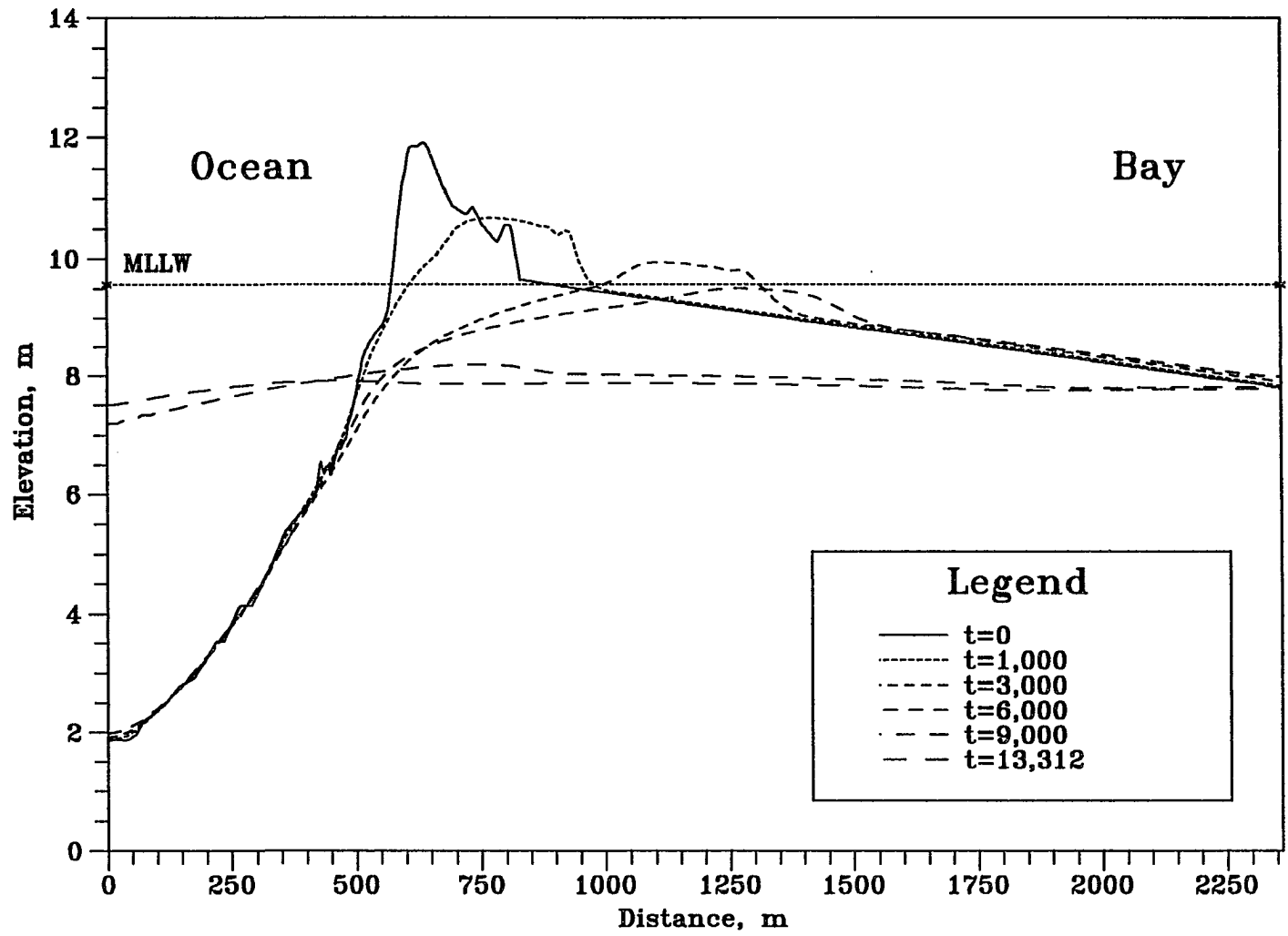


Figure 6.39 Bed Elevation Changes in Stage III/IV at t=0, 1000, 3000, 6000, 9000 and 13312. ($h_{om}=3.5m$, $h_{bm}=3.5m$, $t_{lag}=5hr$, $D_{50}=0.3mm$)

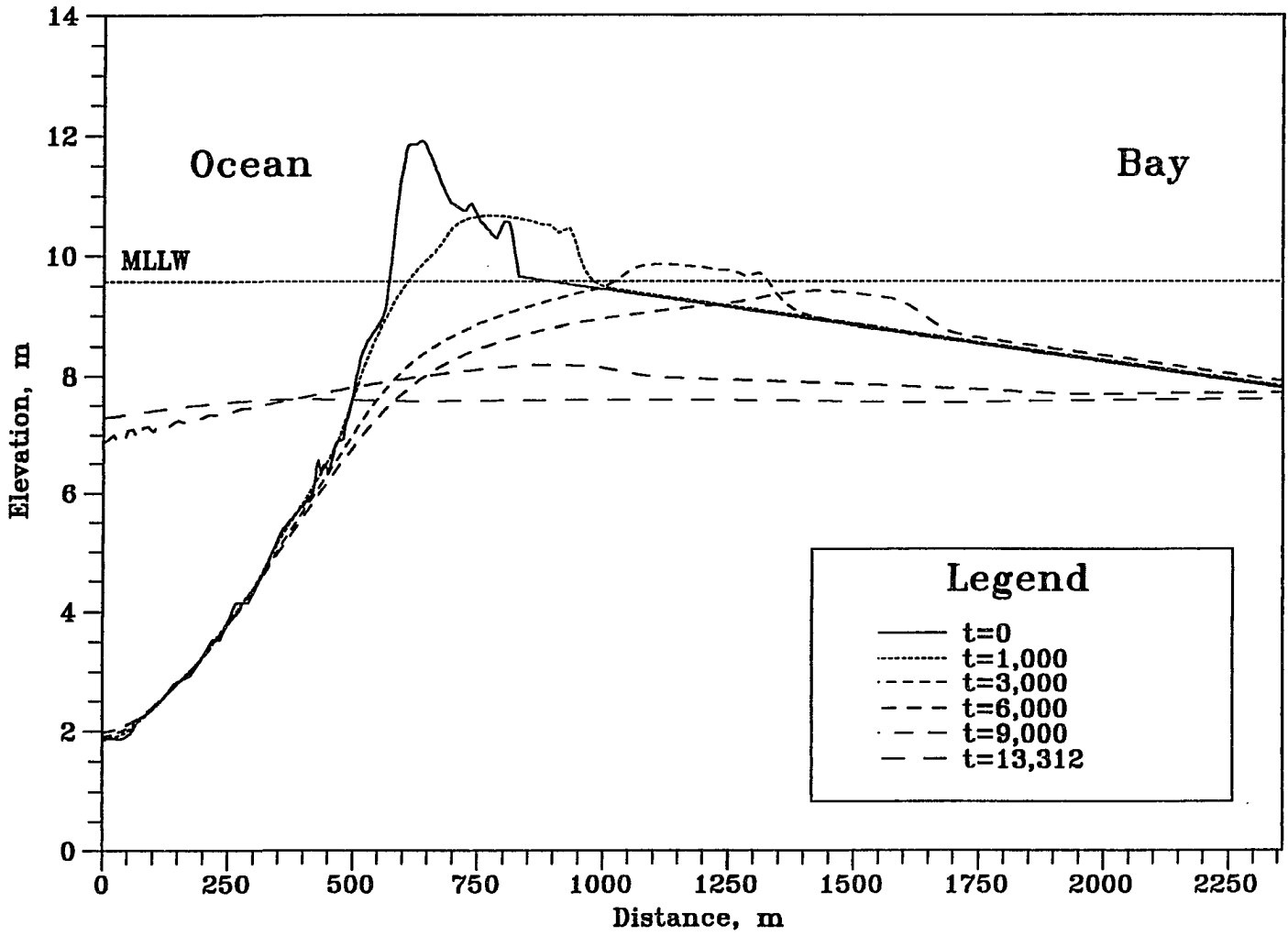


Figure 6.40 Bed Elevation Changes in Stage III/IV at t=0, 1000, 3000, 6000, 9000 and 13312. ($h_{om}=3.5m$, $h_{bm}=3.5m$, $t_{lag}=6hr$, $D_{50}=0.3mm$)

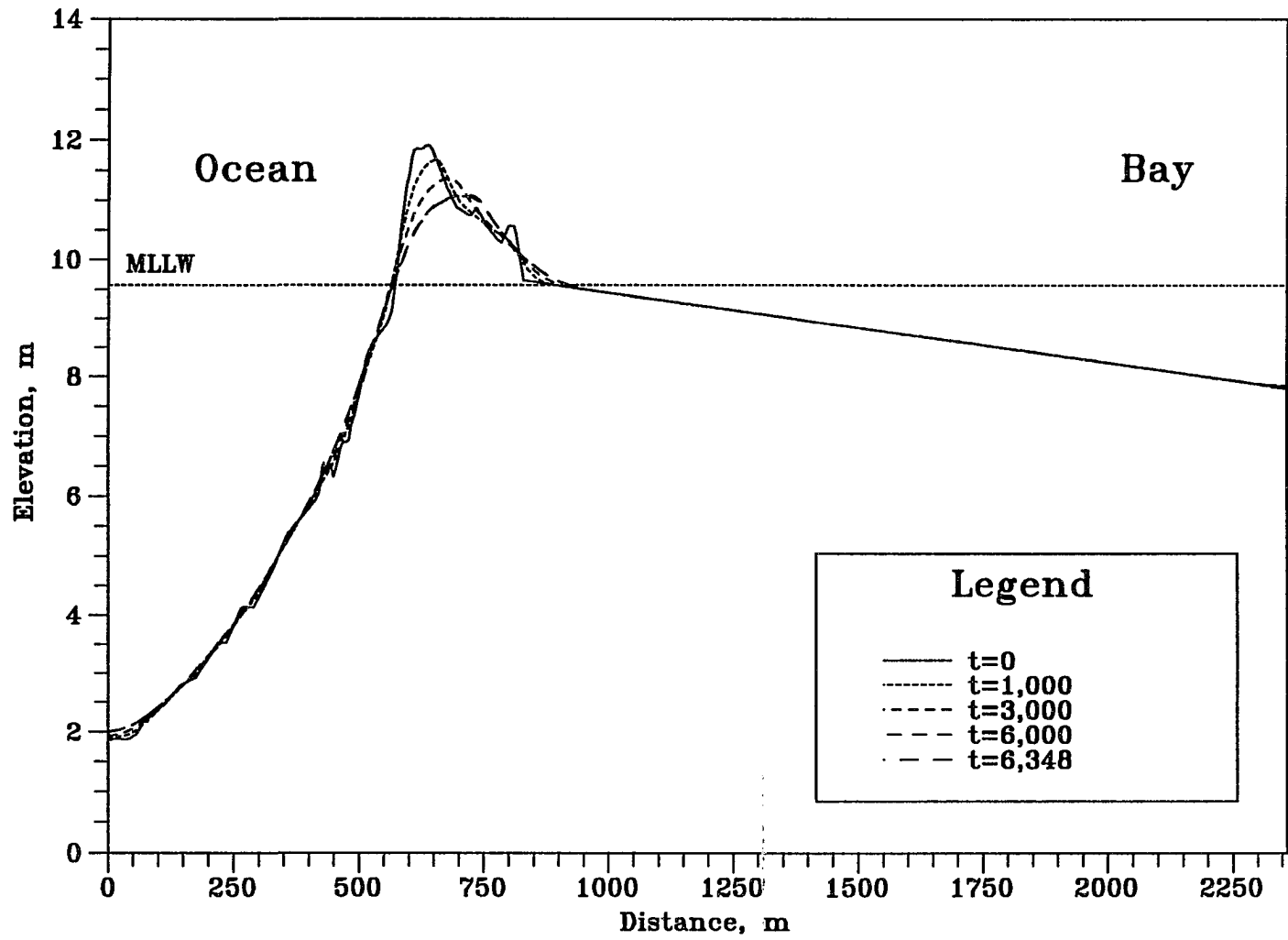


Figure 6.41 Bed Elevation Changes in Stage III/IV at t=0, 1000, 3000, 6000, and 6348. ($h_{om}=3.0m$, $h_{bm}=3.0m$, $t_{lag}=0hr$, $D_{50}=0.3mm$)

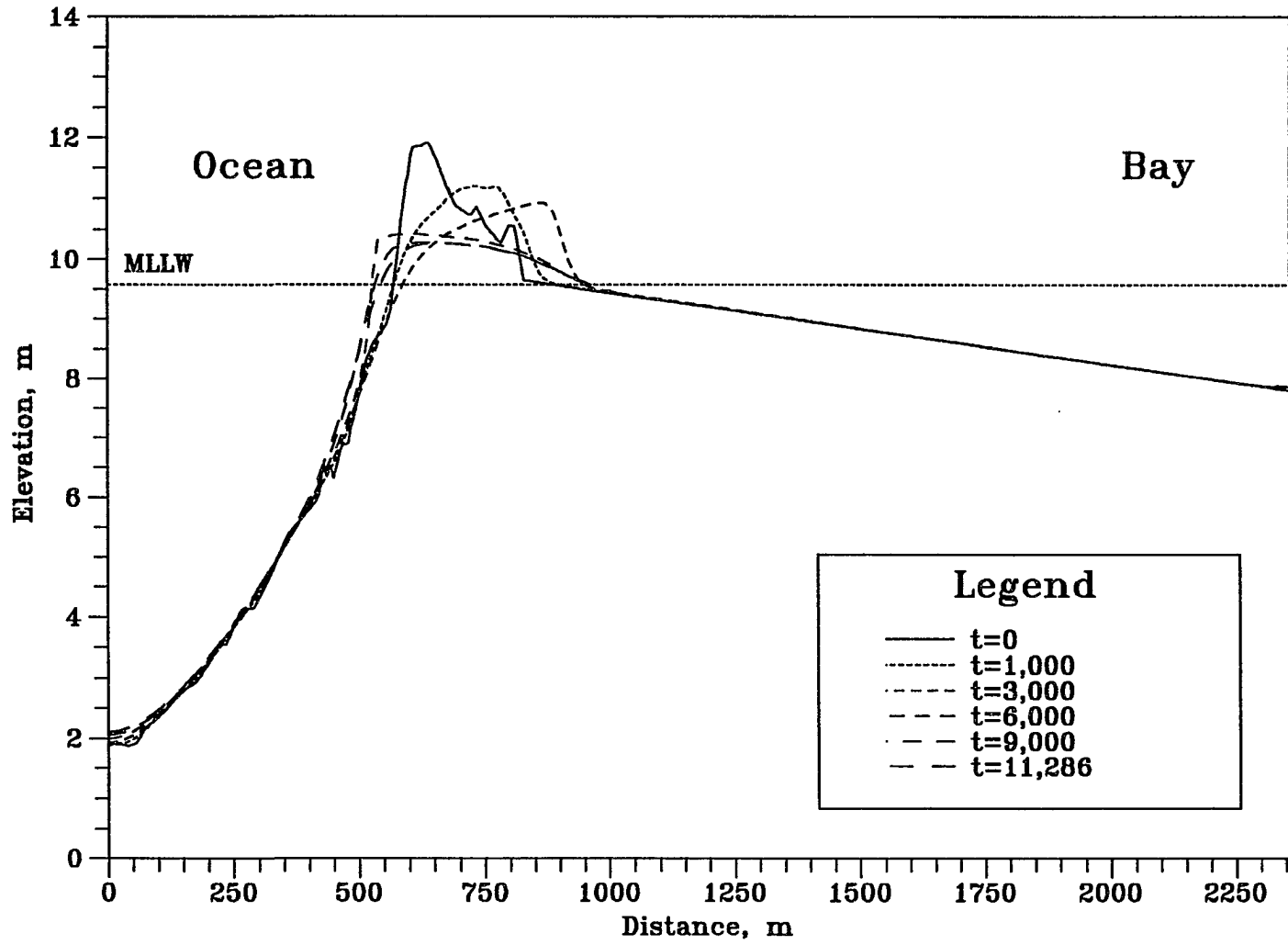


Figure 6.42 Bed Elevation Changes in Stage III/IV at t=0, 1000, 3000, 6000, 9000 and 11286. ($h_{om}=3.0m$, $h_{bm}=3.0m$, $t_{lag}=1hr$, $D_{50}=0.3mm$)

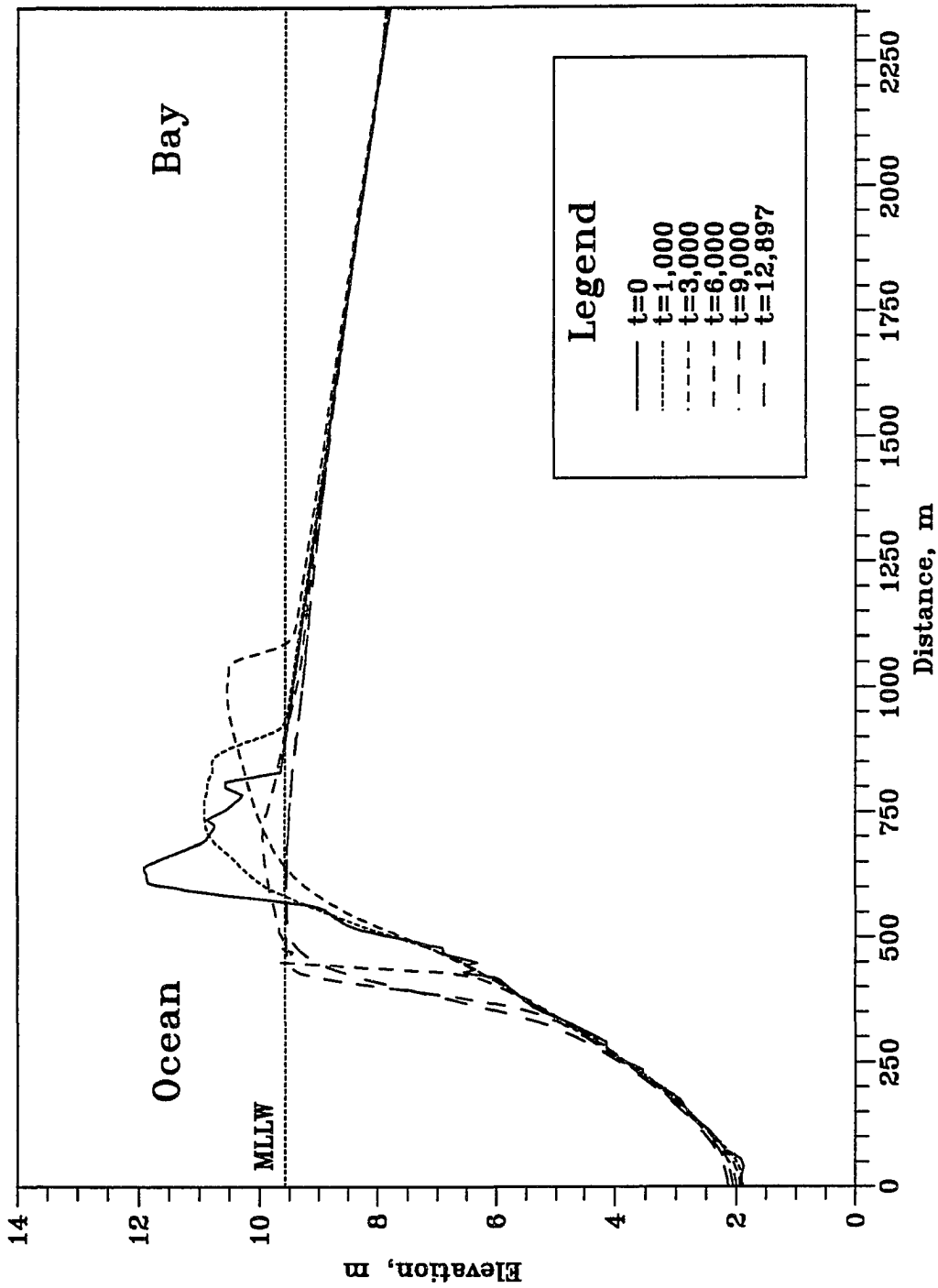


Figure 6.43 Bed Elevation Changes in Stage III/IV at t=0, 1000, 3000, 6000, 9000 and 12897. ($h_{om}=3.0m$, $h_{bm}=3.0m$, $t_{lag}=2hr$, $D_{50}=0.3mm$)

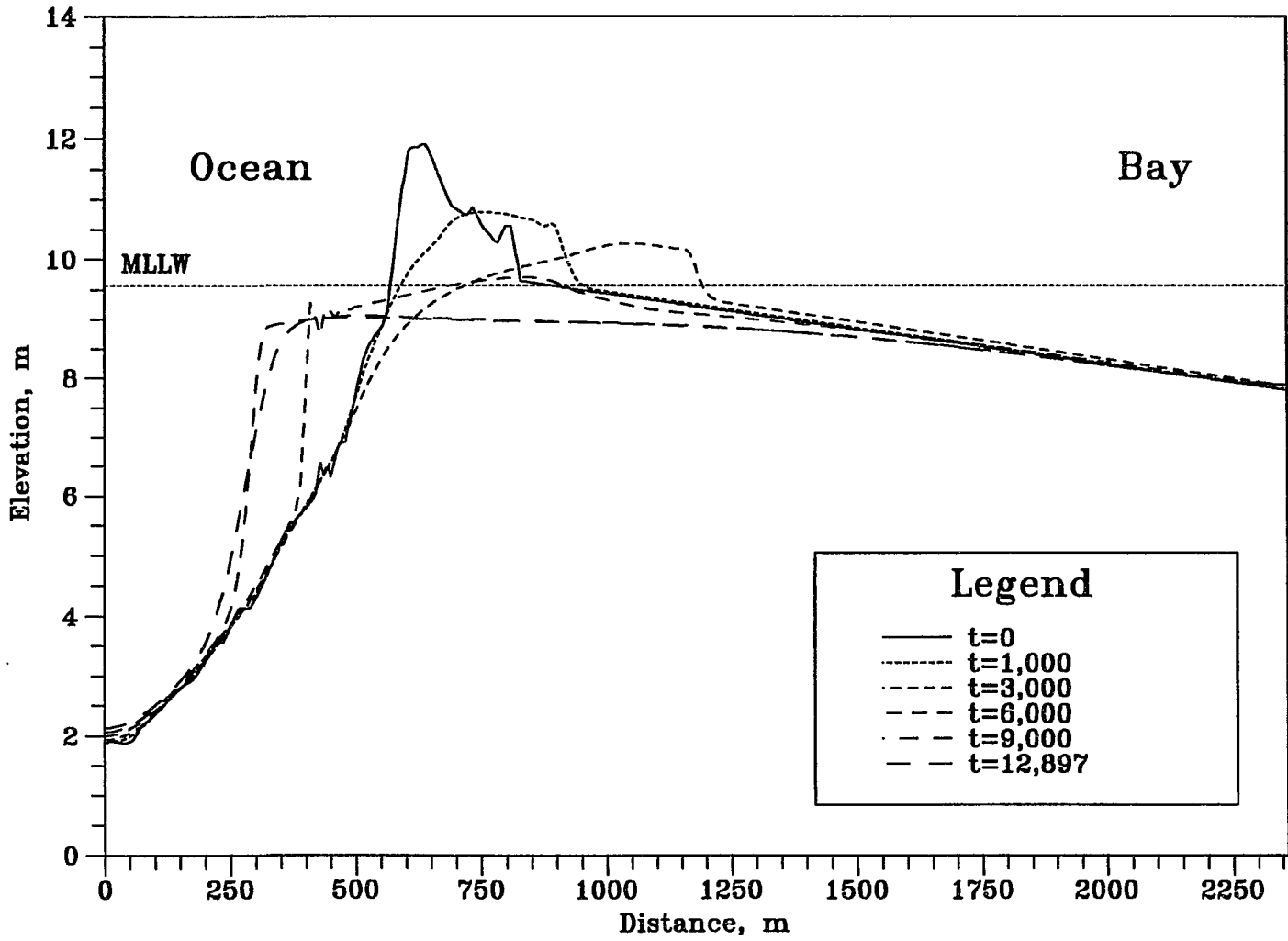


Figure 6.44 Bed Elevation Changes in Stage III/IV at t=0, 1000, 3000, 6000, 9000 and 12897. ($h_{om}=3.0m$, $h_{bm}=3.0m$, $t_{lag}=3hr$, $D_{50}=0.3mm$)

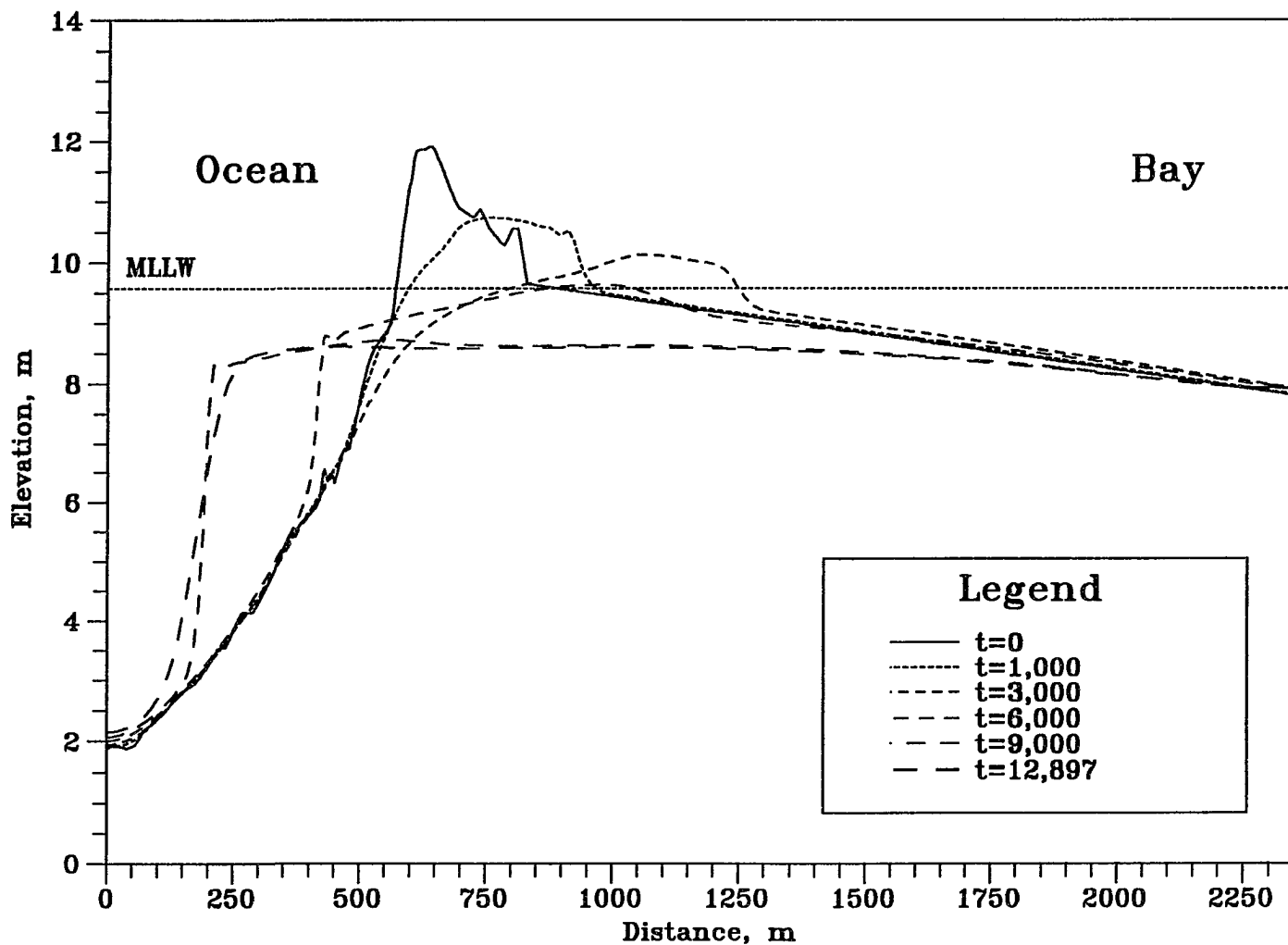


Figure 6.45 Bed Elevation Changes in Stage III/IV at $t=0, 1000, 3000, 6000, 9000$ and 12897 . ($h_{om}=3.0m, h_{bm}=3.0m, t_{lag}=4hr, D_{50}=0.3mm$)

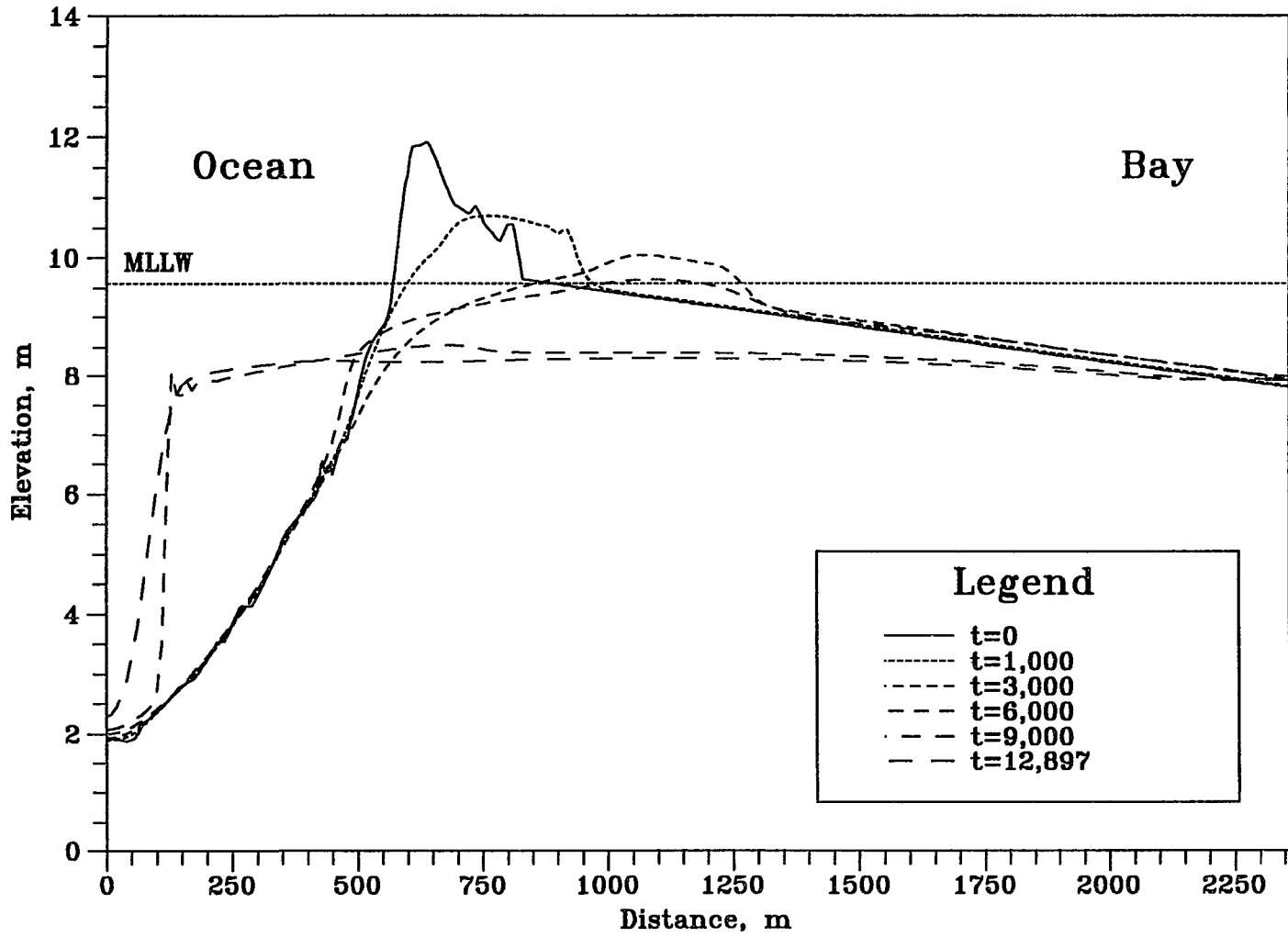


Figure 6.46 Bed Elevation Changes in Stage III/IV at t=0, 1000, 3000, 6000, 9000 and 12897. ($h_{om}=3.0m$, $h_{bm}=3.0m$, $t_{lag}=5hr$, $D_{50}=0.3mm$)

200

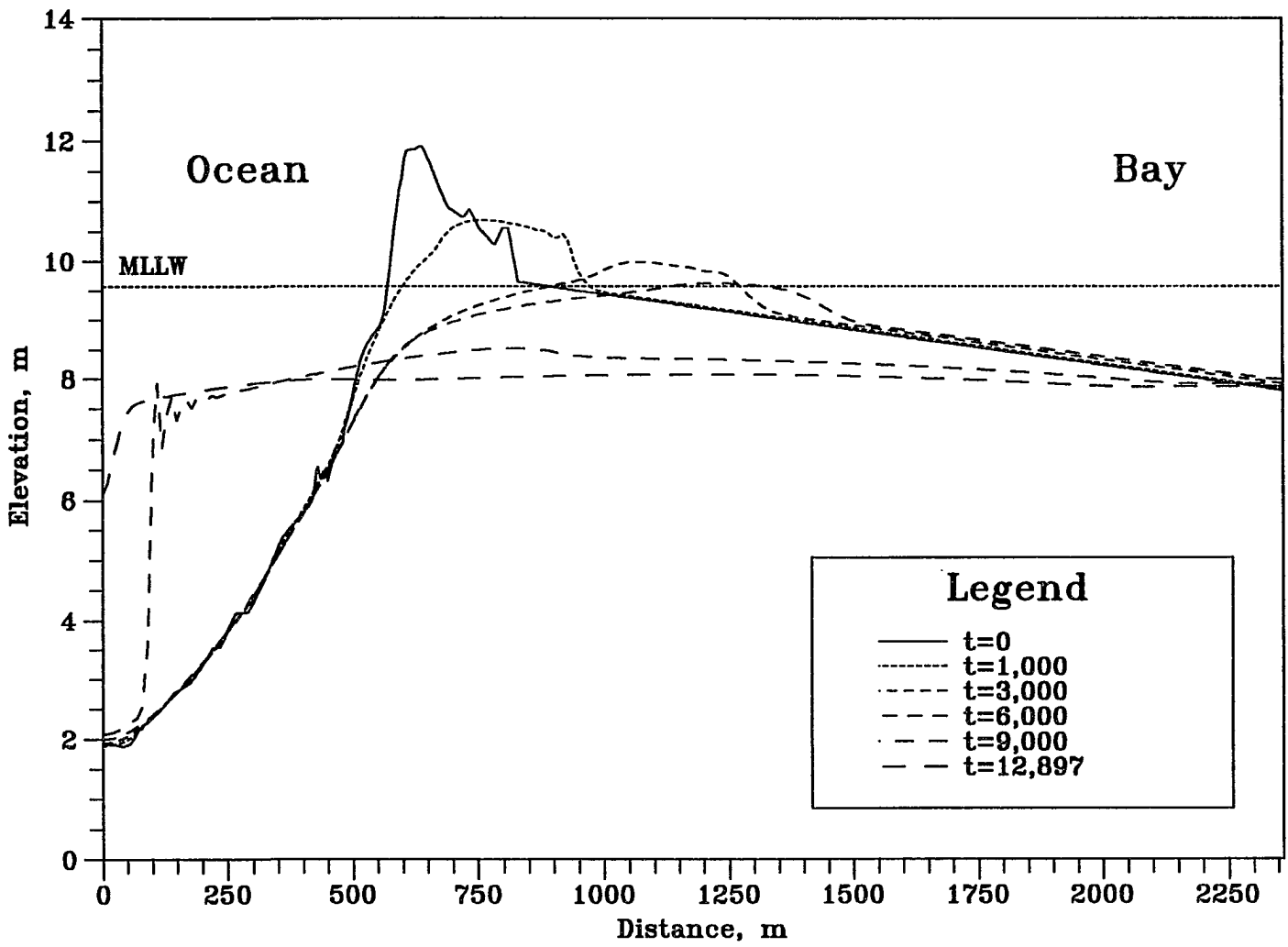


Figure 6.47 Bed Elevation Changes in Stage III/IV at t=0, 1000, 3000, 6000, 9000 and 12897. ($h_{om}=3.0m$, $h_{bm}=3.0m$, $t_{lag}=6hr$, $D_{50}=0.3mm$)

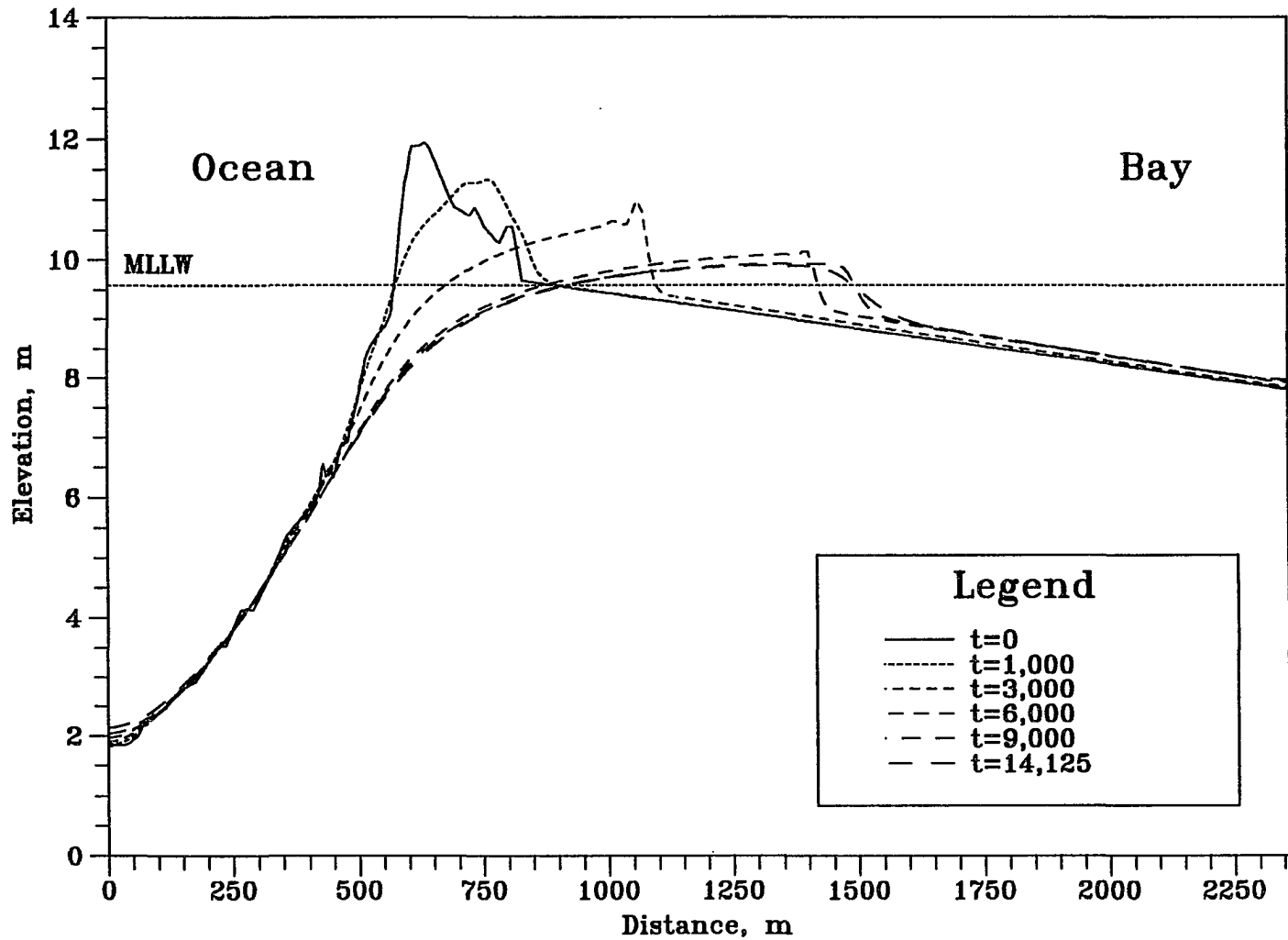


Figure 6.48 Bed Elevation Changes in Stage III/IV at t=0, 1000, 3000, 6000, 9000 and 14125. ($h_{om}=5.0m$, $h_{bm}=4.0m$, $t_{lag}=0hr$, $D_{50}=0.3mm$)

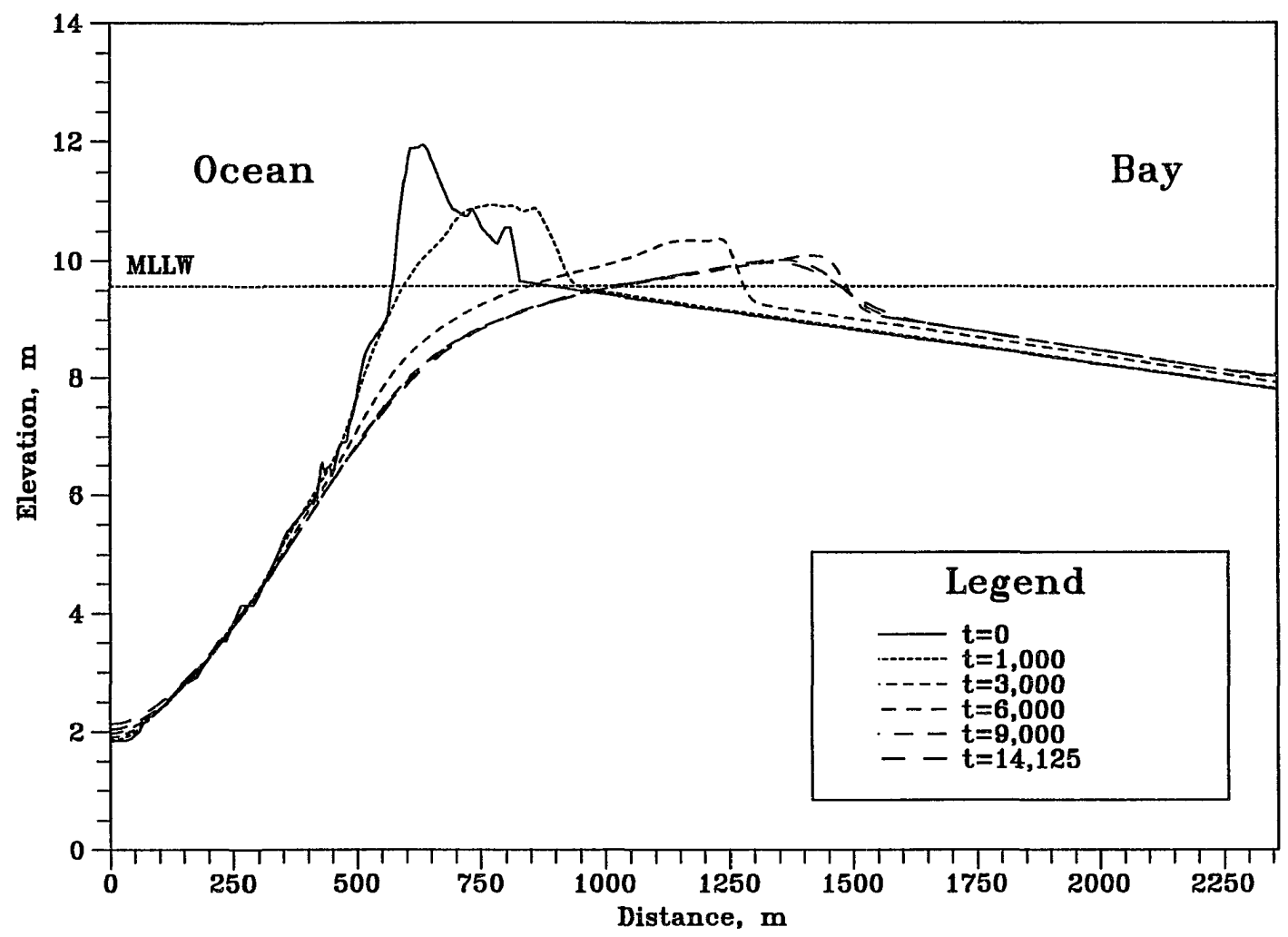


Figure 6.49 Bed Elevation Changes in Stage III/IV at t=0, 1000, 3000, 6000, 9000 and 14125. ($h_{om}=5.0m$, $h_{bm}=4.0m$, $t_{lag}=1hr$, $D_{50}=0.3mm$)

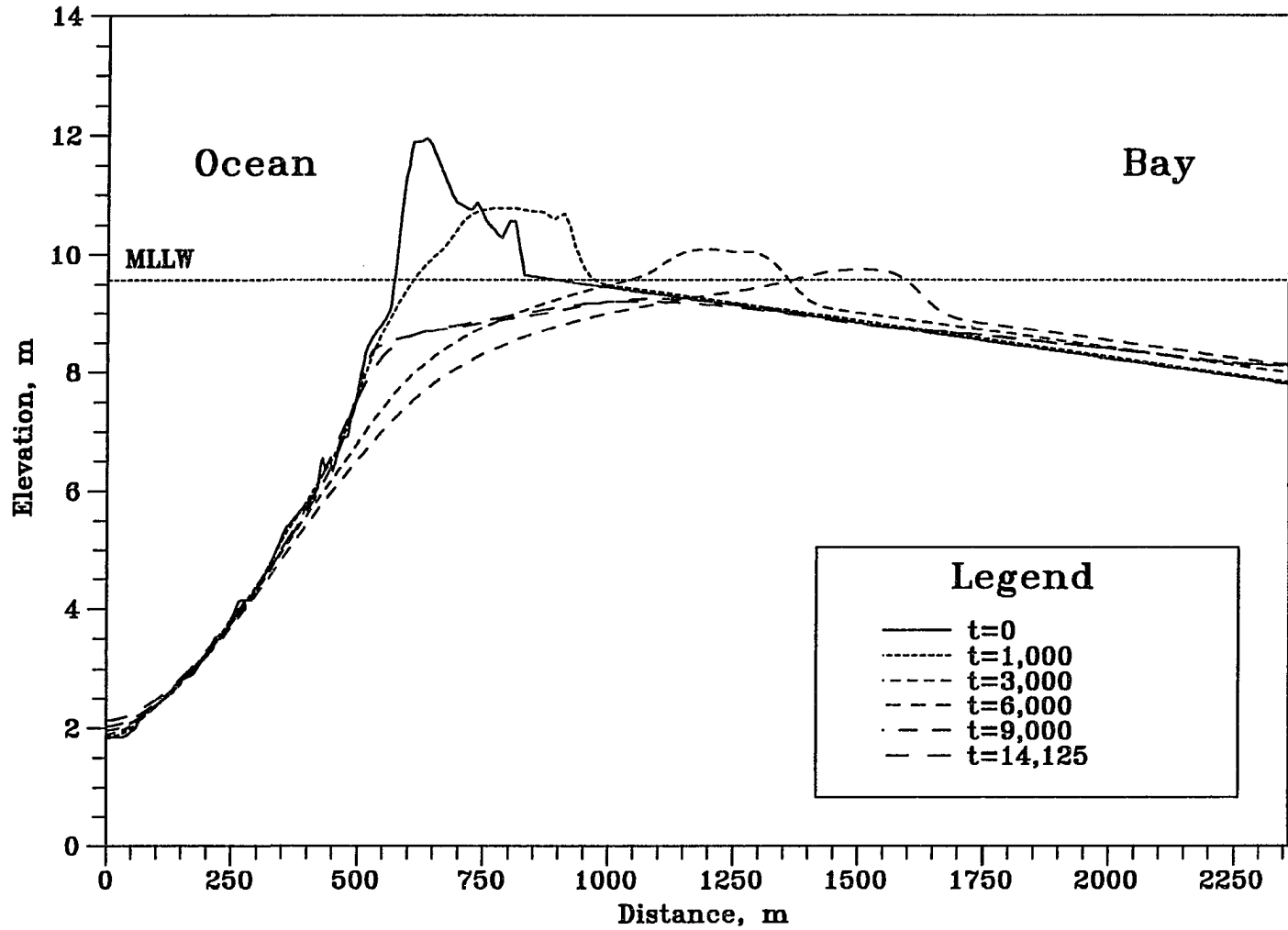


Figure 6.50 Bed Elevation Changes in Stage III/IV at $t=0, 1000, 3000, 6000, 9000$ and 14125 . ($h_{om}=5.0m, h_{bm}=4.0m, t_{lag}=2hr, D_{50}=0.3mm$)

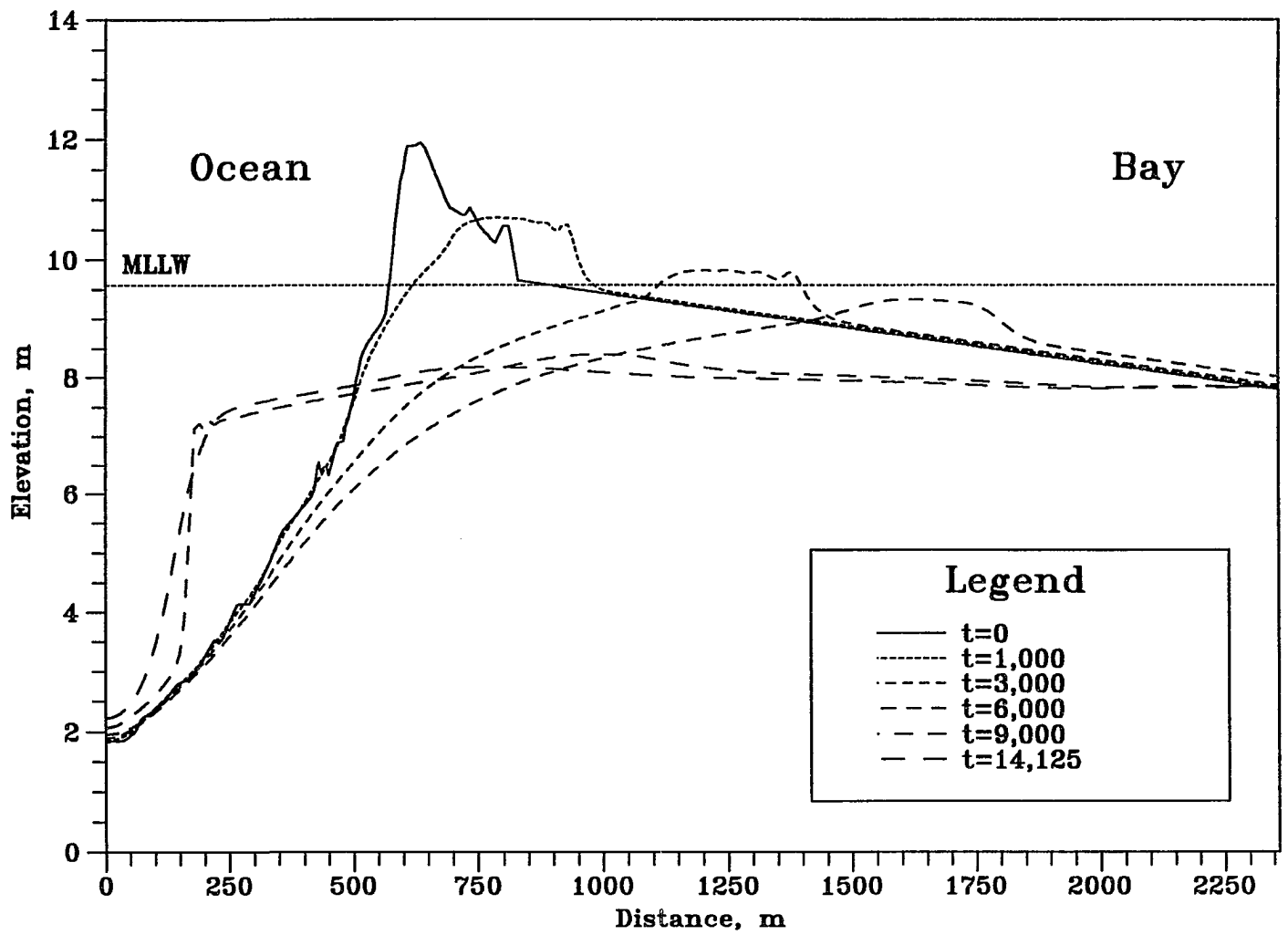


Figure 6.51 Bed Elevation Changes in Stage III/IV at t=0, 1000, 3000, 6000, 9000 and 14125. ($h_{om}=5.0m$, $h_{bm}=4.0m$, $t_{lag}=3hr$, $D_{50}=0.3mm$)

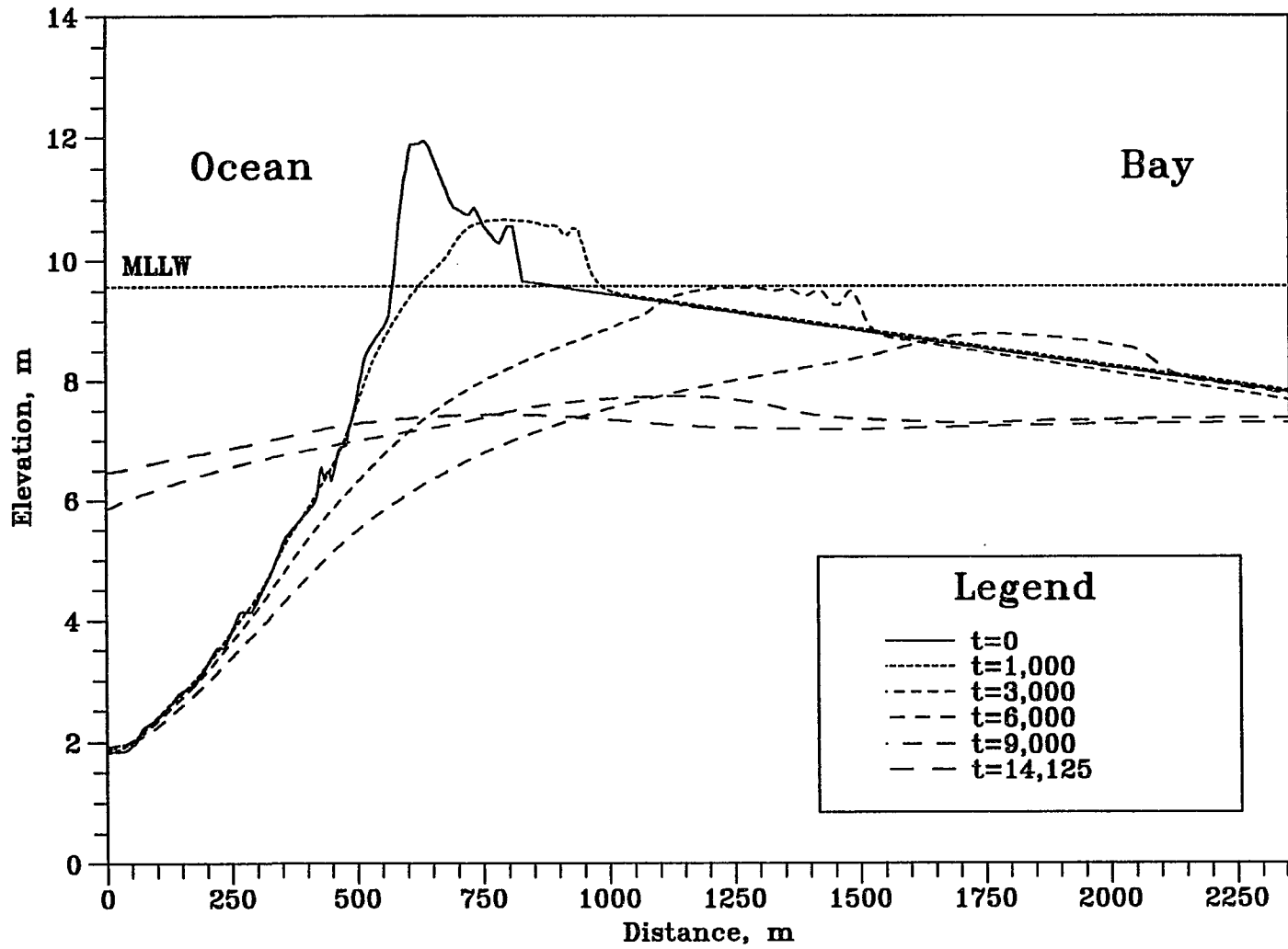


Figure 6.52 Bed Elevation Changes in Stage III/IV at t=0, 1000, 3000, 6000, 9000 and 14125. ($h_{om}=5.0m$, $h_{bm}=4.0m$, $t_{lag}=4hr$, $D_{50}=0.3mm$)

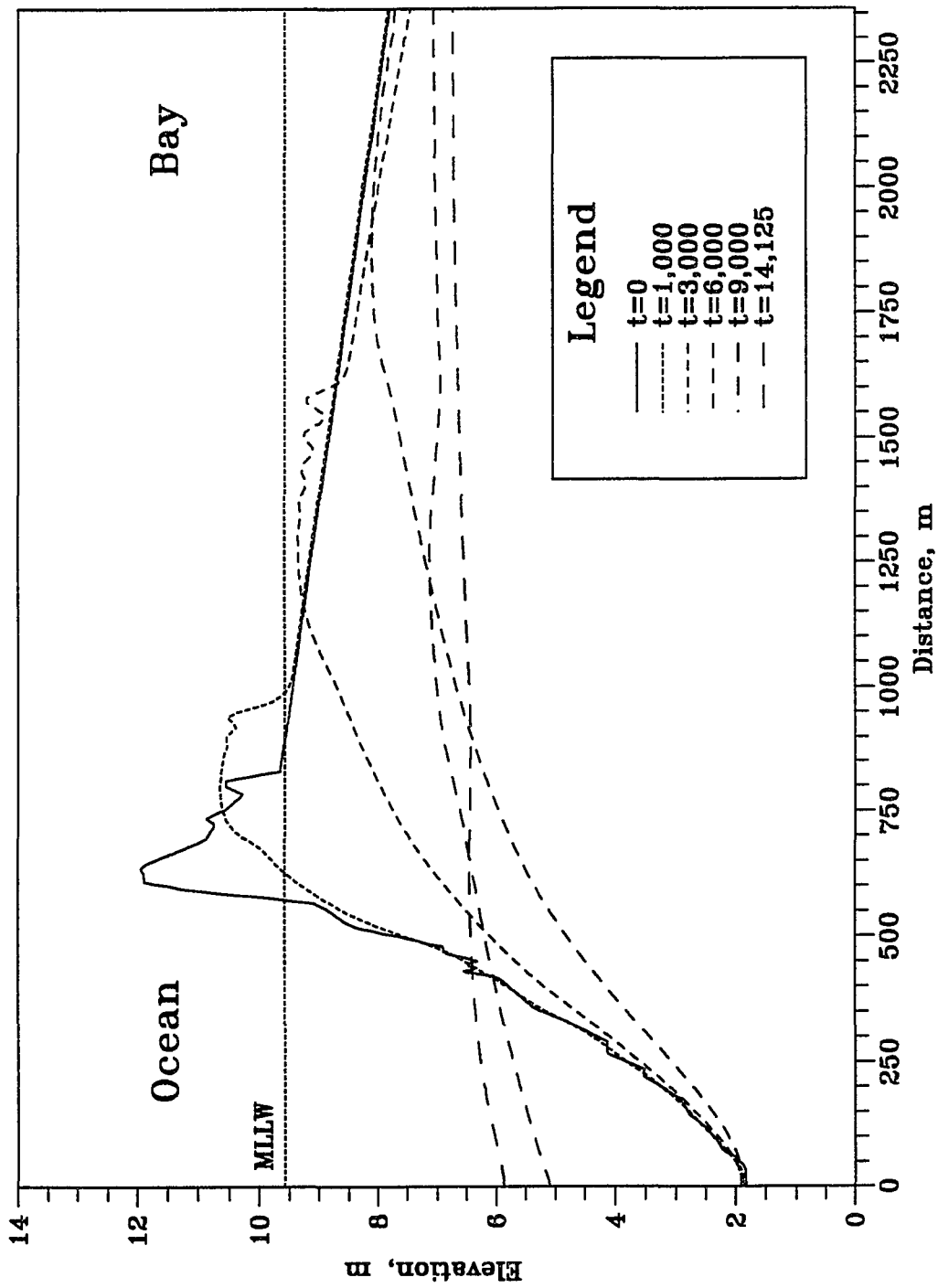


Figure 6.53 Bed Elevation Changes in Stage III/IV at $t=0, 1000, 3000, 6000, 9000$ and 14125 . ($h_{om}=5.0m, h_{bm}=4.0m, t_{lag}=5hr, D_{co}=0.3mm$)

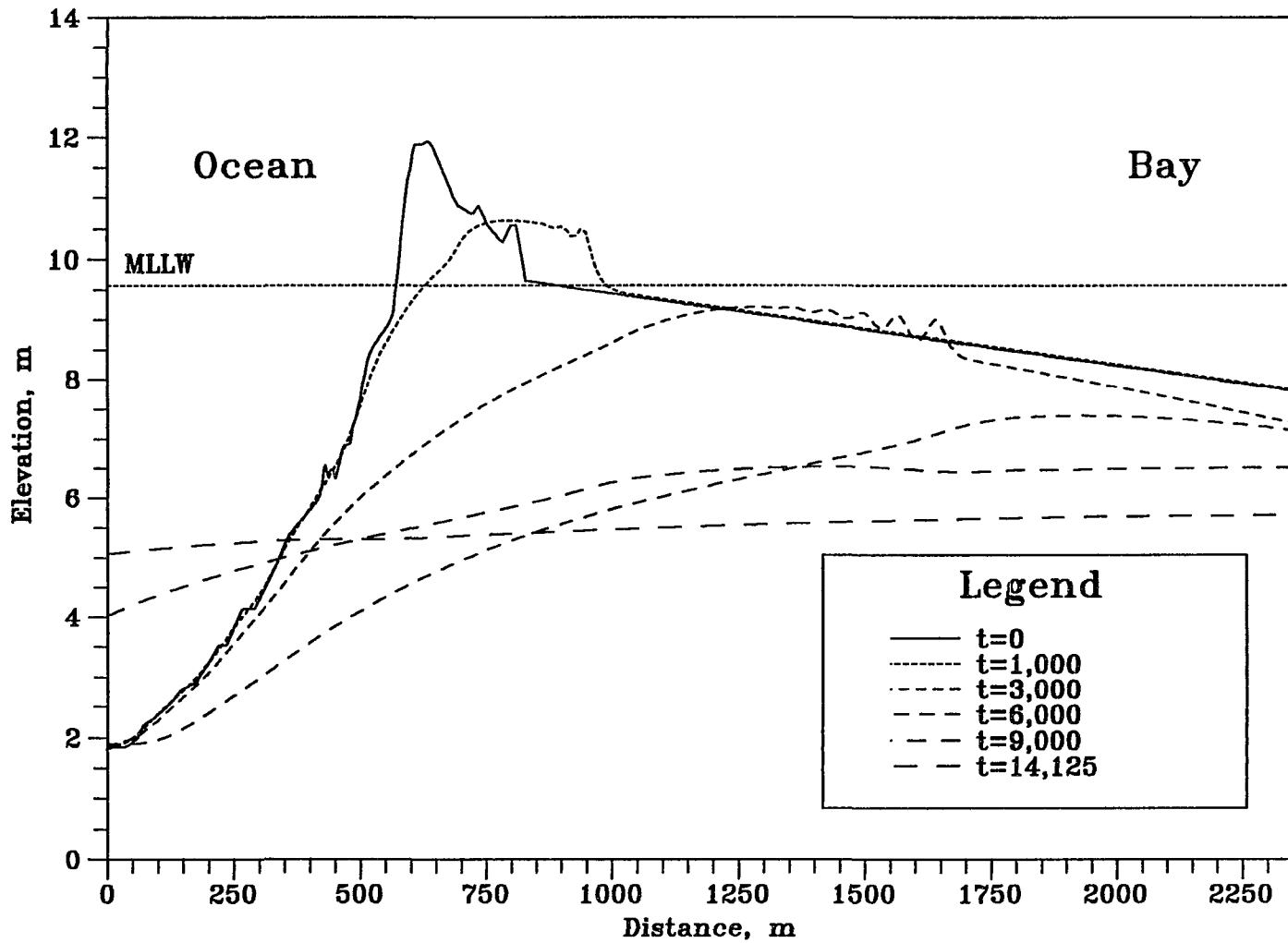


Figure 6.54 Bed Elevation Changes in Stage III/IV at t=0, 1000, 3000, 6000, 9000 and 14125. ($h_{om}=5.0m$, $h_{bm}=4.0m$, $t_{lag}=6hr$, $D_{50}=0.3mm$)

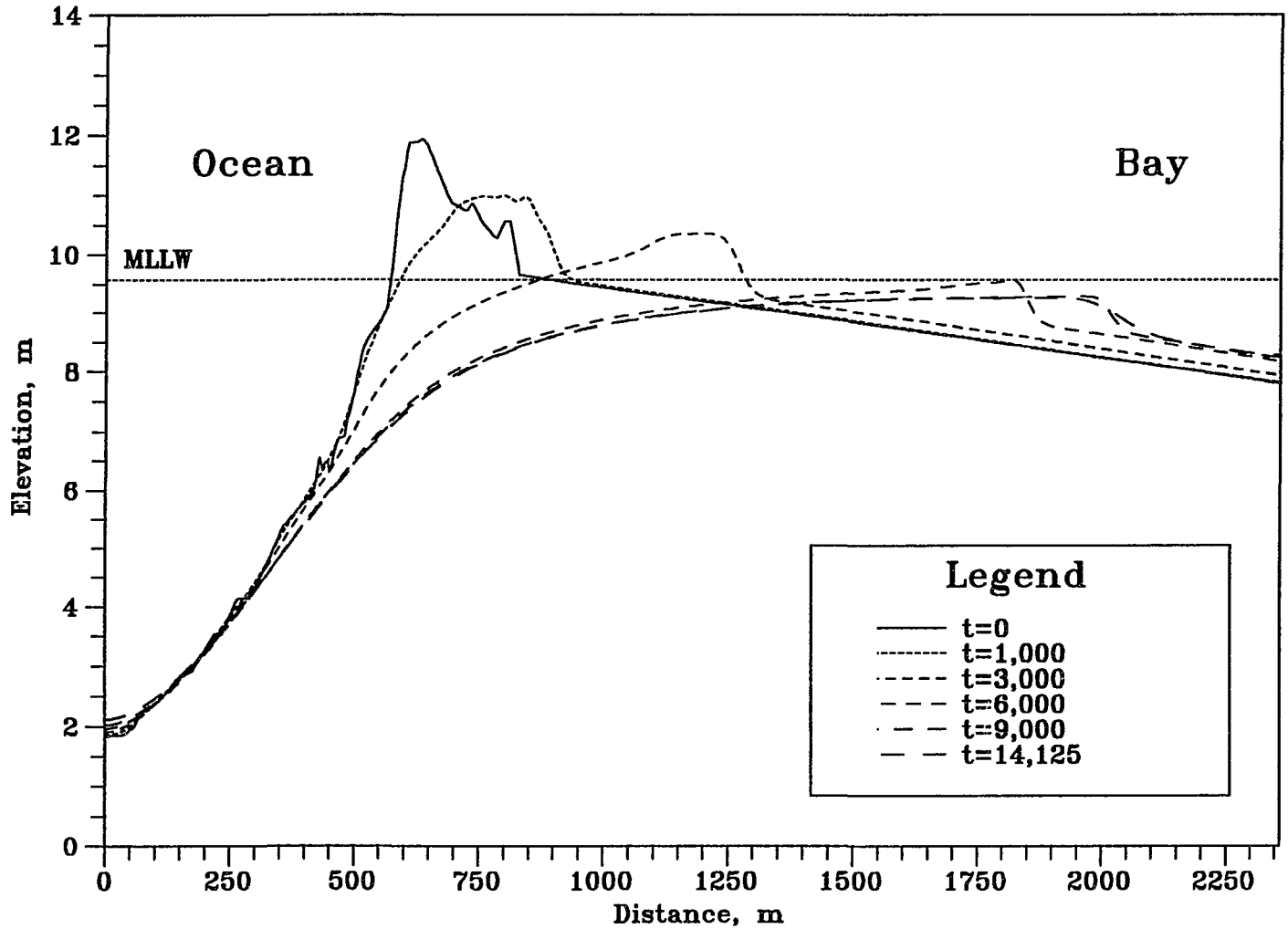


Figure 6.55 Bed Elevation Changes in Stage III/IV at t=0, 1000, 3000, 6000, 9000 and 14125. ($h_{om}=5.0m$, $h_{bm}=3.0m$, $t_{lag}=0hr$, $D_{50}=0.3mm$)

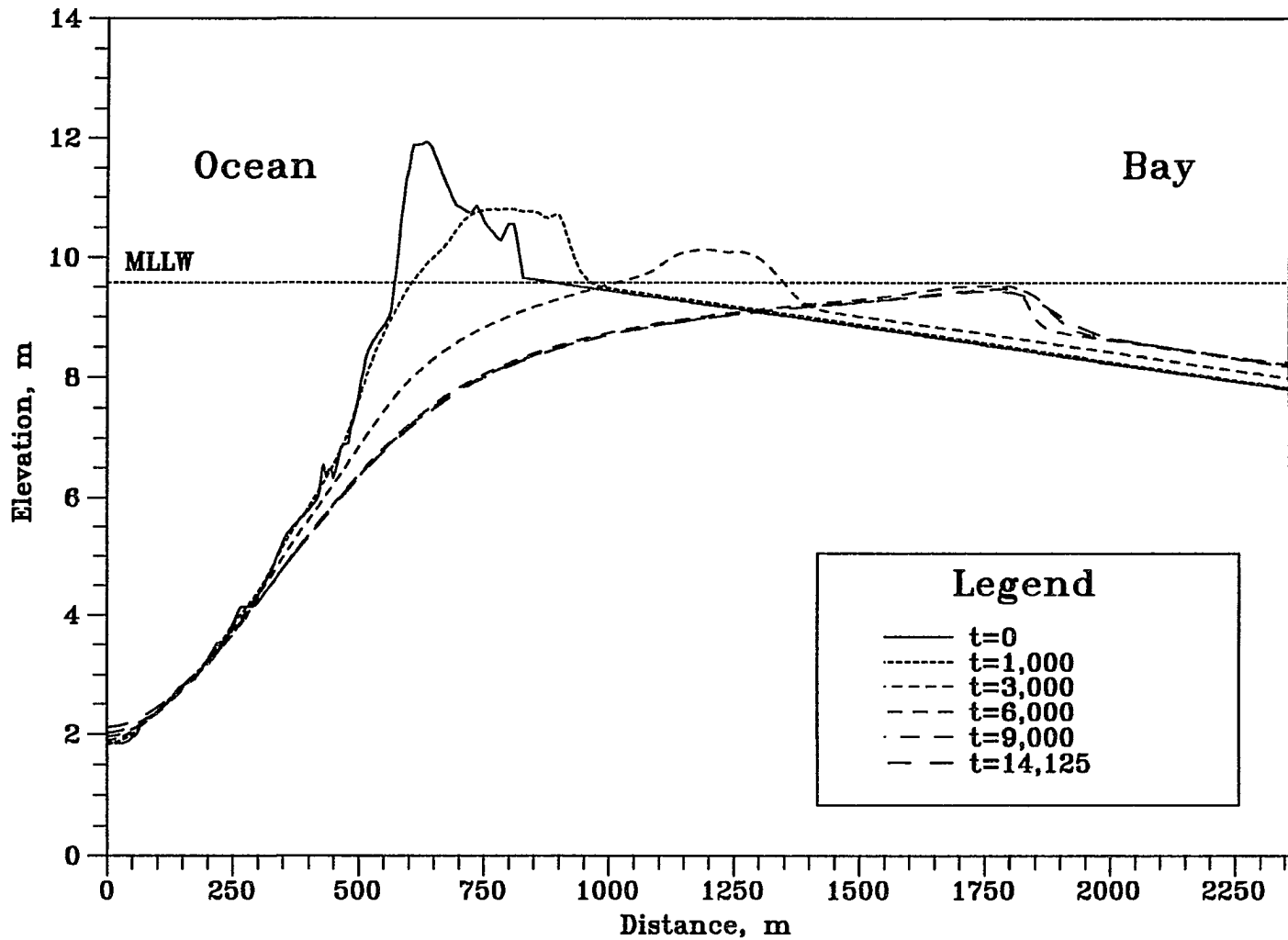


Figure 6.56 Bed Elevation Changes in Stage III/IV at t=0, 1000, 3000, 6000, 9000 and 14125. ($h_{om}=5.0m$, $h_{bm}=3.0m$, $t_{lag}=1hr$, $D_{50}=0.3mm$)

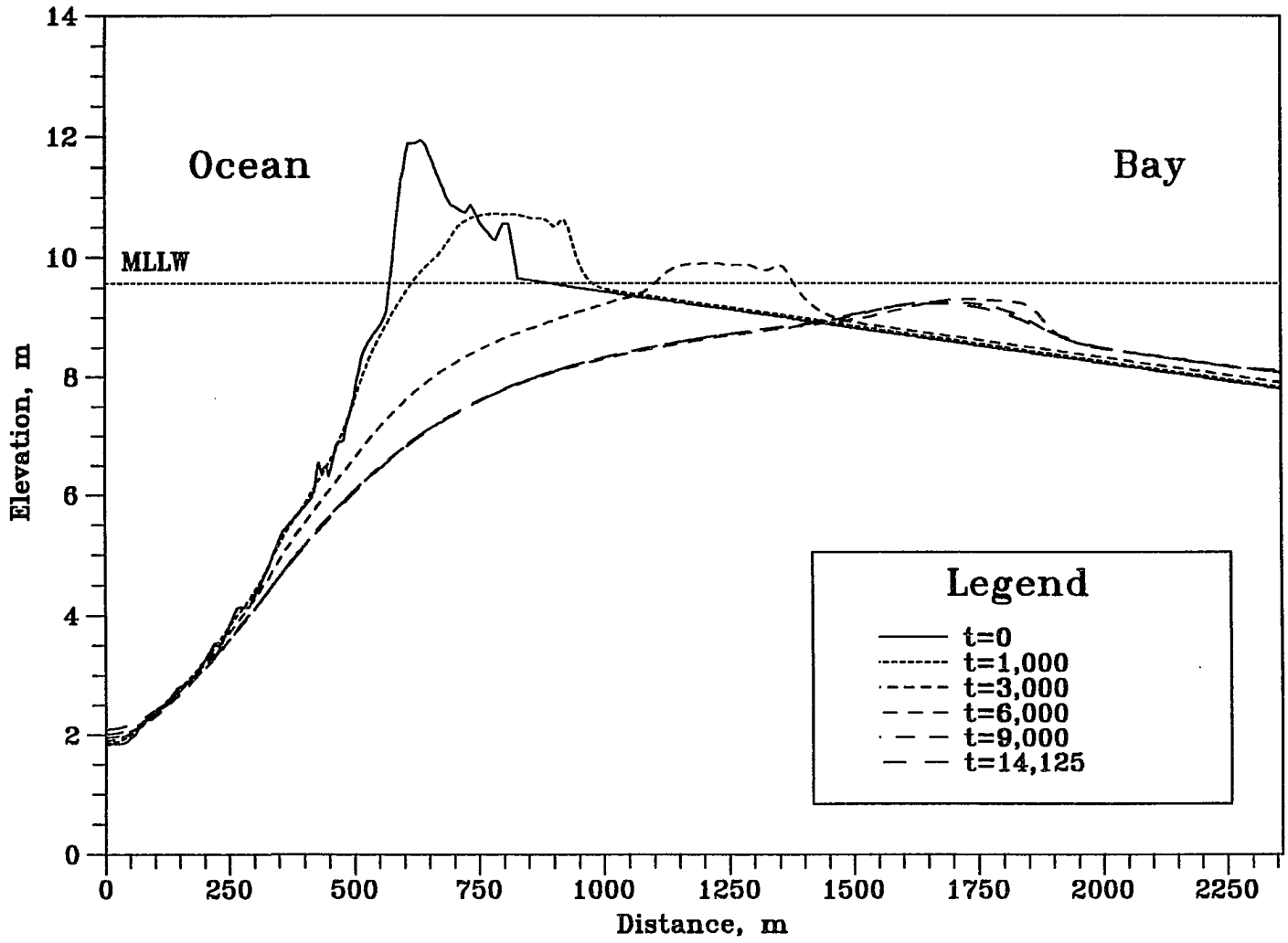


Figure 6.57 Bed Elevation Changes in Stage III/IV at t=0, 1000, 3000, 6000, 9000 and 14125. ($h_{om}=5.0m$, $h_{bm}=3.0m$, $t_{lag}=2hr$, $D_{50}=0.3mm$)

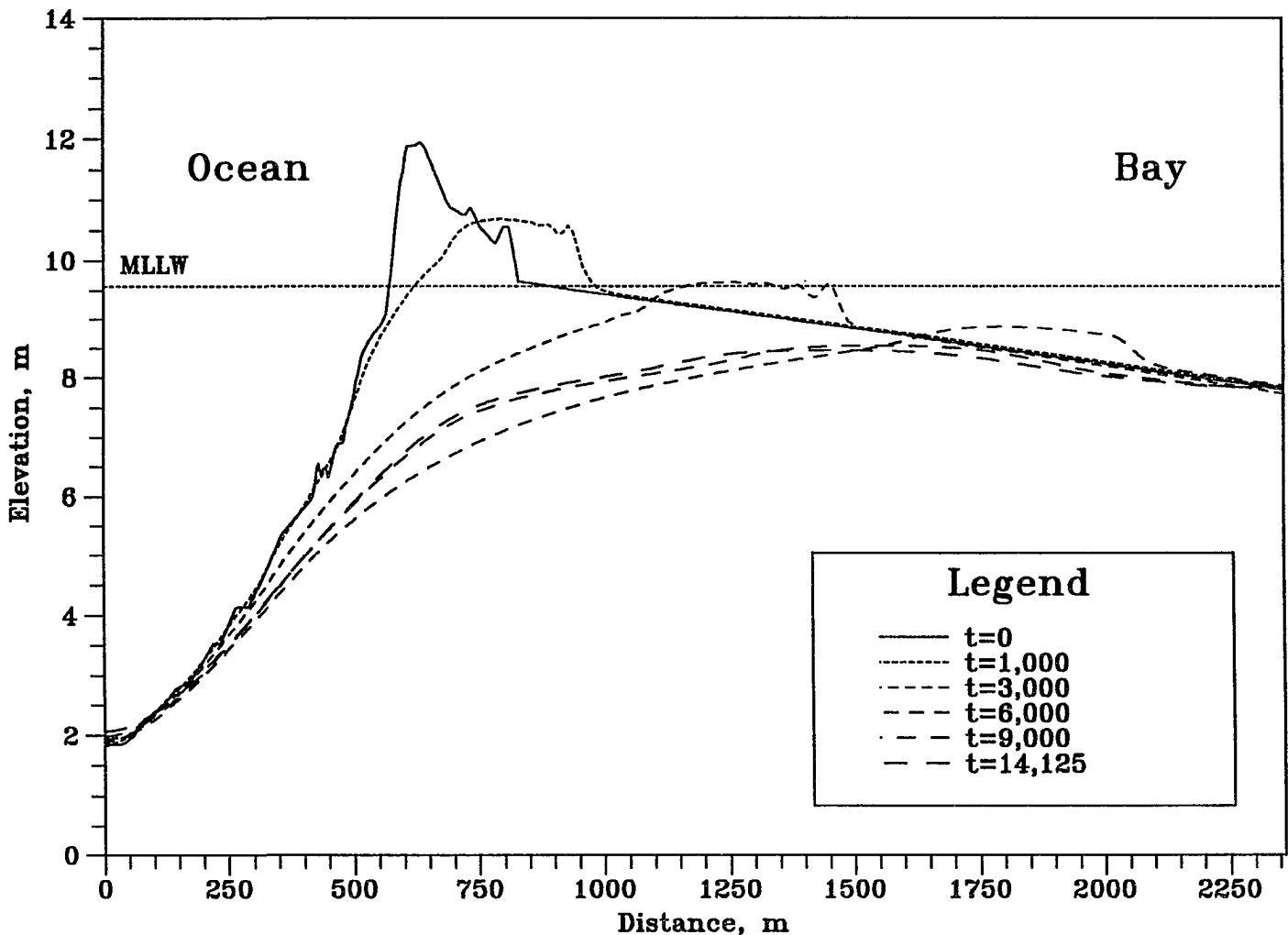


Figure 6.58 Bed Elevation Changes in Stage III/IV at t=0, 1000, 3000, 6000, 9000 and 14125. ($h_{om}=5.0m$, $h_{bm}=3.0m$, $t_{lag}=3hr$, $D_{50}=0.3mm$)

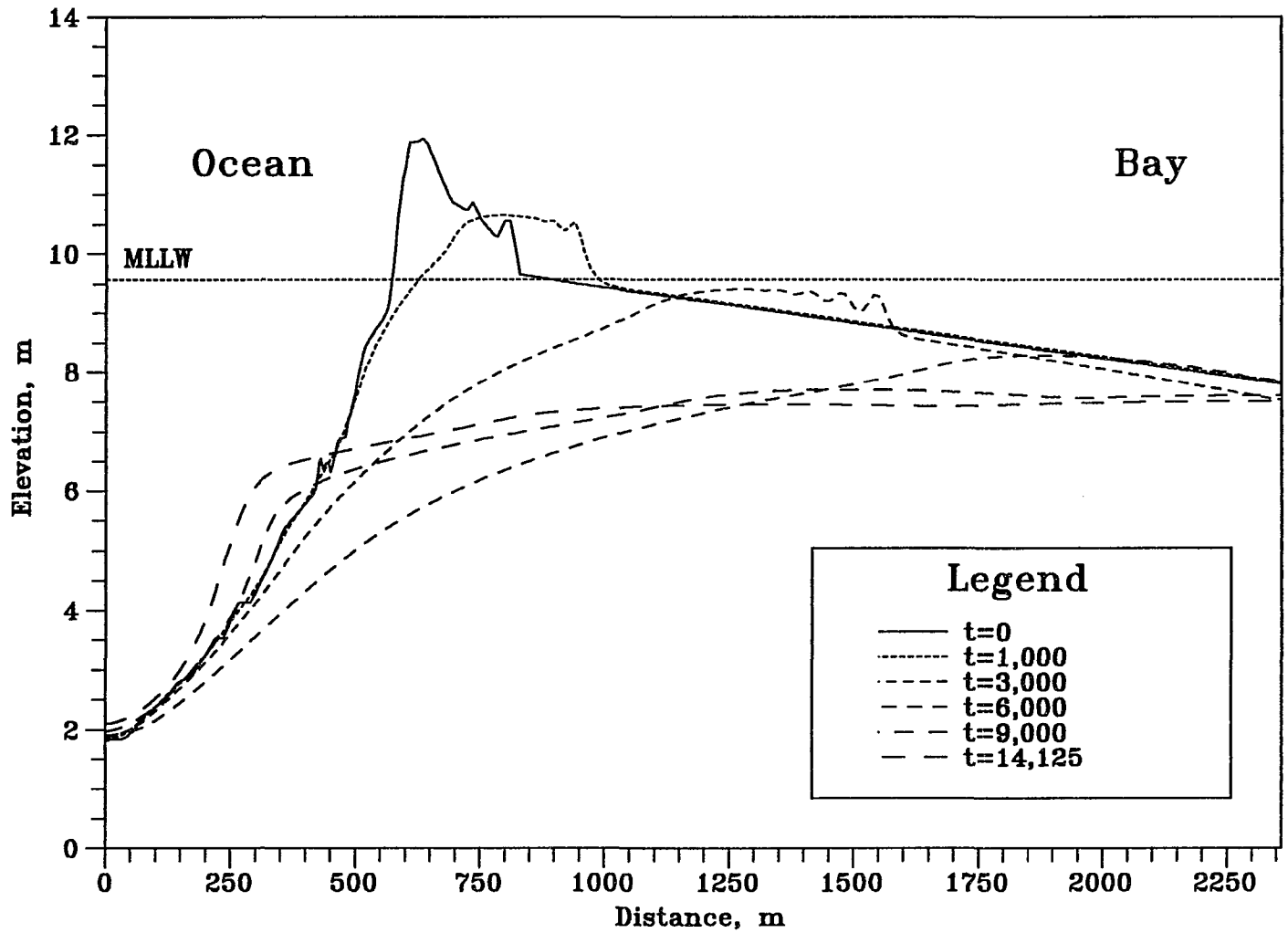


Figure 6.59 Bed Elevation Changes in Stage III/IV at t=0, 1000, 3000, 6000, 9000 and 14125. ($h_{om}=5.0m$, $h_{bm}=3.0m$, $t_{lag}=4hr$, $D_{50}=0.3mm$)

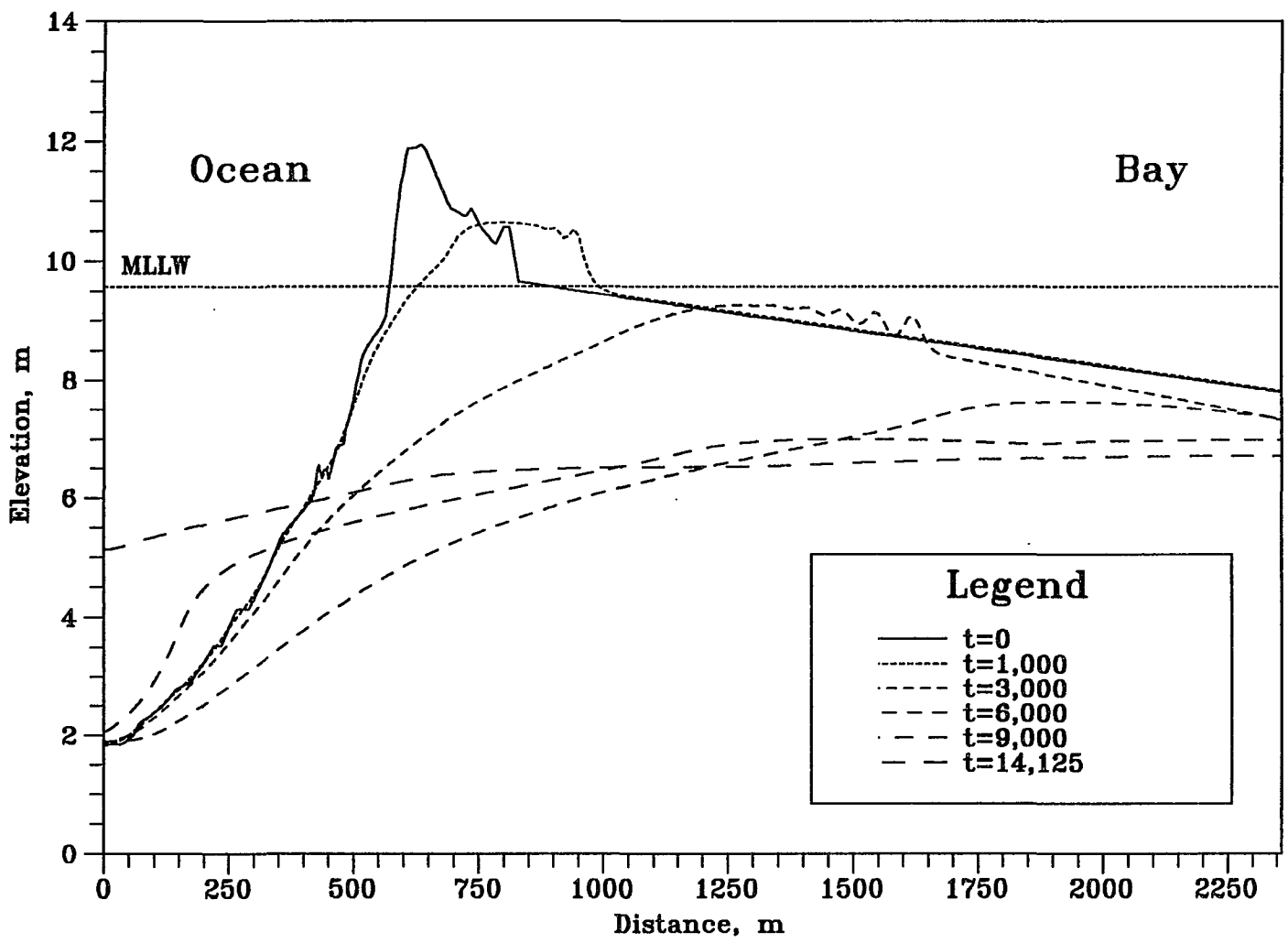


Figure 6.60 Bed Elevation Changes in Stage III/IV at t=0, 1000, 3000, 6000, 9000 and 14125. ($h_{om}=5.0m$, $h_{bm}=3.0m$, $t_{lag}=5hr$, $D_{50}=0.3mm$)

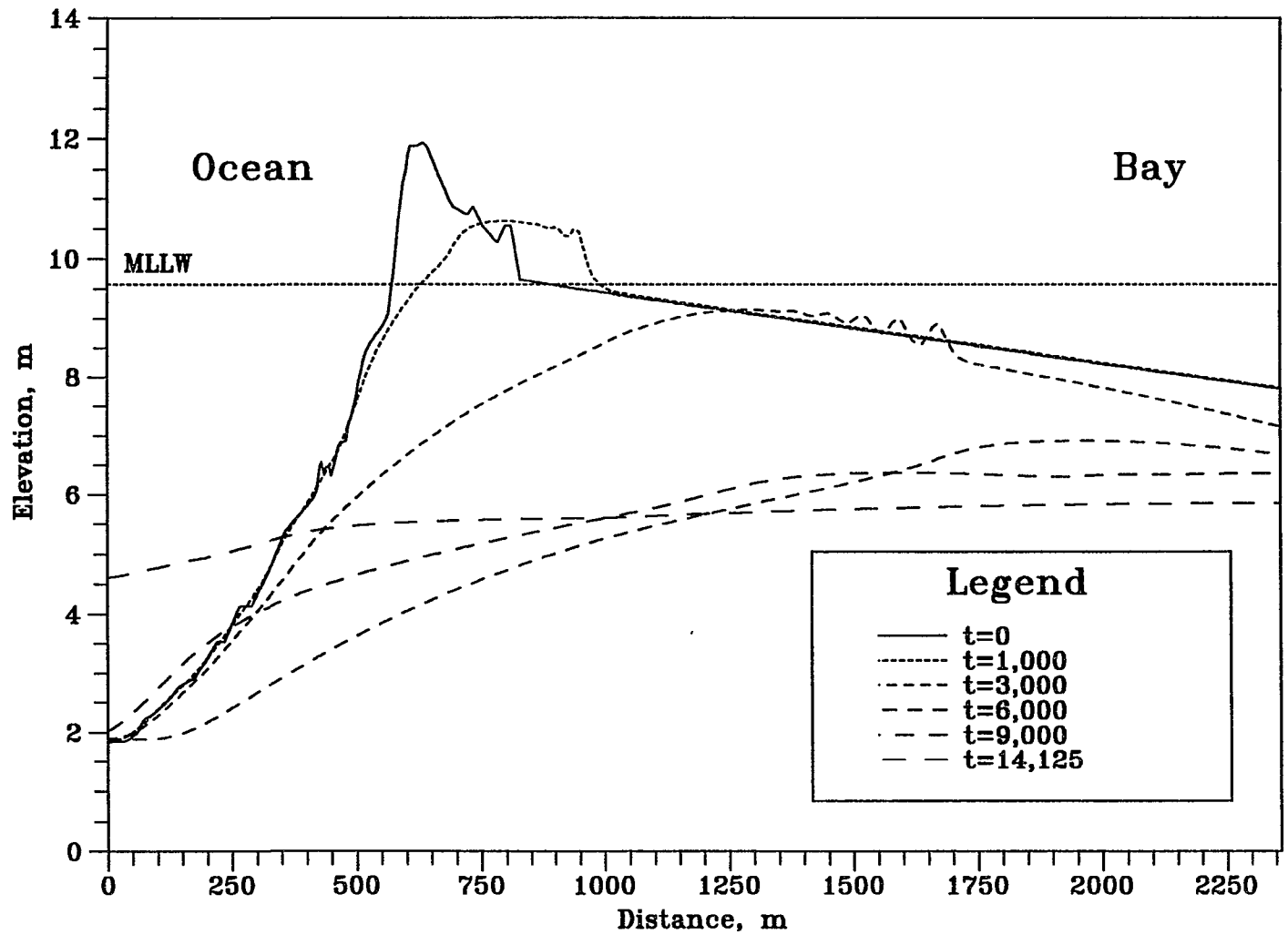


Figure 6.61 Bed Elevation Changes in Stage III/IV at t=0, 1000, 3000, 6000, 9000 and 14125. ($h_{om}=5.0m$, $h_{bm}=3.0m$, $t_{lag}=6hr$, $D_{50}=0.3mm$)

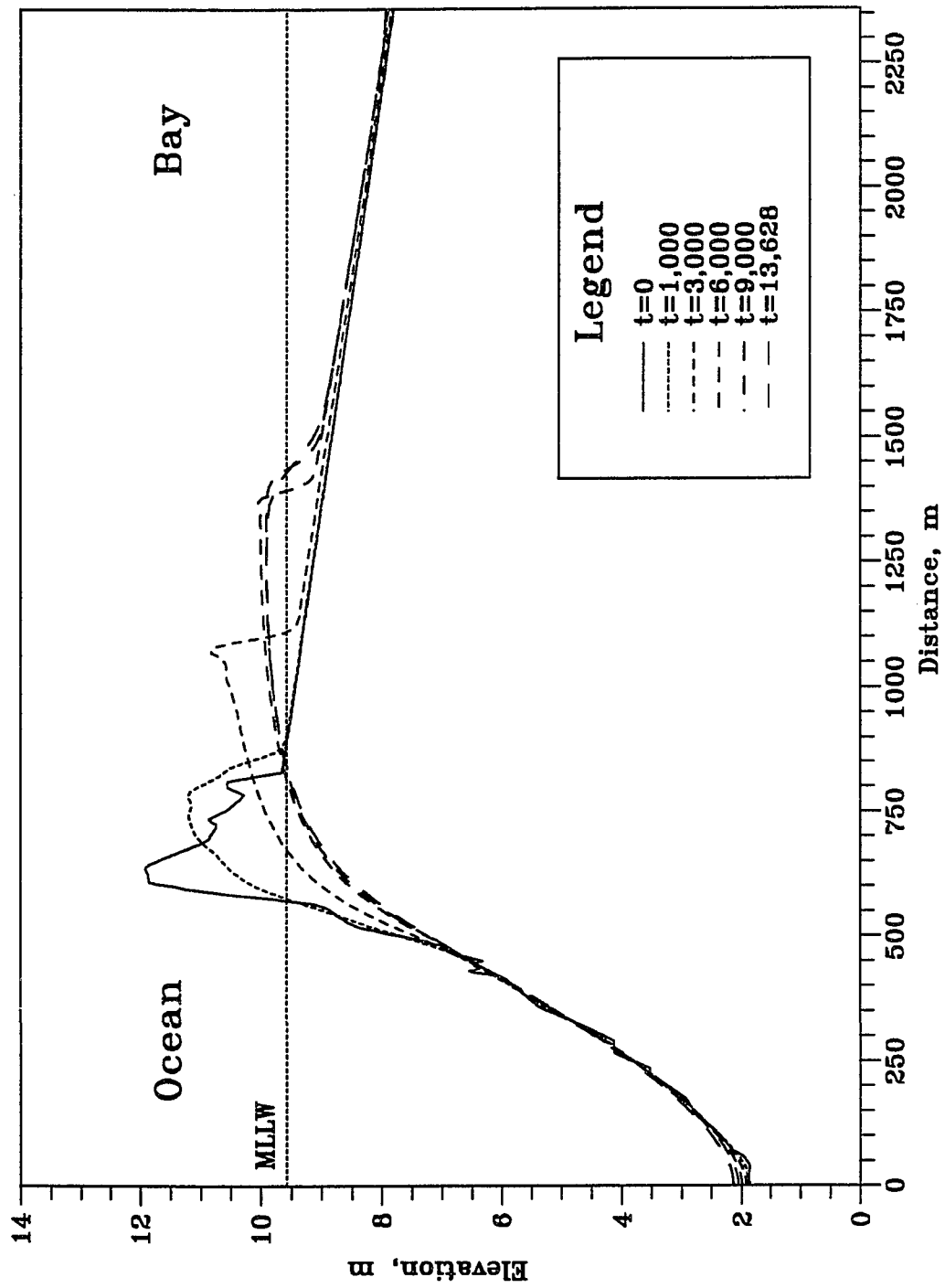


Figure 6.62 Bed Elevation Changes in Stage III/IV at t=0, 1000, 3000, 6000, 9000 and 13628. ($h_{om}=4.0m$, $h_{bm}=3.0m$, $t_{lag}=0hr$, $D_{60}=0.3mm$)

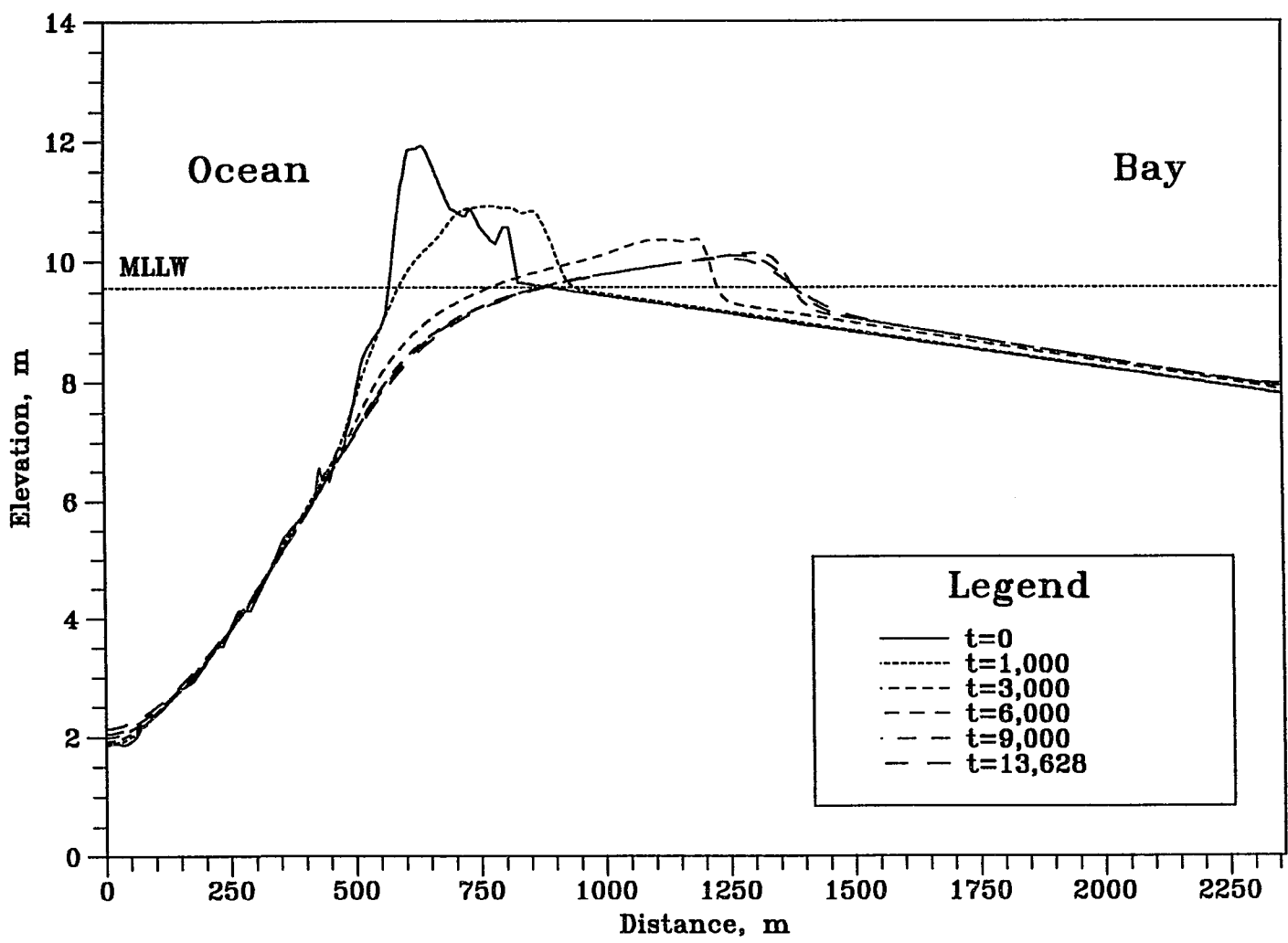


Figure 6.63 Bed Elevation Changes in Stage III/IV at t=0, 1000, 3000, 6000, 9000 and 13628. ($h_{om}=4.0m$, $h_{bm}=3.0m$, $t_{lag}=1hr$, $D_{50}=0.3mm$)

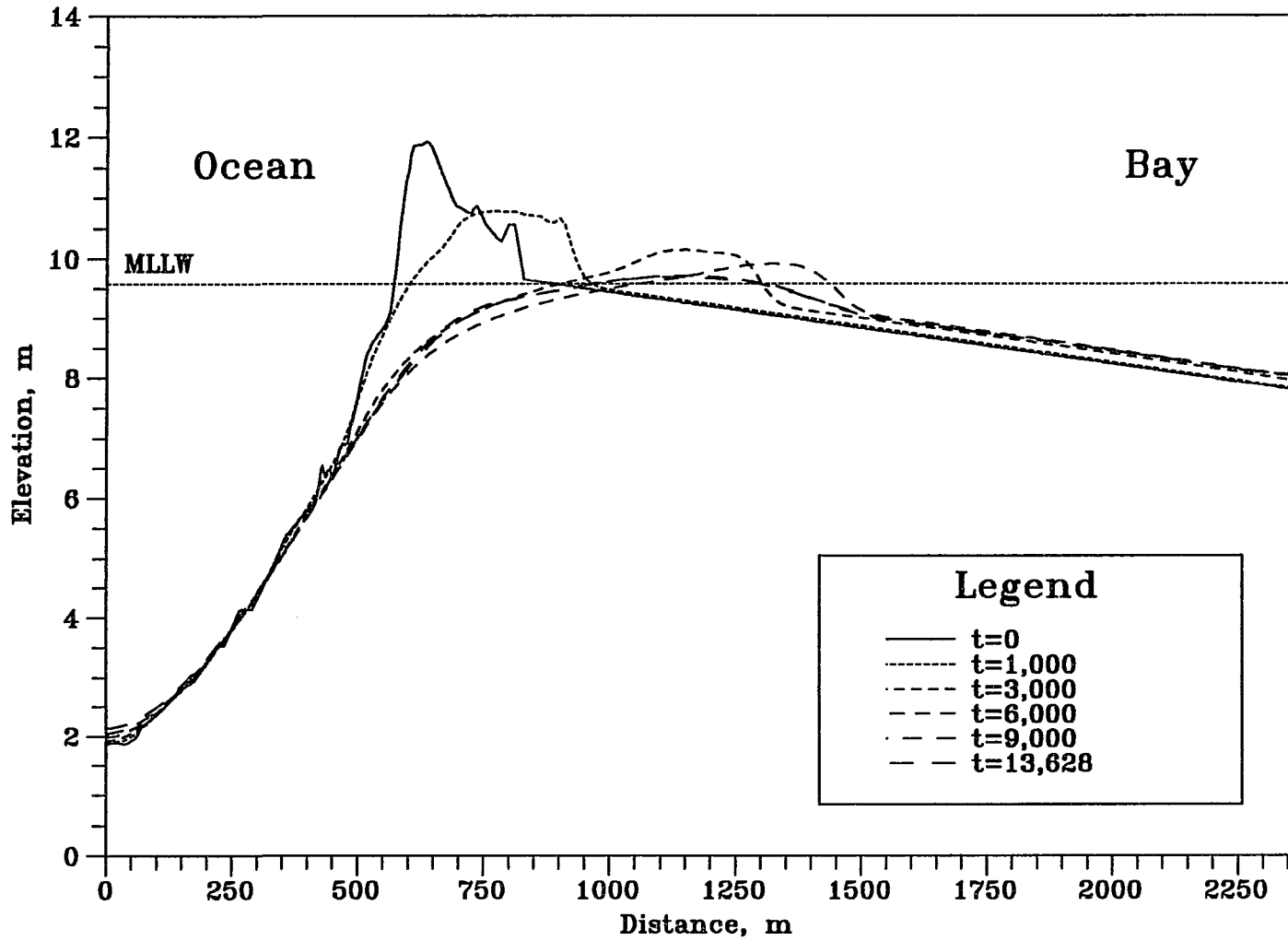


Figure 6.64 Bed Elevation Changes in Stage III/IV at t=0, 1000, 3000, 6000, 9000 and 13628. ($h_{om}=4.0m$, $h_{bm}=3.0m$, $t_{lag}=2hr$, $D_{50}=0.3mm$)

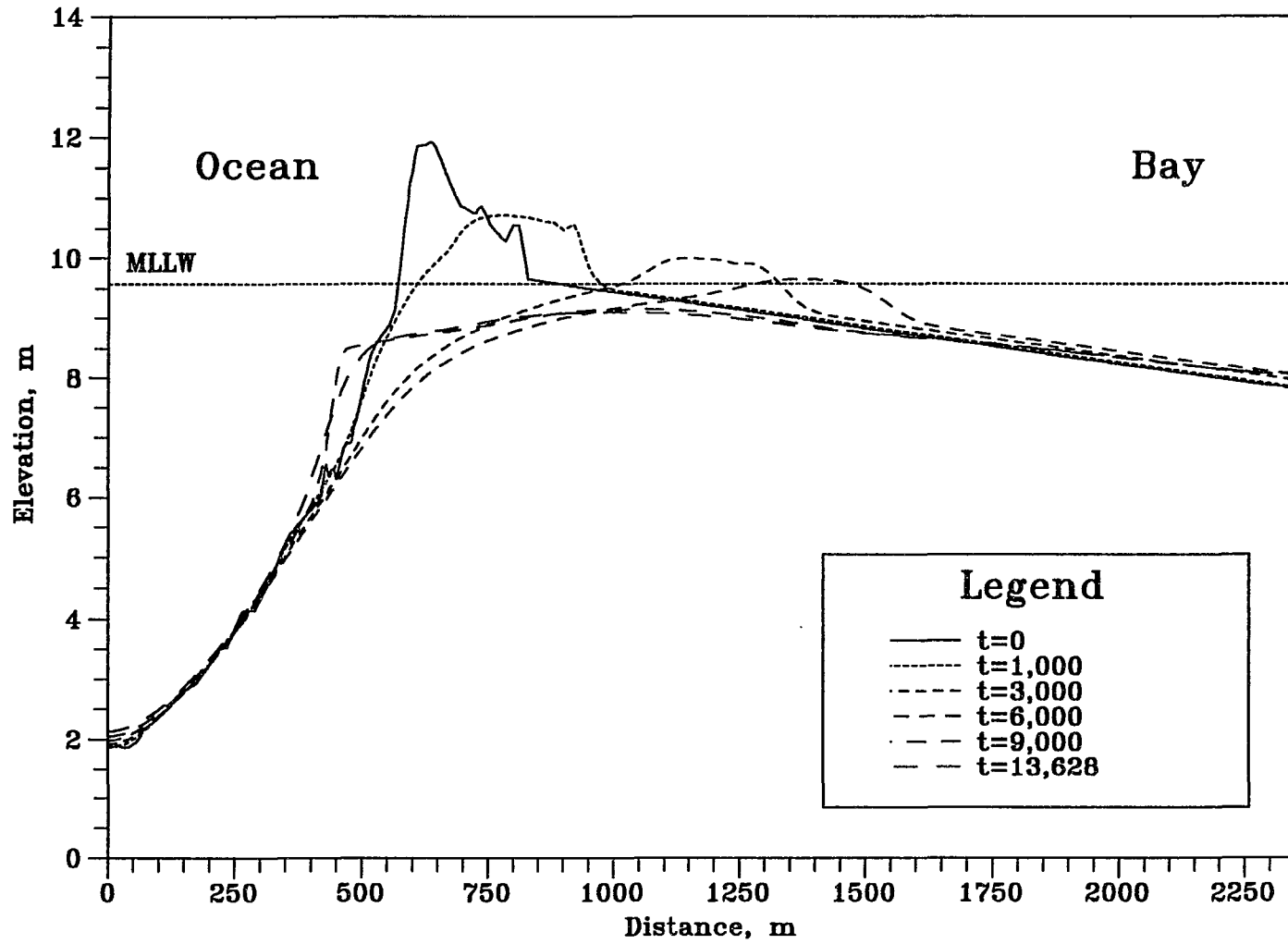


Figure 6.65 Bed Elevation Changes in Stage III/IV at $t=0, 1000, 3000, 6000, 9000$ and 13628 . ($h_{om}=4.0\text{m}$, $h_{bm}=3.0\text{m}$, $t_{lag}=3\text{hr}$, $D_{50}=0.3\text{mm}$)

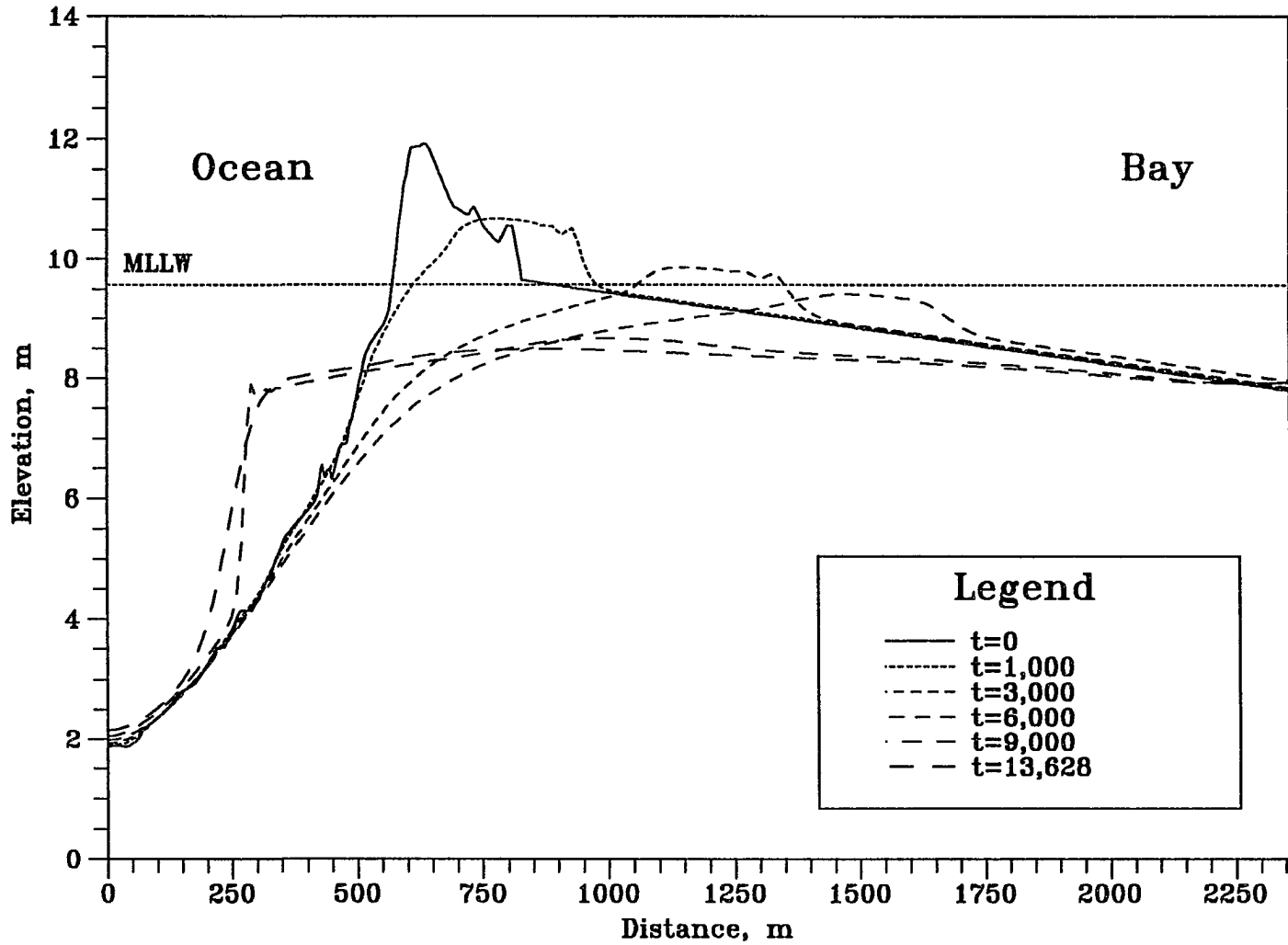


Figure 6.66 Bed Elevation Changes in Stage III/IV at t=0, 1000, 3000, 6000, 9000 and 13628. ($h_{om}=4.0m$, $h_{bm}=3.0m$, $t_{lag}=4hr$, $D_{50}=0.3mm$)

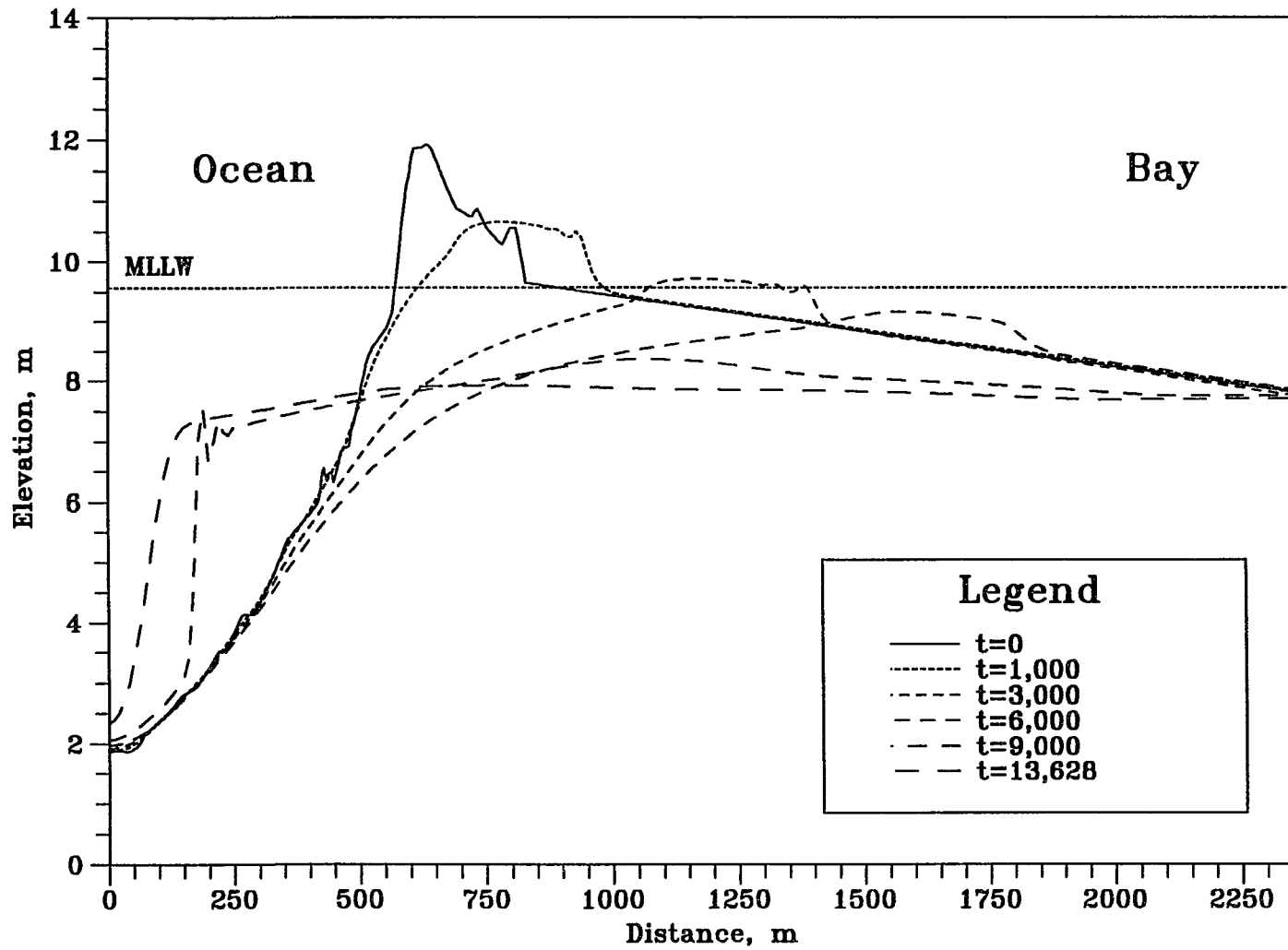


Figure 6.67 Bed Elevation Changes in Stage III/IV at $t=0, 1000, 3000, 6000, 9000$ and 13628 . ($h_{om}=4.0m, h_{bm}=3.0m, t_{lag}=5hr, D_{50}=0.3mm$)

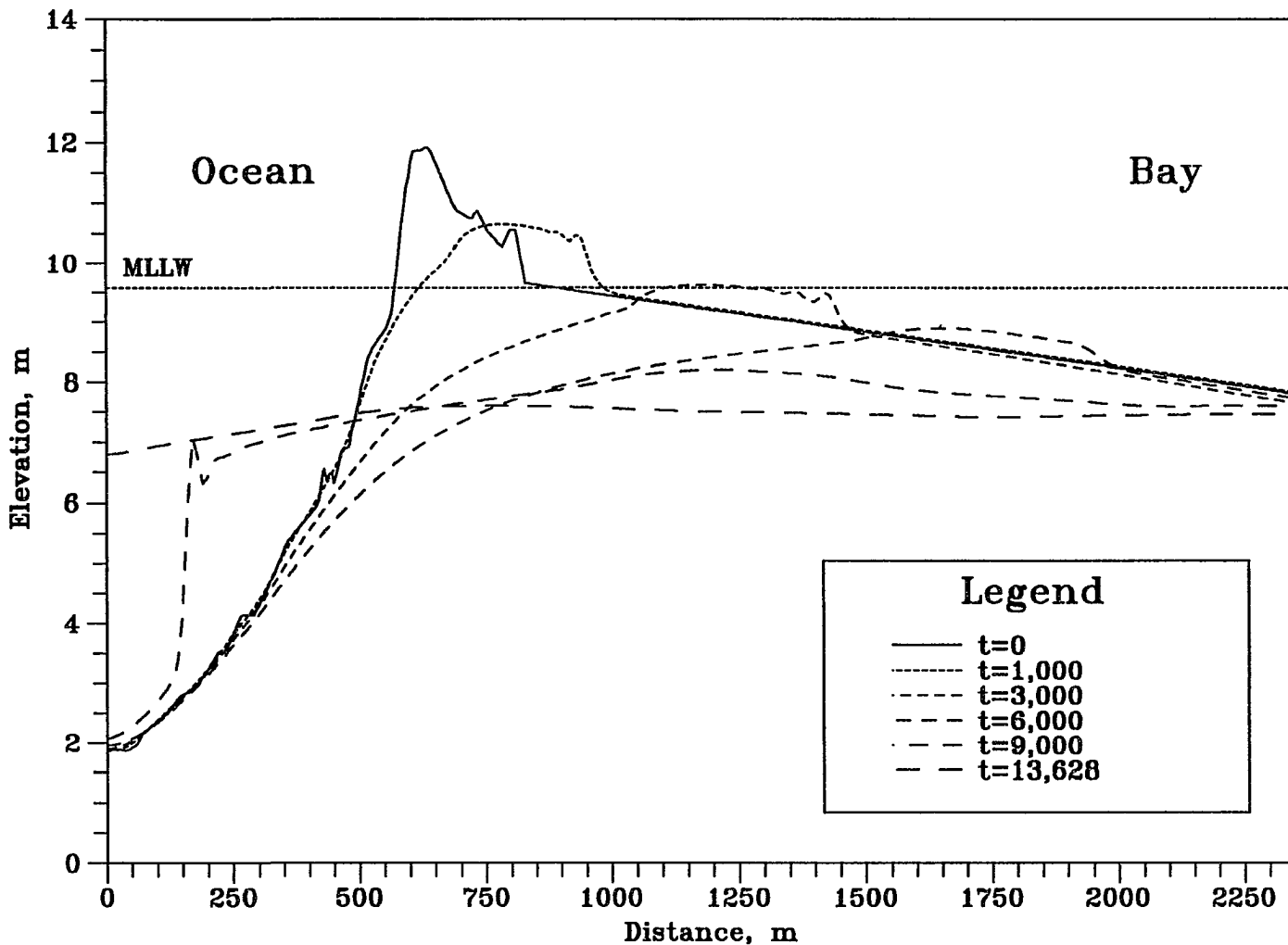


Figure 6.68 Bed Elevation Changes in Stage III/IV at t=0, 1000, 3000, 6000, 9000 and 13628. ($h_{om}=4.0m$, $h_{bm}=3.0m$, $t_{lag}=6hr$, $D_{50}=0.3mm$)

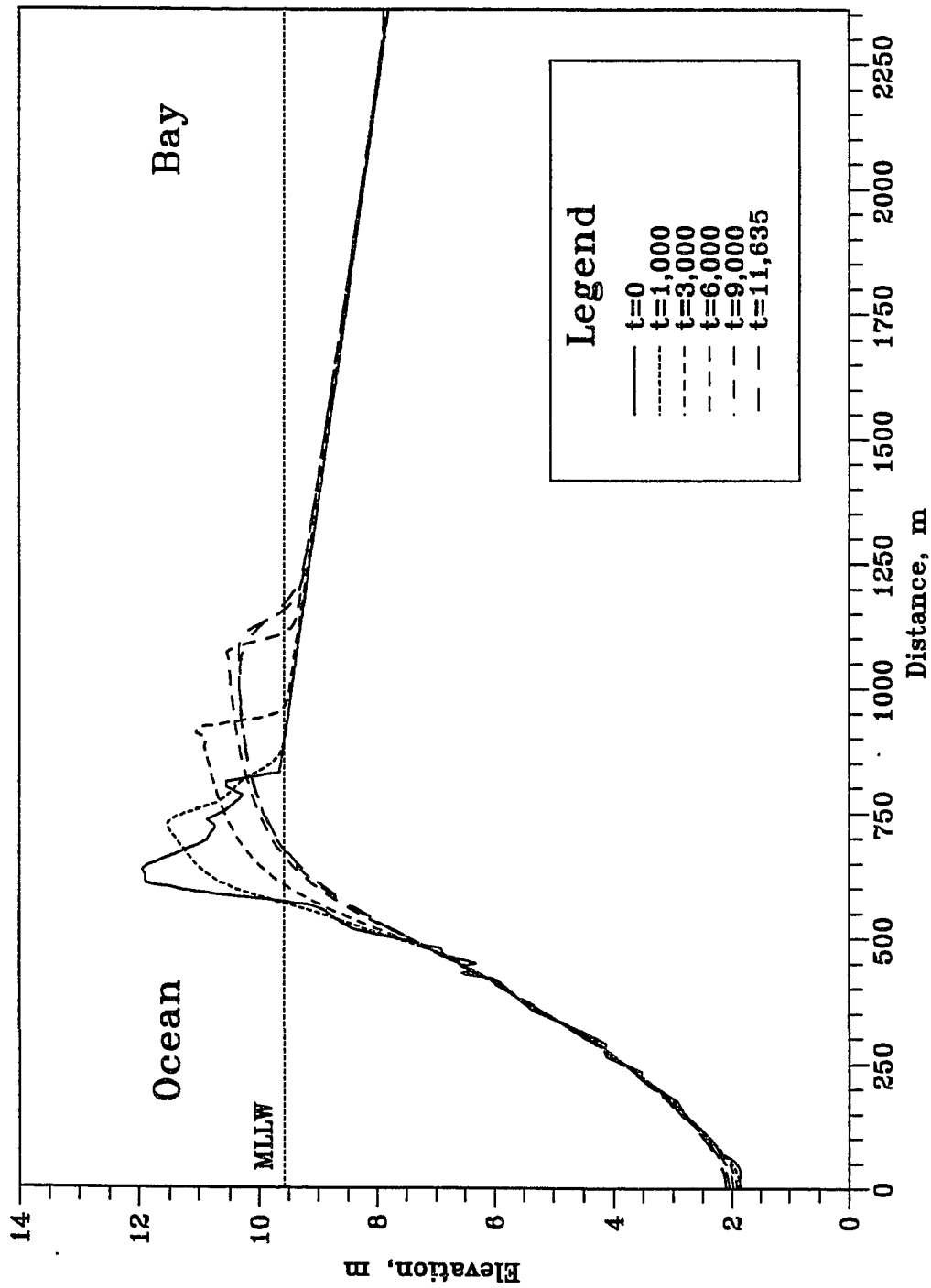


Figure 6.69 Bed Elevation Changes in Stage III/IV at $t=0, 1000, 3000, 6000, 9000$ and 11635 . ($h_{om}=4.5m, h_{bm}=4.0m, t_{lag}=0hr, D_{50}=0.3mm$)

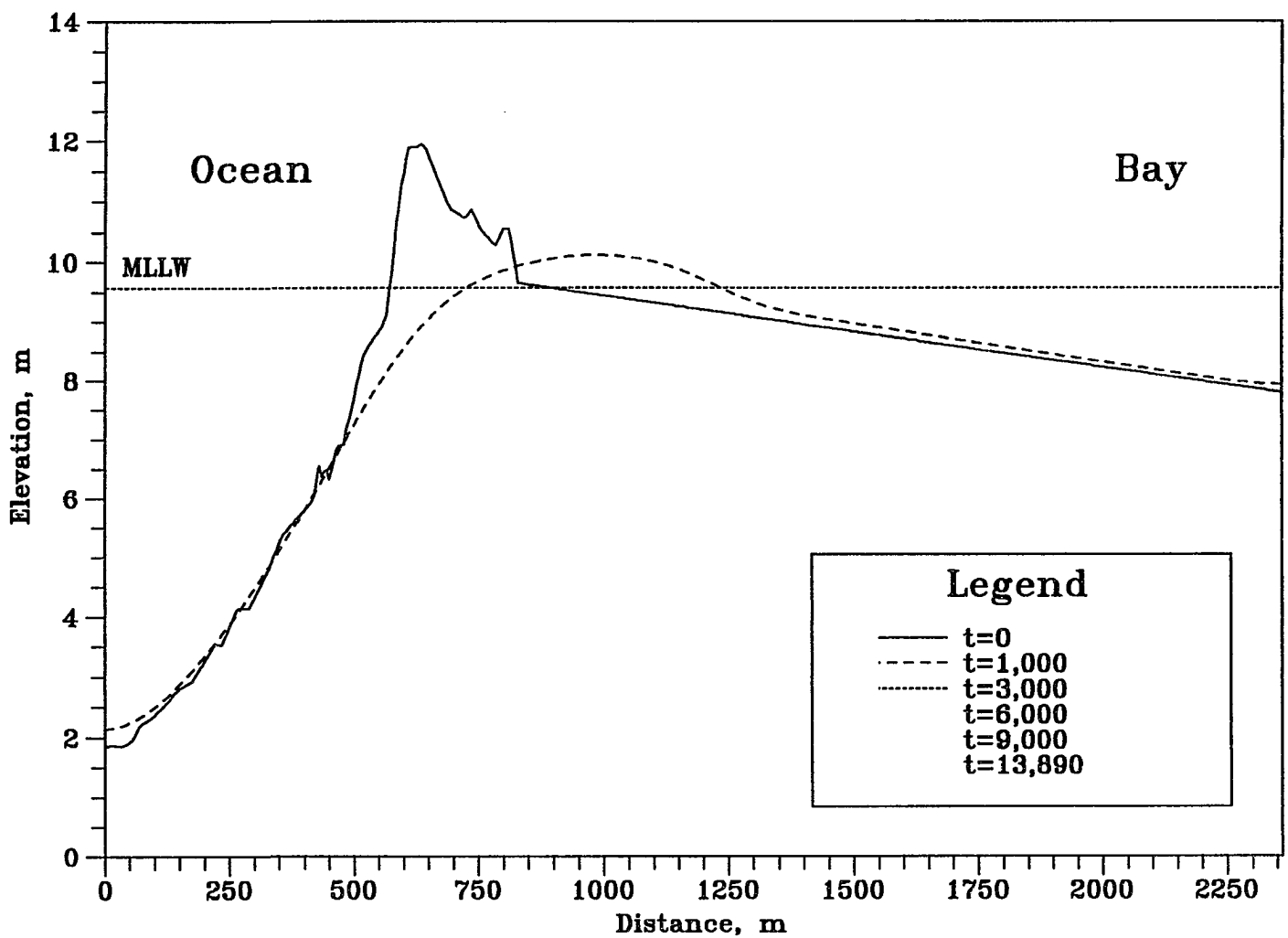


Figure 6.70 Bed Elevation Changes in Stage III/IV at t=0, 1000, 3000, 6000, 9000 and 13890. ($h_{om}=4.5m$, $h_{bm}=4.0m$, $t_{lag}=1hr$, $D_{50}=0.3mm$)

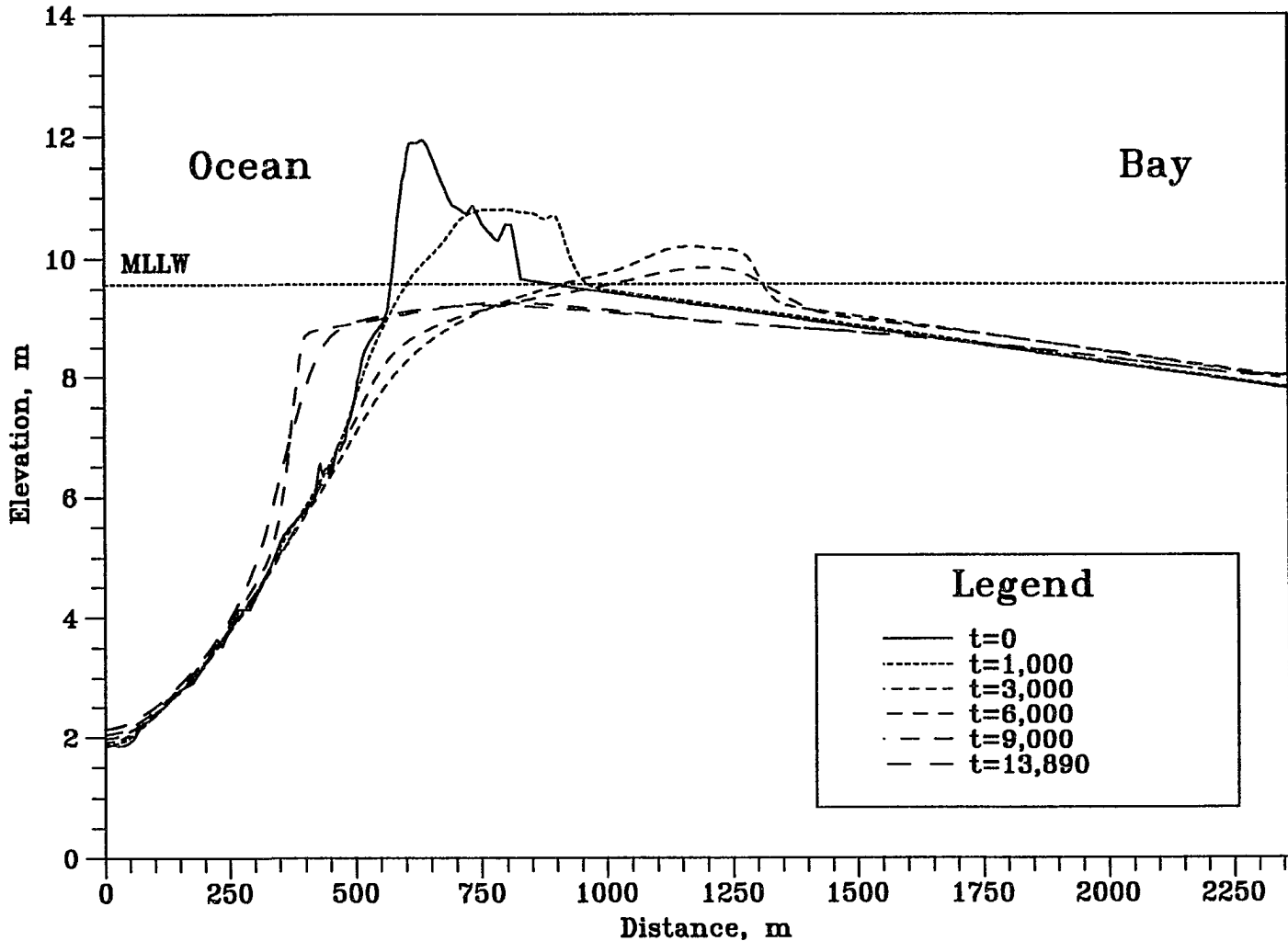


Figure 6.71 Bed Elevation Changes in Stage III/IV at t=0, 1000, 3000, 6000, 9000 and 13890. ($h_{om}=4.5m$, $h_{bm}=4.0m$, $t_{lag}=2hr$, $D_{50}=0.3mm$)

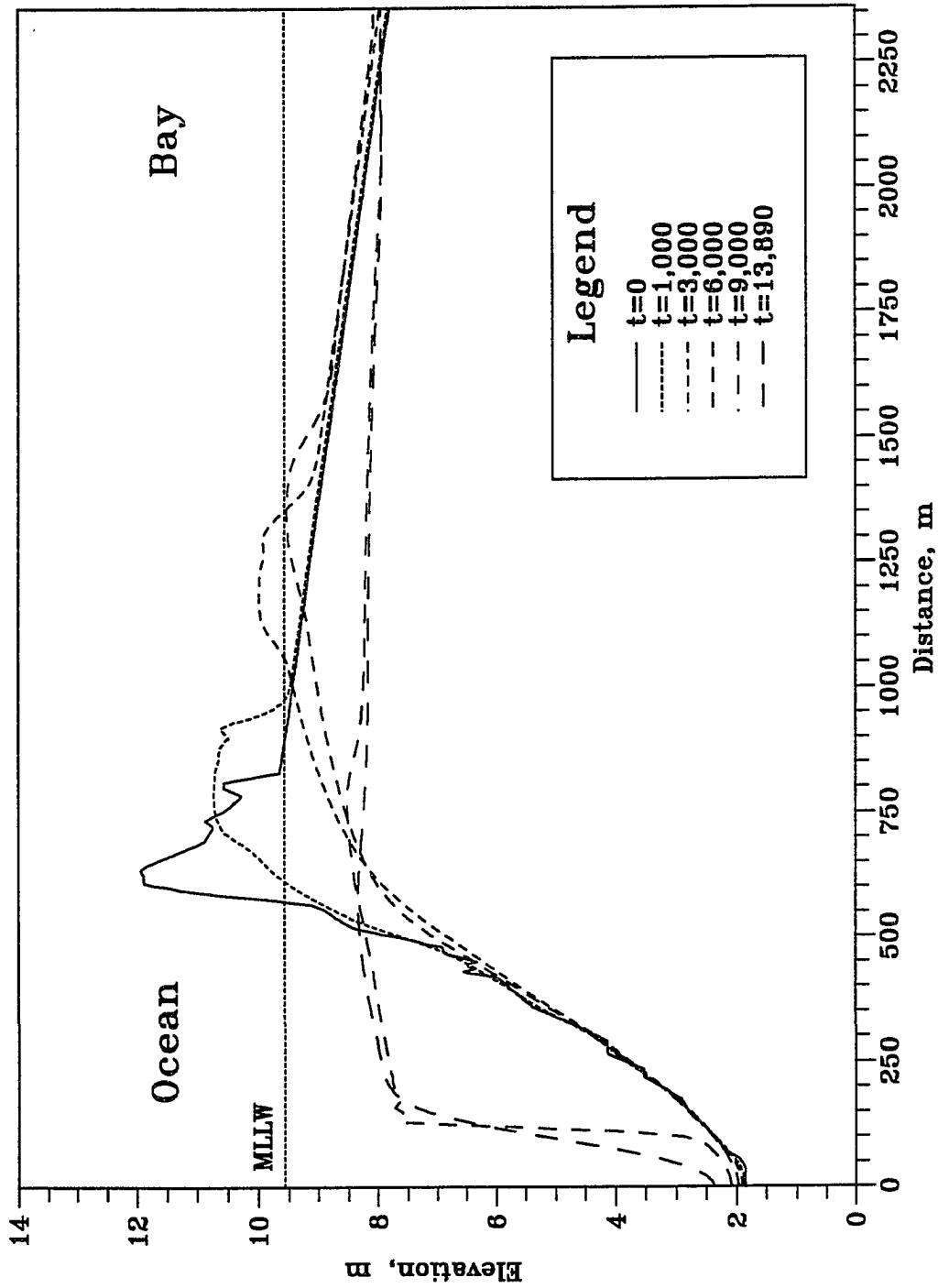


Figure 6.72 Bed Elevation Changes in Stage III/IV at $t=0, 1000, 3000, 6000, 9000$ and 13890 . ($h_{om}=4.5m, h_{bm}=4.0m, t_{lag}=3hr, D_{50}=0.3mm$)

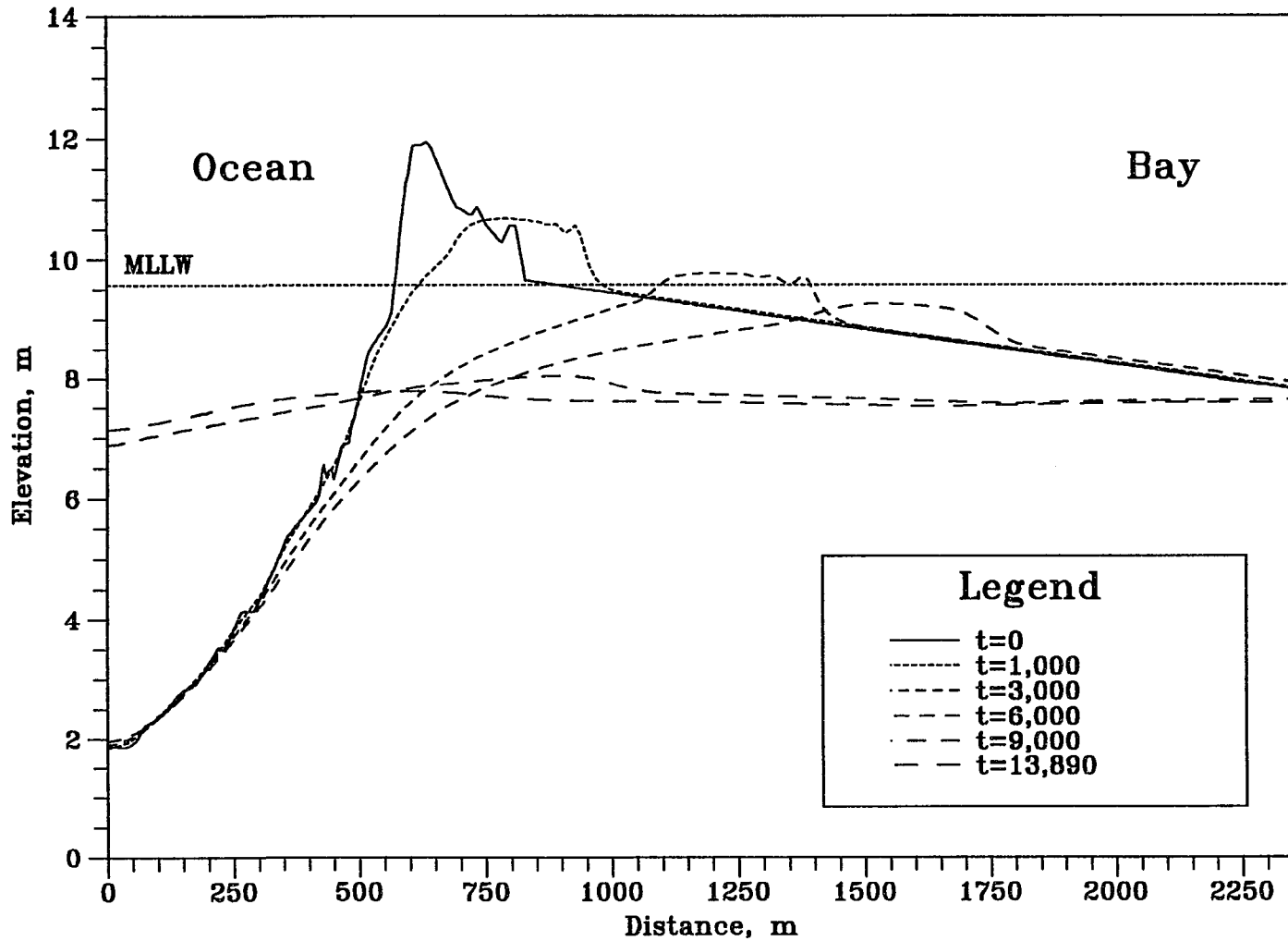


Figure 6.73 Bed Elevation Changes in Stage III/IV at t=0, 1000, 3000, 6000, 9000 and 13890. ($h_{om}=4.5m$, $h_{bm}=4.0m$, $t_{lag}=4hr$, $D_{50}=0.3mm$)

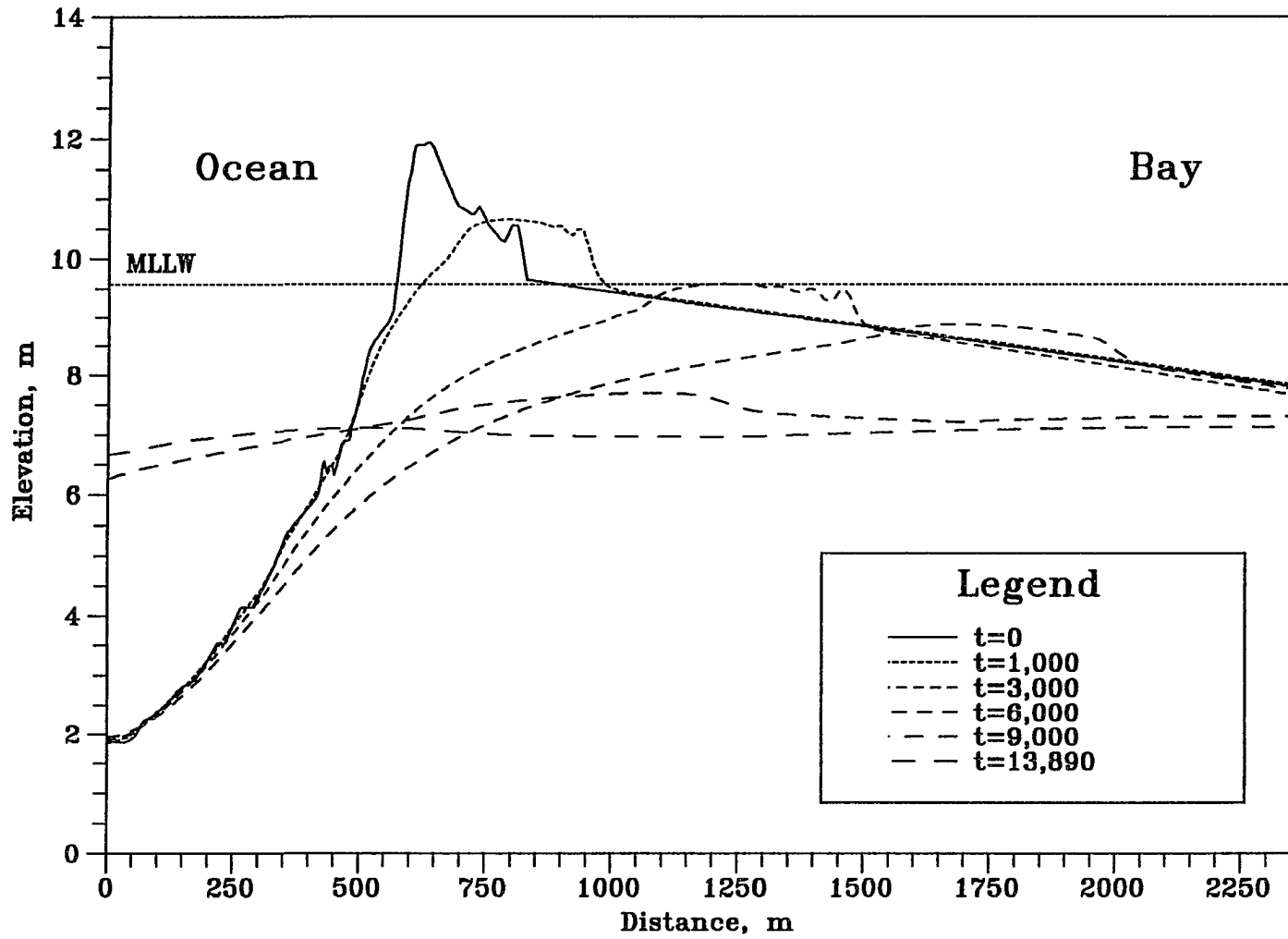


Figure 6.74 Bed Elevation Changes in Stage III/IV at $t=0, 1000, 3000, 6000, 9000$ and 13890 . ($h_{om}=4.5m, h_{bm}=4.0m, t_{lag}=5hr, D_{50}=0.3mm$)

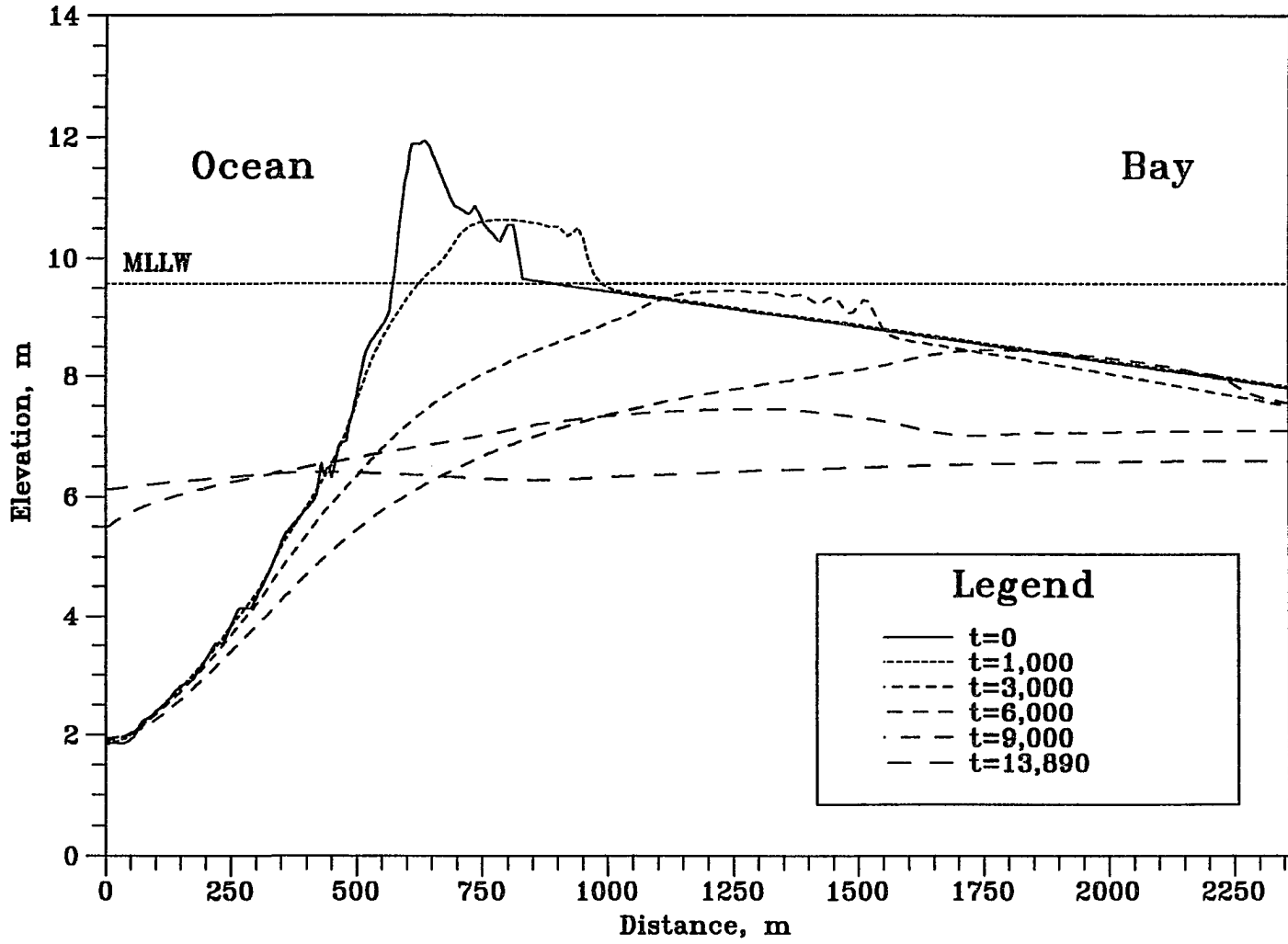


Figure 6.75 Bed Elevation Changes in Stage III/IV at t=0, 1000, 3000, 6000, 9000 and 13890. ($h_{om}=4.5m$, $h_{bm}=4.0m$, $t_{lag}=6hr$, $D_{50}=0.3mm$)

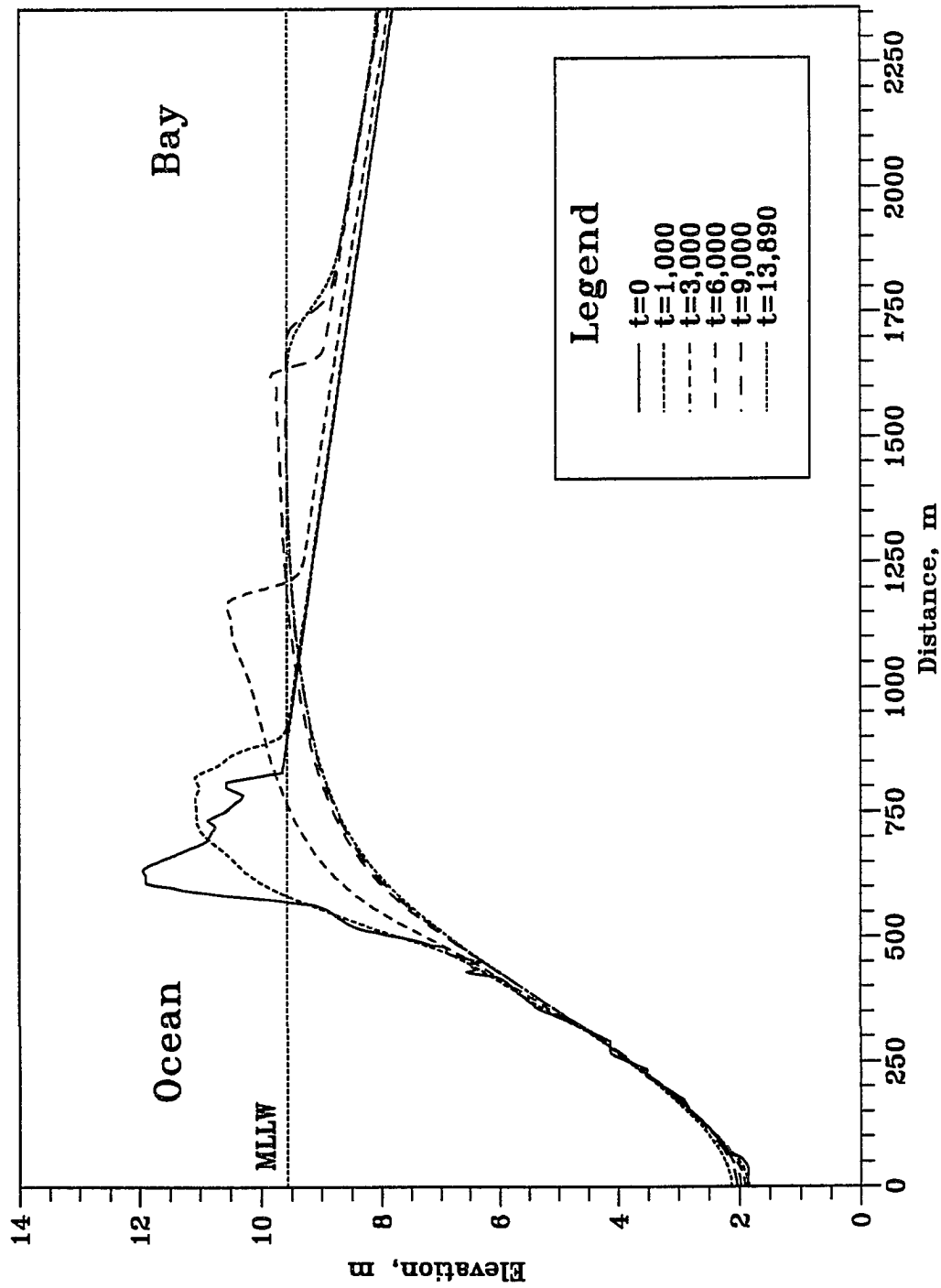


Figure 6.76 Bed Elevation Changes in Stage III/IV at $t=0, 1000, 3000, 6000, 9000$ and 13890 . ($h_{om}=4.5m, h_{bm}=3.0m, t_{ag}=0hr, D_{50}=0.3mm$)

230

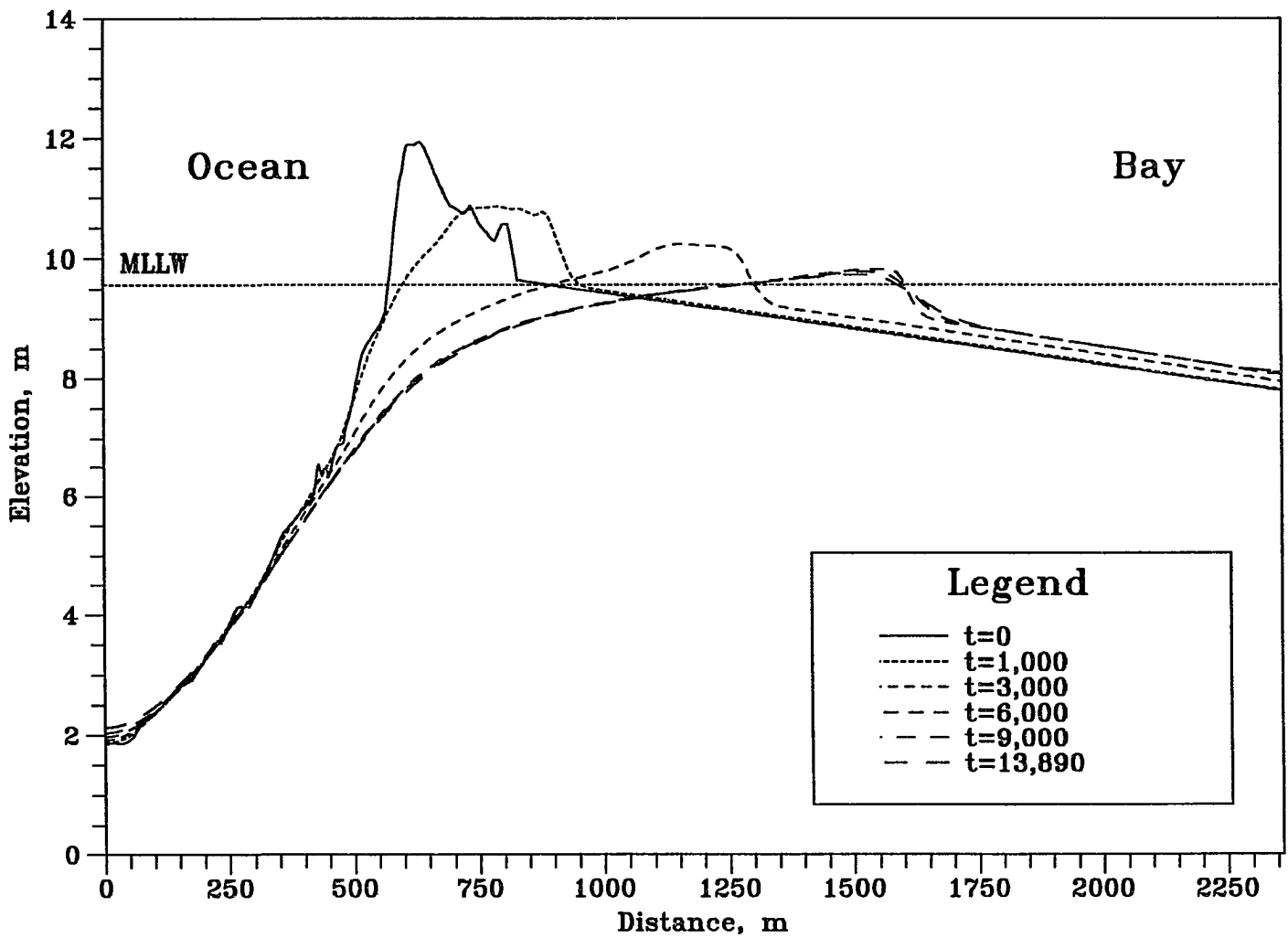


Figure 6.77 Bed Elevation Changes in Stage III/IV at t=0, 1000, 3000, 6000, 9000 and 13890. ($h_{om}=4.5m$, $h_{bm}=3.0m$, $t_{lag}=1hr$, $D_{50}=0.3mm$)

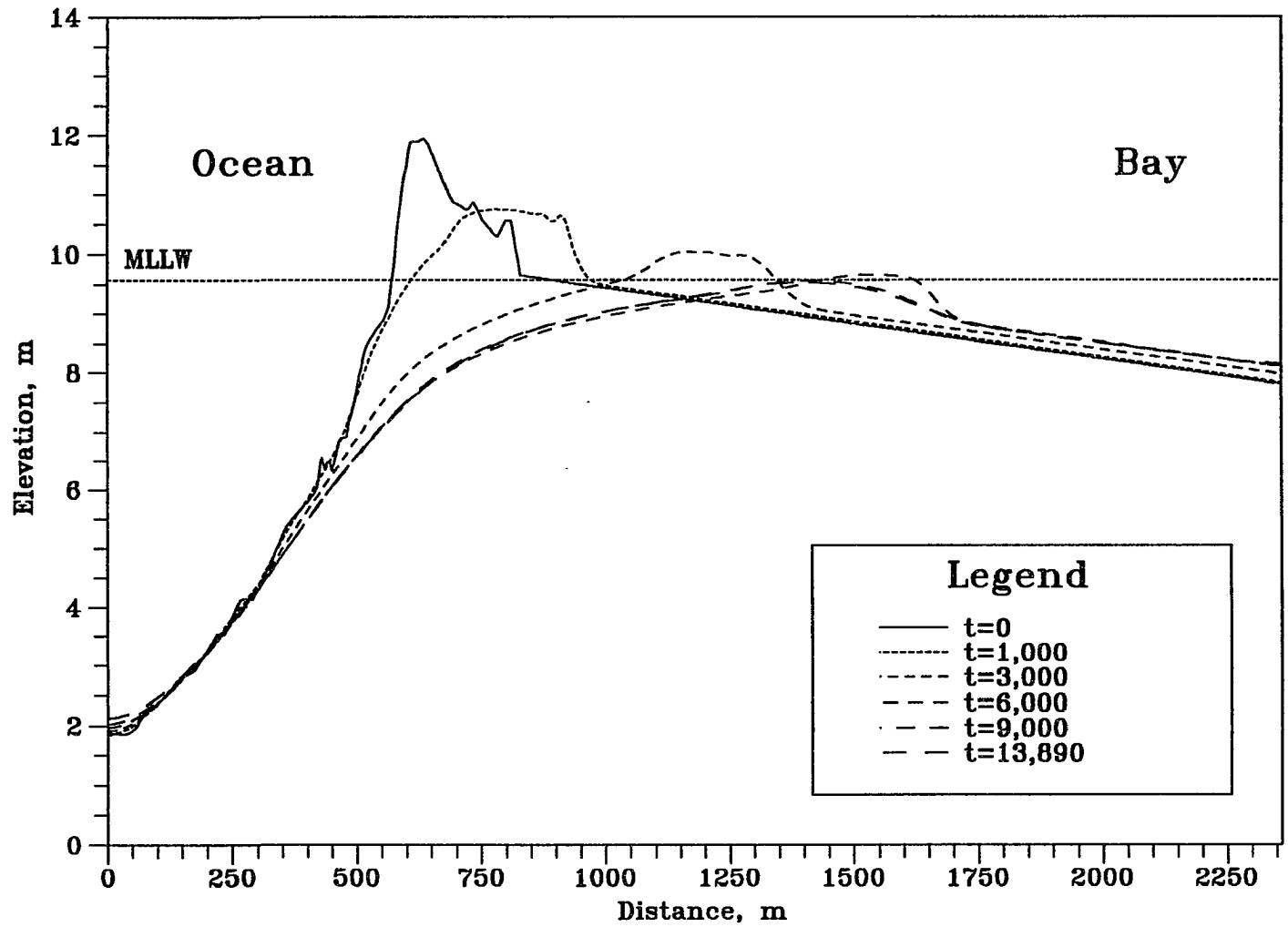


Figure 6.78 Bed Elevation Changes in Stage III/IV at t=0, 1000, 3000, 6000, 9000 and 13890. ($h_{om}=4.5m$, $h_{bm}=3.0m$, $t_{lag}=2hr$, $D_{50}=0.3mm$)

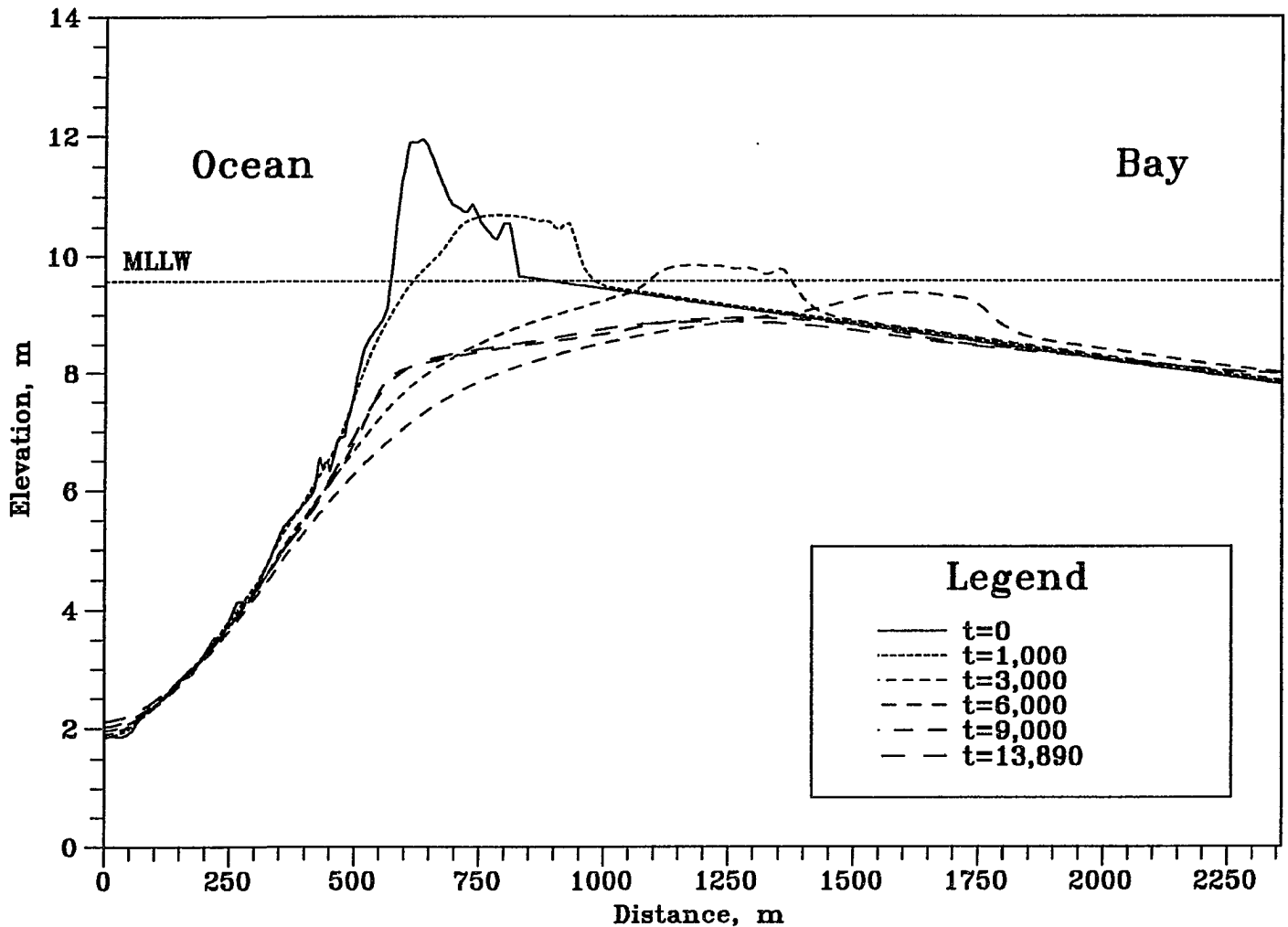


Figure 6.79 Bed Elevation Changes in Stage III/IV at t=0, 1000, 3000, 6000, 9000 and 13890. ($h_{om}=4.5m$, $h_{bm}=3.0m$, $t_{lag}=3hr$, $D_{50}=0.3mm$)

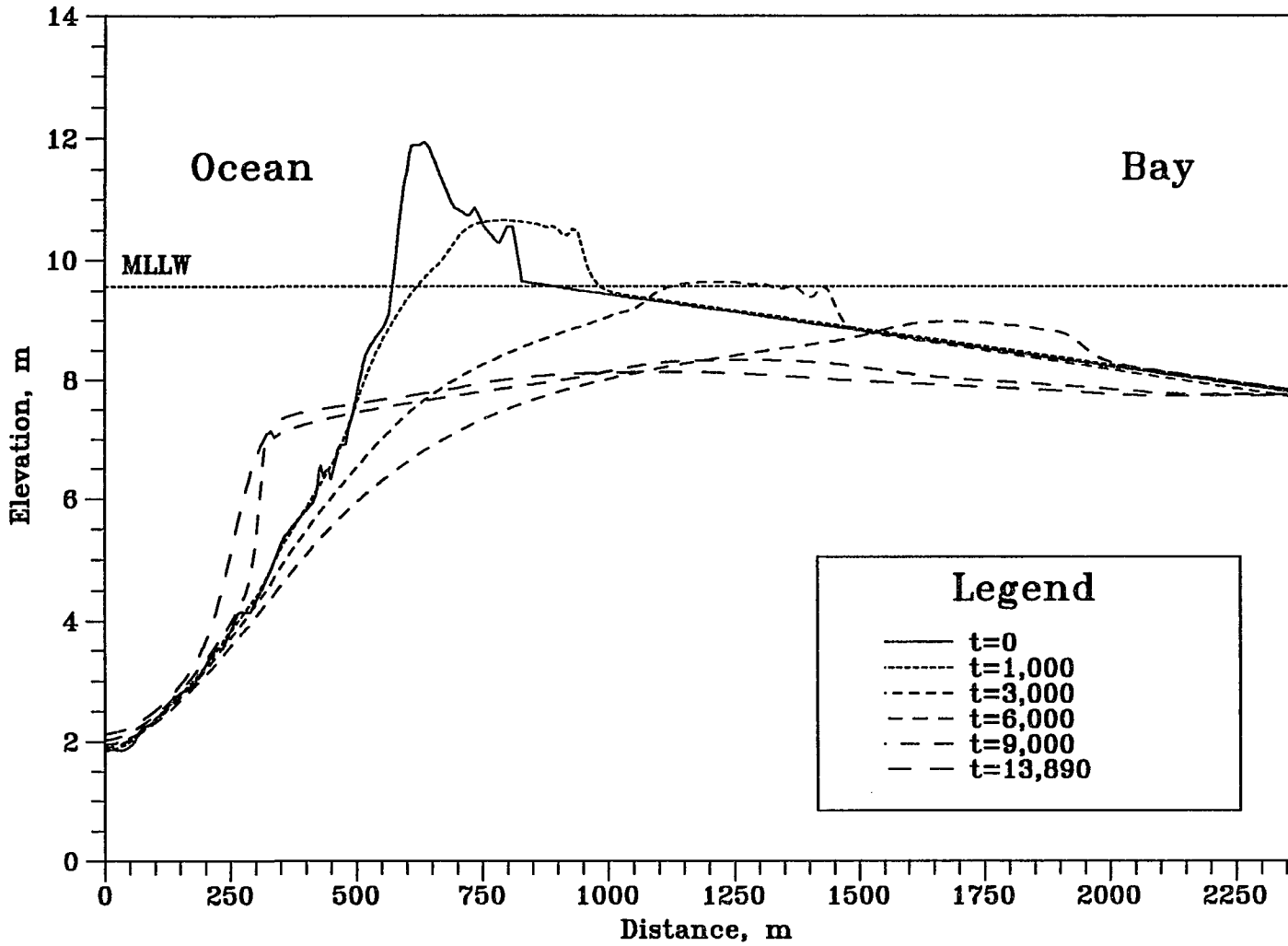


Figure 6.80 Bed Elevation Changes in Stage III/IV at t=0, 1000, 3000, 6000, 9000 and 13890. ($h_{om}=4.5m$, $h_{bm}=3.0m$, $t_{lag}=4hr$, $D_{50}=0.3mm$)

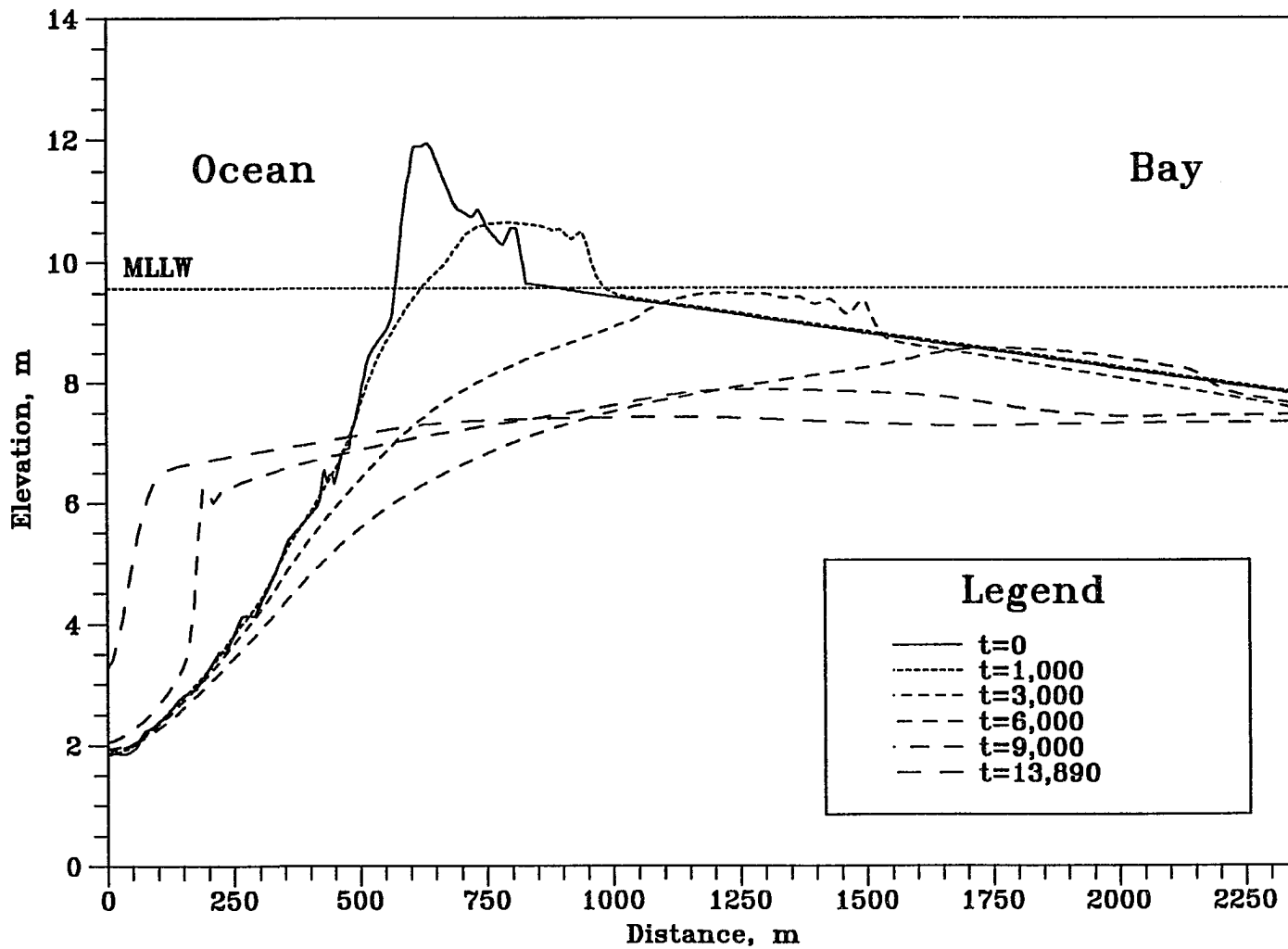


Figure 6.81 Bed Elevation Changes in Stage III/IV at t=0, 1000, 3000, 6000, 9000 and 13890. ($h_{om}=4.5m$, $h_{bm}=3.0m$, $t_{lag}=5hr$, $D_{50}=0.3mm$)

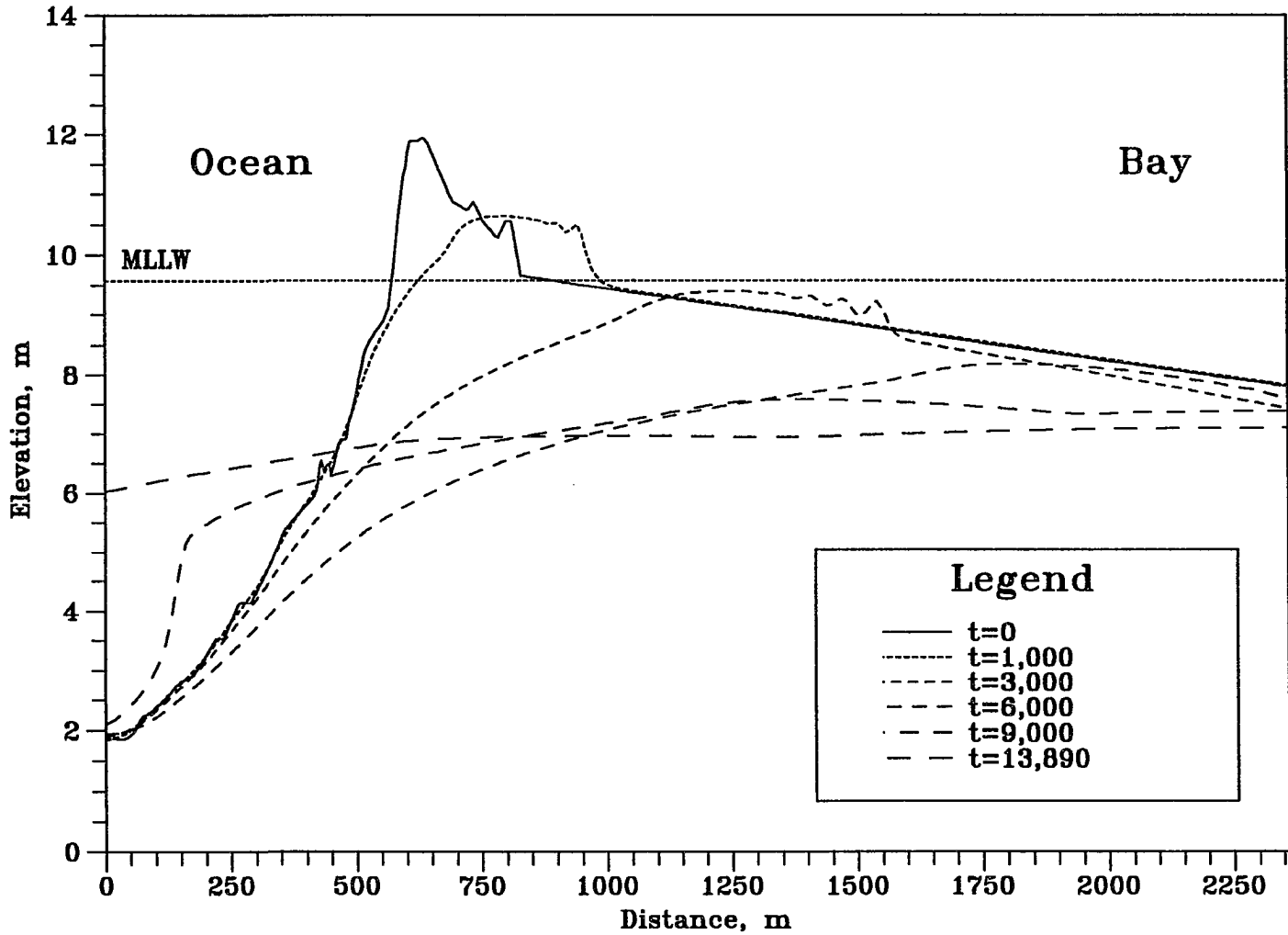


Figure 6.82 Bed Elevation Changes in Stage III/IV at t=0, 1000, 3000, 6000, 9000 and 13890. ($h_{om}=4.5m$, $h_{bm}=3.0m$, $t_{lag}=6hr$, $D_{50}=0.3mm$)

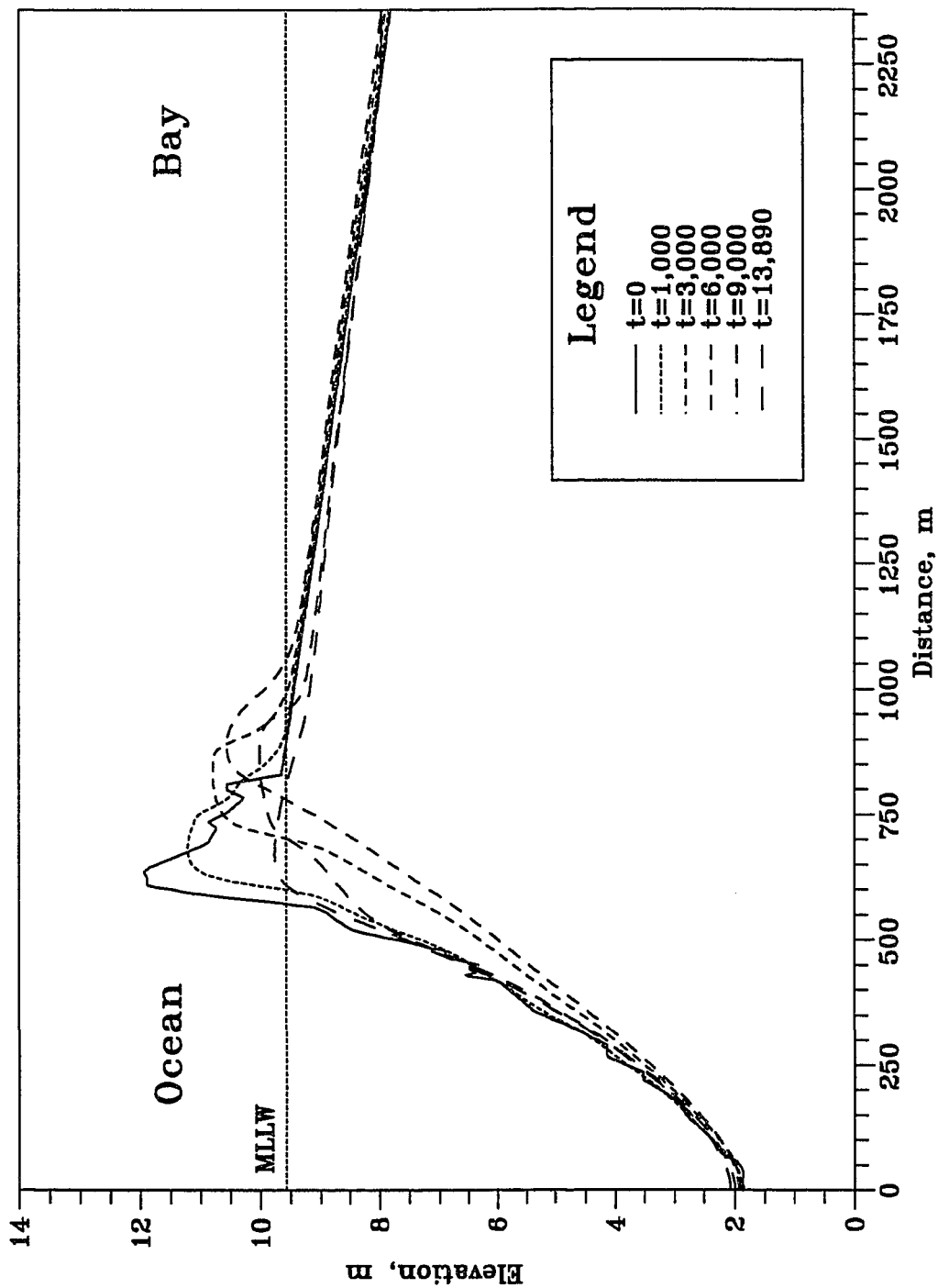


Figure 6.83 Bed Elevation Changes in Stage III/IV at $t=0, 1000, 3000, 6000, 9000$ and 13628 . ($h_{om}=4.0m, h_{bm}=3.0m, t_{ug}=3hr, D_{50}=0.1mm$)

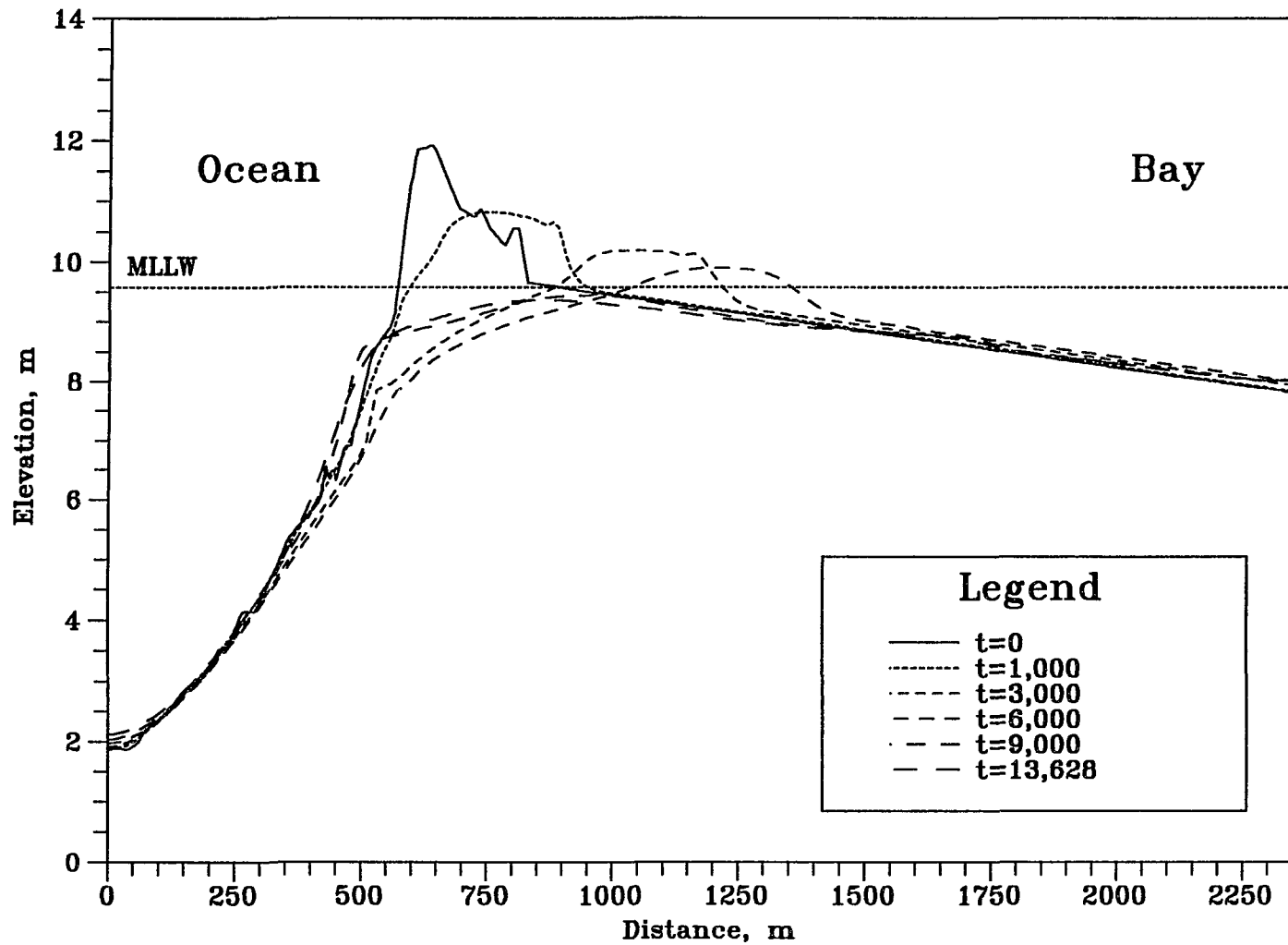


Figure 6.84 Bed Elevation Changes in Stage III/IV at $t=0, 1000, 3000, 6000, 9000$ and 13628 . ($h_{om}=4.0m, h_{bm}=3.0m, t_{lag}=3hr, D_{50}=0.2mm$)

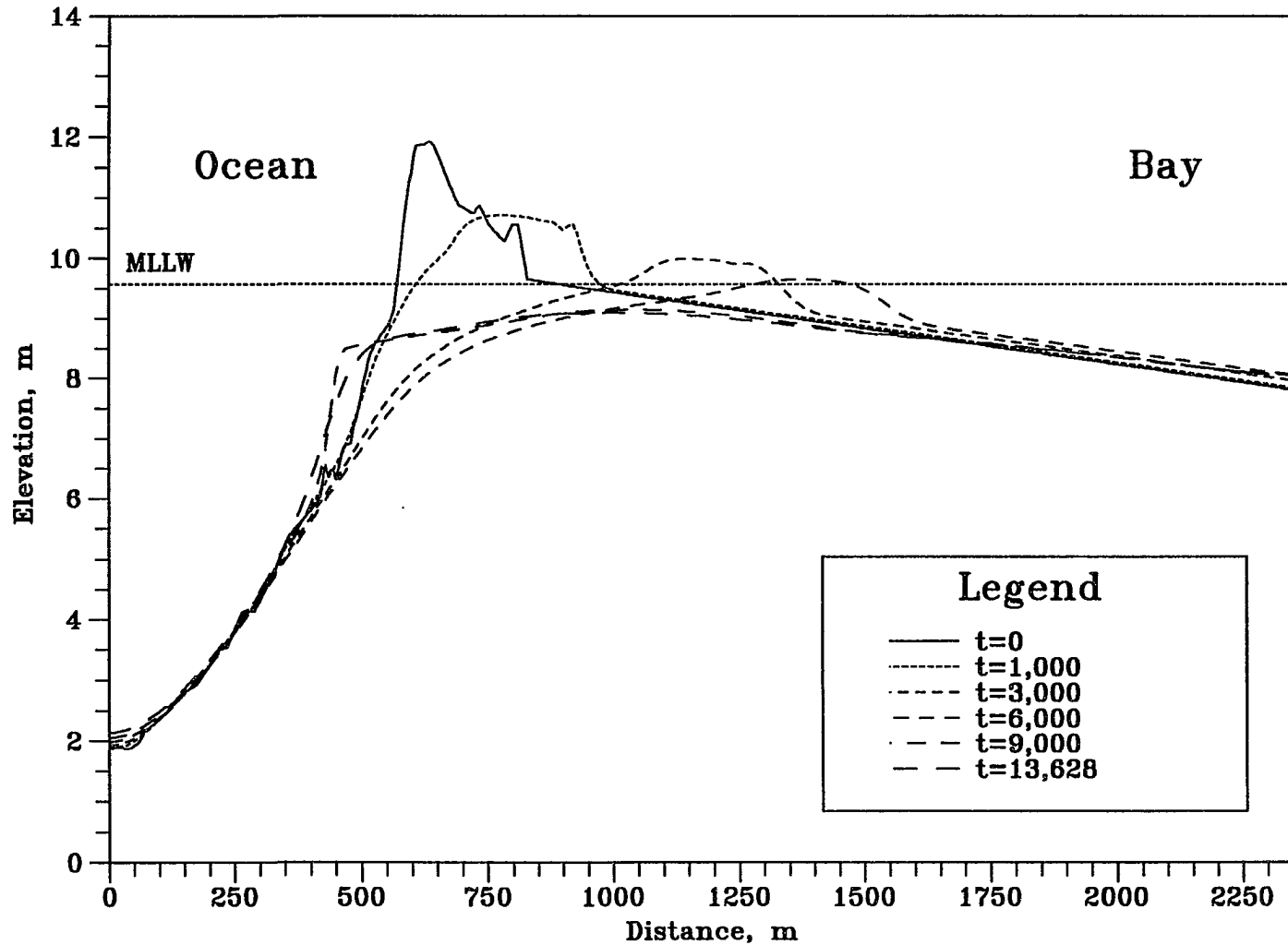


Figure 6.85 Bed Elevation Changes in Stage III/IV at t=0, 1000, 3000, 6000, 9000 and 13628. ($h_{om}=4.0m$, $h_{bm}=3.0m$, $t_{lag}=3hr$, $D_{50}=0.3mm$)

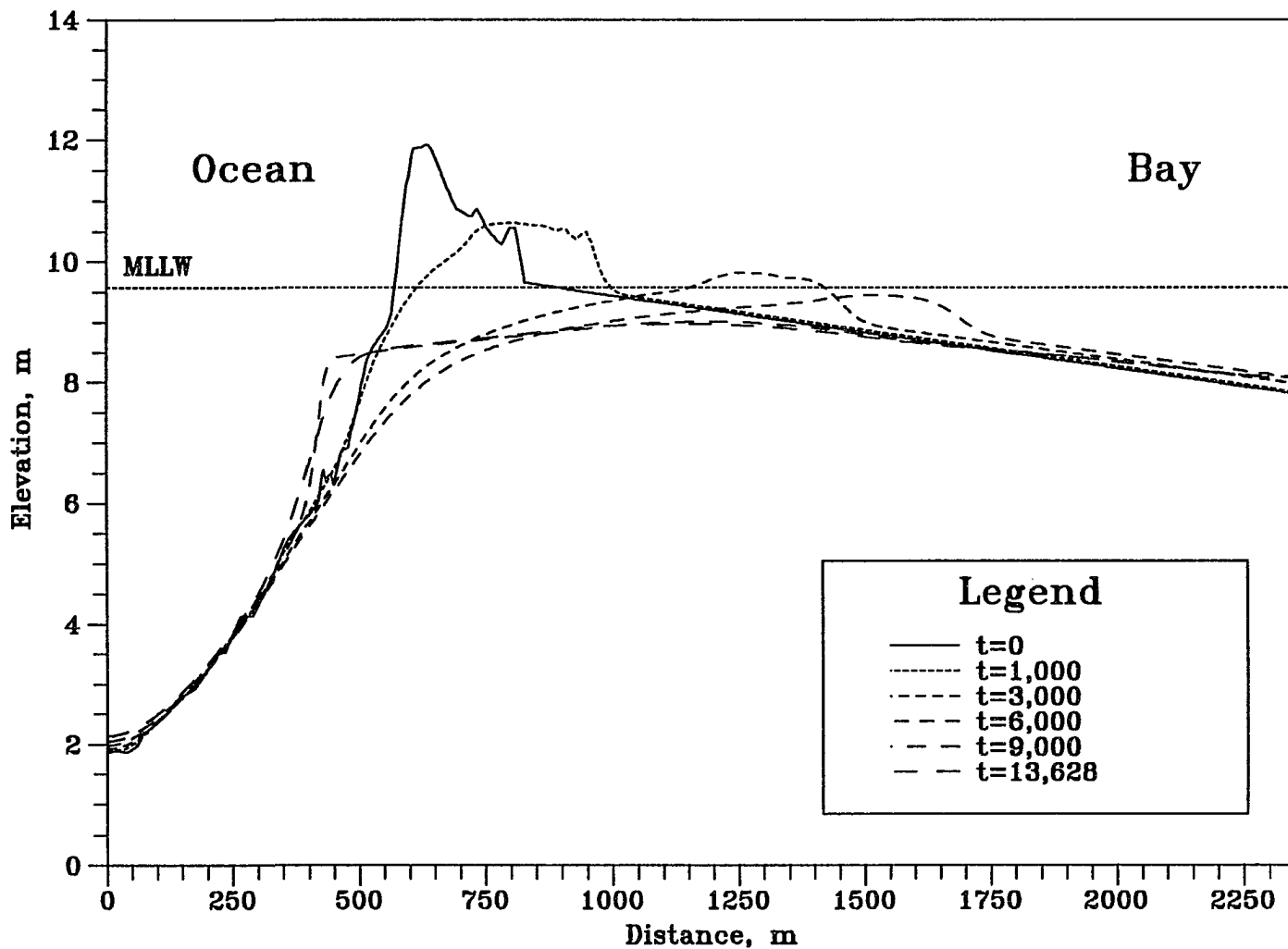


Figure 6.86 Bed Elevation Changes in Stage III/IV at t=0, 1000, 3000, 6000, 9000 and 13628. ($h_{om}=4.0m$, $h_{bm}=3.0m$, $t_{lag}=3hr$, $D_{50}=0.4mm$)

240

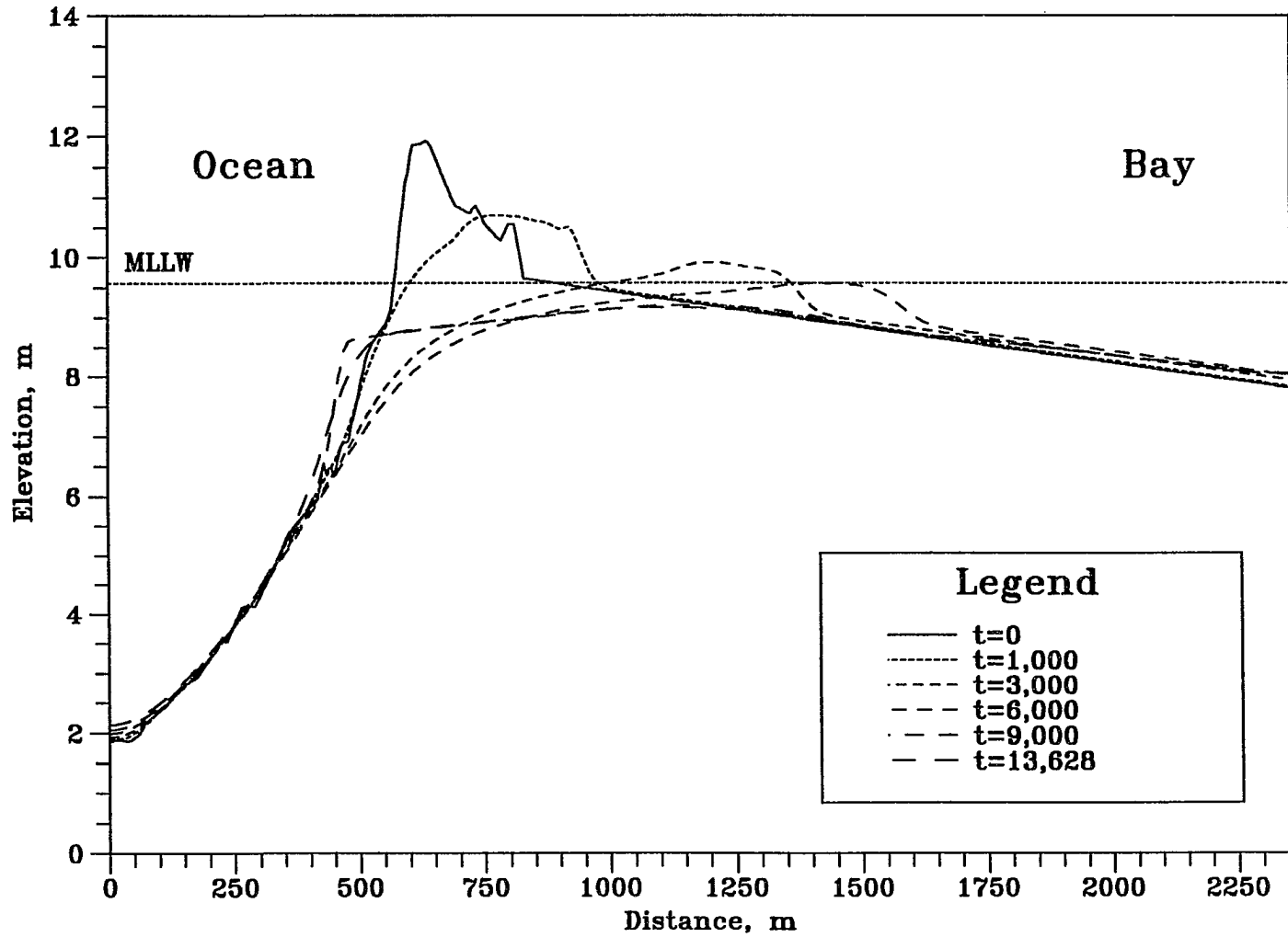


Figure 6.87 Bed Elevation Changes in Stage III/IV at $t=0, 1000, 3000, 6000, 9000$ and 13628 . ($h_{om}=4.0m, h_{bm}=3.0m, t_{lag}=3hr, D_{50}=0.6mm$)

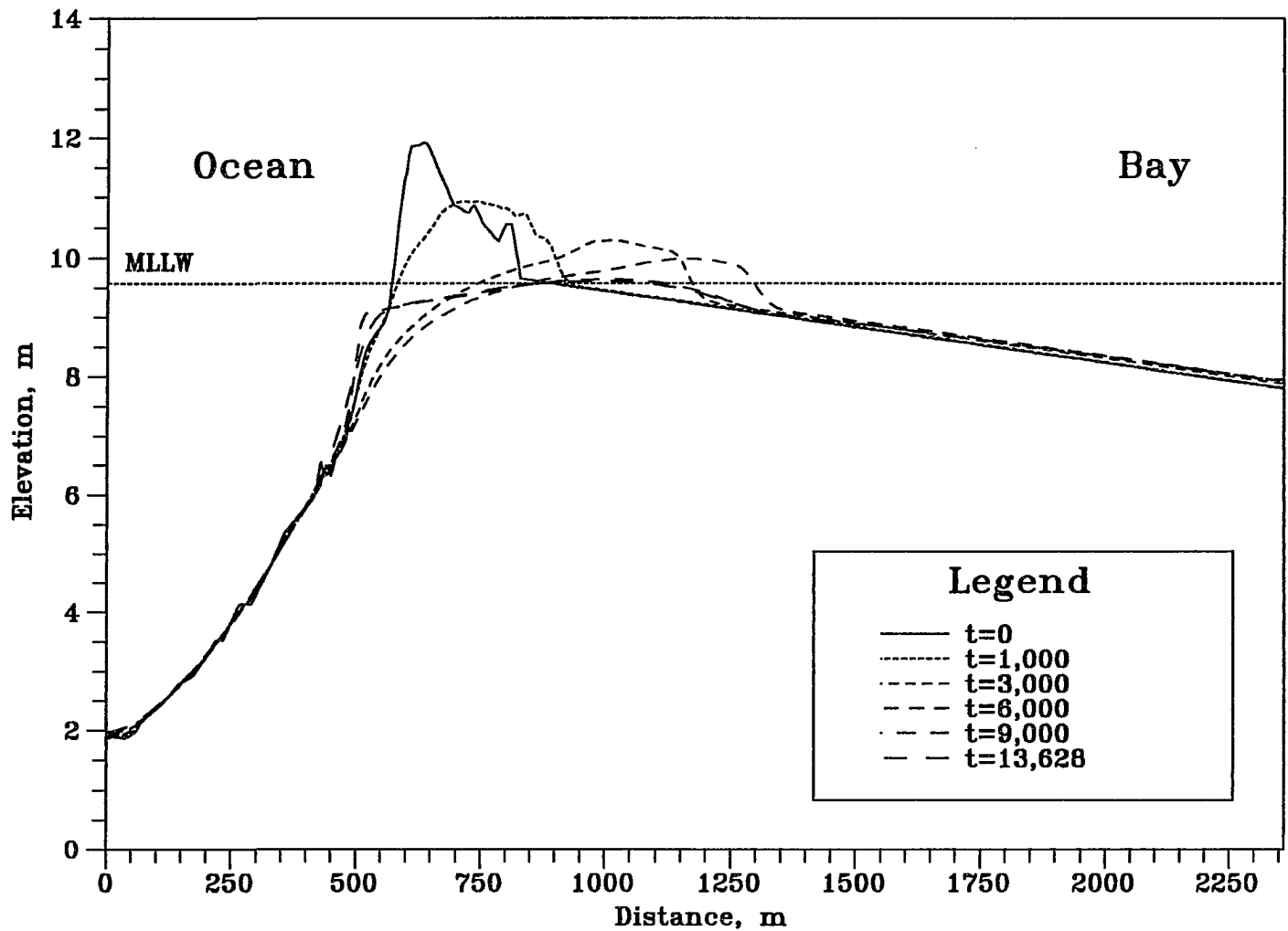


Figure 6.88 Bed Elevation Changes in Stage III/IV at t=0, 1000, 3000, 6000, 9000 and 13628. ($h_{om}=4.0m$, $h_{bm}=3.0m$, $t_{lag}=3hr$, $D_{50}=1.0mm$)

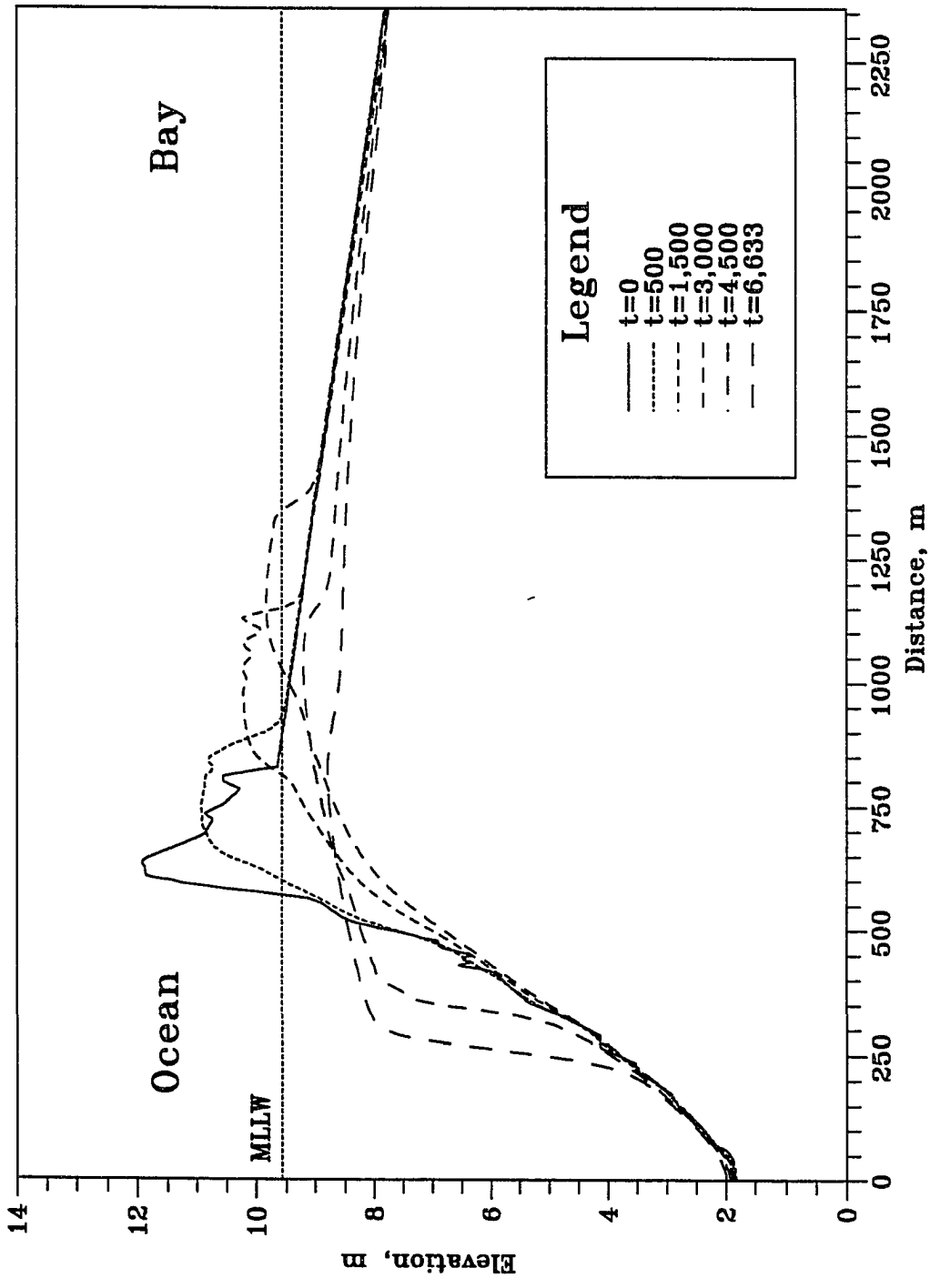


Figure 6.89 Bed Elevation Changes in Stage III/IV at $t=0, 500, 1500, 3000, 4500$ and 6633 . ($h_{om}=4.0m, h_{bm}=3.0m, t_{lag}=3hr, D_{50}=0.3mm, T=12hr$)

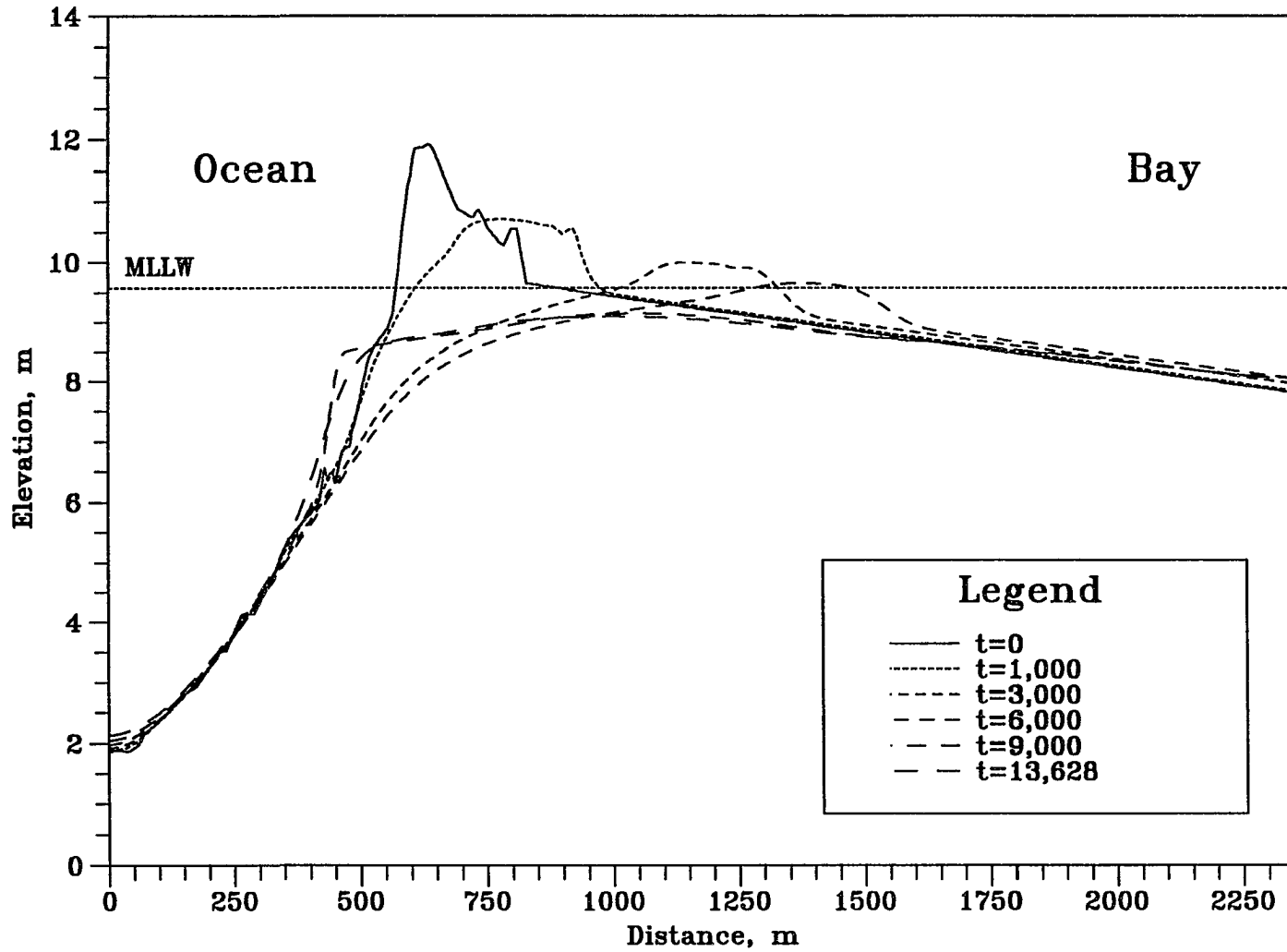


Figure 6.90 Bed Elevation Changes in Stage III/IV at $t=0, 1000, 3000, 6000, 9000$ and 13628 . ($h_{om}=4.0\text{m}$, $h_{bm}=3.0\text{m}$, $t_{1\sigma}=3\text{hr}$, $D_{50}=0.3\text{mm}$, $T=24\text{hr}$)

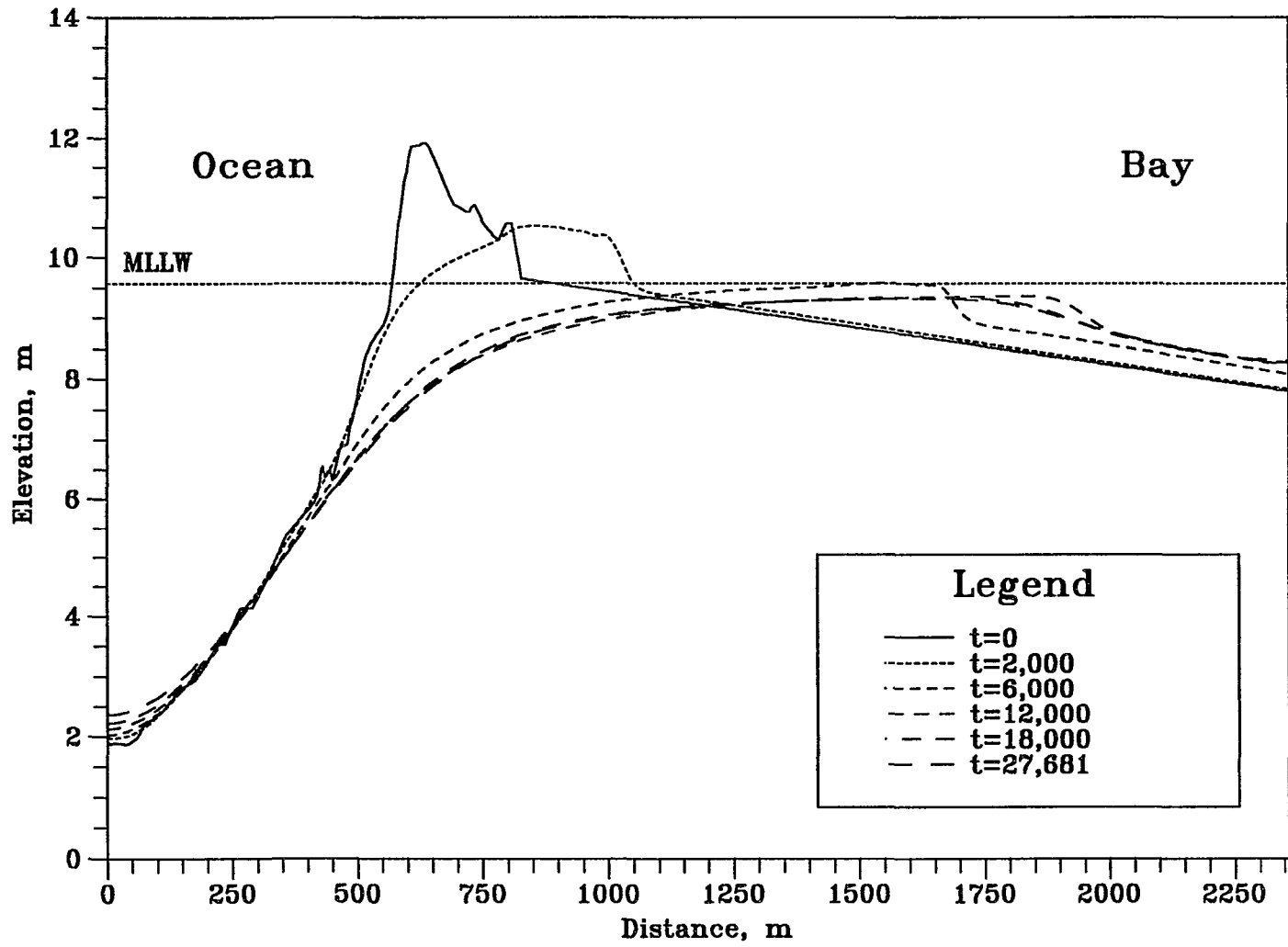


Figure 6.91 Bed Elevation Changes in Stage III/IV at $t=0, 2000, 6000, 12000, 18000$ and 27681 . ($h_{om}=4.0m$, $h_{bm}=3.0m$, $t_{lag}=3hr$, $D_{50}=0.3mm$, $T=48hr$)

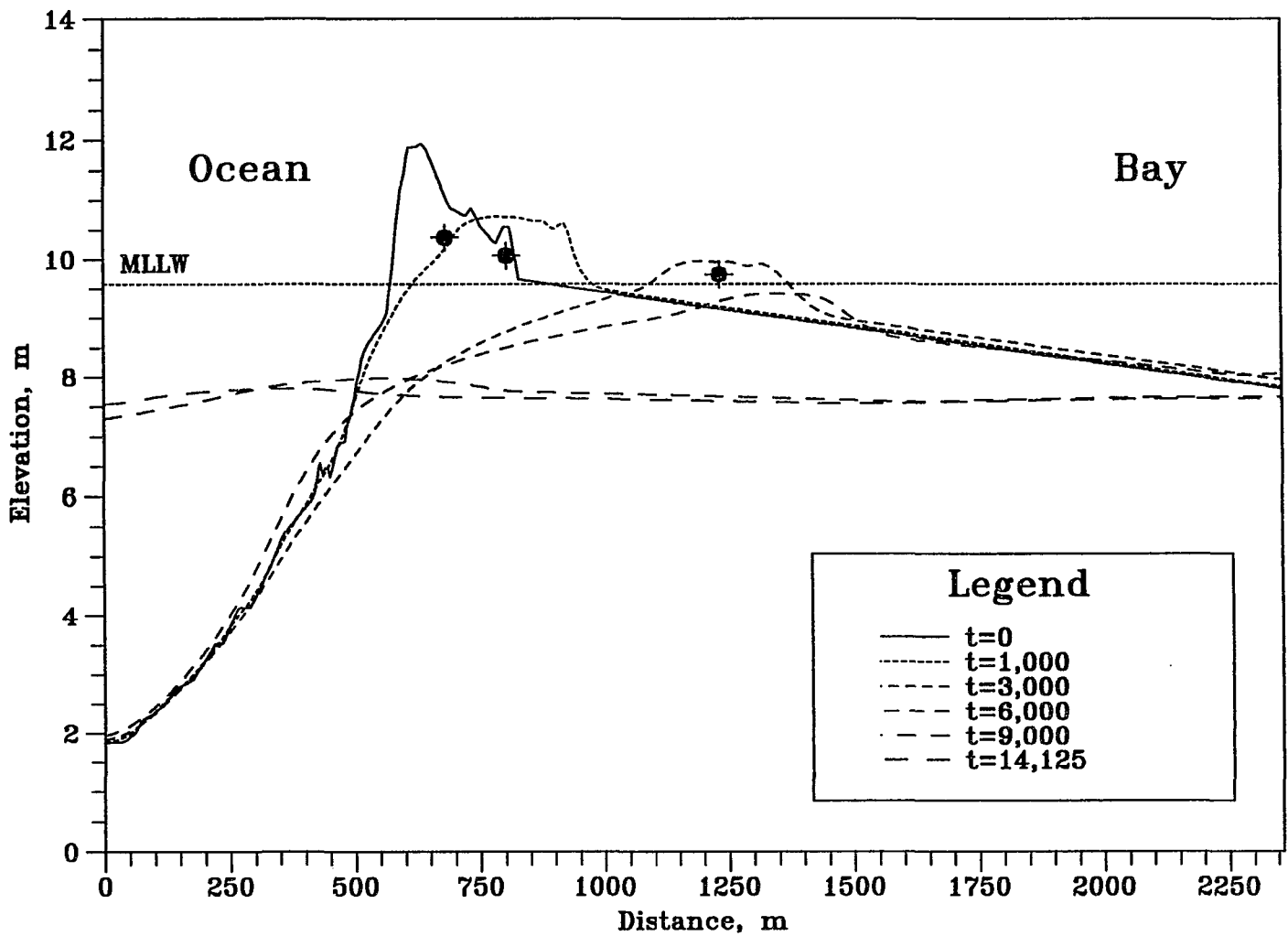


Figure 6.92 Bed Elevation Changes with Centroids of the Dune above MLLW in Stage III/IV at t=0, 1000, 3000, 6000, 9000 and 14125. ($h_{om}=5m$, $h_{bm}=5m$, $t_{lag}=3hr$, $D_{50}=0.3mm$)

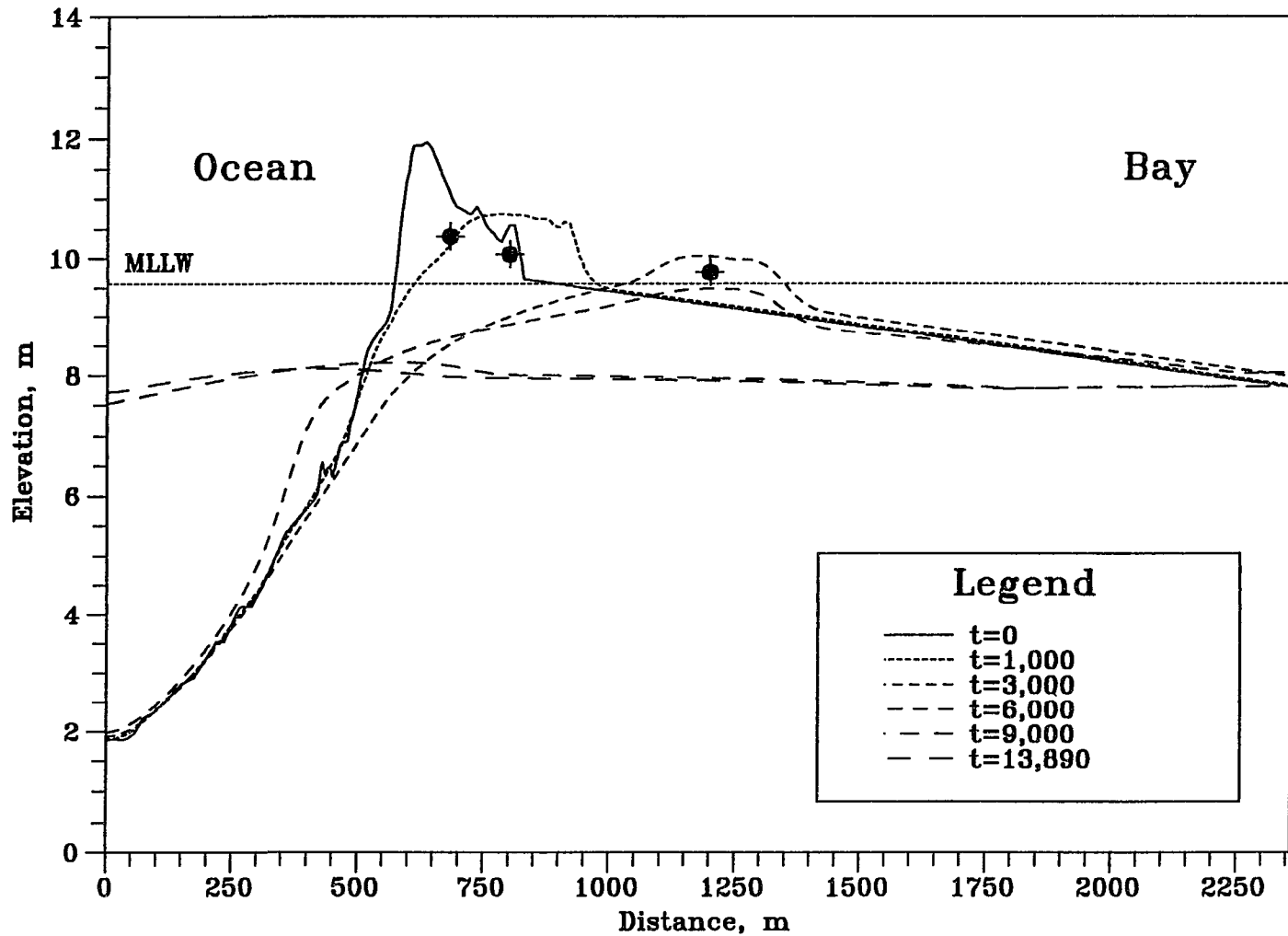


Figure 6.93 Bed Elevation Changes with Centroids of the Dune above MLLW in Stage III/IV at t=0, 1000, 3000, 6000, 9000 and 13890. ($h_{om}=4.5m$, $h_{bm}=4.5m$, $t_{lag}=3hr$, $D_{50}=0.3mm$)

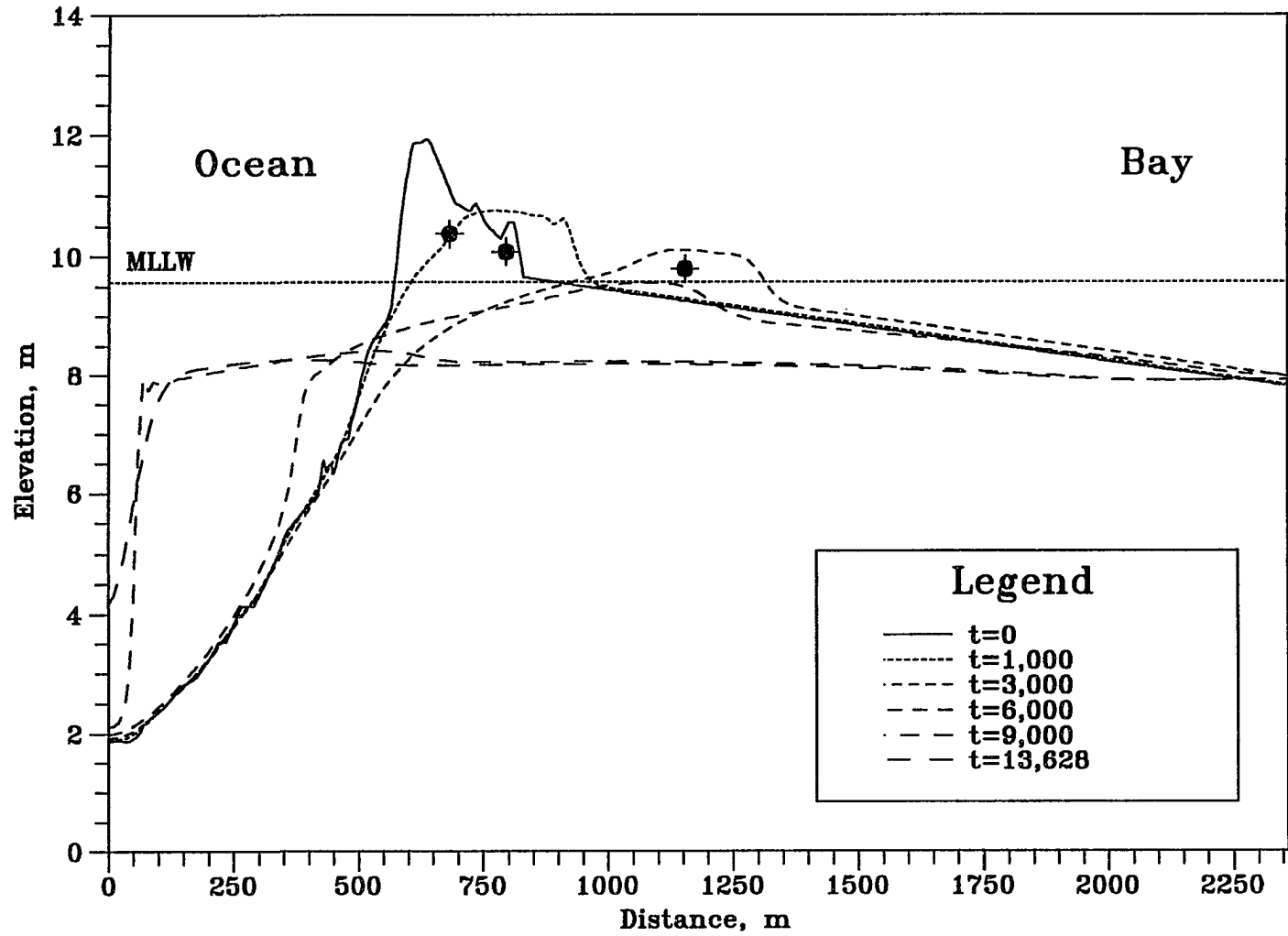


Figure 6.94 Bed Elevation Changes with Centroids of the Dune above MLLW in Stage III/IV at t=0, 1000, 3000, 6000, 9000 and 13628. ($h_{om}=4.0m$, $h_{bm}=4.0m$, $t_{lag}=3hr$, $D_{50}=0.3mm$)

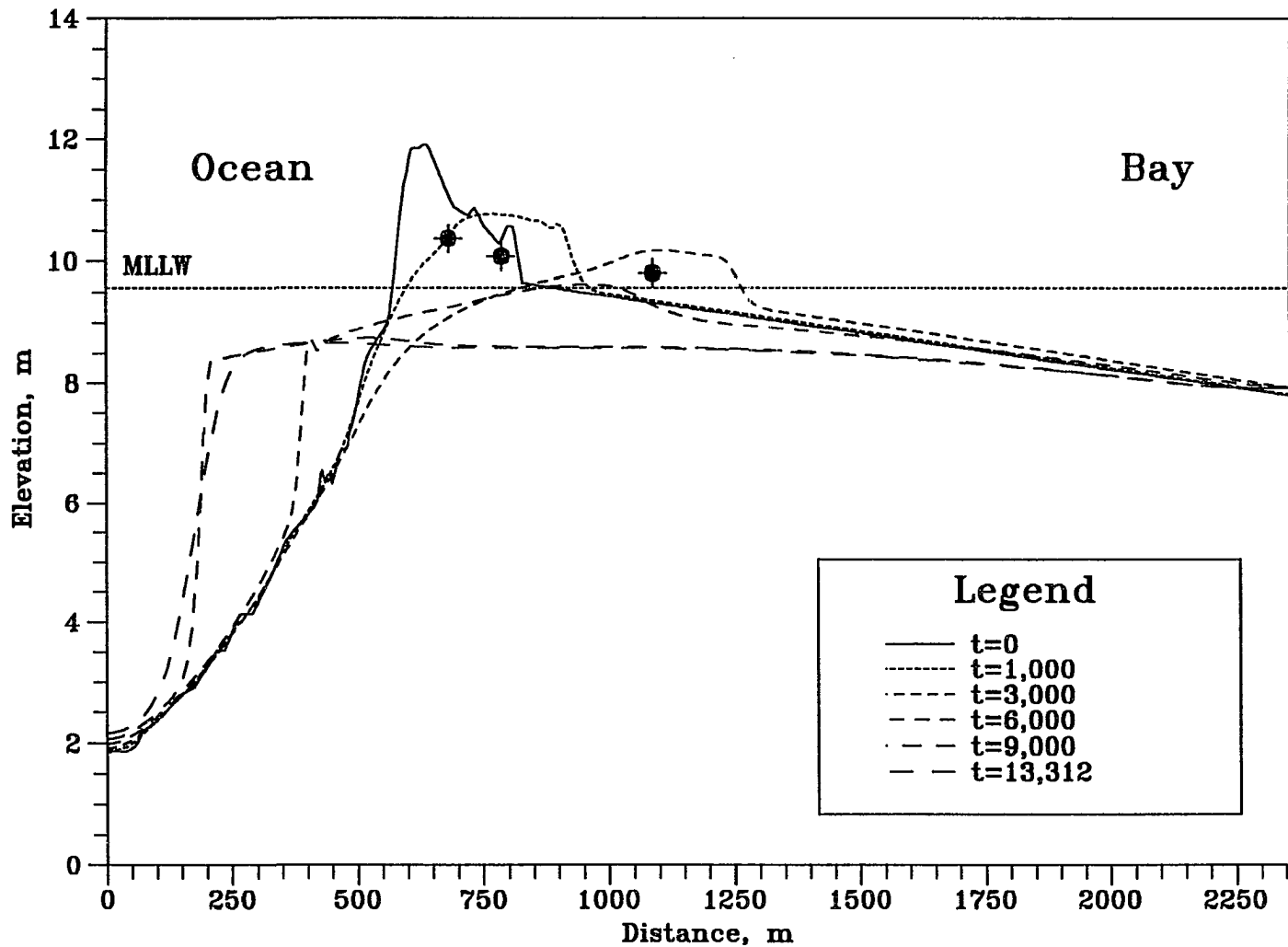


Figure 6.95 Bed Elevation Changes with Centroids of the Dune above MLLW in Stage III/IV at $t=0, 1000, 3000, 6000, 9000$ and 13312 . ($h_{om}=3.5m, h_{bm}=3.5m, t_{lag}=3hr, D_{50}=0.3mm$)

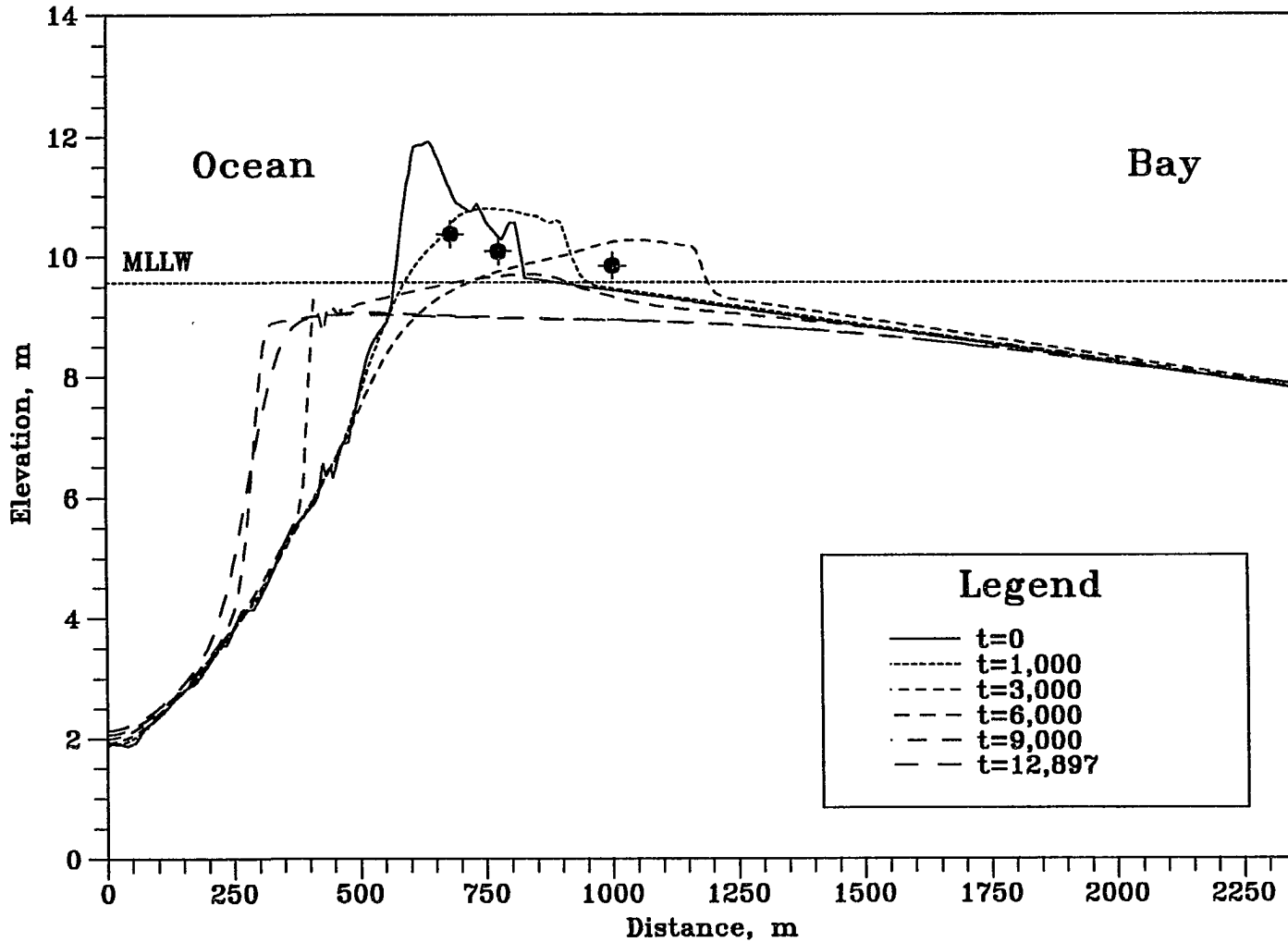


Figure 6.96 Bed Elevation Changes with Centroids of the Dune above MLLW in Stage III/IV at t=0, 1000, 3000, 6000, 9000 and 12897. ($h_{om}=3.0m$, $h_{bm}=3.0m$, $t_{lag}=3hr$, $D_{80}=0.3mm$)

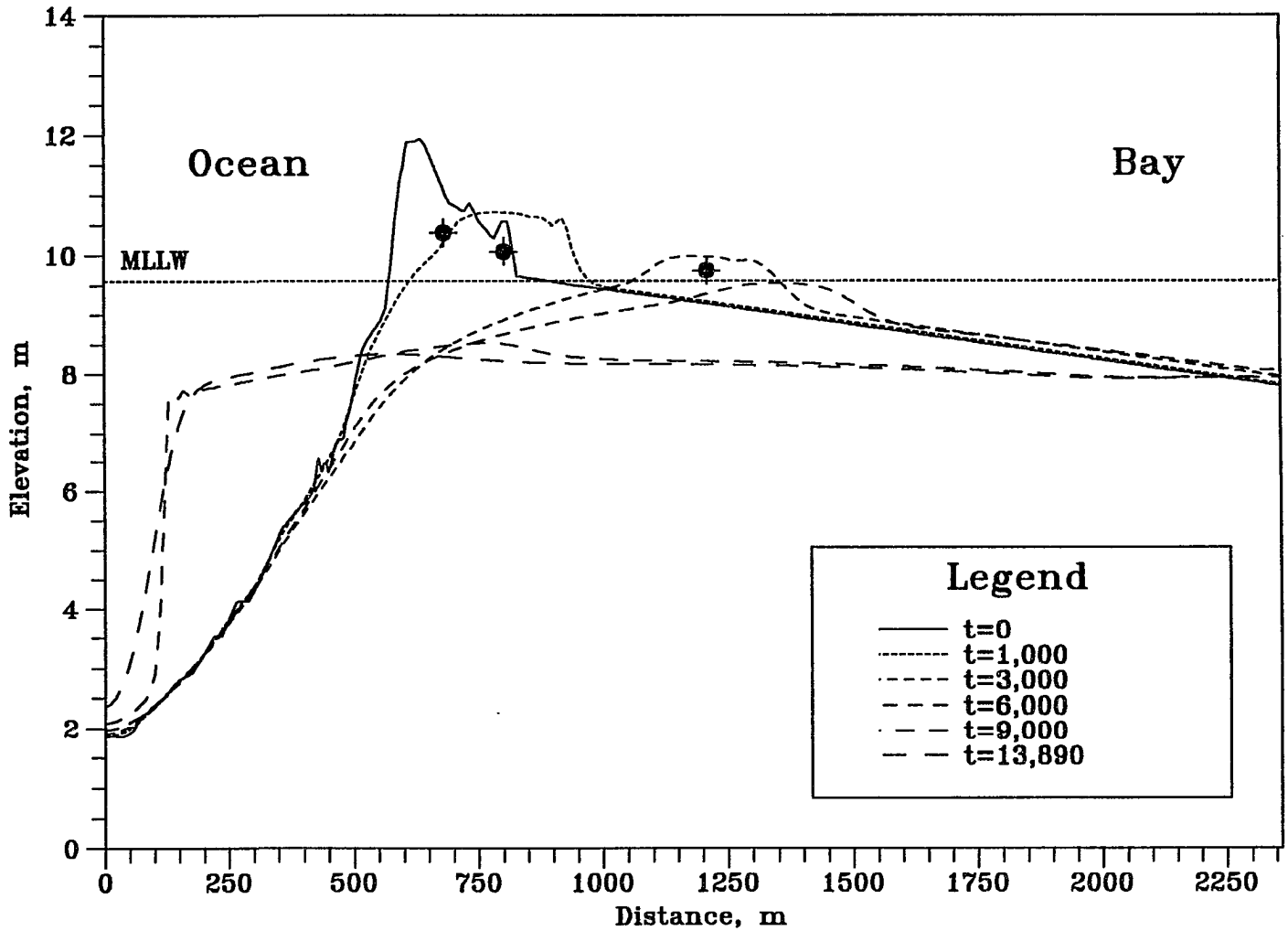


Figure 6.97 Bed Elevation Changes with Centroids of the Dune above MLLW in Stage III/IV at t=0, 1000, 3000, 6000, 9000 and 13890. ($h_{om}=4.5m$, $h_{bm}=4.0m$, $t_{lag}=3hr$, $D_{50}=0.3mm$)

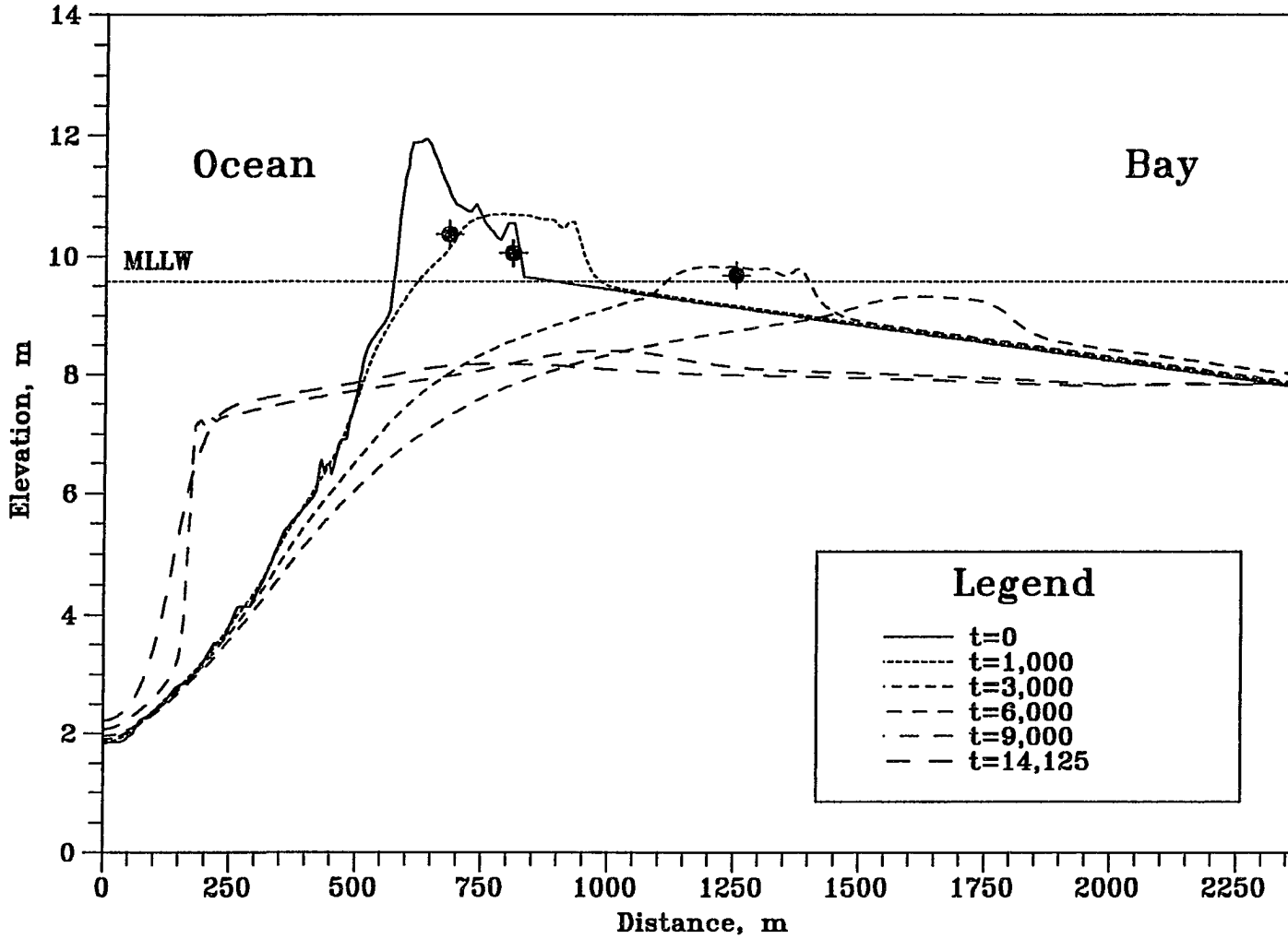


Figure 6.98 Bed Elevation Changes with Centroids of the Dune above MLLW in Stage III/IV at $t=0, 1000, 3000, 6000, 9000$ and 14125 .
 ($h_{om}=5.0m, h_{bm}=4.0m, t_{lag}=3hr, D_{50}=0.3mm$)

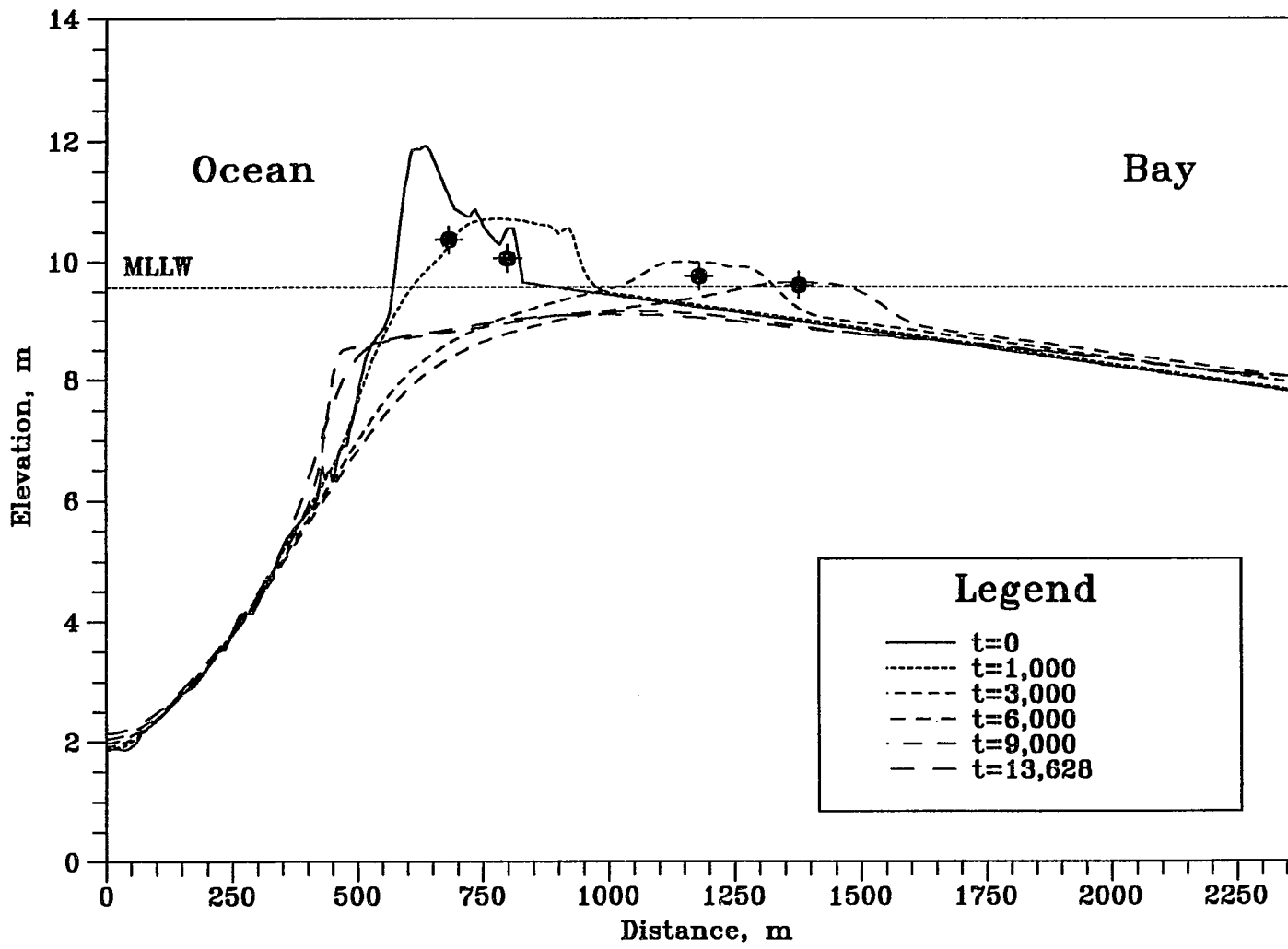


Figure 6.99 Bed Elevation Changes with Centroids of the Dune above MLLW in Stage III/IV at t=0, 1000, 3000, 6000, 9000 and 13628. ($h_{om}=4.0m$, $h_{bm}=3.0m$, $t_{lag}=3hr$, $D_{50}=0.3mm$)

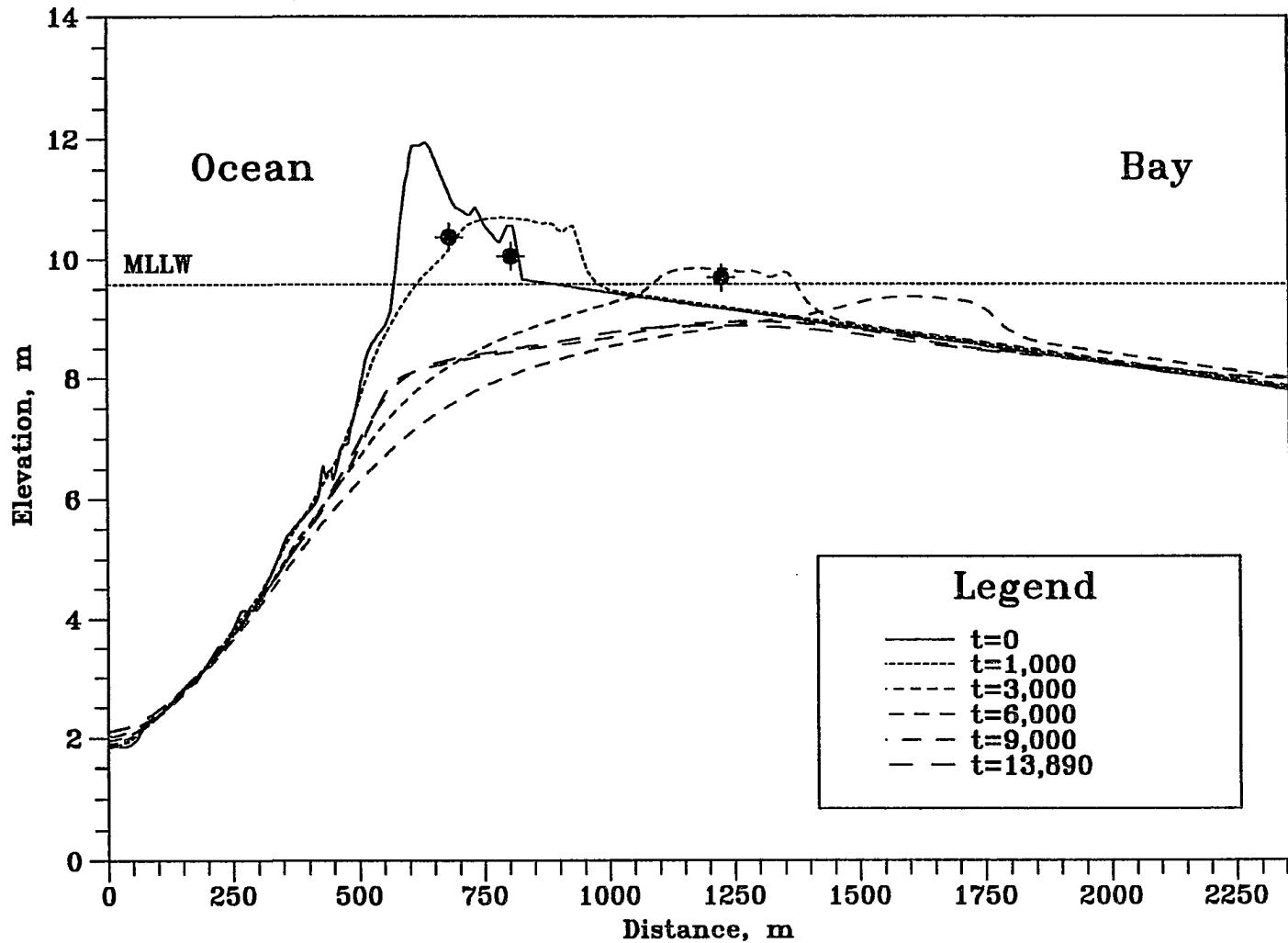


Figure 6.100 Bed Elevation Changes with Centroids of the Dune above MLLW in Stage III/IV at t=0, 1000, 3000, 6000, 9000 and 13890. ($h_{om}=4.5m$, $h_{bm}=3.0m$, $t_{lag}=3hr$, $D_{50}=0.3mm$)

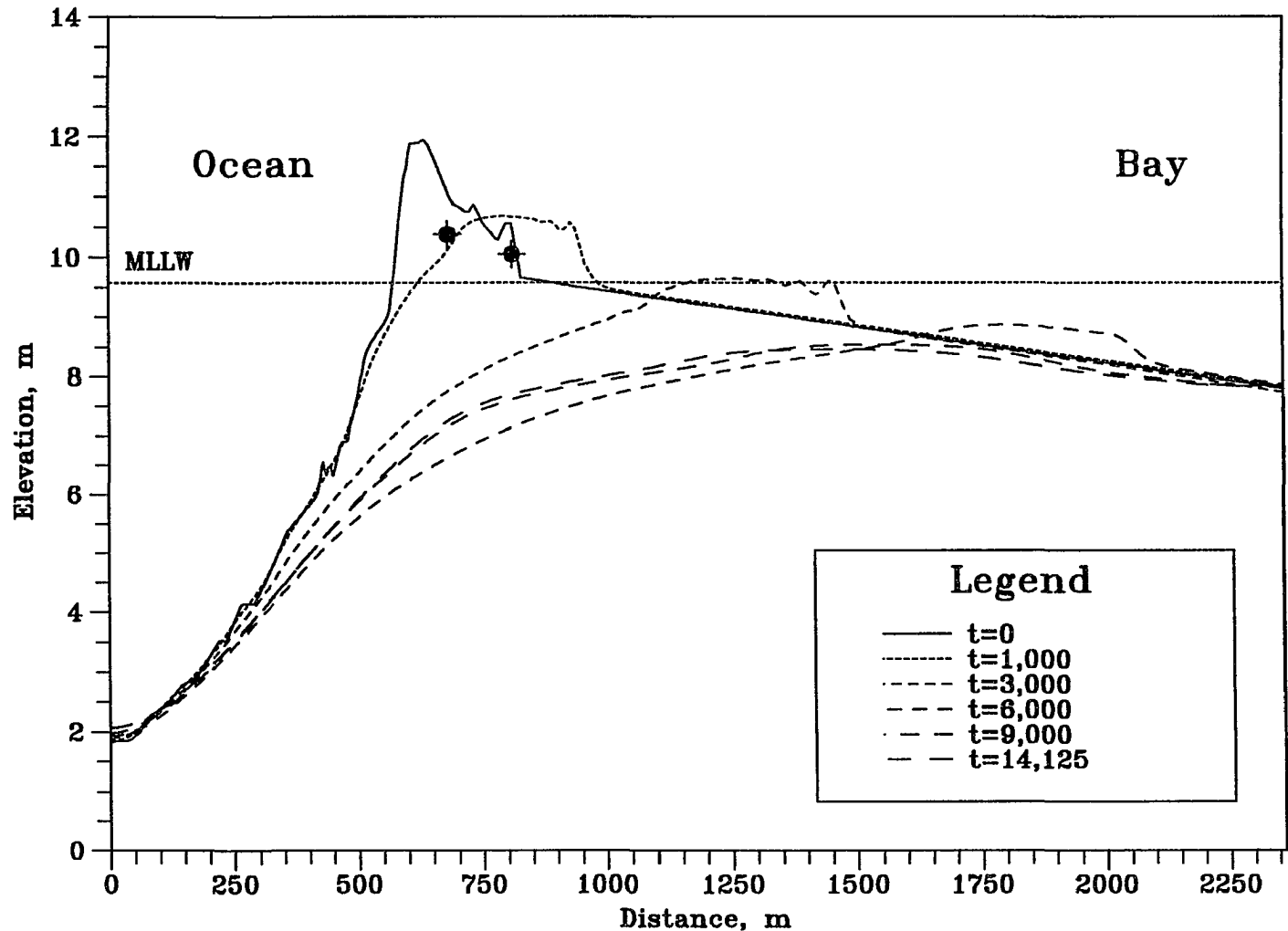


Figure 6.101 Bed Elevation Changes with Centroids of the Dune above MLLW in Stage III/IV at t=0, 1000, 3000, 6000, 9000 and 14125. ($h_{om}=5.0m$, $h_{bm}=3.0m$, $t_{lag}=3hr$, $D_{50}=0.3mm$)

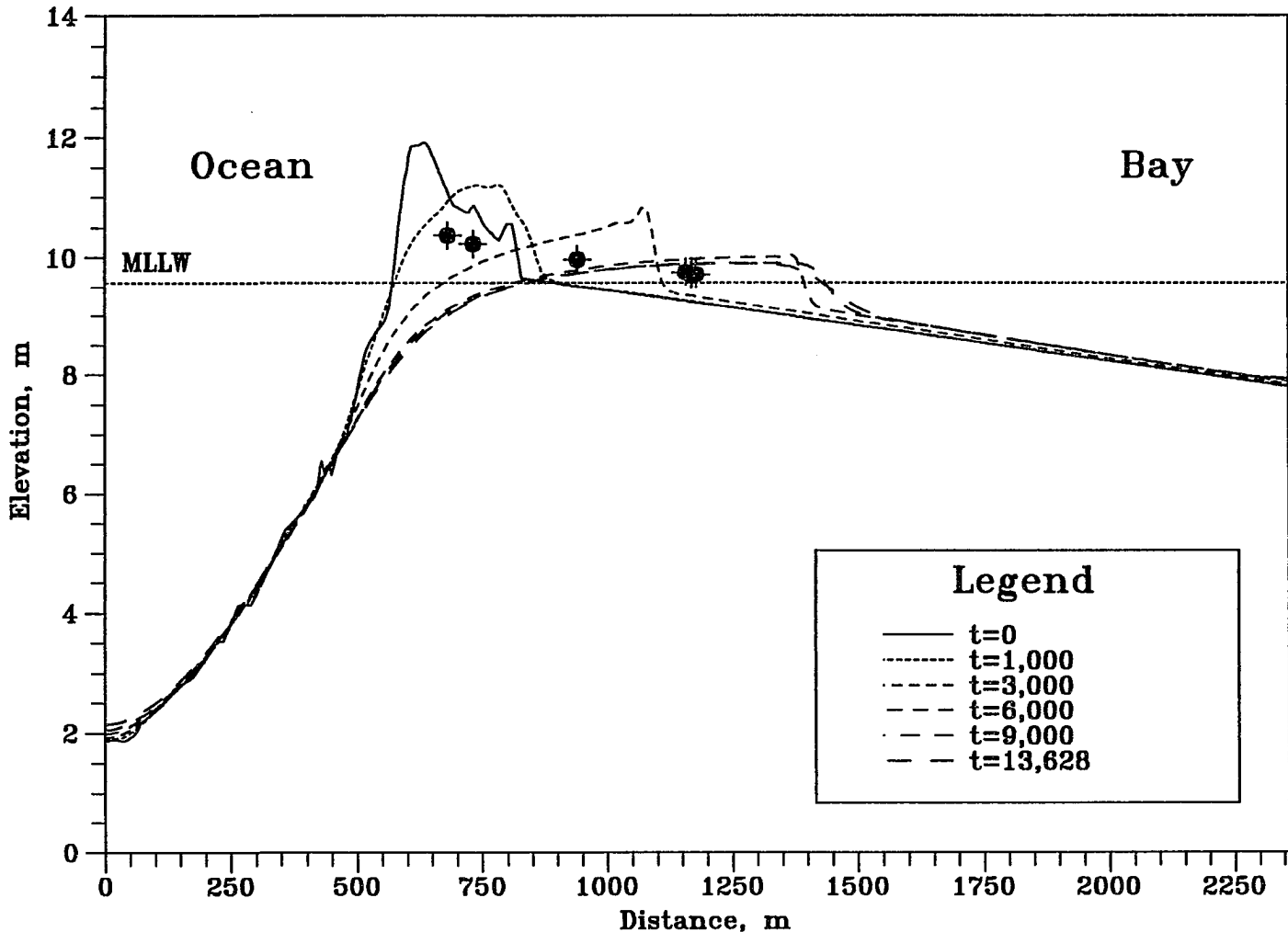


Figure 6.102 Bed Elevation Changes with Centroids of the Dune above MLLW in Stage III/IV at t=0, 1000, 3000, 6000, 9000 and 13628. ($h_{om}=4.0m$, $h_{bm}=3.0m$, $t_{lag}=0hr$, $D_{50}=0.3mm$)

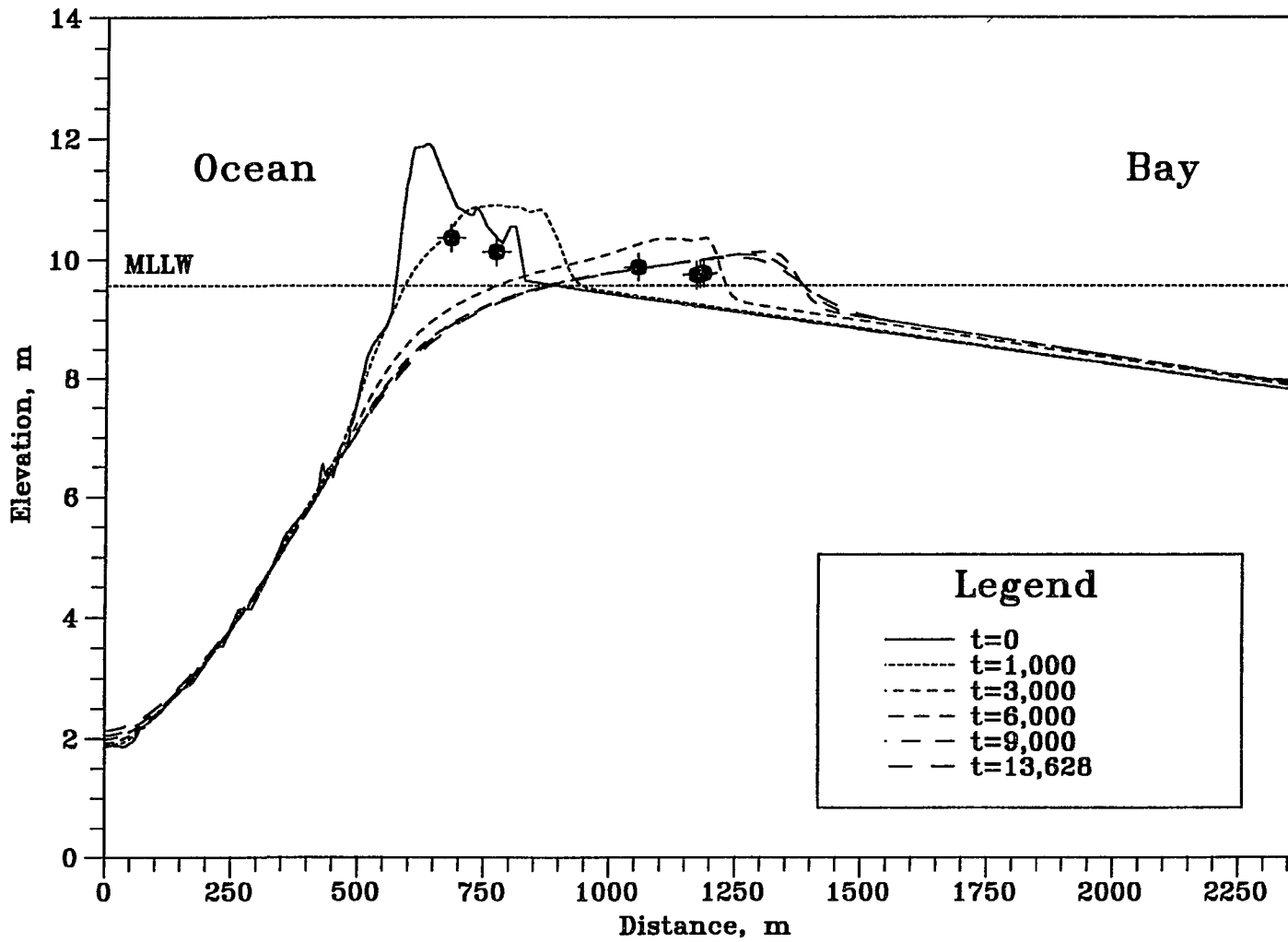


Figure 6.103 Bed Elevation Changes with Centroids of the Dune above MLLW in Stage III/IV at t=0, 1000, 3000, 6000, 9000 and 13628. ($h_{om}=4.0m$, $h_{bm}=3.0m$, $t_{lag}=1hr$, $D_{50}=0.3mm$)

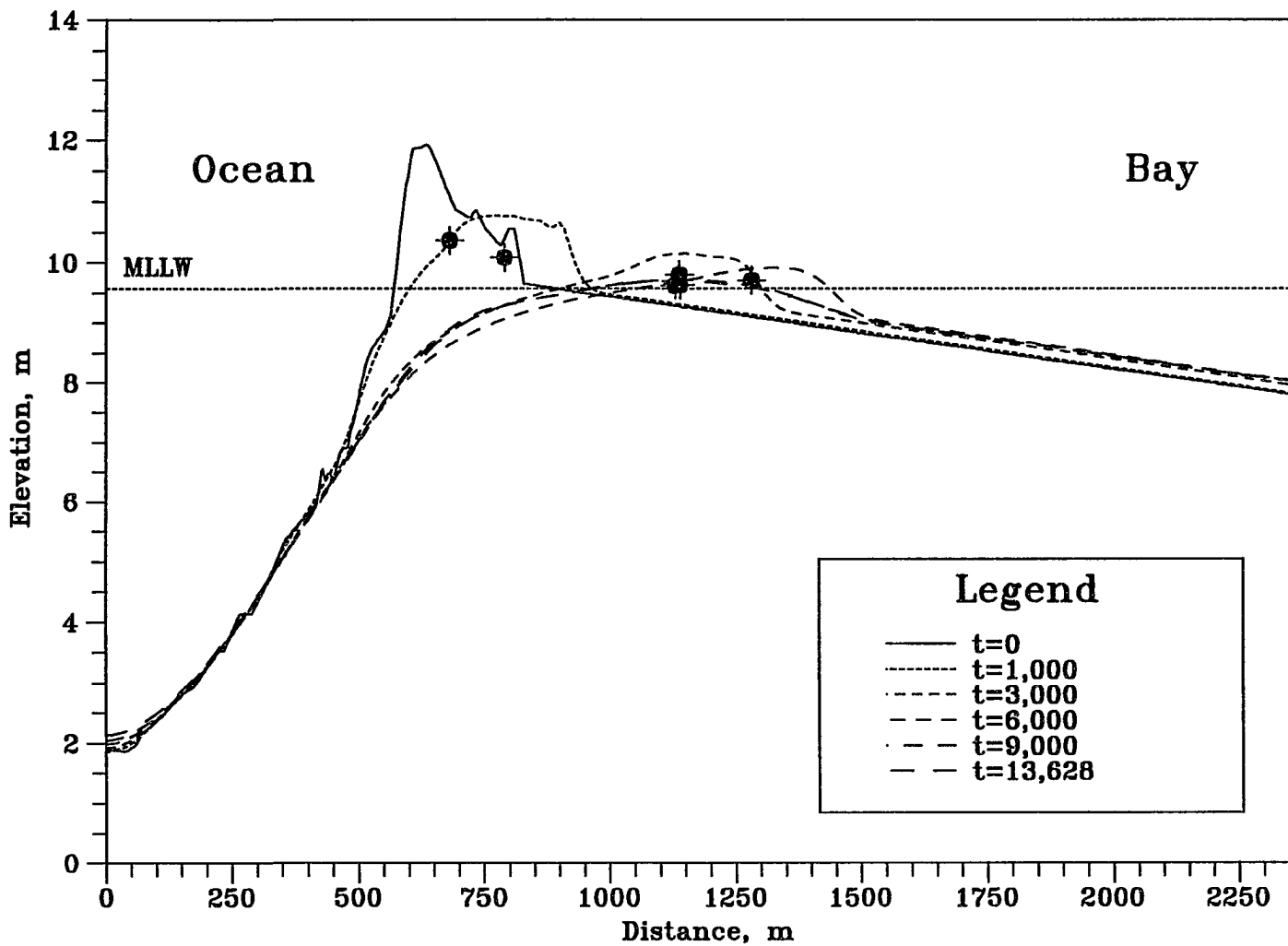


Figure 6.104 Bed Elevation Changes with Centroids of the Dune above MLLW in Stage III/IV at $t=0, 1000, 3000, 6000, 9000$ and 13628 . ($h_{om}=4.0m, h_{bm}=3.0m, t_{lag}=2hr, D_{50}=0.3mm$)

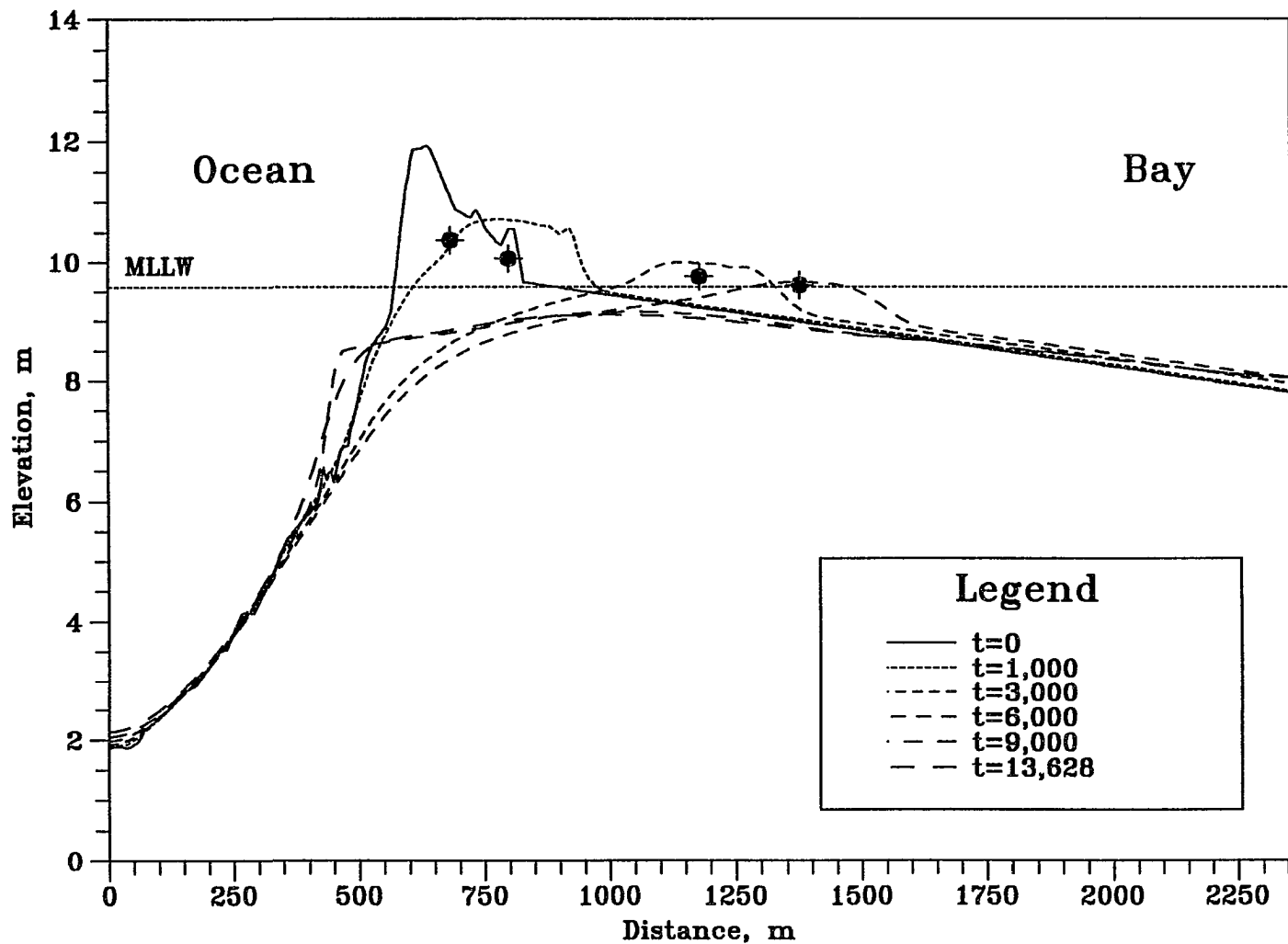


Figure 6.105 Bed Elevation Changes with Centroids of the Dune above MLLW in Stage III/IV at t=0, 1000, 3000, 6000, 9000 and 13628. ($h_{om}=4.0m$, $h_{bm}=3.0m$, $t_{1sg}=3hr$, $D_{50}=0.3mm$)

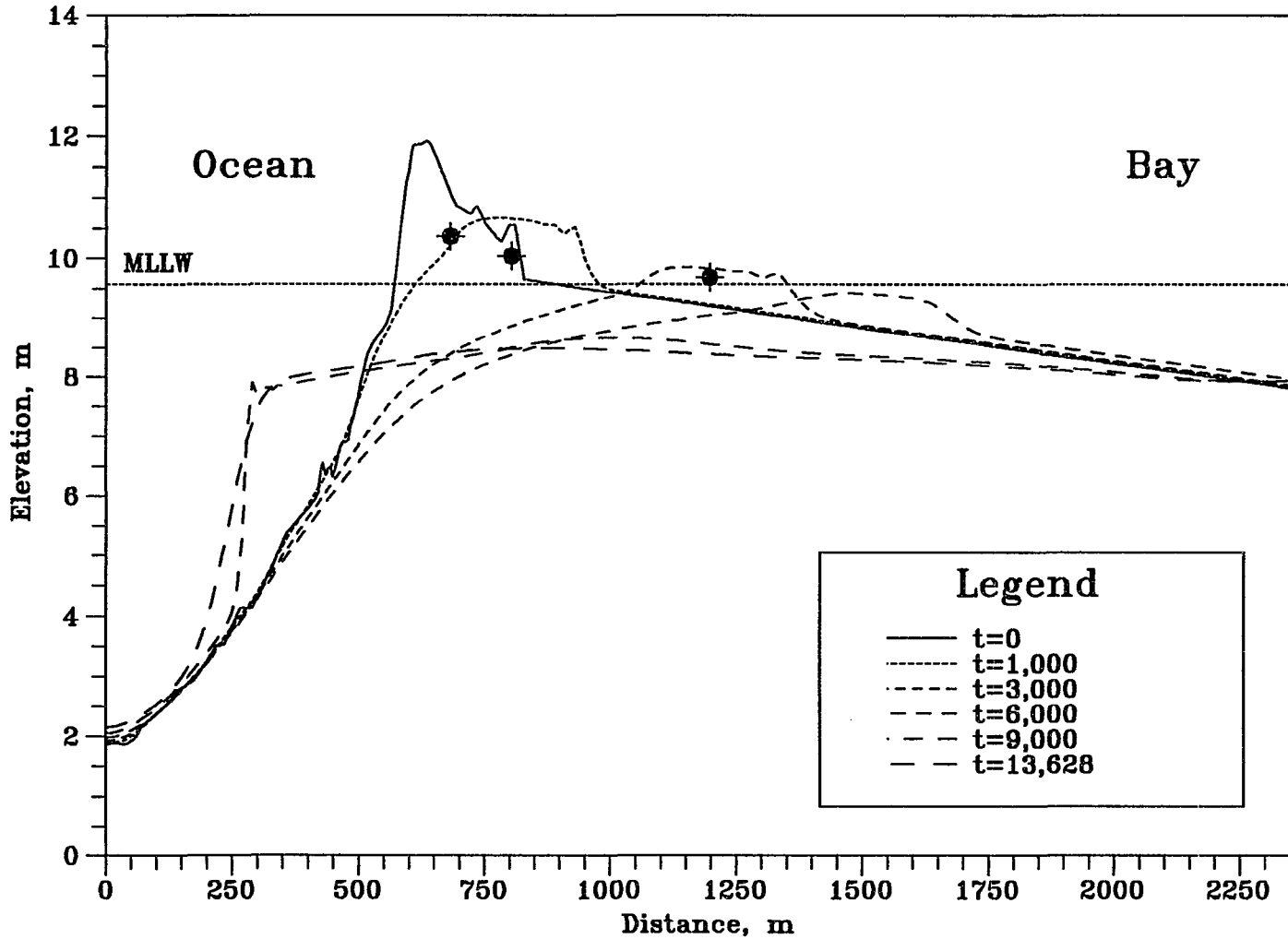


Figure 6.106 Bed Elevation Changes with Centroids of the Dune above MLLW in Stage III/IV at t=0, 1000, 3000, 6000, 9000 and 13628. ($h_{om}=4.0m$, $h_{bm}=3.0m$, $t_{leg}=4hr$, $D_{50}=0.3mm$)

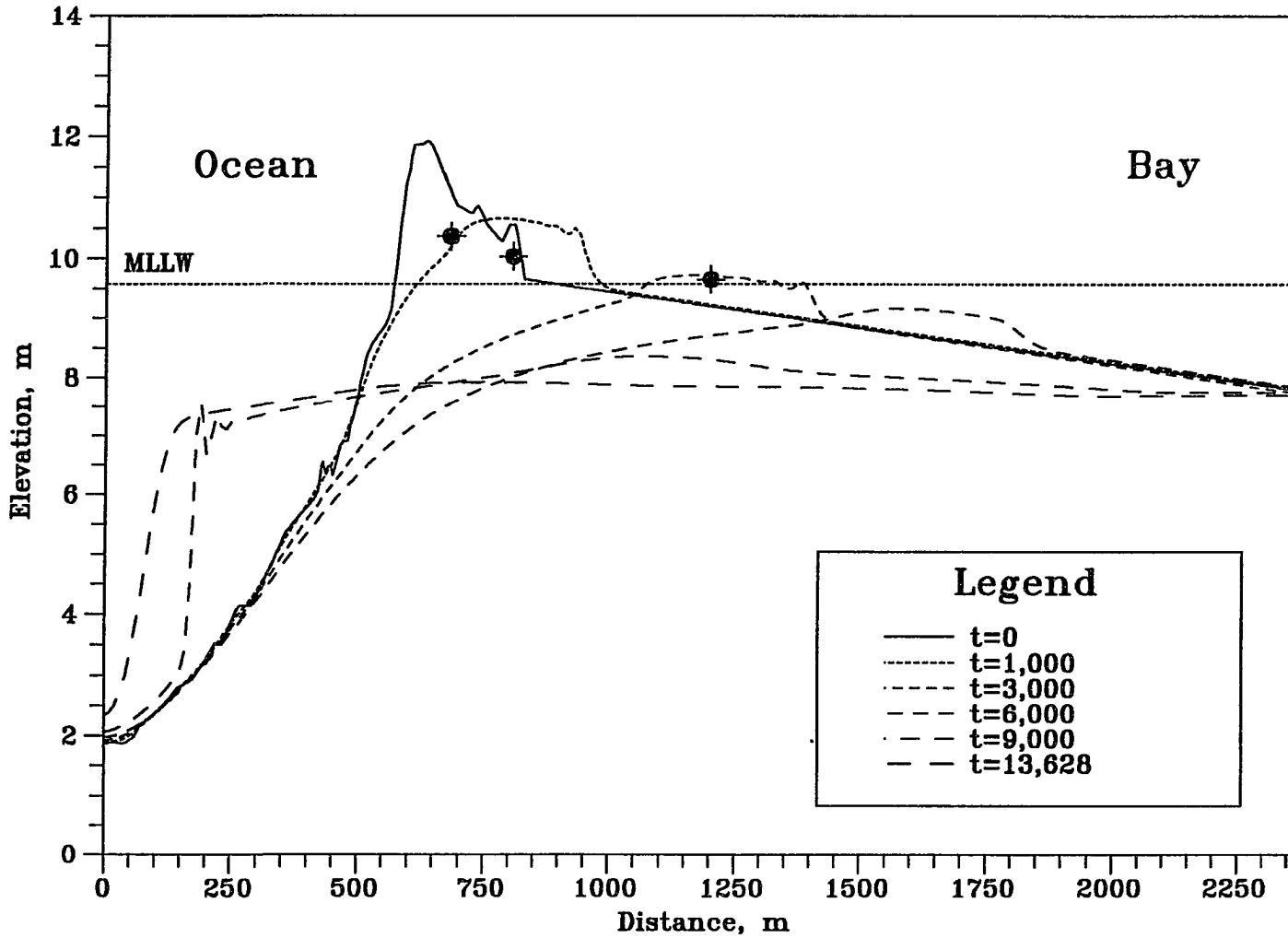


Figure 6.107 Bed Elevation Changes with Centroids of the Dune above MLLW in Stage III/IV at t=0, 1000, 3000, 6000, 9000 and 13628. ($h_{om}=4.0m$, $h_{bm}=3.0m$, $t_{lag}=5hr$, $D_{50}=0.3mm$)

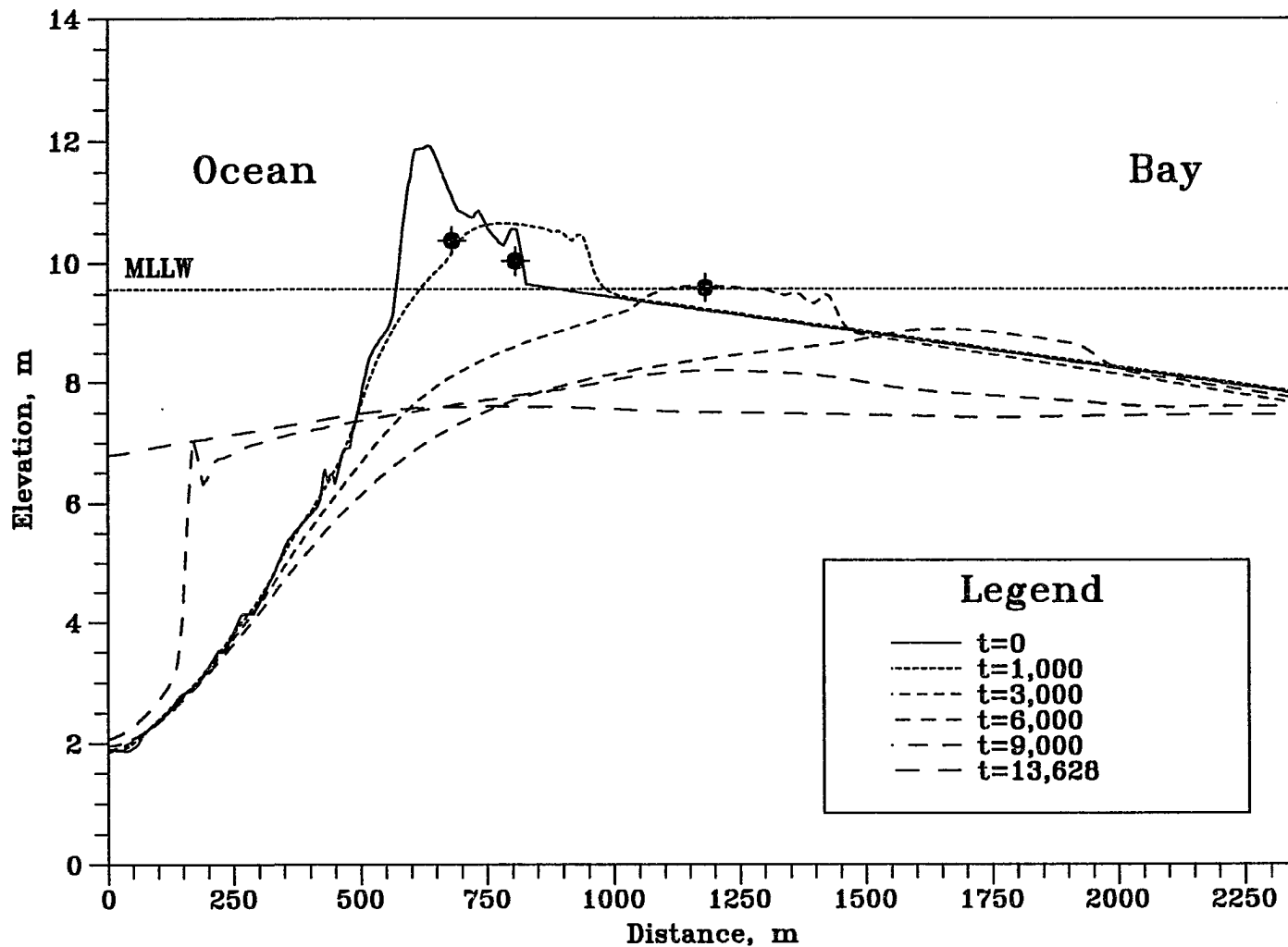


Figure 6.108 Bed Elevation Changes with Centroids of the Dune above MLLW in Stage III/IV at $t=0, 1000, 3000, 6000, 9000$ and 13628 .
 ($h_{om}=4.0m, h_{bm}=3.0m, t_{lag}=6hr, D_{50}=0.3mm$)

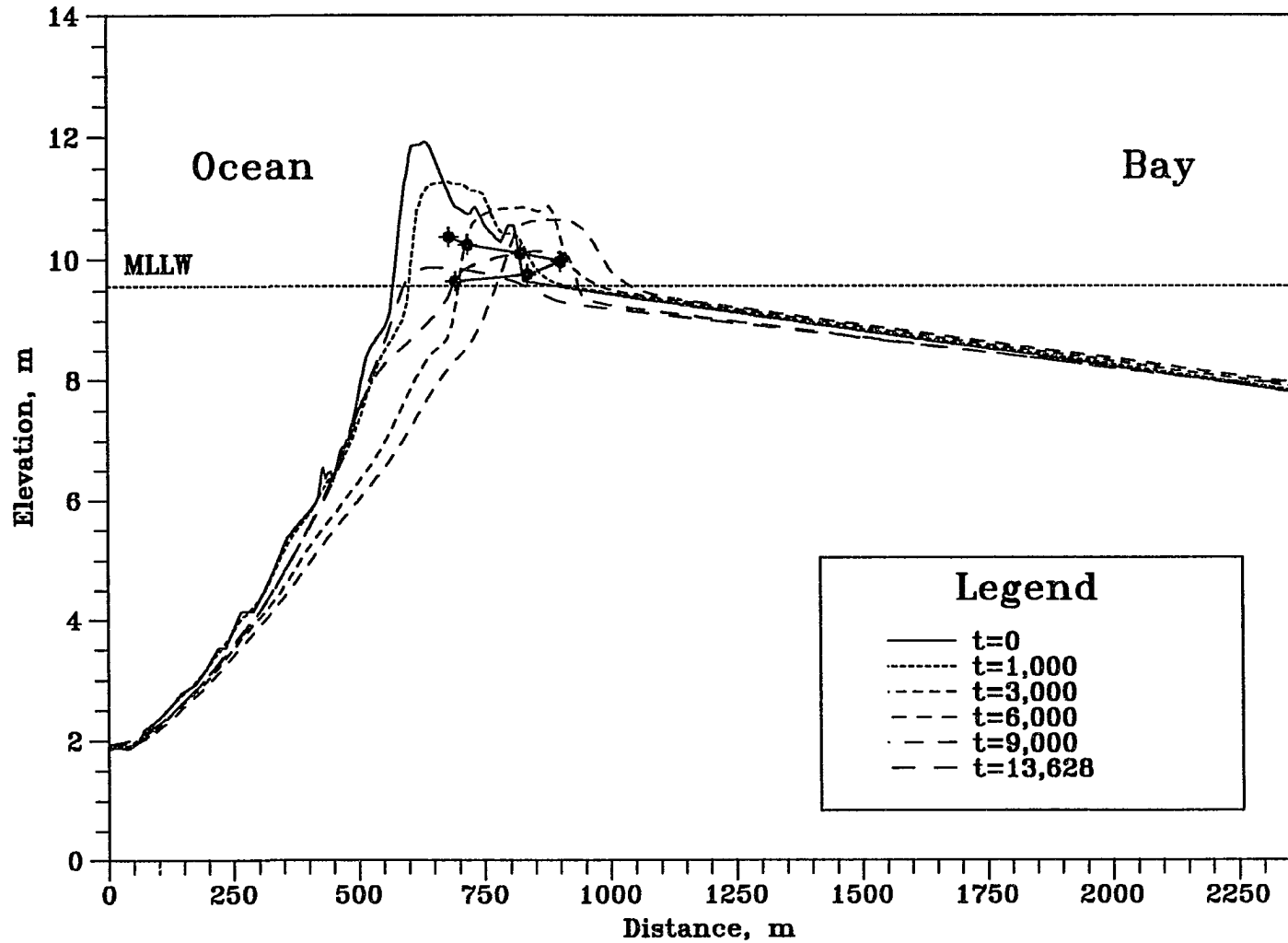


Figure 6.109 Bed Elevation Changes with Centroids of the Dune above MLLW in Stage III/IV at t=0, 1000, 3000, 6000, 9000 and 13628. ($h_{om}=4.0m$, $h_{bm}=3.0m$, $t_{1\%g}=3hr$, $D_{50}=0.1mm$)

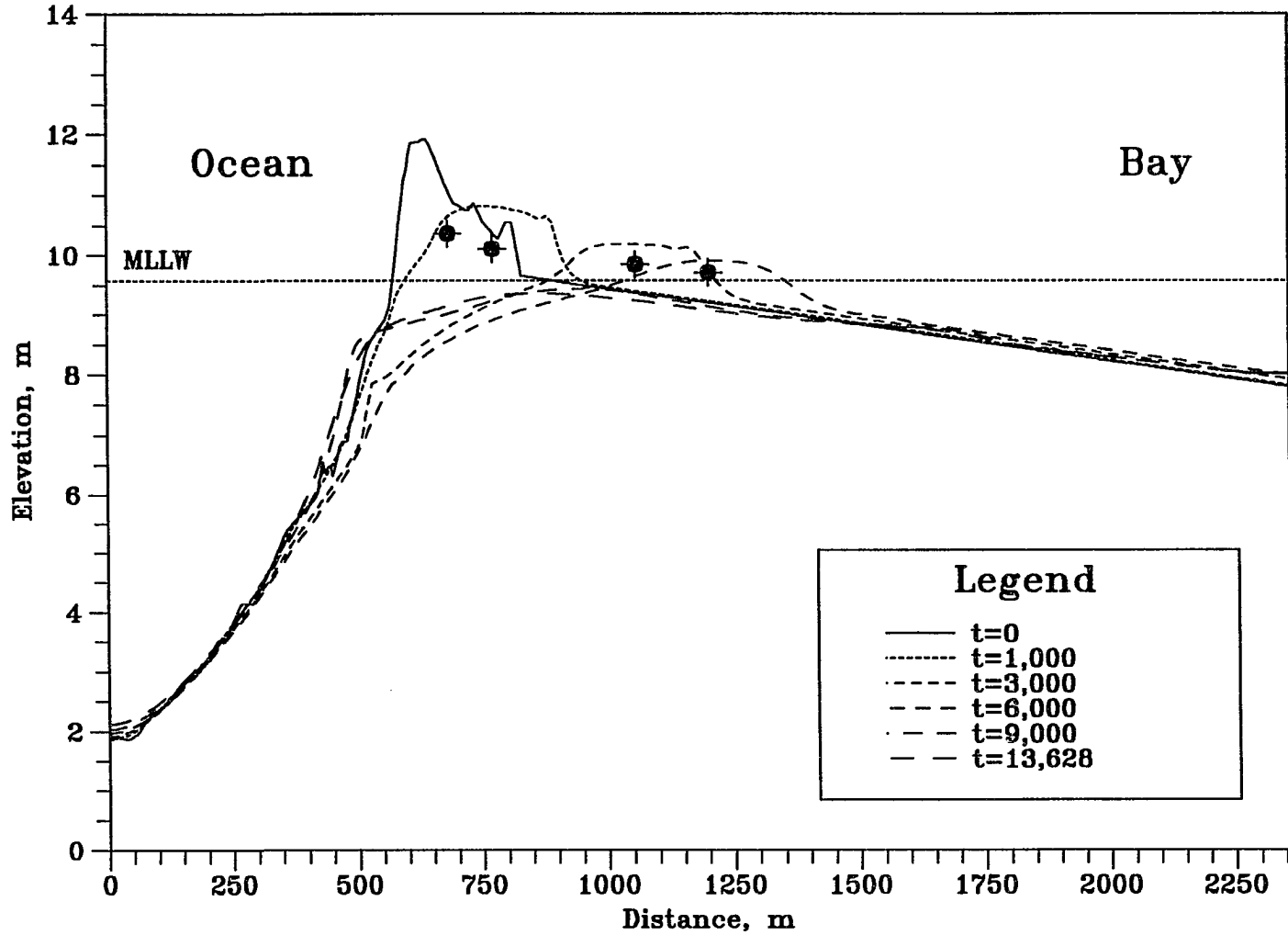


Figure 6.110 Bed Elevation Changes with Centroids of the Dune above MLLW in Stage III/IV at t=0, 1000, 3000, 6000, 9000 and 13628. ($h_{om}=4.0m$, $h_{bm}=3.0m$, $t_{lag}=3hr$, $D_{50}=0.2mm$)

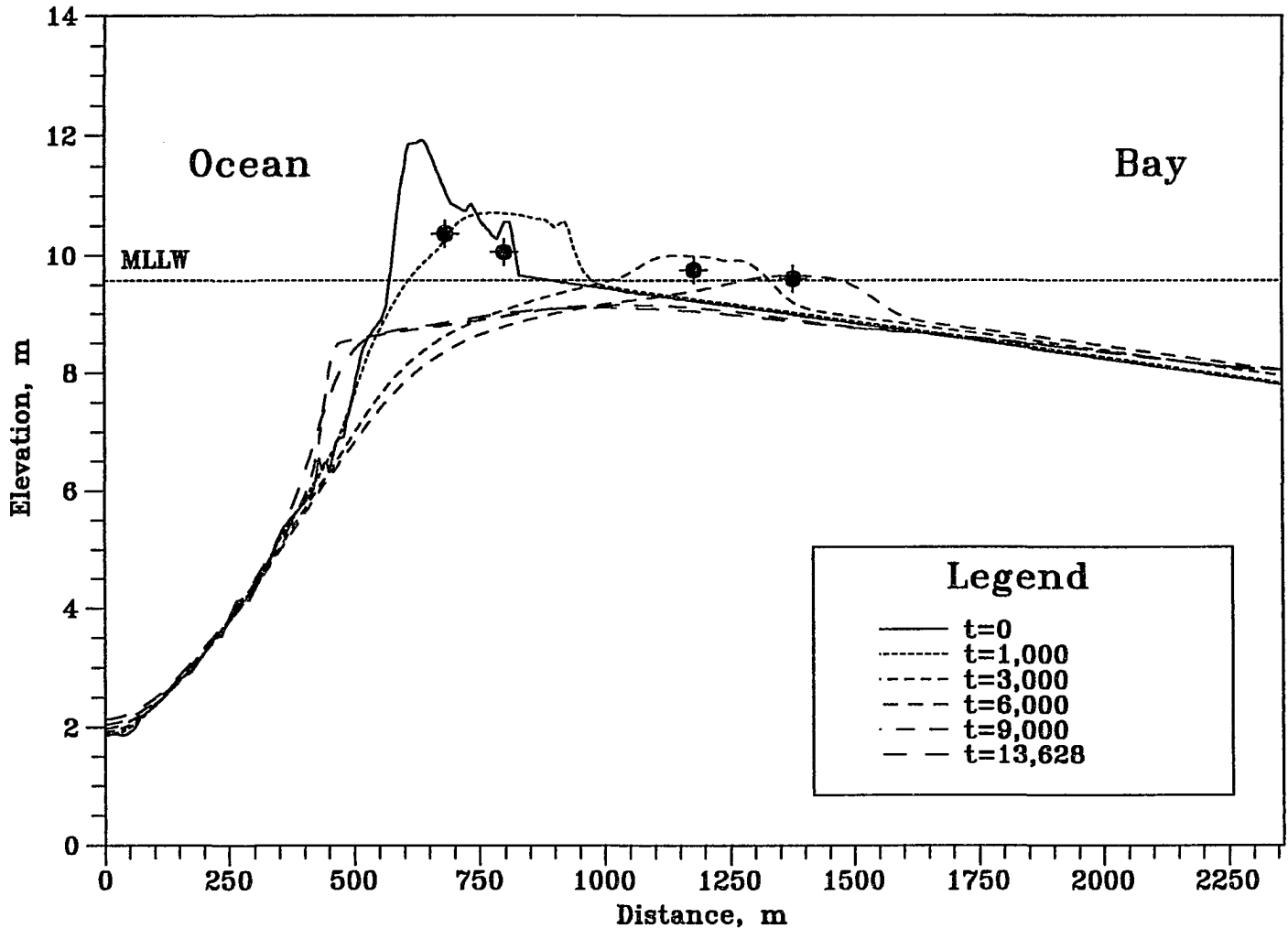


Figure 6.111 Bed Elevation Changes with Centroids of the Dune above MLLW in Stage III/IV at t=0, 1000, 3000, 6000, 9000 and 13628. ($h_{om}=4.0m$, $h_{bm}=3.0m$, $t_{lag}=3hr$, $D_{50}=0.3mm$)

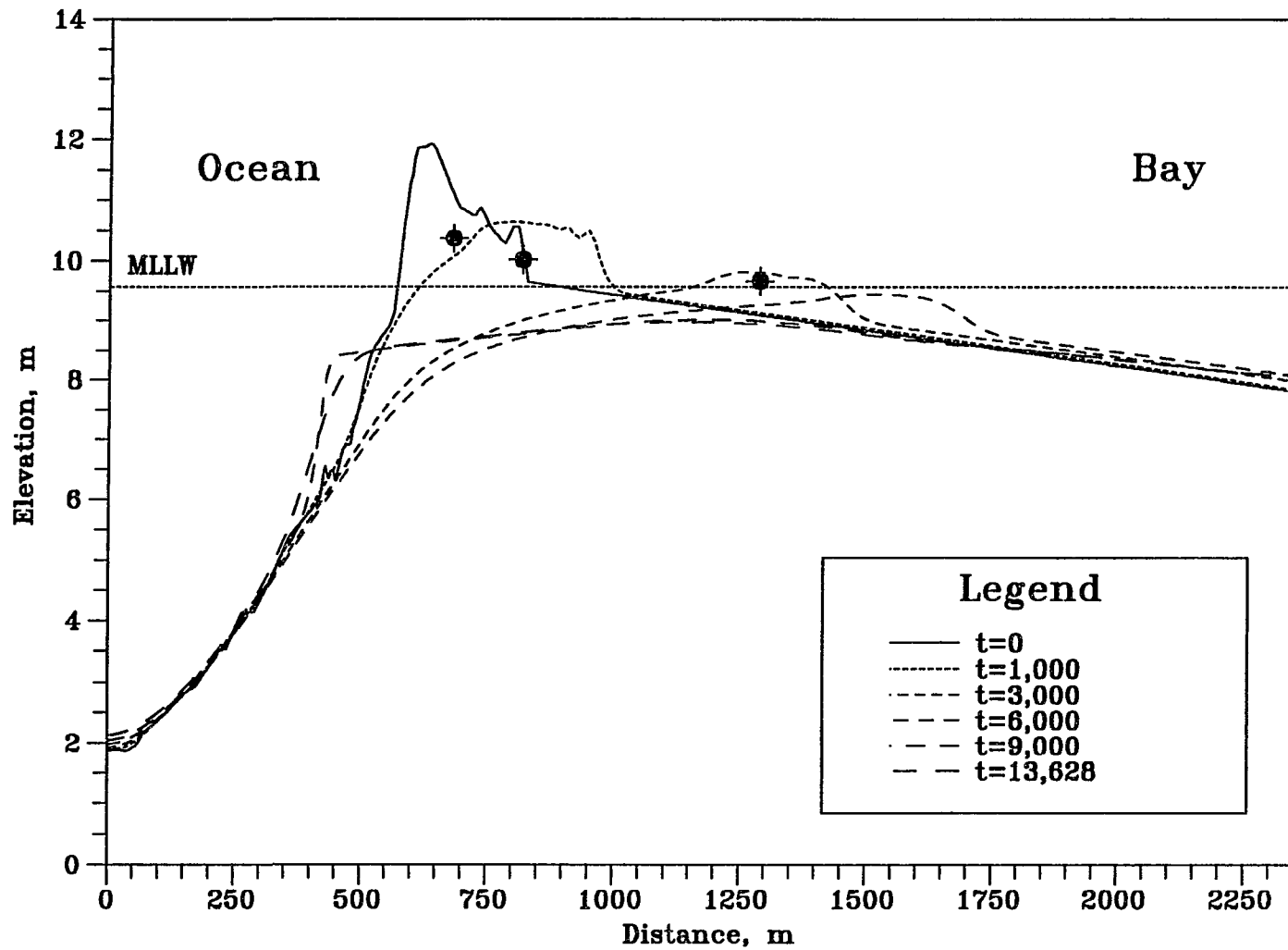


Figure 6.112 Bed Elevation Changes with Centroids of the Dune above MLLW in Stage III/IV at t=0, 1000, 3000, 6000, 9000 and 13628. ($h_{om}=4.0m$, $h_{bm}=3.0m$, $t_{lag}=3hr$, $D_{50}=0.4mm$)

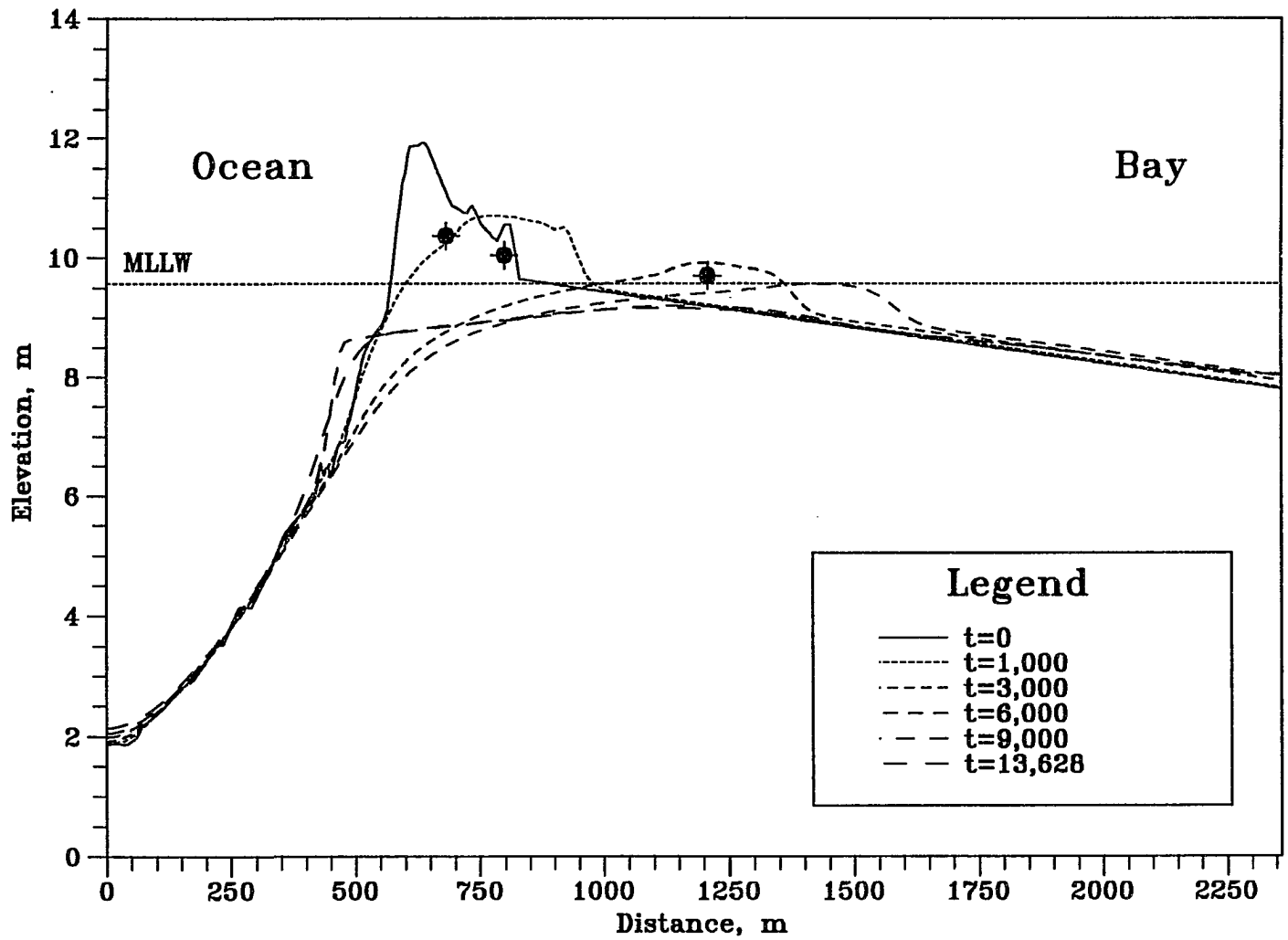


Figure 6.113 Bed Elevation Changes with Centroids of the Dune above MLLW in Stage III/IV at $t=0, 1000, 3000, 6000, 9000$ and 13628 . ($h_{om}=4.0m, h_{bm}=3.0m, t_{lag}=3hr, D_{50}=0.6mm$)

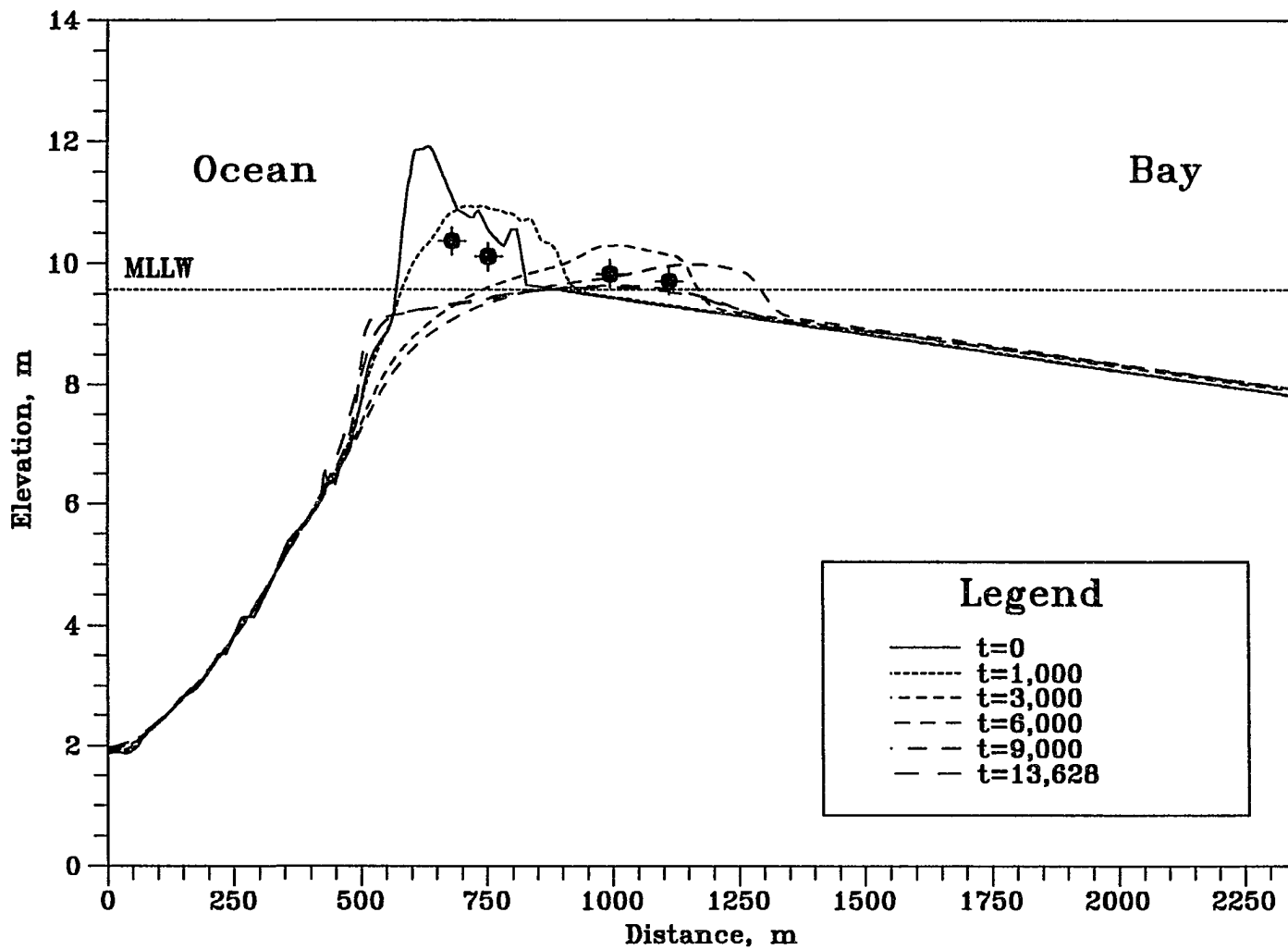


Figure 6.114 Bed Elevation Changes with Centroids of the Dune above MLLW in Stage III/IV at t=0, 1000, 3000, 6000, 9000 and 13628. ($h_{om}=4.0m$, $h_{bm}=3.0m$, $t_{lag}=3hr$, $D_{50}=1.0mm$)

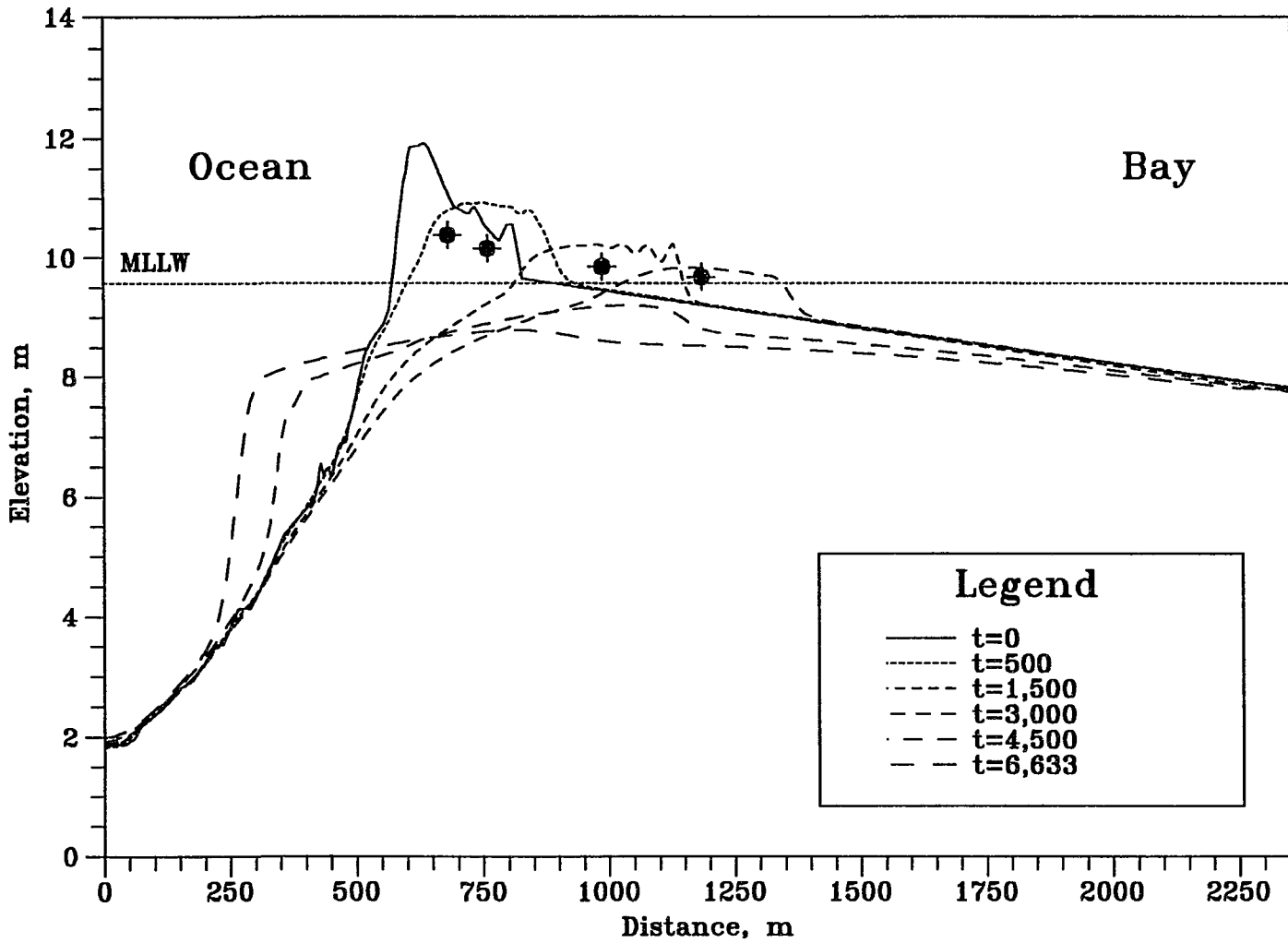


Figure 6.115 Bed Elevation Changes with Centroids of the Dune above MLLW in Stage III/IV at t=0, 500, 1500, 3000, 4500 and 6633. ($h_{om}=4.0\text{m}$, $h_{bm}=3.0\text{m}$, $t_{lag}=3\text{hr}$, $D_{50}=0.3\text{mm}$, $T=12\text{hr}$)

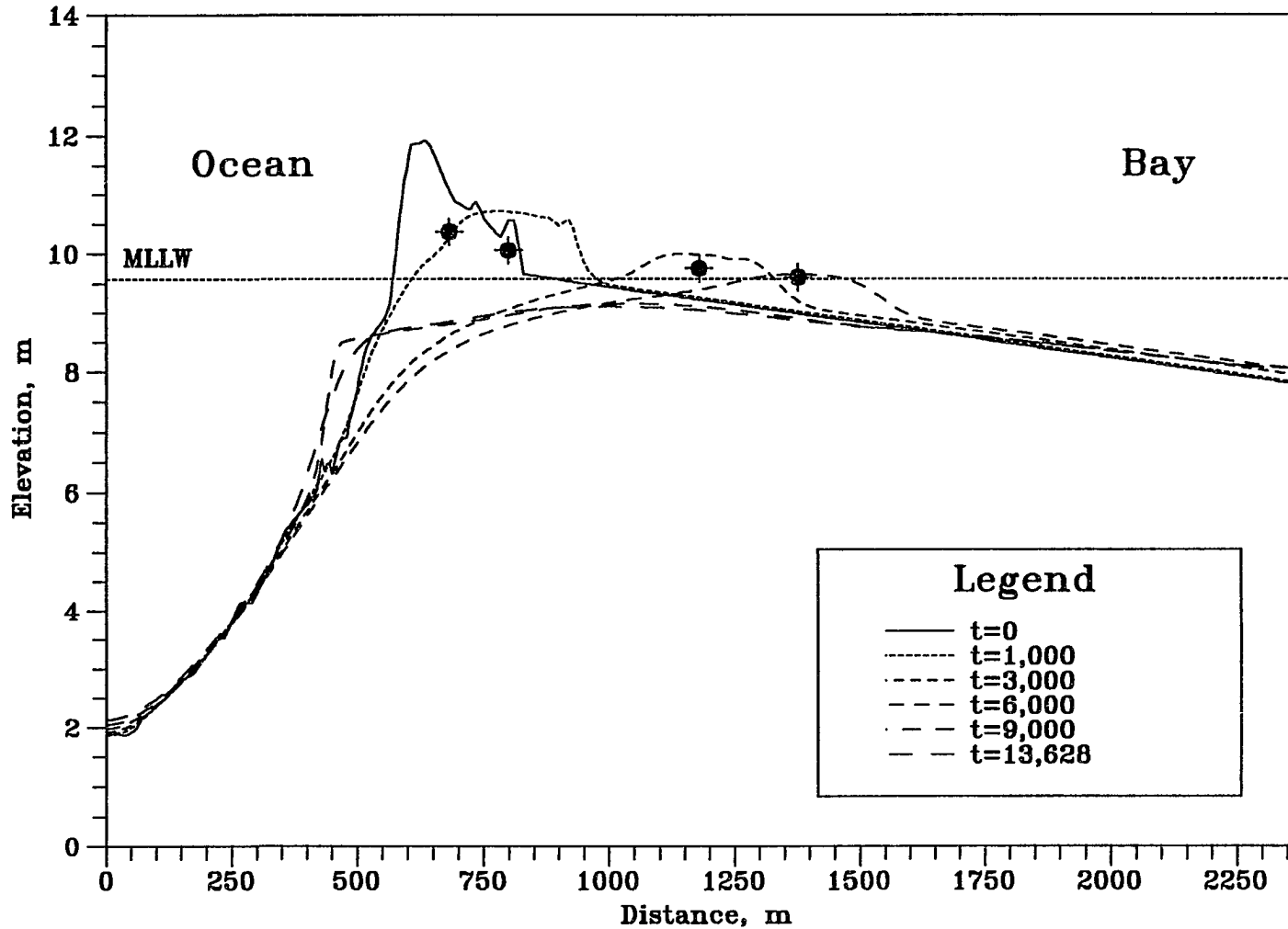


Figure 6.116 Bed Elevation Changes with Centroids of the Dune above MLLW in Stage III/IV at $t=0, 1000, 3000, 6000, 9000$ and 13628 .
 ($h_{om}=4.0\text{m}$, $h_{bm}=3.0\text{m}$, $t_{lag}=3\text{hr}$, $D_{50}=0.3\text{mm}$, $T=24\text{hr}$)

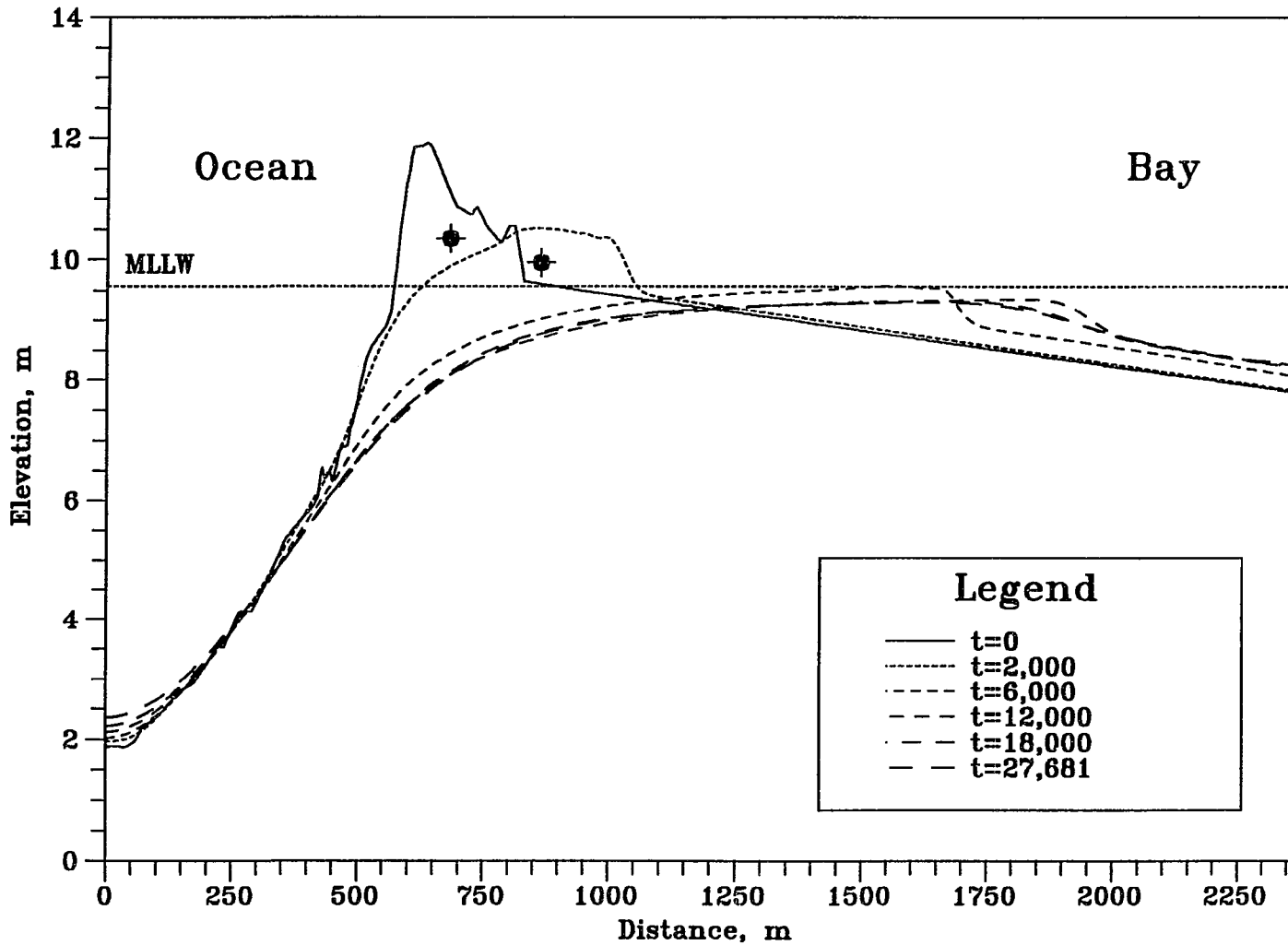


Figure 6.117 Bed Elevation Changes with Centroids of the Dune above MLLW in Stage III/IV at t=0, 2000, 6000, 12000, 18000 and 27681. ($h_{om}=4.0m$, $h_{bm}=3.0m$, $t_{lag}=3hr$, $D_{50}=0.3mm$, $T=48hr$)

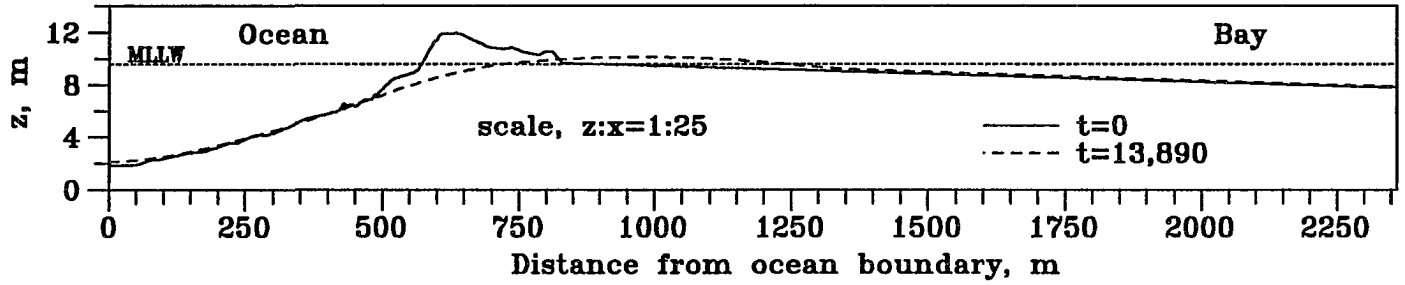


Figure 6.118 Bed Elevation Changes in Stage III/IV at t=0 and 14125.
($h_{om}=4.5m$, $h_{bm}=4.0m$, $t_{lag}=1hr$, $D_{50}=0.3mm$)

271

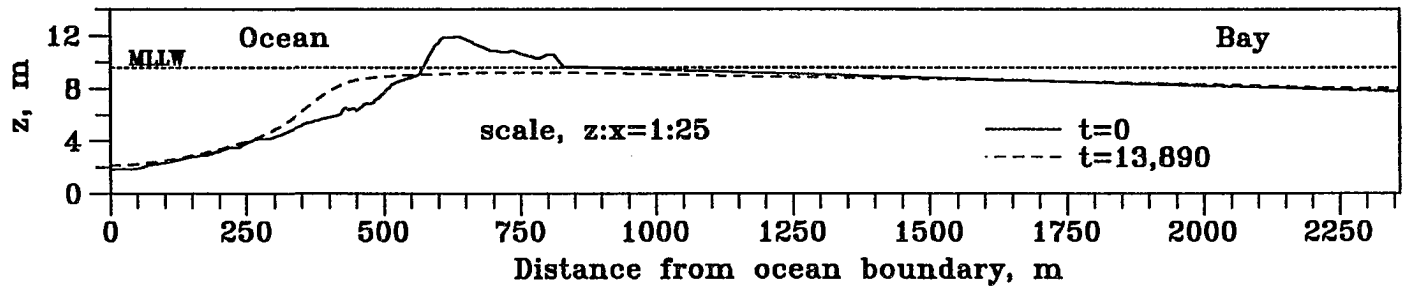


Figure 6.119 Bed Elevation Changes in Stage III/IV at t=0 and 14125.
($h_{om}=4.5m$, $h_{bm}=4.0m$, $t_{lag}=2hr$, $D_{50}=0.3mm$)

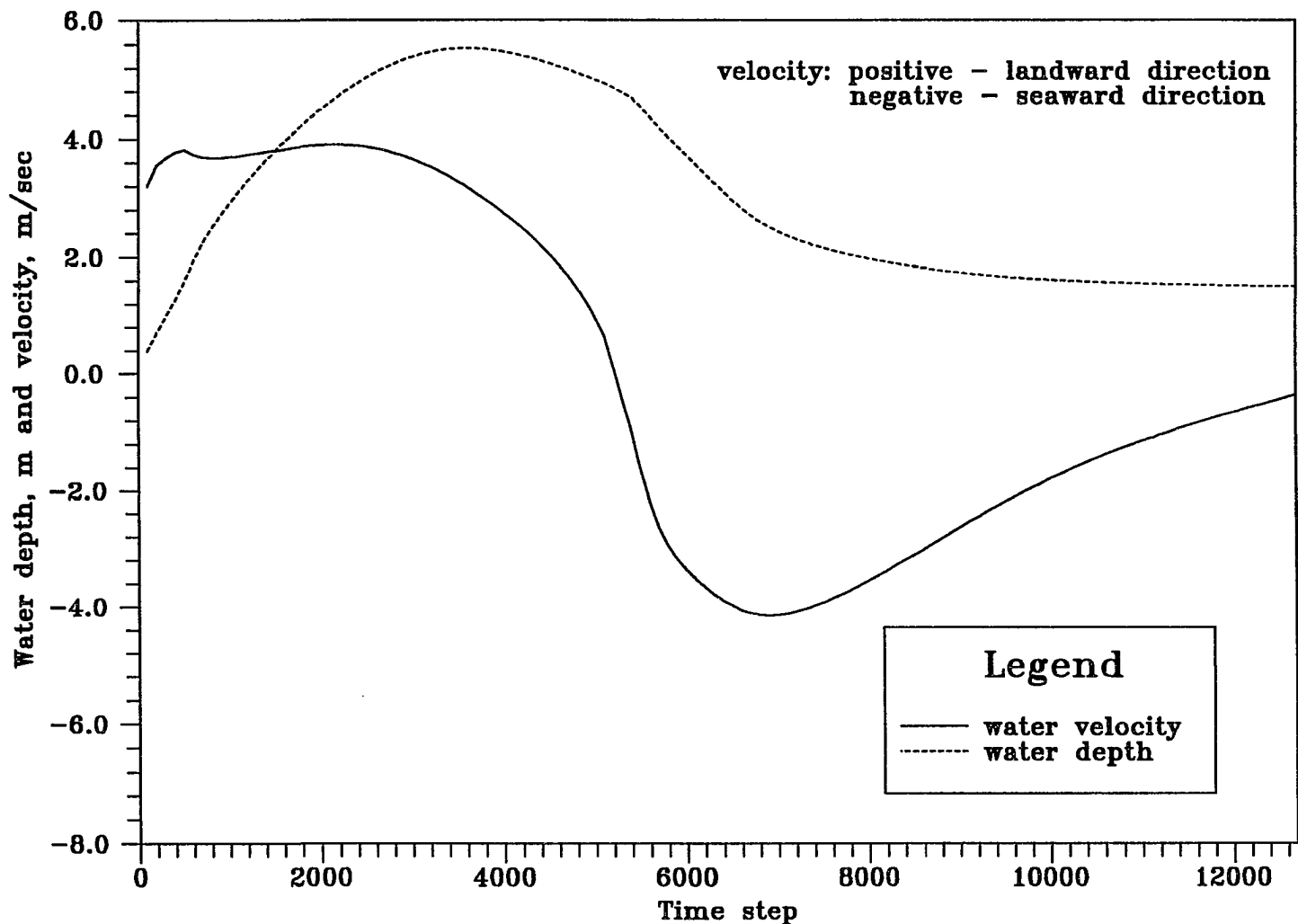


Figure 6.120 Water Depth and Velocity Variation at the Initial Top of Dune. ($h_{om}=4.0m$, $h_{bm}=3.0m$, $t_{lag}=3hr$, $D_{50}=0.3mm$ and $\Delta t=4sec$)

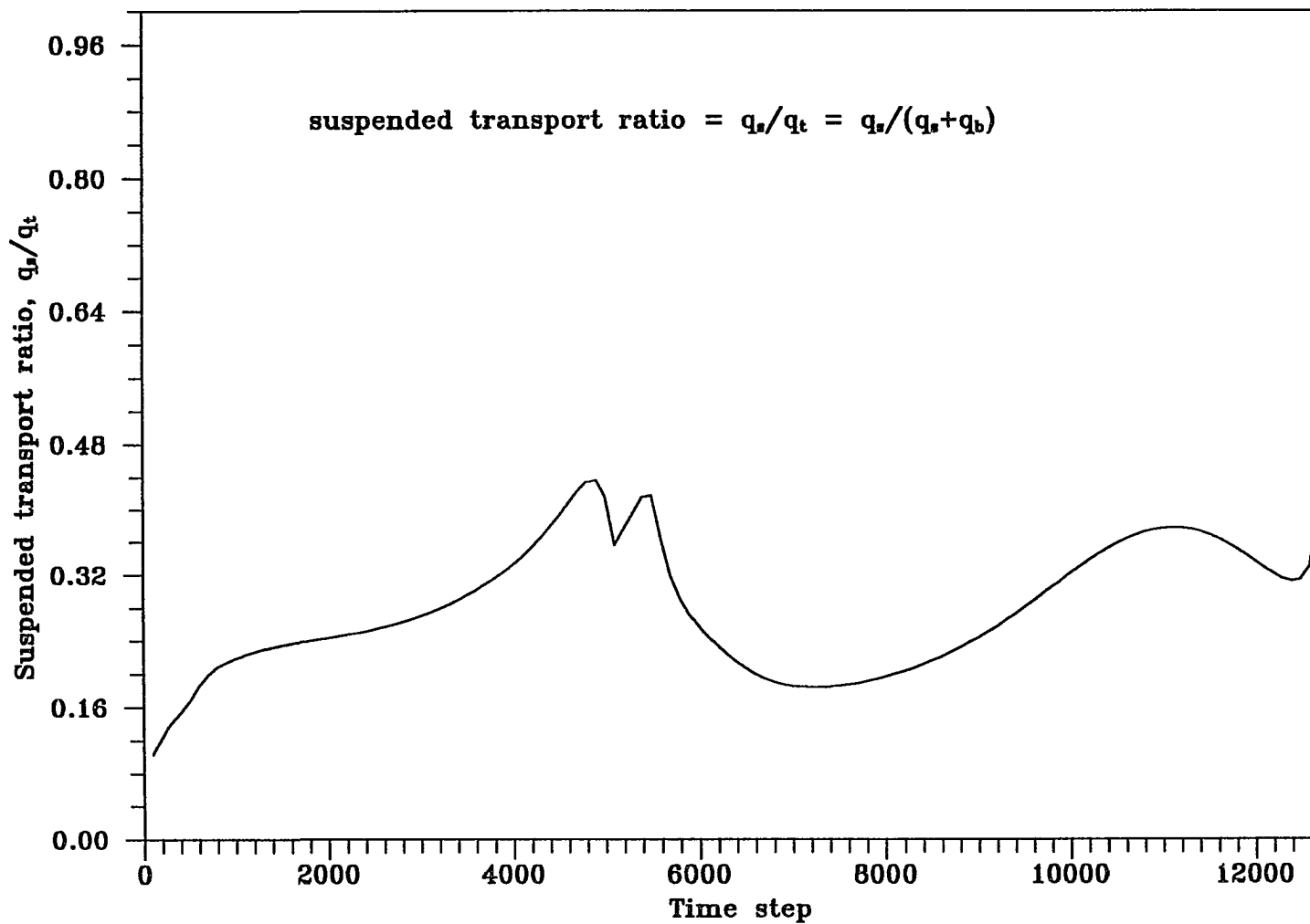


Figure 6.121 Suspended Sediment Transport Ratio at the Initial Top of Dune. ($h_{om}=4.0m$, $h_{bm}=3.0m$, $D_{50}=0.3mm$, $t_{lag}=3hr$ and $\Delta t=4sec$)

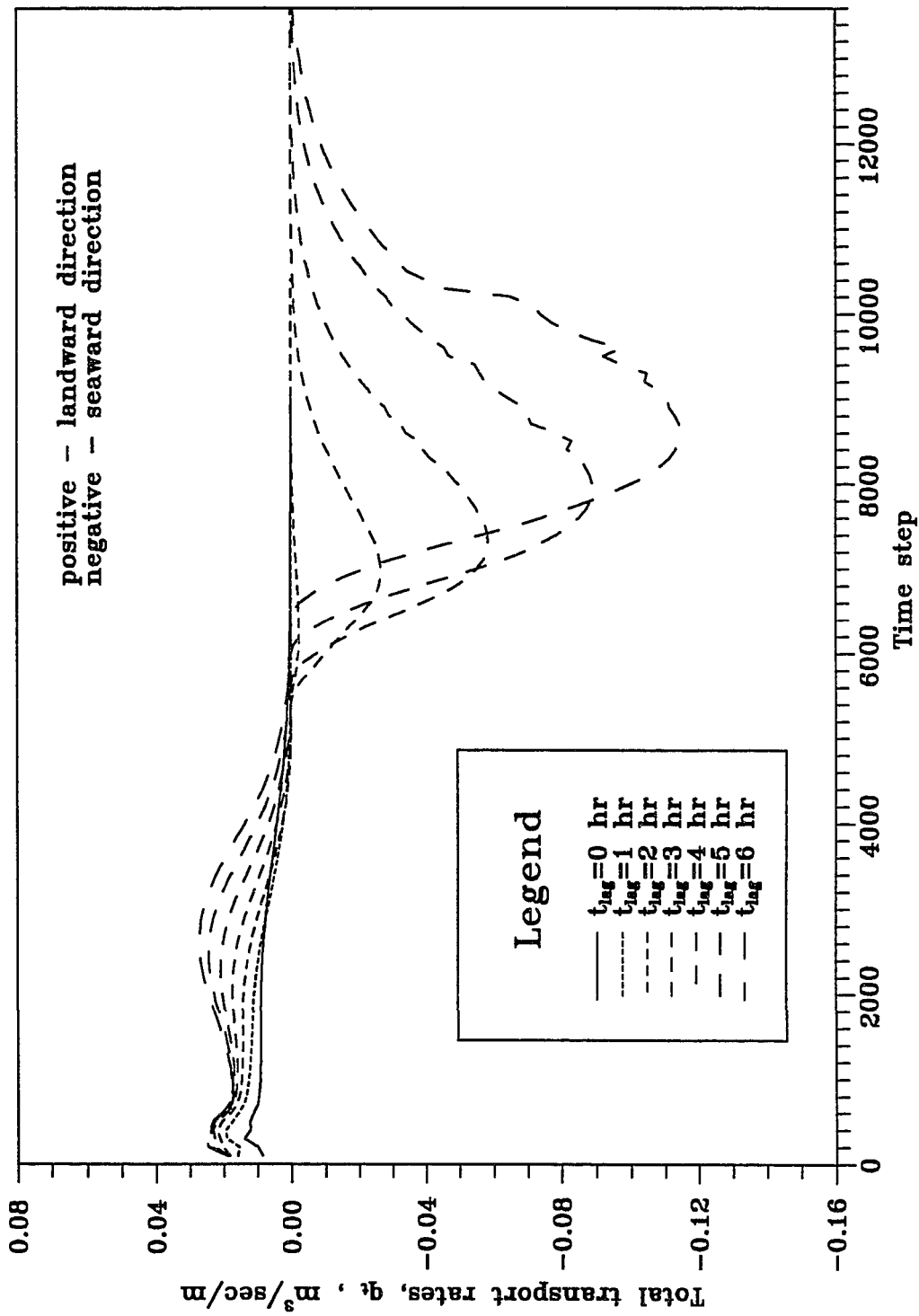


Figure 6.122 Total Sediment Transport Rates at the Initial Top of Dune.
 ($h_{om}=4.0m$, $h_{bm}=3.0m$, $D_{50}=0.3mm$, $T=24hr$ and $\Delta t=4sec$)

7.0 DISCUSSIONS AND ANALYSES OF RESULTS

7.1 Stage I - Dune / Beach Erosion

Profile change is sensitive to storm duration, surge shape, and wave height and period, in addition to peak stage. In the SBEACH model, the higher storm surge level with shorter duration produces less erosion than a storm of lower surge but longer duration. This fact is well presented in Table 6.35 (p.140). The volume loss, ΔV above MLLW in Storm No.1 (duration, $t=8.0hr$) is $1.20 m^3/m$ but $2.40 m^3/m$ in Storm No.5 with longer duration, $t=9.3hr$. Also, dune crest elevation change, Δz in Storm No.1 gives a little lower value than that in Storm No.5.

No significant volume losses are shown in overall simulations because eroded volume from the dune crest area is redistributed closer to foreshore and overwashed to behind the dune crest. The maximum volume loss in percentage, ΔV , among all simulation is 0.69% of initial barrier volume above MLLW.

7.2 Stage II - Overwash / Overland Flow

The Lax-Wendroff scheme is developed for the overland flow computation which is used for an initial condition of Stages III and IV. Also, the method of characteristics (MOC) is used to compute additional boundary data at both boundaries.

During overland flow computation with an initial base flow, some computational difficulties may develop due to steep and irregular bottom profiles. In this situation, it is recommended to change the base flow depth and use bigger weighting factor for both water

depth and velocity in the dissipative interface.

The calculated water surface profiles between the top of the dune and the end of the barrier islands are plotted in Figure 6.11 (p.152). There is no instability shown over the computational domain. Minimum water depth ($\approx 0.1m$) is obtained along the steep slope in the upper reach and the maximum water depth of $0.3m$ is shown in the lower reach where bay water meets with ocean flood water. The calculated water velocity variations are also plotted in Figure 6.12 (p.153). Water flow velocities are varied from 0.6 to $2.3m/sec$.

Although super-critical flow is developed along the steep slope, the Lax-Wendroff scheme certainly maintains the stable flow computation.

The range of $0.03 \sim 0.05m$ in base flow gave satisfactory results and a weighting factor of 0.25 in dissipative interface was useful to provide some dissipation and to suppress nonlinear instabilities in a controlled manner.

7.3 Stage III and IV - Storm Tides

In this section, the following parameters are analyzed from the model test results in terms of volume changes, centroid positions and retreat speeds of the dune above MLLW.

- *Storm surge levels at ocean and bay, h_{om} and h_{bm}*
- *Time lag, t_{lag}*
- *Sediment grain size, D_{50} and D_{90}*
- *Storm duration, T*

7.3.1 Storm Surge Level

Storm surge level is one of the most significant factors in determining profile changes and barrier dune retreat rates. Also, the peak surge level *difference* between ocean and bay boundaries determines flow conditions and directions over the whole computational domain.

The relative volume changes above MLLW for five different storm surge levels ($h_{om}=h_{bm}$) are shown in Figure 7.1 with the remaining parameters fixed ($t_{lag}=3.0hr$, $D_{50}=0.3mm$ and $T=24hr$). It is clearly indicated that the higher storm surge level (*i.e.* $h_{om}=h_{bm}=5.0m$) has more rapidly increased the volume erosion rate than the lower levels. At 3,000 time step, the relative volume change in the lowest storm surge level ($h_{om}=h_{bm}=3.0m$) is about 0.62 but 0.24 in highest levels. This is further clarified in Figure 7.2 using dune retreat speed which is computed from the distances and time intervals between two adjacent centroids. The fastest retreat speed ($\approx 0.05m/sec$) comes from the biggest storm surge level.

Most of the barrier volume above MLLW disappears after 4,000 time steps for higher surge levels and 6,000 time steps for lower surge levels.

Different storm surge levels between ocean and bay are analyzed and plotted in Figure 7.3 for relative volume changes and Figure 7.4 for dune retreat speeds. The biggest hydraulic stage difference ($\Delta h=h_{om}-h_{bm}=2.0m$) results in the largest volume change 0.02 and the fastest dune retreat speed about 0.09m/sec at 3,000 time steps.

Therefore, it can be generally concluded that the storms with larger hydraulic stage differences and higher ocean surge levels produce more erosion and faster dune retreat speeds than storms with lower stage differences. Detailed individual profile evolutions are shown in Figures 6.92 through 6.101 (p.245-254).

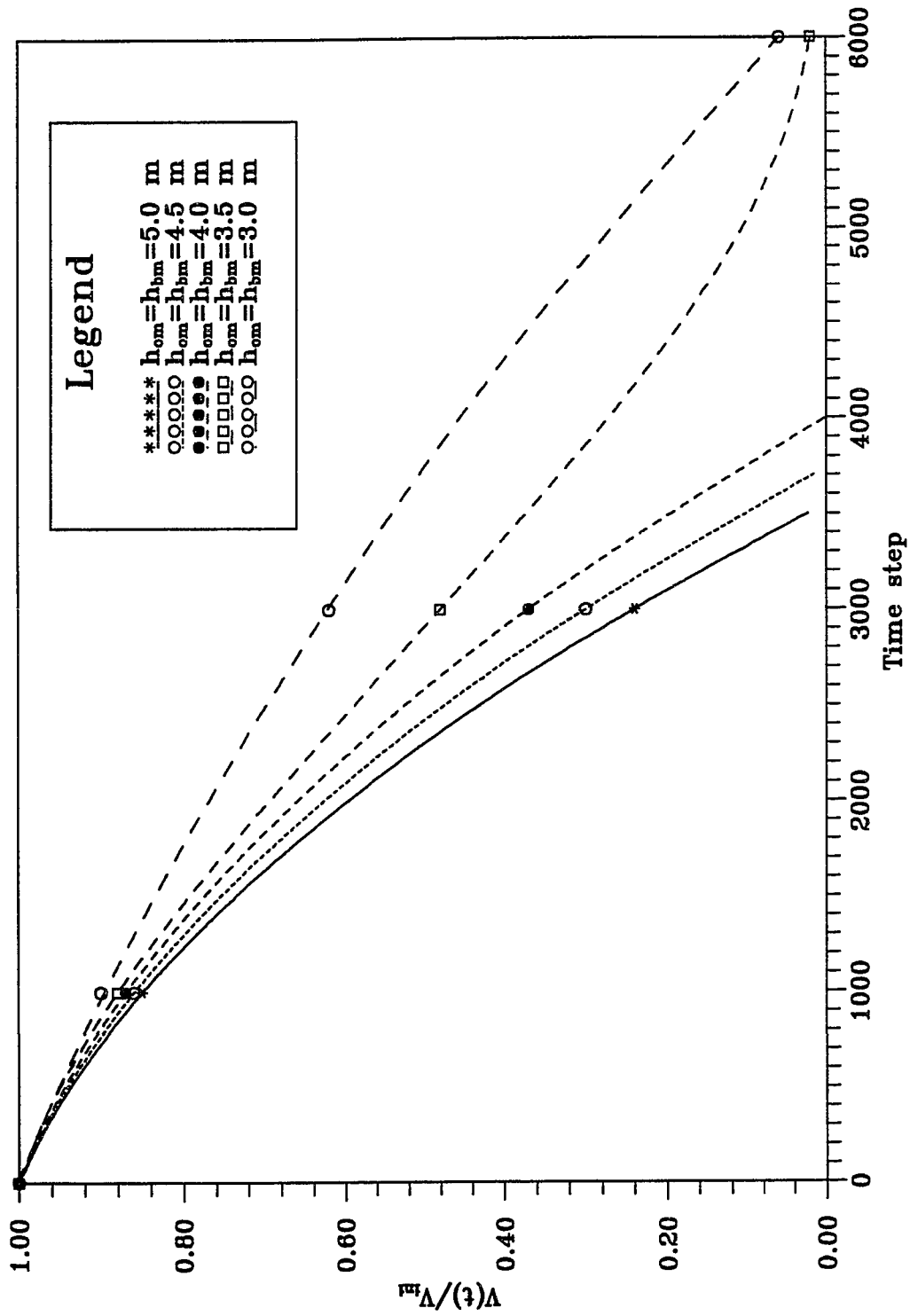


Figure 7.1 Volume Changes above MLLW for Five Different Storm Surge Levels. ($t_{lag}=3hr$, $D_{50}=0.3mm$ and $T=24hr$)

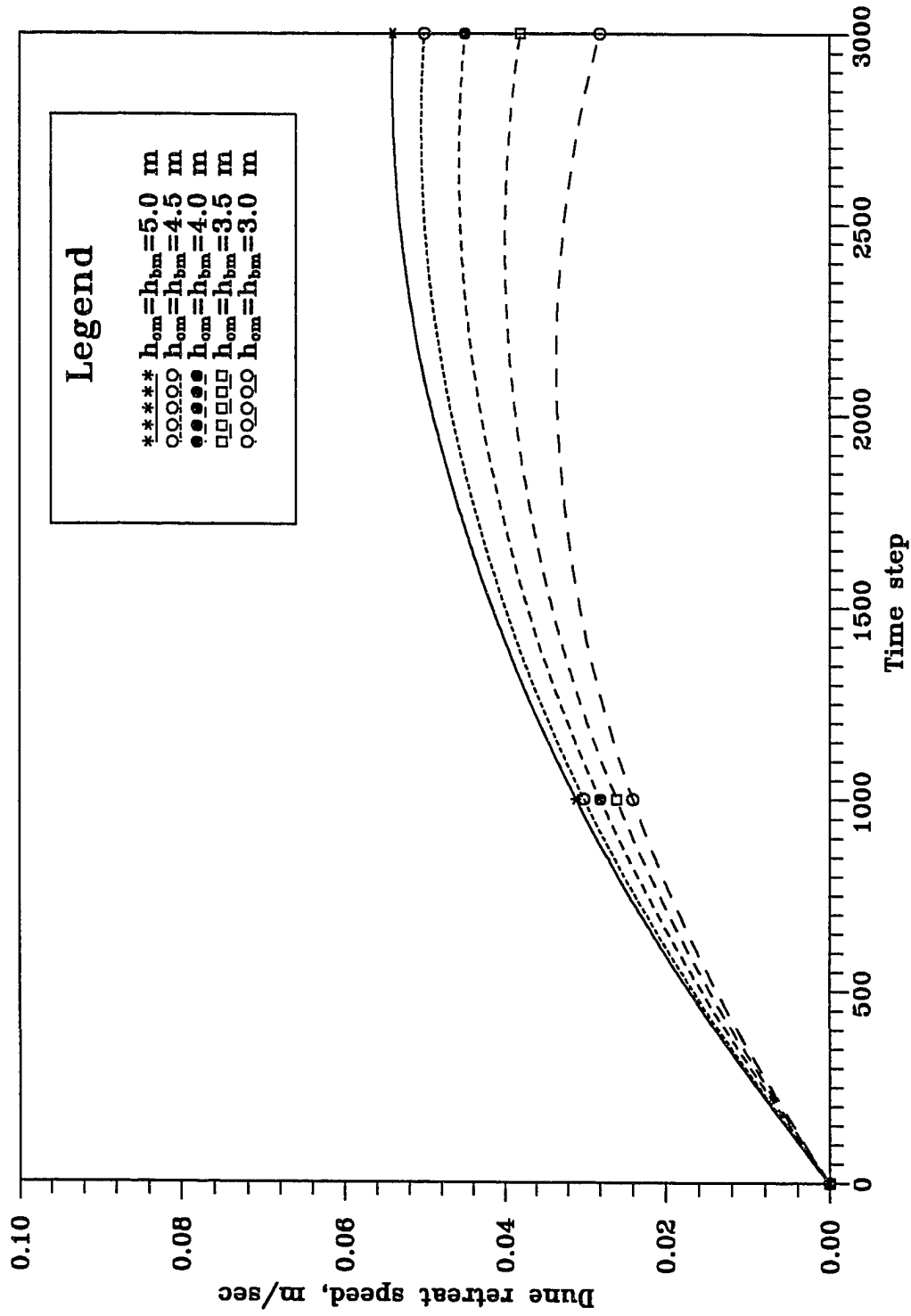


Figure 7.2 Dune Retreat Speeds above MLLW for Five Different Storm Surge Levels. ($t_{lag} = 3hr$, $D_{60} = 0.3mm$ and $T = 24hr$)

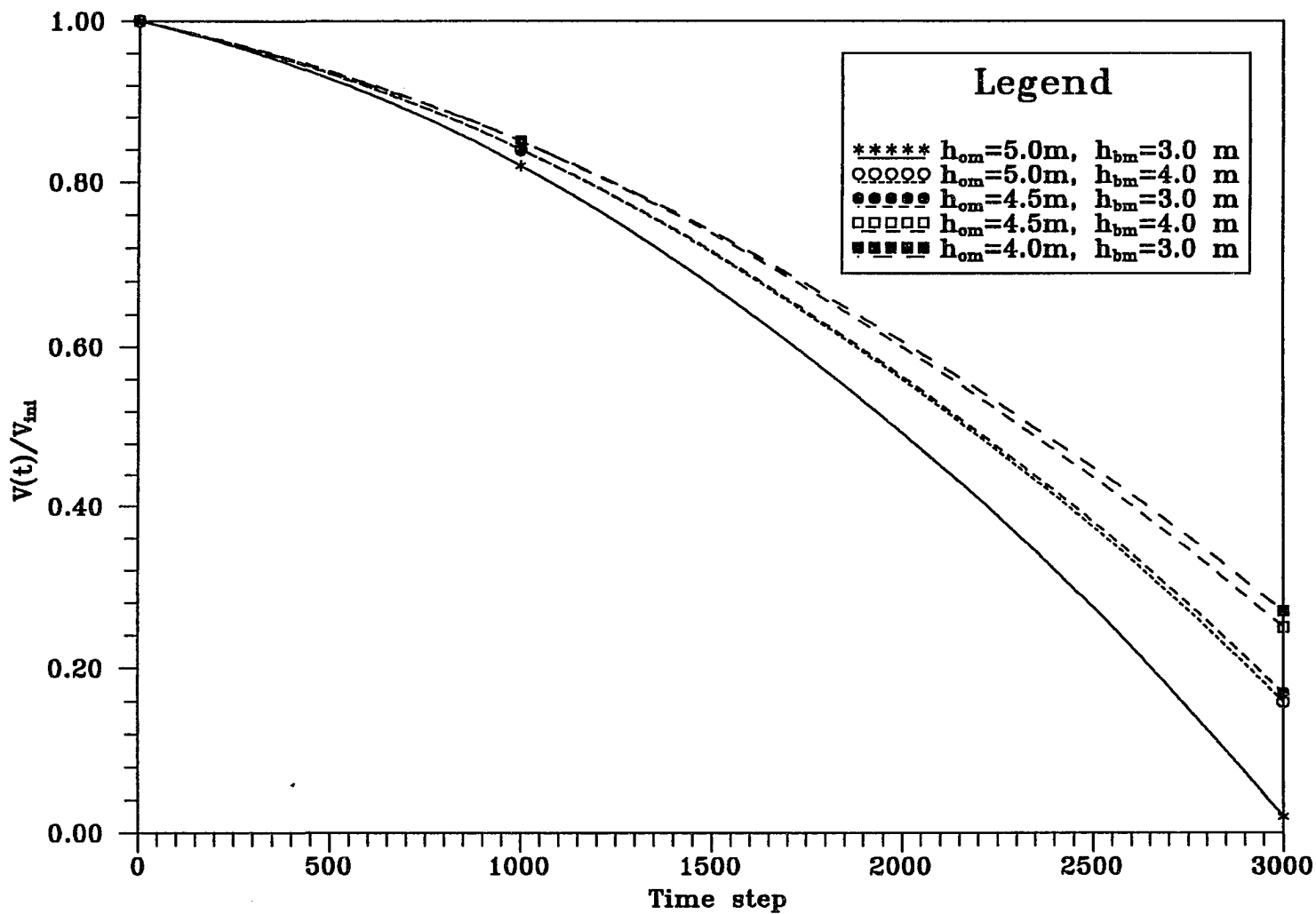


Figure 7.3 Volume Changes above MLLW for Five Different Storm Surge Levels.
 ($t_{lag}=3hr, D_{50}=0.3mm$ and $T=24hr$)

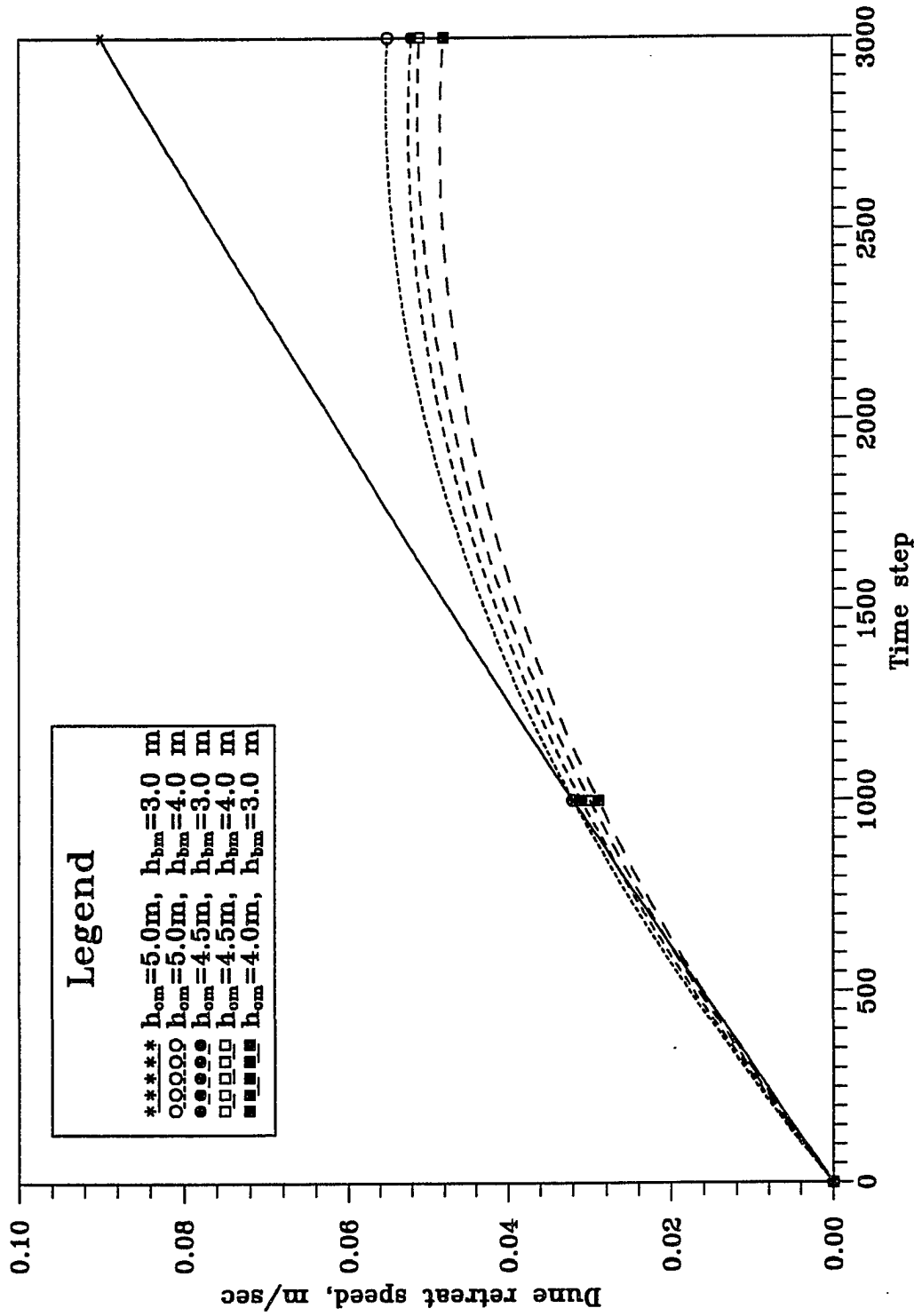


Figure 7.4 Dune Retreat Speeds above MLLW for Five Different Storm Surge Levels. ($t_{lag}=3\text{hr}$, $D_{50}=0.3\text{mm}$ and $T=24\text{hr}$)

7.3.2 Time Lag

In determining the flow directions in this study (*i.e.* ocean to bay and/or bay to ocean across barrier dunes), the time lag in storm surge levels between ocean and bay is apparently one of the major factors. From zero to six hour time lags are incorporated with fixed remaining parameters in the model tests because in general, a six-hour time lag is equivalent to the time difference between high tide and low tide.

The relative volume changes for various time lags between ocean and bay water levels are presented in Figure 7.5. The barrier dunes move to bay side about 400-500m for shorter time lags (0.0~2.0hr) with significant erosion but still maintain barrier volumes above MLLW at the end of simulations. However, for the longer time lags (3.0~6.0hr) the barrier dunes are completely eroded through either direction at the middle of the simulations. Eroded materials are transported along the water flows, and deposited in the bay for shorter time lags and in the ocean for longer time lags (see, Figures 6.102~6.108 and Figure 6.122).

It is difficult to clearly separate Stage IV from Stage III because many parameters are involved in determining a flow direction. However, the water velocity variation, total sediment transport rate and negative dune retreat speed in Figures 6.120, 6.122 and 7.6, respectively, provide excellent information for understanding ebbing flows of eroded sediment materials above MLLW.

The larger time lag gives the faster retreat speeds and volume changes, and vice versa. It becomes readily apparent through Figure 7.7, which indicates the relationships among relative volume changes, dune retreat speeds and time lags at $t=3,000$ time level.

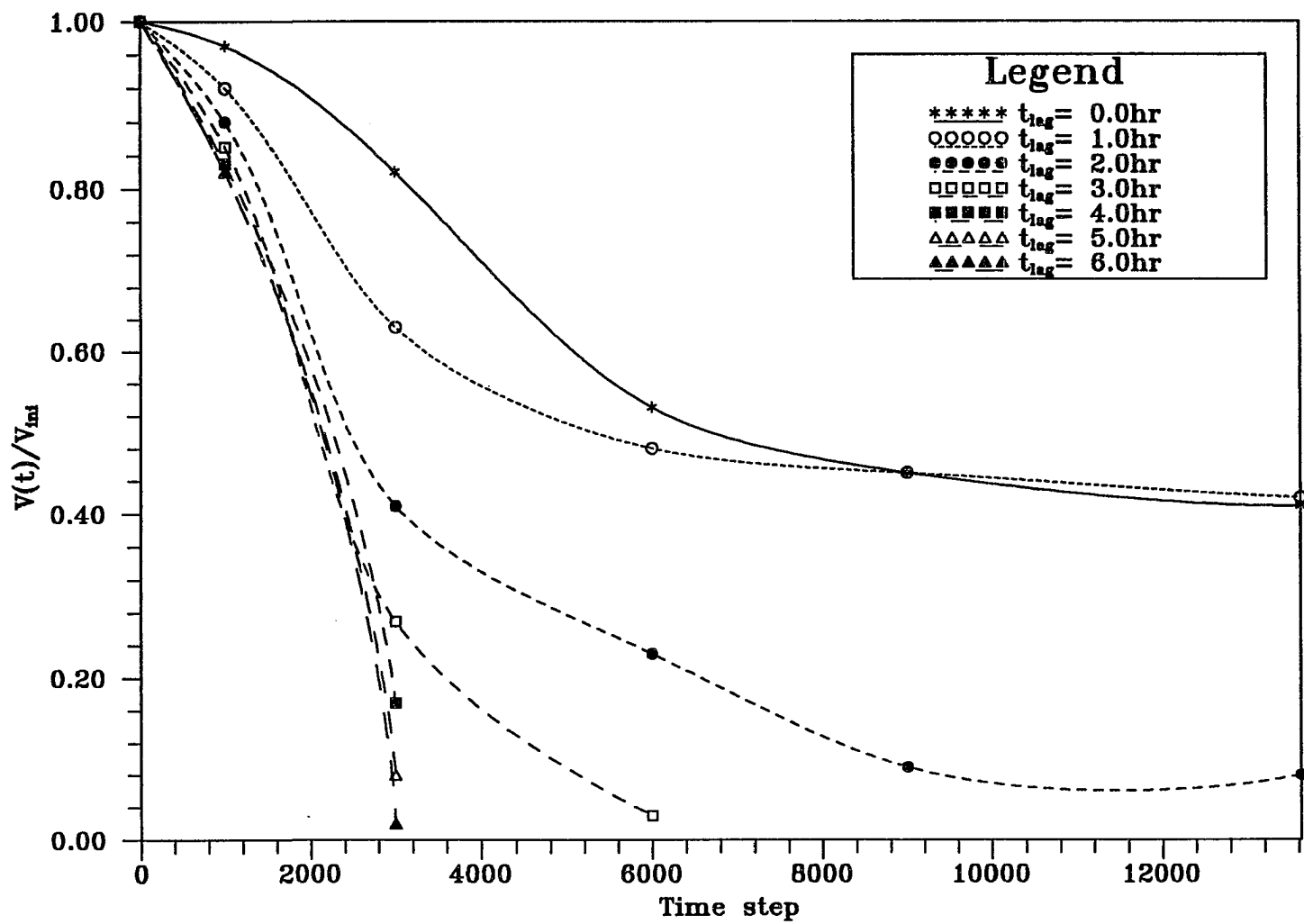


Figure 7.5 Volume Changes above MLLW for Various Time Lags.
 ($h_{om}=4.0m$, $h_{bm}=3.0m$, $D_{60}=0.3mm$ and $T=24hr$)

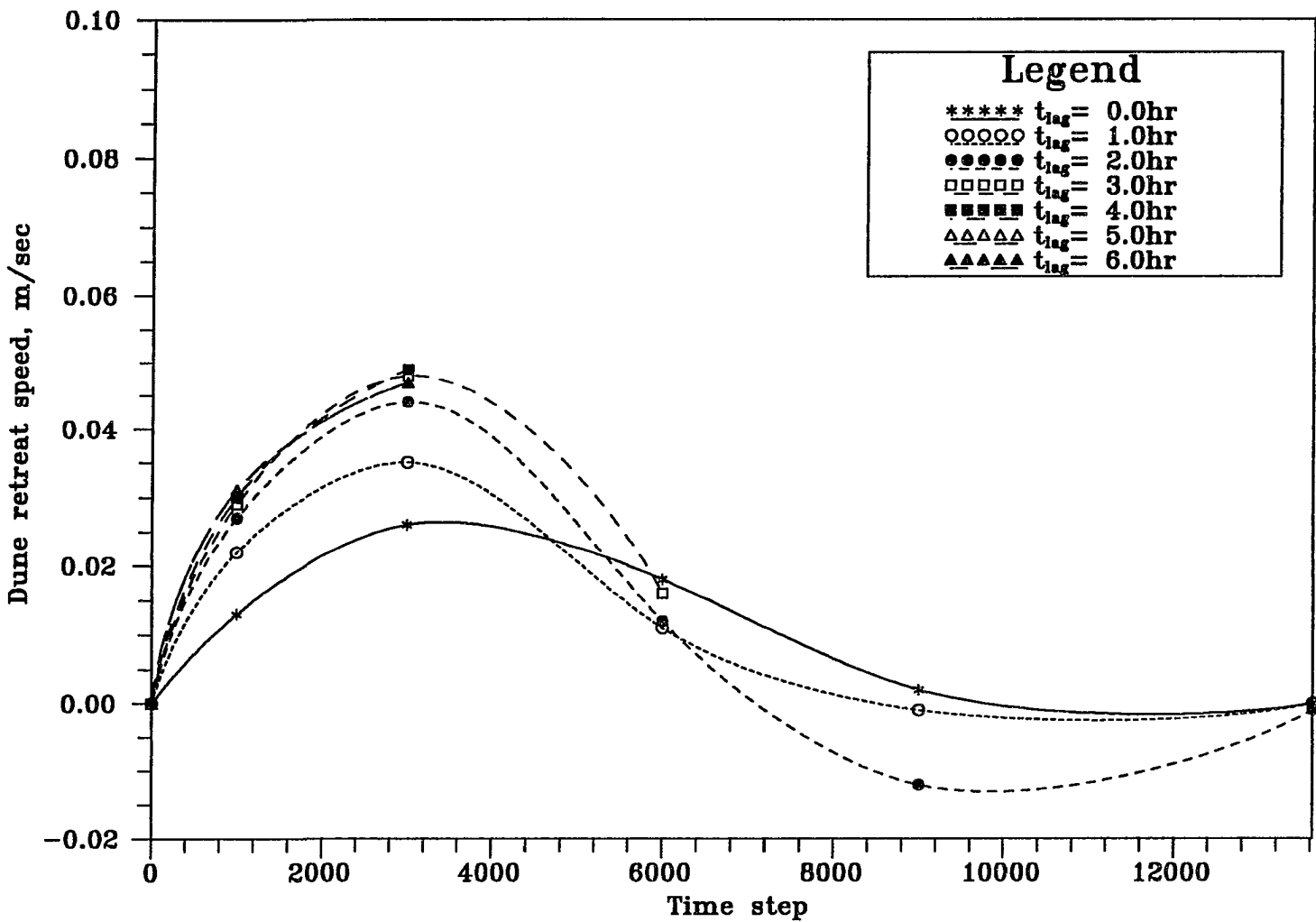


Figure 7.6 Dune Retreat Speeds above MLLW for Various Time Lags.
 ($h_{om}=4.0m$, $h_{bm}=3.0m$, $D_{50}=0.3mm$ and $T=24hr$)

285

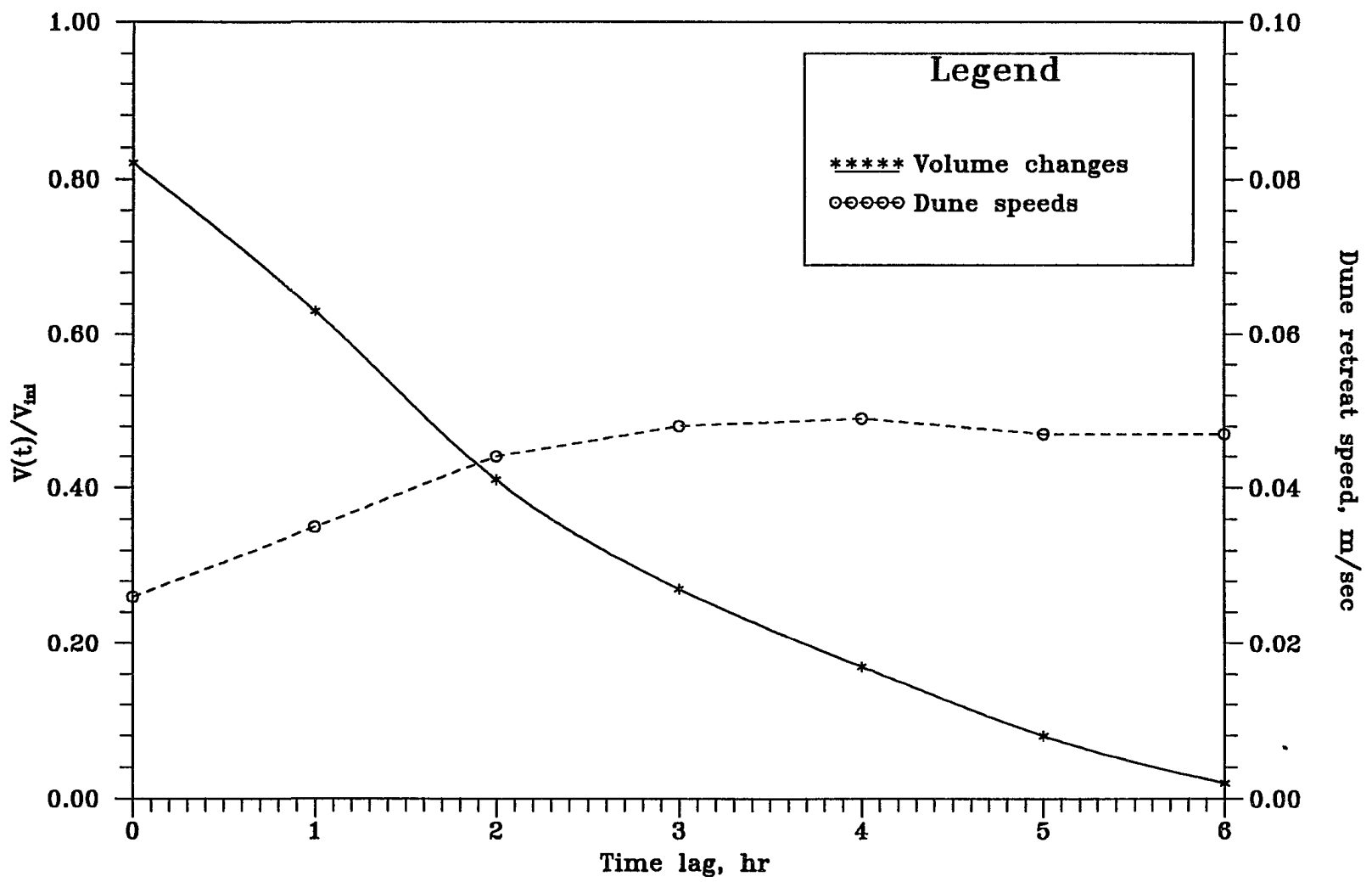


Figure 7.7 Volume Changes and Dune Retreat Speeds above MLLW for Various Time Lags at $t=3000$. ($h_{om}=4.0m$, $h_{bm}=3.0m$, $D_{50}=0.3mm$ and $T=24hr$)

7.3.3 Sediment Grain Size

The transport of sediment particles by a flow of water depends on the size of the bed material particles and the flow conditions. In this study, six different grain sizes are investigated for the sensitivity analyses. Grain size is one of the model parameters that significantly affects the movement of the centroids of barrier dunes.

Figure 7.8 shows the relative volume changes for various sand diameters. Median grain size, $D_{50}=0.1mm$ results in the least volume change but $D_{50}=0.4mm$ gives the fastest volume losses. In van Rijn's (1984a and b) sediment transport formulas, it is assumed that the sediment transport rate can be described sufficiently accurately by two dimensionless parameters only, a dimensionless *particle parameter*, D , and a *transport stage parameter*, T . The T -parameter expresses the mobility of the particles in terms of the stage of movement relative to the critical stage for initiation of motion according to the Shields curve. In the Shields curve (van Rijn, 1984a), it is seen that the minimum critical bed-shear velocity, which generally gives maximum sediment transport, occurs at $D_{50}\approx 0.4\text{--}0.5mm$ and Figure 2.46 in Vanoni (1975, p102) shows minimum critical velocity occurs at $D_{50}\approx 0.2\text{--}0.5mm$.

Dune retreat speeds for various sand diameters are presented in Figure 7.9. Median grain size, $D_{50}=0.4mm$ results in maximum retreat speed and $D_{50}=0.1mm$ gives minimum values for the entire computational domain. The above results are graphically summarized in Figure 7.10 for both relative volume changes and dune retreat speeds with various grain sizes at $t=3,000$ time level.

The curve for the volume changes indicated as the solid line in Figure 7.10 follows the Shields curve in a similar manner, so sensitivity tests of the numerical model for sand

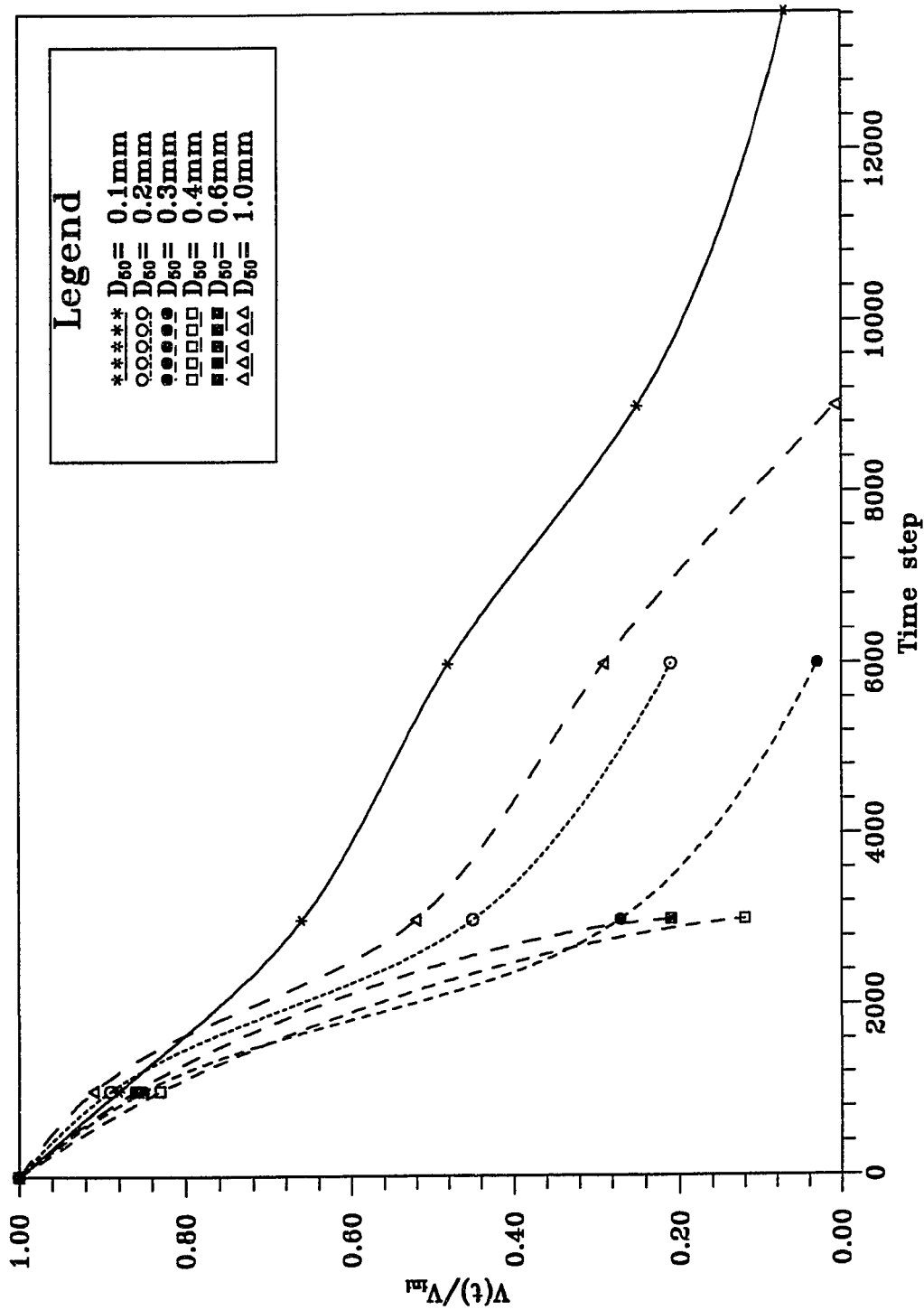


Figure 7.8 Volume Changes above MLLW for Various Sand Diameters.
 ($h_{om}=4.0\text{m}$, $h_{bm}=3.0\text{m}$, $t_{ag}=3.0\text{hr}$ and $T=24\text{hr}$)

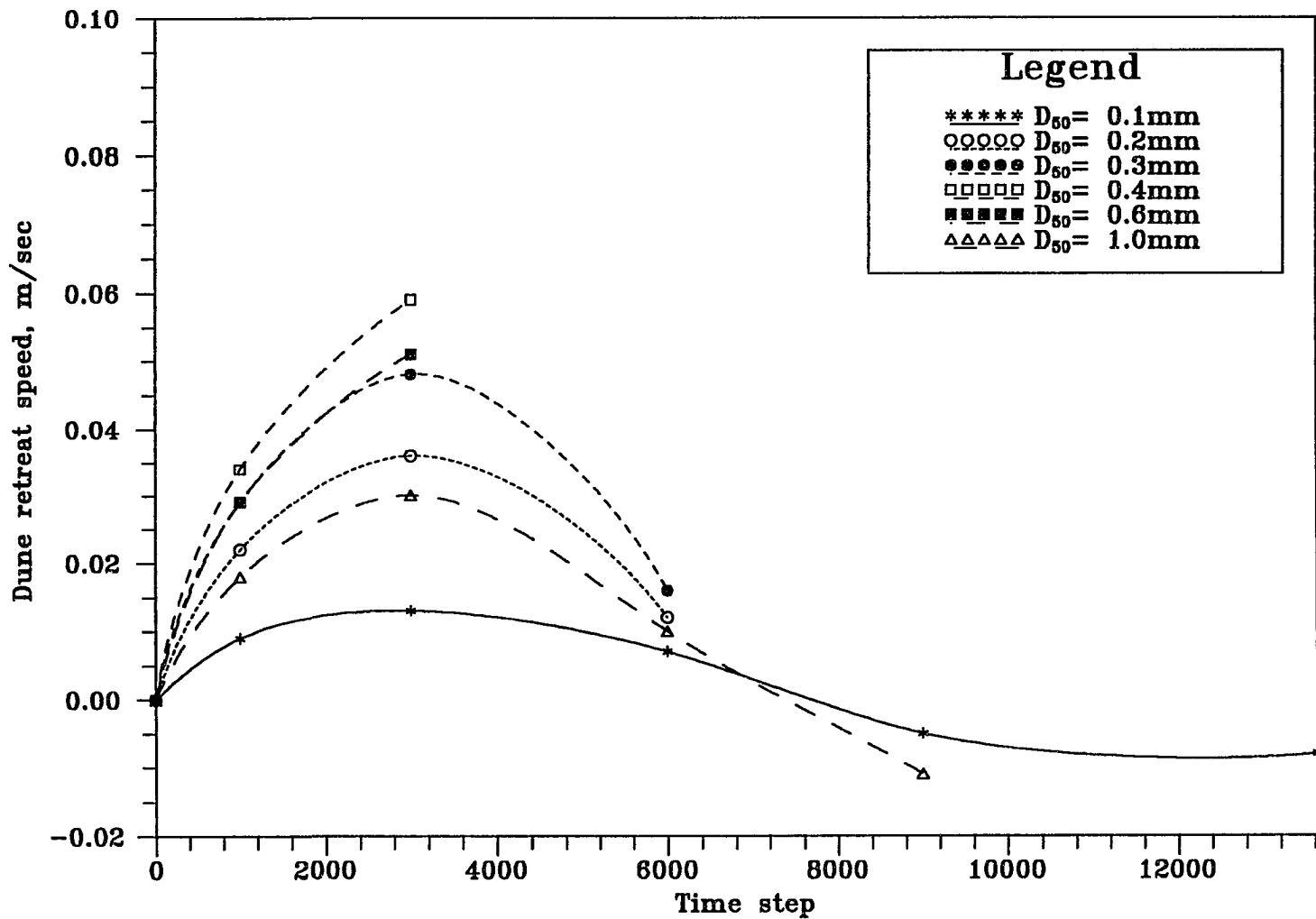


Figure 7.9 Dune Retreat Speeds above MLLW for Various Sand Diameters.
 ($h_{om}=4.0m$, $h_{bm}=3.0m$, $t_{lag}=3.0hr$ and $T=24hr$)

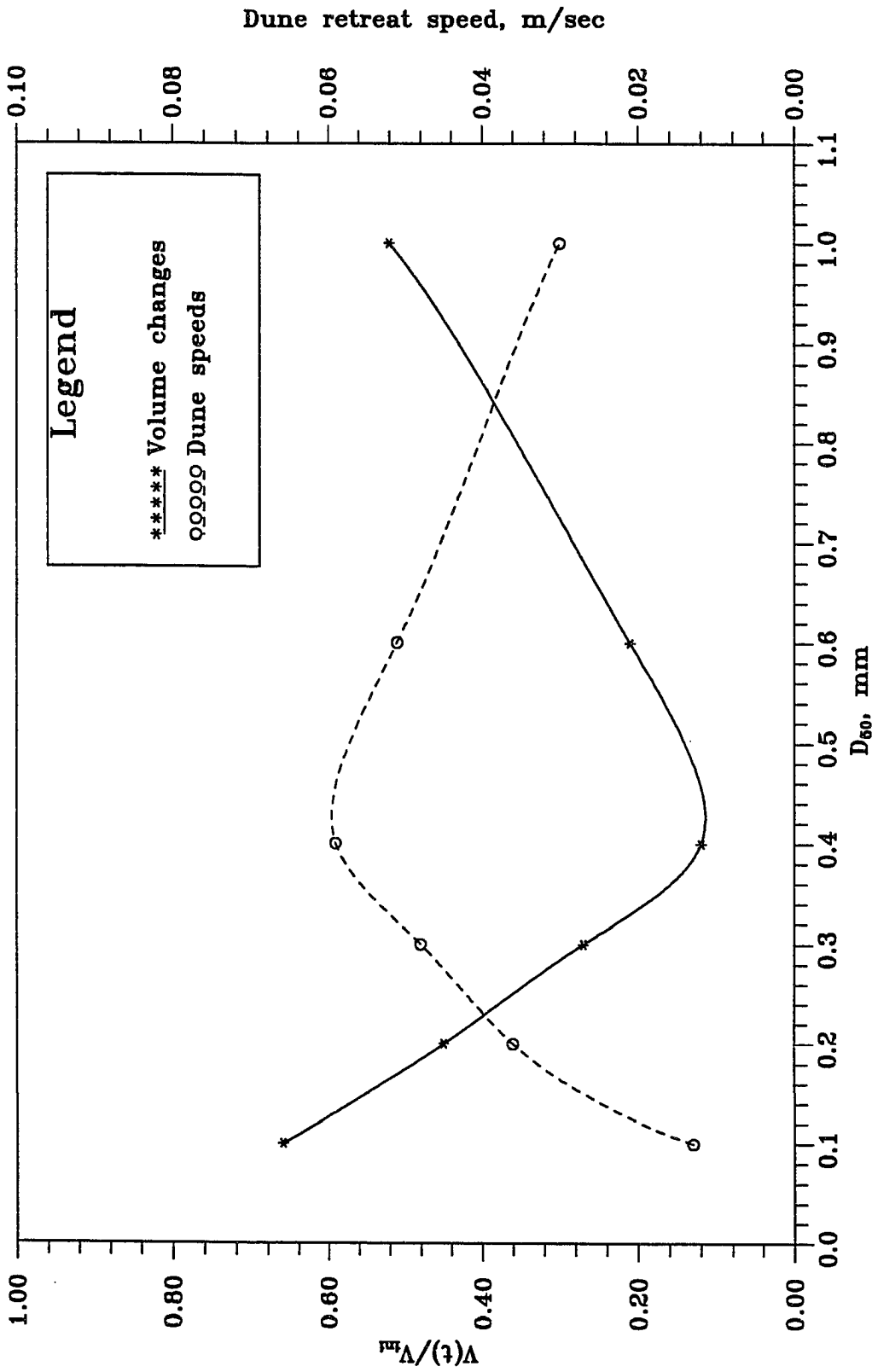


Figure 7.10 Volume Changes and Dune Retreat Speeds above MLLW for Various D_{50} at $t=3000$. ($h_{om}=4.0m$, $h_{bm}=3.0m$, $t_{ag}=3.0hr$ and $T=24hr$)

diameters can be concluded to give successful results.

7.3.4 Storm Duration

The water flow characteristics are strongly affected by the shape of the surge hydrograph which is determined from the storm duration and the peak surge level. In the case of a fixed peak surge level, shorter storm duration produces more rapid changes in flow depth and velocity than in longer duration. This is well defined in Figures 7.11 and 7.12 for relative volume change and dune retreat speed, respectively.

Barrier volumes above MLLW are completely eroded during simulations in all cases. A shorter duration storm moves eroded sediment to the ocean side and longer duration distributes eroded sediment over the bay area. In longer duration, there are no distinct sediment flows from bay to ocean due to mild water flow characteristics. Because the hydraulic stage difference between ocean and bay in shorter duration is much greater than that of longer duration, the faster dune retreat speed and strong ebbing flood flow are produced from shorter duration storm. Detailed results for volume changes, retreat speeds and centroid positions of barrier dune are summarized in Table 6.40 (p.165).

7.4 General Discussion

In this study, the major task was to develop the numerical model for water motion and sediment transport.

The Lax-Wendroff two-step explicit scheme was successfully developed and run to provide initial conditions for subsequent stages. Also, the method of characteristics was well

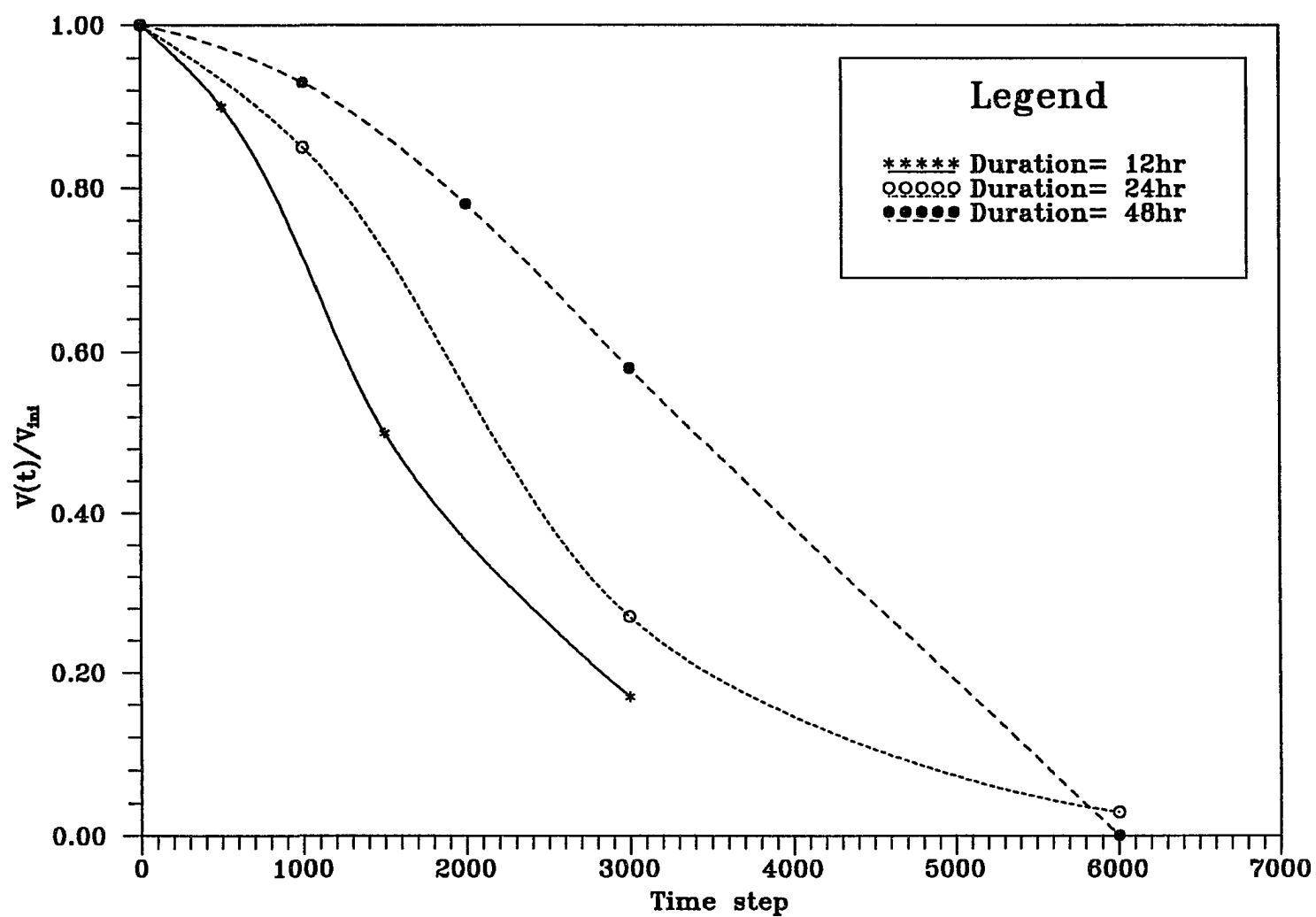


Figure 7.11 Volume Changes above MLLW for Various Storm Durations.
($h_{om}=4.0m$, $h_{bm}=3.0m$, $t_{lag}=3.0hr$ and $D_{50}=0.3mm$)

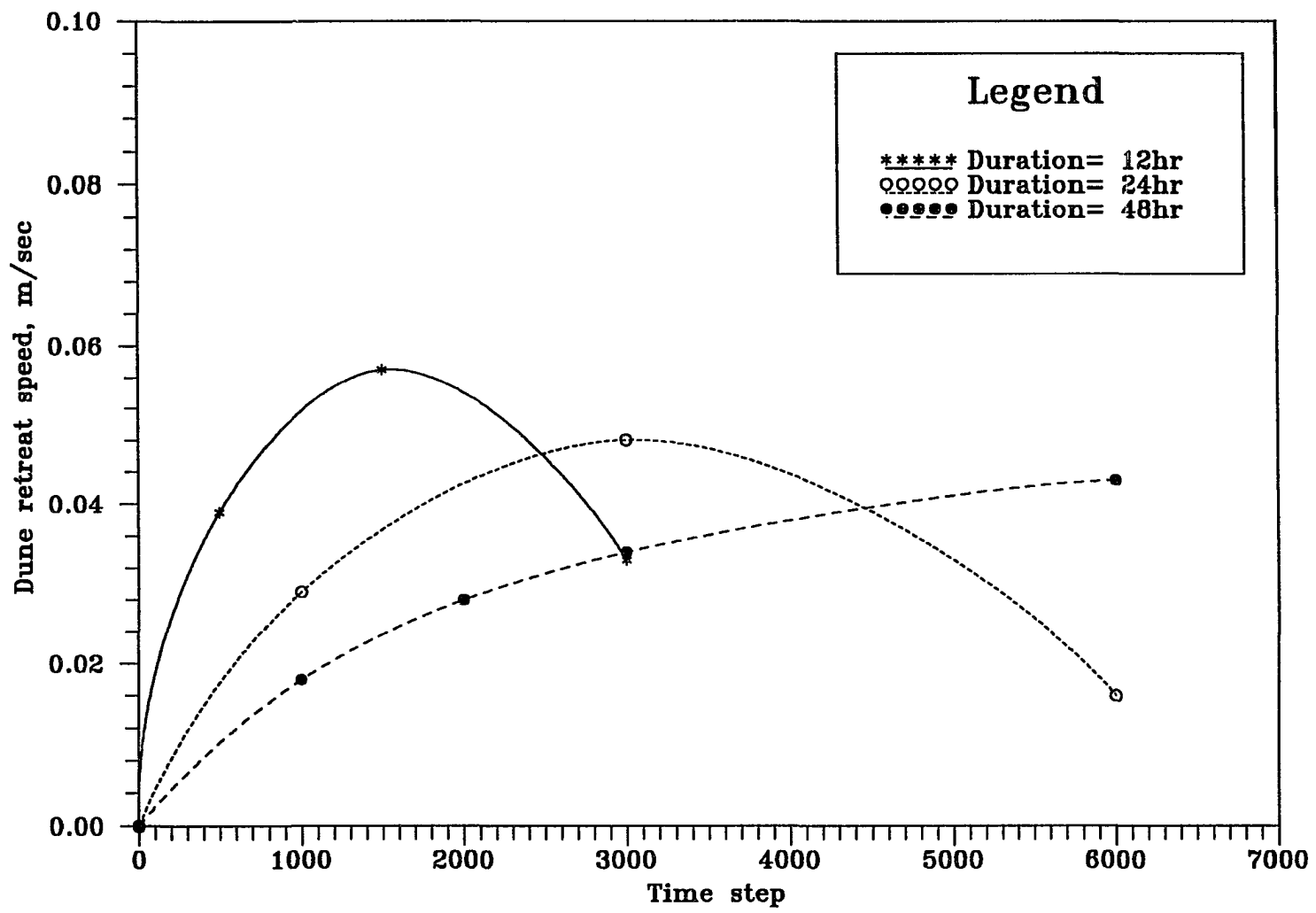


Figure 7.12 Dune Retreat Speeds above MLLW for Various Storm Durations.
($h_{om}=4.0m$, $h_{bm}=3.0m$, $t_{lag}=3.0hr$ and $D_{50}=0.3mm$)

incorporated within the Lax-Wendroff scheme to provide additional boundary data.

The Preissmann implicit four-point box scheme was also developed for the storm tide simulations and an explicit scheme was incorporated for a numerical integration of the sediment continuity equation.

Standard tests (static, cosine swing and shock tests) for a fixed boundary gave good verification of each numerical codes. Also, the volume conservation tests on numerical computations brought a confirmation about the accuracy of linked numerical models.

The model tests (sensitivity tests) revealed which boundary conditions or parameters are critical to transport the most sediment landward (Stage III) and seaward (Stages I and IV) in the model.

Finally, the volume changes in each stage for 24 hour storm duration ($h_{om}=4.0m$, $h_{bm}=3.0m$, $t_{lag}=3.0hr$ and $D_{50}=0.3mm$) are plotted in Figure 7.13. Most of the eroded volumes above MLLW are mainly derived not by the wave actions (Stage I, dune / beach erosion) but by the water motions (Stages III and IV, storm tidal flows).

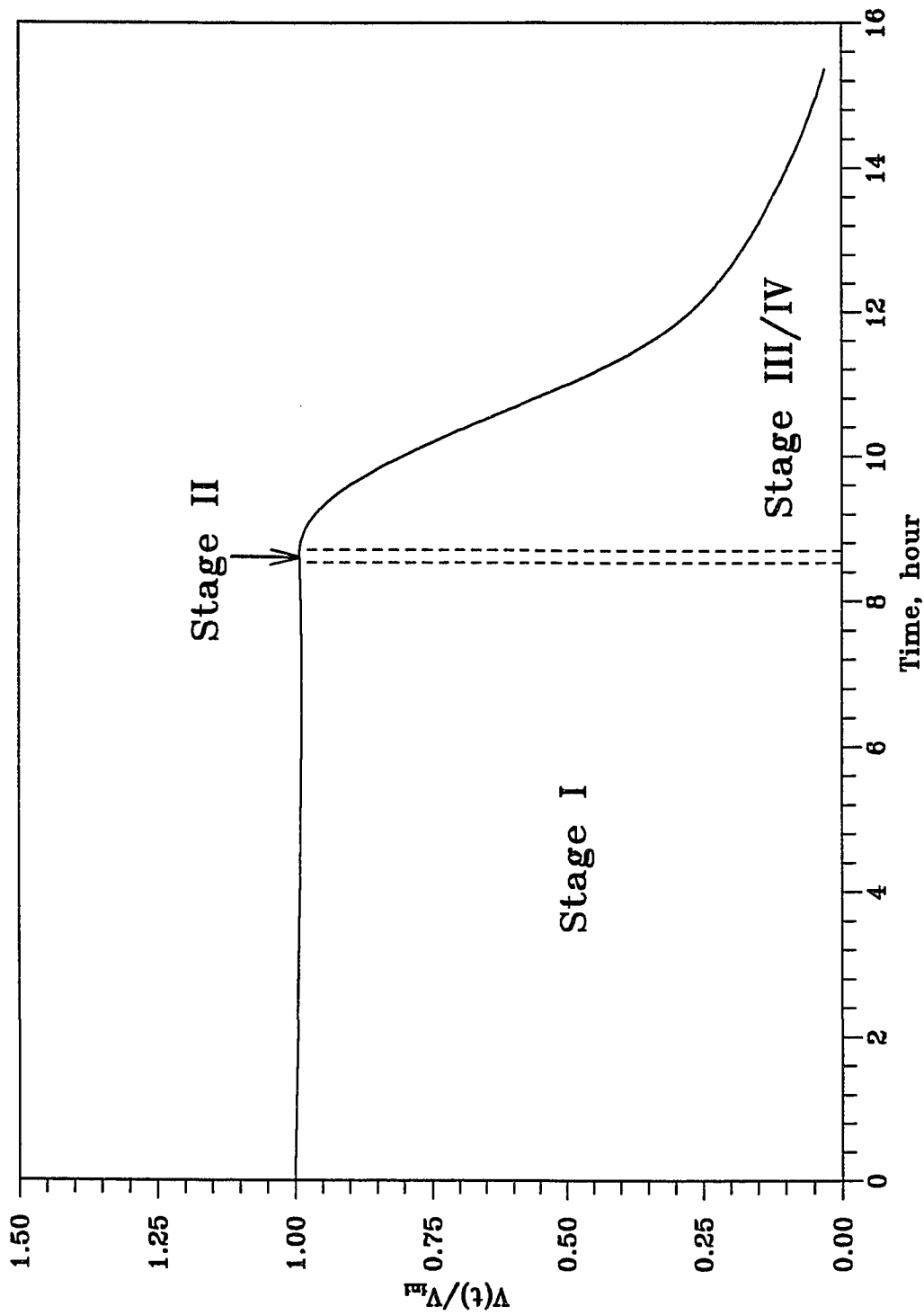


Figure 7.13 Volume Changes in Each Stage above MLLW for 24 Hours Storm Duration. ($h_{om}=4.0m$, $h_{pm}=3.0m$, $t_{sf}=3.0hr$ and $D_{50}=0.3mm$)

8.0 CONCLUSIONS AND RECOMMENDATIONS

8.1 Conclusions

The summarized conclusions are classified into two categories as: (1) the performances and properties of the numerical models and (2) the results of the numerical model tests.

Three different numerical codes are incorporated in this study: (1) the SBEACH for dune/beach erosion, (2) the Lax-Wendroff scheme with MOC for overwash/overland flow and (3) the Preissmann scheme with the FTCS scheme for storm tidal floods and resulting profile evolutions. The following concluding summaries are derived from the various numerical experiments.

- Overall applicabilities and performances of the SBEACH model for simulating dune/beach erosion were successful and satisfactory.
- The Lax-Wendroff two-step scheme, which is written in momentum conservation form, could handle mixed sub- and super-critical flows directly, with no regard for the directional nature of the computation.
- The method of characteristics (MOC) provides a particularly transparent procedure to obtain additional boundary data at both boundaries.
- The Lax-Wendroff scheme is capable of furnishing proper initial conditions within ten to twenty minutes of simulation for the next stages.
- A small depth of initial base flow about $0.03\text{-}0.05\text{m}$ provides a good technique to

overcome a dry bed situation.

- The double sweep solution method provides an efficient way to solve linearized equation systems in the Preissmann scheme.
- The spatial weighting factor, $\psi=0.5$ and time weighting factor, $\theta \geq 0.65$ lead to an unconditionally stable scheme.
- The Preissmann scheme as written is not directly capable of handling super-critical flows but introduction of a control function to suppress the convective acceleration term makes it possible to maintain a subcritical flow characteristic structure.
- The forward time centered space explicit scheme for the sediment continuity equation produces growing oscillations (*i.e.* wiggles) which result in numerical instability, but the dissipative interface with $\gamma=1/50 \sim 1/20$ was successfully introduced to control growing wiggles.
- In situations with more rapid changes in flow direction and/or magnitude, it is necessary to adjust the weighting factor, γ in the dissipative interface to give more local dissipation for the stability of the numerical scheme.
- The program correctness for both the Lax-Wendroff and Preissmann schemes was verified and confirmed as excellent through the standard tests.
- The accuracy of the integrated numerical models was examined through volume conservation tests, and it is concluded that the integrated models provide accurate solutions without any notable numerical errors.

Within the range of the physical parameters considered, the following conclusions

are drawn from the results of the numerical model tests.

- The relative volume change, centroid position and dune retreat speed provide a fundamental indicator of the state of the barrier islands.
- The peak surge level difference between ocean and bay boundaries regulates flow conditions and directions, and larger hydraulic stage difference produces greater volume loss and faster dune retreat speed.
- The eroded sediments are mainly transported to the bay when smaller time lags are employed and to the ocean when larger time lags are employed.
- Time lags for most open barrier-bay systems (*i.e.* many segmented barrier islands with many existing tidal inlets) are relatively short so that eroded sediments are mainly transported to the bay sides.
- In inundated barrier breaching mode represented with unit width for the relatively closed barrier-bay systems (*e.g.* Sandbridge Back bay-barrier), bay side water levels are influenced by both storm tidal flows through existing tidal inlets and ocean flood flows over the eroded barrier dunes. In that case, both hydraulic stage difference and time lag between ocean and bay will be relatively small, so sediment transports toward the bay side are apparently predicted.
- However, in localized breaching mode for the closed barrier-bay systems, the barriers generally remain above the maximum storm surge level except at localized spots where breaching occurs, so bay side water levels are mainly influenced by storm tidal flows through existing tidal inlets. An assumption is that the tidal prism in the bay

is large enough that it must be followed to justify the above outcome. In this mode, hydraulic stage difference and time lag can be relatively greater than those of inundated breaching mode, so sediment transports toward ocean side will occur.

- Median grain size, $D_{50}=0.4mm$ gave maximum volume losses and retreat speeds.
- Grain size turned out to be one of the model parameters that significantly affects the movements of the centroid of barrier dune.
- In the SBEACH model, profile changes are most sensitive to storm durations.
- The fast dune retreat speeds and strong ebbing flows result from the shorter duration storms because stage difference in shorter duration is much greater than that in longer duration.
- It can be summarized from the above facts that the most sediments are transported landward by larger peak storm surge difference with shorter time lag and longer duration, and seaward by smaller peak storm surge difference with longer time lag and shorter storm duration.
- The numerical model has properly responded to the changes of each model parameter; therefore, it is concluded that the model can produce *reasonable* results.

8.2 Recommendations

Future research for refining and extending the capabilities of the numerical models will be directed toward improved understanding and modeling of sediment transport associated with dune overtopping, dune breach growth and complex tidal and sediment flows through breached barrier islands.

Considering the scope of the present research, the following recommendations are discussed for further investigations.

- The Lax-Wendroff scheme could also be used in Stages III and IV for the sediment transport computation under the conditions with the computational time because its time step is limited by the stability condition.
- The bed-form (ripples, bed dunes, etc.) influence on the boundary resistance term in the momentum equation for water flows in Stages III/IV should be investigated to determine the relative magnitude of influence on these *plane bed* results.
- Various geometric sections characterized by barrier width, dune crest elevation, dune base width and average barrier elevation can be considered as further calibration parameters.
- Bathymetric, topographic map data with oceanographic data for both the ocean and bay during the historic storm events will be extremely valuable for the field calibrations and verifications of the numerical models.
- Breaking (or non-breaking) wave propagation over the eroded barrier islands should be incorporated within the future models.
- Laboratory and field experiments for breach growth (width) are necessary for the next two-dimensional model development (*i.e.* localized breaching mode).
- The development of a depth-averaged, two-dimensional (horizontal) model for the water motion and sediment transport in coupled or uncoupled modes will be the next effort for a better understanding of breaching and tidal dynamics through the barrier-bay and inlets systems.

REFERENCES

- Abbott, M.B., 1979. "Computational hydraulics : elements of the theory of free surface flows." Pitman Pub., London.
- Abbott, M.B.,and Basco, D.R., 1989. "Computational fluid dynamics." Longman Scientific & Technical, pp.425.
- Abbott, M.B., and Cunge, J.A. (eds.), 1982. "Engineering applications of computational hydraulics." Vol.1, Pitman Pub., Massachusetts.
- Ackers, P.,and White, W., 1973. "Sediment transport: new approach and analysis." *J. Hydr. Div.*, ASCE, Vol.99, No.HY11.
- Airy, G.B., 1845. "Tides and waves." *Encyc. Metrop.*, Art.192.
- Akanbi, A.A., and Katopodes, N.D., 1988. "Model for flood propagation on initially dry land." *J. Hydr. Eng.*, ASCE, Vol.116, No.7.
- Akan, A.O., 1976. "Unsteady shallow water flow on porous media." Ph.D. Dissertation, Civil Eng. Dept., University of Illinois at Urbana-Champaign.
- Akan, A.O., and Yen, B.C., 1981. "Mathematical model of shallow water flow over porous media." *J. Hydr. Eng.*, ASCE, Vol.107, No.HY4.
- Allen, J.R.L., 1970. "The avalanching of granular solids on dune and similar slopes." *J. Geology*, Vol.78, No.3, pp. 326-351.
- Amein, M., 1968. "An implicit method for numerical flood routing." *Water Resources Research*, 4(4), pp. 719-726.
- Amein, M., and Fang, C.S., 1970. "Implicit flood routing in natural channels." *J. Hydr. Eng.*, ASCE, Vol.96, No. HY12.
- Aubrey, D.G., and Weishar, L.(eds.), 1988. "Hydrodynamics and sediment dynamics of tidal inlets." Lecture Notes on Coastal and Estuarine Studies, Vol.29, Springer-Verlag New York, Inc.
- Basco, D.R., 1977. "On numerical accuracy in computational hydraulics." *Proc. 25th Annual Hydr. Div. Spec. Conf.*, ASCE, College Station, TX, pp.179-186.
- Basco, D.R., 1990. "The effect of seawalls on long-term shoreline change rates for the

- southern Virginia ocean coastline." *Proc. 22nd Conf. Coastal Eng.*, Delft, The Netherlands, pp.1292-1305.
- Basco, D.R., 1996. Personal Communication.
- Basco, D.R., and Shin, C.S., 1992 and 1993. "Unpublished SBEACH model parameters calibration works for the CERC." U.S. Army Eng. Waterway Exp. Sta., Vicksburg, MS.
- Bathurst, J.C., Graf, W.H., and Cao, H.H., 1987. "Bed-load discharge equations for steep mountain rivers." *Sediment Transport in Gravel-Bed Rivers*, C.R. Thorne, J.C. Bathurst and R.D. Hey, eds., John Wiley and Sons Ltd., New York, N.Y.
- Battjes, J.A., and Janssen, J.P.F.M., 1978. "Energy loss and set-up due to wave breaking of random waves." *Proc. 16th Conf. Coastal Eng.*, Hamburg, Germany.
- Bruun, P., 1962. "Sea-level rise as a cause of shore erosion." *J. Waterways and Harbors Div.*, ASCE, Vol.88, No. ww1, pp.117-130.
- Bruun, P., 1978. "Stability of tidal inlets: theory and engineering." New York, Elsevier Scientific Pub. Co., pp.510.
- Bruun, P., 1983. "Review of conditions for uses of the Bruun Rule of erosion." *Coastal Engineering*, 7, pp. 77-89.
- Chang, F.F.M., and Richards, D.L., 1971. "Deposition of sediment in transient flow." *J. Hydr. Eng.*, ASCE, Vol.97, No.HY6.
- Chen, Y.H., 1973. "Mathematical modeling of water and sediment routing in natural channels." Ph.D. Thesis, Colorado State Univ., Fort Collins, Colorado.
- Coleman, N.L., 1970. "Flume studies of the sediment transfer coefficient." *Water Resources*, Vol.6, No.3.
- Correia, L.-R.P., Krishnappan, B.G., and Graf, W.H., 1992. "Fully coupled unsteady mobile boundary flow model." *J. Hydr. Eng.*, ASCE, Vol.118, No.3.
- Cunge, J.A., Holly, F.M., and Verwey Jr, A., 1980. "Practical aspects of computational river hydraulics." Pitman Pub. Inc., London.
- Dally, W.R., 1990. "Stochastic modeling of surf climate." *Proc. 22nd Conf. Coastal Eng.*, Delft, The Netherlands.

- Dally, W.R., Dean, R.G., and Dalrymple, R.A., 1985a. "Wave height variation across beaches of arbitrary profile." *J. Geophys. Res.*, Vol.90, No.C6, pp.11917-11927.
- Dally, W.R., Dean, R.G., and Dalrymple, R.A., 1985b. "A model for breaker decay on beaches." *Proc. 19th Conf. Coastal Eng.*, pp.82-98.
- Dean, R.G., 1976. "Beach Erosion: Causes, processes, and remedial measures." *CRC Reviews in Environmental Control*, CRC Press, 6(3): pp.259-296.
- Dean, R.G., 1977. "Equilibrium beach profiles: U.S. Atlantic and Gulf Coasts." Dept. Civil Eng., Ocean Eng. Rept. No.12, Univ. of Delaware, Newark, DE.
- Dean, R.G., 1984. "Applications of equilibrium beach profile concepts." *Coastal Engineering Abstracts*, ASCE, pp140-141.
- Dean, R.G., 1987. "Coastal Sediment Processes: toward engineering solutions." *Proc. Coastal Sediments'87*, ASCE, pp.1-24.
- Dolan, R.H., 1985. "Sandbridge beach and back bay, Virginia." Tech. Rept. Coastal Research Assoc., Inc., Charlottesville, Virginia, pp.120.
- Ebersole, B.A., 1987. "Measurements and prediction of wave height decay in the surf zone." *Proc. Coastal Hydrodynamics*, ASCE, pp.1-16.
- Edelmann, T., 1968. "Dune erosion during storm conditions." *Proc. 11th Conf. Coastal Eng.*, London, pp.719-722.
- Edelmann, T., 1972. "Dune erosion during storm conditions." *Proc. 13th Conf. Coastal Eng.*, Vancouver, pp.1305-1312.
- Engelund, F., and Hansen, E., 1967. "A monograph on Sediment transport." Technisk Forlag, Copenhagen, Denmark.
- Escoffier, F.F., 1940. "The stability of tidal inlets." *Shore and Beach*, Vol.8, pp.114-115.
- Escoffier, F.F., 1972. "Hydraulics and stability of tidal inlets." U.S. Army Corps of Eng., GITI Report 13, pp.72.
- Evans, E.P., 1977. "The behavior of a mathematical model of open channel flow." *Proc. 17th IAHR*, Baden-Baden, 2:pp.173-180.
- Fessenden, F.W., and Scott, S.C., 1989. "The coastal beach at Nauset Beach, Chatham, Mass.: a case study." In *Barrier Islands: process and management*, ASCE, New York,

pp.138-149.

- Fread, D.L., 1974. "Numerical properties of implicit four-point finite difference equations of unsteady flow." National Weather Service, TM HYDRO-18, Washington, DC.
- Galvin, C.J., 1969. "Breaker travel and choice of design wave height." *J. Waterways and Harbors Div.*, ASCE, Vol.95, No.2, pp.175-200.
- Giese, G.S., 1978. "The barrier beaches of Chatham, Mass." Rept., Provincetown Center for Coastal Studies.
- Giese, G.S., Liu, T.T., and Aubrey, D.G., 1989. "Impacts of tidal formation on the physical characteristics of a barrier beach-estuary system." In *Barrier Island: process and management*, ASCE, New York, pp.150-158.
- Goldsmith, V., 1972. "Coastal processes of a barrier island complex and adjacent ocean floor: Monomoy Island-Nauset Spit, Cape Cod, Mass." unpublished Ph.D. thesis, Univ. of Massachusetts, pp.469.
- Havnø, K., and Brorsen, M., 1986. "A general mathematical modeling system for flood forecasting and flood control." *Proc. International Conf. Hydr. Floods and Flood Control*, Cambridge, UK; BHRA, Stevenage.
- Holly, F.M., Jr., and Rahuel, J.-L., 1990. "New numerical/physical framework for mobile-bed modeling." *J. Hydraulic Research*, Vol.28, No.4, pp.401-416.
- Hsu, S.M., and Holly, F.M., Jr., 1992. "Conceptual bed-load transport model and verification for sediment mixtures." *J. Hydr. Eng.*, ASCE, Vol.118, No.8.
- Jain, S.C., 1981. "River bed aggradation due to overloading." *J. Hydr. Eng.*, ASCE, Vol.107, No.HY1.
- Jaramillo, W.F., and Jain, S.C., 1984. "Aggradation and degradation of alluvial-channel beds." *J. Hydr. Eng.*, ASCE, Vol.110, No.8.
- Katopodes, N.D., 1990. "Observability of surface irrigation advance." *J. Irrigation and Drainage Eng.*, Vol.116, No.5, pp.656-675.
- Katopodes, N.D., and Strelkoff, T., 1978. "Computing two-dimensional dam break waves." *J. Hydr. Div.*, ASCE, Vol.104, No.HY9.
- Katopodes, N.D., Tang, J.-H., and Clemmens, A.J., 1990. "Estimation of surface irrigation parameters." *J. Irrigation and Drainage Eng.*, Vol.116, No.5, pp.676-696.

- Kajima, R., Shimizu, T., Maruyama, K., and Saito, S., 1983. "Experiments of beach profile change with a large wave flume." *Proc. 18th Conf. Coastal Eng.*, pp.1385-1404.
- Keulegan, G.H., 1967. "Tidal flow in entrances: Water-level fluctuations of basins in communication with seas." U.S. Army Corps of Eng., Committee on Tidal Hydraulics, Tech. Bull. 14, pp.89.
- Kobayashi, N., 1987. "Review of wave transformation and cross-shore sediment transport processes in surf zones." *J. Coastal Res.*, Vol.4, No.3: pp.435-445.
- Kriebel, D.L., 1982. "Beach and dune response to hurricanes." Unpublished MS thesis, Univ. of Delaware, Newark, DE.
- Kriebel, D.L., 1986. "Verification study of a dune erosion model." *Shore and Beach*, Vol.54, No.3.
- Kriebel, D.L., and Dean, R.G., 1984. "Beach and dune response to severe storms." *Proc. 19th Conf. Coastal Eng.*, Houston, pp.1587-1599.
- Kriebel, D.L., and Dean, R.G., 1985. "Numerical simulation of time-dependent beach and dune erosion." *Coastal Eng.*, Vol.9, pp.221- 245.
- Kriebel, D.L., and Dally, W.R., and Dean, R.G., 1986a. "Beach profile response following severe erosion events." Report UFL/COEL-86/016, Coastal and Oceanographical Dept., University of Florida, Gainesville, FL.
- Kriebel, D.L., and Dally, W.R., and Dean, R.G., 1986b. "Undistorted Froude model for surf zone sediment transport." *Proc. 20th Conf. Coastal Eng.*, Taipei, Taiwan, pp.1296-1310.
- Lai, C., 1989. "A numerical scale model for simulating unsteady-alluvial channel flow." Tech. Rept. prepared for Sedimentation Comm., Interagency Advis. Comm. on Water Data, pp.72.
- Lai, C., 1991. "Modeling alluvial-channel flow by multimode characteristics method." *J. Eng. Mechanics*, Vol.117, No.1, pp.32-53.
- Larson, M., 1988. "Quantification of beach profile change." Rept. No.1008, Dept. Water Res. Eng., Univ. of Lund, Lund, Sweden.
- Larson, M., and Kraus, N.C., 1989. "SBEACH: numerical model for simulating storm-induced beach change." Tech. Rept. CERC-89-9, CERC, U.S. Army Eng. Waterway Exp. Sta., Vicksburg, MS.

- Larson, M., Kraus, N.C., and Byrnes, M.R., 1990. 'SBEACH: numerical model for simulating storm-induced beach change; Rept.2: numerical formulation and model tests." Tech. Rept. CERC-89-9, CERC, U.S. Army Eng. Waterway Exp. Sta., Vicksburg, MS.
- Lax, P.D., and Wendroff, B., 1960. "System of conservation laws." *Comm. Pure and Applied Math.*, 13: pp.217-237.
- Leatherman, S.P., 1988. "Barrier island handbook." Laboratory for coastal research, Univ. of Maryland, College Park, 3rd ed., pp.63.
- Leffler, M.W., Baron, C.F., Scarborough, B.L., and Hathaway, K.R., 1993. "Annual data summary for 1991, CERC field research facility." U.S. Army Corps of Engineers, WES, CERC, TR-CERC-93-9.
- Lyn, D.A., 1987. "Unsteady sediment-transport modeling." *J. Hydr. Eng.*, ASCE, Vol.113, No.1, pp.1-15.
- Lyn, D.A., and Goodwin, P., 1987. "Stability of a general Preissmann scheme." *J. Hydr. Eng.*, ASCE, Vol.113, No.1, pp.16-28.
- Mahmood, K., and Yevjevich, V. (eds.), 1975. "Unsteady flow in open channels." Water Resources Publ., Fort Collins, Colorado.
- Mahmood, K., and Ponce, V.M., 1976. "Mathematical modeling of sedimentation transients in sand-bed channels." Rept. CER75-76- KM-VMP28, Eng. Res. Center, Colorado State Univ., Fort Collins, Colorado.
- McBride, R.A., 1986. "The origin, evolution, orientation, and distribution of shoreface-attached sand ridges and their relationship to tidal inlets, north Atlantic shelf, USA." Unpublished MS thesis, Louisiana State Univ., Baton Rouge, Louisiana, pp.180.
- McClennen, C.E., 1979. "Nauset Spit: model of cyclical breaching and spit regeneration during coastal retreat." In eastern section field trip guide book; Cape Cod national seashore, Boulder, Colorado.
- Moore, B.D., 1982. "Beach profile evolution in response to changes in water level and wave height." Unpublished MS thesis, Univ. of Delaware, Newark, Delaware.
- O'Brien, M.P., 1931. "Estuary tidal prisms related to entrance areas." *Civil Eng.*, May.
- Oertel, G.F., 1988. "Processes of sediment exchange between tidal inlets, ebb deltas and barrier islands." Lecture Notes on Coastal and Estuarine Studies, Vol.29 in

Hydrodynamics and Sediment Dynamics of Tidal Inlets, Aubrey, D.G. and Weishar, L. (eds.), Springer-Verlag New York, Inc.

Park, I. And Jain, S.C., 1986. "River-bed profiles with imposed sediment load." *J. Hydr. Eng.*, ASCE, Vol.112, No.4.

Park, I. And Jain, S.C., 1987. "Numerical simulation of degradation of alluvial channel beds." *J. Hydr. Eng.*, ASCE, Vol.113, No.7.

Pierce, J.W., 1970. "Tidal inlets and washover fans." *J. Geology*, Vol.78, pp.230-234.

Ponce, V.M., and Simons, D.B., 1977. "Shallow water propagation in open channel flow." *J. Hydr. Eng.*, ASCE, Vol.103, No.HY12.

Ponce, V.M., Indlekofer, H., and Simons, D.B., 1979. "The convergence of implicit bed transient models." *J. Hydr. Div.*, ASCE, Vol.105, No.HY4.

Preissmann, A., 1961. "Propagation des intumescences dans les canaux et rivières." 1st Congress de l'Assoc. Francaise de Calcul Grenoble, pp.433-442.

Rahuel, J.L., Holly, F.M., Chollet, J.P., Belleudy, P.J., and Yang, G., 1989. "Modeling of riverbed evolution for bedload sediment mixtures." *J. Hydr. Eng.*, ASCE, Vol.115, No.11.

Richtmyer, R.D., 1963. "A survey of difference methods for nonsteady fluid dynamics." NCAR Tech. Note 63-2, Boulder, Colorado.

van Rijn, L.C., 1984a. "Sediment transport, part I: bed load transport." *J. Hydr. Eng.*, ASCE, Vol.110, No.10.

van Rijn, L.C., 1984b. "Sediment transport, part II: suspended load transport." *J. Hydr. Eng.*, ASCE, Vol.110, No.11.

van Rijn, L.C., 1984c. "Sediment transport, part III: bed forms and alluvial roughness." *J. Hydr. Eng.*, ASCE, Vol.110, No.12.

de Saint Venant, A.J.C., 1871. "Theory of unsteady water flow, with application to river floods and to propagation of tides in river channels." French Academy of Science, Vol.73, pp.148-154,237-240.

Schoonees, J.S., and Theron, A.K., 1995. "Evaluation of 10 cross-shore sediment transport / morphological models." *Coastal Engineering*, 25, pp. 1-41.

- Shields, A., 1936. "Anwendung der aehnlichkeits mechanik und der turbulenzforschung auf die geschiebewegung." Mitt. Preuss. Versuchanst. Wasserbau Schiffbau, Berlin, 26: 1-26.
- Soni, J.P., Garde, R.J., and Raju, K.G.R., 1980. "Aggradation in streams due to overloading." *J. Hydr. Eng.*, ASCE, Vol.106, No.HY1.
- Stauble, D.K.(ed.), 1989. "Barrier islands: process and management." ACES, Volume published as series of papers from the Coastal Zone 89 Conf.
- Stauble, D.K., Eiser, W.C., Birkemeier, W.A., Hales, L.Z., and Seabergh, W.C., 1990. "Erosion characteristics of Hurricane Hugo on the beaches of South Carolina." *Shore and Beach*, Vol.58, No.4.
- Steetzel, H.J., 1993. "Cross-shore transport during storm surges." Ph.D. Thesis, Delft University of Tech., Delft, The Netherlands.
- Stone, G.W., Grymes III, J.M., Robbins, K.D., Underwood, S.G., Steyer, G.D., and Muller, R.A., 1993. "A chronologic overview of climatological and hydrological aspects associated with Hurricane Andrew and its morphological effects along the Louisiana coast, U.S.A." *Shore and Beach*, Vol.61, No.2.
- Svendsen, I.A., 1987. "Analysis of surf zone turbulence." *J. Geophysical Res.*, Vol.92, No.C5, pp.5115-5124.
- Swart, D.H., 1976. "Predictive equations regarding coastal transports." *Proc. 15th Conf. Coastal Eng.*, Honolulu, pp.1113-1132.
- Tayfur, G., Kavvas, M.L., Govindaraju, R.S., and Storm, P.E., 1993. "Applicability of St. Venant equations for two-dimensional overland flows over rough infiltrating surfaces." *J. Hydr. Eng.*, ASCE, Vol.119, No.1.
- U.S. Army, 1989. "Beach erosion control and hurricane protection, Virginia Beach, Virginia." Phase II-General Design Memo., Vol.III, Corps of Engineers, Norfolk District Office.
- Vanoni, V.A. (ed.), 1975. "Sedimentation engineering.", ASCE.
- Vellinga, P., 1982. "Beach and dune erosion during storm surges." *Coastal Engineering*, 6, pp.361-387.
- Vellinga, P., 1983. "Predictive computational model for beach and dune erosion during storm surges." *Proc. Coastal Structures'83*, ASCE, pp. 806-819.

- Voogt, H.L., van Rijn, L.C., and van den Berg, J.H., 1991. "Sediment transport of fine sands at high velocities." *J. Hydr. Eng.*, ASCE, Vol.117, No.7.
- de Vries, M., 1965. "Considerations about non-steady bed-load transport." *Proc. 11th Congress, Int. Ass. of Hydraulic Res.*, Vol.3, paper 3.8, Leningrad, USSR.
- de Vries, M., 1973. "River-bed variations-aggradation and degradation." Delft Hydr. Lab. Publ. No.107.
- de Vries, M., 1975. "A morphological time scale for rivers." *Proc. 14th Congress, Int. Ass. of Hydraulic Res.*, Vol.2, paper B3, SaoPaulo, Brazil.
- White, W.R., Milli, H., and Crabbe, C., 1973. "Sediment transport: an appraisal of available methods." Hydr. Res. Station, Wallingford.
- Wilson, K.C., 1987. "Analysis of bed-load motion at high shear stress." *J. Hydr. Eng.*, ASCE, Vol.113, No.1.
- Wilson, K.C., and Nnadi, F.N., 1990. "Behavior of mobile beds at high shear stress." *Proc. 22nd Conf. Coastal Eng.*, Delft, The Netherlands.
- Zanke, U., 1977. "Berechnung der Sinkgeschwindigkeiten von Sedimenten." *Mitt. des Franzius-Instituts für Wasserbau*, Heft46, Seite243, Tech. Univ., Hannover, Germany.

APPENDIX A

The appendix presents a flow chart of overall simulation and a user interface *Configuration File* which allows entry and manipulation of the *start* file containing basic information necessary for executing **SBEACH**. The configuration file is separated into five sections: A - Model Setup; B - Waves/Water Elevation/Wind; C - Beach; D - Beach Fill; E - Seawall/Revetment.

To run SBEACH, five types of input data are required :

- *Initial beach profile data.*
- *Median grain size representative of the surf zone and beach.*
- *Time series of water level.*
- *Time series (or constant) of wave height and period.*
- *Values of model parameters.*

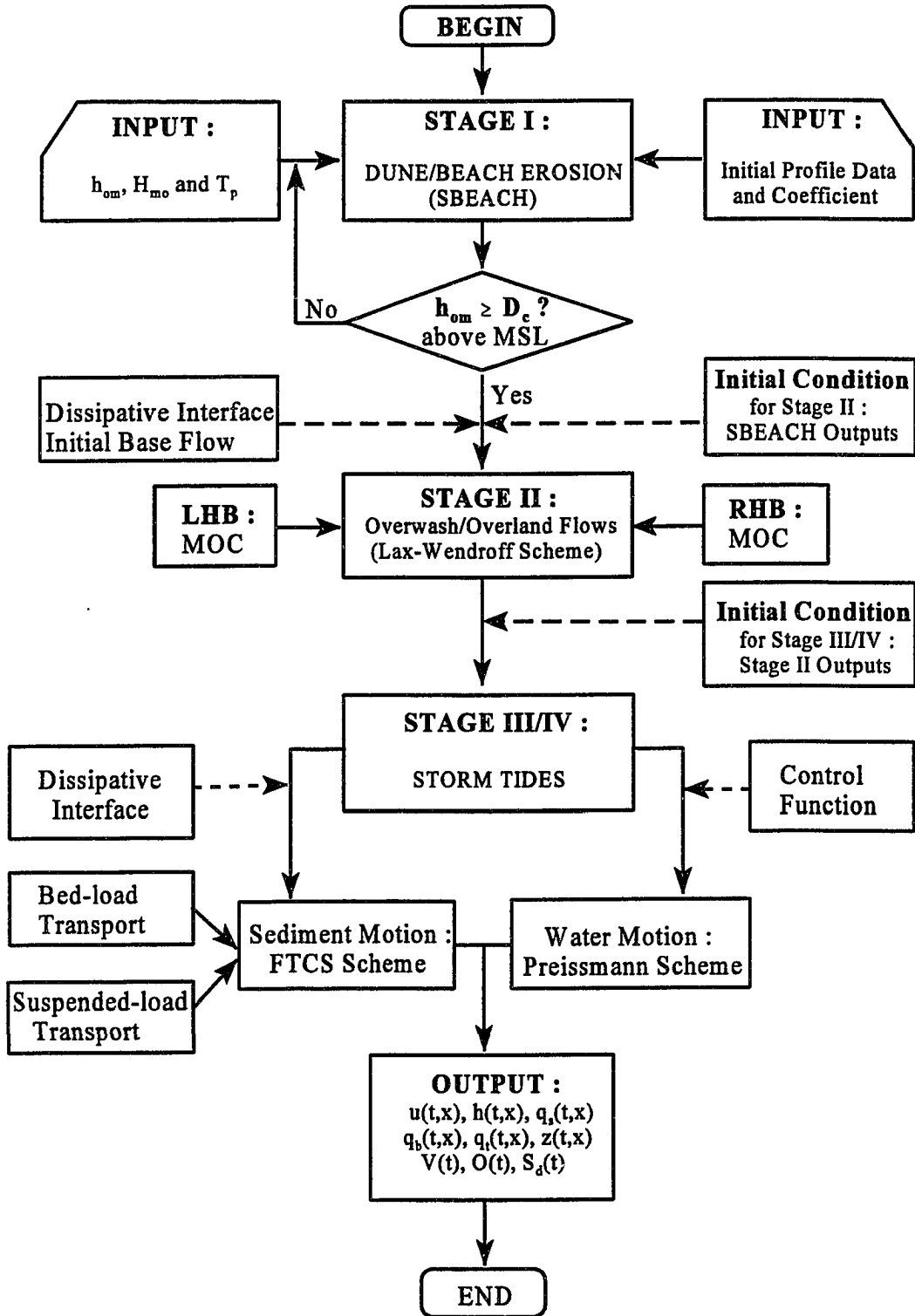
Output data are reported in four files :

- **__.PRC** : *Calculated profile data at intermediate and final time steps.*
- **__.XVR** : *Calculated maximum wave height, water elevation plus setup, water depth and volume change.*
- **__.LOG** : *A record of various coastal processes (i.e. accretion, erosion, overwash, boundary limited runup and inundation).*
- **__.RPT** : *A record of input data, as well as output parameters.*

(.PRC, .XVR, .LOG, and .RPT are file extensions)

If the water level at the ocean boundary exceeds the eroded dune crest elevation, then simulation is stopped (need trial and error). The data format of final calculated profile in **__.PRC** is then modified and used as initial bottom boundary conditions for the subsequent Stages II, III and IV.

FLOW CHART



```

*****
*   SBEACH model configuration file:   1000.CFG   *
*****

```

A----- MODEL SETUP -----A

```

A.1  RUN TITLE: TITLE
      1000 year return period
A.2  INPUT UNITS (SI=1, AMERICAN CUST.=2): UNITS
      1
A.3  TOTAL NUMBER OF CALCULATION CELLS AND POSITION OF LANDWARD BOUNDARY
      RELATIVE TO INITIAL PROFILE: NDX, XSTART
      473      0.00
A.4  GRID TYPE (CONSTANT=0, VARIABLE=1): IDX
      0
A.5  COMMENT: IF GRID TYPE IS VARIABLE, CONTINUE TO A.8
A.6  CONSTANT GRID CELL WIDTH: DXC
      5
A.7  COMMENT: IF GRID TYPE IS CONSTANT CONTINUE TO A.10
A.8  NUMBER OF DIFFERENT GRID CELL REGIONS: NGRID
      0
A.9  GRID CELL WIDTHS AND NUMBER OF CELLS IN EACH REGION FROM LANDWARD
      TO SEAWARD BOUNDARY: (DXV(I), NDXV(I), I=1,NGRID)

A.10 NUMBER OF TIME STEPS AND VALUE OF TIME STEP IN MINUTES: NDT,DT
      96      5.00
A.11 NUMBER OF TIME STEP(S) INTERMEDIATE OUTPUT IS WANTED: NWR
      0
A.12 TIME STEPS OF INTERMEDIATE OUTPUT: (WRI(I), I=1,NWR)

A.13 IS A MEASURED PROFILE AVAILABLE FOR COMPARISON? (NO=0, YES=1):
      ICOMP
      0
A.14 THREE PROFILE ELEVATION CONTOURS (MAXIMUM HORIZONTAL RECESSION OF
      EACH WILL BE DETERMINED): ELV1, ELV2, ELV3
      1.00      0.00      -1.00
A.15 THREE PROFILE EROSION DEPTHS AND REFERENCE ELEVATION (DISTANCE FROM
      POSITION OF REFERENCE ELEVATION ON INITIAL PROFILE TO POSITION OF
      LANDWARD MOST OCCURRENCE OF EACH EROSION DEPTH WILL BE DETERMINED
      EDP1, EDP2, EDP3, REFELV
      0.50      1.00      1.50      0.00
A.16 TRANSPORT RATE COEFFICIENT (m^4/N): K
      1.5e-6
A.17 COEFFICIENT FOR SLOPE-DEPENDENT TERM (m^2/s): EPS
      0.002000
A.18 TRANSPORT RATE DECAY COEFFICIENT MULTIPLIER: LAMM
      0.400000
A.19 WATER TEMPERATURE IN DEGREES C: TEMPC
      20.00

```

B----- WAVES/WATER ELEVATION/WIND -----B

```

B.1  WAVE TYPE (MONOCHROMATIC=1, IRREGULAR=2): WVTYPE
      2

```

B.2 WAVE HEIGHT AND PERIOD INPUT (CONSTANT=0, VARIABLE=1): IWAVE
0

B.3 COMMENT: IF WAVE HEIGHT AND PERIOD ARE VARIABLE, CONTINUE TO B.6

B.4 CONSTANT WAVE HEIGHT AND PERIOD: HIN, T
5.54 15.25

B.5 COMMENT: IF WAVE HEIGHT AND PERIOD ARE CONSTANT, CONTINUE TO B.7

B.6 TIME STEP OF VARIABLE WAVE HEIGHT AND PERIOD INPUT IN MINUTES:
DTWAV
0.00

B.7 WAVE ANGLE INPUT (CONSTANT=0, VARIABLE=1): IANG
0

B.8 COMMENT: IF WAVE ANGLE IS VARIABLE, CONTINUE TO B.11

B.9 CONSTANT WAVE ANGLE: ZIN
0.00

B.10 COMMENT: IF WAVE ANGLE IS CONSTANT, CONTINUE TO B.12

B.11 TIME STEP OF VARIABLE WAVE ANGLE INPUT IN MINUTES: DTANG
0.00

B.12 WATER DEPTH OF INPUT WAVES (DEEPWATER=0): DMEAS
0.00

B.13 IS RANDOMIZATION OF WAVE HEIGHT DESIRED? (NO=0, YES=1): IRAND
1

B.14 COMMENT: IF RANDOMIZATION OF WAVE HEIGHT IS NOT DESIRED, CONTINUE
TO B.16

B.15 SEED VALUE FOR RANDOMIZER AND PERCENT OF VARIABILITY: ISEED, RPERC
4567 20.00

B.16 TOTAL WATER ELEVATION INPUT (CONSTANT=0, VARIABLE=1): IELEV
1

B.17 COMMENT: IF WATER ELEVATION IS VARIABLE CONTINUE TO B.20

B.18 CONSTANT TOTAL WATER ELEVATION: TELEV
1.60

B.19 COMMENT: IF WATER ELEVATION IS CONSTANT, CONTINUE TO B.21

B.20 TIME STEP OF VARIABLE TOTAL WATER ELEVATION INPUT IN MINUTES: DTELV
60.00

B.21 WIND SPEED AND ANGLE INPUT (CONSTANT=0, VARIABLE=1): IWIND
0

B.22 COMMENT: IF WIND SPEED AND ANGLE ARE VARIABLE, CONTINUE TO B.25

B.23 CONSTANT WIND SPEED AND ANGLE: W,ZWIND
0.00 0.00

B.24 COMMENT: IF WIND SPEED AND ANGLE ARE CONSTANT, CONTINUE TO C.

B.25 TIME STEP OF VARIABLE WIND SPEED AND ANGLE INPUT IN MINUTES: DTWIND
0.00

C----- BEACH -----C

C.1 TYPE OF INPUT PROFILE (ARBITRARY=1, SCHEMATIZED=2): TPIN
1

C.2 COMMENT: IF PROFILE TYPE IS ARBITRARY CONTINUE TO C.4

C.3 LOCATION AND ELEVATION OF LANDWARD BOUNDARY, LANDWARD BASE OF DUNE,
LANDWARD CREST OF DUNE, SEAWARD CREST OF DUNE, START OF BERM,
END OF BERM, AND FORESHORE: XLAND, DLAND, XLBDUNE, DLBDUNE, XLCDUNE,
DLCDUNE, XSCDUNE, DSCDUNE, XBERMS, DBERMS, XBERME, DBERME, XFORS, DFORS
0.00 9.00 20.00 9.00 50.00 11.50
70.00 12.00 100.00 5.00 170.00 4.00 200.00 -2.00

```

C.4 DEPTH CORRESPONDING TO LANDWARD END OF SURF ZONE: DFS
    0.30
C.5 EFFECTIVE GRAIN SIZE DIAMETER IN MILLIMETERS: D50
    0.30
C.6 MAXIMUM PROFILE SLOPE PRIOR TO AVALANCHING IN DEGREES: BMAX
    15.00
D----- BEACH FILL -----D
D.1 IS A BEACH FILL PRESENT? (NO=0, YES=1): IBCHFILL
    0
D.2 COMMENT: IF NO BEACH FILL, CONTINUE TO E.
D.3 POSITION OF START AND END OF BEACH FILL RELATIVE
    TO INITIAL PROFILE: XBFS, XBFE
    0.00    0.00
D.4 NUMBER OF REPRESENTATIVE POINTS BETWEEN START
    AND END OF BEACH FILL: NFILL
    0
D.5 LOCATION AND ELEVATION OF REPRESENTATIVE POINTS RELATIVE TO THE
    INITIAL PROFILE: (XF(I), EFILL(I), I=1,NFILL)

E----- SEAWALL/REVTMENT -----E
E.1 IS A SEAWALL PRESENT? (NO=0, YES=1): ISWALL
    0
E.2 COMMENT: IF NO SEAWALL, CONTINUE TO F.
E.3 LOCATION OF SEAWALL RELATIVE TO INITIAL PROFILE: XSWALL
    0.00
E.4 IS SEAWALL ALLOWED TO FAIL? (NO=0, YES =1): ISWFAIL
    0
E.5 COMMENT: IF NO SEAWALL FAILURE, CONTINUE TO F.
E.6 PROFILE ELEVATION AT SEAWALL WHICH CAUSES FAILURE, TOTAL WATER
    ELEVATION AT SEAWALL WHICH CAUSES FAILURE, AND WAVE HEIGHT AT
    SEAWALL WHICH CAUSES FAILURE: PEFAIL, WEFAIL,HFAIL
    0.00    0.00    0.00
F----- COMMENTS -----F
----- END -----

```

APPENDIX B

The appendix presents the complete listing of the following computer programs based on the theory presented in the dissertation. The programs consist of a main and eight subroutines with a function routine for Stages II, III and IV.

- Program **MAIN** : *Defines arguments of variables, and inputs overall constants and parameters.*
- Subroutine **STAGE2** : *Computes Stage II, overwash/overland flows using the Lax-Wendroff scheme.*
- Subroutine **LHB** : *Computes left hand boundary data using the method of characteristics.*
- Subroutine **RHB** : *Computes right hand boundary data using the method of characteristics.*
- Subroutine **NRITER** : *Computes characteristic distances in boundary modules using the Newton-Raphson iteration method.*
- Subroutine **STAGE34** : *Computes Stages III/IV, storm tidal flows using the Preissmann scheme by double sweep solution procedure.*
- Subroutine **SUPER** : *Computes super-critical flows during Stages III/IV, however, this routine is not used in actual calculation.*
- Subroutine **SEDIM1** : *Computes profile evolutions using the FTCS scheme with sediment transport formulas of van Rijn(1984a&b).*
- Subroutine **VOLUME** : *Computes barrier volumes, centroid positions, dune speeds and numerical errors.*
- Function **Y** : *Defines each iterative function for four different type of boundaries in Stage II.*


```

c
c
common ho(500),hn(500),qo(500),qn(500),uo(500),un(500),zo(500),
&      zn(500),yo(500),yn(500),qto(500),qtn(500),pfdist,time,
&      hpeako,hpeakb,tlend,t2time,t2end,t3time,t3end,hini,gr,
&      timelag,d50,d90,phi,xdist(500)
common /first/ hhalf(500), qhalf(500), deltax, deltat, mm, nn,
&      kk, ll, i
common /fourth/etod, emsl, etodz
c
c      Input parameters and constants
c
hpeako=4.
hpeakb=3.
timelag=10800.
pfdist=2360.
time=86400.
phi=3.14159265
gr=9.81
d50=0.0003
d90=0.0004
hini=0.05
c
c      calculation of "tlend".
c
c      "tlend" is the SBEACH running time until water level reaches up
c      to the top of eroded dune ,and this time is also employed for the
c      bay side water level rise with timelag.
c
print *, '***** programmed by Cheol Shik Shin *****'
&
&
c
print *, 'input elevation of top of eroded dune above MSL,etod'
read *, etod
print *, 'input elevation of MSL above datum, emsl'
read *, emsl
c
c      elevation of top of eroded dune above datum, etodz
etodz=etod+emsl
c
tlend=time/(2.*phi)*log(sqrt(hpeako/etod)-sqrt(hpeako/etod-1.))
&      +time/2.
print *, tlend
t2time=1200.
t2end=tlend+t2time
t3time=time-t2end
t3end=t2end+t3time
c
c
c      Calculation of stage II.( Lax-Wendroff scheme )
c
call stage2
print *, 'end of stage 2'
c
c      Calculation of stage III/IV.( Preissmann scheme )
c
call stage34

```



```

stop
end
C
*****
*
*   Stage II is for the initial condition of water flow in stage III *
*   and IV. *
*
*   The Lax-Wendroff two-step scheme is adopted, and the method of *
*   characteristic is elaborated to compute additional boundary data *
*   (i.e. flow rate) at both boundaries. *
*
*   Simulation time is defined as t2time. (about 10-20 min.) *
*
*
*   etod   : the top elevation of the eroded dune above datum *
*   emsl   : the elevation of MSL above datum *
*   etodz  : the elevation of the top of eroded dune above datum *
*   bwlr   : the bay side water level rise during SBEACH with timelag *
*   webz   : the elevation of the water surface above datum at bay *
*
*****
  subroutine stage2
  dimension ff(500), gg(500), fhalf(500), ghalf(500)
  common ho(500), hn(500), qo(500), qn(500), uo(500), un(500), zo(500),
&      zn(500), yo(500), yn(500), qto(500), qtn(500), pfdist, time,
&      hpeako, hpeakb, tlend, t2time, t2end, t3time, t3end, hini, gr,
&      timelag, d50, d90, phi, xdist(500)
  common /first/ hhalf(500), qhalf(500), deltax, deltat, mm, nn,
&      kk, ll, i
  common /fourth/ etod, emsl, etodz
  integer kk, ll, mm, nn, nend
  real cp, cn, crnol, crno2
C
  deltax=10.
  deltat=.5
  mm=t2time/deltat+1
  nn=2*pfdist/deltax+1
C
  data input(x,z) from the modification of the SBEACH outputs
C
  open(unit=9, file='48hom4.dat', status='unknown')
C
  initial condition
C
  elev1=etodz+hini
  bwlr=hpeakb*1./(cosh(2.*phi*(tlend-timelag-time)/2.)/time)**2
  webz=bwlr+emsl
  elev2=webz+hini
C
  print *, 'you will need to confer initial bottom elevation data in
& x, z format'
  print *, '*****'
  print *, 'elevation at top of dune above datum, etodz=', etodz
  print *, 'water surface elevation above datum at bay, webz=', webz
  print *, 'input distance from ocean boundary to top of dune after
& SBEACH, xtod='
  read *, xtod

```

```

    print *, 'input distance from ocean boundary to end of barrier
& island after SBEACH, xebi='
    read *, xebi
c
c   compute initial water depth at ocean and bay.
c
do 10 j=1,nn
read(9,*) xdists(j), zo(j)
    if(xdists(j).lt.xtod) then
        ho(j)=(elev1-zo(j))*1.02
    else if(xdists(j).gt.xebi) then
        ho(j)=(elev2-zo(j))*1.02
    else
        ho(j)=hini
    end if
    uo(j)=0.
    qo(j)=0.
10 continue
c
c   introduce numerical filter for smoothing of initial bottom
c   bathymetry.
c
    gamma=1./16.
90   if (sum .lt. 10) then
        sum=sum+1
        zo(1)=gamma*zo(2)+(1.-gamma)*zo(1)
        zo(nn)=(1.-gamma)*zo(nn)+gamma*zo(nn-1)
c         ho(1)=elev1-zo(1)
c         ho(nn)=elev2-zo(nn)

do 111 j=2,nn-1
zo(j)=gamma*zo(j+1)+(1.-2.*gamma)*zo(j)+gamma*zo(j-1)
c   ho(j)=yo(j)-zo(j)
111 continue
go to 90
end if

c
c   input initial right and left hand boundary data
c
    hinio=ho(1)
    hinib=ho(nn)
c
c
do 30 i=1,mm-1
c
c   start Lax-Wendroff two-step scheme
c
c   n+1/2 step (first step)
c
    nend=(nn-1)/2-1
do 40 j=1,nend
ff(2*j)=(qo(2*j))**2/ho(2*j)+gr*ho(2*j)**2/2.
ff(2*j+2)=(qo(2*j+2))**2/ho(2*j+2)+gr*ho(2*j+2)**2/2.
c
    if(ho(2*j).lt.0.) then
        print *, i, 2*j, ho(2*j)
        stop

```

```

end if
cz1=18.*log10(12.*ho(2*j)/(3.*d90))
cz2=18.*log10(12.*ho(2*j+2)/(3.*d90))
c
gg(2*j)=gr*ho(2*j)*2.*(zo(2*j)-zo(2*j+1))/deltax-gr*qo(2*j)*
&      abs(qo(2*j))/(cz1*ho(2*j))**2
gg(2*j+2)=gr*ho(2*j+2)*2.*(zo(2*j+2)-zo(2*j+3))/deltax-gr*
&      qo(2*j+2)*abs(qo(2*j+2))/(cz2*ho(2*j+2))**2
c
hhalf(2*j+1)=(ho(2*j+2)+ho(2*j))/2.-deltat/(2.*deltax)
&      *(qo(2*j+2)-qo(2*j))
qhalf(2*j+1)=(qo(2*j+2)+qo(2*j))/2.-deltat/(2.*deltax)
&      *(ff(2*j+2)-ff(2*j))+deltat/4.*(gg(2*j+2)+gg(2*j))
40 continue
c
c      find qhalf(1) and qhalf(nn) by Method of Characteristic
c
c      Ocean side half step boundary condition
c
hhalf(1)=hinio+hpeako*(1./(cosh(2.*phi*((tlend+deltat*
&      float(i-0.5))-time/2.)/time))**2-1./(cosh(2.*phi*(tlend-
&      time/2.)/time))**2)
c
c      Bay side half step boundary condition
c
hhalf(nn)=hinib+hpeakb*(1./(cosh(2.*phi*((tlend+deltat*
&      float(i-0.5))-(timelag+time/2.)/time))**2-1./(cosh(2.*
&      phi*(tlend-(timelag+time/2.)/time))**2)
c      print *, i+1, hhalf(1), hhalf(nn)
c
c      call n+1/2 step boundary conditions to get qhalf(1), qhalf(nn)
c
kk=1
c
call lhb
c
call rhb
c
c      n+1 step (second-step)
c
do 50 j=1,(nn-1)/2
c
fhalf(2*j-1)=(qhalf(2*j-1))**2/hhalf(2*j-1)+gr*(hhalf(2*j-1))**2
&      /2.
fhalf(2*j+1)=(qhalf(2*j+1))**2/hhalf(2*j+1)+gr*(hhalf(2*j+1))**2
&      /2.
c
cz3=18.*log10(12.*hhalf(2*j-1)/(3.*d90))
cz4=18.*log10(12.*hhalf(2*j+1)/(3.*d90))
c
ghalf(2*j-1)=gr*hhalf(2*j-1)*2.*(zo(2*j-1)-zo(2*j))/deltax-gr*
&      qhalf(2*j-1)*abs(qhalf(2*j-1))/(cz3*hhalf(2*j-1))**2
c
if(j.eq.(nn-1)/2) then
temp=2.*(zo(nn-1)-zo(nn))/deltax
else
temp=2.*(zo(2*j+1)-zo(2*j+2))/deltax
end if

```

```

c
  ghalf(2*j+1)=gr*hhalf(2*j+1)*temp-gr*qhalf(2*j+1)*
&      abs(qhalf(2*j+1))/(cz4*hhalf(2*j+1))**2
c
  hn(2*j)=ho(2*j)-deltat/deltax*(qhalf(2*j+1)-qhalf(2*j-1))
  qn(2*j)=qo(2*j)-deltat/deltax*(fhalf(2*j+1)-fhalf(2*j-1))
&      +deltat/2.*(ghalf(2*j+1)+ghalf(2*j-1))
50  continue
c
c  find q(i+1,1) and q(i+1,nn) by Method of Characteristic
c
c  Ocean side full step boundary condition
c
  hn(1)=hinio+hpeako*(1./(cosh(2.*phi*((tlend+deltat*float(i)
&      )-time/2.)/time))**2-1./(cosh(2.*phi*(tlend-time/2.)/
&      time))**2)
c
c  Bay side full step boundary condition
c
  hn(nn)=hinib+hpeakb*(1./(cosh(2.*phi*((tlend+deltat*
&      float(i)-(timelag+time/2.)/time))**2-1./(cosh(2.*phi*
&      (tlend-(timelag+time/2.)/time))**2)
c
  kk=2
c
  call lhb
c
  call rhb
c
c  introduce dissipative interface on n+1 step for stability
c
  gamma=1./20.
  hn(1)=gamma*hn(2)+(1.-gamma)*hn(1)
  hn(nn)=(1.-gamma)*hn(nn)+gamma*hn(nn-1)
  qn(1)=gamma*qn(2)+(1.-gamma)*qn(1)
  qn(nn)=(1.-gamma)*qn(nn)+gamma*qn(nn-1)
c
  do 42 j=2, (nn-3)/2
  hn(2*j)=gamma*hn(2*j-2)+(1.-2.*gamma)*hn(2*j)+gamma*hn(2*j+2)
  qn(2*j)=gamma*qn(2*j-2)+(1.-2.*gamma)*qn(2*j)+gamma*qn(2*j+2)
42  continue
c
  un(1)=qn(1)/hn(1)
  un(nn)=qn(nn)/hn(nn)
  do 43 j=1, (nn-1)/2
  un(2*j)=qn(2*j)/hn(2*j)
c
43  continue
c
c  stability check
c
  cp=un(2*j)+sqrt(gr*hn(2*j))
  cn=un(2*j)-sqrt(gr*hn(2*j))
  crno1=abs(cp)*deltat/deltax
  crno2=abs(cn)*deltat/deltax
c
  if((crno1.gt. 1.) .or. (crno2.gt. 1.)) then
  print *, 'i+1=', i+1, '2j=', 2*j, 'warning ! Courant No is gt 1.'

```

```

print *, un(2*j), hn(2*j), crno1, crno2
stop
end if
c
if(i.eq.mm-1) go to 33
do 51 j=1, (nn-1)/2
    ho(2*j)=hn(2*j)
    uo(2*j)=un(2*j)
    qo(2*j)=qn(2*j)
c
    print *, 'i=', i, ho(2*j), uo(2*j), qo(2*j)
51 continue
c
c
initialize variables
c
ho(1)=hn(1)
ho(nn)=hn(nn)
uo(1)=un(1)
uo(nn)=un(nn)
qo(1)=qn(1)
qo(nn)=qn(nn)
c
c
write(6,52) I
c
30 continue
c
33 open(unit=10, file='hstge2.dat', status='unknown')
open(unit=11, file='ustge2.dat', status='unknown')
c
write(10,60) hn(1)
write(11,60) un(1)
do 70 j=1, (nn-1)/2
write(10,60) hn(2*j)
write(11,60) un(2*j)
70 continue
write(10,60) hn(nn)
write(11,60) un(nn)
60 format(f10.3)
c
close(unit=10)
close(unit=11)
c
return
end
c
*****
* This subroutine is for the calc. of q(i+1/2,1) and q(i+1,1) at *
* left hand boundary using the Method of Characteristics. *
* * * * *
* Arguments of Variables *
* * * * *
* ll=1 : left hand boundary *
* ll=2 : right hand boundary *
* kk=1 : half step boundary, (n+1/2) *
* kk=2 : full step boundary, (n+1) *
* * * * *
* rni : negative Riemann invariant, m/s *
* rpi : positive Riemann invariant, m/s *
*****

```

```

*       x       : characteristic distance, m
*
*****
      subroutine lhb
      common ho(500),hn(500),qo(500),qn(500),uo(500),un(500),zo(500),
&          zn(500),yo(500),yn(500),qto(500),qtn(500),pfdist,time,
&          hpeako,hpeakb,tlend,t2time,t2end,t3time,t3end,hini,gr,
&          timelag,d50,d90,phi,xdist(500)
      common /first/ hhalf(500), qhalf(500), deltax, deltat, mm, nn,
&          kk, ll, i
      real x, qq, hh, rni
c
      ll=1
      if(kk .eq. 1) then
c
      call nriter(x)
c
      qq=(x*qo(2)+(deltax/2.-x)*qo(1))/(deltax/2.)
      hh=(x*ho(2)+(deltax/2.-x)*ho(1))/(deltax/2.)
      rni=qq/hh-2.*sqrt(gr*hh)
      cz=18.*log10(12.*hh/(3.*d90))
c
      qhalf(1)=hhalf(1)*(rni+2.*sqrt(gr*hhalf(1))+gr*((zo(1)-zo(2))*
&          2./deltax-qq*abs(qq)/cz**2/hh**3)*(deltat/2.))
c
      else
      qhalf(2)=(qhalf(1)+qhalf(3)+qo(2)+qn(2))/4.
      hhalf(2)=(hhalf(1)+hhalf(3)+ho(2)+hn(2))/4.
c
      call nriter(x)
c
      qq=(x*qhalf(2)+(deltax/2.-x)*qhalf(1))/(deltax/2.)
      hh=(x*hhalf(2)+(deltax/2.-x)*hhalf(1))/(deltax/2.)
      rni=qq/hh-2.*sqrt(gr*hh)
      cz=18.*log10(12.*hh/(3.*d90))
c
      qn(1)=hn(1)*(rni+2.*sqrt(gr*hn(1))+gr*((zo(1)-zo(2))*2./deltax-
&          qq*abs(qq)/cz**2/hh**3)*0.5*deltat)
c
      end if
      return
      end
c
*****
*       This subroutine is for the calc. of q(i+1/2,nn) and q(i+1,nn) at
*       right hand boundary using the Method of Characteristics.
*
*****
      subroutine rhb
      common ho(500),hn(500),qo(500),qn(500),uo(500),un(500),zo(500),
&          zn(500),yo(500),yn(500),qto(500),qtn(500),pfdist,time,
&          hpeako,hpeakb,tlend,t2time,t2end,t3time,t3end,hini,gr,
&          timelag,d50,d90,phi,xdist(500)
      common/first/ hhalf(500), qhalf(500), deltax, deltat, mm, nn,
&          kk, ll, i
      integer kk, ll, mm, nn
      real x, qq, hh, rpi
c

```

```

ll=2
if(kk .eq. 1) then
c
call nriter(x)
c
qq=(x*go(nn-1)+(deltax/2.-x)*go(nn))/(deltax/2.)
hh=(x*ho(nn-1)+(deltax/2.-x)*ho(nn))/(deltax/2.)
rpi=qq/hh+2.*sqrt(gr*hh)
cz=18.*log10(12.*hh/(3.*d90))
c
qhalf(nn)=hhalf(nn)*(rpi-2.*sqrt(gr*hhalf(nn))+gr*((zo(nn-1)-
& zo(nn))*2./deltax-qq*abs(qq)/cz**2/hh**3)*0.5*deltat)
c
else
qhalf(nn-1)=(qhalf(nn)+qhalf(nn-2)+go(nn-1)+qn(nn-1))/4.
hhalf(nn-1)=(hhalf(nn)+hhalf(nn-2)+ho(nn-1)+hn(nn-1))/4.
c
call nriter(x)
c
qq=(x*qhalf(nn-1)+(deltax/2.-x)*qhalf(nn))/(deltax/2.)
hh=(x*hhalf(nn-1)+(deltax/2.-x)*hhalf(nn))/(deltax/2.)
rpi=qq/hh+2.*sqrt(gr*hh)
cz=18.*log10(12.*hh/(3.*d90))
c
qn(nn)=hn(nn)*(rpi-2.*sqrt(gr*hn(nn))+gr*((zo(nn-1)-zo(nn))*
& 2./deltax-qq*abs(qq)/cz**2/hh**3)*0.5*deltat)
end if
return
end
c
*****
* This subroutine is for the calculation of a characteristic *
* distance, x using Newton-Raphson iteration method at the both *
* boundaries. *
* *
*****
subroutine nriter(x)
common ho(500),hn(500),go(500),qn(500),uo(500),un(500),zo(500),
& zn(500),yo(500),yn(500),qto(500),qtn(500),pfdist,time,
& hpeako,hpeakb,tlend,t2time,t2end,t3time,t3end,hini,gr,
& timelag,d50,d90,phi,xdist(500)
common/first/ hhalf(500), qhalf(500), deltax, deltat, mm, nn,
& kk, ll, i
real x, y, eps, xmax, y1, y2, dx, yd, xn
c
eps=0.00001*deltax/2.
x=0.25*deltax
xmax=deltax/2.
10 y1=y(x)
c
c check for convergence
c
if(abs(y1) .gt. eps) then
xn=x+0.00001*deltax/2.
y2=y(xn)
yd=(y2-y1)/(0.00001*deltax/2.)
c
c check if results diverge

```



```

*
*   psi   : weighting factor for space
*   theta : weighting factor for time
*
*****
  subroutine stage34
  dimension delz(500)
  common ho(500),hn(500),qo(500),qn(500),uo(500),un(500),zo(500),
&       zn(500),yo(500),yn(500),qto(500),qtn(500),pfdist,time,
&       hpeako,hpeakb,tlend,t2time,t2end,t3time,t3end,hini,gr,
&       timelag,d50,d90,phi,xdist(500)
  common/second/froud(500),ustar(500),hstar(500),
&       pp(500),qq(500),rr(500),f(500),g(500)
  common/third/deltax,deltat,psi,theta,mm,nn,i,j
  common/fifth/tmpv1,tqtn(500)

c
c   Input all constants and parameters.
c
  deltax=10.
  deltat=4.
  psi=0.5
  theta=0.75
  mm=t3time/deltat+1
  nn=pfdist/deltax+1

c
c   input initial condition for sediment transport rate, qt and z
c   rewrite zo(j) from Lax-Wendroff scheme to Preissmann scheme
c
  open(unit=14, file='hom4d.dat', status='unknown')
  do 10 j=1,nn
    zo(j)=zo(2*j-1)
    qto(j)=0.
    write(14,*) xdist(2*j-1), zo(j)
10  continue
c
  close(unit=14)

c
c   input initial condition from the results of stage II, and
c   interpolate initial conditions to fit stage III and IV's grids.
c
  open(unit=10, file='hstge2.dat')
  open(unit=11, file='ustge2.dat')
  read(10,*) (ho(j), j=1,nn+1)
  read(11,*) (uo(j), j=1,nn+1)

c
c
  do 80 j=2,nn-1
  ho(j)=(ho(j)+ho(j+1))/2.
  uo(j)=(uo(j)+uo(j+1))/2.
  yo(j)=ho(j)+zo(j)
80  continue
  ho(nn)=ho(nn+1)
  uo(nn)=uo(nn+1)
  yo(nn)=ho(nn)+zo(nn)
  yo(1)=ho(1)+zo(1)
  hinib=ho(nn)
  hinio=ho(1)

c

```

```

open(unit=18, file='1000.dat', status='unknown')
open(unit=19, file='3000.dat', status='unknown')
open(unit=20, file='6000.dat', status='unknown')
open(unit=21, file='9000.dat', status='unknown')
open(unit=22, file='final.dat', status='unknown')
C
C initialize variables for volume conservation checks, and
C for boundary conditions
C
tqtn(1)=0.0
tqtn(nn)=0.0
delz(1)=0.
delz(nn)=0.
delzl=0.
delznn=0.
C
open(unit=40, file='dummy.out', status='unknown')
C
do 30 I=1,nn-1
C
delzl=delzl+delz(1)
delznn=delznn+delz(nn)
C
C Input right hand boundary condition
C
hn(nn)=hinib+hpeakb*(1./(cosh(2.*phi*((t2end+deltat*
& float(i)-(timelag+time/2.))/time))**2-1./(cosh(2.*
& phi*(t2end-(timelag+time/2.))/time))**2)+delznn
C
m=0
f(nn)=0.
g(nn)=hn(nn)
C
C First sweep to get all f and g (from j=nn-1 to 1).
C
do 40 j=1,nn-1
ustar(j)=(uo(j+1)+uo(j))/2.
hstar(j)=(ho(j+1)+ho(j))/2.
40 continue
C
41 do 50 j=2,nn
jj=nn-j+1
C
C Introduce control function to suppress the convective accel. term.
C fr : Froud number
C cf : control function
C
fr=abs(ustar(jj)/sqrt(gr*hstar(jj)))
if (fr .gt. 1.) then
cf=0.
else
cf=1.-fr**2
end if
C
chezy=18.*log10(12.*ho(jj)/(3.*d90))
bs=gr/(4.*chezy**2*hstar(jj))*abs(uo(jj)+uo(jj+1))
a1=(1.-psi)/deltat-cf*ustar(jj)*theta/deltax+bs
b2=a1-bs

```

```

b1=-gr*theta/deltax
d1=-b1
c1=psi/deltat+cf*ustar(jj)*theta/deltax+bs
d2=c1-bs
a2=-hstar(jj)*theta/deltax
c2=-a2
c
e11=((1.-psi)/deltat+cf*ustar(jj)*(1.-theta)/deltax)*uo(jj)
e12=(gr*(1.-theta)/deltax)*ho(jj)
e13=(psi/deltat-cf*ustar(jj)*(1.-theta)/deltax)*uo(jj+1)
e14=-(gr*(1.-theta)/deltax)*ho(jj+1)+gr*(zo(jj)-zo(jj+1))/deltax
e1=e11+e12+e13+e14
c
c
e21=(hstar(jj)*(1.-theta)/deltax)*uo(jj)
e22=((1.-psi)/deltat+ustar(jj)*(1.-theta)/deltax)*ho(jj)
e23=-(hstar(jj)*(1.-theta)/deltax)*uo(jj+1)
e24=(psi/deltat-ustar(jj)*(1.-theta)/deltax)*ho(jj+1)
e2=e21+e22+e23+e24
c
c
c
c
Recurrence relations to calculate the initial sweep coefficients
c
f(jj)=-((c2+d2*f(jj+1))*a1-(c1+d1*f(jj+1))*a2)/
& ((c2+d2*f(jj+1))*b1-(c1+d1*f(jj+1))*b2)
g(jj)=((c2+d2*f(jj+1))*(e1-d1*g(jj+1))-(c1+d1*f(jj+1))*
& (e2-d2*g(jj+1)))/((c2+d2*f(jj+1))*b1-(c1+d1*f(jj+1))*b2)
c
c
Calculate new coefficients pp, qq and rr
c
pp(jj+1)=-a1/(c1+d1*f(jj+1))
qq(jj+1)=-b1/(c1+d1*f(jj+1))
rr(jj+1)=(e1-d1*g(jj+1))/(c1+d1*f(jj+1))
50 continue
c
c
Second sweep to get u and h at the n+1 time level.
c
c
Input left hand boundary data and get u.
c
hn(1)=hinio+hpeako*(1./(cosh(2.*phi*((t2end+deltat*float(i)
& )-time/2.)/time))**2-1./(cosh(2.*phi*(t2end-time/2.)/
& time))**2)+delz1
c
un(1)=(hn(1)-g(1))/f(1)
c
c
Calculation of u and h at certain time level and check
c Froud no. ,and find flow status(super- or sub- flow).
c
do 42 j=1,nn-1
c froud(j)=abs(un(j)/sqrt(gr*hn(j)))
c if(froud(j) .ge. 1.) then
c print *, 'super critical flow, i=', i, j, un(j),hn(j)
c
c call super
c
c else
c
c
un(j+1)=pp(j+1)*un(j)+qq(j+1)*hn(j)+rr(j+1)

```

```

hn(j+1)=f(j+1)*un(j+1)+g(j+1)
c
c   end if
42 continue
c
c   Update ustar and hstar.
c
c   if(m.eq.4) goto 32
c
c   do 43 j=1,nn-1
ustar(j)=(un(j+1)+uo(j+1)+un(j)+uo(j))/4.
hstar(j)=(hn(j+1)+ho(j+1)+hn(j)+ho(j))/4.
43 continue
c
m=m+1
go to 41
c
32 call sedim1
c
do 35 j=1,nn
  if(i .eq. 1000) write(18,*) i,xdist(2*j-1),hn(j),un(j),zn(j)
  if(i .eq. 3000) write(19,*) i,xdist(2*j-1),hn(j),un(j),zn(j)
  if(i .eq. 6000) write(20,*) i,xdist(2*j-1),hn(j),un(j),zn(j)
  if(i .eq. 9000) write(21,*) i,xdist(2*j-1),hn(j),un(j),zn(j)
  if(hn(j).lt.0.01 .or. i.eq.nnn-1) go to 36
35 continue
c
go to 38
c
c
36 do 37 j=1,nn
write(22,*) i, xdist(2*j-1), hn(j), un(j), zn(j)
37 continue
c
stop
c
c
38 write(6,33) i, zn(64)
33 format('+',i10,2x,'zn(64)=' , f10.5)
c
c   initialize known values for the next time level
c
delz(1)=zo(1)-zn(1)
delz(nn)=zo(nn)-zn(nn)
c
do 31 j=1,nn
  ho(j)=hn(j)
  uo(j)=un(j)
  zo(j)=zn(j)
  yo(j)=yn(j)
  qto(j)=qtn(j)
31 continue
c
go to next time level
c
30 continue
c

```

```

C
    close(unit=18)
    close(unit=19)
    close(unit=20)
    close(unit=21)
    close(unit=22)
C
    return
    end
C
*****
*   This subroutine is for the calculation of super-critical flows   *
*   from left to right(j=1 to jj) direction, however, this routine  *
*   is not used in actual computation.                               *
*                                                                     *
*****
    subroutine super
    common ho(500),hn(500),qo(500),qn(500),uo(500),un(500),zo(500),
    &      zn(500),yo(500),yn(500),qto(500),qtn(500),pfdist,time,
    &      hpeako,hpeakb,tlend,t2time,t2end,t3time,t3end,hini,gr,
    &      timelag,d50,d90,phi,xdist(500)
    common/second/froud(500),ustar(500),hstar(500),
    &      pp(500),qq(500),rr(500),f(500),g(500)
    common/third/deltax,deltat,psi,theta,mm,nn,i,j
C
    Single sweep to get u & h from left to right
C
    chezy=18.*log10(12.*ho(j)/(3.*d90))
    bs=gr/(4.*chezy**2*hstar(j))*abs(uo(j)+uo(j+1))
    a1=(1.-psi)/deltat-ustar(j)*theta/deltax+bs
    b2=a1-bs
    b1=-gr*theta/deltax
    d1=-b1
    c1=psi/deltat+ustar(j)*theta/deltax+bs
    d2=c1-bs
    a2=-hstar(j)*theta/deltax
    c2=-a2
C
    e11=((1.-psi)/deltat+ustar(j)*(1.-theta)/deltax)*uo(j)
    e12=(gr*(1.-theta)/deltax)*ho(j)
    e13=(psi/deltat-ustar(j)*(1.-theta)/deltax)*uo(j+1)
    e14=-gr*(1.-theta)/deltax*ho(j+1)+gr*(zo(j)-zo(z+1))/deltax
    e1=e11+e12+e13+e14
C
    e21=(hstar(j)*(1.-theta)/deltax)*uo(j)
    e22=((1.-psi)/deltat+ustar(j)*(1.-theta)/deltax)*ho(j)
    e23=-hstar(j)*(1.-theta)/deltax*uo(j+1)
    e24=(psi/deltat-ustar(j)*(1.-theta)/deltax)*ho(j+1)
    e2=e21+e22+e23+e24
C
    Calculation of u and h at time level n+1
C
    un(j+1)=((a2*d1-a1*d2)/(c1*d2-c2*d1))*un(j)+((b2*d1-b1*d2)
    &      / (c1*d2-c2*d1))*hn(j)+(d2*e1-d1*e2)/(c1*d2-c2*d1)
    hn(j+1)=- (c1/d1)*un(j+1)- (a1/d1)*un(j)- (b1/d1)*hn(j)+e1/d1
C
    return
    end

```



```

c
c      cbsv=sqrt(thetacr*(sden-1.)*gr*d50)
c
c      do 10 j=1,nn
c
c      compute Chezy-coefficient related to grains, cprime, effective
c      bed-shear velocity, ebsv and transport stage parameter, tsp.
c
c      cprime=18.*log10(12.*hn(j)/(3.*d90))
c      ebsv=(gr**0.5*abs(un(j)))/cpime
c      if(ebsv .le. cbsv) then
c          tsp=0.0
c          qtn(j)=0.
c          go to 10
c      else
c          tsp=((ebsv)**2-(cbsv)**2)/(cbsv)**2
c      end if
c
c      ***** bed-load transport rate, qb *****
c
c      compute bed-load concentration, cb, thickness of bed-load layer,
c      deltab and particle velocity, ub
c
c      cb=0.18*tsp/shields*co
c      deltab=0.3*shields**0.7*tsp**0.5*d50
c      ub=1.5*tsp**0.6*((sden-1.)*gr*d50)**0.5
c
c      compute bed-load transport
c
c      qb=cb*ub*deltab
c
c      ***** suspended-load transport, qs *****
c
c      compute reference level, a
c
c      ks=3.*d90
c      amin=0.01*hn(j)
c      if(ks .lt. amin) then
c          rla=amin
c      else
c          rla=ks
c      end if
c
c      compute reference concentration, ca
c
c      ca=0.015*(d50*tsp**1.5)/(rla*shields**0.3)
c
c      compute representative particle diameter of suspended sediment,
c      ds.
c      sigmas=geometric standard deviation of bed material
c
c      sigmas=2.5
c      ds=d50*(1.+0.011*(sigmas-1.)*(tsp-25.))
c
c      compute fall velocity of suspended sediment, ws
c
c      if(d50 .lt. 0.0001) then
c          ws=1./18.*(sden-1.)*gr*ds**2/vkin

```

```

else if(d50 .gt. 0.001) then
    ws=1.1*((sden-1.)*gr*ds)**0.5
else
    ws=10.*vkin/ds*((1.+0.01*(sden-1.)*gr*ds**3/temp)
&      **0.5-1.)
end if
c
c compute overall bed-shear velocity, obsv
c
obsv=gr**0.5*abs(un(j))/cprime
c
c compute beta-factor
c
if(obsv .gt. 2.*ws) then
    fbeta=1.+2.*(ws/obsv)**2
else
    fbeta=1.0
end if
c
c compute phi-factor for simplified method
c
fphi=2.5*(ws/obsv)**0.8*(ca/co)**0.4
c
c compute suspension parameter, Z and Z'
c
spz=ws/(fbeta*vonkn*obsv)
spzp=spz+fphi
c
c compute F-factor
c
temp1=(rla/hn(j))**spzp-(rla/hn(j))**1.2
temp2=(1.-rla/hn(j))**spzp*(1.2-spzp)
factor=temp1/temp2
if(i.eq.200) then
c print *, j, temp1, temp2, factor, rla,hn(j),un(j), spz,spzp
c end if
c
c compute suspended load transport, qs
c
qs=factor*abs(un(j))*hn(j)*ca
c
***** compute total load transport rate *****
c
if(un(j).lt.0.) then
    qtn(j)=-qs+qb
else
    qtn(j)=qs+qb
end if
c
c check suspended sediment ratio and un, hn at the initial top of
c dune (j=64) at every 100 time step
c
nnn=100*int(i/100)
if(i.eq.nnn .and. j.eq.64) then
    rs=qs/(qs+qb)
    ruws=obsv/ws
    write(23,*) i, rs, un(j), hn(j), qtn(j)
    write(24,*) ruws, rs

```



```

        end if
c
10  continue
c
c    check numerical dissipation, tmpv1 is actual volume change
c
    tqtn(1)=tqtn(1)+deltat*(qtn(1)+qto(1))/2.
    tqtn(nn)=tqtn(nn)+deltat*(qtn(nn)+qto(nn))/2.
    tmpv1=(tqtn(nn)-tqtn(1))/(1.-po)
c
c
*****  end of sediment transport formulas  *****
c
*****  start sediment continuity equation  *****
c
c    discretization of 1-D sediment transport equation using
c    centered space and forward time explicit scheme.
c
c    calculate new bottom elevation, zn at time level, n+1
c
    do 20 j=2,nn-1
c
        zn(j)=zo(j)-deltat/(2.*deltax*(1.-po))*(qtn(j+1)-qtn(j-1))
c
20  continue
c
*****          boundary conditions          *****
c
c    introduce Newmann type boundary conditions,
c
        zn(1)=zo(1)+2.*(zn(2)-zo(2))-(zn(3)-zo(3))
c
        zn(nn)=zo(nn)+2.*(zn(nn-1)-zo(nn-1))-(zn(nn-2)-zo(nn-2))
c
c    introduce Dirichlet type boundary conditions
c
        zn(1)=zo(1)
        zn(nn)=zo(nn)
c
*****          end of boundary condition          *****
c
c
*****          introduce dissipative interface          *****
c
c    zn(j) is the only variable to employ dissipative interface,
c    however, under certain flow condition hn(j) and un(j) will
c    need this (very rare).
c
    alpha=1./20.
    mmm=20*int(i/20)
c
    if(i.eq.mmm) then
    do 30 j=2,nn-1
        zn(j)=alpha*zn(j-1)+(1.-2.*alpha)*zn(j)+alpha*zn(j+1)
c        hn(j)=alpha*hn(j-1)+(1.-2.*alpha)*hn(j)+alpha*hn(j+1)
c        un(j)=alpha*un(j-1)+(1.-2.*alpha)*un(j)+alpha*un(j+1)
30  continue
c

```

```

      zn(1)=(1.-alpha)*zn(1)+alpha*zn(2)
      zn(nn)=alpha*zn(nn-1)+(1.-alpha)*zn(nn)
c      hn(1)=(1.-alpha)*hn(1)+alpha*hn(2)
c      hn(nn)=alpha*hn(nn-1)+(1.-alpha)*hn(nn)
c      un(1)=(1.-alpha)*un(1)+alpha*un(2)
c      un(nn)=alpha*un(nn-1)+(1.-alpha)*un(nn)
c
      end if
c
c      adjustments of flow characteristics due to sediment motion
c
      do 40 j=1,nn
      qn(j)=un(j)*hn(j)
      yn(j)=hn(j)+zo(j)
      hn(j)=yn(j)-zn(j)
      un(j)=qn(j)/hn(j)
40  continue
c
c      call subroutine "volume" for centroid and volume computation
c
      if(i.eq.1000) call volume
c
      if(i.eq.3000) call volume
c
      if(i.eq.6000) call volume
c
      if(i.eq.9000) call volume
c
      do 43 j=1,nn
      if(i.eq.mm-1 .or. hn(j).lt.0.01) then
          call volume
          go to 44
      end if
43  continue
c
c      adjusted variables are used for the next time step water
c      flow computation.
c
44  return
      end
c
*****
*
*      This routine is for the volume calculation above MLLW( or above *
*      a datum) and for the finding of centroid of the volume. *
*
*      zini(j) : initial profile *
*      zn(j)   : intermediate profile *
*      sumi    : total volume of initial profile above datum *
*      sumf    : total volume of intermediate profile *
*      dmlw   : height adjustment for MLLW to a datum *
*      xbari   : x-location of centroid, xbari=aixi/sumi, of initial *
*              profile *
*      ybari   : y-location of centroid, ybari=aiyi/sumi, of initial *
*              profile *
*      xbarf   : x-location of centroid, xbarf=afx/sumf, of intermed. *
*              profile *
*      ybarf   : y-location of centroid, ybarf=afyf/sumf, of intermed. *
*****

```

```

*           profile
*   xini    : beginning point of volume calculation
*
*****
      subroutine volume
      dimension voli(500), volf(500), zini(500), dist(500)
      common ho(500),hn(500),qo(500),qn(500),uo(500),un(500),zo(500),
&          zn(500),yo(500),yn(500),qto(500),qtn(500),pfdist,time,
&          hpeako,hpeakb,tlend,t2time,t2end,t3time,t3end,hini,gr,
&          timelag,d50,d90,phi,xdist(500)
      common/third/deltax,deltat,psi,theta,mm,nn,i,j
      common/fifth/tmpv1,tqtn(500)
c
c   call initial profile data(unit=14)
c
      open(unit=14, file='hom4d.dat')
      open(unit=25, file='cvc.dat', status='unknown')
c
      read(14,*) (dist(j), zini(j), j=1,nn)
c
      close(unit=14)
c
      adjustment of datum, elevation of MLLW above a profile datum
c
      dmllw=9.57
c
      do 9 j=1,nn
          zini(j)=zini(j)-dmllw
          zn(j)=zn(j)-dmllw
9      continue
c
c   initialization of volume
c
      sumi=0.
      sumf=0.
      aixi=0.
      aiyi=0.
      afxf=0.
      afyf=0.
c
c   calculation of volume and centroid
c
      do 10 j=1,nn-1
c
c   calculation for initial profile
c
      if(zini(j).lt.0. .and. zini(j+1).ge.0.) xini=dist(j+1)
          if(zini(j+1).ge.0. .and. zini(j+2).ge.0.) then
              voli(j)=(zini(j+2)+zini(j+1))*deltax/2.
              aixi=aixi+voli(j)*(dist(j+2)-xini-deltax/2.)
              aiyi=aiyi+voli(j)*(zini(j+2)+zini(j+1))/4.
              sumi=sumi+voli(j)
          else
              voli(j)=0.
          end if
c
c   calculation for final profile
c

```

```

if(zn(j).lt.0. .and. zn(j+1).ge.0.) xfin=dist(j+1)
if(zn(j+1).ge.0. .and. zn(j+2).ge.0.) then
    volf(j)=(zn(j+2)+zn(j+1))*deltax/2.
    afxf=afxf+volf(j)*(dist(j+2)-xfin-deltax/2)
    afyf=afyf+volf(j)*(zn(j+2)+zn(j+1))/4.
    sumf=sumf+volf(j)
    else
        volf(j)=0.
    end if
10 continue
c
c compute centroid, cumulative and percent volume change
c
if(sumf.le.0.) then
go to 22
else
    xbari=aixi/sumi+xini
    ybari=aiyi/sumi+dmlw
    xbarf=afxf/sumf+xfin
    ybarf=afyf/sumf+dmlw
    cumvolc=sumi-sumf
end if
c
c error1 is percent volume loss due to numerical errors
c error2 is percent volume loss through both boundaries
c
error1=(cumvolc-tmpv1)/sumi*100.
error2=tmpv1/sumi*100.
c
c pvolc is percent volume change , error1+error2
c
pvolc=cumvolc/sumi*100.
c
c compute speed of sand dune migration
c
if(i.eq.1000) then
dx=xbarf-xbari
dy=ybarf-ybari
io=0
else
    dx=xbarf-xbarfo
    dy=ybarf-ybarfo
end if
c
spdune=dx/abs(dx)*sqrt(dx**2+dy**2)/((i-io)*deltat)
c
write result in cvc--.out
c
write(25,20) i, sumi, sumf, cumvolc, pvolc, xbari, ybari, xbarf,
& ybarf, spdune,error1,error2
20 format('i=',i6,2x,'sumi=',f10.3,' sumf=',f10.3,' cumvolc=',
& f10.3,2x,'pvolc=',f8.3,/,8x,'xbari=',f9.3,2x,'ybari=',
& f8.3,2x,'xbarf=',f9.3,2x,'ybarf=',f8.3,
& /,10x,'spdune=',f8.3,' error1=',f8.3,' error2=',f8.3,/)
c
c relocate profiles for the flow computation
c
22 do 21 j=1,nn

```

```
zini(j)=zini(j)+dmlw
zn(j)=zn(j)+dmlw
21 continue
c
c set variables to compute dune speed
c
xbarfo=xbarf
ybarfo=ybarf
io=i
c
return
end
```

BIOGRAPHY

The author was born on September 4, 1960 in Jeon Ra Nam-Do, South Korea. He completed his early education up to the high school in there. He received B.C.E. and M.S. degrees in Civil Engineering from Seoul City University in February, 1986 and 1988, respectively. Also, he received another M.S. degree in Civil (Coastal) Engineering from University of Delaware in December, 1991.

He joined Old Dominion University to pursue Ph.D. degree in Civil (Coastal) Engineering and became a candidate in 1994. During his graduate study in ODU, he has been assigned to work on various researches supported by the U.S. Army Corps, CERC, the Commonwealth of Virginia and U.S. Navy as graduate research assistant. He is married to Mee Sung Shin and they have a son, Jang Ho Shin.

He has published the following articles:

Basco, D.R., and Shin, C.S., 1993. "Design wave information for Chesapeake Bay and major tributaries in Virginia." Dept. Civil Eng., *Tech. Rept. No.93-1*, Old Dominion University, Norfolk, Virginia.

Shin, C.S., Basco, D.R., Hill, L., and Baumer, J., 1994. "The application of a wave hindcasting model in Chesapeake Bay." *Proc. International Symp. : Waves-Physical and Numerical Modeling*, University of British Columbia, Vancouver, Canada.

Basco, D.R., and Shin, C.S., 1996. "Dune damage curves and their use to estimate dune maintenance coasts." *Proc. 25th Conf. Coastal Eng.*, Orlando, Florida. (to be appeared)